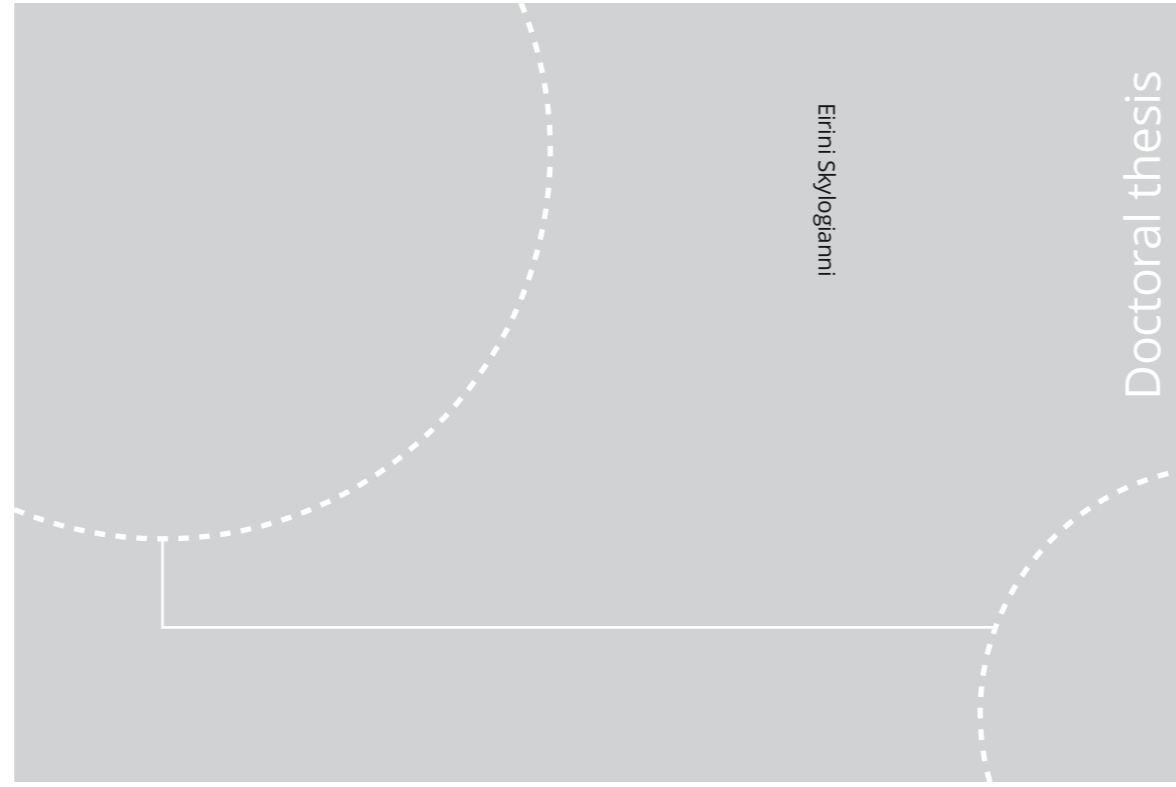


ISBN 978-82-326-4766-8 (printed ver.)  
ISBN 978-82-326-4767-5 (electronic ver.)  
ISSN 1503-8181



Doctoral theses at NTNU, 2020:209

Eirini Skylogianni

# Combined Hydrogen Sulfide Removal and Hydrate Control for Subsea Application

Characterization of Selected Blends

 **NTNU**  
Norwegian University of  
Science and Technology

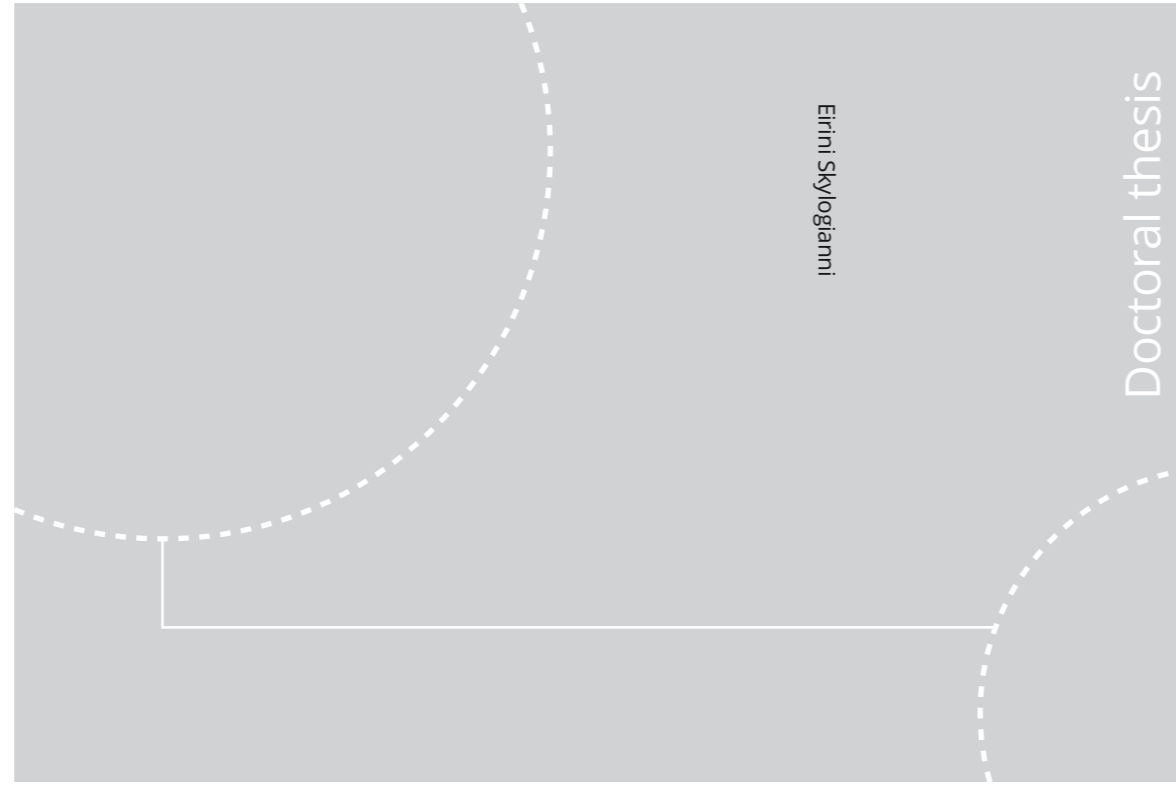
Doctoral theses at NTNU, 2020:209

 NTNU

**NTNU**  
Norwegian University of Science and Technology  
Thesis for the Degree of  
Philosophiae Doctor  
Faculty of Natural Sciences  
Department of Chemical Engineering

 **NTNU**  
Norwegian University of  
Science and Technology

ISBN 978-82-326-4766-8 (printed ver.)  
ISBN 978-82-326-4767-5 (electronic ver.)  
ISSN 1503-8181



Eirini Skylogianni

Doctoral thesis

Doctoral theses at NTNU, 2020:209

Eirini Skylogianni

# Combined Hydrogen Sulfide Removal and Hydrate Control for Subsea Application

Characterization of Selected Blends

Doctoral theses at NTNU, 2020:209

**NTNU**  
Norwegian University of Science and Technology  
Thesis for the Degree of  
Philosophiae Doctor  
Faculty of Natural Sciences  
Department of Chemical Engineering

 **NTNU**  
Norwegian University of  
Science and Technology

 NTNU

 **NTNU**  
Norwegian University of  
Science and Technology

Eirini Skylogianni

# **Combined Hydrogen Sulfide Removal and Hydrate Control for Subsea Application**

Thesis for the Degree of Philosophiae Doctor

Trondheim, June 2020

Norwegian University of Science and Technology  
Faculty of Natural Sciences  
Department of Chemical Engineering



Norwegian University of  
Science and Technology

**NTNU**  
Norwegian University of Science and Technology

Thesis for the Degree of Philosophiae Doctor

Faculty of Natural Sciences  
Department of Chemical Engineering

© Eirini Skylogianni

ISBN 978-82-326-4766-8 (printed ver.)  
ISBN 978-82-326-4767-5 (electronic ver.)  
ISSN 1503-8181

Doctoral theses at NTNU, 2020:209

Printed by NTNU Grafisk senter

# Preface

This thesis is submitted to the Norwegian University of Science and Technology (NTNU) for partial fulfilment of the requirement for the Philosophiae Doctor Degree.

The work was performed at the Department of Chemical Engineering at the Faculty of Natural Sciences under the supervision of Professor Hanna K. Knuutila. Appointed co-supervisors were Professor Hallvard F. Svendsen and Doctor Diego D. D. Pinto. A part of the study was conducted at Mines ParisTech-PSL university in France, under the supervision of Professor Christophe Coquelet.

The research was supported by SUBPRO, a Center for Research-based Innovation within subsea production and processing, which is funded by the Research Council of Norway, major industry partners and NTNU (project number 237893).



# Abstract

After more than a century of oil and gas exploration, fewer and fewer easily accessible reservoirs are available. In order to meet the increasing energy demands, the industry has extended its exploration activities in greater depths and longer distances from the shore, while also focusing its efforts on increasing the efficiency and reducing the environmental footprint of existing and new processes. As a sub-project in the SUBPRO research center for subsea production and processing, this work deals with process intensification for natural gas treatment; the combined hydrogen sulfide removal and hydrate control for subsea application.

The backbone of this process is the identification of a solvent with this dual function. Aqueous or non-aqueous blends of methyldiethanolamine (MDEA) and monoethylene glycol (MEG), as well as highly concentrated aqueous MDEA are promising systems. Thus, the objective of this thesis is to characterize these mixtures and gain knowledge of their physical properties and thermodynamic behavior.

Density and viscosity studies showed that density decreases with temperature and with MDEA concentration, while viscosity increases. It was found that considerably high viscosities are encountered in the amine-glycol systems, reaching 200 mPa·s for the ternary system consisting of 90 wt% MDEA – 5 wt% MEG – 5 wt% H<sub>2</sub>O, and that the model developed in this work can be used for the prediction of the viscosity limits of this process.

High-pressure vapor-liquid equilibrium (VLE) measurements of hydrogen sulfide in 50 wt% aqueous MDEA, 70 wt% aqueous MDEA and 30 wt% MDEA – 40 wt% MEG – 30 wt% H<sub>2</sub>O showed that the effect of total pressure up to 100 bar on the liquid loading of the solvent is within or slightly higher than the experimental uncertainties and that changes in the H<sub>2</sub>S partial pressure is attributed to the non-idealities of the vapor phase. Analyzing the acquired data and literature information on MDEA-glycol systems, it was found that increasing MDEA concentration under constant water content or lowering MEG content under constant amine concentration, leads to higher absorption capacity, manifesting the need for careful choice of MDEA-MEG-H<sub>2</sub>O composition for this combined process. Further, low-pressure VLE data of

carbon dioxide in aqueous and non-aqueous MDEA-MEG blends in combination with Karl-Fischer titration and Nuclear Magnetic Resonance analysis, revealed the reaction of CO<sub>2</sub> with MEG in the presence of MDEA and the formation of glycol carbonate in both aqueous and non-aqueous amine-glycol systems.

In the end, an overall evaluation of the technical performance of the studied solvents was conducted for the combined H<sub>2</sub>S removal and hydrate control for subsea application. It was shown that, although further work is required to conclude the feasibility of this process, MDEA-MEG systems offer the advantage of comprising compounds already employed subsea and seem to possess the properties that were identified as the most important ones.



# Acknowledgement

This PhD work has been an invaluable experience, teaching me a lot and making me grow not only as a scientist, but also as a person. During these years, I was lucky to have many great people around me whom I would like to thank.

First and foremost, I would like to thank my supervisor Professor Hanna K. Knuutila for believing in me and giving me the opportunity to pursue this doctoral degree under her guidance. Thank you for all your support during this project, your advices and feedback. I have learnt a lot and, no matter the occasion, my motivation was always higher walking out of your office.

I would also like to express my gratitude to my co-supervisor Dr. Diego D. D. Pinto for always being there to support me and answer all my questions about the VLE model. Especially during my research stay in France, your encouragement has been tremendous. My thanks also go to Professor Hallvard Svendsen, who was my co-supervisor in the start of this work. Needless to say that his vast knowledge that he gladly shares, is greatly appreciated.

Part of this thesis was undertaken during a 6-month research stay in the laboratory of the Centre of Thermodynamics of Processes of Mines ParisTech-PSL university in France, under the supervision of Professor Christophe Coquelet. Thank you for your guidance and for introducing me to the fascinating world of uncertainties. Special thanks go to Mr. Eric Boonaert and Ing. Alain Valtz for their priceless help in the laboratory work with the high-pressure setup.

For their contribution to the publications produced during this thesis, I am thankful to have worked with Ricardo Wanderley, Cristina Perinu, Ingvild Mundal, Anastasia Trollebø, Blanca Cervantes Gameros, Mari Lilleng, Gro Mogseth and Sigrid Austad. To obtain the experimental data in this work, the laboratory became my second home. I would, therefore, like to thank my “house-mates” Mikael Hammer, Gøril Flatberg, Inna Kim, Sigvart Evjen, Ricardo Wanderley, Vanja Buvik, Ida Bernhardsen and Ardi Hartono for all the help, trainings and discussions we had together. Øystein Jonassen, thank you for the long hours in the lab trying to fix the leakages.

Thanks to all the colleagues and friends from our group and from SUBPRO for the memorable lunches, cake breaks, parties and trips we had together: Kristin, Mohammad, Cristina, Usman, Seniz, Ina, Ram, Vanja, Karen, Visha, Jasper, Tobi, Umesh, Bahareh, Lucas, Are, Marcin, Adriaen, Dinesh, Håvard, Mahdi, Luca and everyone else I might forget. Special thanks to Putta, Ida, Ricardo and Andres; our discussions have meant a lot to me.

To my good friends outside the university; the Italian gang, the Greek community, my friends from the Red Cross, and even my friends in Greece (!), thank you all for making my time in Trondheim so joyful. I miss you already Luca, Roberta, Giancarlo, Claudio, Elisavet, and my dearest friend and best flatmate in the world, Eleni.

Finally, my deepest thanks go to the most important people in my life, my family and my boyfriend, for their unwavering support, understanding and encouragement during the PhD. Talking with you was always the best moment of the day. I am mostly grateful to my mother who, leading by example, taught me to love learning and that with hard work and dedication, I can achieve anything.

# Contents

<b>Preface</b>	<b>i</b>
<b>Abstract</b>	<b>iii</b>
<b>Acknowledgements</b>	<b>v</b>
<b>Nomenclature</b>	<b>xi</b>
<b>Abbreviations</b>	<b>xiv</b>
<b>Chapter 1 Introduction .....</b>	<b>1</b>
1.1 Background.....	1
1.1.1 The subsea vision .....	1
1.1.2 SUBPRO .....	2
1.1.3 Motivation for combined hydrogen sulfide removal and hydrate control .....	3
1.2 Objective of the thesis .....	4
1.3 Outline of the thesis.....	5
1.4 Research Dissemination .....	6
1.4.1 List of journal publications .....	6
1.4.2 List of conference publications and presentations .....	7
Bibliography .....	7
<b>Chapter 2 Technical Background.....</b>	<b>9</b>
2.1 Technology status .....	9
2.1.1 Hydrogen sulfide removal.....	9

2.1.1.1	Technologies .....	10
2.1.1.2	Amine-based process.....	12
2.1.2	Gas dehydration and hydrate inhibition .....	15
2.1.2.1	Gas dehydration.....	15
2.1.2.2	Hydrate inhibition .....	16
2.1.3	Combined hydrogen sulfide removal and hydrate control .....	17
2.1.4	Industrial status .....	25
2.2	Gap Analysis.....	28
2.2.1	Scientific challenges.....	29
2.2.2	Industrial needs and challenges.....	29
2.3	Chemistry.....	30
	Bibliography .....	33
<b>Chapter 3</b>	<b>Density and Viscosity .....</b>	<b>41</b>
3.1	Density and viscosity study for the systems MDEA-MEG and MDEA-MEG-H <sub>2</sub> O .....	42
3.2	Further considerations .....	81
	Bibliography .....	83
<b>Chapter 4</b>	<b>VLE Data for H<sub>2</sub>S-containing Systems.....</b>	<b>85</b>
4.1	Vapor-liquid equilibrium study for the system H <sub>2</sub> S-CH <sub>4</sub> -MDEA-H <sub>2</sub> O .....	87
4.2	Vapor-liquid equilibrium study for the system H <sub>2</sub> S-CH <sub>4</sub> -MDEA-MEG-H <sub>2</sub> O .....	120
4.2.1	Aim of the study .....	120
4.2.2	Experimental work .....	120
4.2.2.1	Materials.....	120

4.2.2.2	Experimental setup and procedure .....	121
4.2.3	Results and discussion.....	122
4.2.3.1	Trends and effects .....	122
4.2.3.2	Comparison with literature.....	128
4.2.3.3	Comparison with 70 wt% aqueous MDEA .....	134
4.2.3.4	Cyclic capacity .....	135
4.2.4	Conclusions .....	137
4.3	Experimental challenges and learnings with high-pressure VLE work .....	138
	Bibliography .....	144
<b>Chapter 5</b>	<b>VLE Data for CO<sub>2</sub>-containing Systems .....</b>	<b>147</b>
5.1	CO <sub>2</sub> solubility in mixtures of MDEA with MEG, MEG -H <sub>2</sub> O, H <sub>2</sub> O and TEG .....	148
<b>Chapter 6</b>	<b>Solvent Evaluation.....</b>	<b>237</b>
6.1	Solvent characterization .....	238
6.1.1	Removal efficiency .....	239
6.1.1.1	Absorption capacity and cyclic capacity .....	239
6.1.1.2	Heat of reaction .....	240
6.1.1.3	Kinetics.....	241
6.1.2	Trouble-free operations .....	242
6.1.2.1	Viscosity.....	242
6.1.2.2	Precipitation .....	242
6.1.2.3	Foaming.....	243
6.1.2.4	Chemical stability and degradation .....	243

6.1.2.5	Corrosion.....	244
6.1.2.6	Volatility.....	245
6.1.3	Environment.....	245
6.1.3.1	Biodegradation and ecotoxicity.....	245
6.1.3.2	Emissions and aerosols.....	246
6.2	Solvent development approach.....	246
6.3	Conclusions .....	249
	Bibliography .....	249
<b>Chapter 7</b>	<b>Conclusions and Recommendations for future work.....</b>	<b>253</b>
7.1	Conclusions .....	253
7.2	Recommendations for future work.....	256
<b>Appendix</b>	<b>.....</b>	<b>259</b>

# Nomenclature

## Latin letters

$a, \alpha$	parameter
$A$	parameter
$A_\Phi$	Debye-Hückel parameter
$b$	parameter
$B$	parameter
$c$	concentration ( $\text{mol}\cdot\text{L}_{\text{sol}}^{-1}$ , $\text{kg}\cdot\text{L}_{\text{sol}}^{-1}$ , $\text{mol}\cdot\text{kg}^{-1}_{\text{solution}}$ ); parameter
$C$	parameter
$c-a$	cation-anion
$d$	parameter
$D$	dielectric constant (-)
$g$	molar Gibbs energy ( $\text{J}\cdot\text{mol}^{-1}$ )
$G$	eNRTL auxiliary function (-)
$H$	Henry's constant ( $\text{kPa}\cdot\text{m}^3\cdot\text{kmol}^{-1}$ , MPa)
$I_x$	Ionic strength in mole fraction scale ( $\text{mol}\cdot\text{m}^{-3}$ )
$k$	Boltzmann constant ( $\text{J}\cdot\text{K}^{-1}$ ); parameter
$k_{1,a}, k_{1,b}, k_{2,a},$ $k_{2,b}, k_{3,a}, k_{3,b}$	parameters for the VLE "soft model"
$l$	parameter
$M, MW$	molecular weight ( $\text{kg}\cdot\text{kmol}^{-1}$ )
$n$	number of moles
$N_A$	Avogadro number ( $\text{mol}^{-1}$ )
$P, p$	pressure (kPa, Pa)
$pK_{\text{ap}}$	autoprotolysis (dissociation) constant
$r_{\text{BORN}}$	Born radius (m)
$R$	universal gas constant ( $\text{J}\cdot\text{mol}^{-1}\cdot\text{K}^{-1}$ , $\text{m}^3\cdot\text{Pa}\cdot\text{K}^{-1}\cdot\text{mol}^{-1}$ )
$R^2$	coefficient of determination

$T$	temperature (K, °C)
$u$	uncertainty
$v, v$	molar volume ( $\text{m}^3 \cdot \text{mol}^{-1}$ )
$V$	volume ( $\text{m}^3$ )
$w$	weight fraction (-)
$x$	liquid phase mole fraction (-)
$X$	eNRTL mole fraction (-)
$y$	gas phase mole fraction (-)
$z$	ionic charge (-)
$Z$	Absolute value of the ionic charge (-); compressibility factor (-)

#### Greek letters

$\alpha$	loading ( $\text{mol acid gas} \cdot \text{mol}^{-1} \text{ MDEA}$ )
$\gamma$	activity coefficient
$\Delta\eta$	Viscosity deviation ( $\text{mPa} \cdot \text{s}$ )
$\varepsilon$	Permittivity ( $\text{F} \cdot \text{m}^{-1}$ )
$\eta$	Viscosity ( $\text{mPa} \cdot \text{s}$ )
$\rho, \rho$	density ( $\text{kg} \cdot \text{m}^{-3}$ ), molar density ( $\text{mol} \cdot \text{cm}^{-3}$ )
$\rho_{\text{pdh}}$	closest approach parameter of the Pitzer-Debye-Hückel formulation (-)
$\tau$	NRTL energy parameter (-)
$\varphi$	fugacity coefficient (-), fluidity ( $\text{P}^{-1}$ )
$\omega$	acentric factor

#### Subscripts

abs	absorption
amb	ambient
ap	autoprotolysis
app	apparent
aq. MDEA	aqueous MDEA
c	critical; combined
calc	calculated value from the model
des	desorption
glob	global, refers to global loading $\alpha_{\text{glob}}$ ( $\text{mol H}_2\text{S in the cell} \cdot \text{mol}^{-1} \text{ MDEA}$ )



i, j, k	component in a mixture
ij	binary, cross parameter
liq	liquid, refers to liquid loading $\alpha_{liq}$ (mol H <sub>2</sub> S·mol <sup>-1</sup> MDEA)
r	reduced
RA	Rackett equation, as in compressibility factor $Z_{RA,i}$ (-)
s	solvent; saturation
tot	total
w	water

### Superscripts

calc	calculated
E, ex	Excess property
exp	experimental value
l	liquid phase
lc	local composition
pdh	Pitzer-Debye-Hückel formulation
phys	physical absorption
pred	predicted value
v	vapor phase

### Other notations

Accent, ex.: $\hat{y}$	estimated variable, not measured
Bold, ex.: $\mathbf{y}$	the variable is an array of variables

# Abbreviations

AAD	Average Absolute Deviation
AARD	Average Absolute Relative Deviation
AMP	2-Amino-2-methyl-1-propanol
ARD	Absolute Relative Deviation
BOD	Biochemical Oxygen Demand
BTEX	Benzene, Toluene, Ethylbenzene and Xylene
CAPEX	Capital expenditure
CCS	Carbon Capture and Storage
CFU	Compact Flotation Unit
CO <sub>2</sub>	Carbon dioxide
DEA	Diethanolamine
DEA-1,2-PD	3-Diethylamino-1,2-propanediol
DEEA	2-Diethylamino-ethanol
DEG	Diethylene glycol
DEPTH	Deep Export Production and Treatment Hub
DIPA	Diisopropanolamine
EC <sub>50</sub>	half maximal effective concentration
eNRTL	electrolyte non-random two-liquid
EOR	Enhanced Oil/hydrocarbon Recovery
EoS	Equation of State
ex.	for example
FID	Flame Ionization Detector
FPD	Freezing Point Depression
FTIR	Fourier-Transform infrared
GC	Gas Chromatograph
H <sub>2</sub> S	Hydrogen sulfide
HSE	Health, Safety and Environment
i.e.	<i>id est</i> (that is)

LNG	Liquified Natural Gas
MDEA	Methyldiethanolamine
MEA	Monoethanolamine
MEG	Monoethylene glycol
min.	minute
NC	Number of components
NCS	Norwegian Continental Shelf
NMR	Nuclear Magnetic Resonance
NP	Number of data points
NS	Number of vapor phase samples for GC analysis
OiW	Oil in Water
OPEX	Operational expenditure
ppm	parts per million
PZ	Piperazine
rpm	revolutions per minute
ROV	Remotely Operated Vehicles
SRB	Sulfate Reducing Bacteria
TCD	Thermal Conductivity Detector
TEA	Triethanolamine
TEG	Triethylene glycol
TIC	total inorganic carbon
TREG	Tetraethylene glycol
TRL	Technology Readiness Level
VLE	Vapor-Liquid Equilibrium
vol	volume, as in composition given in vol%
wt	weight, as in composition given in wt%
2D	two-dimensional
2MPZ	2-methylpiperazine



# Chapter 1

## Introduction

### 1.1 Background

#### 1.1.1 The subsea vision

After more than a century of oil and gas exploration, fewer and fewer easily accessible reservoirs are available. In order to ensure that the future energy demands are met, the petroleum industry is forced to search for resources in longer distances and depths offshore, such as in the Arctic Ocean. In many cases, the harsh environment and safety-related issues do not allow the use of a platform, thus subsea processing has naturally gained grounds (Albuquerque et al., 2013; Økland et al., 2013).

The installation, maintenance and retrieval of the subsea equipment play a significantly more important role than for onshore/topside facilities. Therefore, key elements in subsea processes are the increased efficiency and modularity and the reduced weight, size and complexity, i.e. process intensification. Primary drivers for subsea production and processing are increased recovery and lifetime of existing fields and reduced cost and complexity in future installations. Innovative solutions developed under the “subsea umbrella” could also enable the production of confirmed oil and gas deposits which today are left unexploited due to technical and/or economic reasons (Økland et al., 2013).

Different stakeholders, oil companies, suppliers and service companies, share the vision of an ensemble of subsea-qualified and standardized equipment and processes which, in the short-term, leads to elimination of topside/offshore processing and direct export to pipeline/onshore and, in the long-term, direct export from the reservoir to the market (Ruud et al., 2015). The subsea vision is illustrated in Figure 1.1 describing Statoil’s “Subsea Factory”. It comprises bulk separation of oil-water-gas, treatment, storage and pumping of oil to export, treatment and

injection of produced water and treatment and compression of gas to export. The “Subsea Factory” has been transformed to “Remotely Operated Factory” in Equinor, which comprises of both topside and subsea technologies (Samuelsberg, 2017). Any monitoring and intervention required is performed by ROVs (Remotely Operated Vehicles), since the operating depths and temperatures are prohibitive for human activity. Various solutions exist already for use subsea (single-phase or multi-phase pumps, bulk separators, dry and wet compressors), though variations of the “factories” are expected depending on the maturity of the field (Økland et al., 2013). The industry is working intensely in identifying the technology gaps to be closed for the realization of reliable, efficient and sustainable subsea production and processing.

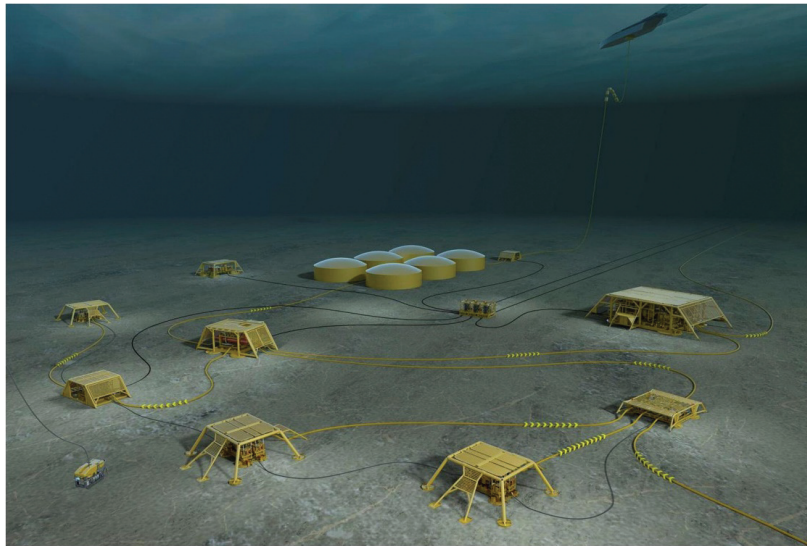


Figure 1.1. Statoil's Subsea Factory™ (Equinor, 2019)

### 1.1.2 SUBPRO

Many of the pieces of the subsea processing “puzzle” are in place, yet there is the need for new and innovative solutions in order to maximize recovery and add potential on the fields under development. In those efforts, the industrial and academic community joined forces in 2015 forming a center for research-based innovation within subsea production and processing, called SUBPRO. The center is established in the Norwegian University of Science and Technology (NTNU), which together with industrial players in the subsea field, aim to address challenges

for subsea applications (SUBPRO, 2019). The center is funded by the Research Council of Norway and several major international oil companies and subsea system suppliers. Our industrial partners as per January 2020 are Aker Solutions, DNV GL, Equinor, Kongsberg Digital, Lundin Petroleum, Neptune Energy and Total.

SUBPRO activities are present in the departments of Chemical Engineering, Mechanical and Industrial Engineering, Geoscience and Petroleum as well as the department of Engineering Cybernetics in NTNU and they are divided in five research areas:

1. Field Architecture
2. Reliability, Availability, Maintenance and Safety
3. Separation - Fluid Characterization
- 4. Separation - Process Concepts**
5. System Control

The work presented in this thesis belongs to the research area of Separations – Process Concepts and deals with process intensification for natural gas treatment. It entails combining two well-established processes in one, i.e. acid gas removal and water removal/hydrate control, to allow for improved flow assurance and direct export of natural gas to pipeline or to the shore.

### **1.1.3 Motivation for combined hydrogen sulfide removal and hydrate control**

Both hydrogen sulfide (H<sub>2</sub>S) removal and dehydration/hydrate inhibition in natural gas treatment are necessary processes for safe and reliable operations. The presence of hydrogen sulfide in produced gas creates safety hazards for operations, most important of which is corrosion, and results in an export gas of lower value. Water is commonly present in the gas when produced from the reservoir, while water is also introduced to the gas via other gas treating processes, such as H<sub>2</sub>S removal using aqueous solvents. Pipelines used for gas transportation have quality restrictions related to the content of water, hydrogen sulfide, carbon dioxide and heavy hydrocarbons in order to maintain integrity and ensure safety (Stewart and Arnold, 2011). If these requirements cannot be met, oil wells may need to be closed.

Today, on a typical platform hydrogen sulfide is removed by triazine while triethylene glycol (TEG) is used for gas dehydration. In addition, monoethylene glycol (MEG) is injected in the well flowlines for hydrate inhibition, giving in total three different chemical systems (Campbell, 1998). Simplifying the chemical systems or moving equipment and process elements subsea could be a way to ensure better energy efficiency and utilization of the resources.

While a process for the simultaneous removal of acid gases and water vapor in one stage can lead to higher efficiency and improved flow assurance, it also aims to provide a solution to a significant industrial challenge; field souring. The term denotes the increasing concentration of sulfur compounds observed in the course of production of a reservoir, mainly due to seawater injection during enhanced oil/hydrocarbons recovery (EOR) activities. Triazine cannot treat high H<sub>2</sub>S concentrations, while it has also been observed that mitigation strategies do not perform as expected and the H<sub>2</sub>S content keeps increasing (Mitchell et al., 2010).

The core challenge for the combined hydrogen sulfide and hydrate control process is the determination of a chemical compound, which will serve both as a hydrate inhibitor and as an H<sub>2</sub>S removal agent. The characterization of the proposed solvent is the backbone of this process, which should also be regenerative. Aqueous methyldiethanolamine (MDEA) and aqueous monoethylene glycol are traditionally used today for the selective removal of H<sub>2</sub>S over CO<sub>2</sub> and for hydrate control, respectively. Therefore, mixtures of MDEA-MEG as well as highly concentrated MDEA are promising candidates for such a process. Knowledge of the physical properties, thermodynamic behavior and kinetics of the proposed system is necessary for the successful process design, development and optimization.

## **1.2 Objective of the thesis**

The main objective of this work was to determine the necessary thermodynamics and physical properties to characterize aqueous and non-aqueous mixtures of methyldiethanolamine and monoethylene glycol, as potential solvents to be used for the combined hydrogen sulfide and hydrate control subsea.

Simulation work in the initial stage of this investigation revealed the necessity for more experimental data in order to develop and study the feasibility of such a process. In this



direction, our efforts were focused in obtaining vapor-liquid equilibrium (VLE) experiments with either hydrogen sulfide or carbon dioxide in MDEA-MEG solutions. Alongside the MDEA-MEG system, one of the objectives of the thesis was to evaluate the H<sub>2</sub>S removal capacity for highly concentrated aqueous MDEA, due to the affinity of MDEA for water. The physical properties, density and viscosity of MDEA-MEG and MDEA-MEG-H<sub>2</sub>O systems were investigated and possible limitations for subsea application were evaluated.

### 1.3 Outline of the thesis

The thesis is a collection of published or submitted papers.

**Chapter 2** presents a literature review on hydrogen sulfide removal and water control technologies as well as the state-of-the-art and gap analysis in offshore/subsea application.

**Chapter 3** presents the study of the density and viscosity of MDEA-MEG and MDEA-MEG-H<sub>2</sub>O systems.

**Chapter 4** and **Chapter 5** consist of the VLE studies performed with H<sub>2</sub>S and with CO<sub>2</sub>, respectively. In the former chapter, a section is dedicated on the experimental challenges encountered at high-pressure VLE measurements.

In **Chapter 6**, a general evaluation of the proposed solvents' technical performance is conducted in the framework of a simplified guide for solvent development.

**Chapter 7** is the concluding chapter with recommendations for future work.

The experimental apparatuses used in this work are presented through-out the thesis depending on the study, however, a detailed description of all devices and techniques is given in the **Appendix** to facilitate the reader with interest in the experimental methodology. References are given in every chapter to allow for an easy access to the literature sources. For those chapters which consist of published work with its own references, these are not repeated in the end of the chapter.

## 1.4 Research Dissemination

As part of the doctoral studies, experimental work, modeling of the obtained data and supervision of master students, connected to SUBPRO, were performed. Most of the results have been published or will be published, either in conferences or in peer-reviewed journals. A list of the dissemination results follows.

### 1.4.1 List of journal publications

- I. Skylogianni, E., Wanderley, R.R., Austad, S.S., Knuutila, H.K., 2019. Density and Viscosity of the Nonaqueous and Aqueous Mixtures of Methyl-diethanolamine and Monoethylene Glycol at Temperatures from 283.15 to 353.15 K. *J. Chem. Eng. Data* 64, 5415–5431. <https://doi.org/10.1021/acs.jced.9b00607>  
*The first author carried out the literature review, supervised the third author (summer student), produced most of the experimental data and was the main responsible for writing the article.*
- II. Skylogianni, E., Mundal, I., Pinto, D.D.D., Coquelet, C., Knuutila, H.K., 2020. Hydrogen sulfide solubility in 50 wt% and 70 w% aqueous methyl-diethanolamine at temperatures from 283 to 393 K and total pressures from 500 to 10000 kPa. *Fluid Phase Equilibria* 511, 112498. <https://doi.org/10.1016/j.fluid.2020.112498>  
*The first author carried out the literature review, produced, analyzed and fitted the data to models and was the main responsible for writing the article.*
- III. Skylogianni, E., Perinu, C., Gameros, B.Y.C., Knuutila, H.K. Carbon Dioxide Solubility in Methyl-diethanolamine – Monoethylene Glycol – Water and Methyl-diethanolamine – Triethylene Glycol Mixtures. Accepted in the *Journal of Chemical Thermodynamics*.  
*The first author produced 60% of the VLE experimental data, supervised the third author (master student), treated, analyzed and fitted the data to models and was the main responsible for writing the manuscript.*

## 1.4.2 List of conference publications and presentations

1. Skylogianni, E., Lilleng, M.I., Knuutila, H.K., Combined Hydrogen Sulfide Removal and Hydrate Control for Subsea Application - Simulation Study. IEEE Techno-Ocean 2016, October 6-8<sup>th</sup>, Kobe. (paper and poster)
2. Skylogianni, E., Pinto, D.D.D., Mogseth, G., Knuutila, H.K., Challenges and literature review on combined H<sub>2</sub>S/H<sub>2</sub>O removal for subsea application. 4<sup>th</sup> Trondheim Gas Technology Conference - TGTC 2016, December 5<sup>th</sup>, Trondheim. (oral presentation)
3. Skylogianni, E., Mundal, I., Pinto, D.D.D., Knuutila, H.K., Coquelet, Christophe, Vapor-Liquid Equilibrium Data for the Systems H<sub>2</sub>S-MDEA-H<sub>2</sub>O and CH<sub>4</sub>-H<sub>2</sub>S-MDEA-H<sub>2</sub>O at High Solvent Concentrations and High Pressures. AIChE Annual Meeting 2017, October 29<sup>th</sup>, Minneapolis. (oral presentation)
4. Skylogianni, E., Knuutila, H.K., Process intensification: Hydrogen sulfide and hydrate control for subsea application. Gas Processors Association – GPA Europe Spring Conference 2019, May 14-17<sup>th</sup>, Amsterdam. (paper and oral presentation)

## Bibliography

- Albuquerque, F.A., Vianna, F.L.V., Alves, R.P., Kuchpil, C., Morais, M.G.G., Orlowski, R.T.C., Moraes, C.A.C., RIBEIRO, O., 2013. Subsea Processing Systems: Future Vision, in: OTC-24161-MS. Presented at the Offshore Technology Conference, Offshore Technology Conference, OTC, p. 14. <https://doi.org/10.4043/24161-MS>
- Campbell, J.M., 1998. Planning the system, in: Gas Conditioning and Processing. Oklahoma, USA, pp. 23–44.
- Equinor, 2019. Invisible platforms - The subsea revolution: making platforms invisible - equinor.com [WWW Document]. URL <https://www.equinor.com/en/magazine/the-final-frontier.html> (accessed 2.5.20).
- Mitchell, A.F., Anfindsen, H., Brurås Hårvik, A.-M., Hustad, B.M., 2010. A Review of Reservoir Souring for three North Sea Fields. Presented at the NACE Corrosion 2010 Conference & Expo.
- Økland, O., Davies, S., Ramberg, R.M., Rognø, H., 2013. Steps to the Subsea Factory, in: OTC-24307-MS. Offshore Technology Conference, OTC. <https://doi.org/10.4043/24307-MS>

- Ruud, T., Idrac, A., McKenzie, L.J., Høy, S.H., 2015. All Subsea: A Vision for the Future of Subsea Processing. Presented at the Offshore Technology Conference, Offshore Technology Conference. <https://doi.org/10.4043/25735-MS>
- Samuelsberg, A., 2017. Statoil Remotely Operated Factory (ROFTM). Presented at the Subsea Operations Conference, Haugesund.
- Stewart, M., Arnold, K., 2011. Part 1 - Gas Sweetening, in: Arnold, M.S. (Ed.), Gas Sweetening and Processing Field Manual. Gulf Professional Publishing, Boston, pp. 1–140.
- SUBPRO, 2019. SUBPRO [WWW Document]. URL <https://www.ntnu.edu/subpro/> (accessed 3.13.19).

## Chapter 2

# Technical Background

*This chapter provides the technology status and literature review for the combined hydrogen sulfide removal and hydrate control and identifies the challenges for its subsea application.*

## 2.1 Technology status

### 2.1.1 Hydrogen sulfide removal

Hydrogen sulfide is a colorless, very toxic and flammable gas, which is extremely corrosive in the presence of water. In the oil and gas industry, hydrogen sulfide is found as a compound of crude oil, natural gas or dissolved in water. The concentration of hydrogen sulfide in non-associated gas varies typically from a few ppm to 500 ppm, while in associated gas H<sub>2</sub>S can be found into the percent levels (Schulz, 2013). Natural gas containing hydrogen sulfide and other sulfur compounds is called “sour” and a typical transport specification of natural gas is 4 ppm allowable H<sub>2</sub>S content (Stewart and Arnold, 2011).

Thermal decomposition of organic materials and sulfate reducing bacteria (SRB) activity result in hydrogen sulfide formation (Amosa et al., 2010). Although the mechanisms are not yet fully understood, there is consensus in the industry that water injection during secondary recovery leads to reservoir souring, i.e. the increasing H<sub>2</sub>S concentration in the course of production of a reservoir (Mitchell et al., 2017). It is evident that good HSE practices impose that the removal of hydrogen sulfide takes place in an as early stage as possible.

### 2.1.1.1 Technologies

The chemical substances used to remove hydrogen sulfide from natural gas are called scavengers. H<sub>2</sub>S scavengers can be categorized based on their state of matter, solid or liquid, their ability to be regenerated and reused or the technology they are using, i.e. absorption, adsorption, biotechnology, membranes or cryogenic distillation. Table 2.1 shows an overview of the different technologies available today for the removal of H<sub>2</sub>S in natural gas processing (Amosa et al., 2010; GATEkeeper, 2014; Shah et al., 2017; Stewart and Arnold, 2011). The main advantages and disadvantages are presented from a viewpoint of subsea/offshore suitability. For example, the fact that in many processes elemental sulfur is formed and precipitates is listed under the disadvantages, since formation of solids can jeopardize safe and trouble-free operations subsea.

Solid scavengers are very effective in removing hydrogen sulfide by adsorption down to trace levels and this is the reason why molecular sieves are used in liquified natural gas (LNG) treatment plants where there is a 2 ppm requirement (Stewart and Arnold, 2011). Capital expenditure (CAPEX) is significant, but the operating costs are lower than with liquid scavengers in addition to their predictability in their removal rates and change of media. The latter is time- and labor-intensive, which is an important drawback of solid scavengers. Liquid scavengers' main advantage over solid ones is the requirements for smaller space and weight. Liquid scavengers accommodate higher operating costs, but their use offers more flexibility in terms of retrofitting an existing facility and adapting to flow and composition changes. On the contrary, the use of biological scavengers is mainly limited due to the sensitivity of the system and limited operating conditions they have. Moreover, H<sub>2</sub>S selective removal by membranes is researched today because of their great space and weight advantages. For treating high H<sub>2</sub>S-concentration reservoirs, cryogenic distillation has been proposed in combination with amine unit for complete gas sweetening (Axens Solutions, 2017).

It is apparent that today an engineer has a great range of different gas sweetening processes to choose from. The selection is based on a variety of factors such as H<sub>2</sub>S concentration, amount of gas to be treated, operating conditions (pressure and temperature), residence time, operational expenditure (OPEX) and CAPEX considerations and space and weight limitations;

Table 2.1 Technologies for hydrogen sulfide removal in gas processing.

Technology	State of matter	Chemical	Regenerative	Advantages	Disadvantages
Adsorption	Solid	Metal Oxides	No	<ul style="list-style-type: none"> <li>- removal to trace levels</li> <li>- high reliability</li> <li>- predictable in removal rate and change cycle</li> </ul>	<ul style="list-style-type: none"> <li>- labor- and time-intensive change of media</li> <li>- pyrophoric waste</li> </ul>
Adsorption	Solid	Zeolites	Yes	<ul style="list-style-type: none"> <li>- removal to trace levels</li> <li>- high selectivity</li> </ul>	<ul style="list-style-type: none"> <li>- requires gas stream for regeneration, which must also be treated</li> </ul>
Absorption	Liquid	Triazines	No	<ul style="list-style-type: none"> <li>- selective over CO<sub>2</sub> and reactive with mercaptans</li> <li>- inexpensive, biodegradable and disposable in overboard waters reaction product</li> <li>- high selectivity</li> </ul>	<ul style="list-style-type: none"> <li>- unreacted triazine is highly toxic to aquatic life</li> <li>- scaling or precipitation issues</li> <li>- contact and efficiency reduction if the chemical is diluted with water</li> <li>- possible hydrate formation</li> <li>- HSE issues (formaldehyde: carcinogen)</li> <li>- HSE issues (handling)</li> </ul>
Absorption	Liquid	Aldehydes	No	<ul style="list-style-type: none"> <li>- high reaction rate</li> </ul>	<ul style="list-style-type: none"> <li>- corrosion</li> </ul>
Absorption	Liquid	Strong oxidizers	No	<ul style="list-style-type: none"> <li>- removal to trace levels</li> <li>- mature technology</li> </ul>	<ul style="list-style-type: none"> <li>- degradation</li> </ul>
Absorption	Liquid	Amine solutions	Yes	<ul style="list-style-type: none"> <li>- high selectivity</li> </ul>	<ul style="list-style-type: none"> <li>- precipitation of elemental sulfur</li> </ul>
Absorption	Liquid	Redox systems	Yes	<ul style="list-style-type: none"> <li>- regeneration by contact with air, thus no heat requirement</li> </ul>	<ul style="list-style-type: none"> <li>- difficult separation of sulfur from the liquid</li> </ul>
Bacterial respiration	Liquid	Biological scavengers	No	<ul style="list-style-type: none"> <li>- effective removal</li> </ul>	<ul style="list-style-type: none"> <li>- limited operating temperatures</li> <li>- formation of mercaptans and elemental sulfur</li> </ul>
Membranes	-	-	-	<ul style="list-style-type: none"> <li>- compact design, light and small</li> </ul>	<ul style="list-style-type: none"> <li>- low selectivity</li> </ul>
Cryogenic distillation	-	-	-	<ul style="list-style-type: none"> <li>- for reservoirs with high H<sub>2</sub>S content</li> <li>- production of high-pressure liquid H<sub>2</sub>S for re-injection to the reservoir</li> </ul>	<ul style="list-style-type: none"> <li>- only bulk removal</li> <li>- combined with amine unit</li> </ul>

the latter being probably the most significant consideration for subsea applications. Today, liquid solvents dominate in the oil and gas industry offshore; triazines for direct injection topside or amines in the form of amine towers topside, when there is also the need for carbon dioxide removal. Triazine H<sub>2</sub>S scavengers are able to remove only small amounts of H<sub>2</sub>S and require attention in their application to avoid precipitation of overspent chemical (Schulz, 2013). Absorption by aqueous amines is the most mature technology of all. Amine solutions are regenerative, therefore, suitable for treating gas with high hydrogen sulfide concentrations and provide potential for production from reservoirs that are today closed. Compared to other regenerative processes, they are advantageous since they neither include solid elements with their corresponding high weight and need for adsorption media change nor precipitates are formed, as in the case of redox processes. Moreover, by selecting the proper amine, selective removal of H<sub>2</sub>S can be achieved.

### **2.1.1.2 Amine-based process**

Chemical absorption with amine-based solvents is the most mature process for carbon dioxide and hydrogen sulfide removal (Stewart and Arnold, 2011). In this process, the acid gases chemically react with the amine-based absorbent to form acid/base salts in an exothermic reversible reaction. Then, the absorbent can be regenerated by means of heat, where the reactions are reversed and the captured acid gas is desorbed.

Amines are organic compounds derived from ammonia, NH<sub>3</sub>, with substitution of one or all of the hydrogens with alkyl or aryl groups. Depending on whether one, two or all three hydrogens are replaced, they are categorized in primary, secondary and tertiary amines, respectively. Factors like the CO<sub>2</sub>/H<sub>2</sub>S concentration, pressure, temperature and purity requirement, decide the choice of the amine. Monoethanolamine (MEA), diethanolamine (DEA), methyl-diethanolamine (MDEA), diglycolamine (DGA) and diisopropanolamine (DIPA) are of principal commercial interest for gas purification. Different amines and concentration of the solutions lead to different acid gas loadings, selectivity and degradation of the amine.

For the simultaneous removal of CO<sub>2</sub> and H<sub>2</sub>S, primary and secondary amines can be used. In case selective hydrogen sulfide removal is required, tertiary amines, such as MDEA, are preferred. The reason is that the rate of reaction of H<sub>2</sub>S is much higher than the rate of reaction with CO<sub>2</sub> in aqueous tertiary amines. Tertiary amines react with hydrogen sulfide through a



proton transfer reaction, a typical acid-base reaction, thus the reaction is instantaneous. On the contrary, carbon dioxide is practically removed by its reaction with the water of the solution and this reaction is slow. More information about the chemistry of the system are provided later in section 2.3.

A typical flow diagram for amine-based gas sweetening is shown in Figure 2.1. It is a typical MEA-based gas sweetening process, however, there are no significant variations when other amines are used. The main parts of the process are the absorber/contactor and the desorber/still. The gas to be treated enters in the bottom of a contactor tower and flows counter-current with an amine solution. Typically, the sweetened gas leaves the top of the absorber towards a dehydration unit before being considered ready for sale. The amine solution, lean in acid gas, enters the absorber from the top and moving downwards, it removes the acid compounds of the gas. Having stripped the gas from H<sub>2</sub>S and CO<sub>2</sub>, the now rich in acid gas, amine solution leaves the absorber from the bottom towards the still or stripper. Before entering it, it passes through an amine-amine heat exchanger, where it is pre-heated by the hot regenerated lean amine.

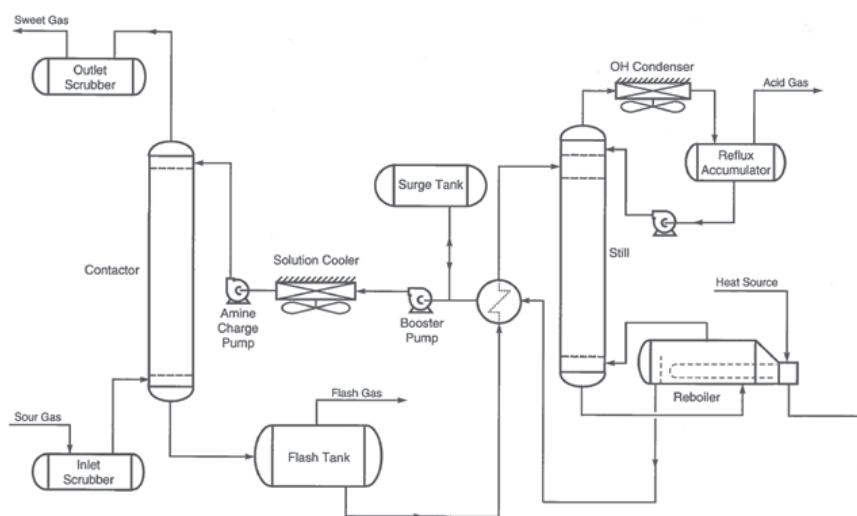


Figure 2.1. Process flow for typical ethanolamine sweetening unit (Campbell, 1998a)

Inside the still, the absorbent is regenerated. The rich solution flows downward through the column while steam and vapor from the reboiler enters from the bottom. The reboiler vapor strips the acid gases from the rich solution as, by adding heat, the reaction is reversed and CO<sub>2</sub> and H<sub>2</sub>S are released from the amine. The acid gases and the steam leave the top of the stripper and pass overhead through a condenser, where most of the steam and any remaining amine are

cooled and condensed. The acid gases are sent for further processing while the water-amine solution is returned to the top of the stripper as reflux. Lean amine solution from the bottom of the stripper column is pumped through the amine-amine heat exchanger and then through a water or air-cooled exchanger before entering the top of the absorber. The process necessitates the use of a water or air-cooled exchanger because the amine-amine heat exchanger is not adequate to sufficiently cool the lean amine down to the required temperature. This is because the rich amine solution used in the heat exchanger comes out of the absorber at elevated temperature due to the heat of reaction released when acid gases react with amines. Hydrogen sulfide cannot be released in the atmosphere and typically it is processed in a Claus unit for the production of elemental sulfur.

Main disadvantage of the amine-based processes is the high energy requirement for the regeneration of the solvent, which constitutes the largest source of OPEX. These high energy needs come mainly from the heating duties in the reboiler which should suffice to provide the heat to rise the temperature of the solvent to the reboiler temperature (sensible heat), the heat to produce stripping steam (latent heat) and the heat to reverse the exothermic reaction between acid gases and the amine solutions in the absorber (heat of absorption). Researchers aim to minimize the heating duties via selection/development of solvents with low regeneration requirements and configuration optimization or both (Liang et al., 2016). Variations in configuration include, but are not limited to, addition of intercooling, interheating and split-stream flow modifications (Ahn et al., 2013).

After screening over fifty different amines, Frazier and Kohl proposed already in 1950 the use of aqueous MDEA for the selective removal of hydrogen sulfide over carbon dioxide (Frazier and Kohl, 1950). Since then, aqueous MDEA is an established solvent for H<sub>2</sub>S selective removal and a 50 wt% MDEA solution is considered benchmark in natural gas treatment. The reasons are multiple; ability to meet the 4 ppm specification requirement for pipeline gas, low heat of absorption thus low energy requirements, resistance to degradation, high availability and low cost (Kohl and Nielsen, 1997a). MDEA is also not corrosive and, in fact, it is used as a pH stabilizer in the pipeline (Davoudi et al., 2014). Last but not least, as a polar compound, it has affinity for water rendering highly concentrated MDEA solutions a good candidate for acting both as an H<sub>2</sub>S removal and a dehydrating agent. For all these reasons, we have chosen MDEA in the amine-glycol solvent for the combined hydrogen sulfide removal and hydrate control.

## **2.1.2 Gas dehydration and hydrate inhibition**

Natural gas is often produced from the reservoir saturated with water. In addition, water is added to the gas during the gas sweetening process, which commonly employs aqueous solutions of amines or triazines (GPSA, 2014). Dehydration is the process of removing water to very low content, usually in order to meet sales requirements for water dew point. Presence of water in the producing gas assists corrosion and can lead to hydrate formation and condensation of free water in processing and transportation facilities. Hydrates are physical combinations of water and other small molecules, such as methane, to produce solids with an “ice-like” appearance. In extreme cases of hydrate formation, accumulation of hydrates can result in clogging valves, fittings and even pipelines. Hydrate inhibition is the process where a chemical, able to control the hydrate formation and its rate, is injected in the pipeline to ensure hydrate-free gas transportation (Campbell, 1998b; Kohl and Nielsen, 1997b). The specification for water dew point is -18 °C at 69 bar (Christensen, 2011).

### **2.1.2.1 Gas dehydration**

According to Campbell (Campbell, 1998b), absorption-, adsorption-, condensation- and membrane-based methods can be used for natural gas dehydration. The most common method for meeting pipeline and sales specification is absorption with triethylene glycol (TEG) solutions, while for deep dehydration (0.1 ppm water in gas) in LNG plants, it is adsorption with molecular sieves. Condensation is used together with the injection of a hydrate inhibitor to eliminate hydrate formation risks. Membranes utilize the difference in permeability of different compounds to separate them from a gas stream and today researchers are working towards improved selectivity for water and reduced methane loss.

Absorption of water in glycols is an established dehydration process and mostly used in the industry, since already the 1930s. Its success emerges from the fact that the glycols are very hydrophilic, can be easily regenerated, have low cost, are neither corrosive nor volatile, are unreactive and insoluble in hydrocarbons. TEG is preferred over other glycols because it is easier to regenerate and presents lower solvent losses. Highly concentrated TEG solutions are used to physically absorb the water from the gas in a similar configuration as in acid gas removal with amines, with a contactor and a stripping still playing the central role. A typical glycol dehydration unit is shown in Figure 2.2.

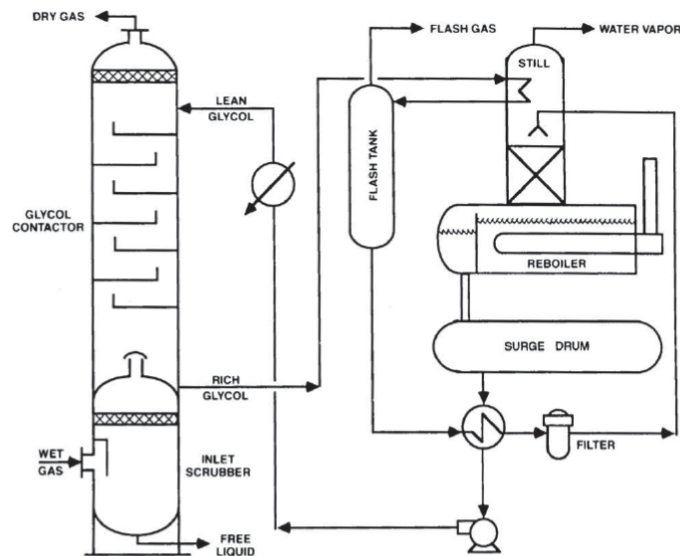


Figure 2.2. Process flow for typical glycol dehydration unit (GPSA, 2014)

Wet gas enters at the bottom of the contactor (absorber) and as it flows upwards, counter-current with the glycol solution, water vapor is stripped by the lean, regenerated, glycol. Water-rich glycol is removed from the bottom of the contactor, passes through the reflux condenser coil at the top of the regenerator and then enters the flash tank where most of the soluble gas are flashed off. After that, it flows through the rich-lean glycol heat exchanger to the regenerator. In the regenerator, the absorbed water is released from the glycol at near atmospheric pressure by application of heat. The regenerated lean glycol exits the surge drum, gets cooled in the lean-rich glycol exchanger first, and in the glycol cooler afterwards before it is introduced in the top of the absorber.

### 2.1.2.2 Hydrate inhibition

During the transportation of natural gas, it is not necessary to remove all the water vapor but rather control its content in order to avoid hydrates or condensation at the specific temperature and pressure conditions in the pipeline. Hydrate inhibitors serve this purpose and can be divided into equilibrium inhibitors and low dosage inhibitors. The first, which are commonly monoethylene glycol or methanol, lower the freezing point of water, while the second decelerate hydrate growth or restrict the size of the formed hydrates. Equilibrium inhibitors, MEG and methanol, are most commonly used, with MEG being preferred for continuous

operations, mainly due to its lower cost, lower viscosity, and lower solubility in liquid hydrocarbons (GPSA, 2014).

A widely applied technique offshore for flow assurance is the direct injection of aqueous MEG into the multiphase flow or gas phase flow pipeline. Typically, MEG is injected continuously in the wellhead to eliminate the risk of hydrates in the production line. A scrubber might be used to collect the glycol from the gas stream, which is then, with the aid of a pump or utilizing its high pressure, is sent to a stripper for regeneration and re-injection. Often, high concentration of salts in the chemical demand glycol reclamation.

To take this further, managing the dehydration of the gas with MEG offshore/subsea would have the major benefit of using the same chemical for two purposes, hydrate inhibition and dehydration. One less chemical means reduced processing equipment, storage vessels, need for one flow line instead of two, thus, simpler umbilical system. Other advantages are lower viscosity, BTEX solubility in MEG than TEG (Ebeling et al., 1998), toxicity and flammability. The main drawback, compared to TEG is the lower decomposition temperature, i.e. 165 °C for MEG and 206 °C for TEG (Campbell, 1998b), and, therefore, lower regeneration glycol purity.

### **2.1.3 Combined hydrogen sulfide removal and hydrate control**

The concept of the combined hydrogen sulfide and water removal exists since 1939, when A. J. L. Hutchinson patented a gas treating process for the “simultaneous removal of moisture and acid gases from natural gas” to meet pipeline specifications (Hutchinson, 1939). In this process, acid gases and water vapor are removed by means of absorption into a liquid solvent. The configuration of the process is similar to the typical amine-based gas sweetening process; the solvent and the gas flow counter-current in a contactor tower, the sweet gas exits from the top and the rich solvent leaves the contactor from the bottom and continues for regeneration (Figure 2.3). The solvent is regenerated by supplying heat and directed to the top of the contactor for reuse. The liquid solvent is a glycol-amine aqueous solution, whose concentration depends on the composition of the sour wet gas but has always glycol in excess of the amine. Hutchinson claims that a mixture of a glycol, an amine and water will remove acid gases to a high degree of separation and the water vapor down to the saturation or dew point. Suggested concentration

ranges for the compounds are 2-20 vol% amine, 50-90 vol% glycol and 2-30 vol% water, and example constituents are triethanolamine and diethylene glycol.

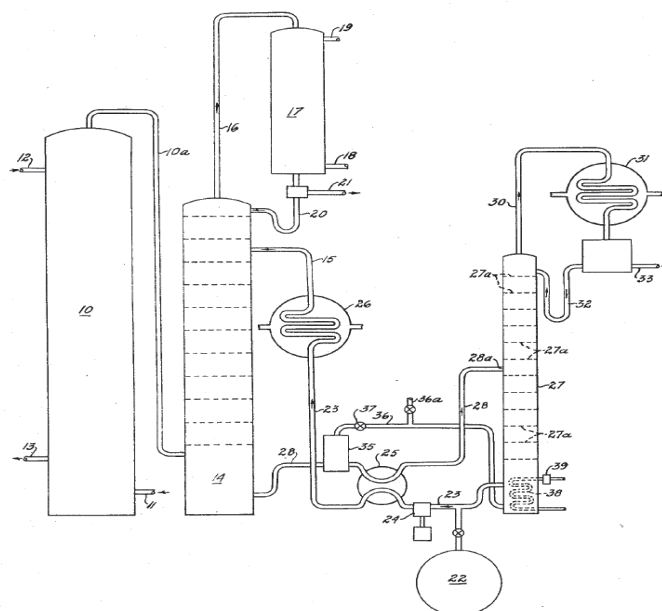


Figure 2.3. Process diagram for Hutchinson's patented gas treatment process (Hutchinson, 1939)

The advantages of the proposed process are multiple: the boiling point of an amine-glycol solution is higher than aqueous amine allowing for more complete regeneration of the amine, the vapor pressure is lower, the glycol is more stable and, thus, resistant to degradation in the presence of the amine, the mixture has lower viscosity than the glycol alone, implying more intimate contact between the gas and the liquid, higher rates of heat exchange and foaming reduction. During tests in a gas plant, Hutchinson found that the presence of the alcohol-part of the glycol makes possible the separation of the absorbed acid gas with very slight boiling of the solution, and that the  $H_2S$  and  $CO_2$  were removed from the amine to a far greater extent, compared to water-amine mixtures. Moreover, the presence of the amine improves the capacity of the glycol for dehydration, even when the addition of the amine is accompanied by an increase in the water content of the solvent. Last, the temperature required to regenerate the solutions was significantly reduced.

After Hutchinson, different configurations have been proposed for combined hydrogen sulfide removal and hydrate control. First, McCartney proposed that the sour wet gas is contacted in

the same absorption tower first with an acid gas removing solvent and then with a water removing solvent (glycol), each one of the solvents having their own separate desorber. The acid gas and the water vapor removed in the glycol stripper are directed to the amine stripper for recovery in order to recover possible amine carry-over in the glycol cycle. With these modifications, McCartney addressed the problem of large circulation rates encountered with Hutchinson's process due to the significantly lower amine amount (McCartney, 1948).

Soon after McCartney's patent, another patent was published regarding the simultaneous removal of H<sub>2</sub>S and water (Chapin, 1950). This was an improvement of the process proposed by McCartney. According to Chapin, McCartney's process could result in vaporization and carry-over of glycols from the glycol regeneration cycle into the amine's regeneration cycle, leading eventually to depletion of the glycol solution. As a solution to this problem, Chapin suggested the replacement of the first treating amine-based absorbent with an amine-glycol absorbent. The second treating solution remains of the same type: a mixture of glycol and water for water removal. A side-stream of the lean amine-glycol solution is added to the rich glycol solution to compensate for the glycol carry-over from the glycol stripper.

In 1951, another patent from McCartney was accepted based on his first patent, tackling the problem identified by Chapin (McCartney, 1951). He suggested the use of the same type of solutions for the acid gas and water removal as Chapin; first an amine-glycol solution and then a glycol solution. However, instead of introducing part of the lean amine-glycol solution to the glycol solution, he proposed returning the condensate from the amine-glycol regeneration cycle to the glycol regeneration cycle for use as a reflux assuring condensation of all glycol vapors.

The amine-glycol process, utilizing a solvent comprising monoethanolamine (MEA) and either diethylene or triethylene glycol, was popular in the past for the simultaneous acid gas removal and dehydration of natural gases. The water content had to be kept at or below 5% in these processes in order to be effective as a dehydrating agent. This implies that relatively high temperatures were required in the reboiler resulting to severe corrosion in the heat exchangers, the stripping column, and, under certain operating conditions, the reboiler (Kohl and Nielsen, 1997a). The corrosion problem was due to the materials that were used back then and it was one of the main reasons the use of amine-glycol mixtures for the combined desulfurization and dehydration was abandoned. Another reason was the high amine vaporization losses, a known problem when using MEA solutions.

Several researchers have investigated mixed amine-glycol systems in terms of thermodynamic behavior (VLE), kinetics and physical properties (density, viscosity, surface tension, diffusivity and physical solubility). An overview is presented in Table 2.2. These scientific works are sorted in chronological order to enhance a discussion about the research interest in amine-glycol solutions in the course of time. Mixtures of the most common amines, monoethanolamine (MEA), diethanolamine (DEA), triethanolamine (TEA), methyldiethanolamine (MDEA), amino-methyl propanol (AMP), diisopropanolamine (DIPA) and the glycols, monoethylene glycol (MEG), diethylene glycol (DEG), triethylene glycol (TEG), tetraethylene glycol (TREG), polyethylene glycol (PEG), studied for CO<sub>2</sub> and/or H<sub>2</sub>S removal have been included.

Already since the 1980s there is documented interest in amine-glycol systems, aqueous and non-aqueous. The scope of these works can be divided into four primary areas; determination of interfacial areas and mass transfer coefficients in gas-liquid contactors (Alvarez-Fuster et al., 1981; Sridharan and Sharma, 1976), combined acid gas removal and dehydration (Eimer, 1994; Jelstad, 1997; Poblete, 1997; Shoukat et al., 2019; Tørnqvist, 1991), selective H<sub>2</sub>S removal over CO<sub>2</sub> (Xu et al., 2002a, 2002b) and CO<sub>2</sub> removal from gas streams (most of remaining literature sources in Table 2.2).

The majority of the studies within CO<sub>2</sub>-capture is performed in the framework of water-lean solvents, as an alternative for post-combustion CO<sub>2</sub> removal from flue gases, with the number of publications in the last 10 years being almost the same as the number of all studies during the previous decades. The focus on water-lean solvents stems from their potential advantages in terms of absorption capacity and regeneration heating duties. It is claimed that by substituting some of the aqueous part with another compound (here by glycol), which has higher acid gas physical solubility than water, can lead to higher solvent capacity, at high CO<sub>2</sub> partial pressures (Rivas and Prausnitz, 1979). As far as the regeneration heating duties are concerned, it is suggested that the energy requirements would decrease due to the lower heat of vaporization of water-lean solvents (Leites, 1998; Tan et al., 2011). Based on Raynal et al., the energy requirements only for solvent regeneration in a typical CO<sub>2</sub>-capture process from flue gas, constitute more than 80% of the OPEX (Raynal et al., 2011). Therefore, it is not surprising that increasing focus has been given in this direction.



Table 2.2 Amine-glycol solvents investigated in the literature.

Literature source	Amine	Glycol	System	Acid Gas	Study
(Woertz, 1972)	MEA	TEG	aqueous	CO <sub>2</sub>	VLE, kinetics
(Sridharan and Sharma, 1976)	MEA, DEA	DEG, PEG400	aqueous, non-aqueous	CO <sub>2</sub>	kinetics, density, viscosity, surface tension
(Alvarez-Fuster et al., 1981)	MEA, DEA	MEG	non-aqueous	CO <sub>2</sub>	kinetics
(Oyevaar et al., 1989a)	DEA	MEG	aqueous	CO <sub>2</sub>	VLE
(Oyevaar et al., 1989b)	DEA	MEG	aqueous	CO <sub>2</sub>	density, viscosity, physical solubility, diffusivity
(Oyevaar et al., 1990)	DEA	MEG	aqueous	CO <sub>2</sub>	kinetics
(Tonnqvist, 1991)	MEA, DEA, MDEA	TEG	non-aqueous	CO <sub>2</sub>	VLE
(Davis et al., 1993)	DEA, DIPA	PEG400	non-aqueous	CO <sub>2</sub>	density, viscosity, physical solubility, diffusivity
(Davis and Sandall, 1993)	DEA, DIPA	PEG400	non-aqueous	CO <sub>2</sub>	kinetics
(Eimer, 1994) (Pedersen, 1994)	MDEA	TEG	aqueous, non-aqueous	CO <sub>2</sub> , H <sub>2</sub> S	VLE, kinetic
(Song et al., 1996a)	MEA	MEG	aqueous	-	density, viscosity
(Song et al., 1996b)	MEA	MEG, PEG400	aqueous	CO <sub>2</sub>	VLE
(Song et al., 1997)	MEA	MEG, PEG400	aqueous	CO <sub>2</sub>	VLE
(Jelstad, 1997)	MDEA	MEG	aqueous non-aqueous	H <sub>2</sub> S	VLE
(Poblete, 1997)	MDEA	MEG	aqueous non-aqueous	CO <sub>2</sub> +H <sub>2</sub> S	VLE

Literature source	Amine	Glycol	System	Acid Gas	Study
(Leites, 1998)	MEA	MEG, DEG, TEG, TREG	non-aqueous	CO <sub>2</sub>	VLE
(Tsiirkezos and Molinou, 1999)	MEA	MEG	non-aqueous	-	density, viscosity
(Braun et al., 2001)	AMP	MEG	aqueous	-	density, viscosity
(Xu et al., 2002a)	MDEA	MEG, DEG, TEG, PEG200	non-aqueous	CO <sub>2</sub> +H <sub>2</sub> S	VLE
(Xu et al., 2002b)	MDEA	MEG	non-aqueous	CO <sub>2</sub> , H <sub>2</sub> S, CO <sub>2</sub> +H <sub>2</sub> S	VLE
(Park et al., 2005a)	MEA	PEG20000	aqueous	CO <sub>2</sub>	kinetics, density, viscosity
(Park et al., 2005b)	DEA	MEG	non-aqueous	CO <sub>2</sub>	kinetics, viscosity
(Park et al., 2006a)	TEA	MEG	non-aqueous	CO <sub>2</sub>	kinetics, viscosity
(Park et al., 2006b)	MDEA	MEG	non-aqueous	CO <sub>2</sub>	kinetics, viscosity
(Park et al., 2007)	MDEA	PEG200000	non-aqueous	CO <sub>2</sub>	kinetics, density, viscosity
(Hwang et al., 2010)	DIPA	MEG	non-aqueous	CO <sub>2</sub>	kinetics, viscosity
(Archane et al., 2011)	DEA	PEG400	aqueous	CO <sub>2</sub>	VLE
(Tan et al., 2011)	MEA	TEG	non-aqueous	CO <sub>2</sub>	VLE
(Zheng et al., 2012)	AMP	DEG, TEG	non-aqueous	CO <sub>2</sub>	VLE
(Zheng et al., 2013)	AMP	MEG	non-aqueous	CO <sub>2</sub>	VLE
(Yu et al., 2013)	Piperazine	DEG	aqueous, non-aqueous	CO <sub>2</sub>	mass transfer, viscosity
(F. Yang et al., 2013)	MEA	DGA	aqueous	-	density
(C. Yang et al., 2013)	MDEA	MEG	non-aqueous	-	VLE

Literature source	Amine	Glycol	System	Acid Gas	Study
(Fu et al., 2014a)	MEA, DEA	PEG400	aqueous	-	surface tension
(Fu et al., 2014b)	MEA, DEA, MDEA	PEG400	aqueous	-	viscosity
(Gurylev et al., 2014)	AMP	DEG, TEG, TREG	aqueous	-	density
(Zheng et al., 2015)	AMP	MEG	non-aqueous	CO <sub>2</sub>	kinetics
(Stanimirovic et al., 2016)	MEA	PEG400	non-aqueous	-	viscosity
(Shoukat et al., 2016)	MEA, MDEA	MEG, TEG	non-aqueous	CO <sub>2</sub>	degradation, corrosion
(AlHarooni et al., 2016)	MDEA	MEG	aqueous	-	degradation, corrosion
(Kang et al., 2017b)	MEA	MEG	aqueous, non-aqueous	CO <sub>2</sub>	VLE
(Kang et al., 2017a)	MEA	MEG	aqueous, non-aqueous	CO <sub>2</sub>	kinetics
(Garcia et al., 2018)	MEA	MEG, DEG, TEG	non-aqueous	CO <sub>2</sub>	kinetics, physical solubility, density, viscosity
(Gurylev et al., 2018)	AMP	DEG	aqueous	-	viscosity
(Wanderley et al., 2019)	MEA, 2MPZ, MDEA	MEG	aqueous	CO <sub>2</sub>	VLE, kinetics
(Shoukat et al., 2019)	MDEA, TEA	MEG, TEG	aqueous	CO <sub>2</sub>	degradation, corrosion
(Wanderley et al., 2020)	MEA	MEG	non-aqueous	CO <sub>2</sub>	VLE

Few authors report different motivation for their work. Tsierkezos and Molinou measured the density and viscosity of the binary mixture MEA-MEG in the framework of their continuous work in understanding the properties of MEG-containing blends (Tsierkezos and Molinou, 1999). Davis and co-workers studied the physical properties and kinetics of amine-PEG400 system and actually discussed the carbon dioxide removal by the glycol, being enhanced by adding amines, and not vice-versa (Davis et al., 1993; Davis and Sandall, 1993). Yu et al. investigated the removal of CO<sub>2</sub> in a rotating packed bed reactor by employment of a piperazine-DEG solvent (Yu et al., 2013). The main motivation in utilizing DEG instead of water was to avoid the precipitation which can occur in aqueous piperazine.

All the literature sources relevant to combined acid gas removal and dehydration are conducted in Norway in the 1990s, with the exception of the work of AlHarooni et al. and Braun et al., who also mentioned this dual function along with increased absorption capacity (AlHarooni et al., 2016; Braun et al., 2001). The measurements were mainly performed with aqueous and non-aqueous MDEA-TEG and MDEA-MEG systems. Regarding MDEA-TEG systems, Tørnqvist concluded that MDEA does not react with CO<sub>2</sub> in non-aqueous MDEA-TEG systems, while Eimer observed a reaction between CO<sub>2</sub> and MDEA in “almost water-free” TEG and suggested further investigation (Eimer, 1994; Tørnqvist, 1991). Eimer and Pedersen found that, in the absence of water, the absorption of H<sub>2</sub>S in the combined solvent decreases with increasing glycol content (Eimer, 1994). Therefore, replacing TEG with MEG which is less viscous can be beneficial for reaction kinetics.

Regarding MDEA-MEG, the work was performed in the framework of two master theses (Jelstad, 1997; Poblete, 1997) and showed that H<sub>2</sub>S absorption capacity increases with amine and with water content, though the effect in the latter is small at the studied conditions. Moreover, measurements in the presence of both acid gases, showed that the presence of carbon dioxide leads to reduced H<sub>2</sub>S absorption capacity of the solvent, and this behavior is not affected by the water content in the system. However, the authors mention some disagreements with the literature and the repeatability of the measurements was not evaluated. Xu et al. investigated the selective H<sub>2</sub>S removal in the presence of high CO<sub>2</sub> concentration in non-aqueous MDEA-MEG, after screening several other physical solvents (Xu et al., 2002b). Solubility of H<sub>2</sub>S was found to be slightly lower in MDEA-MEG than MDEA-H<sub>2</sub>O, while CO<sub>2</sub> solubility was greatly decreased. Their results indicate that MDEA-MEG systems are indeed suitable for the selective removal of hydrogen sulfide.

From the above, it is understood that aqueous or non-aqueous blends of MDEA and MEG are promising solvents for the combined H<sub>2</sub>S removal and hydrate control. The fact that aqueous MDEA and aqueous MEG are proven regenerative solutions for H<sub>2</sub>S removal and H<sub>2</sub>O removal, respectively, is the basis for this selection. In the process of simultaneous H<sub>2</sub>S removal and hydrate control, the solvent will be injected in the pipeline which will now act as the absorber and will reach H<sub>2</sub>S and H<sub>2</sub>O content transportation specifications inline. Then the solvent should be separated from the gas stream, for example by using a scrubber or a deliquidizer, directed to a topside facility for regeneration and re-injection. By operating at high pressures and by eliminating the need of a topside absorber entails large potential for space, weight and energy savings. Since this solvent is regenerative, it can also allow production of sour reservoirs that today are closed due to material integrity risks and/or reduced capacity topside. In addition, MDEA-MEG systems are expected to be more effective for H<sub>2</sub>S removal in terms of selectivity and energy requirements in regeneration.

#### **2.1.4 Industrial status**

The onshore or topside technologies used today in the oil and gas operations cannot be directly implemented subsea for various reasons; operations take place at much higher pressures, all components are surrounded by water which poses challenges especially for electrical equipment, the external pressure is higher at high depths, the number and the frequency of maintenance operations must be minimum and more. Over the past few years, many topside technologies have been qualified and reached high Technology Readiness Level (TRL) for subsea application.

One can categorize the subsea developments into those related to oil-water-gas separation, those related to water treatment and those related to oil and gas processing following the separation. Regarding separation, the challenge is the liquid-liquid separation of oil and water and different solutions are available. There are several developed fields with subsea separators in operation. For example, a three-phase gravity separator was installed in Troll field already in 2001 (Rasmussen, 2002), a caisson separator is used in Perdido field (Littell et al., 2011) for gas-liquid separation and a compact pipe separator, called PipeSeparator (Sagatun et al., 2008) has been patented by Hydro and installed in the Marlim field (Orlowski et al., 2012) for three-phase separation.

In the latter, the separated water was treated with hydrocyclones and injected in the production reservoir. Hydrocyclones and water injection pumps are qualified technologies for subsea. Offshore water treatment often includes gas flotation units to meet stringent oil-in-water (OiW) quality requirements, both for re-injection in producing or disposal reservoir as well as for discharge in the sea (30 ppm OiW according to OSPAR convention for the protection of the marine environment in the north-east Atlantic (OSPAR Commission, 2010)). Compact Flotation Units (CFU) technology, specifically designed for subsea application, has been demonstrated and reached TRL 4 in 2019 (Zhao, 2019) while the “Seabox” subsea water treatment TRL 6 technology for water disinfection (“Seabox Subsea Water Treatment Technology,” 2004) is currently being tested at the Ekofisk field (Dirdal, 2019).

Besides separation, subsea multi-phase boosting is a key enabler for the development of remote fields. Both single-phase and multi-phase pumps are available and operated subsea (Forster et al., 2016). Single-phase pumps are commonly used subsea for well streams as well as umbilicals and service fluids. Multi-phase boosting also takes place in several fields, such as in the first to be installed Topacio field (Falcimaigne and Decarre, 2008) and the CLOV field (Total, 2014).

Regarding gas processing, subsea compression has recently been applied successfully: dry compression in Åsgard field (Time and Torpe, 2016) and wet compression in Gulfaks field (Vinterstø et al., 2016). Further, fiscal metering, which is the precise measurement of various properties of the effluent when ownership changes, is planned to be qualified for subsea application this year for gas and the coming years for oil (Faanes, 2020).

However, subsea gas conditioning, including gas sweetening, water dew point control (gas dehydration) and hydrocarbon dew point, is still at its infancy. Main reasons are the complexity of the processes and their utility requirements. In order to meet the specification for CO<sub>2</sub>, amine-based absorption units are operated topside. For example, in Åsgard B field, both CO<sub>2</sub> and H<sub>2</sub>S specifications are met by employment of the amine-based solvent FLEXSORB SE (“Årsrapport 2005 Utslipp fra Åsgardfeltet,” 2005). Many research groups look into membranes for CO<sub>2</sub> separation (Ahmadi et al., 2018) while Aker Solutions is working towards the qualification of membrane technology for the bulk removal of carbon dioxide from natural gas at the seabed and the evaluation of its combination with CO<sub>2</sub> re-injection in the reservoir for EOR purposes (Si Huai Yeaw, 2019). In the Norwegian Continental Shelf (NCS), the reservoirs are characterized by low carbon dioxide content which often does not require its removal to meet transportation specifications. In these cases, amine-processes are not necessary and the

corrosive effect of H<sub>2</sub>S is handled through material selection and H<sub>2</sub>S scavenging. Typically, triazine-based H<sub>2</sub>S scavengers are employed for gas sweetening, either topside or post-separation (Lioliou et al., 2017).

The water content is controlled nowadays subsea in terms of hydrate inhibition. Methanol or, most commonly in the NCS, monoethylene glycol are employed for hydrate control subsea, though pipeline heating has been also considered. For instance, electrically heated pipe-in-pipe technology is used today in Fenja field development (Gyllenhammar et al., 2015; Neptune Energy, 2020). Nevertheless, on-spec water dew point is achieved by gas dehydration, which today takes place either topside or onshore. Gas dehydration with highly concentrated aqueous TEG solution is a very mature and efficient technology widely applied for natural gas dehydration, while dehydration with MEG is investigated by Equinor through Gas-2-Pipe™ concept (Fredheim et al., 2016). Supersonic separation technology is also used today topside for dehydration (Ruud et al., 2015). Technologies with potential for subsea application and unmanned platforms for which research is conducted are both supersonic separation (Brouwer and Epsom, 2003) and membrane technology (Dalane et al., 2019). In DEPTH project, launched by Total and Aker Solutions, these two technologies together with adsorption were considered; the latter mainly due to long lifetime, the elimination of liquid solvent and the extensive knowledge already obtained from LNG plants (Gyllenhammar et al., 2015).

It is important to note that for both subsea and topside, co-current contactors with inline static mixers have been demonstrated to perform better than traditional counter-current towers (Baker and Rogers, 1989; Pyles and Rader, 1989). This type of separators is efficient, compact and lighter than traditional gas-liquid contactors and, thus, they have a lower cost. Commercial gas treating technologies based on inline separation are available for gas dehydration and acid gas removal. cMIST™ and ProDry™ can be used to meet water dew point specifications employing TEG (Dekeyzer et al., 2012; Ramkumar et al., 2017), with the latter having recently been installed topside in Troll B in the NCS (ProSep, 2017). Because of the enhanced mass transfer and shorter contact time, both concepts have been demonstrated to improve the selectivity of H<sub>2</sub>S over CO<sub>2</sub> using aqueous MDEA (Linga and Kalgraff, 2008; Ramkumar, et al., 2019). Moreover, BP Norway and Maersk Oil use ProScav, a natural gas treatment system for efficient injection and mixing of H<sub>2</sub>S scavengers, offshore (RIGZONE, 2009).

Finally, it is generally accepted that in many cases the topside factor will remain and “remotely operated factories” are taking over the “subsea factories” concept. Typical examples are gas

treating processes employing regenerative solvents. Regeneration of acid gas removing solvents takes place at high temperatures which is not energy efficient to be done at the low seabed temperatures. New developments and concepts for unmanned platforms, ex. “Subsea on a stick” (“UWP/Subsea on a Stick®,” n.d.), could support such operations as more cost-effective solutions. In fact, Eriksen and co-workers from FMC Kongsberg Subsea AS patented in 2015 the removal of carbon dioxide from a crude hydrocarbon gas stream by an amine-based absorbent subsea and its regeneration topside, followed by water vapor removal by a glycol-based absorbent subsea and its regeneration topside, where hot high-pressure gas is added to the absorbents to serve as a gas lift to transport the solvent from a subsea treatment unit to topside regenerator (Eriksen et al., 2015).

As one can understand from the above, when it comes to gas conditioning, research is conducted in various technologies and different strategies for flow assurance. Although one universal solution is always desirable, different technologies may be proven more efficient and economical in different fields; therefore, it is important to identify specific needs for individual cases. For example, membrane technology is promising in various applications where bulk removal is desired and when the partial pressure of the permeate is high. This means that for example, it could be used in the pre-treatment of gas streams with exceptionally high H<sub>2</sub>S concentration, like fields in Indonesia with 20% H<sub>2</sub>S, but not in fields which experience field souring and small concentration of hydrogen sulfide are gradually appearing.

The combined removal and hydrate control with one liquid solvent consisting of MDEA-MEG(-H<sub>2</sub>O) is only conceptualized and together with the results of this work aims to reach TRL 1. The challenges in the development and application of a process for the simultaneous removal of H<sub>2</sub>S and control in the water content subsea are identified in the next section.

## 2.2 Gap Analysis

A base case is required in order to identify with some degree of precision the needs and challenges of a process, both in a scientific level and an industrial one. In this work, we consider the idealized case of a stream with low CO<sub>2</sub> content whose only treatment requirements are for meeting H<sub>2</sub>S and water content specifications for safe transportation in the pipeline.



### **2.2.1 Scientific challenges**

The scientific challenges for the development of a process for the simultaneous hydrogen sulfide removal and hydrate control are numerous given that this is a new process. They concern both the characterization of a suitable solvent and the overall configuration of the process.

Regarding solvent development, the optimum MDEA-MEG-water concentration of the solvent must be found to provide adequate desulfurization and dehydration. For this to be decided, a full characterization of the solvent is required. According to the literature review presented in section 2.1.3, few data are available for understanding the thermodynamic and kinetic behavior of the proposed system. Thus, the need for more and with high precision data arises. In addition, there are not any information about either the dehydrating capacity or the physical properties of MDEA-MEG solvents, i.e. density, viscosity, surface tension. Degradation and corrosion studies are limited and have been only performed in the presence of carbon dioxide, and not hydrogen sulfide. The above should be evaluated in the presence of high pressure and at temperatures relevant to the absorption subsea and the regeneration topside. After obtaining all these information, a suitable composition can be chosen for optimizing the selectivity of the solvent for H<sub>2</sub>S.

In the matter of process configuration, primary scientific challenge is the regeneration scheme of MDEA-MEG solvent, mainly due to possible solvent degradation at regeneration temperatures. Aqueous MDEA is regenerated at 130 °C and aqueous MEG at 165 °C because they start decomposing at higher temperatures. Bearing in mind that it is the lowest degradation temperature of the two that will dictate the regeneration thermal conditions, i.e. 130 °C, stripping of MEG might be insufficient and schemes utilizing vacuum, stripping gas, or other should be evaluated. Degradation and corrosion issues both in the pipeline and the stripper should also be studied.

### **2.2.2 Industrial needs and challenges**

As mentioned earlier in section 2.1.3, currently there is no application of a subsea process for the combined H<sub>2</sub>S removal and hydrate control. Compact and efficient systems could enable subsea operations in remote areas, in great distances from the shore and great depths (Økland et al., 2013). According to the technology developments, however, the concept of subsea

treatment and topside regeneration is already patented and is considered technically feasible. Inline gas-liquid contactors, subsea compressors and fiscal metering are available technologies. For industrial application, the process needs to be adjustable to various operating conditions as the reservoir properties are subject to significant variations over its lifetime. Another aspect of increasing significance is the utilization and transportation of umbilical chemicals, which respect the international and national environmental regulations, such as ecotoxicity and biodegradability.

The ultimate challenge for the industry is certainly to prove the technical alongside the economic feasibility of the process. Elimination of topside reactors as well as operation at high pressures, both in absorption and desorption, aim to the reduction of the total costs, through both lower CAPEX and OPEX.

## 2.3 Chemistry

In this section, the chemical reactions undergone in the systems studied in this work are presented. They include the reactions between hydrogen sulfide and carbon dioxide with MDEA-MEG solvents.

Alkanolamines carry one amino group (one basic nitrogen atom, N) and at least one hydroxyl group, -OH. The alkalinity of the amines comes from the amino group, while the solubility in aqueous solutions is thanks to the hydroxyl group (Kohl and Nielsen, 1997a). The alkaline environment the amines form is the reason why they are good absorbents of acid gases.

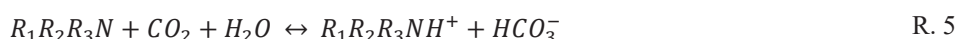
In the following reactions, MDEA (methyldiethanolamine,  $\text{CH}_3\text{N}(\text{C}_2\text{H}_4\text{OH})_2$ ) is denoted by the general form of tertiary amines,  $\text{R}_1\text{R}_2\text{R}_3\text{N}$ , where R stands for any alkyl or aryl group. Hydrogen sulfide reacts instantaneously with MDEA, through a proton-transfer reaction (R. 1).



In aqueous systems, the reactions taking place are often written including the water (R. 2 - R. 4), though the overall reaction is the same as R. 1.



The overall reaction between carbon dioxide and aqueous tertiary amines is given in R. 5.



Two mechanisms have been proposed regarding the role of the amine in the reaction path; one suggests the role of the amine as a catalyst to promote the hydrolysis of carbon dioxide (Donaldson and Nguyen, 1980) and the other suggests the direct reaction of carbon dioxide with the tertiary amine to form a zwitterion (Yu et al., 1985).

Regarding the first proposed mechanism, Donaldson and Nguyen (Donaldson and Nguyen, 1980) rejected the possibility for direct reaction of the tertiary amine with CO<sub>2</sub> and suggested that the amine serves as catalyst accelerating the reaction of carbon dioxide with water. The reactions proposed according to this theory, which is widely embraced by the scientific community, are presented below:



Carbon dioxide reacts with water in aqueous solutions with bicarbonate ions as products. Further dissociation of carbonic acid, from bicarbonate to carbonate also takes place but it can be considered negligible at amine pK<sub>a</sub> values < 10.8 at 25 °C. Since the pK<sub>a</sub> of MDEA is 8.3, this reaction is not listed (Yu et al., 1985). The formation reaction of bicarbonate is slow (R. 6 - R. 8). Contrary to primary and secondary amines which can directly react with CO<sub>2</sub> by losing their proton and forming carbamate (RNHCOO<sup>-</sup>) in a relatively fast reaction, tertiary amines do not have any hydrogen atom available. Therefore, carbon dioxide is forced to form bicarbonate

via the slow route. Donaldson and Nguyen (Donaldson and Nguyen, 1980) also discussed the formation of monoalkyl carbonate in the case that one of the R- groups of the tertiary amine is an alcohol, but concluded that the formation of an alkyl carbonate is not possible. This implies, that in non-aqueous systems, carbon dioxide will remain unreacted.

As far as the second proposed mechanism is concerned, Yu et al. (Yu et al., 1985) proposed the formation of an intermediate in reaction R. 6 as the product of CO<sub>2</sub>-amine reaction and addressed the question of what kind of intermediate could that be. They suggested an unstable zwitterion to be formed on the nitrogen atom of the tertiary amine. According to this theory, the zwitterion then reacts with H<sub>2</sub>O to form the more stable protonated amine and bicarbonate ion (R. 10 - R. 11 ). This implies that bicarbonate cannot be formed in water-free systems.



Recent studies have shown that in both aqueous and non-aqueous tertiary amines, alkyl carbonates can be formed (Behrens et al., 2017; Rainbolt et al., 2011), meaning that both theories seem to have correct and incorrect elements. Based on the latest findings, the theory of Yu et al. (Yu et al., 1985) seems to hold in terms of a direct reaction of carbon dioxide with tertiary amines and the formation of a zwitterionic product. However, the reaction product is not formed on the nitrogen atom of the amine, but instead on the O<sup>-</sup> of one of the present hydroxyl groups. In the interim, the theory of Donaldson and Nguyen (Donaldson and Nguyen, 1980) is correct about the role of the aqueous amine as a facilitator in carbon dioxide hydration, although their dismissal of alkyl carbonate formation is false.

In spite of the mechanism, it is proven that the kinetics of aqueous tertiary amines with CO<sub>2</sub> is slow. Fast kinetics are exhibited with H<sub>2</sub>S and it is this difference that renders tertiary amines suitable solvents for selective removal of hydrogen sulfide over CO<sub>2</sub>. In spite of the much faster reaction of H<sub>2</sub>S compared to the reaction of CO<sub>2</sub>, the latter still limits the H<sub>2</sub>S selectivity that aqueous tertiary amines can attain because the bicarbonate concentration in the bulk phase of the liquid affects the driving force available for hydrogen sulfide absorption (Yu et al., 1985). It is noted that any advantage for H<sub>2</sub>S selectivity disappears at extended times that will allow the formation of the CO<sub>2</sub> reaction products.

## Bibliography

- Ahmadi, M., Janakiram, S., Dai, Z., Ansaloni, L., Deng, L., 2018. Performance of Mixed Matrix Membranes Containing Porous Two-Dimensional (2D) and Three-Dimensional (3D) Fillers for CO<sub>2</sub> Separation: A Review. *Membranes* 8, 50. <https://doi.org/10.3390/membranes8030050>
- Ahn, H., Luberti, M., Liu, Z., Brandani, S., 2013. Process configuration studies of the amine capture process for coal-fired power plants. *International Journal of Greenhouse Gas Control* 16, 29–40. <https://doi.org/10.1016/j.ijggc.2013.03.002>
- AlHarooni, K., Pack, D., Iglauer, S., Gubner, R., Ghodkay, V., Barifcani, A., 2016. Analytical Techniques for Analyzing Thermally Degraded Monoethylene Glycol with Methyl Diethanolamine and Film Formation Corrosion Inhibitor. *Energy Fuels* 30, 10937–10949. <https://doi.org/10.1021/acs.energyfuels.6b02116>
- Alvarez-Fuster, C., Midoux, N., Laurent, A., Charpentier, J.C., 1981. Chemical kinetics of the reaction of CO<sub>2</sub> with amines in pseudo m–nth order conditions in polar and viscous organic solutions. *Chemical Engineering Science* 36, 1513–1518. [https://doi.org/10.1016/0009-2509\(81\)85112-3](https://doi.org/10.1016/0009-2509(81)85112-3)
- Amosa, M.K., Mohammed, I.A., Yaro, S.A., 2010. Sulphide Scavengers in Oil and Gas Industry – A Review. *Nafta* 61, 85–98.
- Archane, A., Fürst, W., Provost, E., 2011. Influence of Poly(ethylene oxide) 400 (PEG400) on the Absorption of CO<sub>2</sub> in Diethanolamine (DEA)/H<sub>2</sub>O Systems. *J. Chem. Eng. Data* 56, 1852–1856. <https://doi.org/10.1021/je100854j>
- Årsrapport 2005 Utslipp fra Åsgardfeltet [WWW Document], 2005. URL <https://docplayer.me/60170477-Arsrapport-2005-utslipp-fra-asgardfeltet-hno-asg-myn-0357.html> (accessed 2.10.20).
- Axens Solutions, 2017. SPREX technology [WWW Document]. URL <https://www.axens.net/product/process-licensing/20131/sprex.html/> (accessed 2.27.20).
- Baker, J.R., Rogers, J.A., 1989. High Efficiency Co-current Contactors for Gas Conditioning Operations. Presented at the Laurence Reid Gas Conditioning Conference, Oklahoma, USA.
- Behrens, R., von Harbou, E., Thiel, W.R., Böttinger, W., Ingram, T., Sieder, G., Hasse, H., 2017. Monoalkylcarbonate Formation in Methyldiethanolamine–H<sub>2</sub>O–CO<sub>2</sub>. *Ind. Eng. Chem. Res.* 56, 9006–9015. <https://doi.org/10.1021/acs.iecr.7b01937>
- Braun, N.O., Persson, U.Å., Karlsson, H.T., 2001. Densities and Viscosities of Mono(ethylene glycol) + 2-Amino-2-methyl-1-propanol + Water. *J. Chem. Eng. Data* 46, 805–808. <https://doi.org/10.1021/je010004z>
- Brouwer, J.M., Epsom, H.D., 2003. Twister Supersonic Gas Conditioning for Unmanned Platforms and Subsea Gas Processing. Presented at the Offshore Europe, Society of Petroleum Engineers. <https://doi.org/10.2118/83977-MS>
- Campbell, J.M., 1998a. Amine-based processes, in: *Gas Conditioning and Processing*. Oklahoma, USA.
- Campbell, J.M., 1998b. Glycol Dehydration, in: *Gas Conditioning and Processing*. Oklahoma, USA, pp. 333–394.
- Chapin, W.F., 1950. Purification and dehydration of gases. US2518752 A.

- Christensen, K.O., 2011. Water content of high pressure natural gas: Data, prediction and experience from field. Presented at the Trondheim Gas Technology Conference, Trondheim, Norway.
- Dalane, K., Hillestad, M., Deng, L., 2019. Subsea natural gas dehydration with membrane processes: Simulation and process optimization. *Chemical Engineering Research and Design* 142, 257–267. <https://doi.org/10.1016/j.cherd.2018.12.027>
- Davis, R.A., Menendez, R.E., Sandall, O.C., 1993. Physical, thermodynamic, and transport properties for carbon dioxide and nitrous oxide in solutions of diethanolamine or di-2-propanolamine in polyethylene glycol. *J. Chem. Eng. Data* 38, 119–124. <https://doi.org/10.1021/je00009a029>
- Davis, R.A., Sandall, O.C., 1993. Kinetics of the reaction of carbon dioxide with secondary amines in polyethylene glycol. *Chemical Engineering Science* 48, 3187–3193. [https://doi.org/10.1016/0009-2509\(93\)80204-4](https://doi.org/10.1016/0009-2509(93)80204-4)
- Davoudi, M., Heidari, Y., Safadoost, A., Samieirad, S., 2014. Chemical injection policy for internal corrosion prevention of South Pars sea-pipeline: A case study. *Journal of Natural Gas Science and Engineering* 21, 592–599. <https://doi.org/10.1016/j.jngse.2014.09.017>
- Dekeyzer, E., Christensen, K.O., Voldum, K., Nillson, C., Grønn, T., 2012. ProDry - Robust Contactor for Moderate Water Dew Point Reduction. Presented at the Laurance Reid Gas Conditioning Conference, Oklahoma, USA.
- Dirdal, E., 2019. Subsea Water Treatment Pilot Testing at the Ekofisk Field in the North Sea. Presented at the Offshore Technology Conference, Offshore Technology Conference. <https://doi.org/10.4043/29552-MS>
- Donaldson, T.L., Nguyen, Y.N., 1980. Carbon Dioxide Reaction Kinetics and Transport in Aqueous Amine Membranes. *Industrial & Engineering Chemistry Fundamentals* 19, 260–266. <https://doi.org/10.1021/i160075a005>
- Ebeling, H.O., Lyddon, L.G., Covington, K.K., 1998. Reduce Emissions and Operating Costs with Appropriate Glycol Selection, in: Seventy-Seventh Annual Convention - Gas Processors Association. Presented at the Annual Convention. Gas Processors Association (GPA), GPA, Texas, USA.
- Eimer, D., 1994. Simultaneous removal of water and hydrogen sulphide from natural gas (Dr. Ing thesis). NTNU, Trondheim.
- Eriksen, S., Hop, B.I., Ruud, T., 2015. Offshore processing method and system. US20150013539 A1.
- Faanæs, A., 2020. Industrial input.
- Falcimaigne, J., Decarre, S., 2008. *Multiphase Production: Pipeline Transport, Pumping and Metering*. Editions OPHRYS.
- Forster, L., Mesquita Paes, T., Baker, R., Thati, D., Antilley, D., Hawthorn, K., Burke, J., Mendoza, A., Allen, J., McKee, M., Albaugh, E.K., Davis, D., 2016. 2016 Worldwide Survey Of Subsea Processing: Separation, Compression, and Pumping System [WWW Document]. Offshore. URL <https://www.offshore-mag.com/resources/maps-posters/whitepaper/14034369/2016-worldwide-survey-of-subsea-processing-separation-compression-and-pumping-system> (accessed 2.10.20).
- Frazier, H.D., Kohl, A.L., 1950. Selective Absorption of Hydrogen Sulfide from Gas Streams. *Ind. Eng. Chem.* 42, 2288–2292. <https://doi.org/10.1021/ie50491a032>

- Fredheim, A.O., Johnsen, C.G., Johannessen, E., Kojen, G.P., 2016. Gas-2-Pipe™, A Concept for Treating Gas to Rich Gas Quality in a Subsea or Unmanned Facility, in: OTC-27147-MS. Offshore Technology Conference, OTC. <https://doi.org/10.4043/27147-MS>
- Fu, D., Du, L., Wang, H., 2014a. Experiment and model for the surface tension of MEA-PEG400 and DEA-PEG400 aqueous solutions. *The Journal of Chemical Thermodynamics* 69, 132–136. <https://doi.org/10.1016/j.jct.2013.10.016>
- Fu, D., Zhang, P., Du, L., Dai, J., 2014b. Experiment and model for the viscosities of MEA-PEG400, DEA-PEG400 and MDEA-PEG400 aqueous solutions. *The Journal of Chemical Thermodynamics* 78, 109–113. <https://doi.org/10.1016/j.jct.2014.06.017>
- Garcia, M., Knuutila, H.K., Aronu, U.E., Gu, S., 2018. Influence of substitution of water by organic solvents in amine solutions on absorption of CO<sub>2</sub>. *International Journal of Greenhouse Gas Control* 78, 286–305. <https://doi.org/10.1016/j.ijggc.2018.07.029>
- GATEkeeper, 2014. Introduction to H<sub>2</sub>S scavenging.
- GPSA, 2014. Dehydration, in: *Engineering Data Book*. Section 20. Gas Processors Suppliers Association, Tulsa, Oklahoma.
- Gurylev, V., Soriano, A.N., Caparanga, A.R., Li, M.-H., Adornado, A.P., 2018. Viscosities of diethylene glycol (DEG) + 2-amino-2-methyl-1-propanol (AMP) + water. *IOP Conf. Ser.: Earth Environ. Sci.* 191, 012088. <https://doi.org/10.1088/1755-1315/191/1/012088>
- Gurylev, V., Soriano, A.N., Eleazar, E.G., Caparanga, A.R., Li, M.-H., 2014. Densities of aqueous glycol-amine systems containing (DEG or TEG or TREG) as glycol and 2-amino-2-methyl-1-propanol as amine, in: 1. Presented at the Philippine Institute of Chemical Engineers, PICHE Journal, Manila, Philippines, pp. 21–29.
- Gyllenhammar, E., Boireau, C., Riviere, L., Ulvestad, A., 2015. Deep Offshore Gas Fields: A New Challenge for the Industry. Presented at the Offshore Technology Conference, Offshore Technology Conference. <https://doi.org/10.4043/25802-MS>
- Hutchinson, A.J.L., 1939. Process for treating gases. US2184596 A.
- Hwang, K.-S., Park, S.-W., Park, D.-W., Oh, K.-J., Kim, S.-S., 2010. Absorption of carbon dioxide into diisopropanolamine solutions of polar organic solvents. *Journal of the Taiwan Institute of Chemical Engineers* 41, 16–21. <https://doi.org/10.1016/j.jtice.2009.05.009>
- Jelstad, A., 1997. Gass-væske likevektsstudier for hydrogensulfid. Norwegian University of Science and Technology, Trondheim, Norway.
- Kang, M.-K., Cho, J.-H., Lee, J.-H., Lee, S.-S., Oh, K.-J., 2017a. Kinetic Reaction Characteristics of Quasi-Aqueous and Nonaqueous Sorbents for CO<sub>2</sub> Absorption Using MEA/H<sub>2</sub>O/Ethylene Glycol. *Energy Fuels* 31, 8383–8391. <https://doi.org/10.1021/acs.energyfuels.7b00768>
- Kang, M.-K., Jeon, S.-B., Cho, J.-H., Kim, J.-S., Oh, K.-J., 2017b. Characterization and comparison of the CO<sub>2</sub> absorption performance into aqueous, quasi-aqueous and non-aqueous MEA solutions. *International Journal of Greenhouse Gas Control* 63, 281–288. <https://doi.org/10.1016/j.ijggc.2017.05.020>
- Kohl, A.L., Nielsen, R.B., 1997a. Chapter 2 - Alkanolamines for Hydrogen Sulfide and Carbon Dioxide Removal, in: *Gas Purification*. Gulf Professional Publishing, Houston, pp. 40–186.
- Kohl, A.L., Nielsen, R.B., 1997b. Chapter 11 - Absorption of Water Vapor by Dehydrating Solutions, in: *Gas Purification*. Gulf Professional Publishing, Houston, pp. 946–1021.

- Leites, I.L., 1998. Thermodynamics of CO<sub>2</sub> solubility in mixtures monoethanolamine with organic solvents and water and commercial experience of energy saving gas purification technology. *Energy Conversion and Management* 39, 1665–1674. [https://doi.org/10.1016/S0196-8904\(98\)00076-4](https://doi.org/10.1016/S0196-8904(98)00076-4)
- Liang, Z., Fu, K., Idem, R., Tontiwachwuthikul, P., 2016. Review on current advances, future challenges and consideration issues for post-combustion CO<sub>2</sub> capture using amine-based absorbents. *Chinese Journal of Chemical Engineering* 24, 278–288. <https://doi.org/10.1016/j.cjche.2015.06.013>
- Linga, H., Kalgraff, B.H., 2008. Boosting your H<sub>2</sub>S-Selectivity in Sour Gas Treatment. Presented at the Sour Oil and Gas Advanced Technology - SOGAT 2008.
- Lioliou, M.G., Sandrød, J., Stipanicev, M., Birketveit, Ø., 2017. Qualification and field performance of subsea H<sub>2</sub>S scavenger injection. Presented at the Oilfield Chemistry Symposium, Geilo.
- Littell, H.S., Jessup, J.W., Schoppa, W.W., Seay, M.R., Coulon, T.D., 2011. Perdido Startup: Flow Assurance and Subsea Artificial Lift Performance. Presented at the Offshore Technology Conference, Offshore Technology Conference. <https://doi.org/10.4043/21716-MS>
- McCartney, E.R., 1948. Gas purification and dehydration process. US2435089 A.
- Mitchell, A.F., Skjevrak, I., Waage, J., 2017. A Re-Evaluation of Reservoir Souring Patterns and Effect of Mitigation in a Mature North Sea Field, in: SPE International Conference on Oilfield Chemistry. Presented at the SPE International Conference on Oilfield Chemistry, Society of Petroleum Engineers, Montgomery, Texas, USA. <https://doi.org/10.2118/184587-MS>
- Neptune Energy, 2020. Fenja [WWW Document]. Neptune Energy. URL <https://www.neptuneenergy.com/field/fenja/> (accessed 2.10.20).
- Økland, O., Davies, S., Ramberg, R.M., Rognø, H., 2013. Steps to the Subsea Factory, in: OTC-24307-MS. Offshore Technology Conference, OTC. <https://doi.org/10.4043/24307-MS>
- Orlowski, R., Euphemio, M.L.L., Euphemio, M.L., Andrade, C.A., Guedes, F., Tosta da Silva, L.C., Pestana, R.G., de Cerqueira, G., Lourenço, I., Pivari, A., Witka, A., Folhadella, H., Pacheco, L., Kronemberger, S., Vilela, J., 2012. Marlim 3 Phase Subsea Separation System - Challenges and Solutions for the Subsea Separation Station to Cope with Process Requirements. Presented at the Offshore Technology Conference, Offshore Technology Conference. <https://doi.org/10.4043/23552-MS>
- OSPAR Commission, 2010. Discharges, Spills and Emissions from Offshore Oil and Gas Installations. OSPAR Commission: London, UK.
- Oyevaar, M.H., Fontein, H.J., Westerterp, K.R., 1989a. Equilibria of carbon dioxide in solutions of diethanolamine in aqueous ethylene glycol at 298 K. *J. Chem. Eng. Data* 34, 405–408. <https://doi.org/10.1021/jc00058a010>
- Oyevaar, M.H., Morssinkhof, R.W.J., Westerterp, K.R., 1990. The kinetics of the reaction between CO<sub>2</sub> and diethanolamine in aqueous ethyleneglycol at 298 K: a viscous gas—liquid reaction system for the determination of interfacial areas in gas—liquid contactors. *Chemical Engineering Science* 45, 3283–3298. [https://doi.org/10.1016/0009-2509\(90\)80220-9](https://doi.org/10.1016/0009-2509(90)80220-9)
- Oyevaar, M.H., Morssinkhof, R.W.J., Westerterp, K.R., 1989b. Density, viscosity, solubility, and diffusivity of carbon dioxide and nitrous oxide in solutions of diethanolamine in aqueous ethylene glycol at 298 K. *J. Chem. Eng. Data* 34, 77–82. <https://doi.org/10.1021/jc00055a022>



- Park, S.-W., Choi, B.-S., Lee, J.-W., 2007. Influence of polyethylene oxide on absorption of carbon dioxide into aqueous N-methyldiethanolamine solution. *Korean J. Chem. Eng.* 24, 431–435. <https://doi.org/10.1007/s11814-007-0074-y>
- Park, S.-W., Choi, B.-S., Lee, J.-W., 2006a. Chemical absorption of carbon dioxide with triethanolamine in non-aqueous solutions. *Korean J. Chem. Eng.* 23, 138–143. <https://doi.org/10.1007/BF02705705>
- Park, S.-W., Choi, B.-S., Lee, J.-W., 2005a. Chemical Absorption of Carbon Dioxide into Aqueous PEO Solution of Monoethanolamine. *Separation Science and Technology* 40, 3261–3275. <https://doi.org/10.1080/01496390500423623>
- Park, S.-W., Lee, Joon-Wook, Choi, B.-S., Lee, Jae-Wook, 2006b. Absorption of carbon dioxide into non-aqueous solutions of N-methyldiethanolamine. *Korean J. Chem. Eng.* 23, 806–811. <https://doi.org/10.1007/BF02705932>
- Park, S.-W., Lee, Joon-Wook, Choi, B.-S., Lee, Jae-Wook, 2005b. Reaction Kinetics of Carbon Dioxide with Diethanolamine in Polar Organic Solvents. *Separation Science and Technology* 40, 1885–1898. <https://doi.org/10.1081/SS-200064536>
- Pedersen, E.K., 1994. Absorpsjonslikevekter for H<sub>2</sub>S i ikke vandige aminløsninger (Report Supplement), Simultan fjerning av vann og H<sub>2</sub>S fra naturgass. NTNU, Trondheim, Norway.
- Poblete, A.T.C., 1997. Gass-væske likevektsstudier for hydrogensulfid. Norwegian University of Science and Technology, Trondheim, Norway.
- ProSep, 2017. Prosep Awarded Contract For Statoil's Troll B ZMP Project [WWW Document]. ProSep. URL <https://www.prosep.com/prosep-awarded-contract-statoils-troll-b-zmp-project/> (accessed 2.16.20).
- Pyles, S., Rader, R.G., 1989. Single Stage Co-current Contactor Replaces Trayed Column on Offshore Platform for Dehydration. Presented at the 12th Annual Energy - Sources Technology Conference Exhibition, Houston, Texas.
- Rainbolt, J.E., Koech, P.K., Yonker, C.R., Zheng, F., Main, D., Weaver, M.L., Linehan, J.C., Heldebrant, D.J., 2011. Anhydrous tertiary alkanolamines as hybrid chemical and physical CO<sub>2</sub> capture reagents with pressure-swing regeneration. *Energy Environ. Sci.* 4, 480–484. <https://doi.org/10.1039/C0EE00506A>
- Ramkumar, S., Grave, E.J., Larnholm, P.-R., Thierens, D., 2017. cMIST TM: Novel, Compact Dehydration System for Reducing Size and Weight. Presented at the Offshore Technology Conference, Offshore Technology Conference. <https://doi.org/10.4043/27746-MS>
- Ramkumar, S., Philbrook, S., Santhanam, P., Cullinane, T., Northrop, S., 2019. Compact, Selective H<sub>2</sub>S Removal Technology. Presented at the Sour Oil and Gas Advanced Technology - SOGAT 2019, Abu Dhabi, UAE.
- Rasmussen, A.W., 2002. Troll Pilot Technology- The Next Step. Presented at the Offshore Technology Conference, Offshore Technology Conference. <https://doi.org/10.4043/14258-MS>
- Raynal, L., Bouillon, P.-A., Gomez, A., Broutin, P., 2011. From MEA to demixing solvents and future steps, a roadmap for lowering the cost of post-combustion carbon capture. *Chemical Engineering Journal*, Special Section: Symposium on Post-Combustion Carbon Dioxide Capture 171, 742–752. <https://doi.org/10.1016/j.cej.2011.01.008>

- RIGZONE, 2009. Oil Majors Tap ProSep to Supply Proprietary Technologies [WWW Document]. URL [https://www.rigzone.com/news/oil\\_gas/a/78014/oil\\_majors\\_tap\\_prosep\\_to\\_supply\\_proprietary\\_technologies/](https://www.rigzone.com/news/oil_gas/a/78014/oil_majors_tap_prosep_to_supply_proprietary_technologies/) (accessed 2.16.20).
- Rivas, O.R., Prausnitz, J.M., 1979. Sweetening of sour natural gases by mixed-solvent absorption: Solubilities of ethane, carbon dioxide, and hydrogen sulfide in mixtures of physical and chemical solvents. *AIChE J.* 25, 975–984. <https://doi.org/10.1002/aic.690250608>
- Ruud, T., Idrac, A., McKenzie, L.J., Høy, S.H., 2015. All Subsea: A Vision for the Future of Subsea Processing. Presented at the Offshore Technology Conference, Offshore Technology Conference. <https://doi.org/10.4043/25735-MS>
- Sagatun, S.I., Gramme, P., Lie, G., Horgen, O.J., Ruud, T., Storvik, M., 2008. The Pipe Separator - Simulations and Experimental Results. Presented at the Offshore Technology Conference, Offshore Technology Conference. <https://doi.org/10.4043/19389-MS>
- Schulz, M., 2013. Integration of H<sub>2</sub>S scavengers with amine plants. Presented at the Laurance Reid Gas Conditioning.
- Seabox Subsea Water Treatment Technology [WWW Document], 2004. URL <https://www.nov.com/products/seabox-subsea-water-treatment-technology> (accessed 2.8.20).
- Shah, M.S., Tsapatsis, M., Siepmann, J.I., 2017. Hydrogen Sulfide Capture: From Absorption in Polar Liquids to Oxide, Zeolite, and Metal–Organic Framework Adsorbents and Membranes. *Chem. Rev.* 117, 9755–9803. <https://doi.org/10.1021/acs.chemrev.7b00095>
- Shoukat, U., Baumeister, E., Pinto, D.D.D., Knuutila, H.K., 2019. Thermal stability and corrosion of tertiary amines in aqueous amine and amine-glycol-water solutions for combined acid gas and water removal. *Journal of Natural Gas Science and Engineering* 62, 26–37. <https://doi.org/10.1016/j.jngse.2018.11.025>
- Shoukat, U., Fytianos, G., Knuutila, H.K., 2016. Thermal stability and corrosion studies of amines for combined acid gas removal and hydrate control for subsea gas treatment systems, in: 2016 Techno-Ocean (Techno-Ocean). Presented at the 2016 Techno-Ocean (Techno-Ocean), pp. 176–180. <https://doi.org/10.1109/Techno-Ocean.2016.7890641>
- Si Huai Yeaw, 2019. Subsea Processing – Beyond Pump and Compressor.
- Song, J.-H., Park, S.-B., Yoon, J.-H., Lee, H., Lee, K.-H., 1997. Solubility of Carbon Dioxide in Monoethanolamine + Ethylene Glycol + Water and Monoethanolamine + Poly(ethylene glycol) + Water at 333.2 K. *J. Chem. Eng. Data* 42, 143–144. <https://doi.org/10.1021/je960203w>
- Song, J.-H., Park, S.-B., Yoon, J.-H., Lee, H., Lee, K.-H., 1996a. Densities and Viscosities of Monoethanolamine + Ethylene Glycol + Water. *J. Chem. Eng. Data* 41, 1152–1154. <https://doi.org/10.1021/je9601366>
- Song, J.-H., Yoon, J.-H., Lee, H., Lee, K.-H., 1996b. Solubility of Carbon Dioxide in Monoethanolamine + Ethylene Glycol + Water and Monoethanolamine + Poly(ethylene glycol) + Water. *J. Chem. Eng. Data* 41, 497–499. <https://doi.org/10.1021/je9502758>
- Sridharan, K., Sharma, M.M., 1976. New systems and methods for the measurement of effective interfacial area and mass transfer coefficients in gas–liquid contactors. *Chemical Engineering Science* 31, 767–774. [https://doi.org/10.1016/0009-2509\(76\)80049-8](https://doi.org/10.1016/0009-2509(76)80049-8)
- Stanimirovic, A., Zivkovic, E., Majstorovic, D., Kijevcanin, M., 2016. Transport properties of binary liquid mixtures - candidate solvents for optimized flue gas cleaning processes. *J. Serb Chem Soc* 81, 1427–1439. <https://doi.org/10.2298/JSC160623083S>

- Stewart, M., Arnold, K., 2011. Part 1 - Gas Sweetening, in: Arnold, M.S. (Ed.), Gas Sweetening and Processing Field Manual. Gulf Professional Publishing, Boston, pp. 1–140.
- Tan, J., Shao, H., Xu, J., Du, L., Luo, G., 2011. Mixture Absorption System of Monoethanolamine–Triethylene Glycol for CO<sub>2</sub> Capture. *Ind. Eng. Chem. Res.* 50, 3966–3976. <https://doi.org/10.1021/ie101810a>
- Time, N.P., Torpe, H., 2016. Subsea Compression - Åsgard Subsea Commissioning, Start-Up and Operational Experiences. Presented at the Offshore Technology Conference, Offshore Technology Conference. <https://doi.org/10.4043/27163-MS>
- Tørnqvist, M., 1991. Absorpsjon av karbondioksid i ikke-vandige systemer. NTNU, Trondheim, Norway.
- Total, 2014. ANGOLA - CLOV | WikiTotal [WWW Document]. URL <https://wiki.total/en/angola-clov> (accessed 2.10.20).
- Tsierkezos, N.G., Molinou, I.E., 1999. Densities and Viscosities of Ethylene Glycol Binary Mixtures at 293.15 K. *J. Chem. Eng. Data* 44, 955–958. <https://doi.org/10.1021/je990059p>
- UWP/Subsea on a Stick® [WWW Document], n.d. . Kvaerner - UWP/Subsea on a Stick®. URL <https://www.kvaerner.com/Products/Subsea-on-a-Stick/> (accessed 3.13.19).
- Vinterstø, T., Birkeland, B., Ramberg, R.M., Davies, S., Hedne, P.E., 2016. Subsea Compression - Project Overview. Presented at the Offshore Technology Conference, Offshore Technology Conference. <https://doi.org/10.4043/27172-MS>
- Wanderley, R.R., Pinto, D.D.D., Knuutila, H.K., 2020. Investigating opportunities for water-lean solvents in CO<sub>2</sub> capture: VLE and heat of absorption in water-lean solvents containing MEA. *Separation and Purification Technology* 231, 115883. <https://doi.org/10.1016/j.seppur.2019.115883>
- Wanderley, R.R., Yuan, Y., Rochelle, G.T., Knuutila, H.K., 2019. CO<sub>2</sub> solubility and mass transfer in water-lean solvents. *Chemical Engineering Science* 202, 403–416. <https://doi.org/10.1016/j.ces.2019.03.052>
- Woertz, B.B., 1972. Experiments with solvent-amine-water for removing co<sub>2</sub> from gas. *The Canadian Journal of Chemical Engineering* 50, 425–427. <https://doi.org/10.1002/cjce.5450500321>
- Xu, H.-J., Zhang, C.-F., Zheng, Z.-S., 2002a. Selective H<sub>2</sub>S Removal by Nonaqueous Methyl-diethanolamine Solutions in an Experimental Apparatus. *Ind. Eng. Chem. Res.* 41, 2953–2956. <https://doi.org/10.1021/ie0109253>
- Xu, H.-J., Zhang, C.-F., Zheng, Z.-S., 2002b. Solubility of Hydrogen Sulfide and Carbon Dioxide in a Solution of Methyl-diethanolamine Mixed with Ethylene Glycol. *Ind. Eng. Chem. Res.* 41, 6175–6180. <https://doi.org/10.1021/ie020375o>
- Yang, C., Feng, Y., Cheng, B., Zhang, P., Qin, Z., Zeng, H., Sun, F., 2013. Vapor–Liquid Equilibria for Three Binary Systems of N-Methylethanolamine, N-Methyl-diethanolamine, and Ethylene Glycol at P = (40.0, 30.0, and 20.0) kPa. *J. Chem. Eng. Data* 58, 2272–2279. <https://doi.org/10.1021/je400373d>
- Yang, F., Wang, X., Wang, W., Liu, Z., 2013. Densities and Excess Properties of Primary Amines in Alcoholic Solutions. *J. Chem. Eng. Data* 58, 785–791. <https://doi.org/10.1021/je3013205>

- Yu, C.-H., Wu, T.-W., Tan, C.-S., 2013. CO<sub>2</sub> capture by piperazine mixed with non-aqueous solvent diethylene glycol in a rotating packed bed. *International Journal of Greenhouse Gas Control* 19, 503–509. <https://doi.org/10.1016/j.ijggc.2013.10.014>
- Yu, W.-C., Astarita, G., Savage, D.W., 1985. Kinetics of carbon dioxide absorption in solutions of methyldiethanolamine. *Chemical Engineering Science* 40, 1585–1590. [https://doi.org/10.1016/0009-2509\(85\)80101-9](https://doi.org/10.1016/0009-2509(85)80101-9)
- Zhao, H., 2019. CFU Pilot JIP.
- Zheng, C., Tan, J., Wang, Y.J., Luo, G.S., 2013. CO<sub>2</sub> Solubility in a Mixture Absorption System of 2-Amino-2-methyl-1-propanol with Ethylene Glycol. *Ind. Eng. Chem. Res.* 52, 12247–12252. <https://doi.org/10.1021/ie401805n>
- Zheng, C., Tan, J., Wang, Y.J., Luo, G.S., 2012. CO<sub>2</sub> Solubility in a Mixture Absorption System of 2-Amino-2-methyl-1-propanol with Glycol. *Ind. Eng. Chem. Res.* 51, 11236–11244. <https://doi.org/10.1021/ie3007165>
- Zheng, C., Zhao, B., Wang, K., Luo, G., 2015. Determination of kinetics of CO<sub>2</sub> absorption in solutions of 2-amino-2-methyl-1-propanol using a microfluidic technique. *AIChE Journal* 61, 4358–4366. <https://doi.org/10.1002/aic.14972>

## Chapter 3

# Density and Viscosity

*This chapter presents experimental measurements and modeling of density and viscosity of aqueous and non-aqueous mixtures of methyldiethanolamine and monoethylene glycol.*

In the first part of this chapter, the physical properties density and viscosity of the systems MDEA-MEG and MDEA-MEG-H<sub>2</sub>O were studied at temperatures from 283.15 to 353.15 K and ambient pressure (journal publication I). In the binary systems, the amine content varied from 5 to 90 wt%. The effect of water was studied in the ternary systems by varying its concentration from 5 to 50 wt%. Both density and viscosity measurements showed good repeatability and reproducibility. Excess molar volumes and viscosity deviations upon mixing were derived from the experimental data. They indicate strong non-ideality of the mixtures at the studied conditions, which have been explained by the attractive intermolecular forces and structural effects in the mixtures. Non-random two-liquid-based models were used to successfully predict both density and viscosity, while a comparison was performed with the Aspen liquid mixture viscosity model. The average absolute relative deviations (AARDs) were found to be less than 0.4% for density and 3% for viscosity for both models for the binary and the ternary systems. Special focus has been given on the uncertainty of the measurements; therefore, a comprehensive uncertainty analysis is included in the Supporting information of the following published article.

In the second part of the chapter, further considerations in the application of MEG-MDEA and MEG-MDEA-H<sub>2</sub>O solvents for the combined hydrogen sulfide removal and hydrate control subsea are discussed. The discussion focuses on the high viscosity of the proposed systems that may clash with processing equipment requirements. The effects of pressure and acid gas loading of the solvent are examined and it is shown that the model developed in this work can be used for the prediction of the viscosity limits of this process.

### **3.1 Density and viscosity study for the systems MDEA-MEG and MDEA-MEG-H<sub>2</sub>O**

#### **Journal publication I**

Skylogianni, E., Wanderley, R.R., Austad, S.S., Knuutila, H.K., 2019. Density and Viscosity of the Nonaqueous and Aqueous Mixtures of Methyldiethanolamine and Monoethylene Glycol at Temperatures from 283.15 to 353.15 K. *J. Chem. Eng. Data* 64, 5415–5431. <https://doi.org/10.1021/acs.jced.9b00607>.

Reprinted (adapted) with permission from The Journal of Chemical and Engineering Data. Copyright 2019 American Chemical Society.

# Paper I

...the ...

...the ...

...the ...

...the ...

...the ...

...the ...

...the ...

...the ...

...the ...

...the ...

...the ...

...the ...

...the ...

...the ...


...the ...

...the ...


...the ...



# Density and Viscosity of the Nonaqueous and Aqueous Mixtures of Methyldiethanolamine and Monoethylene Glycol at Temperatures from 283.15 to 353.15 K

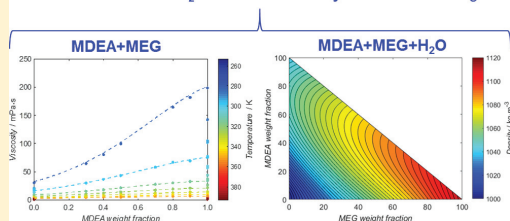
Eirini Skylogianni, Ricardo R. Wanderley, Sigrid S. Austad, and Hanna K. Knuutila\*

Department of Chemical Engineering, Norwegian University of Science and Technology, 7034 Trondheim, Norway

 Supporting Information

**ABSTRACT:** Nonaqueous and aqueous mixtures of methyldiethanolamine and monoethylene glycol form promising absorbents for the combined hydrogen sulfide removal and hydrate control, necessary in natural gas processing. In this direction, the density and viscosity of the binary and ternary systems were measured and modeled in the temperature range of  $T = 283.15\text{--}353.15\text{ K}$  and at ambient pressure. Excess molar volumes and viscosity deviations from ideality were also calculated. The water content varied from 5 to 50 wt % and the amine content from 5 to 90 wt %. Both density and viscosity were modeled using nonrandom two-liquid-based models.

Regarding the density modeling, the average absolute relative deviations (AARDs) were found to be less than 0.4% for the binary subsystems and equal to 0.3% for the ternary system. Viscosity modeling results show higher AARD, though always lower than 3.0% for both binary and ternary solutions.

Solvent for combined  $\text{H}_2\text{S}$  removal and dehydration of natural gas

## 1. INTRODUCTION

Acid gas removal with the aid of amines is a common industrial process, for example, in oil refineries and natural gas treatment plants among others. Commercial amines are monoethanolamine, diglycolamine, and methyldiethanolamine (MDEA), the latter being most suitable for the selective removal of hydrogen sulfide ( $\text{H}_2\text{S}$ ) over carbon dioxide ( $\text{CO}_2$ ).<sup>1</sup> In oil and gas production, hydrate control or dehydration is an equally necessary process as gas sweetening. Typically, glycols such as monoethylene glycol (MEG) and triethylene glycol are used, respectively, to prevent hydrate formation during gas transportation and to reach water content specifications.<sup>2,3</sup> Moreover, the focus of oil and gas companies on subsea operations encourages process intensification concepts, where modules with respect to size, weight, and complexity are developed.<sup>4</sup> Such a concept is the combined removal of acid gases and water vapors in one step only, first conceived and patented by Hutchinson<sup>5</sup> and later further developed by McCartney<sup>6,7</sup> and Chapin.<sup>8</sup> In this direction, our group investigates the feasibility of the simultaneous acid gas removal and hydrate control process with nonaqueous and aqueous MDEA–MEG mixtures.

As in every new process analysis, the evaluation of the combined acid gas and water vapor removal by an amine–glycol-based solvent requires the knowledge of the thermodynamic behavior, reaction kinetics, and physical properties of the system. This study focuses on some of the physical properties of the system, namely, density and viscosity, which play a crucial role in the successful design and operation of a separation process. Nookuea et al. studied the effect of various thermophysical properties on the design of an absorber for  $\text{CO}_2$  capture

and concluded that liquid density and viscosity have the most significant impact on the packing height.<sup>9</sup> Especially for subsea applications, the low temperature experienced in the seabed dramatically changes the solvent viscosity, affecting the overall mass transfer and hydrodynamics of the system. In fact, viscosity specifications related to the pumpability of injected chemicals apply for offshore/subsea operations. Therefore, the objective of this study is to provide experimental measurements and develop auxiliary models for density and viscosity as a tool for assessing the successful employment of the binary MDEA–MEG or the ternary MDEA–MEG– $\text{H}_2\text{O}$  systems for natural gas purification.

The literature is rich in density and viscosity studies for aqueous MDEA solutions due to their broad applicability in  $\text{CO}_2$  capture and selective  $\text{H}_2\text{S}$  removal. Several authors report densities<sup>10–14</sup> and viscosities<sup>11–19</sup> of MDEA– $\text{H}_2\text{O}$  mixtures. Moreover, the measurement of the density and viscosity of pure MDEA has been presented as a validation for the experimental method of density and viscosity measurements.<sup>20</sup> A sufficient amount of data exists also for MEG– $\text{H}_2\text{O}$  system densities and viscosities.<sup>21–26</sup> A comprehensive, though not exhaustive, list is shown in Table 1. The combination of amines and glycols has also been studied in the literature;<sup>27–30</sup> however, to the best of our knowledge, no data on the density or the viscosity of the MDEA–MEG or MDEA–MEG– $\text{H}_2\text{O}$  mixtures are reported. In addition, although for pure monoethylene glycol and its solutions with water, density and viscosity measurements have

Received: June 26, 2019

Accepted: October 25, 2019

Published: November 25, 2019

**Table 1.** Literature Review on the Density and Viscosity Measurements of Aqueous MDEA and Aqueous MEG Systems at Ambient Pressure

system	molar fraction, $x_1$	property	temperature (K)	source
MDEA (1)	0–1	density	283.15–363.15	Bernal-García et al. <sup>10</sup>
H <sub>2</sub> O (2)	0.0165–1	density	288.15–333.15	Al-Ghawas et al. <sup>11</sup>
	0.0165–1	viscosity	288.15–333.15	
	0.0364, 0.0608	density	303.15–333.15	Li and Lie <sup>12</sup>
	0.0364–1	viscosity	303.15–353.15	
	0.0165–1	density	288.15–333.15	Paul and Mandal <sup>13</sup>
	0.0165–1	viscosity	288.15–333.15	
	0.1–1	density	293.15–333.15	Yin et al. <sup>14</sup>
	0.1–1	viscosity	293.15–333.15	
	0–1	viscosity	298.15–353.15	Teng et al. <sup>15</sup>
	0–1	viscosity	313.15–363.15	Bernal-García et al. <sup>16</sup>
	0–1	viscosity	303.15–323.15	Chowdhury et al. <sup>18</sup>
	0.0447–1	viscosity	293.15–353.15	Pinto et al. <sup>17</sup>
	0.0165–0.1313	viscosity	333.15–373.15	Rinker et al. <sup>19</sup>
	1	density	296.15–470.15	DiGuillo et al. <sup>31</sup>
	1	viscosity	293.15–424.15	
	1	density	298.15–323.15	Álvarez et al. <sup>32</sup>
	1	viscosity	298.15–323.15	
	1	viscosity	298.15–343.15	Henni et al. <sup>33</sup>
	1	viscosity	303.15–343.15	Baek et al. <sup>20</sup>
	1	viscosity	303.15–353.15	Haghtalab and Shojaean <sup>34</sup>
	1	viscosity	303.15–313.15	Akbar and Murugesan <sup>35</sup>
MEG (1)	0–1	density	298.15	Hayduk and Malik <sup>21</sup>
H <sub>2</sub> O (2)	0–1	viscosity	298.15	
	0–1	density	263.15–423.15	Bohne et al. <sup>22</sup>
	0–1	viscosity	263.15–373.15	
	0.25–0.75	density	296.15–445.15	Sun and Teja <sup>23</sup>
	0–1	viscosity	284.15–449.15	
	0–1	density	273.15–363.15	Afzal et al. <sup>26</sup>
	0–0.72	density	293.15	Tsierkezos and Molinou <sup>36</sup>
	0–0.72	viscosity	293.15	
	0–1	density	293.15–353.15	Yang et al. <sup>24</sup>
	0–1	viscosity	293.15–353.15	
	0–1	density	283.15–313.15	Tsierkezos and Molinou <sup>25</sup>
	0–1	viscosity	283.15–313.15	
	0–1	viscosity	298.15	Jerome et al. <sup>37</sup>
	0–1	viscosity	298.15	Dunstan <sup>38</sup>
	1	viscosity	298.15–373.15	Rumble <sup>39</sup>

been reported at low temperatures, even down to 263 K,<sup>22,24,26</sup> only Bernal-García et al.<sup>10</sup> report densities at 283.15 K for pure MDEA and its aqueous solutions. We have not found reported viscosities of pure MDEA or aqueous MDEA in the existing literature at such low temperature.

In this work, density and viscosity measurements of the binary system MDEA–MEG and the ternary system MDEA–MEG–H<sub>2</sub>O are presented in the temperature range of  $T = 283.15$ – $353.15$  K and at a pressure of 0.1020 MPa. The binary system was studied in the whole concentration range, from pure MDEA to pure MEG. For the ternary system of aqueous MDEA–MEG–H<sub>2</sub>O, we varied the water concentration from 5 to 50 wt % to demonstrate the impact of water content on the physical properties of the amine–glycol system studied. Both density and viscosity were modeled for the pure components and binary and ternary systems using the data obtained in this work as well as the data presented in Table 1.

## 2. EXPERIMENTAL AND COMPUTATIONAL METHODS

**2.1. Materials.** Information on the chemicals used is provided in Table 2. The chemicals were used as received

from the supplier without further purification. For the aqueous mixtures composed of MDEA–MEG–H<sub>2</sub>O, deionized water was used. The solutions were prepared gravimetrically in a METTLER PM1200 scale with an accuracy of  $1 \times 10^{-6}$  kg, and MDEA concentration was verified for each system by acid–base titration. Magnetic stirring prior to measurements for at least 8 h ensured solution homogeneity.

**2.2. Experimental Methods.** **2.2.1. Density Measurements.** The densities of all solutions were measured with an Anton Paar Density Meter DMA 4500M. Millipore water and dry air were used for the calibration of this apparatus, as explained by Hartono et al.,<sup>40</sup> whereas pure water, MDEA, and MEG were used as reference fluids for the apparatus validation. We studied the repeatability of the density measurements (set A) at selected temperatures at low and high concentrations of MDEA–MEG, as well as at 353.15 K for the aqueous system due to the risk of water vaporization. A reproducibility study (set C) was also performed by preparing fresh solutions and experimentally determining the density of the pure components and the binary system at low and high concentrations. The results show excellent repeatability and reproducibility with

Table 2. Chemical Sample Table

component	IUPAC name	CAS	supplier	mass fraction
N-methyldiethanolamine (MDEA)	2-[2-hydroxyethyl(methyl)amino]ethanol	105-59-9	Sigma-Aldrich	≥0.99
monoethylene glycol (MEG)	ethane-1,2-diol	107-21-1	Sigma-Aldrich	0.998

average absolute relative deviations (AARDs) equal to 0.01 and 0.02%, respectively.

**2.2.2. Viscosity Measurements.** Viscosity measurements were performed in a Lovis 2000 M microviscometer, connected in series to the density meter. The sample is introduced to a temperature-controlled capillary block with an accuracy of 0.02 K, where the Hoppel's falling ball method is employed. In our experiments, a capillary of a  $1.59 \times 10^{-3}$  m diameter with a gold ball was used, allowing for the measurement of viscosities up to approximately 60 mPa s. The apparatus validation is presented in Section 3. The validation revealed an AARD from the reference liquid value of 2.88%. The repeatability (set A) and reproducibility (set C) of the viscosity measurements were studied similarly to density measurements, and the AARDs were 0.76 and 0.69%, respectively.

An Xsample 452 H sample filling module is integrated into the density meter and microviscometer for automatic sampling, cleaning, and drying. The measurements always started with an air check and measurement of Millipore water samples, which were distributed in approximately every other three samples, allowing for a continuous check of the results as well as an additional cleaning medium.

For viscosities outside the limits of the available capillary in the microviscometer, an Anton Paar MCR 100 rheometer with a double-gap measuring cell (DG-26.7) was used. A detailed description of the apparatus and experimental and calibration procedure is given by Hartono et al.<sup>40</sup> The measurement repeatability was studied for all systems at 283.15 K, and we concluded that the repeatability of the instrument is good since the maximum absolute relative deviation (MARD) is 2.05% and the AARD is 0.5%. Solutions measurable in the microviscometer were also measured in the rheometer to determine the viscosity reproducibility with the two different instruments. We conducted the study primarily at 283.15 K and calculated a 2.72% MARD and 1.07% AARD.

In all our experiments, at least two measurements were taken and the average is reported as the measured property of the solution. Moreover, acid–base titration was employed to determine the amine concentration of samples also after the measurements to ensure that no vaporization had occurred. The concentration of all samples remained unchanged even after the experiments conducted at 353.15 K.

**2.3. Computational Methods.** **2.3.1. Model Parametrization.** The parametrization procedure has been carried following the particle swarm optimization algorithm described by Poli et al.<sup>41</sup> and Ghosh et al.<sup>42</sup> and previously successfully implemented by Evjen et al.<sup>43</sup> and Pinto and Svendsen.<sup>44</sup> As before, the lbest topology was chosen with  $\omega = 0.7298$  as the inertia factor and  $\varphi_1 = \varphi_2 = 1.49618$  as acceleration coefficients. The objective function  $\epsilon$  to be minimized is given by eq 1, where  $y$  is the output one is set to estimate,  $u$  is a set of input variables, and  $\theta$  is a set of model parameters. NP is the total number of points used for the parametrization routine.

$$\epsilon(u, y, \theta) = \sum_{i=1}^{\text{NP}} \frac{(y_i - \hat{y}_i(u, \theta))^2}{y_i \cdot \hat{y}_i(u, \theta)} \quad (1)$$

Furthermore, the quality of the fitting has been evaluated by two complementary criteria: the average absolute relative deviation (AARD) and the maximum absolute deviation (MAD) as defined by eqs 2 and 3

$$\text{AARD} = \frac{100}{\text{NP}} \cdot \sum_{i=1}^{\text{NP}} \left| \frac{y_i - \hat{y}_i}{y_i} \right| \quad (2)$$

$$\text{MAD} = \max(|y - \hat{y}|) \quad (3)$$

The same overall parametrization procedure has been applied for the modeling of both density and viscosity. In general lines, one initially needs to estimate the properties of single components. The properties of binaries and ternaries are then calculated by the use of a simple mixing rule and an additional term that accounts for excess properties. In this work, the fitting is carried over the global data set, meaning that unitary, binary, and ternary data sets are all coupled together in the evaluation of the objective function  $\epsilon$  and accounted for in the AARD and in the MAD calculation. However, it is a good optimization practice to fit the excess property models first to each individual binary data set, thus generating a periphery of initial guesses for the fitting of the global data set. This has been the procedure carried throughout this study. A list of the symbols used in the remainder of this work is given in the nomenclature provided at the end of the article.

**2.3.2. Modeling of Density.** The typical approach employed for the estimation of multicomponent system densities goes through the modeling of excess molar volumes ( $v^E$ ). Once the  $v^E$  of a mixture is calculated, its density can be recovered by eq 4.

$$\rho = \frac{\sum_{i=1}^{\text{NC}} x_i \cdot \text{MW}_i}{v^E + \sum_{i=1}^{\text{NC}} x_i \cdot \frac{\text{MW}_i}{\rho_i}} \quad (4)$$

Following the example of Pinto et al.,<sup>45</sup> a modified Rackett equation of the form shown in eqs 5–7 was employed for the calculation of  $\hat{\rho}_i$ . This calculation requires the estimation of single molar volumes in eq 5 using the Rackett compressibility factor  $Z_{\text{RA},i}$  described in eq 6. The parameters in these equations are the critical temperature  $T_{\text{C},i}$  and critical pressure  $p_{\text{C},i}$  for each pure component and the reduced temperature and pressure. Furthermore, three parameters ( $\hat{A}_i$ ,  $\hat{B}_i$ , and  $\hat{C}_i$ ) have to be fitted for the obtention of  $Z_{\text{RA},i}$ .

$$\hat{v}_i(p, T) = \frac{R \cdot T_{\text{C},i}}{p_{\text{C},i}} \cdot \hat{Z}_{\text{RA},i}^{1+(1-T_{\text{r},i})^{2/7}} \quad (5)$$

$$\hat{Z}_{\text{RA},i}(p, T) = \exp \left[ \hat{A}_i + \frac{\hat{B}_i}{p_{\text{r},i}} + \hat{C}_i \ln(T_{\text{r},i}) \right] \quad (6)$$

$$\hat{\rho}_i(p, T) = \frac{\text{MW}_i}{\hat{v}_i} \quad (7)$$

The estimation of the single-component molar volumes  $\hat{v}_i$  is followed by the estimation of the excess properties  $\hat{v}^E$  of binary and ternary mixtures. In the previous work carried out by Evjen

et al.,<sup>43</sup> the Redlich–Kister (RK) equation fulfilled this duty. However, as seen in that study, the RK equation demands that at least six parameters are fitted for each binary mixture so that a good agreement between experimental and estimated densities is obtained. These binary estimations must additionally be coupled with an extra  $\hat{v}^E$  model for the estimation of ternary densities.<sup>46,47</sup> Such a correction demands additional parameters and fittings in the forms proposed differently by several distinct authors, like Cibulka,<sup>48</sup> Nagata and Tamura,<sup>49</sup> Redlich and Kister,<sup>50</sup> and Singh et al.<sup>51</sup> Most of these models have at least three extra parameters, meaning that  $6 \cdot \text{NC} + 3 = 21$  empirical parameters must be found for the description of the density of ternary solutions. This poses the disadvantages of having to choose one among several  $\hat{v}^E$  models in the literature and fitting an unordinary number of coefficients. This also means that the quality of the ternary data fitting is wholly dependent on the quality of the binary data fitting.

An alternative to this has been suggested by Pinto and Knuutila<sup>52</sup> for the direct fitting of ternary density data. This model, henceforth called the NRTL-DVOL, is explicitly based on the nonrandom two-liquid (NRTL) model and has the form outlined in eqs 8–11.

$$\hat{v}^E(x, T) = R \cdot T \cdot \sum_{i=1}^{\text{NC}} x_i \frac{\sum_{j=1}^{\text{NC}} \hat{\tau}_{ji} \cdot \hat{G}_{ji} \cdot x_j}{\sum_{k=1}^{\text{NC}} \hat{G}_{ki} \cdot x_k} \quad (8)$$

$$\hat{G}_{ij}(T) = \exp(-\alpha_{ij} \cdot \hat{\tau}_{ij}) \quad (9)$$

$$\hat{\tau}_{ij}(T) = \hat{a}_{ij} + \frac{\hat{b}_{ij}}{T} \quad (10)$$

$$\hat{a}_{ii} = 0; \hat{b}_{ii} = 0; \hat{\alpha}_{ij} = \hat{\alpha}_{ji} \quad (11)$$

The expressions shown in eqs 8–11 demand the fitting of  $\hat{a}_{ij}$  and  $\hat{b}_{ij}$ . Meanwhile,  $R$  is a fixed parameter of the model and its value is  $R = 6.48803$ . The nonrandomness parameter  $\alpha_{ij}$  is set alternatively at  $\alpha_{ij} = 0.1, 0.2, \text{ or } 0.3$ , and the optimization routines are performed once for each of these values. In this work, a global  $\alpha_{ij} = \alpha$  was implemented for each study, meaning that a single  $\hat{a}$  was chosen for the binary–ternary systems instead of one for each binary.

**2.3.3. Modeling of Viscosity.** Similar to that of density, the modeling of the viscosity requires the “excess viscosity” of the mixture or more correctly the viscosity deviations from ideality upon mixing. In this work, viscosity deviations  $\Delta\eta$  were calculated from the experimental measurements using eqs 12–13.<sup>53,54</sup>

$$\ln(\eta^{\text{id}}) = \sum_{i=1}^{\text{NC}} x_i \ln(\eta_i) \quad (12)$$

$$\Delta\eta = \eta - \eta^{\text{id}} \quad (13)$$

where  $\eta^{\text{id}}$  is the viscosity of the ideal mixture;  $x_i$  and  $\eta_i$  are the molar fraction and viscosity of the pure component  $i$ , respectively;  $\eta$  is the measured viscosity of the mixture; and  $\Delta\eta$  is the viscosity deviation upon mixing.

There are several approaches for modeling the viscosity of binary liquid mixtures. However, only the models of Song et al.<sup>55</sup> and Pinto and Svendsen<sup>44</sup> offer an easy extension toward the calculation of ternary mixtures. The former is usually called the Aspen liquid mixture viscosity model, whereas the latter was named the NRTL-DVIS model. Both of them are reliant on good estimates of pure component viscosities. Therefore, the

viscosities of pure MDEA and MEG were fitted to the Vogel equation, which has a generic form shown in eq 14.

$$\ln(\hat{\eta}_i(T)) = \hat{A}_i + \frac{\hat{B}_i}{T - \hat{C}_i} \quad (14)$$

Meanwhile, the viscosity of pure water can be estimated by the correlation of Bingham and Jackson<sup>56</sup> given in eqs 15 and 16.

$$\varphi_{\text{H}_2\text{O}}(T) = 2.1482 \cdot [(T - 281.585) + \sqrt{8078.4 + (T - 281.585)^2}] - 120 \quad (15)$$

$$\hat{\eta}_{\text{H}_2\text{O}}(T) = \frac{100}{\varphi_{\text{H}_2\text{O}}} \quad (16)$$

The viscosity of mixtures is estimated by the addition of an excess viscosity term, different from the one displayed in eqs 12 and 13, as shown in eq 17. Following the initial suggestion of Song et al.,<sup>55</sup> the mass fractions  $w_i$  are better weights for the mixture calculations than the molar fractions  $x_i$ .

$$\ln(\hat{\eta}(w, T)) = \sum_{i=1}^{\text{NC}} w_i \cdot \ln(\hat{\eta}_i(T)) + \ln(\hat{\eta}^E(w, T)) \quad (17)$$

Moreover, the form that this excess term  $\hat{\eta}^E$  can take is what differs the Aspen liquid mixture viscosity model from the NRTL-DVIS model. Following the Aspen liquid mixture viscosity model, this term is calculated by eqs 18–21. These equations require that four different sets of parameters,  $\hat{a}_{ij}$ ,  $\hat{b}_{ij}$ ,  $\hat{c}_{ij}$ , and  $\hat{d}_{ij}$ , are estimated for each binary pair.

$$\ln(\hat{\eta}^E(w, T)) = \sum_{i=1}^{\text{NC}} \sum_{j>i}^{\text{NC}} \hat{k}_{ij} \cdot w_i \cdot w_j \ln(\hat{\eta}_{ij}) + \sum_{i=1}^{\text{NC}} w_i \cdot \left[ \sum_{j \neq i}^{\text{NC}} w_j \cdot (\hat{l}_{ij} \ln(\hat{\eta}_{ij}))^{1/3} \right]^3 \quad (18)$$

$$\ln(\hat{\eta}_{ij}) = \frac{\ln(\hat{\eta}_i) - \ln(\hat{\eta}_j)}{2} \quad (19)$$

$$\hat{k}_{ij}(T) = \hat{a}_{ij} + \frac{\hat{b}_{ij}}{T} \quad (20)$$

$$\hat{l}_{ij}(T) = \hat{c}_{ij} + \frac{\hat{d}_{ij}}{T} \quad (21)$$

Similarly, the NRTL-DVIS model also requires that 12 parameters be estimated. Its form is very similar to that of the NRTL-DVOL since both come from the same approach of modeling excess properties with the general shape of the NRTL excess Gibbs energy equation. The model is described by eqs 22–25.

$$\ln(\hat{\eta}^E(w, T)) = R \cdot \sum_{i=1}^{\text{NC}} w_i \cdot \frac{\sum_{j=1}^{\text{NC}} \hat{\tau}_{ji} \cdot \hat{G}_{ji} \cdot w_j}{\sum_{k=1}^{\text{NC}} \hat{G}_{ki} \cdot w_k} \quad (22)$$

$$\hat{G}_{ij}(T) = \exp(-\alpha_{ij} \cdot \hat{\tau}_{ij}) \quad (23)$$

$$\hat{\tau}_{ij}(T) = \hat{a}_{ij} + \frac{\hat{b}_{ij}}{T} \quad (24)$$

**Table 3. Experimental and Indicative Literature Values of the Density  $\rho/\text{kg m}^{-3}$  for Pure Water, MEG, and MDEA at Temperatures  $T = 283.15\text{--}353.15\text{ K}$  and Pressure near  $p = 0.1\text{ MPa}$** 

T/K	$\rho/\text{kg m}^{-3}$								
	water			MEG			MDEA		
	Spieweck and Bettin <sup>57</sup>	Yang et al. <sup>24</sup>	this work	Afzal et al. <sup>26</sup>	Yang et al. <sup>24</sup>	this work	Bernal-García et al. <sup>10</sup>	Al-Ghawas et al. <sup>11</sup>	this work
283.15	999.699		999.9	1120.23		1120.0	1047.53		1048.0
298.15	997.043		997.2	1109.77		1109.9	1037.86	1037.4	1036.8
313.15	992.212	992.2	992.3	1099.17	1093.6	1098.8	1026.52	1026.7	1025.4
323.15	988.030	988.1	988.3	1092.02	1084.7	1091.6	1018.88	1019.4	1017.7
333.15	983.191	983.2	983.5	1084.78	1076.4	1085.0	1011.43	1012.3	1010.0
343.15	977.759	977.8	978.1	1077.42	1067.5	1077.6	1003.32		1002.2
353.15	971.785	971.8	972.3	1069.95	1060.0	1070.1	995.41		994.6
AARD (%) <sup>a</sup>			0.03			0.33			0.12

$${}^a\text{AARD (\%)} = \frac{100}{\text{NP}} \sum_{i=1}^{\text{NP}} \left| \frac{\rho_i^{\text{exp}} - \rho_i^{\text{lit}}}{\rho_i^{\text{lit}}} \right|$$

**Table 4. Experimental Values of Density  $\rho/\text{kg m}^{-3}$  for {MDEA (1) + MEG (2)} as a Function of Weight Fraction  $w$  and Temperature  $T$  at Pressure  $p = 0.1020\text{ MPa}$ <sup>a</sup>**

$w_1$	$\rho/\text{kg m}^{-3}$					
	283.15 K		298.15 K		313.15 K	
	set A	set A	set A (1)	set A (2)	set A (3)	set C
0.000	1120.0 ± 0.2	1109.9 ± 0.3	1098.8 ± 0.3	1099.3 ± 0.3		1099.3 ± 0.3
0.300 ± 0.003	1101.8 ± 0.2	1090.9 ± 0.2	1079.9 ± 0.1	1079.9 ± 0.1	1079.9 ± 0.1	1080.0 ± 0.1
0.400 ± 0.003	1095.1 ± 0.2	1084.3 ± 0.2	1073.2 ± 0.1	1073.2 ± 0.1		
0.500 ± 0.004	1088.1 ± 0.2	1077.2 ± 0.2	1066.0 ± 0.1	1066.0 ± 0.1		
0.700 ± 0.006	1073.3 ± 0.2	1062.1 ± 0.2	1050.7 ± 0.1	1050.8 ± 0.1		
0.800 ± 0.008	1065.4 ± 0.2	1054.0 ± 0.2	1042.5 ± 0.1	1042.6 ± 0.1		
0.900 ± 0.009	1057.2 ± 0.2	1045.6 ± 0.2	1034.1 ± 0.1	1034.1 ± 0.1	1034.1 ± 0.1	1034.0 ± 0.1
1.000 ± 0.011	1048.0 ± 0.2	1036.8 ± 0.2	1025.4 ± 0.1	1025.4 ± 0.1		1025.1 ± 0.1
$w_1$	323.15 K		333.15 K			
0.000	set A	set A (1)	set A (2)	set C		
0.300 ± 0.003	1091.6 ± 0.1	1085.0 ± 0.1		1084.9 ± 0.1		
0.400 ± 0.003	1072.5 ± 0.1	1065.1 ± 0.1	1065.0 ± 0.1	1065.2 ± 0.1		
0.500 ± 0.004	1065.7 ± 0.1	1058.1 ± 0.1				
0.700 ± 0.006	1058.5 ± 0.1	1050.9 ± 0.1				
0.800 ± 0.008	1043.1 ± 0.1	1035.4 ± 0.1				
0.900 ± 0.009	1034.9 ± 0.1	1027.2 ± 0.1				
1.000 ± 0.011	1026.4 ± 0.1	1018.7 ± 0.1	1018.7 ± 0.1	1018.6 ± 0.1		
	1017.7 ± 0.1	1010.0 ± 0.1		1010.0 ± 0.1		
$w_1$	343.15 K		353.15 K			
0.000	set A	set A (1)	set A (2)	set C		
0.300 ± 0.003	1077.6 ± 0.1	1070.1 ± 0.1		1070.1 ± 0.1		
0.400 ± 0.003	1057.4 ± 0.1	1049.7 ± 0.1	1049.7 ± 0.1	1049.8 ± 0.1		
0.500 ± 0.004	1050.5 ± 0.1	1042.7 ± 0.1				
0.700 ± 0.006	1043.1 ± 0.1	1035.3 ± 0.1				
0.800 ± 0.008	1027.5 ± 0.1	1019.7 ± 0.1				
0.900 ± 0.009	1019.3 ± 0.1	1011.5 ± 0.1				
1.000 ± 0.011	1010.9 ± 0.1	1003.1 ± 0.1	1003.1 ± 0.1	1002.8 ± 0.1		
	1002.2 ± 0.1	994.6 ± 0.1		994.4 ± 0.1		

<sup>a</sup>Weight fractions and densities are reported with their expanded uncertainties (0.95 level of confidence). Expanded uncertainties not included above are  $U(T) = 0.02\text{ K}$  and  $U(p) = 0.0030\text{ MPa}$ .

$$\hat{a}_{ij} = 0; \hat{b}_{ij} = 0; \hat{\alpha}_{ij} = \hat{\alpha}_{ji} \quad (25)$$

All of the remarks made regarding the NRTL-DVOL model apply to the NRTL-DVIS model. Once again, a value of  $R = 6.48803$  was set as a fixed parameter of the equations, whereas  $\alpha_{ij} = \alpha$  was set alternatively to  $\alpha = 0.1, 0.2,$  and  $0.3$  for each optimization routine.

### 3. RESULTS AND DISCUSSION

The results of density  $\rho$  and viscosity  $\eta$  measurements and modeling for the binary mixtures of MDEA–MEG and the ternary mixtures of MDEA–MEG–H<sub>2</sub>O are presented below.

**3.1. Density.** The densities of pure water, monoethylene glycol, and methyl-diethanolamine were measured and compared

Table 5. Experimental Values of Density  $\rho/\text{kg m}^{-3}$  for {MDEA (1) + MEG (2) + Water (3)} as a Function of Weight Fraction  $w$  and Temperature  $T$  at Pressure  $p = 0.1020 \text{ MPa}$ <sup>a</sup>

		$\rho/\text{kg m}^{-3}$				
		283.15 K	298.15 K	313.15 K	323.15 K	333.15 K
$w_1$	$w_2$	set A	set A	set A	set A	set A
0.050 ± 0.002	0.900 ± 0.003	1114.1 ± 0.2	1103.7 ± 0.3	1093.1 ± 0.1	1086.4 ± 0.6	1079.1 ± 0.7
0.900 ± 0.013	0.050 ± 0.010	1057.6 ± 0.2	1046.3 ± 0.3	1034.8 ± 0.1	1027.5 ± 0.6	1019.8 ± 0.7
0.300 ± 0.003	0.600 ± 0.003	1196.6 ± 0.2	1086.1 ± 0.3	1075.1 ± 0.1	1068.2 ± 0.6	1060.7 ± 0.7
0.600 ± 0.006	0.300 ± 0.006	1078.5 ± 0.2	1067.6 ± 0.3	1056.3 ± 0.1	1049.1 ± 0.6	1041.5 ± 0.7
0.100 ± 0.002	0.600 ± 0.002	1090.1 ± 0.2	1080.5 ± 0.3	1070.3 ± 0.1	1063.4 ± 0.6	1056.8 ± 0.7
0.300 ± 0.003	0.400 ± 0.003	1081.2 ± 0.2	1071.2 ± 0.3	1060.9 ± 0.1	1053.8 ± 0.6	1047.1 ± 0.7
0.600 ± 0.006	0.100 ± 0.006	1067.8 ± 0.2	1057.4 ± 0.3	1046.5 ± 0.1	1039.4 ± 0.6	1031.7 ± 0.7
0.250 ± 0.002	0.250 ± 0.002	1061.0 ± 0.2	1052.2 ± 0.3	1043.2 ± 0.1	1036.6 ± 0.6	1030.5 ± 0.7
		343.15 K		353.15 K		
$w_1$	$w_2$	set A	set A (1)	set A (2)	set C	
0.050 ± 0.002	0.900 ± 0.003	1071.8 ± 0.7	1064.5 ± 0.9	1064.6 ± 0.9		
0.900 ± 0.013	0.050 ± 0.010	1012.0 ± 0.7	1004.2 ± 0.9	1004.2 ± 0.9		
0.300 ± 0.003	0.600 ± 0.003	1053.2 ± 0.7	1045.6 ± 0.9	1045.7 ± 0.9	1045.7 ± 0.9	
0.600 ± 0.006	0.300 ± 0.006	1033.6 ± 0.7	1025.8 ± 0.9	1025.8 ± 0.9		
0.100 ± 0.002	0.600 ± 0.002	1049.4 ± 0.7	1042.0 ± 0.9	1042.2 ± 0.9		
0.300 ± 0.003	0.400 ± 0.003	1039.5 ± 0.7	1031.8 ± 0.9	1031.9 ± 0.9		
0.600 ± 0.006	0.100 ± 0.006	1023.7 ± 0.7	1015.7 ± 0.9	1015.8 ± 0.9		
0.250 ± 0.002	0.250 ± 0.002	1023.5 ± 0.7	1016.1 ± 0.9	1016.1 ± 0.9	1016.2 ± 0.9	

<sup>a</sup>Weight fractions and densities are reported with their expanded uncertainties (0.95 level of confidence). Expanded uncertainties not included above are  $U(T) = 0.02 \text{ K}$  and  $U(p) = 0.0030 \text{ MPa}$ .

to values from the literature for validation purposes. Our measured densities were compared against the literature sources presented in Table 1 and, to be more specific, against data reported by Bernal-García et al.,<sup>10</sup> Hayduk and Malik,<sup>21</sup> Yang et al.,<sup>24</sup> Tsierkezos and Molinou,<sup>25</sup> and Spieweck and Bettin<sup>57</sup> for water; data reported by Hayduk and Malik,<sup>21</sup> Bohne et al.,<sup>22</sup> Afzal et al.,<sup>26</sup> Yang et al.,<sup>24</sup> and Tsierkezos and Molinou<sup>25</sup> for MEG; and data reported by Bernal-García et al.,<sup>10</sup> Al-Ghawas et al.,<sup>11</sup> Álvarez et al.,<sup>32</sup> Paul and Mandal,<sup>13</sup> and Yin et al.<sup>14</sup> for MDEA. The average absolute relative deviation (AARD) is 0.01% for water, 0.30% for MEG, and 0.10% for MDEA, demonstrating that our measurements are in good agreement with the data already reported in the literature. Indicative literature data sets are given in Table 3, selected because they cover as many temperatures studied in this work as possible. The AARDs using those two sources for each component were found to be 0.03, 0.33, and 0.12% for water, MEG, and MDEA, respectively.

Tables 4 and 5 show the measured densities in this work for the nonaqueous and aqueous MEG–MDEA mixtures, respectively, as a function of weight fraction  $w$  and temperature  $T$  at ambient pressure. The expanded uncertainties with a 0.95 level of confidence of composition and density are provided for each system and temperature. In addition to the weight fractions, molar fractions  $x_i$  and the corresponding uncertainties can be found in the Supporting Information. As mentioned earlier, the repeatability of the density measurements is excellent, as one can see in the results. It is observed that the density of the binary mixtures of MDEA–MEG decreases with temperature and with MDEA concentration. These trends are better illustrated in Figure 1, presenting the experimental densities for the binary system MDEA–MEG and the estimates generated by the NRTL-DVOL model. Similar figures for MDEA–H<sub>2</sub>O and MEG–H<sub>2</sub>O are provided in the Supporting Information. The density of MEG–H<sub>2</sub>O is similar to the one for MDEA–MEG, whereas the one for the binary MDEA–H<sub>2</sub>O varies in the way

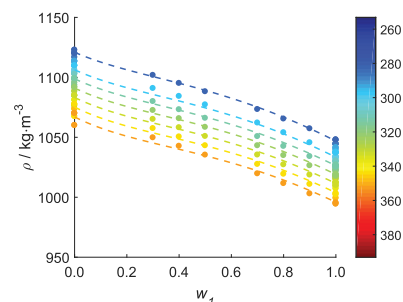


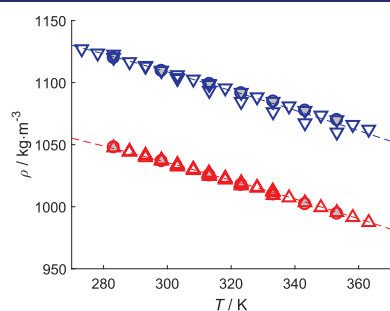
Figure 1. Binary data set of densities for {MDEA (1) + MEG (2)} and estimations generated by the NRTL-DVOL model. The temperature at which each experimental point (solid circle) was measured is color-coded by the bar on the right side. The temperatures at which the estimates were made were 283.15 K (dark-blue dashed line), 298.15 K (capri-blue dashed line), 313.15 K (aqua dashed line), 323.15 K (green dashed line), 343.15 K (lime-green dashed line), 343.15 K (yellow dashed line), and 353.15 K (orange dashed line).

that it increases with MDEA concentration but only up to approximately  $w_1 = 0.7$  after which it starts decreasing. This behavior is due to the excess molar volumes upon mixing of MDEA and H<sub>2</sub>O and is discussed in detail in Section 3.3. The trend of decreasing density with temperature and amine content applies to the ternary systems as well, given that the amount of water in the solution is constant. The generated density contour plots for the ternary system can be found in the Supporting Information.

As explained in Section 2, a modified Rackett equation was employed for the fitting of the single-component data sets shown in Table 1. The results of the fitting are presented in Table 6 and Figure 2. The values of MW,  $T_C$ , and  $p_C$  were obtained from Yaws.<sup>58</sup> The fitting for water was not performed

**Table 6. Parameters and Results for the Fittings of the Modified Rackett Equation**

parameter	MDEA	MEG	water <sup>52</sup>
MW (kg kmol <sup>-1</sup> )	119.16	62.07	18.02
T <sub>c</sub> (K)	675	720	647.1
p <sub>c</sub> (MPa)	3.88	8.20	22.064
A	-1.4003	-1.4021	-1.4937
B̂	-3.0132 × 10 <sup>-6</sup>	-0.7670 × 10 <sup>-6</sup>	6.6495 × 10 <sup>-6</sup>
Ĉ	-0.03542	-0.02230	-9.868
AARD (%)	0.07	0.19	0.35
MAD (kg m <sup>-3</sup> )	2.36	7.68	15.82

**Figure 2.** Experimental single-component density of MDEA both obtained in the literature (red open triangle up) and as produced in this work (red circle filled in gray) and of MEG both obtained in the literature (blue open triangle down) and as produced in this work (blue circle filled in gray), and corresponding estimations with the modified Rackett equation for MDEA (red dashed line) and MEG (blue dashed line).

in this study, but the parameters for its modified Rackett equation were obtained from Pinto and Knuutila.<sup>52</sup> As such, we merely report the parameters obtained by these authors without checking their significance, though it should be pointed out that the parameter  $B$  obtained by Pinto and Knuutila<sup>52</sup> of  $6.6495 \times 10^{-6}$  could be set to zero with no noticeable effects on the performance of the model. Although the results for the fitting of MEG are worse than those of MDEA, this is arguably due to the scatter in experimental data found for MEG in the literature, as evidenced by Figure 2. The density data of pure MEG reported by Yang et al.<sup>24</sup> is partially responsible for this scatter, as their values are consistently lower than those obtained by other researchers (see the bifurcation in the blue data points in Figure 2), particularly at higher temperatures. However, the data set from Yang et al.<sup>24</sup> contains pure water density measurements in excellent agreement with the literature, and their collection of pure MEG density measurements is off by only 1% when compared to other published data. Therefore, we have decided to keep their data set in our parametrization procedure.

Table 7 shows the results for the fitting with the NRTL-DVOL model. The fitting was done by minimizing the objective function eq 1 with the entire data set of unitary, binary, and ternary solutions. Moreover, since the parameters found for the NRTL-DVOL fitting are valid for estimating binary as well as ternary data, Table 7 shows first the AARD and MAD obtained for the binaries and then that obtained for the global data set. It can be seen that the AARDs are very small for the three binaries and that the deviations for the MEG–water binary case are the worst. This will be discussed further with the aid of

**Table 7. Parameters and Results for the NRTL-DVOL Equation Fitted for the Global Data Set**

Parameters of the NRTL-DVOL Model (1 = MDEA, 2 = MEG, 3 = Water)					
$\hat{a}_{12}$	-0.59445	$\hat{a}_{13}$	-0.77567	$\hat{a}_{23}$	0.44978
$\hat{a}_{21}$	0.63227	$\hat{a}_{31}$	0.83786	$\hat{a}_{32}$	-0.44286
$\hat{b}_{12}$	-20.026	$\hat{b}_{13}$	-24.830	$\hat{b}_{23}$	-118.93
$\hat{b}_{21}$	21.832	$\hat{b}_{31}$	29.961	$\hat{b}_{32}$	117.49
$\alpha_{ij} = \alpha = 0.1$ ; $R = 6.48803$					
Fitting Results in Terms of Binary Data Sets					
MDEA–MEG		MDEA–water		MEG–water	
AARD (%)	0.14	AARD (%)	0.16	AARD (%)	0.38
MAD (kg m <sup>-3</sup> )	7.68	MAD (kg m <sup>-3</sup> )	5.63	MAD (kg m <sup>-3</sup> )	28.75
Fitting Results in Terms of the Global Data Set					
AARD (%)				0.26	
MAD (kg m <sup>-3</sup> )				28.75	

**Figure 3.** Overall, the fitting results are quite good and show that the densities of both binary and ternary mixtures can be estimated with a high degree of confidence.

The parity plots exhibited in Figure 3a,b reinforce that the fitting of the NRTL-DVOL model for the global data set is good, with only a few remarkable features. One of them is the higher deviations observed for binary data regarding MEG–water mixtures (cyan cross), which account for the largest share in the decoupling between model and experimental data. Figure 3a evidences that this decoupling is the strongest at lower densities or, conversely, at higher temperatures (Figure 3b). This can be explained by the scatter of data points at these specific conditions and by the original scatter of pure MEG data observed already in Figure 2. Other decoupling trends, such as that for MDEA–water binary mixtures at higher temperatures (green asterisk), are an unfortunate consequence of fitting parameters for such a wide range of temperatures and compositions. Nevertheless, for all systems, besides one MEG–water data point, the deviations are not higher than 1%. One can also observe the absolute relative deviations (ARDs) between measured and estimated values for ternary systems in Table S1 in the Supporting Information.

**3.2. Viscosity.** The viscosities of pure water, monoethylene glycol, and methyl-diethanolamine were measured and compared to values from the literature for validation purposes. At temperatures higher than 323.15 K, it was not possible to measure the viscosity of pure water. Similar to that of the density study, our measured viscosities were compared against all of the literature sources presented in Table 1. The data used for the validation are from Teng et al.,<sup>15</sup> Bernal-García et al.,<sup>16</sup> Chowdhury et al.,<sup>18</sup> Pinto et al.,<sup>17</sup> Li and Lie,<sup>12</sup> and Yin et al.<sup>14</sup> for MDEA and from Hayduk and Malik,<sup>21</sup> Bohne et al.,<sup>22</sup> Tsierekos and Molinou,<sup>25</sup> Yang et al.,<sup>24</sup> Jerome et al.,<sup>37</sup> and Dunstan<sup>38</sup> for MEG. For water, the same references as previously mentioned for MEG validation were used, in addition to Teng et al.,<sup>15</sup> Bernal-García et al.,<sup>16</sup> and Chowdhury et al.<sup>18</sup> The AARDs are 2.40, 3.78, and 2.71% for water, MEG, and MDEA, respectively. The AARDs for viscosity are higher than for density, indicating the more challenging nature of viscosity measurements compared to the density ones. The data obtained agree satisfactorily with the data already reported in the literature, with the exception of pure MEG at 283.15 K. Indicative reference sources and their corresponding AARDs are given in Table 8.

The measured viscosities for the nonaqueous and aqueous MDEA–MEG and corresponding expanded uncertainties with a 0.95 level of confidence are shown in Tables 9 and 10,

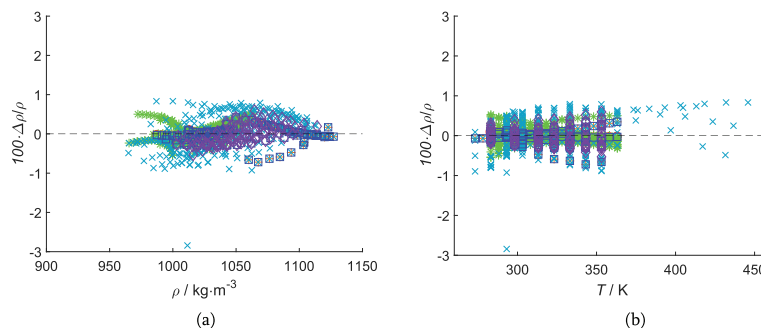


**Figure 3.** Deviations in terms of differences between experimental and estimated densities divided by experimental densities regarding estimations made with the NRTL-DVOL model, and how they vary the experimental densities themselves (a) and with temperature (b). The data sets are distributed in terms of pure MDEA data (red open circle), pure MEG data (orange plus), binary MDEA–water data (green asterisk), binary MEG–water data (cyan cross), binary MDEA–MEG data (blue open square), and ternary data (purple open diamond).

**Table 8. Experimental and Indicative Literature Values of Viscosity  $\eta$ /mPa s for Pure Water, MEG, and MDEA at Temperatures  $T = 283.15$ – $353.15$  K and Pressure near  $p = 0.1$  MPa**

T/K	$\eta$ /mPa s									
	water			MEG				MDEA		
	IAPWS 2008 <sup>59</sup>	Yang et al. <sup>24</sup>	this work	Tsierkezos and Molinou <sup>25</sup>	Bohne et al. <sup>22</sup>	Yang et al. <sup>24</sup>	this work	Teng et al. <sup>15</sup>	Li and Lie <sup>12</sup>	this work
283.15	1.3059		1.32	30.5126			34.07			198.15
298.15	0.8900		0.91		16.630		17.27	77.190		75.37
313.15	0.6527	0.653	0.67	9.5348	9.407	9.443	9.69	34.110	34.3085	35.05
323.15	0.5465	0.547	0.57			6.992	6.81		21.6716	21.96
333.15					5.030	5.06	5.28	14.300	14.3856	14.83
343.15						3.987	4.06	9.849	9.9789	10.29
353.15					3.068	3.021	3.21	7.115	7.0875	7.40
AARD (%) <sup>a</sup>				2.79			4.30			3.15

$${}^a\text{AARD} (\%) = \frac{100}{\text{NP}} \sum_{i=1}^{\text{NP}} \left| \frac{\eta_i^{\text{exp}} - \eta_i^{\text{th}}}{\eta_i^{\text{th}}} \right|$$

respectively. The repeatability of density measurements was excellent, whereas the one for viscosity is lower, though still satisfactory. As presented earlier in Section 2, set A consists of the measurements conducted in the microviscometer, set B consists of the ones conducted in the rheometer, and set C includes all of the measurements performed to study the reproducibility of the obtained data.

As expected, viscosity increases as temperature decreases. Actually, a rather dramatic increase with temperature is observed especially for MDEA, exhibiting a viscosity of 7.4 mPa s at 353.15 K and a viscosity of 198.1 mPa s at 283.15 K. The variation of viscosity for MEG at the temperature limits of the study is far smaller than for MDEA. The same temperature effect is shown for the multicomponent systems, whose viscosity is also increasing with increasing amine concentration. The binary system MDEA–H<sub>2</sub>O exhibits its maximum viscosity value for MDEA concentration of approximately 95 wt % and then decreases (see the Supporting Information for a graphical presentation). Viscosity extremums (minimum, maximum, or both) are not uncommon,<sup>60</sup> and several authors have observed such behavior in amine–water systems.<sup>15,16,18,45,61</sup> The lower the temperature is, the more pronounced the maximum in the viscosity curve is. This behavior is not followed for the MDEA–MEG or MEG–H<sub>2</sub>O binary system, as indicated in Figures 4 and S5, which show the binary plots generated by comparing the fitted NRTL-DVIS model and real experimental data.

The observed viscosity behavior is further discussed in Section 3.3.

According to the modeling procedure described in the previous section, the Vogel equation was employed for the estimation of the pure component viscosity. The results for the parametrization of the Vogel equation, presented in Table 11, show that the viscosities of the pure components are predicted with a satisfactory accuracy. Although the scatter observed for density data is not seen in the viscosity data, the huge variation of viscosity values with temperature (see Figure 5) generates AARDs worse than those observed for the fitting of density models. This variation with temperature makes the fitting of viscosity models more difficult than that of density models, as will be seen briefly.

Both the Aspen liquid mixture viscosity model and the NRTL-DVIS model were tested. One data point from our measurements for the MDEA–MEG binary system was excluded as an outlier ( $T = 283.15$  K,  $w_1 = 0.7$ ). The data fitting parameters and results are shown in Tables 12 and 13 for the Aspen model and the NRTL-DVIS model, respectively. Overall, the Aspen liquid mixture viscosity model showed a slightly worse performance than the NRTL-DVIS equation, returning AARD = 4.39% and MAD = 16.64 mPa s, whereas the latter showed AARD = 2.97% and MAD = 12.62 mPa s. For the Aspen model, these deviations are more noticeable at lower temperature and viscosity ranges, though they are also present at higher



Table 9. Experimental Values of Viscosity  $\eta/\text{mPa s}$  for {MDEA (1) + MEG (2)} as a Function of Weight Fraction  $w$  and Temperature  $T$  at Pressure  $p = 0.1020 \text{ MPa}$ <sup>a</sup>

$w_1$	$\eta/\text{mPa s}$					
	283.15 K			298.15 K		
	Set A	Set B (1)	Set B (2)	Set A	Set B (1)	Set B (2)
0.000	34.40 ± 4.52	33.92 ± 4.06	33.88 ± 4.06	17.28 ± 1.08	-	17.25 ± 1.08
0.300 ± 0.003	-	64.34 ± 4.10	64.37 ± 4.10	30.43 ± 1.08	-	-
0.400 ± 0.003	-	80.69 ± 4.06	80.69 ± 4.06	36.57 ± 1.08	-	-
0.500 ± 0.004	-	99.66 ± 4.08	-	43.44 ± 1.09	43.65 ± 2.61	-
0.700 ± 0.006	-	-	-	-	58.07 ± 2.61	-
0.800 ± 0.008	-	164.27 ± 4.27	-	-	66.59 ± 2.62	-
0.900 ± 0.009	-	181.33 ± 4.42	-	-	69.21 ± 2.61	-
1.000 ± 0.011	-	197.93 ± 4.20	198.37 ± 4.20	-	75.87 ± 2.62	74.87 ± 1.08
	313.15 K					
$w_1$	Set A (1)	Set A (2)	Set A (3)	Set B	Set C	
0.000	9.42 ± 1.06	9.82 ± 1.06	-	-	9.83 ± 1.06	
0.300 ± 0.003	15.74 ± 1.04	15.87 ± 1.04	15.87 ± 1.04	-	16.07 ± 1.04	
0.400 ± 0.003	18.43 ± 1.04	18.61 ± 1.04	-	-	-	
0.500 ± 0.004	21.20 ± 1.06	21.58 ± 1.06	-	21.97 ± 0.49	-	
0.700 ± 0.006	27.33 ± 1.07	27.96 ± 1.07	27.88 ± 1.07	-	-	
0.800 ± 0.008	30.30 ± 1.06	30.68 ± 1.06	-	-	-	
0.900 ± 0.009	32.80 ± 1.06	33.38 ± 1.06	33.23 ± 1.06	32.39 ± 0.48	33.46 ± 1.06	
1.000 ± 0.011	34.82 ± 1.07	35.30 ± 1.07	-	34.99 ± 0.48	35.07 ± 1.07	
	323.15 K		333.15 K		343.15 K	
$w_1$	Set A	Set A (1)	Set A (2)	Set C	Set A	
0.000	6.81 ± 0.36	5.26 ± 0.47	-	5.30 ± 0.47	4.06 ± 0.46	
0.300 ± 0.003	10.80 ± 0.34	7.76 ± 0.47	7.82 ± 0.47	7.88 ± 0.47	5.75 ± 0.46	
0.400 ± 0.003	12.43 ± 0.34	8.82 ± 0.47	-	-	6.45 ± 0.46	
0.500 ± 0.004	14.20 ± 0.34	9.94 ± 0.47	-	-	7.17 ± 0.46	
0.700 ± 0.006	17.75 ± 0.34	12.17 ± 0.47	-	-	8.61 ± 0.46	
0.800 ± 0.008	19.48 ± 0.34	13.26 ± 0.47	-	-	9.26 ± 0.46	
0.900 ± 0.009	20.91 ± 0.34	14.08 ± 0.47	14.16 ± 0.47	14.13 ± 0.47	9.81 ± 0.46	
1.000 ± 0.011	21.96 ± 0.38	14.76 ± 0.47	-	14.90 ± 0.47	10.29 ± 0.53	
	353.15 K					
$w_1$	set A (1)	set A (2)	set C			
0.000	3.20 ± 0.31	-	3.22 ± 0.31	-		
0.300 ± 0.003	4.44 ± 0.31	4.43 ± 0.31	4.46 ± 0.31	-		
0.400 ± 0.003	4.89 ± 0.31	-	-	-		
0.500 ± 0.004	5.36 ± 0.31	-	-	-		
0.700 ± 0.006	6.32 ± 0.31	-	-	-		
0.800 ± 0.008	6.76 ± 0.31	-	-	-		
0.900 ± 0.009	7.12 ± 0.31	7.13 ± 0.31	7.13 ± 0.31	-		
1.000 ± 0.011	7.42 ± 0.31	7.37 ± 0.31	7.42 ± 0.31	-		

<sup>a</sup>Weight fractions and viscosities are reported with their expanded uncertainties (0.95 level of confidence). Expanded uncertainties not included above are  $U(T) = 0.02 \text{ K}$  and  $U(p) = 0.0030 \text{ MPa}$ .

temperatures and viscosities. The previously discussed maximum exhibited in the MDEA–H<sub>2</sub>O system toward higher concentrations of MDEA is particularly problematic for the Aspen model to follow (see figures in the [Supporting Information](#)). This difficulty in modeling strong nonideal behavior also arises with the NRTL-DVIS equation but to a much smaller extent. Comparison between the results of the NRTL-DVIS model and the Aspen liquid viscosity model shows that the fitting of the individual binaries returns higher or similar (for the MEG–H<sub>2</sub>O system) AARDs and MADs than the latter.

In [Table 13](#), one can notice that the largest deviation between estimated and experimental data is obtained for the ternary system, which not only can show high viscosity variations but is

also subject to the nonidealities of mixing three very distinct components. The absolute relative deviations (ARDs) between measured and estimated values for ternary systems can be observed in [Table S2](#) in the Supporting Information.

[Figure 6a,b](#) shows the parity plots between experimental and predicted viscosity data. These figures show that the maximum deviations incurred by the NRTL-DVIS model are on the order of 20%, though the vast majority of these are within 10%. The largest deviations are obtained for the MDEA–water binary system (green asterisks) and the MDEA–MEG–H<sub>2</sub>O ternary system (purple open diamond). These are the conditions under which the widest span of viscosities is observed, which could be the main reason for the fitting difficulties encountered. [Figure 6b](#) suggests that there is no significant trend between the deviations

**Table 10.** Experimental Values of Viscosity  $\eta/\text{mPa s}$  for {MDEA (1) + MEG (2) + Water (3)} as a Function of Weight Fraction  $w$  and Temperature  $T$  at Pressure  $p = 0.1020 \text{ MPa}^a$ 

		$\eta/\text{mPa s}$				
		283.15 K			298.15 K	
$w_1$	$w_2$	Set A	Set B (1)	Set B (2)	Set A (1)	Set A (2)
0.050 ± 0.002	0.900 ± 0.003	30.86 ± 4.52	30.06 ± 4.08	30.67 ± 4.08	15.80 ± 1.08	-
0.900 ± 0.013	0.050 ± 0.010	-	201.93 ± 5.06	206.07 ± 5.06	-	79.59 ± 2.61
0.300 ± 0.003	0.600 ± 0.003	47.03 ± 4.53	47.20 ± 4.07	-	22.51 ± 1.08	22.43 ± 1.08
0.600 ± 0.006	0.300 ± 0.006	-	103.16 ± 4.60	-	43.92 ± 1.08	-
0.100 ± 0.002	0.600 ± 0.002	13.13 ± 4.52	12.93 ± 4.06	12.95 ± 4.06	7.27 ± 1.08	-
0.300 ± 0.003	0.400 ± 0.003	22.48 ± 4.52	22.26 ± 4.06	22.37 ± 4.06	11.52 ± 1.08	-
0.600 ± 0.006	0.100 ± 0.006	58.83 ± 4.53	58.74 ± 4.07	58.74 ± 4.07	25.09 ± 1.08	-
0.250 ± 0.002	0.250 ± 0.002	9.61 ± 4.52	9.91 ± 4.06	9.73 ± 4.06	5.35 ± 1.08	5.30 ± 1.08
		313.15 K	323.15 K	333.15 K	343.15 K	
$w_1$	$w_2$	Set A	Set A	Set A	Set A	
0.050 ± 0.002	0.900 ± 0.003	9.02 ± 1.04	6.49 ± 0.34	4.86 ± 0.47	3.76 ± 0.46	-
0.900 ± 0.013	0.050 ± 0.010	34.90 ± 1.04	21.70 ± 0.34	14.25 ± 0.47	9.76 ± 0.46	-
0.300 ± 0.003	0.600 ± 0.003	12.01 ± 1.04	8.32 ± 0.34	6.03 ± 0.47	4.50 ± 0.46	-
0.600 ± 0.006	0.300 ± 0.006	20.96 ± 1.04	13.60 ± 0.34	9.33 ± 0.47	6.63 ± 0.46	-
0.100 ± 0.002	0.600 ± 0.002	4.40 ± 1.04	3.36 ± 0.34	2.57 ± 0.47	2.04 ± 0.46	-
0.300 ± 0.003	0.400 ± 0.003	6.44 ± 1.04	4.73 ± 0.34	3.51 ± 0.47	2.70 ± 0.46	-
0.600 ± 0.006	0.100 ± 0.006	12.15 ± 1.04	8.18 ± 0.34	5.75 ± 0.47	4.15 ± 0.46	-
0.250 ± 0.002	0.250 ± 0.002	3.25 ± 1.04	2.46 ± 0.34	1.92 ± 0.47	1.55 ± 0.46	-
		353.15 K				
$w_1$	$w_2$	Set A (1)	Set A (2)	set C		
0.050 ± 0.002	0.900 ± 0.003	2.96 ± 0.31	2.98 ± 0.31	-	-	-
0.900 ± 0.013	0.050 ± 0.010	6.96 ± 0.31	6.96 ± 0.31	-	-	-
0.300 ± 0.003	0.600 ± 0.003	3.47 ± 0.31	3.47 ± 0.31	3.47 ± 0.31	-	-
0.600 ± 0.006	0.300 ± 0.006	4.89 ± 0.31	4.88 ± 0.31	-	-	-
0.100 ± 0.002	0.600 ± 0.002	1.66 ± 0.31	1.66 ± 0.31	-	-	-
0.300 ± 0.003	0.400 ± 0.003	2.12 ± 0.31	2.13 ± 0.31	-	-	-
0.600 ± 0.006	0.100 ± 0.006	3.10 ± 0.31	3.13 ± 0.31	-	-	-
0.250 ± 0.002	0.250 ± 0.002	1.25 ± 0.31	1.26 ± 0.31	1.26 ± 0.31	-	-

<sup>a</sup>Weight fractions and viscosities are reported with their expanded uncertainties (0.95 level of confidence). Expanded uncertainties not included above are  $U(T) = 0.02 \text{ K}$  and  $U(p) = 0.0030 \text{ MPa}$ .

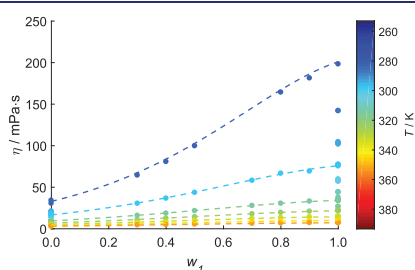


**Figure 4.** Binary data set of viscosities for {MDEA (1) + MEG (2)} and estimations generated by the NRTL-DVIS model. The temperature at which each experimental point (solid circle) was measured is color-coded by the bar on the right side. The temperatures at which the estimates were made were 283.15 K (dark-blue dashed line), 298.15 K (capri-blue dashed line), 313.15 K (aqua dashed line), 323.15 K (green dashed line), 333.15 K (lime-green dashed line), 343.15 K (yellow dashed line), and 353.15 K (orange dashed line).

and the temperature, whereas Figure 6a shows that the model may underestimate the viscosities of binary MDEA–water systems and ternary systems at somewhat higher viscosities (noticed by the scatter of green asterisk and purple open diamond above the zero line).

**Table 11.** Parameters and Results for the Fittings of the Vogel Equation

parameter	MDEA	MEG
$\hat{A}$	-4.3997	-3.8670
$\hat{B}$	1302.2	1087.1
$\hat{C}$	148.94	135.50
AARD (%)	1.10	2.47
MAD (mPa s)	3.76	2.46

**3.3. Excess Properties.** To further understand the molecular interactions of the system MDEA–MEG–H<sub>2</sub>O, we calculated the excess molar volume  $v^E$  and viscosity deviations  $\Delta\eta$  of the mixtures from the experimental results. For the calculation of excess molar volume  $v^E$ , we used eq 4. The calculated excess molar volumes and their uncertainties are shown in Table 14 and Figure 7 for MDEA–MEG and in Table 15 for MDEA–MEG–H<sub>2</sub>O.

For the binary system, excess molar volumes are negative in the whole range of compositions and temperatures studied in this work. Volume reduction upon mixing indicates the presence of charge-transfer and complex-forming interactions between MDEA and MEG, whereas it can also be the result of structural effects such as interstitial accommodation.<sup>46,62</sup> Both MDEA and MEG are polar molecules; therefore, dipole–dipole interactions should be present between the partial negative charge of one

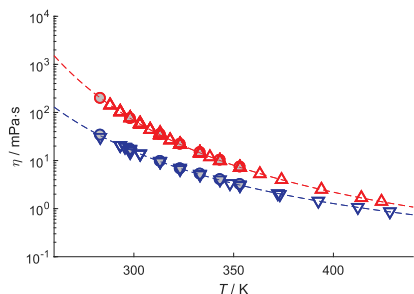


**Figure 5.** Experimental single-component viscosity of MDEA both obtained in the literature (red open triangle up) and as produced in this work (red  $\circ$  filled in gray) and of MEG both obtained in the literature (blue open triangle up) and as produced in this work (blue circle filled in gray), and corresponding estimations with the Vogel equation for MDEA (red dashed line) and MEG (blue dashed line).

**Table 12. Parameters and Results for the Aspen Liquid Mixture Viscosity Model Fitted for the Global Data Set**

Parameters of the Aspen Liquid Mixture Viscosity Model (1 = MDEA, 2 = MEG, 3 = Water)					
$\hat{a}_{12}$	2.59783	$\hat{a}_{13}$	-1.37707	$\hat{a}_{23}$	0.02792
$\hat{b}_{12}$	-0.42333	$\hat{b}_{13}$	0.53470	$\hat{b}_{23}$	-0.16100
$\hat{c}_{12}$	2.74959	$\hat{c}_{13}$	-0.10402	$\hat{c}_{23}$	0.24937
$\hat{d}_{12}$	-0.98385	$\hat{d}_{13}$	-0.32799	$\hat{d}_{23}$	0.10408
Fitting Results in Terms of Binary Data Sets					
	MDEA–MEG		MDEA–water		MEG–water
AARD (%)	2.41	AARD (%)	6.55	AARD (%)	2.22
MAD (mPa s)	6.77	MAD (mPa s)	16.64	MAD (mPa s)	2.28
Fitting Results in Terms of the Global Data Set					
AARD (%)					4.39
MAD (mPa s)					16.64

**Table 13. Parameters and Results for the NRTL-DVIS Equation Fitted for the Global Data Set**

Parameters of the NRTL-DVIS Model (1 = MDEA, 2 = MEG, 3 = Water)					
$\hat{a}_{12}$	-0.75876	$\hat{a}_{13}$	-2.4116	$\hat{a}_{23}$	0.02129
$\hat{a}_{21}$	0.34081	$\hat{a}_{31}$	-0.81471	$\hat{a}_{32}$	5.4190
$\hat{b}_{12}$	442.83	$\hat{b}_{13}$	1710.7	$\hat{b}_{23}$	-46.130
$\hat{b}_{21}$	-244.71	$\hat{b}_{31}$	-180.36	$\hat{b}_{32}$	6636.7
$\alpha_{ij} = \alpha = 0.3$ ; $R = 6.48803$					
Fitting Results in Terms of Binary Data Sets					
	MDEA–MEG		MDEA–water		MEG–water
AARD (%)	1.83	AARD (%)	2.98	AARD (%)	2.64
MAD (mPa s)	5.19	MAD (mPa s)	9.69	MAD (mPa s)	2.15
Fitting Results in Terms of the Global Data Set					
AARD (%)					2.97
MAD (mPa s)					12.62

molecule and the partial positive charge of another molecule. Additionally, autoprotolysis of MEG is reported in the literature<sup>63,64</sup> in the presence of MDEA, implying the breakage of the hydrogen bonding as a MEG molecule is losing its proton. In this case, dipole-ion forces between MDEA, which acts as an electron donor, and the cations formed from MEG autoprotolysis would appear. A minimum seems to occur between  $x_1 = 0.4$  and  $0.5$  ( $w_1 = 0.82$  and  $w_2 = 0.87$ ), indicating that these attractive

intermolecular forces are the strongest when the molar ratio between MDEA and MEG is close to 1:1.

As far as the temperature effect is concerned, Figure 7 shows that the deviations from ideality become smaller when the temperature increases. This is expected and can be explained by the increase of the kinetic energy and weakening of the intermolecular forces at higher temperatures. In some cases, the calculated excess volumes at different temperatures overlap. However, a closer look at the uncertainties listed in Table 14 reveals that the observed overlaps lie within the uncertainty. Details about the uncertainty analysis of the excess molar volumes can be found in the Supporting Information.

The excess molar volumes for the ternary system are also negative, as one could speculate given the negative deviations observed for the binary subsystems. Negative excess volumes have been reported for MEG–H<sub>2</sub>O by several researchers,<sup>23,25,26</sup> with the exception of Yang et al.<sup>24</sup> who reported positive  $v^E$  at  $T = 313.15$ – $353.15$  K and  $w_1 = 0.1$  and  $0.2$ . However, one would expect that the miscibility of the mixture and the known affinity of MEG for water would lead to negative excess molar volumes. As mentioned earlier, the excess volume is a contribution of both intermolecular forces and structural effects. For the MEG–H<sub>2</sub>O system, the dominating attractive intermolecular forces due to the polarity of the molecules contribute to negative  $v^E$ . In addition, the structure of the water molecule has cavities due to its hydrogen bonds; therefore, it is expected that these empty spaces will be filled partially by other molecules, such as MEG and MDEA, leading also to negative excess volumes.<sup>61,65,66</sup> Negative deviations from ideality have also been reported for the MDEA–H<sub>2</sub>O system.<sup>10,14</sup> The MDEA protonation reaction with water is known in the literature,<sup>1</sup> resulting in the formation of strong hydrogen bonds in the mixture. Therefore, higher compactness is expected for the MDEA–H<sub>2</sub>O system in comparison with MEG–H<sub>2</sub>O due to its strong hydrogen bonding. This is confirmed by the magnitude of their excess molar volumes; at 313.15 K, for example, the minimum  $v^E$  is ca.  $-1.2$  cm<sup>3</sup> mol<sup>-1</sup> for MDEA–H<sub>2</sub>O and ca.  $-0.3$  cm<sup>3</sup> mol<sup>-1</sup> for MEG–H<sub>2</sub>O. The extreme minimum of  $-1.2$  cm<sup>3</sup> mol<sup>-1</sup> appears at the amine mole fraction close to  $x_1 = 0.3$  ( $w_1 = 0.75$ ), which is reflected in the previously mentioned maximum in density, observed at the same mole fraction for MDEA–H<sub>2</sub>O mixtures. Therefore, the negative excess volumes for the ternary system would be the result of mainly the dipole-ion forces between MDEA and MEG and hydrogen bonds between MDEA and water.

As mentioned in Section 2.3, the viscosity deviations were calculated according to eqs 12 and 13. Calculation results and viscosity deviation uncertainties are shown in Table 16 and Figure 8 for MDEA–MEG and in Table 17 for MDEA–MEG–H<sub>2</sub>O.

The viscosity deviations for the binary systems MDEA–H<sub>2</sub>O, MEG–H<sub>2</sub>O, and MDEA–MEG and the ternary system MDEA–MEG–H<sub>2</sub>O are positive according to the literature and the additional findings of this work. The positive viscosity deviations from ideality are expected based on the observed negative molar volumes, which indicate the presence of strong molecular interactions between these three chemical compounds, as discussed earlier. The strong hydrogen bonds in MDEA–H<sub>2</sub>O and dipole-ion forces in MDEA–MEG hinder the fluid to flow, leading to a viscosity increase with MDEA concentration, as observed in Figures S4 (Supporting Information) and 4, respectively. The former system exhibits a viscosity increase with amine content up to approximately 95 wt % ( $x_1 = 0.75$ ).<sup>14</sup>

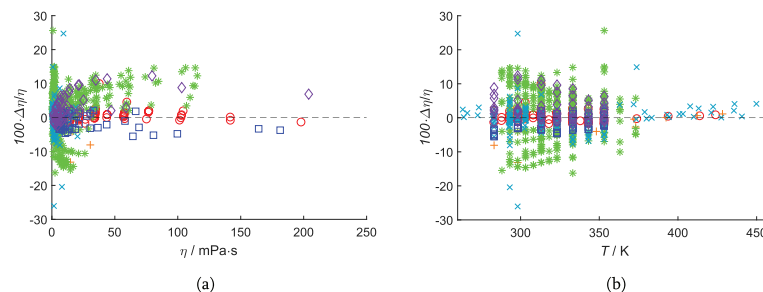


**Figure 6.** Deviations in terms of differences between experimental and estimated viscosities divided by experimental viscosities regarding estimations made with the NRTL-DVIS model, and how they vary with the experimental viscosities themselves (a) and with temperature (b). The data sets are distributed in terms of pure MDEA data (red open circle), pure MEG data (orange plus), binary MDEA–water data (green asterisk), binary MEG–water data (cyan cross), binary MDEA–MEG data (blue open square), and ternary data (purple open diamond).

**Table 14.** Excess Molar Volumes  $v^E/\text{cm}^3 \text{mol}^{-1}$  for {MDEA (1) + MEG (2)} as a Function of Weight Fraction  $w$  and Temperature  $T$  at Pressure  $p = 0.1020 \text{ MPa}$ <sup>a</sup>

$w_1$	$v^E/\text{cm}^3 \text{mol}^{-1}$			
	$T = 283.15 \text{ K}$	$T = 298.15 \text{ K}$	$T = 313.15 \text{ K}$	$T = 323.15 \text{ K}$
0.000	0.000	0.000	0.000	0.000
$0.300 \pm 0.003$	$-0.267 \pm 0.007$	$-0.247 \pm 0.008$	$-0.255 \pm 0.009$	$-0.268 \pm 0.006$
$0.400 \pm 0.003$	$-0.326 \pm 0.008$	$-0.319 \pm 0.008$	$-0.326 \pm 0.008$	$-0.335 \pm 0.006$
$0.500 \pm 0.004$	$-0.367 \pm 0.009$	$-0.357 \pm 0.009$	$-0.363 \pm 0.009$	$-0.374 \pm 0.007$
$0.700 \pm 0.006$	$-0.386 \pm 0.012$	$-0.368 \pm 0.011$	$-0.368 \pm 0.011$	$-0.373 \pm 0.010$
$0.800 \pm 0.008$	$-0.336 \pm 0.014$	$-0.307 \pm 0.013$	$-0.307 \pm 0.012$	$-0.306 \pm 0.012$
$0.900 \pm 0.009$	$-0.241 \pm 0.018$	$-0.192 \pm 0.018$	$-0.187 \pm 0.017$	$-0.182 \pm 0.017$
$1.000 \pm 0.011$	0.000	0.000	0.000	0.000
$w_1$	$T = 333.15 \text{ K}$	$T = 343.15 \text{ K}$	$T = 353.15 \text{ K}$	
0.000	0.000	0.000	0.000	
$0.300 \pm 0.003$	$-0.246 \pm 0.004$	$-0.237 \pm 0.004$	$-0.230 \pm 0.004$	
$0.400 \pm 0.003$	$-0.307 \pm 0.004$	$-0.308 \pm 0.004$	$-0.295 \pm 0.004$	
$0.500 \pm 0.004$	$-0.351 \pm 0.006$	$-0.341 \pm 0.006$	$-0.328 \pm 0.006$	
$0.700 \pm 0.006$	$-0.354 \pm 0.009$	$-0.341 \pm 0.009$	$-0.326 \pm 0.009$	
$0.800 \pm 0.008$	$-0.293 \pm 0.011$	$-0.281 \pm 0.011$	$-0.264 \pm 0.010$	
$0.900 \pm 0.009$	$-0.172 \pm 0.016$	$-0.174 \pm 0.016$	$-0.155 \pm 0.017$	
$1.000 \pm 0.011$	0.000	0.000	0.000	

<sup>a</sup>Weight fractions and excess molar volumes are reported with their expanded uncertainties (0.95 level of confidence). Expanded uncertainties not included above are  $U(T) = 0.02 \text{ K}$  and  $U(p) = 0.0030 \text{ MPa}$ .

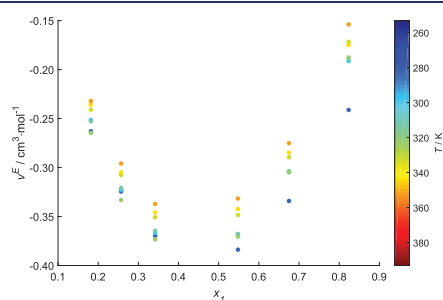


**Figure 7.** Excess molar volumes for {MDEA (1) + MEG (2)} as a function of molar fraction and at temperatures 283.15 K (dark-blue points), 298.15 K (capri-blue points), 313.15 K (aqua points), 323.15 K (green points), 333.15 K (lime-green points), 343.15 K (yellow points), and 353.15 K (orange points).

It is possible that until this point, the attractive hydrogen bonds predominate over the weaker molecule/ionlike forces. After

this point, the abundance of amines or unavailability of water to protonate the amine could lead to a greater contribution from the rest of the forces present in the system.

The temperature increase results in lower viscosity deviations due to the weakening of the intermolecular forces. Moreover, it is observed that, unlike in the case of excess volumes of MDEA–MEG where the minima were found at constant amine concentration between  $x_1 = 0.4$  and  $0.5$  for all temperatures studied in this work, the viscosity deviation maxima seem to appear at around  $x_1 = 0.5$  and shift at higher mole fractions as the temperature decreases. In addition, there is a mismatch between the amine concentration at which the min  $v^E$  and max  $\Delta\eta$  appear. This mismatch has also been observed for the binary MDEA–H<sub>2</sub>O. According to Yin et al.<sup>14</sup> and Sathyanarayana et al.,<sup>67</sup> this behavior can be explained by the effects based on the shape, size, and structure of the molecules, which are able to dominate over the intermolecular effects and even reverse the sign of the viscosity deviation.

The density and viscosity models developed in this work serve as an assessment tool for the successful employment of the

**Table 15.** Excess Molar Volumes  $v^E/\text{cm}^3 \text{mol}^{-1}$  for {MDEA (1) + MEG (2) + Water (3)} as a Function of Weight Fraction  $w$  and Temperature  $T$  at Pressure  $p = 0.1020 \text{ MPa}$ <sup>a</sup>

$w_1$	$w_2$	$v^E/\text{cm}^3 \text{mol}^{-1}$			
		$T = 283.15 \text{ K}$	$T = 298.15 \text{ K}$	$T = 313.15 \text{ K}$	$T = 323.15 \text{ K}$
0.050 ± 0.002	0.900 ± 0.003	-0.210 ± 0.008	-0.181 ± 0.009	-0.179 ± 0.006	-0.211 ± 0.020
0.900 ± 0.013	0.050 ± 0.010	-0.707 ± 0.021	-0.670 ± 0.023	-0.657 ± 0.019	-0.674 ± 0.039
0.300 ± 0.003	0.600 ± 0.003	-0.571 ± 0.007	-0.533 ± 0.009	-0.514 ± 0.005	-0.533 ± 0.019
0.600 ± 0.006	0.300 ± 0.006	-0.856 ± 0.012	-0.815 ± 0.013	-0.792 ± 0.010	-0.801 ± 0.024
0.100 ± 0.002	0.600 ± 0.002	-0.508 ± 0.004	-0.455 ± 0.005	-0.421 ± 0.002	-0.407 ± 0.012
0.300 ± 0.003	0.400 ± 0.003	-0.724 ± 0.005	-0.666 ± 0.006	-0.633 ± 0.004	-0.613 ± 0.012
0.600 ± 0.006	0.100 ± 0.006	-1.089 ± 0.007	-1.026 ± 0.008	-0.985 ± 0.005	-0.969 ± 0.015
0.250 ± 0.002	0.250 ± 0.002	-0.570 ± 0.003	-0.512 ± 0.004	-0.489 ± 0.003	-0.466 ± 0.009
$w_1$	$w_2$	$T = 333.15 \text{ K}$	$T = 343.15 \text{ K}$	$T = 353.15 \text{ K}$	
0.050 ± 0.002	0.900 ± 0.003	-0.179 ± 0.024	-0.180 ± 0.024	-0.191 ± 0.032	
0.900 ± 0.013	0.050 ± 0.010	-0.667 ± 0.046	-0.659 ± 0.045	-0.648 ± 0.059	
0.300 ± 0.003	0.600 ± 0.003	-0.504 ± 0.022	-0.500 ± 0.022	-0.497 ± 0.029	
0.600 ± 0.006	0.300 ± 0.006	-0.783 ± 0.028	-0.765 ± 0.027	-0.751 ± 0.036	
0.100 ± 0.002	0.600 ± 0.002	-0.395 ± 0.014	-0.379 ± 0.014	-0.372 ± 0.018	
0.300 ± 0.003	0.400 ± 0.003	-0.608 ± 0.015	-0.590 ± 0.014	-0.573 ± 0.019	
0.600 ± 0.006	0.100 ± 0.006	-0.940 ± 0.018	-0.913 ± 0.018	-0.887 ± 0.024	
0.250 ± 0.002	0.250 ± 0.002	-0.466 ± 0.011	-0.456 ± 0.011	-0.441 ± 0.014	

<sup>a</sup>Weight fractions and excess molar volumes are reported with their expanded uncertainties (0.95 level of confidence). Expanded uncertainties not included above are  $U(T) = 0.02 \text{ K}$  and  $U(p) = 0.0030 \text{ MPa}$ .

**Table 16.** Viscosity Deviations  $\Delta\eta/\text{mPa s}$  for {MDEA (1) + MEG (2)} as a Function of Weight Fraction  $w$  and Temperature  $T$  at Pressure  $p = 0.1020 \text{ MPa}$ <sup>a</sup>

$w_1$	$\Delta\eta/\text{mPa s}$			
	$T = 283.15 \text{ K}$	$T = 298.15 \text{ K}$	$T = 313.15 \text{ K}$	$T = 323.15 \text{ K}$
0.000	0.00	0.00	0.00	0.00
0.300 ± 0.003	17.34 ± 4.01	7.82 ± 1.36	3.63 ± 0.82	2.36 ± 0.50
0.400 ± 0.003	27.03 ± 4.06	11.32 ± 1.37	5.02 ± 0.97	3.22 ± 0.50
0.500 ± 0.004	37.45 ± 5.09	14.97 ± 1.68	6.54 ± 0.83	4.04 ± 0.50
0.700 ± 0.006		19.30 ± 2.87	8.10 ± 0.91	4.80 ± 0.51
0.800 ± 0.008	52.26 ± 6.24	19.83 ± 3.02	7.38 ± 1.03	4.45 ± 0.54
0.900 ± 0.009	35.98 ± 8.99	11.06 ± 3.69	5.10 ± 1.13	3.04 ± 0.69
1.000 ± 0.011	0.00	0.00	0.00	0.00
$w_1$	$T = 333.15 \text{ K}$	$T = 343.15 \text{ K}$	$T = 353.15 \text{ K}$	
0.000	0.00	0.00	0.00	
0.300 ± 0.003	1.44 ± 0.43	0.94 ± 0.64	0.69 ± 0.28	
0.400 ± 0.003	1.93 ± 0.57	1.29 ± 0.64	0.91 ± 0.37	
0.500 ± 0.004	2.42 ± 0.57	1.59 ± 0.63	1.09 ± 0.37	
0.700 ± 0.006	2.86 ± 0.56	1.85 ± 0.61	1.24 ± 0.36	
0.800 ± 0.008	2.65 ± 0.57	1.65 ± 0.61	1.11 ± 0.35	
0.900 ± 0.009	1.71 ± 0.49	1.07 ± 0.64	0.74 ± 0.26	
1.000 ± 0.011	0.00	0.00	0.00	

<sup>a</sup>Weight fractions and viscosity deviations are reported with their expanded uncertainties (0.95 level of confidence). Expanded uncertainties not included above are  $U(T) = 0.02 \text{ K}$  and  $U(p) = 0.0030 \text{ MPa}$ .

binary MDEA–MEG or the ternary MDEA–MEG–H<sub>2</sub>O systems at various temperature conditions. An example is the use of the developed viscosity model to construct viscosity contour plots, such as Figure 9, to identify the viscosity limits for operational reasons in a specific process. To read Figure 9, one can directly find the weight fraction of MEG in the X axis and the weight fraction of MDEA in the Y axis so that the remainder of the mass will be assigned to water. In  $X = Y = 0$ , therefore, what is seen is the viscosity of pure water.

If one is concerned with avoiding a certain limiting viscosity when employing a MDEA–MEG–H<sub>2</sub>O solution, for example, 200 mPa s at 278.15 K, Figure 9 shows that systems with more

than 80 wt % MDEA approach or even exceed the viscosity specification and are not suitable. Alternatively, if one wants to find the viscosity of an 80 wt % MDEA–15 wt % MEG–5 wt % H<sub>2</sub>O, one should read 80 in the Y axis and 15 in the X axis and find their viscosity at the point their imaginary lines intersect. At 288.15 K however, any composition for the ternary system respects the viscosity limit of 200 mPa s.

In addition, similar to the observations made for the aqueous MDEA exhibiting the maximum viscosity at approximately 95 wt % MDEA, experimentally determined viscosities for the ternary system 90 wt % MDEA–5 wt % MEG–5 wt % H<sub>2</sub>O are also higher than those for the pure amine at temperatures lower than

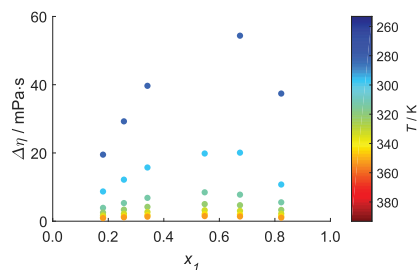


**Figure 8.** Viscosity deviations  $\Delta\eta$  for {MDEA (1) + MEG (2)} as a function of molar fraction and at temperatures 283.15 K (dark-blue points), 298.15 K (capri-blue points), 313.15 K (aqua points), 323.15 K (green points), 333.15 K (lime-green points), 343.15 K (yellow points), and 353.15 K (orange points).

313.15 K. Therefore, the addition of water as a means of reducing the viscosity, for example, to reach the viscosity specifications, should be used cautiously and after advising Figure 9. Naturally, knowing that the NRTL-DVIS model is underestimating the viscosities of MDEA-rich solutions, some additional attention should be paid. Overall, the models have been checked at temperatures outside the temperature range they were developed at, and it is observed that they are able to capture the trends for both density and viscosity. However, since the model is not validated outside the 283.15–353.15 K range as there are no experimental data available for the systems MDEA–MEG and MDEA–MEG–H<sub>2</sub>O, any extrapolation must be performed with caution.

#### 4. CONCLUSIONS

New density and viscosity data were obtained for the systems MDEA–MEG and MDEA–MEG–H<sub>2</sub>O at temperature

**Table 17.** Viscosity Deviations  $\Delta\eta/\text{mPa s}$  for {MDEA (1) + MEG (2) + Water (3)} as a Function of Weight Fraction  $w$  and Temperature  $T$  at Pressure  $p = 0.1020 \text{ MPa}$ <sup>a</sup>

$w_1$	$w_2$	$\Delta\eta/\text{mPa s}$			
		$T = 283.15 \text{ K}$	$T = 298.15 \text{ K}$	$T = 313.15 \text{ K}$	$T = 323.15 \text{ K}$
$0.050 \pm 0.002$	$0.900 \pm 0.003$	$9.13 \pm 2.75$	$4.50 \pm 1.16$	$2.43 \pm 1.10$	$1.73 \pm 0.40$
$0.900 \pm 0.013$	$0.050 \pm 0.010$	$154.38 \pm 6.08$	$57.22 \pm 3.18$	$12.53 \pm 2.10$	$13.63 \pm 0.59$
$0.300 \pm 0.003$	$0.600 \pm 0.003$	$31.30 \pm 3.11$	$14.00 \pm 0.79$	$3.54 \pm 1.06$	$4.62 \pm 0.36$
$0.600 \pm 0.006$	$0.300 \pm 0.006$	$84.45 \pm 4.11$	$34.27 \pm 1.11$	$11.31 \pm 1.07$	$9.53 \pm 0.35$
$0.100 \pm 0.002$	$0.600 \pm 0.002$	$8.10 \pm 2.44$	$4.29 \pm 1.08$	$1.42 \pm 1.04$	$1.82 \pm 0.34$
$0.300 \pm 0.003$	$0.400 \pm 0.003$	$17.48 \pm 2.44$	$8.57 \pm 1.08$	$3.49 \pm 1.04$	$3.21 \pm 0.34$
$0.600 \pm 0.006$	$0.100 \pm 0.006$	$53.89 \pm 2.44$	$22.20 \pm 1.08$	$9.26 \pm 1.04$	$6.69 \pm 0.34$
$0.250 \pm 0.002$	$0.250 \pm 0.002$	$7.10 \pm 2.44$	$3.63 \pm 0.76$	$1.55 \pm 1.04$	$1.50 \pm 0.34$
$w_1$	$w_2$	$T = 333.15 \text{ K}$	$T = 343.15 \text{ K}$	$T = 353.15 \text{ K}$	
$0.050 \pm 0.002$	$0.900 \pm 0.003$	$1.15 \pm 0.51$	$0.86 \pm 0.53$	$0.65 \pm 0.26$	
$0.900 \pm 0.013$	$0.050 \pm 0.010$	$8.47 \pm 0.57$	$5.49 \pm 0.52$	$3.71 \pm 0.26$	
$0.300 \pm 0.003$	$0.600 \pm 0.003$	$3.17 \pm 0.48$	$2.25 \pm 0.48$	$1.66 \pm 0.19$	
$0.600 \pm 0.006$	$0.300 \pm 0.006$	$6.25 \pm 0.48$	$4.24 \pm 0.47$	$2.98 \pm 0.22$	
$0.100 \pm 0.002$	$0.600 \pm 0.002$	$1.34 \pm 0.47$	$1.03 \pm 0.46$	$0.81 \pm 0.22$	
$0.300 \pm 0.003$	$0.400 \pm 0.003$	$2.30 \pm 0.47$	$1.71 \pm 0.46$	$1.29 \pm 0.22$	
$0.600 \pm 0.006$	$0.100 \pm 0.006$	$4.59 \pm 0.47$	$3.20 \pm 0.46$	$2.32 \pm 0.22$	
$0.250 \pm 0.002$	$0.250 \pm 0.002$	$1.15 \pm 0.47$	$0.90 \pm 0.46$	$0.70 \pm 0.18$	

<sup>a</sup>Weight fractions and viscosity deviations are reported with their expanded uncertainties (0.95 level of confidence). Expanded uncertainties not included above are  $U(T) = 0.02 \text{ K}$  and  $U(p) = 0.0030 \text{ MPa}$ .

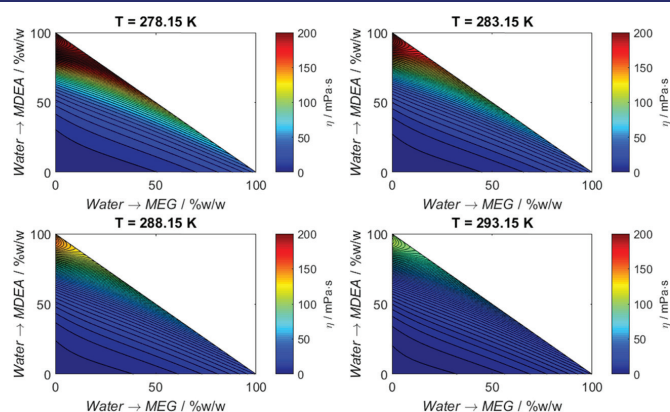


**Figure 9.** Viscosity plots for MDEA–MEG–water ternary mixtures at four different temperatures (278.15, 283.15, 288.15, and 293.15 K). The viscosity values are color-coded by the bar on the right side.

$T = 283.15\text{--}353.15\text{ K}$  due to the potential application of the mixture for the combined  $\text{H}_2\text{S}$  removal and hydrate control in natural gas processing. The measurements showed good repeatability and reproducibility, and the excess molar volume and viscosity deviations upon mixing were calculated. Negative excess molar volumes and positive viscosity deviations indicated the strong nonideality of the mixtures at the studied compositions and temperatures. Density has been modeled successfully using the NRTL-DVOL model, exhibiting AARDs lower than 0.4%. The Aspen liquid mixture viscosity model and the NRTL-DVIS model were employed for the estimation of the viscosity data obtained in this work. They both perform satisfactorily, with the latter yielding slightly better results. The results for the parametrization of the NRTL-DVIS model showed AARDs lower than 3%.

## ■ ASSOCIATED CONTENT

### Supporting Information

The Supporting Information is available free of charge at <https://pubs.acs.org/doi/10.1021/acs.jced.9b00607>.

Experimental and predicted densities with the NRTL-DVOL model; experimental and predicted viscosities with the NRTL-DVIS model; experimental and predicted viscosities with the Aspen liquid mixture viscosity model; uncertainty analysis (PDF)

## ■ AUTHOR INFORMATION

### Corresponding Author

\*E-mail: [hanna.knuutila@ntnu.no](mailto:hanna.knuutila@ntnu.no).

### ORCID

Hanna K. Knuutila: 0000-0003-2057-1743

### Author Contributions

The manuscript was written through contributions of all authors. All authors have given approval to the final version of the manuscript.

### Funding

This work was carried out as a part of Subsea Production and Processing (SUBPRO), a Research-based Innovation Centre within Subsea Production and Processing. The authors gratefully acknowledge the financial support from SUBPRO, which is financed by the Norwegian University of Science and Technology (NTNU), major industry partners, and the Research Council of Norway (RCN) under project number 237893. The authors also acknowledge the financial support from the Faculty of Natural Sciences of NTNU.

### Notes

The authors declare no competing financial interest.

## ■ NOMENCLATURE

### Symbols

$a_{ij}$ , $b_{ij}$ , $c_{ij}$ , $d_{ij}$ , $G_{ij}$ , $k_{ij}$	binary parameters for the density and viscosity models (DVOL, DVIS, and Aspen liquid mixture viscosity models)
$l_{ij}$ , $\alpha_{ij}$ , $\tau_{ij}$	single-component parameters for the individual density and viscosity models (Rackett and Vogel)
$A_i$ , $B_i$ , $C_i$	single-component parameters for the individual density and viscosity models (Rackett and Vogel)
$MW_i$	molar weight of component $i$ (kg mol)
NC	number of components
NP	number of points
$p$	pressure (Pa)
$p_{C,i}$	critical pressure of component $i$ (Pa)

$p_{r,i}$	reduced pressure of component $i$
$R$	ideal gas constant ( $\text{m}^3 \text{ Pa K}^{-1} \text{ mol}^{-1}$ )
$T$	temperature (K)
$T_{C,i}$	critical temperature of component $i$ (K)
$T_{r,i}$	reduced temperature of component $i$
$v_i$	molar volume of component $i$ ( $\text{m}^3 \text{ mol}^{-1}$ )
$v^E$	excess molar volume of a mixture ( $\text{m}^3 \text{ mol}^{-1}$ )
$Z_{RA,i}$	compressibility factor of component $i$ as obtained by the Rackett equation
$w_i$	mass fraction of component $i$ in a mixture
$x_i$	molar fraction of component $i$ in a mixture

### Greek Letters

$\Delta\eta$	viscosity deviation (mPa s)
$\eta$	viscosity (mPa s)
$\eta_i$	viscosity of single component $i$ (mPa s)
$\hat{\eta}_{ij}$	binary parameter for the Aspen liquid mixture viscosity model (mPa s)
$\eta^E$	excess viscosity (mPa s)
$\rho$	density ( $\text{kg m}^{-3}$ )
$\rho_i$	density of single component $i$ ( $\text{kg m}^{-3}$ )
$\varphi_{\text{H}_2\text{O}}$	water fluidity ( $\text{p}^{-1}$ )

### Other Notations

accent, e.g.,  $\hat{y}$  estimated variable, not measured  
bold, e.g.,  $\mathbf{y}$  variable is an array of variables

## ■ REFERENCES

- (1) Kohl, A. L.; Nielsen, R. B. *Gas Purification*, 5th ed.; Gulf Professional Publishing: Houston, 1997.
- (2) Campbell, J. M. Glycol Dehydration. *Gas Conditioning and Processing*; J. M. Campbell and Company: Oklahoma, 1998; Vol. 2, pp 333–394.
- (3) Stewart, M.; Arnold, K. Part 2—Gas Processing. In *Gas Sweetening and Processing Field Manual*; Arnold, M. S., Ed.; Gulf Professional Publishing: Boston, 2011; pp 141–155.
- (4) Albuquerque, F. A.; Vianna, F. L. V.; Alves, R. P.; Kuchpil, C.; Morais, M. G. G.; Orłowski, R. T. C.; Moraes, C. A. C.; Ribeiro, O. In *Subsea Processing Systems: Future Vision*, Offshore Technology Conference: OTC, OTC-24161-MS, 2013; p 14.
- (5) Hutchinson, A. J. L. Process for Treating Gases. US2,184,596A, Oct 24, 1939.
- (6) McCartney, E. R. Gas Purification and Dehydration Process. US2,435,089A, Jan 27, 1948.
- (7) McCartney, E. R. Extraction of Acidic Impurities and Moisture from Gases. US2,547,278A, April 3, 1951.
- (8) Chapin, W. F. Purification and Dehydration of Gases. US2,518,752A, Aug 15, 1950.
- (9) Nookuea, W.; Tan, Y.; Li, H.; Thorin, E.; Yan, J. Impacts of Thermo-Physical Properties of Gas and Liquid Phases on Design of Absorber for  $\text{CO}_2$  Capture Using Monoethanolamine. *Int. J. Greenhouse Gas Control* **2016**, *52*, 190–200.
- (10) Bernal-García, J. M.; Ramos-Estrada, M.; Iglesias-Silva, G. A.; Hall, K. R. Densities and Excess Molar Volumes of Aqueous Solutions of N-Methyl-diethanolamine (MDEA) at Temperatures from (283.15 to 363.15) K. *J. Chem. Eng. Data* **2003**, *48*, 1442–1445.
- (11) Al-Ghawas, H. A.; Hagewiesche, D. P.; Ruiz-Ibanez, G.; Sandall, O. C. Physicochemical Properties Important for Carbon Dioxide Absorption in Aqueous Methyl-diethanolamine. *J. Chem. Eng. Data* **1989**, *34*, 385–391.
- (12) Li, M.-H.; Lie, Y.-C. Densities and Viscosities of Solutions of Monoethanolamine + N-Methyl-diethanolamine + Water and Monoethanolamine + 2-Amino-2-Methyl-1-Propanol + Water. *J. Chem. Eng. Data* **1994**, *39*, 444–447.
- (13) Paul, S.; Mandal, B. Density and Viscosity of Aqueous Solutions of (N-Methyl-diethanolamine + Piperazine) and (2-Amino-2-Methyl-1-Propanol + Piperazine) from (288 to 333) K. *J. Chem. Eng. Data* **2006**, *51*, 1808–1810.

- (14) Yin, Y.; Fu, T.; Zhu, C.; Ma, Y. Volumetric and Viscometric Study and FT-IR Analysis of Binary and Ternary Mixtures of 1-Butyl-3-Methylimidazolium Tetrafluoroborate, Methyl-diethanolamine and Water. *J. Mol. Liq.* **2017**, *243*, 664–676.
- (15) Teng, T. T.; Maham, Y.; Hepler, L. G.; Mather, A. E. Viscosity of Aqueous Solutions of N-Methyl-diethanolamine and Diethanolamine. *J. Chem. Eng. Data* **1994**, *39*, 290–293.
- (16) Bernal-García, J. M.; Galicia-Luna, L. A.; Hall, K. R.; Ramos-Estrada, M.; Iglesias-Silva, G. A. Viscosities for Aqueous Solutions of N-Methyl-diethanolamine from 313.15 to 363.15 K. *J. Chem. Eng. Data* **2004**, *49*, 864–866.
- (17) Pinto, D. D. D.; Johnsen, B.; Awais, M.; Svendsen, H. F.; Knuutila, H. K. Viscosity Measurements and Modeling of Loaded and Unloaded Aqueous Solutions of MDEA, DMEA, DEEA and MAPA. *Chem. Eng. Sci.* **2017**, *171*, 340–350.
- (18) Chowdhury, F. I.; Akhtar, S.; Saleh, M. A. Viscosities and Excess Viscosities of Aqueous Solutions of Some Diethanolamines. *J. Mol. Liq.* **2010**, *155*, 1–7.
- (19) Rinker, E. B.; Oelschlager, D. W.; Colussi, A. T.; Henry, K. R.; Sandall, O. C. Viscosity, Density, and Surface Tension of Binary Mixtures of Water and N-Methyl-diethanolamine and Water and Diethanolamine and Tertiary Mixtures of These Amines with Water over the Temperature Range 20–100 Degree C. *J. Chem. Eng. Data* **1994**, *39*, 392–395.
- (20) Baek, J.-I.; Yoon, J.-H.; Eum, H.-M. Physical and Thermodynamic Properties of Aqueous 2-Amino-2-Methyl-1,3-Propanediol Solutions. *Int. J. Thermophys.* **2000**, *21*, 1175–1184.
- (21) Hayduk, W.; Malik, V. K. Density, Viscosity, and Carbon Dioxide Solubility and Diffusivity in Aqueous Ethylene Glycol Solutions. *J. Chem. Eng. Data* **1971**, *16*, 143–146.
- (22) Bohne, D.; Fischer, S.; Obermeier, E. Thermal, Conductivity, Density, Viscosity, and Prandtl-Numbers of Ethylene Glycol-Water Mixtures. *Bunsen-Ges. Phys. Chem., Ber.* **1984**, *88*, 739–742.
- (23) Sun, T.; Teja, A. S. Density, Viscosity, and Thermal Conductivity of Aqueous Ethylene, Diethylene, and Triethylene Glycol Mixtures between 290 K and 450 K. *J. Chem. Eng. Data* **2003**, *48*, 198–202.
- (24) Yang, C.; Ma, P.; Jing, F.; Tang, D. Excess Molar Volumes, Viscosities, and Heat Capacities for the Mixtures of Ethylene Glycol + Water from 273.15 K to 353.15 K. *J. Chem. Eng. Data* **2003**, *48*, 836–840.
- (25) Tsierekos, N. G.; Molinou, I. E. Thermodynamic Properties of Water + Ethylene Glycol at 283.15, 293.15, 303.15, and 313.15 K. *J. Chem. Eng. Data* **1998**, *43*, 989–993.
- (26) Afzal, W.; Mohammadi, A. H.; Richon, D. Volumetric Properties of Mono-, Di-, Tri-, and Polyethylene Glycol Aqueous Solutions from (273.15 to 363.15) K: Experimental Measurements and Correlations. *J. Chem. Eng. Data* **2009**, *54*, 1254–1261.
- (27) Braun, N. O.; Persson, U. Å.; Karlsson, H. T. Densities and Viscosities of Mono(Ethylene Glycol) + 2-Amino-2-Methyl-1-Propanol + Water. *J. Chem. Eng. Data* **2001**, *46*, 805–808.
- (28) Song, J.-H.; Park, S.-B.; Yoon, J.-H.; Lee, H.; Lee, K.-H. Densities and Viscosities of Monoethanolamine + Ethylene Glycol + Water. *J. Chem. Eng. Data* **1996**, *41*, 1152–1154.
- (29) Li, L.; Zhang, J.; Li, Q.; Guo, B.; Zhao, T.; Sha, F. Density, Viscosity, Surface Tension, and Spectroscopic Properties for Binary System of 1,2-Ethanediamine+diethylene Glycol. *Thermochim. Acta* **2014**, *590*, 91–99.
- (30) Zhao, T.; Zhang, J.; Li, L.; Guo, B.; Gao, L.; Wei, X. Excess Properties and Spectroscopic Studies for the Binary System 1,2-Ethanediamine+polyethylene Glycol 300 at T = (293.15, 298.15, 303.15, 308.15, 313.15, and 318.15) K. *J. Mol. Liq.* **2014**, *198*, 21–29.
- (31) DiGiulio, R. M.; Lee, R. J.; Schaeffer, S. T.; Brasher, L. L.; Teja, A. S. Densities and Viscosities of the Ethanolamines. *J. Chem. Eng. Data* **1992**, *37*, 239–242.
- (32) Álvarez, E.; Gómez-Díaz, D.; La Rubia, M. D.; Navaza, J. M. Densities and Viscosities of Aqueous Ternary Mixtures of 2-(Methylamino)Ethanol and 2-(Ethylamino)Ethanol with Diethanolamine, Triethanolamine, N-Methyl-diethanolamine, or 2-Amino-1-Methyl-1-Propanol from 298.15 to 323.15 K. *J. Chem. Eng. Data* **2006**, *51*, 955–962.
- (33) Henni, A.; Maham, Y.; Tontiwachwuthikul, P.; Chakma, A.; Mather, A. E. Densities and Viscosities for Binary Mixtures of N-Methyl-diethanolamine plus Triethylene Glycol Monomethyl Ether from 25 Degrees C to 70 Degrees C and N-Methyl-diethanolamine plus Ethanol Mixtures at 40 Degrees C. *J. Chem. Eng. Data* **2000**, *45*, 247–253.
- (34) Haghtalab, A.; Shojaean, A. Volumetric and Viscometric Behaviour of the Binary Systems of N-Methyl-diethanolamine and Diethanolamine with 1-Butyl-3-Methylimidazolium Acetate at Various Temperatures. *J. Chem. Thermodyn.* **2014**, *68*, 128–137.
- (35) Akbar, M. M.; Murugesan, T. Thermophysical Properties for the Binary Mixtures of 1-Hexyl-3-Methylimidazolium Bis-(Trifluoromethylsulfonyl)Imide [Hmim][Tf2N]+N-Methyl-diethanolamine (MDEA) at Temperatures (303.15 to 323.15) K. *J. Mol. Liq.* **2012**, *169*, 95–101.
- (36) Tsierekos, N. G.; Molinou, I. E. Transport Properties of 2:2 Symmetrical Electrolytes in (Water+ethylene Glycol) Binary Mixtures at T = 293.15 K. *J. Chem. Thermodyn.* **2006**, *38*, 1422–1431.
- (37) Jerome, F. S.; Tseng, J. T.; Fan, L. T. Viscosities of Aqueous Glycol Solutions. *J. Chem. Eng. Data* **1968**, *13*, 496.
- (38) Dunstan, A. E. IV.—The Viscosity of Liquid Mixtures. Part II. *J. Chem. Soc., Trans.* **1905**, *87*, 11–17.
- (39) Rumble, J. *CRC Handbook of Chemistry and Physics*; CRC Press, 2017.
- (40) Hartono, A.; Mba, E. O.; Svendsen, H. F. Physical Properties of Partially CO<sub>2</sub> Loaded Aqueous Monoethanolamine (MEA). *J. Chem. Eng. Data* **2014**, *59*, 1808–1816.
- (41) Poli, R.; Kennedy, J.; Blackwell, T. Particle Swarm Optimization. *Swarm Intell.* **2007**, *1*, 33–57.
- (42) Ghosh, S.; Das, S.; Kundu, D.; Suresh, K.; Abraham, A. Inter-Particle Communication and Search-Dynamics of Lbest Particle Swarm Optimizers: An Analysis. *Inf. Sci.* **2012**, *182*, 156–168.
- (43) Evjen, S.; Wanderley, R.; Fiksdahl, A.; Knuutila, H. K. Viscosity, Density, and Volatility of Binary Mixtures of Imidazole, 2-Methylimidazole, 2,4,5-Trimethylimidazole, and 1,2,4,5-Tetramethylimidazole with Water. *J. Chem. Eng. Data* **2019**, *64*, 507–516.
- (44) Pinto, D. D. D.; Svendsen, H. F. An Excess Gibbs Free Energy Based Model to Calculate Viscosity of Multicomponent Liquid Mixtures. *Int. J. Greenhouse Gas Control* **2015**, *42*, 494–501.
- (45) Pinto, D. D. D.; Monteiro, J. G. M.-S.; Johnsen, B.; Svendsen, H. F.; Knuutila, H. Density Measurements and Modelling of Loaded and Unloaded Aqueous Solutions of MDEA (N-Methyl-diethanolamine), DMEA (N,N-Dimethylethanolamine), DEEA (Diethylethanolamine) and MAPA (N-Methyl-1,3-Diaminopropane). *Int. J. Greenhouse Gas Control* **2014**, *25*, 173–185.
- (46) Iloukhani, H.; Almasi, M. Densities and Excess Molar Volumes of Binary and Ternary Mixtures Containing Acetonitrile + Acetophenone + 1,2-Pentanediol: Experimental Data, Correlation and Prediction by PFP Theory and ERAS Model. *J. Solution Chem.* **2011**, *40*, 284–298.
- (47) Acevedo, I. L.; Pedrosa, G. C.; Katz, M. Excess Molar Volumes and Excess Viscosities of N-Butylamine + 1,4-Dioxane + Carbon Tetrachloride System at 298.15 K. *Can. J. Chem.* **1991**, *69*, 1006–1010.
- (48) Cibulka, I. Estimation of Excess Volume and Density of Ternary Liquid Mixtures of Non-Electrolytes from Binary Data. *Collect. Czech. Chem. Commun.* **1982**, *47*, 1414–1419.
- (49) Nagata, I.; Tamura, K. Excess Molar Enthalpies for the Methanol-1-Butanol-Benzene System at 25. Degree. *C. J. Chem. Eng. Data* **1988**, *33*, 283–285.
- (50) Redlich, O.; Kister, A. T. Algebraic Representation of Thermodynamic Properties and the Classification of Solutions. *Ind. Eng. Chem.* **1948**, *40*, 345–348.
- (51) Singh, P. P.; Nigam, R. K.; Sharma, S. P.; Aggarwal, S. Molar Excess Volumes of Ternary Mixtures of Nonelectrolytes. *Fluid Phase Equilib.* **1984**, *18*, 333–344.
- (52) Pinto, D. D. D.; Knuutila, H. K. Density Calculations of Aqueous Amine Solutions Using an Excess Gibbs Based Model. *Braz. J. Chem. Eng.* **2019**.



- (53) Arrhenius, S. Über Die Innere Reibung Verdünnter Wässeriger Lösungen. *Z. Phys. Chem.* **1887**, *1*, 285–298.
- (54) Grunberg, L.; Nissan, A. H. Mixture Law for Viscosity. *Nature* **1949**, *164*, 799–800.
- (55) Song, Y.; Mathias, P. M.; Tremblay, D.; Chen, C.-C. Liquid Viscosity Model for Polymer Solutions and Mixtures. *Ind. Eng. Chem. Res.* **2003**, *42*, 2415–2422.
- (56) Bingham, E. C.; Jackson, R. F. Standard Substances for the Calibration of Viscometers. *J. Wash. Acad. Sci.* **1917**, *7*, 53–55.
- (57) Spieweck, F.; Bettin, H. Review: Solid and Liquid Density Determination/Übersicht: Bestimmung Der Dichte von Festkörpern Und Flüssigkeiten. *TM, Tech. Mess.* **1992**, *59*, 285–292.
- (58) Yaws, C. L. *Yaws' Critical Property Data for Chemical Engineers and Chemists*; Knovel: Norwich, NY, 2012.
- (59) IAPWS R12-08: Viscosity of Ordinary Water. <http://www.iapws.org/relguide/viscosity.html> (accessed Jun 7, 2019).
- (60) Qunfang, L.; Yu-Chun, H. Correlation of Viscosity of Binary Liquid Mixtures. *Fluid Phase Equilib.* **1999**, *154*, 153–163.
- (61) Hartono, A.; Svendsen, H. F. Density, Viscosity, and Excess Properties of Aqueous Solution of Diethylenetriamine (DETA). *J. Chem. Thermodyn.* **2009**, *41*, 973–979.
- (62) Raffee, H. R.; Ranjbar, S.; Poursalman, F. Densities and Viscosities of Binary and Ternary Mixtures of Cyclohexanone, 1,4-Dioxane and Isooctane from T = (288.15 to 313.15)K. *J. Chem. Thermodyn.* **2012**, *54*, 266–271.
- (63) Eimer, D. *Gas Treating: Absorption Theory and Practice*; John Wiley & Sons, Inc.: Chichester, West Sussex, 2014.
- (64) Barzagli, F.; Lai, S.; Mani, F. Novel Non-Aqueous Amine Solvents for Reversible CO<sub>2</sub> Capture. *Energy Procedia* **2014**, *63*, 1795–1804.
- (65) Wang, X.; Kang, K.; Wang, W.; Tian, Y. Volumetric Properties of Binary Mixtures of 3-(Methylamino)Propylamine with Water, N-Methyldiethanolamine, N,N-Dimethylethanolamine, and N,N-Diethylethanolamine from (283.15 to 363.15) K. *J. Chem. Eng. Data* **2013**, *58*, 3430–3439.
- (66) Maham, Y.; Teng, T. T.; Hepler, L. G.; Mather, A. E. Densities, Excess Molar Volumes, and Partial Molar Volumes for Binary Mixtures of Water with Monoethanolamine, Diethanolamine, and Triethanolamine from 25 to 80 °C. *J. Solution Chem.* **1994**, *23*, 195–205.
- (67) Sathyanarayana, B.; Ranjithkumar, B.; Savitha Jyostna, T.; Satyanarayana, N. Densities and Viscosities of Binary Liquid Mixtures of N-Methylacetamide with Some Chloroethanes and Chloroethenes at T = 308.15 K. *J. Chem. Thermodyn.* **2007**, *39*, 16–21.

## Supporting Information

Density and Viscosity for the Non-aqueous and Aqueous Mixtures of  
Methyldiethanolamine and Monoethylene Glycol at Temperatures from  
283.15 K to 353.15 K

*Eirini Skylogianni, Ricardo R. Wanderley, Sigrid S. Austad, Hanna K. Knuutila\**

Department of Chemical Engineering, Norwegian University of Science and Technology, 7034  
Trondheim, Norway

\* Corresponding author. E-mail: [hanna.knuutila@ntnu.no](mailto:hanna.knuutila@ntnu.no)

### A. EXPERIMENTAL AND PREDICTED DENSITIES WITH NRTL-DVOL MODEL

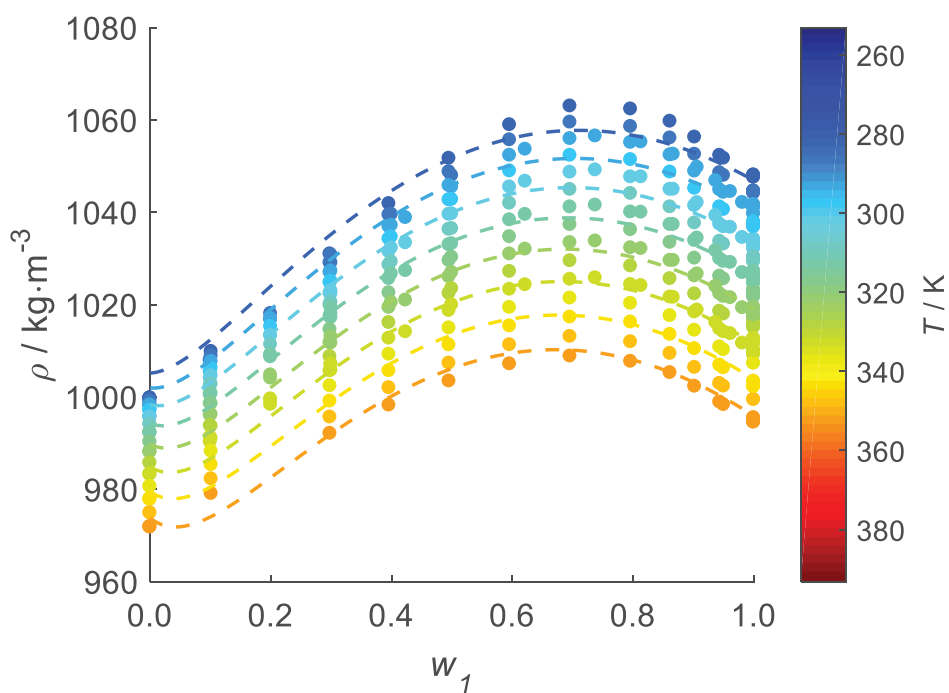


**Figure S1.** Binary data-set of densities for MDEA (1) – water (3) mixtures and estimations generated by the NRTL-DVOL model. The temperature in which each experimental point (●) was measured is color-coded by the bar on the right side. The temperatures in which the estimates were made were 283.15 K (dark blue dashed line), 293.15 K (denim blue dashed line), 303.15 K (light blue dashed line), 313.15 K (aqua dashed line), 323.15 K (green dashed line), 333.15 K (lime green dashed line), 343.15 K (yellow dashed line) and 353.15 K (orange dashed line).

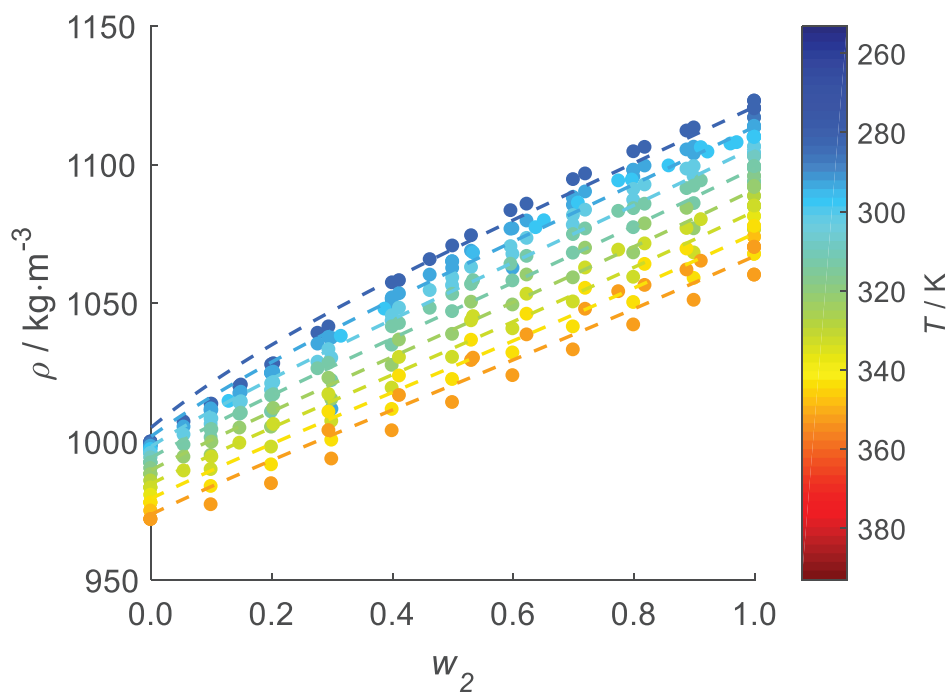


**Figure S2.** Binary data-set of densities for MEG (2)–water (3) mixtures and estimations generated by the NRTL-DVOL model. The temperature in which each experimental point (●) was measured is color-coded by the bar on the right side. The temperatures in which the estimates were made were 283.15 K (dark blue dashed line), 293.15 K (denim blue dashed line), 303.15 K (light blue dashed line), 313.15 K (aqua dashed line), 323.15 K (green dashed line), 333.15 K (lime green dashed line), 343.15 K (yellow dashed line) and 353.15 K (orange dashed line).

These figures do not show data obtained at temperatures below 283.15 K nor above 353.15 K, although such data points were employed in the parametrization. Remarkably, the scatter of binary MEG-water density data exhibited in **Figure S2** (more evident at high temperatures such as 343.15

K and 353.15 K) is one of the main reasons for the worse performance of the NRTL-DVOL model in this scenario. The relatively large amount of data at higher temperatures, where data gathering is certainly more difficult and prone to uncertainties, could be another cause for deviations.

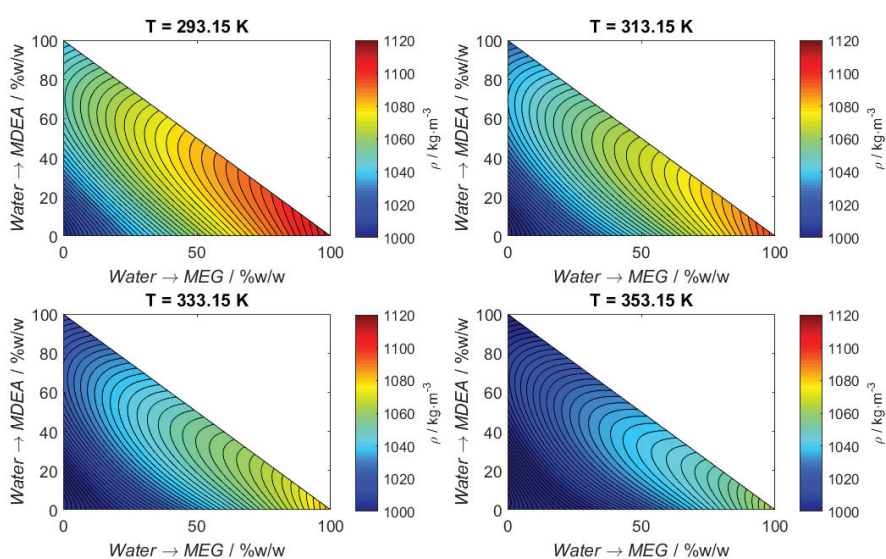


**Figure S3.** Density plots for MDEA-MEG-water ternary mixtures in four different temperatures (293.15 K, 313.15 K, 333.15 K and 353.15 K). The density values are color-coded by the bar on the right side.

The ability of the model to estimate the density and describe its behavior with temperature and composition is perceptible by the  $\rho$ - $w$ - $T$  graphs for the binary system. This is not possible by the figures generated for the ternary system, therefore the modelled values and Absolute Relative Deviations (ARDs) are provided in **Table S1** below.

**Table S1:** Experimental and Predicted Values of Density  $\rho / \text{kg}\cdot\text{m}^{-3}$  for {MDEA (1) + MEG (2) + Water (3)}

$T / \text{K}$	$w_1$	$w_2$	$\rho / \text{kg}\cdot\text{m}^{-3}$	$\hat{\rho} / \text{kg}\cdot\text{m}^{-3}$	ARD%
283.15	$0.050 \pm 0.002$	$0.900 \pm 0.003$	1114.1	1112.0	0.19
	$0.900 \pm 0.013$	$0.050 \pm 0.010$	1057.6	1055.3	0.21
	$0.300 \pm 0.003$	$0.600 \pm 0.003$	1096.6	1094.8	0.17
	$0.600 \pm 0.006$	$0.300 \pm 0.006$	1078.5	1078.2	0.03
	$0.100 \pm 0.002$	$0.600 \pm 0.002$	1090.1	1086.7	0.31
	$0.300 \pm 0.003$	$0.400 \pm 0.003$	1081.2	1080.3	0.09
	$0.600 \pm 0.006$	$0.100 \pm 0.006$	1067.8	1065.1	0.26
	$0.250 \pm 0.002$	$0.250 \pm 0.002$	1061.0	1062.9	0.18
298.15	$0.050 \pm 0.002$	$0.900 \pm 0.003$	1103.7	1100.9	0.25
	$0.900 \pm 0.013$	$0.050 \pm 0.010$	1046.3	1045.4	0.08
	$0.300 \pm 0.003$	$0.600 \pm 0.003$	1086.1	1084.3	0.16
	$0.600 \pm 0.006$	$0.300 \pm 0.006$	1067.6	1068.3	0.06
	$0.100 \pm 0.002$	$0.600 \pm 0.002$	1080.5	1076.3	0.39
	$0.300 \pm 0.003$	$0.400 \pm 0.003$	1071.2	1071.1	0.02
	$0.600 \pm 0.006$	$0.100 \pm 0.006$	1057.4	1056.0	0.12
	$0.250 \pm 0.002$	$0.250 \pm 0.002$	1052.2	1054.3	0.20
313.15	$0.050 \pm 0.002$	$0.900 \pm 0.003$	1093.1	1089.6	0.32
	$0.900 \pm 0.013$	$0.050 \pm 0.010$	1034.8	1035.0	0.02
	$0.300 \pm 0.003$	$0.600 \pm 0.003$	1075.1	1073.6	0.14
	$0.600 \pm 0.006$	$0.300 \pm 0.006$	1056.3	1057.9	0.15
	$0.100 \pm 0.002$	$0.600 \pm 0.002$	1070.3	1066.1	0.40
	$0.300 \pm 0.003$	$0.400 \pm 0.003$	1060.9	1061.7	0.08
	$0.600 \pm 0.006$	$0.100 \pm 0.006$	1046.5	1046.5	0.01
	$0.250 \pm 0.002$	$0.250 \pm 0.002$	1043.2	1045.7	0.24
323.15	$0.050 \pm 0.002$	$0.900 \pm 0.003$	1086.4	1082.0	0.40
	$0.900 \pm 0.013$	$0.050 \pm 0.010$	1027.5	1027.8	0.03
	$0.300 \pm 0.003$	$0.600 \pm 0.003$	1068.2	1066.3	0.17
	$0.600 \pm 0.006$	$0.300 \pm 0.006$	1049.1	1050.8	0.16
	$0.100 \pm 0.002$	$0.600 \pm 0.002$	1063.4	1059.3	0.39
	$0.300 \pm 0.003$	$0.400 \pm 0.003$	1053.8	1055.3	0.14
	$0.600 \pm 0.006$	$0.100 \pm 0.006$	1039.4	1040.0	0.05

	$0.250 \pm 0.002$	$0.250 \pm 0.002$	1036.6	1039.8	0.31
333.15	$0.050 \pm 0.002$	$0.900 \pm 0.003$	1079.1	1074.2	0.46
	$0.900 \pm 0.013$	$0.050 \pm 0.010$	1019.8	1020.3	0.06
	$0.300 \pm 0.003$	$0.600 \pm 0.003$	1060.7	1058.9	0.17
	$0.600 \pm 0.006$	$0.300 \pm 0.006$	1041.5	1043.4	0.19
	$0.100 \pm 0.002$	$0.600 \pm 0.002$	1056.7	1052.5	0.40
	$0.300 \pm 0.003$	$0.400 \pm 0.003$	1047.0	1048.9	0.18
	$0.600 \pm 0.006$	$0.100 \pm 0.006$	1031.7	1033.1	0.14
	$0.250 \pm 0.002$	$0.250 \pm 0.002$	1030.5	1033.8	0.33
343.15	$0.050 \pm 0.002$	$0.900 \pm 0.003$	1071.8	1066.3	0.52
	$0.900 \pm 0.013$	$0.050 \pm 0.010$	1011.9	1012.7	0.07
	$0.300 \pm 0.003$	$0.600 \pm 0.003$	1053.2	1051.3	0.18
	$0.600 \pm 0.006$	$0.300 \pm 0.006$	1033.6	1035.9	0.22
	$0.100 \pm 0.002$	$0.600 \pm 0.002$	1049.4	1045.7	0.36
	$0.300 \pm 0.003$	$0.400 \pm 0.003$	1039.5	1042.3	0.27
	$0.600 \pm 0.006$	$0.100 \pm 0.006$	1023.7	1026.1	0.23
	$0.250 \pm 0.002$	$0.250 \pm 0.002$	1023.5	1027.8	0.42
353.15	$0.050 \pm 0.002$	$0.900 \pm 0.003$	1064.5	1058.2	0.59
	$0.900 \pm 0.013$	$0.050 \pm 0.010$	1004.2	1004.8	0.06
	$0.300 \pm 0.003$	$0.600 \pm 0.003$	1045.6	1043.6	0.20
	$0.600 \pm 0.006$	$0.300 \pm 0.006$	1025.8	1028.1	0.23
	$0.100 \pm 0.002$	$0.600 \pm 0.002$	1042.1	1038.9	0.31
	$0.300 \pm 0.003$	$0.400 \pm 0.003$	1031.8	1035.6	0.36
	$0.600 \pm 0.006$	$0.100 \pm 0.006$	1015.7	1018.9	0.31
	$0.250 \pm 0.002$	$0.250 \pm 0.002$	1016.1	1021.5	0.53

## B. EXPERIMENTAL AND PREDICTED VISCOSITIES WITH NRTL-DVIS MODEL

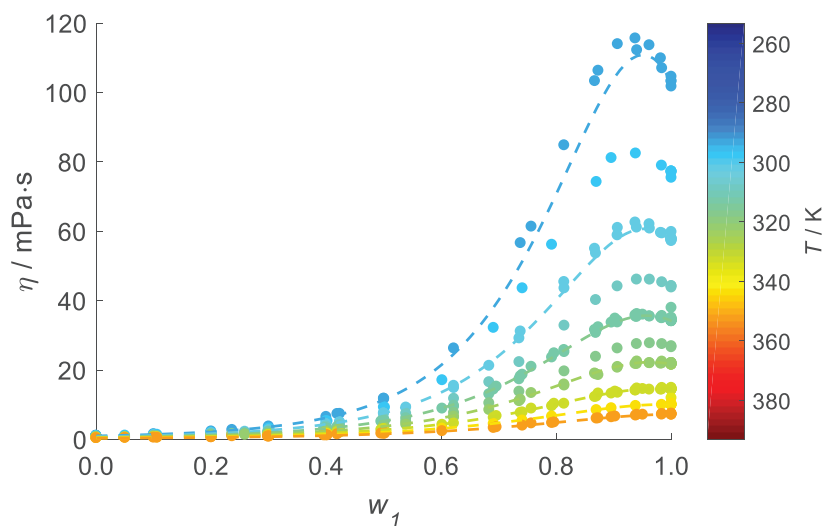


**Figure S4.** Binary data-set of viscosities for MDEA (1) – water (3) mixtures and estimations generated by the NRTL-DVIS model. The temperature in which each experimental point (●) was measured is color-coded by the bar on the right side. The temperatures in which the estimates were made were 293.15 K (denim blue dashed line), 303.15 K (light blue dashed line), 313.15 K (aqua dashed line), 323.15 K (green dashed line), 333.15 K (lime green dashed line), 343.15 K (yellow dashed line) and 353.15 K (orange dashed line).



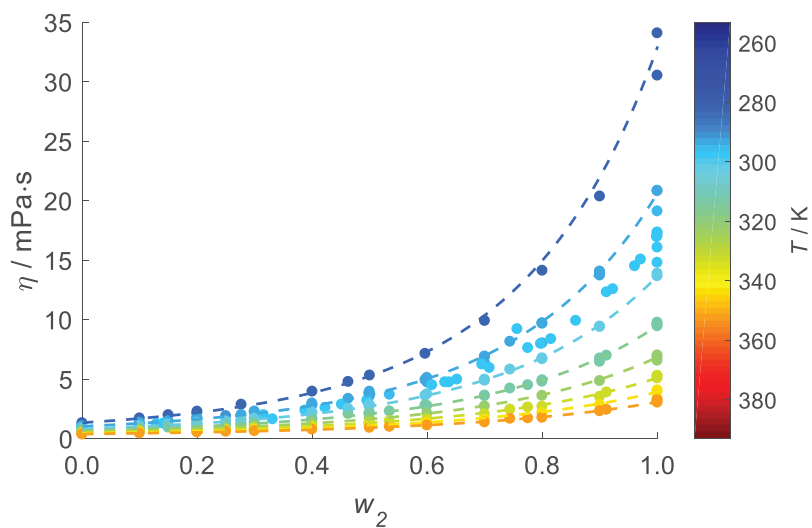


**Figure S5.** Binary data-set of viscosities for MEG (2) – water (3) mixtures and estimations generated by the NRTL-DVIS model. The temperature in which each experimental point (●) was measured is color-coded by the bar on the right side. The temperatures in which the estimates were made were 283.15 K (dark blue dashed line), 293.15 K (denim blue dashed line), 303.15 K (light blue dashed line), 313.15 K (aqua dashed line), 323.15 K (green dashed line), 333.15 K (lime green dashed line), 343.15 K (yellow dashed line) and 353.15 K (orange dashed line).

The ability of the model to estimate the viscosity and describe its behavior with temperature and composition is perceptible by the  $\eta$ - $w$ - $T$  graphs for the binary system. This is not possible by the figures generated for the ternary system, therefore the modelled values and Absolute Relative Deviations (ARDs) are provided in **Table S2** below.

**Table S2:** Experimental and Predicted Values of Viscosity  $\eta$  / mPa·s for {MDEA (1) + MEG (2) + Water (3)}

$T$ /K	$w_1$	$w_2$	$\eta$ / mPa·s	$\hat{\eta}$ / mPa·s	ARD%
283.15	$0.050 \pm 0.002$	$0.900 \pm 0.003$	30.53	30.49	0.13
	$0.900 \pm 0.013$	$0.050 \pm 0.010$	204.00	195.32	4.25
	$0.300 \pm 0.003$	$0.600 \pm 0.003$	47.11	45.75	2.89
	$0.600 \pm 0.006$	$0.300 \pm 0.006$	103.16	90.54	12.23
	$0.100 \pm 0.002$	$0.600 \pm 0.002$	13.00	13.65	5.00
	$0.300 \pm 0.003$	$0.400 \pm 0.003$	22.37	22.88	2.31
	$0.600 \pm 0.006$	$0.100 \pm 0.006$	58.91	50.84	13.70
	$0.250 \pm 0.002$	$0.250 \pm 0.002$	9.75	10.76	10.34
298.15	$0.050 \pm 0.002$	$0.900 \pm 0.003$	15.80	15.48	2.03
	$0.900 \pm 0.013$	$0.050 \pm 0.010$	79.59	73.76	7.32
	$0.300 \pm 0.003$	$0.600 \pm 0.003$	22.47	21.72	3.33
	$0.600 \pm 0.006$	$0.300 \pm 0.006$	43.92	38.73	11.81
	$0.100 \pm 0.002$	$0.600 \pm 0.002$	7.27	7.42	2.10
	$0.300 \pm 0.003$	$0.400 \pm 0.003$	11.52	11.60	0.72
	$0.600 \pm 0.006$	$0.100 \pm 0.006$	25.09	23.10	7.95
	$0.250 \pm 0.002$	$0.250 \pm 0.002$	5.33	5.92	11.07
313.15	$0.050 \pm 0.002$	$0.900 \pm 0.003$	9.02	8.82	2.24
	$0.900 \pm 0.013$	$0.050 \pm 0.010$	34.90	33.00	5.44
	$0.300 \pm 0.003$	$0.600 \pm 0.003$	12.01	11.69	2.65
	$0.600 \pm 0.006$	$0.300 \pm 0.006$	20.96	19.10	8.85
	$0.100 \pm 0.002$	$0.600 \pm 0.002$	4.40	4.48	1.78
	$0.300 \pm 0.003$	$0.400 \pm 0.003$	6.44	6.58	2.24
	$0.600 \pm 0.006$	$0.100 \pm 0.006$	12.15	11.86	2.36
	$0.250 \pm 0.002$	$0.250 \pm 0.002$	3.25	3.59	10.41
323.15	$0.050 \pm 0.002$	$0.900 \pm 0.003$	6.49	6.37	1.87
	$0.900 \pm 0.013$	$0.050 \pm 0.010$	21.70	20.77	4.30
	$0.300 \pm 0.003$	$0.600 \pm 0.003$	8.32	8.16	1.94
	$0.600 \pm 0.006$	$0.300 \pm 0.006$	13.60	12.67	6.80
	$0.100 \pm 0.002$	$0.600 \pm 0.002$	3.36	3.35	0.28
	$0.300 \pm 0.003$	$0.400 \pm 0.003$	4.73	4.73	0.05
	$0.600 \pm 0.006$	$0.100 \pm 0.006$	8.18	8.02	2.00

	$0.250 \pm 0.002$	$0.250 \pm 0.002$	2.45	2.68	9.35
333.15	$0.050 \pm 0.002$	$0.900 \pm 0.003$	4.86	4.76	2.11
	$0.900 \pm 0.013$	$0.050 \pm 0.010$	14.25	13.70	3.86
	$0.300 \pm 0.003$	$0.600 \pm 0.003$	6.03	5.90	2.06
	$0.600 \pm 0.006$	$0.300 \pm 0.006$	9.33	8.75	6.19
	$0.100 \pm 0.002$	$0.600 \pm 0.002$	2.57	2.58	0.19
	$0.300 \pm 0.003$	$0.400 \pm 0.003$	3.51	3.51	0.05
	$0.600 \pm 0.006$	$0.100 \pm 0.006$	5.75	5.60	2.57
	$0.250 \pm 0.002$	$0.250 \pm 0.002$	1.92	2.06	7.11
343.15	$0.050 \pm 0.002$	$0.900 \pm 0.003$	9.76	3.65	62.57
	$0.900 \pm 0.013$	$0.050 \pm 0.010$	3.76	9.41	150.61
	$0.300 \pm 0.003$	$0.600 \pm 0.003$	4.50	4.40	2.26
	$0.600 \pm 0.006$	$0.300 \pm 0.006$	6.63	6.25	5.72
	$0.100 \pm 0.002$	$0.600 \pm 0.002$	2.04	2.03	0.52
	$0.300 \pm 0.003$	$0.400 \pm 0.003$	2.70	2.67	1.03
	$0.600 \pm 0.006$	$0.100 \pm 0.006$	4.15	4.03	2.97
	$0.250 \pm 0.002$	$0.250 \pm 0.002$	1.55	1.62	4.56
353.15	$0.050 \pm 0.002$	$0.900 \pm 0.003$	2.97	2.87	3.24
	$0.900 \pm 0.013$	$0.050 \pm 0.010$	6.96	6.69	3.79
	$0.300 \pm 0.003$	$0.600 \pm 0.003$	3.47	3.37	2.95
	$0.600 \pm 0.006$	$0.300 \pm 0.006$	4.88	4.59	5.94
	$0.100 \pm 0.002$	$0.600 \pm 0.002$	1.66	1.64	1.33
	$0.300 \pm 0.003$	$0.400 \pm 0.003$	2.13	2.08	2.21
	$0.600 \pm 0.006$	$0.100 \pm 0.006$	3.12	2.97	4.79
	$0.250 \pm 0.002$	$0.250 \pm 0.002$	1.26	1.29	2.97

C. EXPERIMENTAL AND PREDICTED VISCOSITIES WITH ASPEN LIQUID MIXTURE  
VISCOSITY MODEL

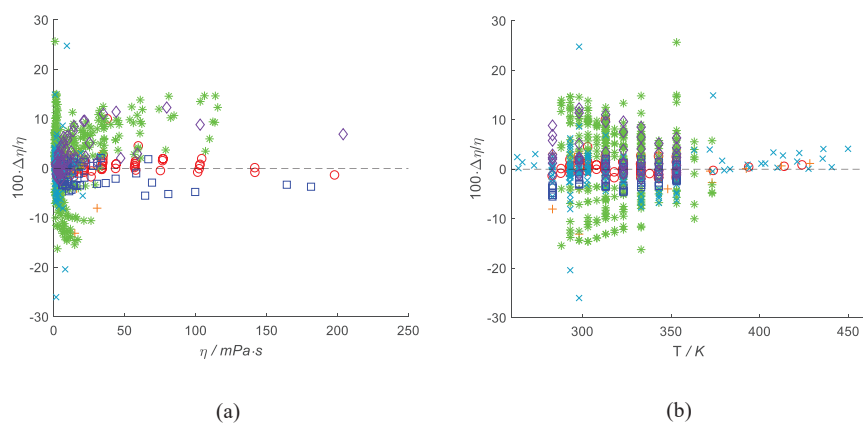


**Figure S6.** Deviations in terms of differences between experimental and estimated viscosities divided by experimental viscosities regarding estimations made with the Aspen liquid mixture viscosity model, and how they vary with the experimental viscosities themselves (a) and with temperature (b). The data-sets are distributed in terms of pure MDEA data (red  $\circ$ ), pure MEG data (orange  $+$ ), binary MDEA-water data (green  $*$ ), binary MEG-water data (cyan  $\times$ ), binary MDEA-MEG data (blue  $\square$ ) and ternary data (purple  $\diamond$ ).

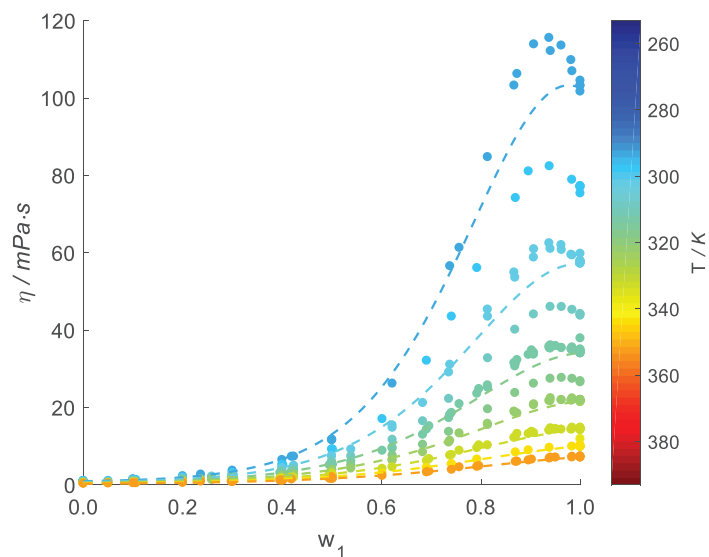


**Figure S7.** Binary data-set of viscosities for MDEA (1) – water (3) mixtures and estimations generated by the Aspen liquid mixture viscosity model. The temperature in which each experimental point (●) was measured is color-coded by the bar on the right side. The temperatures in which the estimates were made were 293.15 K (denim blue dashed line), 303.15 K (light blue dashed line), 313.15 K (aqua dashed line), 323.15 K (green dashed line), 333.15 K (lime green dashed line), 343.15 K (yellow dashed line) and 353.15 K (orange dashed line).

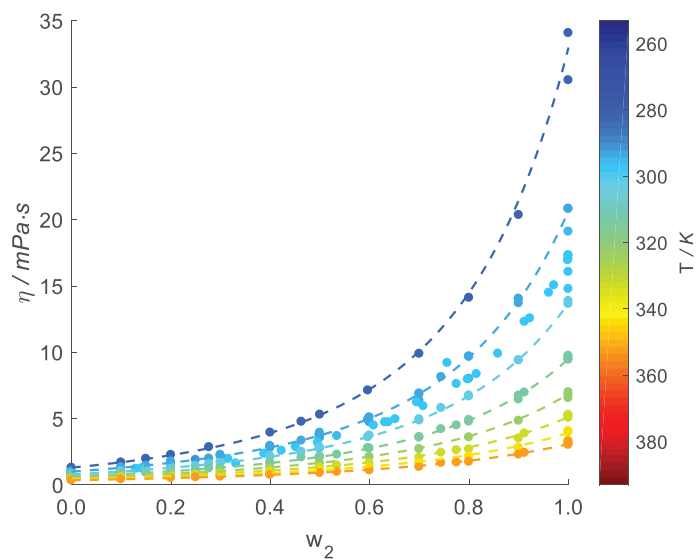


**Figure S8.** Binary data-set of viscosities for MEG (2) – water (3) mixtures and estimations generated by the Aspen liquid mixture viscosity model. The temperature in which each experimental point (●) was measured is color-coded by the bar on the right side. The temperatures in which the estimates were made were 283.15 K (dark blue dashed line), 293.15 K (denim blue dashed line), 303.15 K (light blue dashed line), 313.15 K (aqua dashed line), 323.15 K (green dashed line), 333.15 K (lime green dashed line), 343.15 K (yellow dashed line) and 353.15 K (orange dashed line).

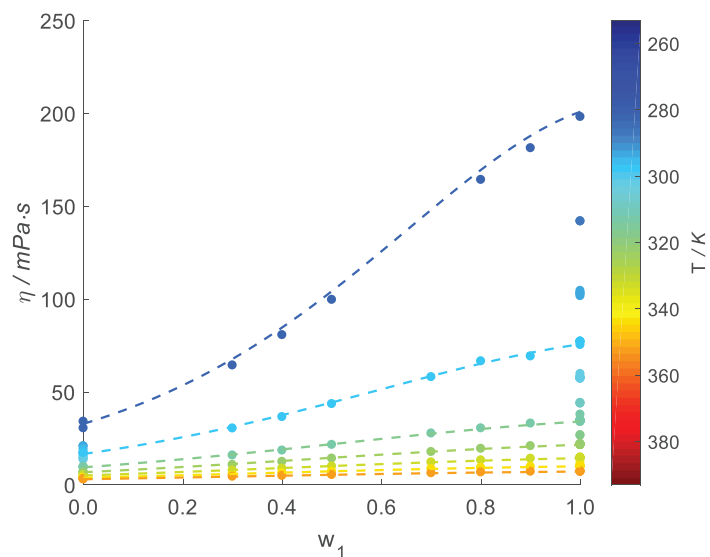


**Figure S9.** Binary data-set of viscosities for MDEA (1) – MEG (2) mixtures and estimations generated by the Aspen liquid mixture viscosity model. The temperature in which each experimental point (●) was measured is color-coded by the bar on the right side. The temperatures in which the estimates were made were 283.15 K (dark blue dashed line), 298.15 K (capri blue dashed line), 313.15 K (aqua dashed line), 323.15 K (green dashed line), 333.15 K (lime green dashed line), 343.15 K (yellow dashed line) and 353.15 K (orange dashed line).

## D. UNCERTAINTY ANALYSIS

### Uncertainty of Composition

1. Expressed in weight basis (weight fraction,  $w$ )

a. Binary system, where MDEA (1) and MEG (2).

The standard uncertainty of the weight fractions of a binary mixture is the same for each component. Given that the weight fraction is given by:

$$w_1 = \frac{m_1}{m_1 + m_2} \quad (1)$$

where  $m$ : mass. Using the Law of propagation of uncertainty, the uncertainty in weight fractions is defined as:

$$u(w_1) = \left(\frac{\partial w_1}{\partial m_1}\right)^2 u(m_1) + \left(\frac{\partial w_1}{\partial m_2}\right)^2 u(m_2) \quad (2)$$

The uncertainty is found:

$$u(w) = u(w_1) = u(w_2) = \frac{u(m)}{(m_1 + m_2)^2} \sqrt{m_1^2 + m_2^2} \quad (3)$$

where  $u(m)$  is the uncertainty of the mass.

b. Ternary system, where MDEA (1), MEG (2) and H<sub>2</sub>O (3).

Similarly, the uncertainty of the weight fractions of a ternary system are found to be:

$$u(w_1) = \frac{u(m)}{(m_1 + m_2 + m_3)^2} \sqrt{2 m_1^2 + (m_2 + m_3)^2} \quad (4)$$

$$u(w_2) = \frac{u(m)}{(m_1 + m_2 + m_3)^2} \sqrt{2 m_2^2 + (m_1 + m_3)^2} \quad (5)$$

$$u(w_3) = \frac{u(m)}{(m_1 + m_2 + m_3)^2} \sqrt{2 m_3^2 + (m_1 + m_2)^2} \quad (6)$$



2. Expressed in molar basis (mole fraction,  $x$ )

a. Binary system, where MDEA (1) and MEG (2).

The standard uncertainty of the molar fractions of a binary mixture is the same for each component. Given that the molar fraction is:

$$x_1 = \frac{\frac{m_1}{M_1}}{\frac{m_1}{M_1} + \frac{m_2}{M_2}} = \frac{m_1 M_2}{m_1 M_2 + m_2 M_1} \quad (7)$$

where  $m$ : mass and  $M$ : molecular weight, following the same methodology as before, the uncertainty is found to be:

$$u(x_1) = u(x_2) = \frac{M_1 M_2}{(m_1 M_2 + m_2 M_1)^2} u(m) \sqrt{m_1^2 + m_2^2} \quad (8)$$

b. Ternary system, where MDEA (1), MEG (2) and H<sub>2</sub>O (3).

The uncertainty of the molar fractions of a ternary system found to be:

$$u(x_1) = \frac{u(m)}{(m_1 M_2 M_3 + m_2 M_1 M_3 + m_3 M_1 M_2)^2} \dots$$

$$\dots \sqrt{(m_2 M_1 M_2 M_3^2 + m_3 M_1 M_2^2 M_3)^2 + (m_1 M_1 M_2 M_3^2)^2 + (m_1 M_1 M_2^2 M_3)^2} \quad (9)$$

$$u(x_2) = \frac{u(m)}{(m_1 M_2 M_3 + m_2 M_1 M_3 + m_3 M_1 M_2)^2} \dots$$

$$\dots \sqrt{(m_1 M_1 M_2 M_3^2 + m_3 M_1^2 M_2 M_3)^2 + (m_2 M_1 M_2 M_3^2)^2 + (m_2 M_1 M_2^2 M_3)^2} \quad (10)$$

$$u(x_3) = \frac{u(m)}{(m_1 M_2 M_3 + m_2 M_1 M_3 + m_3 M_1 M_2)^2} \dots$$

$$\dots \sqrt{(m_1 M_1 M_2^2 M_3 + m_2 M_1^2 M_2 M_3)^2 + (m_3 M_1 M_2^2 M_3)^2 + (m_3 M_1^2 M_2^2)^2} \quad (11)$$

The combined standard uncertainty of the mass includes both the accuracy of the scale,  $u_{scale}(m) = 1 \cdot 10^{-6}$  kg, and the purity of the chemicals used. It is calculated by the equation:

$$u(m) = \sqrt{u_{scale}^2(m) + u_{purity,i}^2(m)} \quad (12)$$

$u_{\text{purity}}(m)$  is calculated for each component, and it is equal to  $a/\sqrt{3}$  assuming uniform distribution is followed, given that no further information is available. The numerator,  $a$ , is the maximum deviation from the measured value, i.e. purity%·mass. Therefore, for each system a different  $u(m)$  is estimated. It is assumed that the water used in this work is 100% pure.

The calculated uncertainties are presented in **Table S3** and **Table S4**.

**Table S3:** Composition in Weight Fraction  $w$  and Molar Fraction  $x$  and their Standard Uncertainties for {MDEA (1) + MEG (2)}

$w_1$	$u(w_1) = u(w_2)$	$x_1$	$u(x_1) = u(x_2)$
0.000	0.000	0.000	0.000
0.300	0.001	0.183	0.001
0.400	0.002	0.258	0.001
0.500	0.002	0.342	0.002
0.700	0.003	0.549	0.004
0.800	0.004	0.676	0.005
0.900	0.005	0.824	0.008
1.000	0.006	1.000	0.011

**Table S4:** Composition in Weight Fraction  $w$  and Molar Fraction  $x$  and their Standard Uncertainties for {MDEA (1) + MEG (2) + Water (3)}

$w_1$	$w_2$	$w_3$	$u(w_1)$	$u(w_2)$	$u(w_3)$	$x_1$	$x_2$	$x_3$	$u(x_1)$	$u(x_2)$	$u(x_3)$
0.050	0.900	0.050	0.001	0.001	0.001	0.024	0.820	0.156	0.001	0.002	0.003
0.900	0.050	0.050	0.007	0.005	0.005	0.677	0.072	0.250	0.018	0.007	0.020
0.300	0.600	0.100	0.002	0.002	0.002	0.142	0.545	0.313	0.001	0.002	0.004
0.600	0.300	0.101	0.003	0.003	0.003	0.326	0.313	0.361	0.004	0.003	0.009
0.100	0.600	0.300	0.001	0.001	0.001	0.031	0.356	0.613	0.000	0.000	0.001
0.300	0.400	0.300	0.001	0.001	0.001	0.098	0.252	0.650	0.001	0.001	0.003
0.600	0.100	0.300	0.003	0.003	0.003	0.216	0.069	0.715	0.002	0.002	0.006
0.250	0.250	0.500	0.001	0.001	0.001	0.062	0.119	0.819	0.000	0.001	0.002

## Uncertainty of Density $\rho$

In accordance to the NIST Requirements for Data Tables, the combined expanded uncertainty  $U(\rho)$  with level of confidence 0.95 was calculated for the density;  $U(\rho) = 2 \cdot u(\rho)$ .

In order to take into account both uncertainty deriving from the repeatability of the measurement,  $u_{rep}(\rho)$ , as well as the uncertainty deriving from the instrument calibration,  $u_{cal}(\rho)$ , the uncertainty of density is calculated according to:

$$u(\rho) = \sqrt{u_{rep}^2(\rho) + u_{cal}^2(\rho)} \quad (13)$$

The repeatability is calculated by the standard deviation of the means. The uncertainty of the calibration is calculated by the equation below, taking into account both the repeatability of the calibration measurements,  $u_{cal,rep}(\rho)$ , and their accuracy  $u_{cal,ref}(\rho)$  against the reference fluid. Water was used as the reference fluid for the calibration.

$$u_{cal}(\rho) = \sqrt{u_{cal,rep}^2(\rho) + u_{cal,ref}^2(\rho)} \quad (14)$$

The repeatability in the calibration measurements is calculated by the standard deviation of the means, while for the uncertainty of the calibration a Uniform Distribution (Type B) is assumed. It is found that the contribution of  $u_{cal,ref}$  and  $u_{cal,rep}$  to  $u_{cal}(\rho)$  are similar. Moreover,  $u_{cal}(\rho)$  was the main contributor to  $u(\rho)$  since the repeatability of the density was excellent.

The results of the uncertainty analysis for the density measurements are given in **Table S5**.

**Table S5:** Maximum uncertainty for the Density  $u(\rho) / \text{kg}\cdot\text{m}^{-3}$  as a Function of Temperature  $T$ .

$T/\text{K}$	$u_{rep}(\rho)$	$u_{cal}(\rho)$	$u(\rho)$	$U(\rho)$
283.15	0.005	0.104	0.104	0.209
298.15	0.130	0.078	0.151	0.303
313.15	0.146	0.065	0.160	0.319
323.15	0.010	0.292	0.292	0.584
333.15	0.010	0.350	0.350	0.701
343.15	0.005	0.349	0.349	0.699
353.15	0.052	0.468	0.471	0.942

## Uncertainty of Viscosity $\eta$

In accordance to the NIST Requirements for Data Tables, the combined expanded uncertainty  $U(\eta)$  with level of confidence 0.95 was calculated;  $U(\eta) = 2 \cdot u(\eta)$ .

The method used for uncertainty calculations is similar to the method presented for the uncertainty of density. The main difference is that pure MDEA and pure MEG were used as reference fluids, due to the large viscosity range covered in this work and because those are the main components of the systems studied. The same method is used for both instruments employed in this work, namely a LOVIS 2000 M microviscometer and an Anton Paar MCR 100 rheometer.

The uncertainty of viscosity is calculated according to:

$$u(\eta) = \sqrt{u_{rep}^2(\eta) + u_{cal}^2(\eta)} \quad (15)$$

The repeatability is calculated by the standard deviation of the means. The uncertainty of the calibration is calculated by the equation below, taking into account both the repeatability of the calibration measurements,  $u_{cal,rep}(\eta)$ , and their accuracy  $u_{cal,ref}(\eta)$  against the reference fluids.

$$u_{cal}(\rho) = \sqrt{u_{cal,rep}^2(\eta) + u_{cal,ref}^2(\eta)} \quad (16)$$

The repeatability in the calibration measurements is calculated by the standard deviation of the means, while for the uncertainty of the calibration a Uniform Distribution (Type B) is assumed. The contribution of  $u_{cal,ref}$  is the main contribution to  $u_{cal}(\eta)$ .

The results of the uncertainty analysis for the viscosity are given in **Table S6** and **Table S7**.

**Table S6:** Maximum uncertainty for the Viscosity  $u(\eta)$  / mPa·s using the LOVIS 2000 M microviscometer as a Function of Temperature  $T$ .

$T/K$	$u_{rep}(\eta)$	$u_{cal}(\eta)$	$u(\eta)$	$U(\eta)$
283.15	0.116	2.262	2.265	4.530
298.15	0.044	0.540	0.542	1.084
313.15	0.142	0.518	0.522	1.075
323.15	0.092	0.168	0.192	0.383
333.15	0.008	0.234	0.235	0.469
343.15	0.130	0.229	0.264	0.528
353.15	0.008	0.153	0.153	0.306

**Table S7:** Maximum uncertainty for the Viscosity  $u(\eta)$  / mPa·s using the Anton Paar MCR 100 rheometer as a Function of Temperature  $T$ .

$T/K$	$u_{rep}(\eta)$	$u_{cal}(\eta)$	$u(\eta)$	$U(\eta)$
283.15	1.507	2.031	2.529	5.059
298.15	0.136	1.305	1.312	2.625
313.15	0.029	0.242	0.244	0.487
323.15	-	-	-	-
333.15	-	-	-	-
343.15	-	-	-	-
353.15	-	-	-	-

### Uncertainty of Excess Molar Volume $v^E$

According to the Law of propagation of uncertainty, and given that the excess molar volume  $v^E$  for the binary {MDEA (1) + MEG (2)} was calculated by Equation (17):

$$v^E = M_1 x_1 \left( \frac{1}{\rho} - \frac{1}{\rho_1} \right) + M_2 x_2 \left( \frac{1}{\rho} - \frac{1}{\rho_2} \right) \quad (17)$$

the uncertainty can be calculated by:

$$u(v^E) = \left( \left( \frac{M_1 x_1 + M_2 x_2}{\rho^2} \right)^2 u(\rho)^2 + \left( M_1 \left( \frac{1}{\rho} - \frac{1}{\rho_1} \right) u(x_1) \right)^2 + \left( M_2 \left( \frac{1}{\rho} - \frac{1}{\rho_2} \right) u(x_2) \right)^2 + \left( \frac{M_1 x_1}{\rho_1^2} u(\rho_1) \right)^2 + \left( \frac{M_2 x_2}{\rho_2^2} u(\rho_2) \right)^2 \right)^{1/2} \quad (18)$$

For the ternary {MDEA (1) + MEG (2) + H<sub>2</sub>O (3)}, the corresponding equation is:

$$u(v^E) = \left( \left( \frac{M_1 x_1 + M_2 x_2 + M_3 x_3}{\rho^2} \right)^2 u(\rho)^2 + \left( M_1 \left( \frac{1}{\rho} - \frac{1}{\rho_1} \right) u(x_1) \right)^2 + \left( M_2 \left( \frac{1}{\rho} - \frac{1}{\rho_2} \right) u(x_2) \right)^2 + \left( M_3 \left( \frac{1}{\rho} - \frac{1}{\rho_3} \right) u(x_3) \right)^2 + \left( \frac{M_1 x_1}{\rho_1^2} u(\rho_1) \right)^2 + \left( \frac{M_2 x_2}{\rho_2^2} u(\rho_2) \right)^2 + \left( \frac{M_3 x_3}{\rho_3^2} u(\rho_3) \right)^2 \right)^{1/2} \quad (19)$$

### Uncertainty of Viscosity Deviations $\Delta\eta$

According to the Law of propagation of uncertainty, and given that the viscosity deviation of the mixture was calculated by Equation (20):

$$\Delta\eta = \eta + \eta^{id} = \eta + \sum_1^{N_C} x_i \ln(\eta_i) \quad (20)$$

the uncertainty for the binary and the ternary can be calculated by the generic equation:

$$u(\Delta\eta) = \sqrt{\left( u(\eta)^2 + \left( \sum_1^{N_C} x_i \ln(\eta_i) \right)^2 \sum_1^{N_C} \ln(\eta_i)^2 u(x_i)^2 + \frac{x_i^2}{\eta_i^2} u(\eta_i)^2 \right)} \quad (21)$$

## 3.2 Further considerations

The work presented in section 3.1 provides measurements of density and viscosity of unloaded non-aqueous and aqueous MDEA-MEG systems at ambient pressure and temperatures relevant for subsea application. Based on the obtained data and data reported in the literature, a predictive model was developed for density and viscosity. Both properties are important for the design and operation of this process, however, viscosity requires special attention because it can be a showstopper if its value is outside the operation range of the processing equipment.

In this process, the solvent would be injected in the pipeline, dispersed in the gas stream with a mixer, separated from the gas stream possibly in a scrubber, then boosted at the nearest platform for topside regeneration and, at last, transported through the umbilical line to the injection point for reuse. Therefore, the data and model in this work concern mainly the conditions of the transportation of the fluid from the regeneration to the injection point and mainly the pumping specifications. Viscosity information of the H<sub>2</sub>S-loaded solvent would be beneficial for defining the requirements of the scrubber and possible boosting system to the topside facility. Due to the material incompatibility of the components of the density meter and viscometer used in this work with hydrogen sulfide, measurements of the loaded systems were not performed.

However, it has been reported in the literature that the viscosity of aqueous MDEA decreases upon hydrogen sulfide absorption, contrary to the typical viscosity increase observed in CO<sub>2</sub>-loaded alkanolamine solutions (Fu et al., 2012; Pinto et al., 2017; Shokouhi et al., 2015; Weiland et al., 1998). To the author's best knowledge, there are only two available literature sources for H<sub>2</sub>S-loaded MDEA-H<sub>2</sub>O solution; the works of Rinker and co-workers (Rinker et al., 2000) and Shokouhi and Ahmadi (Shokouhi and Ahmadi, 2016). Rinker et al. measured density and viscosity at 298 K from 10 wt% to 50 wt% aqueous MDEA and at 313 K 50 wt% aqueous MDEA and loading,  $\alpha$ , up to 0.5 mol H<sub>2</sub>S/mol MDEA. Shokouhi and Ahmadi performed density and viscosity measurements with a 46.78 wt% MDEA-H<sub>2</sub>O at 313, 328 and 373 K and loading in the whole range from 0 to 1 mol H<sub>2</sub>S/mol MDEA. They both found that the density is increasing with increasing H<sub>2</sub>S absorption, while the viscosity is decreasing, with the exception of the data obtained at 373 K. At this temperature, the trend was not clear and the viscosity seemed unaffected. The maximum deviation in viscosity observed between  $\alpha = 0$  and  $\alpha = 0.5$  was 27% at 298 K with 50 wt% aqueous MDEA.

The reason the viscosity decreases with hydrogen sulfide absorption in aqueous MDEA is not understood. Further, there are only few viscosity data reported for water-H<sub>2</sub>S mixture (Murphy and Gaines, 1974). Viscosity measurements of water saturated with H<sub>2</sub>S indicate that the viscosity is higher than that of pure water. It is important to note that the measurements concern total pressures of 18 bar and 303 K and the unloaded system was pressurized using nitrogen. The deviation was 5%. As far as the viscosity and density of H<sub>2</sub>S loaded pure or aqueous MEG is concerned, it has not been possible to find reported data. Reported data on the solubility of pure hydrogen sulfide in pure MEG show that the amount of absorbed H<sub>2</sub>S is low, thus, no significant viscosity effects are expected (Short et al., 1983). Therefore, one would expect that the viscosity of MDEA-MEG solvents would follow the trends of the aqueous amine and decrease after hydrogen sulfide had been absorbed.

High pressure will also influence the viscosity of the solvent. It is expected that the higher the pressure, the higher the viscosity of the liquid solvent will be (Poling et al., 1987). Indeed, both density and viscosity increased with increasing pressure in the work of Sobrino et al. (Sobrino et al., 2016) with aqueous MDEA from 10 wt% to 50 wt% MDEA in the temperature range from 293 to 353 K and pressure range from 10 to 1200 bar. The data for 10 wt% MDEA-H<sub>2</sub>O follow the trend of pure water viscosity; at low temperatures the viscosity initially decreases upon pressure, exhibits a minimum and afterwards, starts increasing, while at higher temperatures, above 303 K, the viscosity increases monotonically with pressure (Horne and Johnson, 1966). At higher amine concentrations, it seems that this behavior of water viscosity is absent, and pressure increase results in increasing viscosity at all temperatures studied. However, the effect is small with maximum relative viscosity change observed upon pressurization to 100 bar, to be 2%, which is lower than the relative expanded uncertainty, 2.9%, reported in the work of Sobrino et al. (Sobrino et al., 2016). Practically, the unloaded or lean solvent to be injected and the loaded solvent after the scrubber, will be in similar pressure, only difference being the pressure drop in the inline separator.

Input from the industrial partners of SUBPRO asserted that the high viscosities of the non-aqueous systems studied, which reaches 200 mPa·s at 283 K for a 90 wt% MDEA – 5 wt% MEG – 5 wt% H<sub>2</sub>O, do not pose any difficulties in their application subsea in terms of processing equipment requirements. This information, coupled with the fact that the viscosity is expected to decrease in MDEA-MEG and MDEA-MEG-H<sub>2</sub>O systems upon H<sub>2</sub>S loading, signifies that the model provided in this work can predict the maximum viscosity to be



encountered in the process. This is true under the premise of minimal carbon dioxide absorption. In addition, assuming that the effect of pressure in the proposed combined solvents shall be of the same magnitude as for aqueous MDEA, the viscosity changes due to high pressure are within the accuracy of the model.

## Bibliography

- Fu, D., Chen, L., Qin, L., 2012. Experiment and model for the viscosity of carbonated MDEA–MEA aqueous solutions. *Fluid Phase Equilibria* 319, 42–47. <https://doi.org/10.1016/j.fluid.2012.01.029>
- Horne, R.A., Johnson, D.S., 1966. The Viscosity of Water under Pressure. *J. Phys. Chem.* 70, 2182–2190. <https://doi.org/10.1021/j100879a018>
- Murphy, J.A., Gaines, G.L., 1974. Density and viscosity of aqueous hydrogen sulfide solutions at pressures to 20 atm. *J. Chem. Eng. Data* 19, 359–362. <https://doi.org/10.1021/je60063a015>
- Pinto, D.D.D., Johnsen, B., Awais, M., Svendsen, H.F., Knuutila, H.K., 2017. Viscosity measurements and modeling of loaded and unloaded aqueous solutions of MDEA, DMEA, DEEA and MAPA. *Chem. Eng. Sci.* 171, 340–350. <https://doi.org/10.1016/j.ces.2017.05.044>
- Poling, B.E., Prausnitz, J.M., O'Connell, J.P., 1987. *The properties of gases and liquids*.
- Rinker, E.B., Colussi, A.T., McKnight, N.L., Sandall, O.C., 2000. Effect of Hydrogen Sulfide Loading on the Density and Viscosity of Aqueous Solutions of Methyldiethanolamine. *J. Chem. Eng. Data* 45, 254–256. <https://doi.org/10.1021/je9902286>
- Shokouhi, M., Ahmadi, R., 2016. Measuring the density and viscosity of H<sub>2</sub>S-loaded aqueous methyldiethanolamine solution. *The Journal of Chemical Thermodynamics* 102, 228–236. <https://doi.org/10.1016/j.jct.2016.06.007>
- Shokouhi, M., Jalili, A.H., Samani, F., Hosseini-Jenab, M., 2015. Experimental investigation of the density and viscosity of CO<sub>2</sub>-loaded aqueous alkanolamine solutions. *Fluid Phase Equilibria* 404, 96–108. <https://doi.org/10.1016/j.fluid.2015.06.034>
- Short, I., Sahgal, A., Hayduk, W., 1983. Solubility of ammonia and hydrogen sulfide in several polar solvents. *J. Chem. Eng. Data* 28, 63–66. <https://doi.org/10.1021/je00031a019>
- Sobrino, M., Concepción, E.I., Gómez-Hernández, Á., Martín, M.C., Segovia, J.J., 2016. Viscosity and density measurements of aqueous amines at high pressures: MDEA-water and MEA-water mixtures for CO<sub>2</sub> capture. *The Journal of Chemical Thermodynamics* 98, 231–241. <https://doi.org/10.1016/j.jct.2016.03.021>
- Weiland, R.H., Dingman, J.C., Cronin, D.B., Browning, G.J., 1998. Density and Viscosity of Some Partially Carbonated Aqueous Alkanolamine Solutions and Their Blends. *J. Chem. Eng. Data* 43, 378–382. <https://doi.org/10.1021/je9702044>



## Chapter 4

# VLE Data for H<sub>2</sub>S-containing Systems

*This chapter presents vapor-liquid equilibrium data for pure MDEA and H<sub>2</sub>S loaded MDEA-H<sub>2</sub>O and MDEA-MEG-H<sub>2</sub>O systems at high pressures in the presence of methane.*

The first section presents VLE data for the systems H<sub>2</sub>S-CH<sub>4</sub>-MDEA-H<sub>2</sub>O and pure MDEA (journal publication II), and the second section presents VLE data for the combined solvent system H<sub>2</sub>S-CH<sub>4</sub>-MDEA-MEG-H<sub>2</sub>O. The high-pressure equilibrium setup and experimental procedure used are briefly presented, so the reader is advised to refer to the Appendix in the end of this thesis for a comprehensive description. In both studies, the effect of total pressure on the absorption capacity of the solvent is investigated with methane used as makeup gas. Emphasis has been put on identifying and estimating the uncertainties of the measurements and evaluating their role in understanding the results.

The study of H<sub>2</sub>S solubility in aqueous MDEA solutions in the presence of methane, presented in the first section, was performed using MDEA concentrations of 50 wt% and 70 wt%. The former was investigated also for experimental validation purposes. The data show that the effect of total pressure up to 100 bar on the liquid loading of the solvent is within the experimental uncertainties. Increase of the total pressure leads to increase of the partial pressure of hydrogen sulfide, which is the result of the non-idealities in the gas phase at high pressures. Comparison of the H<sub>2</sub>S concentration in the liquid 50 and 70 wt% aqueous MDEA suggests that the contribution of the chemical absorption decreases as the amine content increases. A VLE model employing Peng-Robinson EoS and the electrolyte non-random two-liquid (eNRTL) model is also presented for the system H<sub>2</sub>S-MDEA-H<sub>2</sub>O, and it is shown that it can be used for rough estimations of methane-containing systems at low total pressures. Vapor pressure measurements of pure MDEA are also presented and modeled.

The effect of total pressure on the liquid loading and the H<sub>2</sub>S partial pressure with the 30 wt% MDEA – 40 wt% MEG – 30 wt% H<sub>2</sub>O blend, presented in the second section, are similar to the

findings for the aqueous MDEA systems. In addition, based on the newly obtained data and data reported in the literature, it is shown that increasing MDEA concentration under constant water content and lowering MEG content under constant amine concentration in the amine-glycol-water blends, leads to higher absorption capacity. A reaction mechanism theory is proposed for explaining the increasing solubility of hydrogen sulfide with decreasing glycol content. Moreover, a comparison between 70 wt% aqueous MDEA and the 30 wt% MDEA – 40 wt% MEG – 30 wt% H<sub>2</sub>O solution indicated that the absorption performance of the two solvents at 283 K is similar. Last but not least, the effect of glycol on the cyclic capacity of 30 wt% aqueous MDEA was investigated. It was found that, at the experimental pressure and temperature conditions, the amine-glycol-water system has a higher cyclic capacity than its aqueous counterpart.

The experimental challenges and good-to-know elements are listed in the last section of the chapter, with the most important one being the gas chromatography (GC) analysis of the liquid phase concentration which unfortunately did not match the mass balance. In this chapter, the liquid phase loading was estimated based on the GC analysis of the vapor phase and the mass balance.

## 4.1 Vapor-liquid equilibrium study for the system H<sub>2</sub>S-CH<sub>4</sub>-MDEA-H<sub>2</sub>O

### Journal publication II

Skylogianni, E., Mundal, I., Pinto, D.D.D., Coquelet, C., Knuutila, H.K., 2020. Hydrogen sulfide solubility in 50 wt% and 70 wt% aqueous methyldiethanolamine at temperatures from 283 to 393 K and total pressures from 500 to 10000 kPa. *Fluid Phase Equilibria* 511, 112498. <https://doi.org/10.1016/j.fluid.2020.112498>.

Open access.



## Paper II

...the ...

...the ...

...the ...

...the ...

...the ...

...the ...

...the ...

...the ...

...the ...

...the ...

...the ...

...the ...

...the ...

...the ...

...the ...

...the ...

...the ...





Contents lists available at ScienceDirect

## Fluid Phase Equilibria

journal homepage: [www.elsevier.com/locate/fluid](http://www.elsevier.com/locate/fluid)

## Hydrogen sulfide solubility in 50 wt% and 70 wt% aqueous methyldiethanolamine at temperatures from 283 to 393 K and total pressures from 500 to 10000 kPa



Eirini Skylogianni <sup>a</sup>, Ingvild Mundal <sup>a</sup>, Diego D.D. Pinto <sup>a</sup>, Christophe Coquelet <sup>b</sup>, Hanna K. Knuutila <sup>a,\*</sup>

<sup>a</sup> Department of Chemical Engineering, Norwegian University of Science and Technology, Sem Sælands vei 6, 7034, Trondheim, Norway

<sup>b</sup> Mines ParisTech - PSL University, CTP- Centre of Thermodynamics of Processes, 35 rue Saint Honoré, 77305, Fontainebleau, France

## ARTICLE INFO

## Article history:

Received 26 November 2019

Received in revised form

22 January 2020

Accepted 23 January 2020

Available online 29 January 2020

## Keywords:

Gas processing

Absorption

Hydrogen sulfide

Methane

MDEA

High pressure

Vapor-liquid equilibrium

Vapor pressure

## ABSTRACT

The hydrogen sulfide (H<sub>2</sub>S) absorption capacity of a 70 wt% aqueous methyldiethanolamine (MDEA) solution was investigated in a static-analytic apparatus at temperatures of 283, 353 and 393 K and pressures of 2000, 6000 and 10000 kPa in the presence of methane. New experimental data were also produced for a 50.1 wt% aqueous MDEA at 323 K and pressures of 500 and 3000 kPa as part of the apparatus validation procedure. A model based on electrolyte non-random two-liquid (eNRTL) activity coefficient model to describe the liquid phase and Peng-Robinson Equation of State to describe the vapor phase non-idealities was developed for the system H<sub>2</sub>S-MDEA-H<sub>2</sub>O, which can potentially be used also for the system in the presence of methane at low pressures. Vapor pressure measurements of pure MDEA were also performed in the range of 405–435 K in an ebulliometer and parameters for the Antoine correlation were proposed.

© 2020 The Authors. Published by Elsevier B.V. This is an open access article under the CC BY license (<http://creativecommons.org/licenses/by/4.0/>).

## 1. Introduction

Natural and refinery gas streams usually contain acid gases, carbon dioxide and sulfur compounds, which must be removed in order to ensure trouble-free and safe operations. Typical sulfur compounds are hydrogen sulfide, carbonyl sulfide, mercaptans, with the first one being the most important one as it occurs in the largest concentrations [1]. Hydrogen sulfide (H<sub>2</sub>S) gas content is routinely controlled by absorption into aqueous methyldiethanolamine (MDEA), which can then be thermally regenerated and reused.

A 50 wt% MDEA-H<sub>2</sub>O concentration is considered a benchmark solvent in H<sub>2</sub>S removal, due to its equilibrium behavior and low corrosion. Aqueous MDEA has been long established in the industry due to among others, the amine's availability, low cost and energy requirements, resistance to degradation, ability to meet

the 4 ppm specification requirement for pipeline gas and to selectively remove H<sub>2</sub>S over CO<sub>2</sub>, which often coexist. MDEA owes its latter characteristic to its structure; as a tertiary amine, aqueous MDEA reacts instantaneously with hydrogen sulfide while it requires more time to react with CO<sub>2</sub>. Thus, by regulating the contact time between the solvent and the gas, H<sub>2</sub>S removal to specification and minimum co-absorption of CO<sub>2</sub> can be achieved [2,3].

The motivation of this work has been the investigation of highly concentrated MDEA for the combined H<sub>2</sub>S removal and hydrate control for subsea application. Oil and gas reservoirs are turning sour in the course of time [4,5], which is tackled today by using triazine to control the H<sub>2</sub>S levels [6]. Main disadvantages of employment of triazine are related to the non-regeneration of the solvent, weight, space, transportation and disposal requirements. These constraints are of utmost importance, especially as the available production fields are sourer, deeper and in longer distances from the shore [7]. MDEA is already used offshore as a pH stabilizer [8] facilitating its employment subsea, while the fact that, as a polar

\* Corresponding author.

E-mail address: [hanna.knuutila@ntnu.no](mailto:hanna.knuutila@ntnu.no) (H.K. Knuutila).

compound, it has affinity for water, renders highly concentrated aqueous MDEA a good candidate for acting both as a hydrate inhibitor and as an H<sub>2</sub>S removal agent. The solvent could be used and regenerated offshore, supported by new technological developments, such as “subsea on a stick” [9].

This work is a first step in the investigation of this multifunctional solvent, with focus on the effect of total pressure in the H<sub>2</sub>S removal capacity of the solvent. The measurements were conducted at high pressures, up to 10000 kPa, with methane as the pressurization medium, since it is the main constituent of natural gas. Few researchers have previously studied the effect of high-pressure methane for the systems CH<sub>4</sub>–CO<sub>2</sub>–MDEA–H<sub>2</sub>O [10,11] and CH<sub>4</sub>–H<sub>2</sub>S–MDEA–H<sub>2</sub>O; a detailed literature review for the latter is provided in Section 2.1. The main finding has been that for both CO<sub>2</sub> and H<sub>2</sub>S-contained systems, an increase in total pressure leads to increase in the acid gas partial pressure. To our best knowledge, there are no data reported for the system CH<sub>4</sub>–H<sub>2</sub>S–MDEA–H<sub>2</sub>O and MDEA solutions with concentrations higher than 50 wt% MDEA–H<sub>2</sub>O.

A 50.1 wt% MDEA–H<sub>2</sub>O and a 70 wt% MDEA–H<sub>2</sub>O system were used in this work to obtain vapor–liquid equilibrium data (VLE) with hydrogen sulfide and methane. The new VLE data for the system CH<sub>4</sub>–H<sub>2</sub>S–MDEA–H<sub>2</sub>O with 70 wt% MDEA–H<sub>2</sub>O mixtures were obtained at temperatures of approximately 283, 353 and 393 K and pressures of 2000, 6000 and 10000 kPa. The experiments were performed isothermally and the temperature of 283 K was chosen to simulate the low-temperature subsea conditions while the temperature of 393 K was chosen to simulate the high

regeneration temperature.

## 2. Literature review

### 2.1. H<sub>2</sub>S–MDEA–H<sub>2</sub>O–makeup gas system

An updated list of available VLE data for the system H<sub>2</sub>S–MDEA–H<sub>2</sub>O, including data with makeup gas, is provided in Table 1. The amine concentration is expressed in a weight basis for all reference sources to allow for direct comparisons. Concentrations reported in molarities [12–14] have been converted to weight fractions using the density correlations presented by Bernal–García et al. [15]. The solution preparation temperature was assumed to be 298.15 K due to lack of this information.

As also other authors working with the system H<sub>2</sub>S–MDEA–H<sub>2</sub>O have observed, the available data in the literature are rather scattered, especially at low loadings. The literature data have been evaluated for self-consistency and mutual-consistency with reported data in similar experimental conditions, following Chunxi and Fürst’s approach [16]. This evaluation was performed in order to decide if some data sets would be excluded during our thermodynamic modeling. During the evaluation, the partial pressures for H<sub>2</sub>S from Kuranov et al. [17], Kamps et al. [18] and Sidi-Boumedine et al. [19], who all report total pressures in the absence of makeup gases, were calculated by subtracting the vapor pressure of the solvent calculated by Dalton’s Law (Eq. (1)). The vapor pressure of H<sub>2</sub>O was calculated by the correlations proposed by NIST for the given temperature ranges while the vapor pressure of MDEA was calculated based on the Antoine correlation fitted to

**Table 1**  
Literature VLE data for H<sub>2</sub>S–MDEA–H<sub>2</sub>O including data with makeup gas.

wt.% aq. MDEA	T (K)	P <sub>H<sub>2</sub>S</sub> (kPa)	P <sub>tot</sub> (kPa)	Loading	Makeup gas	Analysis Method		Source	NP
						Vapor Phase	Liquid Phase		
11.8, 23.4, 48.9	298.15, 313.15, 323.15, 373.15, 393.15	0.0013 –5890	–	0.00129 –3.229	Nitrogen (P <sub>H<sub>2</sub>S</sub> < 200 kPa)	GC	Iodometric back-titration with thiosulfate	Jou et al. [12]	153
11.9, 20	298.15, 310.95, 338.75, 388.75	13.23 –1536.6	–	0.18 –2.1703	–	Mass balance	Mass balance	Bhairi, Maddox et al. [26,27] <sup>c, b</sup>	49
23.4	313.15	0.52 –1600	–	0.13 –1.725	–	GC	Iodometric back-titration with thiosulfate	MacGregor and Mather [14] <sup>c, b</sup>	27
35, 50	313.15, 373.15	0.00183 –313	–	0.00410 –1.077	Nitrogen (P <sub>H<sub>2</sub>S</sub> < 350 kPa)	GC	Iodometric back-titration with thiosulfate	Jou et al. [21] <sup>c</sup>	50
29.9	313.15, 333.15, 353.15, 373.15	1.498 –445.7	–	0.082 –0.902	Nitrogen (P <sub>H<sub>2</sub>S</sub> < 200 kPa)	Mass balance (P <sub>H<sub>2</sub>S</sub> < 200 kPa)/ GC (P <sub>H<sub>2</sub>S</sub> > 200 kPa)	Iodometric back-titration with thiosulfate	Li and Shen [13] <sup>c</sup>	43
23.1, 50	313.15, 343.15, 373.15, 393.15	0.0033 –3673	–	0.00240 –1.74	Nitrogen (P <sub>H<sub>2</sub>S</sub> < P <sub>amb</sub> )	Mass balance	Iodometric back-titration with thiosulfate	Huang and Ng [23] <sup>c</sup>	42
23, 50	313.15, 323.15	0.00069 –5.268	96–110	0.00219 –0.313	Nitrogen (P <sub>H<sub>2</sub>S</sub> < P <sub>amb</sub> )	FTIR	FTIR	Rogers et al. [24] <sup>c, b</sup>	30
11.83, 23.63	–298.15, –313.1	0.023 –1.611	–	0.0101 –0.2610	–	Mass balance	Mass balance	Lemoine et al. [28] <sup>c</sup>	29
18.7, 32.2, 48.8	313.16, 333.15, 373.15, 393.15, 413.15	–	165.2 –4895.9	0.48 –1.934	–	Mass balance	Mass balance	Kuranov et al. [17] <sup>c</sup>	71
46.78	313.11, 353.16, 393.15	–	147.9 –2783	0.153 –1.428	–	Mass balance	Mass balance	Kamps et al. [18] <sup>c, b</sup>	26
23.7	–313, –373	–	6.21 –1040	0.039 –1.116	–	Mass balance	Mass balance	Sidi-Boumedine et al. [19] <sup>c, b</sup>	27
23.7	313.2	14–1361	–	0.505 –1.639	–	Mass balance	Mass balance	Zoghi and Shokouhi [22] <sup>c, b</sup>	12
35, 50	283, 298, (313)	0.141 –18.892	690 –6900	0.028 –0.575	Methane	GC	Iodometric back-titration with thiosulfate	Huttenhuis et al. [25]	30
50	323.15	3–278 –700	493 –0.889 <sup>a</sup>	0.096 –0.889 <sup>a</sup>	Methane	GC	Mass balance	Dicko et al. [29] <sup>c</sup>	5
50	322.95, 343.15	31–974 –7090	1480 –1.042	0.267 –1.042	Methane	GC	Titration with silver nitrate	Sadegh et al. [30] <sup>c, b</sup>	39

<sup>a</sup> Global loading.

<sup>b</sup> Reported uncertainty in pressure.

<sup>c</sup> Reported uncertainty in H<sub>2</sub>S loading/mole fraction.

**Table 2**  
Literature VLE, FPD and  $H^E$  data for the binary system MDEA-H<sub>2</sub>O.

Property	wt.% aq. MDEA	T/ $\Delta T_F$ (K)	P (kPa)	Source	NP
VLE	3–78.61	313.15–373.15	6.47–100.40	Kim et al. [33]	61
	10–70	326.15–381.15	13.08–101.67	Xu et al. [34]	34
	30–98.9	350.15–458.65	40–66.7	Voutsas et al. [35]	27
FPD	17.4–39.1	(-3.3)-(-13.8)	101.13	Chang et al. [31]	21
	2.6–39.6	(-0.4)-(-14.2)	101.3	Fosbøl et al. [32]	12
$H^E$	9.6–92.5	298.15–342.45	–	Posey [36]	16
	17.5–96.7	298.15–313.15	–	Maham et al. [37]	26
	41.8–98.4	338.15	–	Maham et al. [38]	9

**Table 3**  
Literature vapor pressure data for pure MDEA.

T (K)	$P^s$ (kPa)	Source	NP
293.69–401.97	0.0006–1.4776	Noll et al. [39]	26
406.69–435.50	2.48–7.98	Kim et al. [33]	7
420.45–513.85	3.68–90.44	Daubert et al. [40]	14
467.39, 479.39, 488.15	20, 30, 40	Yang et al. [41]	3
519.7–738.4	98.59–3985	VonNiederhausen et al. [42]	9

existing and new data as presented in Section 5. **Results and Discussion.**

$$P_{sol}^s = P_{MDEA}^s \cdot X_{MDEA} + P_{H_2O}^s \cdot X_{H_2O} \quad (1)$$

Li and Shen [13] measured H<sub>2</sub>S solubility in 29.9 wt% aqueous MDEA at temperatures up to 373 K. During the evaluation of the data, a sharp increase of partial pressure at loadings >0.7 mol H<sub>2</sub>S/mol MDEA was noticed, resulting in a cross-over of literature data reported for 35 wt% and 50 wt% MDEA-H<sub>2</sub>O solutions. For this reason, the data from Li and Shen [13] were not included in our database used in the model parametrization, as chosen also by Huttenhuis et al. [20].

Jou and coworkers [12,21] have published experimental data for a 48.9 wt% and for a 35 wt% MDEA solution. Two observations can be made for the low loading region: a) the data with a 35 wt% [21] and a 48.9 wt% [12] MDEA solution are very similar and b) the deviations between the data with a 48.9 wt% and a 50 wt% solution look larger than what one would expect with such similar concentrations. Uncertainty information is not available in the first publication of Jou et al. [12], while the authors on their second publication report 3% error in liquid loading and 0.1% full scale (FS) error in pressure. Taking this into account, the deviations related to a) and b) are within the experimental uncertainty. Generally, the data from Jou et al. agree with literature values in different concentrations and temperatures besides at low loadings. For example, good agreement is observed between the data Jou et al. [12] for a 23.4 wt% aqueous MDEA at 313 K and from two other sources [14,22] at loadings > 0.4 mol H<sub>2</sub>S/mol MDEA. Any small deviations are justified in terms of reported experimental uncertainties provided by MacGregor and Mather [14] (pressure, loading, composition) as well as by Zoghi and Shokouhi [22] (pressure and composition). At lower loadings, significant deviations are seen between the data by Jou et al. [12] and MacGregor and Mather [14]

**Table 4**  
Chemical sample table.

Component	IUPAC name	CAS	Supplier	Purity	Analysis method
N-methyldiethanolamine (MDEA)	2-[2-hydroxyethyl(methyl) amino] ethanol)	105-59-9	Sigma-Aldrich	≥99 wt%	GC
Water	Oxidane	–	–	Ultra-pure	–
Hydrogen sulfide	Sulfane	7783-06-4	Air Liquide	≥99.5 vol%	GC
Methane	Methane	74-82-8	Air Liquide	≥99.995 vol%	GC

compared to Huang and Ng [23] as well as Rogers et al. [24]. These differences are difficult to explain by the reported uncertainties only. At higher loadings, some inconsistencies are also seen, for example, the data from Kuranov and coworkers [17] for a 32.3 wt% amine solution are close to the data reported for a 50 wt% MDEA solution [12,23].

No pattern was identified between the analysis method and the uncertainty of the results. Unfortunately, often the uncertainty in loading, which could enlighten the reasons for the scatter observed at low loadings, is not reported. The literature sources reporting uncertainties in either pressure or loading are marked in Table 1. In addition, the differences observed in the reported data could also be attributed to the purity of the chemicals. Although most of the authors report the use relatively high-purity chemicals (>98–99 wt % MDEA, >99 vol% H<sub>2</sub>S), the chemical's aging (contamination, contact with atmospheric humidity, light degradation etc.) could also have contributed to the differences observed.

## 2.2. MDEA-H<sub>2</sub>O system

Vapor-liquid equilibrium (VLE), freezing-point depression (FPD) and molar excess enthalpy  $H^E$  data for the binary subsystem MDEA-H<sub>2</sub>O are given in Table 2. The data were used to model the binary system first in order to reduce the number of parameters to be fitted for the ternary system H<sub>2</sub>S-MDEA-H<sub>2</sub>O onwards, as it will be further explained later in Section 4. **Thermodynamic modeling.** Eight points from Chang et al. [31] were excluded due to their deviations from the data by Fosbøl et al. [32].

## 2.3. Pure MDEA

A literature review was also performed for the vapor pressure of MDEA. As seen in Table 3, the data already reported in the literature cover a large range of temperatures, from 293 to 738 K.

## 3. Experimental work

### 3.1. Materials

Information for the chemicals used are provided in Table 4. MDEA was used as received from the supplier without further purification. Ultra-pure Millipore water was used in this work to prepare the aqueous amine solutions. Both the amine and the water

were degassed independently and they were mixed under vacuum to eliminate presence of air during the experiment. The solutions were prepared gravimetrically in a METTLER PM1200 scale with an accuracy of  $1 \cdot 10^{-5}$  kg. The composition uncertainty is the same for each component in a binary mixture as explained in Appendix, and it was found to be  $u(w) = 0.002$  for 50.1 wt% MDEA-H<sub>2</sub>O and  $u(w) = 0.003$  for 70 wt% MDEA-H<sub>2</sub>O. The gases used in this work are hydrogen sulfide and methane as a makeup gas.

### 3.2. Experimental set-ups

**High-pressure VLE.** The high-pressure vapor-liquid equilibrium (VLE) experiments were conducted in an in-house manufacture by ARMINES employing the static-analytic method [43]. The apparatus is designed for measurements with acid gases and can be operated in the pressure range from 0.5 to 19.9 MPa and temperatures, from 223 to 473 K. Temperature regulation with an accuracy of  $\pm 0.01$  K is achieved through immersing the cell into an oil bath. The apparatus is similar to the one previously presented by Ref. [29] and its schematic is given in Fig. 1.

The setup consists of three distinct parts: a) the equipment for filling up the equilibrium cell, i.e. the variable volume press (VVP), the gas bottles and gas tanks, b) the equilibrium cell, including automatic samplers for the gas and the liquid phase(s) and c) the equipment for the analysis of the samples, i.e. the gas chromatograph. Each of these parts consists of various valves and instrumentation. A variable volume press composed by the variable volume pressure cell, a piston and a displacement transducer, was

used to introduce the liquid inside the cell, under vacuum. The transducer measures the piston displacement with an accuracy of  $\pm 1 \cdot 10^{-5}$  m and, by knowing the dimensions of the cell, the exact volume of the solvent introduced was determined. Approximately  $6 \cdot 10^{-6}$  m<sup>3</sup> of solvent were introduced in every experiment. An H<sub>2</sub>S bottle was connected to a gas tank with volume of  $1.61 \cdot 10^{-4} \pm 5 \cdot 10^{-8}$  m<sup>3</sup>, which was further connected to the cell. The presence of a small gas tank between the gas bottle and the cell was dictated as an extra safety barrier in case of leakage of the toxic H<sub>2</sub>S. Pressurization of the cell with methane was done directly from the CH<sub>4</sub> bottle.

The equilibrium cell is a sapphire tube standing between two Hastelloy flanges. Kalrez O-rings are used for sealing the tube. The upper flange accommodates two non-rotating stem loading valves, for H<sub>2</sub>S and for CH<sub>4</sub>, and the lower flange accommodates two more, only one of which was used for the loading of the liquid solution and the discharge of the cell. The temperature is monitored and controlled by two platinum probes and two 100  $\Omega$  Platinum resistance temperature detectors (Pt100) with an uncertainty of  $\pm 0.02$  K. Each of the two located in each flange. They are connected to an HP data acquisition unit and are carefully periodically calibrated. The cell is equipped with two Druck™ pressure transducers, one calibrated for 0–3 MPa and the other for 0–30 MPa pressure range respectively. The transducers are maintained at the temperature they were calibrated at and the uncertainty is 0.6 kPa. The volume of the cell is  $33.12 \cdot 10^{-6} \pm 5 \cdot 10^{-8}$  m<sup>3</sup> (or  $32.24 \cdot 10^{-6}$  m<sup>3</sup> when the low-pressure transducer is isolated). A stirring system is integrated to the cell in order to reduce the time of equilibration

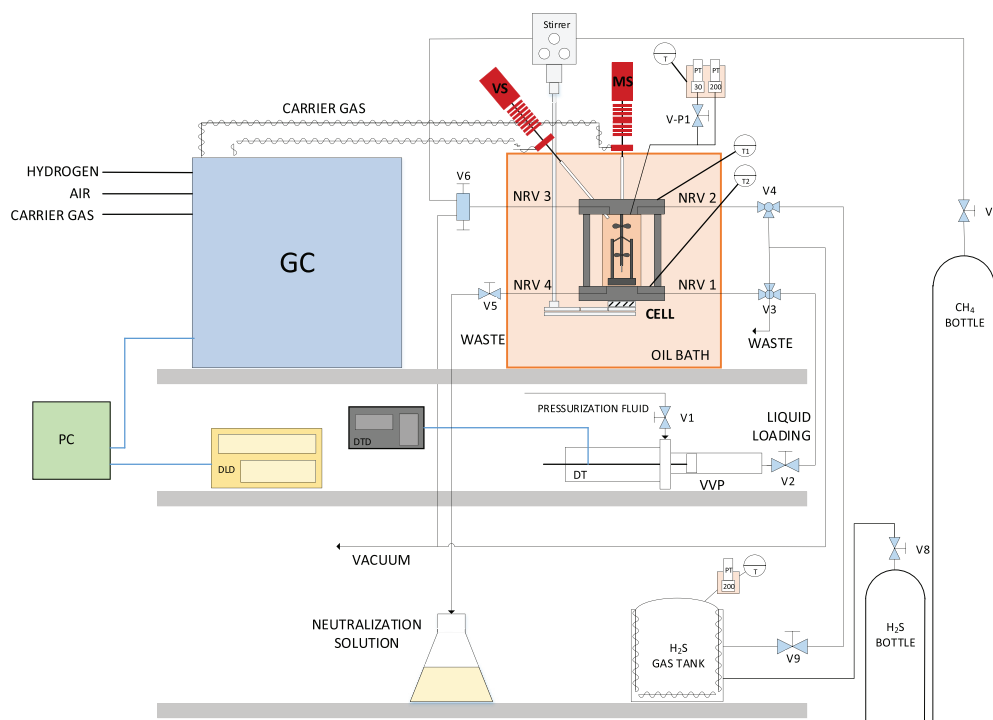


**Fig. 1.** High-pressure VLE setup. DTD: Displacement Transducer Display, DLD: Data Logging Device, DT: Displacement Transducer, GC: Gas Chromatograph, MS: Mobile Sampler for the analysis of liquid phase, NRV: Non-Rotating Valve, PC: Personal Computer for data acquisition, PT: Pressure Transducer, T: Thermocouple, V: Valve, VS: Vapor Sampler for the analysis of gas phase, VVP: variable volume press.

and ensure phase homogeneity. The variable-speed stirrer is composed by a rotating axis inside the cell, two propellers mounted on the rotating axis for stirring both the gas phase and the liquid phase and a magnetic rod mounted on the rotating axis in order to allow for rotation of the axis by a stirring motor located below the cell.

Agilent software BenchLink is used for online monitoring of pressure and temperature, enabling the determination of equilibrium. Once the equilibrium is reached, micro samples can be withdrawn and transferred to the GC for analysis. Automatic sampling is allowed through two capillary samplers (ROLSI®) Armines' patent [44]. Two capillaries are fixed in the cylindrical wall of the cell at levels designed to withdraw vapor and liquid phase samples. The samplers are connected to a PERICHRON model PR-2100 gas chromatograph, through a heated transfer line. The temperature selected is higher than the boiling point of the heaviest component (MDEA) to avoid any sample condensation. The chromatograph is equipped with a thermal conductivity detector (TCD) and a flame ionization detector (FID), and WINILAB III software is used for GC acquisition and treatment.

**Ebulliometer.** A modified Swietoslawski ebulliometer was used, described earlier in detail by Kim et al. [33]. The apparatus can be operated at temperatures up to 473 K and at sub-atmospheric and atmospheric pressure. The temperatures were measured with calibrated Pt100 resistance thermosensors with an uncertainty of  $\pm 0.05$  K. A DP1520 pressure controller from Druck™ was used, calibrated against a BeamexC5 calibrator with an accuracy of  $\pm 0.03$  kPa. The solution is accommodated inside a  $2 \cdot 10^{-4}$  m<sup>3</sup> glass equilibrium still and the set-up allows for the sampling of both the vapor and the liquid phase.

### 3.3. Experimental procedure

**High-pressure VLE.** After thorough cleaning with hot deionized (DI) water and ethanol, the cell and tubings were left to dry and set to vacuum during the previous night. The solution was prepared under vacuum directly inside the VVP and the solution preparation temperature was approximately 298 K. Back-pressure of ca. 500 kPa of methane was applied to the VVP. The solution was introduced inside the cell, and the end displacement position was recorded, so as the exact amount of solution added could be calculated. The cell was immersed into the bath, the stirrer was turned on, the temperature of the experiment was set and the system was left to equilibrate. Temperature stabilization required approximately 30–60 min, after which the vapor pressure of the solution was recorded.

The desired global loading, i.e. mol of H<sub>2</sub>S inside the cell per mol of amine, was first decided and based on the PVT conditions of the H<sub>2</sub>S gas tank before and after the filling of the cell, the amount of H<sub>2</sub>S introduced was determined. The calculations were performed using REFPROP software [45] and a Helmholtz energy-based equation of state developed by Ref. [46] for pure H<sub>2</sub>S was used. The global loading was, thus, calculated by:

$$n_{H_2S} = n_{H_2S,tank}^{before} - n_{H_2S,tank}^{after} \quad (2)$$

$$\alpha_{glob} = \frac{n_{H_2S}}{n_{MDEA}} \quad (3)$$

For the experiments with the 50.1 wt% MDEA aqueous solution, initially a small amount of H<sub>2</sub>S was introduced and it was left to equilibrate. Reaction of H<sub>2</sub>S and MDEA is fast and equilibrium was reached within 1 h. Because the total pressure was lower than the minimum required pressure of 500 kPa for the ROLSI® samplers and GC to function, methane was added up to 500 kPa. Equilibrium

was reached in approximately 1 h, and the sampling started. In our experiments, sampling and analysis was conducted only for the vapor phase. Higher loadings were reached by adding more H<sub>2</sub>S into the cell and repeating the above-mentioned procedure.

For the 70 wt% MDEA solution VLE investigation, two series of experiments were conducted based on the global loading, one for 0.2 and one for 0.5 mol H<sub>2</sub>S/mol MDEA approximately. The experimental procedure varies in the way that after equilibrium was reached, methane was added in 3 stages, up to 2000, 6000 and 10000 kPa. At each pressure level, sampling and analysis of the vapor phase was performed upon equilibrium. The experiments were performed under isothermal conditions, at 283, 353 and 393 K. At the end of the experiment, the cell was depressurized and emptied safely through a caustic solution (NaOH) in order to neutralize the system. At each temperature, a new experiment was conducted using fresh solution. We aimed at having the same global loading at all temperatures, however it was not practically possible to reach exactly the same loadings in every experiment. The study at each temperature and global loading lasted approximately one week.

The analysis of vapor phase concentration was performed in a GC equipped with a Porapak-R column R80/100 mesh (length 2 m, diameter 2 mm) from RESTEK. The carrier gas was helium at a flow rate of 20 ml/min. A constant temperature program at 363 K was used for the quantification of both methane and hydrogen sulfide. Analysis at 383 K was also performed to check for water presence in the vapor phase. In order to check the repeatability of the measurements and to perform uncertainty analysis, five samples at least were withdrawn, the first two of them usually were required to saturate the transfer lines in terms of adsorption. Disturbance to equilibrium was considered negligible due to the small volume of each sample.

Knowing the pressure, temperature and the composition of the vapor phase, the density of the vapor phase was estimated using REFPROP software [45]. The amount of n<sub>H<sub>2</sub>S</sub> in the vapor and liquid phase and finally the H<sub>2</sub>S loading in the liquid phase, liquid loading  $\alpha$ , were calculated according to Eq. (4) - Eq. (7).

$$n_{tot}^v = \rho^v \cdot V^v \quad (4)$$

$$n_i^v = n_{tot}^v \cdot y_i \quad (5)$$

$$n_i^l = n_{tot} - n_i^v \quad (6)$$

$$\alpha = \frac{n_{H_2S}^l}{n_{MDEA}} \quad (7)$$

where  $\rho^v$  is the molar density of the gas mixture, calculated using REFPROP and  $V^v$  is the volume of the vapor phase. The latter is the difference between the volume of the cell, ca.  $33 \cdot 10^{-6}$  m<sup>3</sup>, which is known from our calibration data and the volume of the liquid which was estimated by the correlations proposed by Ref. [15], assuming that the effect of pressure in the liquid volume is negligible. Bernal-García and coworkers measured the density of aqueous MDEA in the whole composition range at temperature range of 263.15–363.15 K and, based on their data, calculated the excess molar volumes of the binary systems. For our calculations at the temperature of 393 K which was not studied in the aforementioned work, the excess molar volume was extrapolated. It is worth mentioning that the deviations in number of moles of H<sub>2</sub>S calculated by the Ideal Gas Law equation and REFPROP employing the most up-to-date Helmholtz energy-based EoS led to deviations in the liquid loading lower than 1.5% at 283 and 353 K, while the deviations were higher at 393 K (max 2.7%). For more accurate

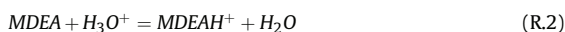
results, we used the results based on the latter.

**Ebulliometer.** Approximately  $0.8 \cdot 10^{-4} \text{ m}^3$  of liquid was charged inside the still, preceding purge with nitrogen. The desired temperature was set and equilibrium was assumed after 10 min of stable pressure and temperature. The vapor pressure of MDEA was measured at the temperature range of 405–435 K. Validation of the apparatus was performed by measuring the vapor pressure of water and a 1.5% maximum error from the literature was found in equilibrium pressure.

#### 4. Thermodynamic modeling

**High pressure VLE.** An in-house MATLAB-based rigorous model has been developed to describe the chemical and phase equilibrium for the system  $\text{H}_2\text{S}$ -MDEA- $\text{H}_2\text{O}$ . The same algorithm has been previously used to successfully describe  $\text{CO}_2$ -amine- $\text{H}_2\text{O}$  systems relevant to carbon capture processes [47,48]. Peng-Robinson EoS [49] with the original alpha function was employed to describe the non-idealities of the vapor phase, coupled with the traditional van der Waals one-fluid mixing rules. The binary interaction parameters for Peng-Robinson EoS in this work were set to zero. To account for the non-idealities in the liquid phase, the electrolyte non-random two-liquid (eNRTL) model [50] was utilized. The models are presented in the Appendix. The required critical parameters and acentric factors for pure components are given in Supplementary Information (Section A).

The chemical reactions assumed in the liquid phase are the ionization of water, the protonation of MDEA and the dissociation of  $\text{H}_2\text{S}$  (R. 1-3). The second dissociation reaction of hydrogen sulfide, from bisulfide to sulfide, is not considered in our model due to the low concentration of  $\text{S}^{2-}$  in the solution and in order to reduce the number of parameters in the model [16].



The chemical equilibrium constants as well as Henry's constant for hydrogen sulfide are described by Eq. (8), parametrized according to Table 5, where  $x$  stands for either the chemical equilibrium constant  $K_{\text{eq}}$  or Henry's constant  $H_{\text{H}_2\text{S}}$ . Temperature is expressed in K and Henry's constant for hydrogen sulfide in  $\text{kg}\cdot\text{atm}$ .

$$\ln(x) = A + \frac{B}{T} + C \ln(T) + DT \quad (8)$$

The vapor pressure for hydrogen sulfide and water is estimated using the Riedel correlation (Eq. (9)) where  $T$  expressed in K and  $P^{\text{sat}}$  in Pa. The parameters are presented in Table 6. MDEA vapor pressure has been measured in this work and fitted to Antoine correlation. The Antoine parameters used in this work can be found in Section 1.5.2.

**Table 5**  
Mole fraction-based parameters for Eq. (8), reported only with their significant digits.

	A	B	C	D	Reference
Chemical Equilibrium constant for R. 1	132.89	-13445	-22.477	0	Posey [36]
Chemical Equilibrium constant for R. 2	-60.03	-1974	7.533	0	Oscarson et al. [51]
Chemical Equilibrium constant for R. 3	214.58	-12995	-33.547	0	Posey [36]
Henry's constant for $\text{H}_2\text{S}$	342.595	-13237	-55.0551	0.05957	Edwards et al. [52]

**Table 6**  
Parameters for pure component vapor pressure correlations for Eq. (9).

Component	Model	A	B	C	D	E	Reference
$\text{H}_2\text{S}$	Riedel	106.47	-5018	-13.306	-0.09	-0.13	DIPPR [53]
$\text{H}_2\text{O}$	Riedel	73.649	-7258	-7.304	4.2E-06	2	DIPPR [53]

$$\ln(P^{\text{sat}}) = A + \frac{B}{T} + C \ln(T) + DT^E \quad (9)$$

A sensitivity analysis was performed to evaluate the significant numbers in the parameters retrieved from the literature. In Tables 5 and 6 the parameters are provided only with their significant digits.

The adjustable parameters for the eNRTL model are the non-randomness factors,  $\alpha$ , and the energy parameters,  $\tau_{ij}$ . The optimization of the  $\text{H}_2\text{S}$ -MDEA- $\text{H}_2\text{O}$  system requires the regression of a total of 78 parameters. In order to reduce this high number of parameters to be adjusted, the following steps have been taken:

- I) All non-randomness factors  $\alpha$  have been given fixed values according to Table 7.
- II) The energy parameters for the subsystem  $\text{H}_2\text{S}$ - $\text{H}_2\text{O}$  have been fixed to the default values used in Aspen Plus V10 simulation software (Table 7).
- III) The energy parameters for the subsystem MDEA- $\text{H}_2\text{O}$  have been fixed to the values obtained by the regression of the literature data presented in Subsection 2.2 MDEA- $\text{H}_2\text{O}$  system.

As a result, the number of parameters is reduced to 36. The temperature dependency of the energy parameters is described by Eq. (10), where  $a_{ij}$  and  $b_{ij}$  were fitted to experimental data.

$$\tau_{ij} = a_{ij} + \frac{b_{ij}}{T} \quad (10)$$

The fixed non-randomness factors and fixed energy parameter values are presented in Table 7, where  $m$  denotes molecule and  $c$ - $a$  cation-anion (salt). The non-randomness factors were fixed at 0.2 for molecule-molecule and water-salt interactions, and at 0.1 for the  $\text{H}_2\text{S}$ -salt and MDEA-salt interactions, according to Hessen and coworkers [54].

The optimization routine used in this work is Particle Swarm Optimization (PSO), developed by Kennedy and Eberhart [55]. This algorithm allows for the optimization of continuous non-linear functions, using particle swarm methodology. The advantage of this optimization routine is that it uses random initialization, thus, unlike other optimization methods, its convergence is not dependent on the first approximations. In order to avoid local minima and find an optimal solution, local best topology was used [56,57]. The PSO parameters are swarm size of 40, maximum number of iterations 600 in 3 loops which terminate once the optimized value deviates more than  $10^{-4}$  (tolerance criterion) from its preceding one or if less than 1% improvement is achieved during 60 iterations. The minimization of the absolute average relative deviation (AARD)

**Table 7**  
Fixed parameters of eNRTL model used in this work.

Non-randomness factors, $\alpha$					
Components					
i	j	ij	ji	-	-
m	m	0.2	0.2		
H <sub>2</sub> O	c-a	0.2	0.2		
H <sub>2</sub> S	c-a	0.1	0.1		
MDEA	c-a	0.1	0.1		
Energy parameters, $\tau_{ij}$					
Components					
i	j	ij	ji	ij	ji
H <sub>2</sub> O	H <sub>2</sub> S	0	0	0	0
H <sub>2</sub> O	H <sub>3</sub> O <sup>+</sup> -OH <sup>-</sup>	8	-4	0	0
H <sub>2</sub> O	H <sub>3</sub> O <sup>+</sup> -HS <sup>-</sup>	8	-4	0	0
H <sub>2</sub> S	H <sub>3</sub> O <sup>+</sup> -OH <sup>-</sup>	15	-8	0	0
H <sub>2</sub> S	H <sub>3</sub> O <sup>+</sup> -HS <sup>-</sup>	15	-8	0	0

shown in Eq. (11), was chosen as the objective function, where  $Y$  was either the partial pressure of H<sub>2</sub>S,  $P_{H_2S}$ , or the total pressure,  $P_{tot}$ .

$$F_{obj}(\%) = \frac{1}{N} \sum_i \frac{|Y_i^{exp} - Y_i^{pred}|}{Y_i^{exp}} \cdot 100 \quad (11)$$

## 5. Results and Discussion

### 5.1. Experimental results

**High-pressure VLE.** The experimental vapor-liquid equilibrium data obtained in this work with 50.1 wt% and 70 wt% MDEA solution for the system CH<sub>4</sub>-H<sub>2</sub>S-MDEA-H<sub>2</sub>O at various pressures and temperatures are presented in Table 8 and Table 9. As mentioned earlier, knowing the experimental uncertainty of reported data could possibly help us understand the scatter observed in the data for the system H<sub>2</sub>S-MDEA-H<sub>2</sub>O. Therefore, we performed a thorough investigation of our measurements' uncertainty in order to properly evaluate our data and conclude on the impact of experimental uncertainty on our results.

We have reported the combined uncertainties employing the Law of propagation of uncertainty according to NIST guidelines

[58]. The new data are accompanied by the standard uncertainties for total pressure and temperature as well as the combined uncertainties for the partial pressure of hydrogen sulfide, the global and the liquid loading. It was found that the main contributor to the uncertainty of the partial pressure of H<sub>2</sub>S is the total pressure of the system, as can be observed by the increasing uncertainty of  $P_{H_2S}$  for increasing total pressure. The main contribution to the global loading uncertainty is associated with the loading itself, while the uncertainty of the liquid loading is mostly affected by the uncertainty of the total moles of H<sub>2</sub>S introduced in the cell. The repeatability of our measurements was taken into account by virtue of the multiple samples analyzed on the GC at each equilibrium pressure and temperature. The complete uncertainty analysis can be found in Supplementary Information.

Table 8 and Fig. 2 reveal information regarding both the reproducibility of the measurements in this work as well as their comparison with the literature for the system CH<sub>4</sub>-H<sub>2</sub>S-MDEA-H<sub>2</sub>O with a 50–50.1 wt% MDEA solution at approximately 323 K. The measured vapor fractions of methane and hydrogen sulfide are reported in Supplementary Information together with the uncertainty analysis. Our measurements in the presence of 500 kPa of methane were performed in two different experiments, and as one can observe in the figure, the same behavior is followed and the measurements can be reproduced. The data obtained in this work are in agreement with the data reported by Dicko et al. [29] under

**Table 8**

Experimental vapor-liquid equilibrium data and their corresponding combined uncertainties at total pressure of 500 kPa (and one measurement at total pressure 3000 kPa) and temperature of 323 K for the system CH<sub>4</sub>-H<sub>2</sub>S-MDEA-H<sub>2</sub>O and 50.1 wt% aqueous MDEA<sup>a</sup>. Methane is used as makeup gas.

$T$	$P_{tot}$	$P_{H_2S}$	$u_c(P_{H_2S})$	$\alpha_{glob}$	$u_c(\alpha_{glob})$	$\alpha_{liq}$	$u_c(\alpha_{liq})$	NS
K	kPa	kPa	kPa	mol H <sub>2</sub> S global/mol MDEA	mol H <sub>2</sub> S global/mol MDEA	mol H <sub>2</sub> S liquid/mol MDEA	mol H <sub>2</sub> S liquid/mol MDEA	
322.98	493.81	2.99	0.03	0.096	0.003	0.095	0.001	9
322.98	480.01	11.27	0.12	0.214	0.005	0.211	0.002	9
322.98	500.72	49.11	0.43	0.490	0.005	0.477	0.002	7
322.98	604.01	177.59	1.20	0.822	0.006	0.775	0.003	10
					Experiment 2			
322.98	493.92	2.60	0.02	0.085	0.003	0.084	0.002	6
322.98	493.50	22.33	0.19	0.312	0.004	0.303	0.002	6
322.98	498.13	72.79	0.56	0.588	0.006	0.559	0.003	8
322.98	530.82	139.10	0.93	0.760	0.013	0.703	0.006	5
322.98	545.53	168.46	1.06	0.820	0.039	0.751	0.020	9
322.98	3106.96	179.67	1.52	0.820	0.039	0.745	0.020	8

<sup>a</sup> Standard uncertainties not included above are  $u(T) = 0.02$  K,  $u(P) = 0.6$  kPa.

**Table 9**

Experimental vapor-liquid equilibrium data and their corresponding combined uncertainties as a function of total pressure and temperature for the system CH<sub>4</sub>-H<sub>2</sub>S-MDEA-H<sub>2</sub>O and 70 wt% aqueous MDEA<sup>a</sup>. Methane is used as makeup gas.

T K	P <sub>tot</sub> kPa	P <sub>H<sub>2</sub>S</sub> kPa	u <sub>c</sub> (P <sub>H<sub>2</sub>S</sub> ) kPa	α <sub>glob</sub>		u <sub>c</sub> (α <sub>glob</sub> )		α <sub>liq</sub>		u <sub>c</sub> (α <sub>liq</sub> )	NS
				mol H <sub>2</sub> S global/mol MDEA	mol H <sub>2</sub> S liquid/mol MDEA	mol H <sub>2</sub> S global/mol MDEA	mol H <sub>2</sub> S liquid/mol MDEA	mol H <sub>2</sub> S liquid/mol MDEA	mol H <sub>2</sub> S liquid/mol MDEA		
283.00	2011.87	3.48	0.03	0.232	0.003	0.231	0.003	9			
283.00	6030.85	3.85	0.05	0.232	0.003	0.231	0.003	10			
283.00	10052.50	4.68	0.04	0.232	0.003	0.231	0.003	7			
352.99	1976.07	106.23	0.92	0.239	0.002	0.211	0.002	5			
352.99	3954.66	108.30	0.98	0.239	0.002	0.210	0.002	10			
352.99	5957.76	108.03	1.03	0.239	0.002	0.210	0.002	7			
352.99	7976.36	111.95	1.04	0.239	0.002	0.209	0.002	6			
352.99	9988.18	111.42	1.12	0.239	0.002	0.208	0.002	6			
393.00	2024.40	375.10	1.46	0.246	0.002	0.167	0.002	8			
392.99	5979.36	376.17	1.72	0.246	0.002	0.165	0.002	10			
393.00	9925.29	364.18	1.97	0.246	0.002	0.167	0.002	8			
283.00	1975.74	13.13	0.15	0.488	0.002	0.484	0.002	7			
283.00	5990.55	17.37	0.28	0.488	0.002	0.482	0.002	5			
283.00	10045.17	21.56	0.24	0.488	0.002	0.480	0.002	6			
352.92	2006.00	264.36	1.30	0.478	0.002	0.415	0.002	7			
352.92	5980.37	281.97	1.57	0.478	0.002	0.408	0.002	8			
352.92	9975.23	300.30	1.67	0.478	0.002	0.402	0.002	8			
393.05	974.22	834.43	0.49	0.484	0.002	0.304	0.003	3			
393.00	2034.17	818.12	2.26	0.484	0.002	0.308	0.003	8			
393.01	5893.45	806.74	3.34	0.484	0.002	0.309	0.003	7			
393.00	9915.85	809.32	3.68	0.484	0.002	0.307	0.003	9			

<sup>a</sup> Standard uncertainties not included above are  $u(T) = 0.02$  K,  $u(P) = 0.6$  kPa.

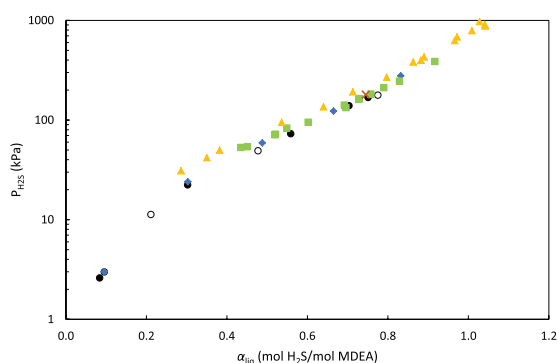


**Fig. 2.** Equilibrium H<sub>2</sub>S partial pressures as a function of liquid loading and total pressure for 50 wt% MDEA-H<sub>2</sub>O at 323 K. ● P<sub>tot</sub> = 500 kPa (This work, Experiment 1), ○ P<sub>tot</sub> = 500–600 kPa (This work, Experiment 2), ◆ P<sub>tot</sub> = 500–700 kPa [29], ■ P<sub>tot</sub> = 1500 kPa [30], × P<sub>tot</sub> = 3000 kPa (This work), ▲ P<sub>tot</sub> = 7000 kPa [30].

similar conditions. These data together with Sadegh et al.'s data [30] at total pressure of 1500 kPa and 7000 kPa show that, for a given liquid loading, an increase in the total pressure of the system leads to an increase in the H<sub>2</sub>S partial pressure. Our single measurement at total pressure of 3000 kPa for this system follows this trend, too. An exception is the last point reported by Dicko et al. at  $\alpha_{liq} = 0.832$  mol H<sub>2</sub>S/mol MDEA, which also differs from the trend in our data. This point is measured at total pressure 700 kPa but lies between the data reported by Sadegh et al., at 1500 kPa and 7000 kPa total pressure. Here it is important to mention that the measurements reported by Dicko et al. are global loadings, and the liquid loadings shown in Fig. 2 are the ones calculated by the authors.

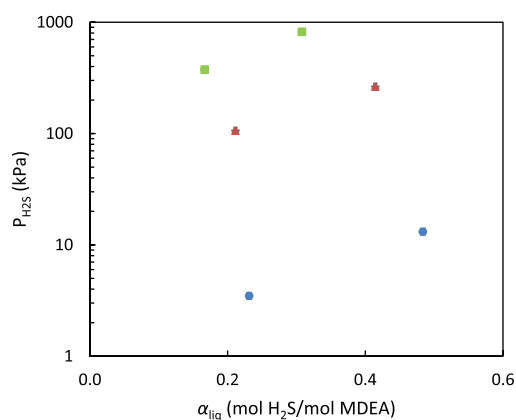


**Fig. 3.** Experimental H<sub>2</sub>S solubility in a 70 wt% MDEA-H<sub>2</sub>O system with methane as makeup gas at total pressure of 2000 kPa at temperature; ● 283 K, ▲ 353 K and ■ 393 K. Error bars for both H<sub>2</sub>S partial pressure and loading are included.

The observation of increased H<sub>2</sub>S partial pressure upon increase in total pressure can be made also for the 70 wt% aqueous MDEA system for the temperatures of 283 K and 353 K. The deviations in partial pressure are higher for higher global loadings. On the other hand, the liquid loading remains unchanged at 283 K while the one at 353 K seems to decrease. At 393 K, not clear trends are shown. This behavior is noticed for all global loadings, though the fact that the water present in the vapor phase could not be quantified through the GC analysis, and it was therefore calculated based on the vapor pressure of the solvent under the assumption that it was constant with increasing total pressures, might have its share on



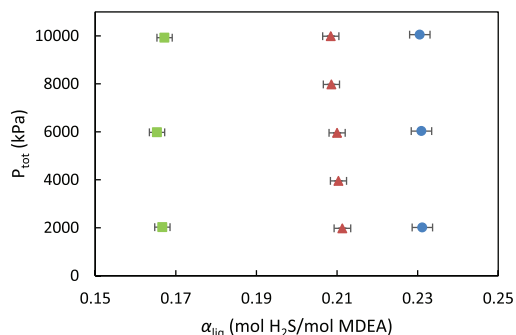


**Fig. 4.** H<sub>2</sub>S liquid phase loading of a 70 wt% MDEA-H<sub>2</sub>O system with methane as makeup gas as a function of total pressure and temperature: ● 283 K, ▲ 353 K and ■ 393 K. Error bars for both total pressure and liquid loading are included.

the latter. The effect of temperature is the expected one given the exothermic nature of the chemical reactions; the lower the temperature, the higher the absorption of H<sub>2</sub>S in the liquid phase at constant partial pressure of hydrogen sulfide. The features discussed above are illustrated in Fig. 3 and Fig. 4. It is worth mentioning that error bars representing the uncertainty in pressures and loadings are included in the figures, however uncertainties in pressure are too low to be visible.

Although there is a clear trend of the pressure effect on the partial pressure of H<sub>2</sub>S, taking into account the uncertainties, it can be seen that the deviations in liquid loading are similar to the experimental uncertainty. In fact, at 283 K and for global loading 0.232, no change at all in liquid loading is observed. The fact that hydrogen sulfide is chemically bound to the amine reinforces the argument that the differences in loading are due to uncertainty in measurements. The amount of methane dissolved in the liquid phase is too low to have an impact on the reaction of hydrogen sulfide with the amine solution which is an exothermic reaction whose reversion requires high amounts of energy. Overall, it is observed that the effect of increasing the total pressure from 2000 kPa to 10000 kPa in terms of H<sub>2</sub>S loading in a 70 wt% aqueous MDEA at temperatures of 283 K, 353 K and 393 K is not significant and, in most cases, it is within or very close to experimental uncertainty.

As Sadegh et al. [30] showed, taking into account the gas

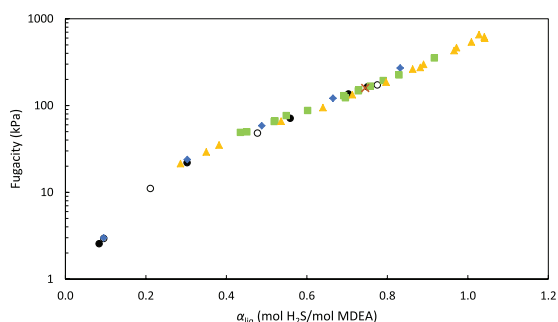


**Fig. 5.** Equilibrium H<sub>2</sub>S fugacities as a function of liquid loading and total pressure for 50 wt% MDEA-H<sub>2</sub>O at 323 K. ●  $P_{\text{tot}} = 500$  kPa (This work, Experiment 1), ○  $P_{\text{tot}} = 500\text{--}600$  kPa (This work, Experiment 2), ◆  $P_{\text{tot}} = 500\text{--}700$  kPa [29], ■  $P_{\text{tot}} = 1500$  kPa [30], ×  $P_{\text{tot}} = 3000$  kPa (This work, Experiment 2), ▲  $P_{\text{tot}} = 7000$  kPa [30].

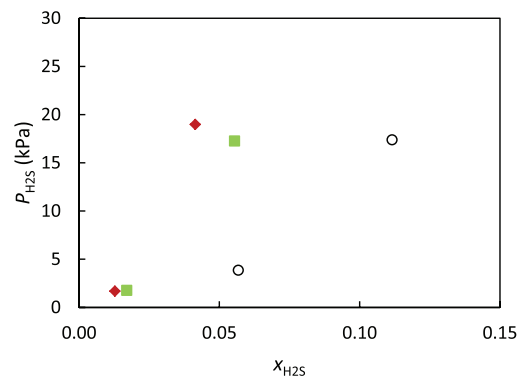


**Fig. 6.** Hydrogen sulfide molar concentration in the liquid phase for the system CH<sub>4</sub>-H<sub>2</sub>S-MDEA-H<sub>2</sub>O as a function of partial pressure and amine concentration at total pressures 6000–6900 kPa and at 283 K; ◆ 35 wt% MDEA-H<sub>2</sub>O [25], ■ 50 wt% MDEA-H<sub>2</sub>O [25], ○ 70 wt% MDEA-H<sub>2</sub>O (This work).

fugacities is adequate to explain the deviations of the equilibrium H<sub>2</sub>S pressures at different total pressures for a 50 wt% aqueous MDEA. Indeed, Fig. 5 shows how the fugacity exhibits the same behavior for all data obtained in a 50–50.1 wt% MDEA-H<sub>2</sub>O solution in the presence of methane from different literature sources. The figure is similar to one provided by Sadegh et al. [30], this time enriched with our data at total pressure of 500 and 3000 kPa demonstrating the same behavior. The fugacities were calculated using Peng-Robinson EoS with binary interaction parameters set to zero. As far as the data obtained for the 70 wt% aqueous MDEA are concerned, the fugacity can explain the partial pressure trend observed for our data at 283 K and 353 K. At 393 K, the uncertainty in liquid loadings are such that no solid conclusions can be drawn.

The effect of amine concentration was also studied by means of comparison with reported data in the literature at 283 K and 393 K, shown in Fig. 6 and Fig. 7 respectively. Data at 353 K in our range of loading and pressure are not available in the literature, therefore no comparison could be performed. A clear effect of increasing molar concentration with increasing amine concentration and constant H<sub>2</sub>S pressure can be seen in the comparison performed at 283 K. This can be expected since the more amine available, the higher the capacity of the solvent. It is important to state that the literature data are reported only from one reference source [25] where methane makeup gas was also used. Because of the effect of methane presence, we have plotted the available data at similar total pressures; our data only for total pressure of 6000 kPa and the literature data at total pressure of 6900 kPa in order to allow for a fairer comparison. The molar concentration of H<sub>2</sub>S is also increasing with amine content in the solution at 393 K, but only up to 50 wt%. Our data at 70 wt% overlap with the literature data obtained in a 50 wt% aqueous MDEA study. This is illustrated in Fig. 7 where we have only plotted the data with very little methane or with total pressure of 2000 kPa from our work.

Hydrogen sulfide can react directly with MDEA through a typical acid-base reaction [2]. At the same time, the presence of water would enhance the acid gas uptake through the dissolution of hydrogen sulfide as well the protonation of the amine. Therefore, we could identify two possible mechanisms through which H<sub>2</sub>S is absorbed; one directly into the amine and one via water. Moreover, hydrogen sulfide absorption in MDEA-H<sub>2</sub>O is the result of both physical and chemical absorption. Therefore, in order to provide a good discussion about the behavior observed in Figs. 6 and 7, the physical absorption of hydrogen sulfide into MDEA-H<sub>2</sub>O systems

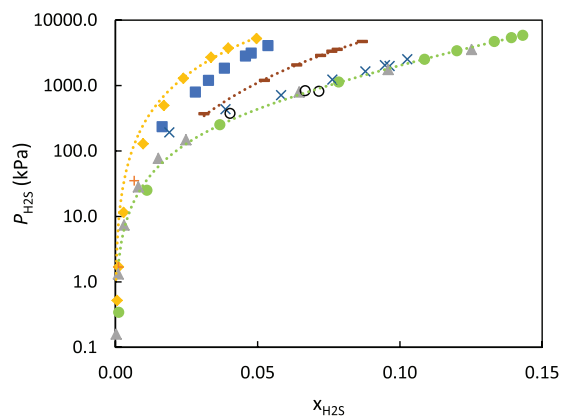


**Fig. 7.** Hydrogen sulfide molar concentration in the liquid phase for the system H<sub>2</sub>S-MDEA-H<sub>2</sub>O as a function of partial pressure and amine concentration at 393 K; ◆ 11.8 wt% MDEA-H<sub>2</sub>O [12], ■ 18.7 wt% MDEA-H<sub>2</sub>O [17], + 23.1 wt% MDEA-H<sub>2</sub>O [23], ● 32.2 wt% MDEA-H<sub>2</sub>O [17], ○ 48.8 wt% MDEA-H<sub>2</sub>O [12], × 48.8 wt% MDEA-H<sub>2</sub>O, ▲ 50 wt% MDEA-H<sub>2</sub>O [23], ○ 70 wt% MDEA-H<sub>2</sub>O (This work).

should be taken into account. To our best knowledge, only Rinker and Sandall [59] have reported such information. They measured H<sub>2</sub>S solubility in protonated aqueous MDEA and their measurements showed that the solubility increases with amine content. Although the available data cover 0–50 wt% MDEA-H<sub>2</sub>O systems, it can be assumed that the same trends would be followed and the physical absorption of H<sub>2</sub>S in to a 70 wt% aqueous MDEA is higher than in a 50 wt% aqueous MDEA.

Based on the above, the fact that  $x_{\text{H}_2\text{S}}$  is not increased with amine content from 50 to 70 wt% at 393 K and constant H<sub>2</sub>S pressure indicates that the contribution of the chemical absorption decreases as the amine content increases. This can be also confirmed by observing the slope of indicative tendency curves in Fig. 7 (better illustrated in Fig. S7 in Supplementary Information, where non-logarithmic scale is used for the y axis). The slope reveals information about the absorption capacity of the systems. It is observed that as the amine composition increases, the  $P$ - $x$  curve has a lower slope (apparent Henry's constant). The lower the slope, the closer to linearity and, thus, higher physical absorption. For example, at 500 kPa, the apparent Henry's constant is 535 kPa m<sup>3</sup>/kmol for 11.8 wt% MDEA-H<sub>2</sub>O and 300 kPa m<sup>3</sup>/kmol for 48.8 wt% MDEA-H<sub>2</sub>O.

**Table 10**  
Experimental vapor pressure  $P^s$ /kPa for pure MDEA<sup>a</sup>.

T (K)	$P^s$ (kPa)				
	Experimental	DIPPR		This work (Table 11)	
		Predicted	ARD (%) <sup>b</sup>	Predicted	ARD (%) <sup>b</sup>
405.34	1.79	1.95	9%	1.79	0%
411.00	2.29	2.53	10%	2.34	2%
415.31	2.79	3.06	10%	2.86	2%
418.58	3.29	3.54	7%	3.31	1%
421.73	3.79	4.05	7%	3.80	0%
424.52	4.29	4.55	6%	4.28	0%
427.21	4.79	5.09	6%	4.80	0%
429.49	5.29	5.59	6%	5.28	0%
431.60	5.79	6.08	5%	5.76	0%
433.49	6.29	6.56	4%	6.22	1%
435.34	6.79	7.05	4%	6.71	1%

<sup>a</sup> Standard uncertainties are  $u(T) = 0.1$  K,  $u(P) = 0.1$  kPa.

<sup>b</sup>  $\text{ARD} (\%) = \left| \frac{P_5^{\text{pred}} - P_5^{\text{exp}}}{P_5^{\text{exp}}} \right| \cdot 100$

**Table 11**  
Parameters for the Antoine correlation for pure MDEA vapor pressure<sup>a</sup>.

	A	B	C
MDEA	$9.676 \pm 0.014$	$-1965.6 \pm 8.9$	$-99.33 \pm 0.69$

<sup>a</sup>  $\log_{10} P^s = A + \frac{B}{T+C}$ , T in K, P in Pa. Temperature range: 294–738 K.

**Table 12**  
AARDs for the fitted  $P_{\text{tot}}$ , FPD and  $H^E$  for the MDEA-H<sub>2</sub>O system.

Variable	Source	AARD (%)
$P_{\text{tot}}$	Kim et al. [33]	1.1
	Xu et al. [34]	1.9
	Voutsas et al. [35]	6.4
	<b>Overall</b>	<b>2.5</b>
FPD	Chang et al. [31]	10.3
	Fosbøl et al. [32]	4.4
	<b>Overall</b>	<b>6.0</b>
$H^E$	Posey [36]	7.6
	Maham et al. [37]	3.1
	Maham et al. [38]	11.5
	<b>Overall</b>	<b>7.4</b>

MDEA-H<sub>2</sub>O at 393 K. This behavior is followed also at higher pressure; at 3000 kPa, the apparent Henry's constant is 1169 kPa m<sup>3</sup>/kmol for 11.8 wt% MDEA-H<sub>2</sub>O and 715 kPa m<sup>3</sup>/kmol for 48.8 wt% MDEA-H<sub>2</sub>O at 393 K. Unfortunately, our data are too few to assess the  $P$ - $x$  linearity for 70 wt% MDEA-H<sub>2</sub>O, nonetheless it can be said that the chemical contribution in the overall H<sub>2</sub>S uptake is decreased. In the case of low temperatures such as in our studied temperature of 283 K, these effects could probably not be visible because the absorption capacity is very high and our data as well as the data reported in the literature are produced for low H<sub>2</sub>S partial pressure.

**Ebulliometer.** The measurements conducted in the ebulliometer are shown in Table 10. The main limitation of ebulliometric measurements is the absence of stirring. Experimental measurement of the vapor pressure of the binary mixtures used in this work was not possible because two phases formed, associated with the high viscosity of pure MDEA, i.e. ca. 77 mPa s at 298.15 K [60–62]. Therefore, only the vapor pressure of MDEA was measured.

## 5.2. Modeling results

In this section, we present first the results from the ebulliometer following by the modeling results for the high-pressure VLE data, since the first ones are used in the model parametrization for the H<sub>2</sub>S-MDEA-H<sub>2</sub>O equilibrium.

**Ebulliometer.** The Antoine correlation was fitted to available data from the literature (Table 3) as well as the newly obtained data of this work, covering a large range of temperatures and pressures. In Table 10, our experimental measurements are compared with the predicted vapor pressures by our fitted Antoine correlation and the DIPPR equation. At the temperature range of 405–435 K studied in this work, the absolute relative deviation (ARD) between the experimental and the estimated value is 7% with DIPPR equation and 1% in our correlation, which has been fitted to available data in the literature covering temperatures from 293 K to 738 K. The new parameters for Antoine correlation proposed for the estimation of the vapor pressure of MDEA, are shown in Table 11. The Average Absolute Relative Deviation (AARD) is 4% for our correlation and 30% for DIPPR. The high deviation for DIPPR equation is mainly due to the vapor pressure predictions at temperatures higher than 530 K, which explains the high AARD. In the fitting, we excluded

**Table 13**  
BIAS<sup>a</sup>, AADs<sup>b</sup> and AARDs<sup>c</sup> for the fitted total pressures,  $P_{\text{tot}}$ , and H<sub>2</sub>S partial pressures,  $P_{\text{H}_2\text{S}}$ , for Cases A, B and C.

Source	Case A				Case B				Case C			
	Pressure range	Bias	AAD	AARD	Pressure range	Bias	AAD	AARD	Pressure range	Bias	AAD	AARD
	kPa	(%)	kPa	(%)	kPa	(%)	kPa	(%)	kPa	(%)	kPa	(%)
Partial pressure, $P_{\text{H}_2\text{S}}$												
Lemoine et al. [28]	0.023–1.611	–42.8	0.1	42.8	0.176–1.611	–27.0	0.2	27.0	0.176–1.611	–23.7	0.1	23.7
Huang and Ng [23]	0.0033–3673	–32.7	80.4	38.8	2.34–3673	–5.0	82.9	8.6	2.34–3673	–2.5	69.0	13.3
Rogers et al. [24]	0.00069–5.268	–25.7	0.1	32.2	0.2–5.268	–12.1	0.2	13.0	0.2–5.268	–6.8	0.2	12.3
MacGregor and Mather [14]	0.52–1600	48.4	19.3	48.7	0.52–1600	36.6	11.5	37.7	0.52–1600	49.0	15.8	49.2
Jou et al. [21]	0.00183–313	–8.1	5.9	23.6	0.295–313	–2.0	3.6	13.0	0.295–313	6.1	5.9	13.4
Jou et al. [12]	0.0013–5890	18.2	125.6	29.7	0.0273–5890	9.5	109.7	17.6	0.0273–5890	13.9	105.7	20.6
Zoghi and Shokouhi [22]	28–1361	24.2	42.4	26.2	14–1361	14.4	32.1	16.4	14–1361	20.4	36.5	22.2
Maddox et al. [27]	13.23–1536.6	–4.9	74.8	15.2	13.23–1536.6	–8.5	78.0	13.4	13.23–1536.6	–6.4	77.1	13.9
Huttenhuis et al. [25]	–	–	–	–	–	–	–	–	0.141–1.495	–35.0	0.3	35.0
Dicko et al. [29]	–	–	–	–	–	–	–	–	3–278	–17.0	11.6	17.0
Sadegh et al. [30]	–	–	–	–	–	–	–	–	53–386	–10.9	11.4	10.9
This work	–	–	–	–	–	–	–	–	2.60–818.12	–20.2	36.5	21.3
<b>Overall</b>		<b>0.9</b>	<b>70.4</b>	<b>30.4</b>		<b>3.5</b>	<b>66.2</b>	<b>17.8</b>		<b>5.1</b>	<b>58.4</b>	<b>20.6</b>
Total pressure, $P_{\text{tot}}$												
Kuranov et al. [17]	165.2–4895.9	–9.6	240.3	12.5	165.2–4895.9	–10.5	241.1	13.6	165.2–4895.9	–10.0	241.5	12.9
Kamps et al. [18]	147.9–2783	–15.2	213.7	16.0	147.9–2783	–20.8	231.5	20.8	147.9–2783	–13.7	173.5	14.2
Sidi-Boumedine et al. [19]	6.21–1040	–10.8	55.4	12.6	6.21–1040	–16.4	70.3	16.7	6.21–1040	–9.9	56.2	11.0
<b>Overall</b>		<b>–11.0</b>	<b>194.4</b>	<b>13.2</b>		<b>–13.9</b>	<b>202.9</b>	<b>15.8</b>		<b>–10.8</b>	<b>187.9</b>	<b>12.7</b>

$$^a \text{BIAS (\%)} = \frac{1}{N} \sum \frac{P_s^{\text{pred}} - P_s^{\text{exp}}}{P_s^{\text{exp}}} \cdot 100,$$

$$^b \text{AAD} = \frac{1}{N} \sum |P_s^{\text{pred}} - P_s^{\text{exp}}|,$$

$$^c \text{AARD (\%)} = \frac{1}{N} \sum \left| \frac{P_s^{\text{pred}} - P_s^{\text{exp}}}{P_s^{\text{exp}}} \right| \cdot 100$$

the data from Kim et al. [33] which are slightly higher than the data obtained on the same conditions by Daubert et al. [40] as well as our measurements. However, including those data leads to modelled vapor pressures with only the slightly higher AARD of 5%.

**High-pressure VLE.** The parameter fitting for the MDEA–H<sub>2</sub>O system returned satisfactory AARDs for all three variables fitted, i.e. VLE ( $P_{\text{tot}}$ ), FPD and  $H^{\text{E}}$ , as described in Sections 2.2 and 4. The calculated AARDs for each variable are shown in Table 12.

The model can predict very well the total pressure of the binary system, as witnessed above by the low AARD. The excess enthalpy  $H^{\text{E}}$  can be well predicted at temperatures of 298.15 and 313.15 K, though the model yields lower excess enthalpies at 338.15 K for MDEA concentrations lower than 85 wt%. At this temperature, the model was fitted to experimental data reported by Maham et al. [38] which shows the highest AARD. The corresponding figures for the total pressure, excess enthalpy and the freezing point depression are presented in Section C of Supplementary Information.

The fixed parameters in Table 7 and the regressed parameters for the binary subsystem MDEA–H<sub>2</sub>O (Supplementary Information) were used for the regression of the ternary system H<sub>2</sub>S–MDEA–H<sub>2</sub>O. Initially, all the data from Table 1 were used for the parametrization of the model, except for the data from Li and Shen, as well as the data in the presence of methane (Case A). The data obtained in the presence of nitrogen were all included. The scatter already discussed earlier at low loadings resulted in high AARD, especially for the data points reported in terms of partial pressure of H<sub>2</sub>S. The high deviations are also attributed to the much lower values of partial pressures in comparison with total ones, leading to higher relative numbers. Therefore, we have decided to also perform the data regression excluding all data at loadings lower than 0.05 mol H<sub>2</sub>S/mol MDEA (Case B). This indeed improved substantially the fitting of the partial pressures, as one can see in the AARDs in Table 13, from approximately 30%–18%. The parity plot for the predicted and experimental values is shown in Fig. 8 while Fig. 9 shows the difference between predicted and experimental H<sub>2</sub>S

partial pressure as a function of the experimental value.

Significant scatter can be seen in the plots above at the lower pressures. At pressures  $P < 1$  kPa, the model underestimates the data from Lemoine et al. [28] while overestimating the data from Jou et al. [12] and MacGregor and Mather [14]. The accuracy of the model is good for the data from Rogers et al. [24] and Jou et al. [21], with some data being underpredicted. The visual observations are depicted on the bias and AARD (%) calculations presented in Table 13. The negative bias whose absolute value is the same as the AARD for Lemoine et al.'s work shows that all data have been underestimated by the model. In addition, the fact that the AARD for this source is 0.2 kPa shows that the high AARD of 27% is due to the low values in partial pressures. At intermediate pressures, the scatter is less pronounced, but still the model overpredicts the data of MacGregor and Mather [14] and Jou et al. [12]. The BIAS and AARDs for these two are –37% and 38% and –27% and 27% respectively, while the rest of the sources show AARDs lower than 17%. At higher pressures, both Figs. 8 and 9 show that the model can predict well the literature data.

Overall, maximum AARD was found for the data from MacGregor and Mather [14] showing an almost 50% AARD in Case A and 38% in Case B. The minimum deviations observed were for the data from Maddox et al. [27] in Case A (13%) and from Huang and Ng [23] in Case B (9%). From the three experimental sets of total pressure, the one reported by Kuranov et al. showed the lowest deviations for both cases. Similar observations were made also by Huttenhuis et al. [20] during the evaluation of their model developed for the H<sub>2</sub>S–MDEA–H<sub>2</sub>O system. Although the model framework they used (electrolyte EoS for both phases) differs from ours, their model predictions also showed highest deviations for the data from MacGregor and Mather and lowest for the data from Maddox et al. [27] and Kuranov et al. [17]. Fig. 10 shows experimental and modelled values for a 50 wt% aqueous MDEA system as a function of temperature in Case B.

The differences in H<sub>2</sub>S partial pressure noticed in the literature

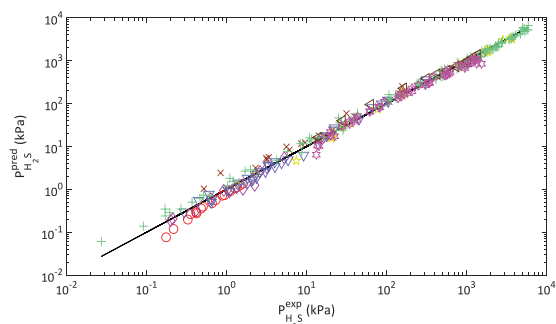


**Fig. 8.** Parity plot for different literature sources;  $\circ$  Lemoine et al. [28],  $\square$  Huang and Ng [23],  $\diamond$  Rogers et al. [24],  $\times$  (MacGregor and Mather [14],  $\nabla$  Jou et al. [21],  $+$  Jou et al. [12],  $\square$  Zoghi and Shokouhi [22],  $\square$  Maddox et al. [27],  $(-)$   $y = x$ .

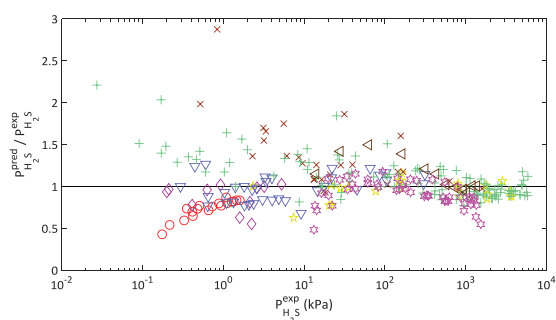


**Fig. 9.** Difference between predicted and experimental  $H_2S$  partial pressure as a function of the experimental value.  $\circ$  Lemoine et al. [28],  $\square$  Huang and Ng [23],  $\diamond$  Rogers et al. [24],  $\times$  MacGregor and Mather [14],  $\nabla$  Jou et al. [21],  $+$  Jou et al. [12],  $\square$  Zoghi and Shokouhi [22],  $\square$  Maddox et al. [27].

data as well as in our data obtained in the presence of methane for relatively low total pressure levels, are comparable to the accuracy of the model. Therefore, since also the effect of methane in the liquid loading has been found to be negligible for a 70 wt% MDEA- $H_2O$ , we also fitted the model to data available in the presence of methane. However, the code was not modified but, instead, the data for partial pressure of  $H_2S$  and loading were used as if methane

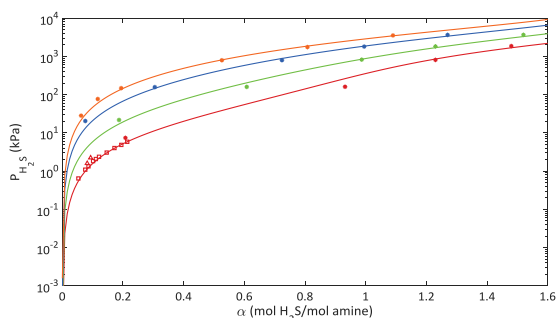


**Fig. 10.** Hydrogen sulfide loading for 50 wt% MDEA- $H_2O$  as a function of partial pressure and temperature; (red) 313 K, (green) 343 K, (blue) 373 K, (orange) 393 K;  $(-)$  model, \* Huang and Ng [23],  $\Delta$  Rogers et al. [24] (1998),  $\square$  Jou et al. [21] (1993). Regression in Case B.

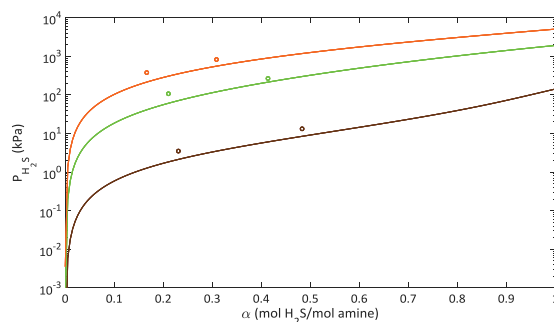


**Fig. 11.** Hydrogen sulfide loading for 70 wt% MDEA- $H_2O$  as a function of partial pressure and temperature; (brown) 283 K, (green) 353 K, (orange) 393 K;  $(-)$  model,  $\circ$  This work. Regression in Case C.

was not present. Only data with maximum total pressure of 2000 kPa were considered, due to the more significant  $P_{H_2S}$  deviations observed at higher pressures in the literature for a 50 wt% aqueous MDEA (Case C). To sum up, three cases were studied:

**Case A.** Regression of all available data in the absence of methane.

**Case B.** Regression of all available data in the absence of methane and loadings  $\alpha > 0.05$  mol  $H_2S$ /mol MDEA.

**Case C.** Regression of all available data in the absence of methane and loadings  $\alpha > 0.05$  mol  $H_2S$ /mol MDEA, and the data in the presence of methane, loadings  $\alpha > 0.05$  mol  $H_2S$ /mol MDEA and maximum total pressures  $P_{tot}$  of 2000 kPa.

The model parameters obtained from the data regression in each case studied are given in Supplementary Information. Fig. 11 shows experimental and modelled values for a 70 wt% aqueous MDEA system as a function of temperature in Case C while Table 13 contains information about each regression in terms of Bias, AADs and AARDs. The performance of the model for a 70 wt% MDEA- $H_2O$  system is good, especially considering the few data available for this solvent concentration. In Table 13, it can be seen that the accuracy of the model does not significantly change upon the addition of the experimental points with methane in the regression. The overall AARD for the partial pressure is altered from 18% to 21%, which is also the AARD calculated for the data published in this work. The data from MacGregor and Mather [14] exhibit again the highest deviations while the measurements reported by Sadegh et al. [30]

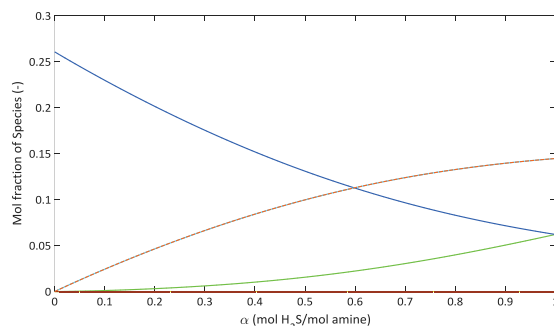


**Fig. 12.** Predicted speciation of  $H_2S$ , MDEA and  $H_2O$  in 70 wt% MDEA- $H_2O$  at 353 K.  $(-)$   $H_2S$ ,  $(-)$  MDEA,  $(-)$   $H_2O$ ,  $(-)$  MDEAH $^+$ ,  $(- -)$  OH $^-$ ,  $(- -)$  HS $^-$ .

in total pressure of 1500 kPa with methane as makeup gas show the lowest deviation, 11%. The slight deterioration of the fitting for the equilibrium  $H_2S$  can be also attributed to the fact that experimental points obtained for high amine concentrations are used, i.e. 70 wt% in this work, but it can also be the result of the sensitivity of the algorithm to the numerical method. To illustrate the latter, we repeated the data regression for Case A. The resulted AARDs were 29.8% and 30.1%, using the exact same data and fixed parameters. As far as the ability of the model to predict the total pressure is concerned, the accuracy has surprisingly improved. This is merely a lucky coincidence due to the fitting of the experimental points for methane-included systems.

Speciation information is necessary in the development of process models for the accurate design and operation of gas processing plants. Speciation results, calculated with the model presented in this work, are provided in Fig. 12 where mole fractions of all the species in the liquid phase are plotted against liquid loading for 70 wt% aqueous MDEA at 353 K. It is shown that as the loading increases, the concentration of MDEA declines and the concentration of protonated amine  $MDEAH^+$  increases. At loadings close to 1, most of the amine has been protonated and the mole fractions of MDEA and  $H_2S$  are equal. The curves representing  $MDEAH^+$  and  $HS^-$  overlap, a behavior expected since the formation of sulfide was not taken into account due to its low concentration, therefore the amount of  $HS^-$  and  $MDEAH^+$  formed are balanced.  $H_3O^+$  and  $OH^-$  also overlap and they are practically zero throughout the loading range. No experimental data were found for the speciation distribution in the  $H_2S$ -MDEA- $H_2O$  system to confirm the model predictions. Speciation graphs for 50.1 wt% and 70 wt% MDEA- $H_2O$  at the temperatures studied in this work are provided in Supplementary Information.

Overall, although the model developed in this work contains MDEA,  $H_2O$ ,  $H_2S$  and the relevant ionic species, it can predict vapor-liquid equilibria for systems containing methane at low total pressures with similar accuracy as the systems in the absence of methane. However, it is recommended to be used only for rough estimations for  $H_2S$ - $CH_4$ -MDEA- $H_2O$  system and a model taking into account the methane solubility to be used if available. This model should not be used for systems with total pressure higher than 2000 kPa, where the gas fugacities change substantially.

## 6. Conclusions

Experimental vapor-liquid equilibrium data were measured for a 50.1 wt% aqueous MDEA at temperature of 323 K and pressure up to 3000 kPa as well as a 70 wt% aqueous MDEA at temperature of 283 K, 353 K and 323 K and pressures up to 10000 kPa, due to their relevance for subsea  $H_2S$  removal of natural gas. Therefore, methane was used as makeup gas. The experimental data indicate that the effect of total pressure on the liquid loading of the solvent is within the experimental uncertainties, while for the 50 wt% MDEA- $H_2O$  system the impact on the partial pressure of hydrogen sulfide is attributed to the non-idealities of the vapor phase and it is lower with decreasing total pressure. The system  $H_2S$ -MDEA- $H_2O$  up to 70 wt% MDEA was modelled employing Peng-Robinson EoS to describe the vapor phase and eNRTL activity coefficient model for the liquid phase. The AARD for the partial pressure of  $H_2S$  and for the total system pressure was found to be 18% and 16% respectively. The effect of including data in the presence of methane and maximum total pressure of 2000 kPa in the data regression was studied and found minimal. However, for higher total pressure and different conditions than the studied ones, the use of models taking into account the methane presence was suggested. Last but not least, new parameters for Antoine correlation were proposed for the estimation of the vapor pressure of MDEA based on our new

measurements and all available literature data covering a wide temperature range.

## Funding

This work was supported by the Norwegian University of Science and Technology (NTNU), major industry partners and the Research Council of Norway (RCN) [project number 237893]. It was carried out as a part of SUBPRO (Subsea Production and Processing), a Research-based Innovation Centre within Subsea Production and Processing.

## Declaration of competing interest

The authors declare that they have no known competing financial interests or personal relationships that could have appeared to influence the work reported in this paper.

## CRediT authorship contribution statement

**Eirini Skylogianni:** Conceptualization, Investigation, Software, Validation, Writing - original draft, Writing - review & editing. **Ingvald Mundal:** Investigation, Software. **Diego D.D. Pinto:** Conceptualization, Investigation, Software, Writing - review & editing, Supervision, Project administration. **Christophe Coquelet:** Investigation, Writing - review & editing, Supervision. **Hanna K. Knuutila:** Conceptualization, Investigation, Writing - review & editing, Supervision, Project administration, Funding acquisition.

## Acknowledgements

The authors acknowledge the valuable help from Mr. Eric Boonaert and Ing. Alain Valtz during the laboratory work with the high-pressure VLE apparatus. Anastasia A. Trollebø is acknowledged for conducting the pure MDEA saturation pressure measurements and Ricardo R. Wanderley for the insightful discussions.

## List of Symbols

### Latin letters

$a$	parameter of Eq. 10
$A_\phi$	Debye-Hückel parameter
$b$	parameter of Eq. 10
$c-a$	cation-anion
$D$	Dielectric constant (–)
$g^{ex}$	Molar excess Gibbs energy (J/mol)
$G$	eNRTL auxiliary function (–)
$H$	Henry's constant (kPa $m^3/kmol$ )
$I_x$	Ionic strength in mole fraction scale (mol/ $m^3$ )
$k$	Boltzmann constant (J/K)
$m$	molecule
$M$	Molecular weight (kg/kmol)
$N_A$	Avogadro number (mol $^{-1}$ )
$P$	Pressure (kPa)
$r_{BORN}$	Born radius (m)
$R$	Gas constant (J mol $^{-1}$ K $^{-1}$ )
$T$	Absolute temperature (K)
$v$	Molar volume (m $^3/mol$ )
$w$	Weight fraction (–)
$x$	Mole fraction (–)
$X$	eNRTL mole fraction (–)
$z$	Ionic charge (–)
$Z$	Absolute value of the ionic charge (–)

**Greek letters**

$\alpha$	Loading (mol H <sub>2</sub> S/mol MDEA)
$\gamma$	Activity coefficient (–)
$\epsilon$	Permittivity (F/m)
$\rho$	Molar density (mol/cm <sup>3</sup> )
$\rho_{pdh}$	Closest approach parameter of the Pitzer-Debye-Hückel formulation (–)
$\tau$	Energy parameter (–)

**Superscripts**

E	Excess property
exp	Experimental value
l	Liquid phase
lc	Local composition
pdh	Pitzer-Debye-Hückel formulation
pred	Predicted value
v	Vapor phase

**Subscripts**

amb	Ambient
c	Critical
glob	Global, refers to global loading $\alpha_{glob}$ (mol H <sub>2</sub> S in the cell/mol MDEA)
i, j, k	Component in a mixture
ij	Cross parameter
liq	Liquid, refers to liquid loading $\alpha_{liq}$ (mol H <sub>2</sub> S/mol MDEA)
s	solvent
w	water

**Abbreviations**

AAD	Average Absolute Deviation
AARD	Average Absolute Relative Deviation
eNRTL	electrolyte Non-Random Two Liquids
EoS	Equation of State
FPD	Freezing Point Depression
FTIR	Fourier-Transform infrared
GC	Gas Chromatography
MDEA	Methyldiethanolamine
NP	Number of data points
NS	Number of vapor phase samples for GC analysis
VLE	Vapor-Liquid Equilibrium

**Appendix A. eNRTL model**

The activity coefficients were calculated by the electrolyte Non-Random Two Liquids (eNRTL) model [50]. The starting point for the description of the liquid phase is the expression of excess Gibbs energy as the sum of two terms; one related to the long-range forces between the ions (first term) and one to the short-range forces between all the species (second term):

$$\frac{g^E}{RT} = \frac{g^{E,pdh}}{RT} + \frac{g^{E,lc}}{RT} \quad A1$$

This equation lead to:

$$\ln \gamma_i = \ln \gamma_i^{pdh} + \ln \gamma_i^{lc} \quad A2$$

The subscript *pdh* denotes Pitzer-Debye-Hückel formulation for the long-range interactions and the subscript *lc* denotes Local Composition model. The formulation of the former is:

$$\frac{g^{E,pdh}}{RT} = - \left( \sum_k x_k \right) \left( \frac{1000}{M_s} \right)^{\frac{1}{2}} \left( \frac{4A_\phi I_x}{\rho_{pdh}} \right) \ln \left( 1 + \rho_{pdh} I_x^{\frac{1}{2}} \right) \quad A3$$

By derivation, the activity coefficient is expressed according to:

$$\ln \gamma_i^{*pdh} = - (1000/M_s)^{\frac{1}{2}} A_\phi \left[ \times \left( 2 \frac{Z_i^2}{\rho_{pdh}} \right) \ln \left( 1 + \rho_{pdh} I_x^{\frac{1}{2}} \right) + \left( Z_i^2 I_x^{\frac{1}{2}} - 2 I_x^{\frac{3}{2}} \right) / \left( 1 + \rho_{pdh} I_x^{\frac{1}{2}} \right) \right] \quad A4$$

where  $I_x$  is the ionic strength and  $A_\phi$  is the Debye-Hückel parameter, expressed as following:

$$I_x = \frac{1}{2} \sum_i Z_i^2 x_i \quad A5$$

$$A_\phi = \frac{1}{3} \left( \frac{2\pi N_o d}{1000} \right)^{\frac{1}{2}} \left( \frac{e^2}{DkT} \right)^{3/2} \quad A6$$

The reference state for the *pdh* term is infinite dilution in the mixed solvent while the reference state for the *lc* term is infinite dilution in water. To account for the excess Gibbs energy of transfer from the infinite dilution in the mixed solvent to the infinite dilution in water, a term is added in the long-range interaction expression. This additional term is described by the Born equation:

$$\frac{g^{E,BORN}}{RT} = - \frac{N_A e^2}{8\pi RT \epsilon_o} \left( \frac{1}{\epsilon_s} - \frac{1}{\epsilon_w} \right) \sum_i x_i z_i^2 \quad A7$$

Further,

$$\ln \gamma_i^{BORN} = \frac{N_A e^2}{8\pi RT \epsilon_o} \left( \frac{1}{\epsilon_s} - \frac{1}{\epsilon_w} \right) z_i^2 \quad A8$$

The short-range contribution is described by the eNRTL model as following:

$$\frac{g^{E,lc}}{RT} = \sum_m X_m \frac{\sum_j X_j G_{jm} \tau_{jm}}{\sum_k X_k G_{km}} + \sum_c X_c \sum_{a'} \frac{X_{a'}}{\sum_k X_k G_{ka'}} \frac{\sum_j X_j G_{jc,a'} \tau_{jc,a'}}{\sum_k X_k G_{ka',c}} + \sum_a X_a \sum_{c'} \frac{X_{c'}}{\sum_k X_k G_{ka,c'}} \frac{\sum_j X_j G_{ja,c'} \tau_{ja,c'}}{\sum_k X_k G_{ka,c'}} \quad A9$$

where  $m, c$  and  $a$  denote molecule, cation and anion, while  $X_j = C_j x_j$  with  $j: m, c, a$  effective local mole fraction. Equations A10 and A11 are given using the ion-like repulsion assumption and the local electroneutrality assumption.

$$G_{cm} = \frac{\sum_a X_a G_{ca,m}}{\sum_{a'} X_{a'}} \quad A10$$

$$G_{am} = \frac{\sum_c X_c G_{ca,m}}{\sum_{c'} X_{c'}} \quad A11$$

The  $G_{ij}$  and  $\tau_{ij}$  parameters are related through the non-randomness parameter,  $a_{ij}$ :

$$G_{ij} = \exp(-a_{ij}\tau_{ij}) \quad A12$$

The equations presented below describe the non-randomness parameters:

$$a_{cm} = \frac{\sum_a X_a a_{ca,m}}{\sum_{a'} X_{a'}} \quad A13$$

$$a_{am} = \frac{\sum_c X_c a_{ca,m}}{\sum_{c'} X_{c'}} \quad A14$$

The energy parameters  $\tau_{mc,ac}$  and  $\tau_{ma,ca}$  are given by:

$$\tau_{mc,ac} = \tau_{cm} - \frac{a_{ca,m}}{a_{mc,ac}} (\tau_{ca,m} - \tau_{m,ca}) \quad A15$$

$$\tau_{ma,ca} = \tau_{am} - \frac{a_{ca,m}}{a_{ma,ac}} (\tau_{ca,m} - \tau_{m,ca}) \quad A16$$

where  $a_{mc,ac} = a_{cm}$  and  $a_{am,ac} = a_{am}$ . The adjustable binary parameters are the non-randomness factors  $a_{ca,m}$ ,  $a_{ca,c'a}$ ,  $a_{ca,c'a}$ ,  $a_{mm'}$ , and the energy parameters  $\tau_{ca,m}$ ,  $\tau_{m,ca}$ ,  $\tau_{ca,c'a}$ ,  $\tau_{c'a,ca}$ ,  $\tau_{ca,c'a}$ ,  $\tau_{c'a,ca}$ ,  $\tau_{m,m'}$ ,  $\tau_{m'm}$ .

From Equation (A9), the activity coefficients are calculated:

For molecules:

$$\begin{aligned} \ln \gamma_m^{lc} = & \frac{\sum_j X_j G_{jm} \tau_{jm}}{\sum_k X_k G_{km}} + \sum_{m'} \frac{X_{m'} G_{mm'}}{\sum_k X_k G_{km'}} \left( \tau_{mm'} - \frac{\sum_k X_k G_{km'} \tau_{km'}}{\sum_k X_k G_{km'}} \right) \\ & + \sum_c \sum_{a'} \frac{X_{a'}}{\sum_{a''} X_{a''}} \frac{X_{c'} G_{mc,a'c}}{\sum_k X_k G_{kc,a'c}} \left( \tau_{mc,a'c} - \frac{\sum_k X_k G_{kc,a'c} \tau_{kc,a'c}}{\sum_k X_k G_{kc,a'c}} \right) \\ & + \sum_a \sum_{c'} \frac{X_{c'}}{\sum_{c''} X_{c''}} \frac{X_{a'} G_{ma,c'a}}{\sum_k X_k G_{ka,c'a}} \left( \tau_{ma,c'a} - \frac{\sum_k X_k G_{ka,c'a} \tau_{ka,c'a}}{\sum_k X_k G_{ka,c'a}} \right) \end{aligned} \quad A17$$

For cations:

$$\begin{aligned} \frac{1}{Z_c} \ln \gamma_c^{lc} = & \sum_{a'} \frac{X_{a'}}{\sum_{a''} X_{a''}} \frac{\sum_k X_k G_{kc,a'c} \tau_{kc,a'c}}{\sum_k X_k G_{kc,a'c}} + \sum_m \frac{X_m G_{cm}}{\sum_k X_k G_{km}} \\ & \left( \tau_{cm} - \frac{\sum_k X_k G_{km} \tau_{km}}{\sum_k X_k G_{km}} \right) + \sum_a \sum_{c'} \frac{X_{c'}}{\sum_{c''} X_{c''}} \frac{X_{a'} G_{ca,c'a}}{\sum_k X_k G_{ka,c'a}} \\ & \left( \tau_{ca,c'a} - \frac{\sum_k X_k G_{ka,c'a} \tau_{ka,c'a}}{\sum_k X_k G_{ka,c'a}} \right) \end{aligned} \quad A18$$

For anions:

$$\begin{aligned} \frac{1}{Z_a} \ln \gamma_a^{lc} = & \sum_{c'} \frac{X_{c'}}{\sum_{c''} X_{c''}} \frac{\sum_k X_k G_{ka,c'a} \tau_{ka,c'a}}{\sum_k X_k G_{ka,c'a}} + \sum_m \frac{X_m G_{am}}{\sum_k X_k G_{km}} \\ & \left( \tau_{am} - \frac{\sum_k X_k G_{km} \tau_{km}}{\sum_k X_k G_{km}} \right) + \sum_c \sum_{a'} \frac{X_{a'}}{\sum_{a''} X_{a''}} \frac{X_c G_{ac,a'c}}{\sum_k X_k G_{kc,a'c}} \\ & \left( \tau_{ac,a'c} - \frac{\sum_k X_k G_{kc,a'c} \tau_{kc,a'c}}{\sum_k X_k G_{kc,a'c}} \right) \end{aligned} \quad A19$$

The expressions of activity coefficients at infinite dilution are then:

$$\ln \gamma_m^{lc,\infty} = \tau_{wm} + G_{mw} \tau_{mw} \quad A20$$

$$\frac{1}{Z_c} \ln \gamma_c^{lc,\infty} = \frac{X_a}{\sum_{a'} X_{a'}} \tau_{wc,ac} + G_{cw} \tau_{cw} \quad A21$$

$$\frac{1}{Z_a} \ln \gamma_a^{lc,\infty} = \frac{X_c}{\sum_{c'} X_{c'}} \tau_{wa,ca} + G_{aw} \tau_{aw} \quad A22$$

By combination of Equations (A2), A4, A7, A18 and A23, the activity coefficient for the liquid phase is found by:

$$\gamma_i = \gamma_i^{pdh} \gamma_i^{BORN} \gamma_i^{lc} / \gamma_i^{lc,\infty} \quad A23$$

where  $i = m, c$  or  $a$  for all components, besides the amine in this work. For MDEA, the symmetric reference state for the short-range interactions contribution,  $\gamma_{MDEA}^{lc,\infty}$  is fixed to 1.

## Appendix B. Peng-Robinson Equation of State

The fugacity coefficients were calculated by Peng-Robinson equation of state [49]:

$$P = \frac{RT}{v-b} - \frac{\alpha a(T)}{v^2 + 2bv - b^2} \quad A24$$

where:

$$a = 0.42724 \frac{R^2 T_c^2}{P_c} \quad A25$$

$$b = 0.07780 \frac{RT_c}{P_c}, \quad a(T) = \left[ 1 + m \left( 1 - T_R^{\frac{1}{2}} \right) \right]^2 \quad A26$$

$$m = 0.37464 + 1.54226\omega - 2.26992\omega^2 \quad A27$$

The traditional van der Waals one-fluid mixing rules were used for the estimation of the gas mixture parameters from the pure components' properties.

$$a a(T) = \sum_i \sum_j x_i x_j (aa(T))_i^{\frac{1}{2}} (aa(T))_j^{\frac{1}{2}} (1 - k_{ij}) \quad A28$$

$$b = \sum_i x_i b_i \quad A29$$

In our work, the binary interaction parameter  $k_{ij}$  is set to zero, so as the eNRTL model parameters are the only ones fitted.

The critical properties used in this work can be found in Supplementary Information.

## Appendix C. Supplementary data

Supplementary data to this article can be found online at <https://doi.org/10.1016/j.fluid.2020.112498>.

## References

- [1] G. Astarita, D.W. Savage, A. Bisio, *Gas Treating with Chemical Solvents*, John Wiley, New York, United States, 1983.
- [2] J.M. Campbell, *Amine-based processes*, in: *Gas Conditioning And Processing*, vol. 4, 1998, Oklahoma, USA.

- [3] A.L. Kohl, R.B. Nielsen, Chapter 2 - alkanolamines for hydrogen sulfide and carbon dioxide removal, in: *Gas Purification*, fifth ed., Gulf Professional Publishing, Houston, 1997, pp. 40–186.
- [4] Z.I. Khatib, J.R. Salanitro, Reservoir souring: analysis of surveys and experience in sour waterfloods, in: Presented at the SPE Annual Technical Conference and Exhibition, 1997, <https://doi.org/10.2118/38795-MS>.
- [5] A. F. Mitchell and S. Asa, "10248: A REVIEW OF RESERVOIR SOURING FOR THREE NORTH SEA FIELDS," p. 8.
- [6] GATEkeeper, H2S Scavenging: Using Triazine, May-2014.
- [7] O. Økland, S. Davies, R.M. Ramberg, H. Rogna, "Steps to the Subsea Factory," in *OTC-24307-MS*, OTC, 2013, <https://doi.org/10.4043/24307-MS>.
- [8] M. Davoudi, Y. Heidari, A. Safadoost, S. Samieirad, Chemical injection policy for internal corrosion prevention of South Pars sea-pipeline: a case study, *J. Nat. Gas Sci. Eng.* 21 (Nov. 2014) 592–599, <https://doi.org/10.1016/j.jngse.2014.09.017>.
- [9] UWP/Subsea on a Stick®, *kvaerner - UWP/Subsea on a Stick®* [Online]. Available, <https://www.kvaerner.com/Products/Subsea-on-a-Stick/>. (Accessed 13 March 2019).
- [10] J. Addicks, G.A. Owren, A.O. Fredheim, K. Tangvik, Solubility of carbon dioxide and methane in aqueous methyldiethanolamine solutions, *J. Chem. Eng. Data* 47 (4) (Jul. 2002) 855–860, <https://doi.org/10.1021/je010292z>.
- [11] Ø. Jonassen, *Equilibrium and Thermal Properties of Selected CO<sub>2</sub>-methane-tertiary Amine Systems; an Experimental and Modelling Study*, NTNU, 2017.
- [12] F.Y. Jou, A.E. Mather, F.D. Otto, Solubility of hydrogen sulfide and carbon dioxide in aqueous methyldiethanolamine solutions, *Ind. Eng. Chem. Process Des. Dev.* 21 (4) (Oct. 1982) 539–544, <https://doi.org/10.1021/i200019a001>.
- [13] M.H. Li, K.P. Shen, Solubility of hydrogen sulfide in aqueous mixtures of monoethanolamine with N-methyldiethanolamine, *J. Chem. Eng. Data* 38 (1) (Jan. 1993) 105–108, <https://doi.org/10.1021/je00009a025>.
- [14] R.J. MacGregor, A.E. Mather, Equilibrium solubility of H<sub>2</sub>S and CO<sub>2</sub> and their mixtures in a mixed solvent, *Can. J. Chem. Eng.* 69 (6) (Dec. 1991) 1357–1366, <https://doi.org/10.1002/cjce.5450690618>.
- [15] J.M. Bernal-García, M. Ramos-Estrada, G.A. Iglesias-Silva, K.R. Hall, Densities and excess molar volumes of aqueous solutions of n-methyldiethanolamine (MDEA) at temperatures from (283.15 to 363.15) K, *J. Chem. Eng. Data* 48 (6) (Nov. 2003) 1442–1445, <https://doi.org/10.1021/je030120x>.
- [16] L. Chunxi, W. Fürst, Representation of CO<sub>2</sub> and H<sub>2</sub>S solubility in aqueous MDEA solutions using an electrolyte equation of state, *Chem. Eng. Sci.* 55 (15) (Aug. 2000) 2975–2988, [https://doi.org/10.1016/S0009-2509\(99\)00550-3](https://doi.org/10.1016/S0009-2509(99)00550-3).
- [17] G. Kuranov, B. Rumpf, N.A. Smirnova, G. Maurer, "Solubility of single gases carbon dioxide and hydrogen sulfide in aqueous solutions of N-methyldiethanolamine in the temperature range 313–413 K at pressures up to 5 MPa, *Ind. Eng. Chem. Res.* 35 (6) (Jan. 1996) 1959–1966, <https://doi.org/10.1021/je950538r>.
- [18] A.P.-S. Kamps, A. Balaban, M. Jödecke, G. Kuranov, N.A. Smirnova, G. Maurer, "Solubility of single gases carbon dioxide and hydrogen sulfide in aqueous solutions of N-methyldiethanolamine at temperatures from 313 to 393 K and pressures up to 7.6 MPa: new experimental data and model extension, *Ind. Eng. Chem. Res.* 40 (2) (Jan. 2001) 696–706, <https://doi.org/10.1021/ie000441r>.
- [19] R. Sidi-Boumedine, S. Horstmann, K. Fischer, E. Provost, W. Fürst, J. Gmehling, Experimental determination of hydrogen sulfide solubility data in aqueous alkanolamine solutions, *Fluid Phase Equil.* 218 (1) (Apr. 2004) 149–155, <https://doi.org/10.1016/j.fluid.2003.11.020>.
- [20] P.J.G. Huttenhuis, N.J. Agrawal, G.F. Versteeg, The solubility of hydrogen sulfide in aqueous N-methyldiethanolamine solutions, *Int. J. Oil Gas Coal Technol.* 1 (4) (2008) 399–424.
- [21] F.-Y. Jou, J.J. Carroll, A.E. Mather, F.D. Otto, The solubility of carbon dioxide and hydrogen sulfide in a 35 wt% aqueous solution of methyldiethanolamine, *Can. J. Chem. Eng.* 71 (2) (Apr. 1993) 264–268, <https://doi.org/10.1002/cjce.5450710213>.
- [22] A.T. Zoghi, M. Shokouhi, Measuring solubility of hydrogen sulphide in aqueous blends of N-methyldiethanolamine and 2-((2-aminoethylamino) ethanol) and correlating by the Deshmukh-Mather model, *J. Chem. Thermodyn.* 100 (2016) 106–115, <https://doi.org/10.1016/j.jct.2016.04.012>.
- [23] S.H. Huang, H.-J. Ng, Solubility of H<sub>2</sub>S and CO<sub>2</sub> in Alkanolamines, *Gas Processors Association*, Sep. 1998, RR-155.
- [24] W.J. Rogers, J.A. Bullin, R.R. Davison, FTIR measurements of acid-gas - methyldiethanolamine systems, *AIChE J.* 44 (11) (1998) 2423–2430.
- [25] P.J.G. Huttenhuis, N.J. Agrawal, J.A. Hogendoorn, G.F. Versteeg, Gas solubility of H<sub>2</sub>S and CO<sub>2</sub> in aqueous solutions of N-methyldiethanolamine, *J. Petrol. Sci. Eng.* 55 (1) (Jan. 2007) 122–134, <https://doi.org/10.1016/j.petrol.2006.04.018>.
- [26] A.M. Bhairi, *Experimental Equilibrium between Acid Gases and Ethanolamine Solutions*, Jul. 1984.
- [27] R.N. Maddox, A.H. Bhairi, J.R. Diers, P.A. Thomas, Equilibrium Solubility of Carbon Dioxide or Hydrogen Sulfide in Aqueous Solutions of Monoethanolamine, Diglycolamine, Diethanolamine and Methyldiethanolamine: Project 841 vol. 104, *Gas Processors Association*, Tulsa, Okla, RR-, 1987.
- [28] B. Lemoine, Y.-G. Li, R. Cadours, C. Bouallou, D. Richon, Partial vapor pressure of CO<sub>2</sub> and H<sub>2</sub>S over aqueous methyldiethanolamine solutions, *Fluid Phase Equil.* 172 (2) (Jul. 2000) 261–277, [https://doi.org/10.1016/S0378-3812\(00\)00383-6](https://doi.org/10.1016/S0378-3812(00)00383-6).
- [29] M. Dicko, C. Coquelet, C. Jarne, S. Northrop, D. Richon, Acid gases partial pressures above a 50 wt% aqueous methyldiethanolamine solution: experimental work and modeling, *Fluid Phase Equil.* 289 (2) (Mar. 2010) 99–109, <https://doi.org/10.1016/j.fluid.2009.11.012>.
- [30] N. Sadegh, K. Thomsen, E. Solbraa, E. Johannessen, G.I. Rudolfsen, O.J. Berg, Solubility of hydrogen sulfide in aqueous solutions of N-methyldiethanolamine at high pressures, *Fluid Phase Equil.* 393 (May 2015) 33–39, <https://doi.org/10.1016/j.fluid.2015.02.016>.
- [31] H.T. Chang, M. Posey, G.T. Rochelle, Thermodynamics of alkanolamine-water solutions from freezing point measurements, *Ind. Eng. Chem. Res.* 32 (10) (1993) 2324–2335.
- [32] P.L. Fosbøl, M.G. Pedersen, K. Thomsen, "Freezing point depressions of aqueous MEA, MDEA, and MEA-MDEA measured with a new apparatus, *J. Chem. Eng. Data* 56 (4) (Apr. 2011) 995–1000, <https://doi.org/10.1021/je100994v>.
- [33] I. Kim, H.F. Svendsen, E. Børresen, "Ebulliometric determination of Vapor-Liquid equilibria for pure water, monoethanolamine, N-methyldiethanolamine, 3-(Methylamino)-propylamine, and their binary and ternary solutions, *J. Chem. Eng. Data* 53 (11) (Nov. 2008) 2521–2531, <https://doi.org/10.1021/je800290k>.
- [34] S. Xu, S. Qing, Z. Zhen, C. Zhang, J.J. Carroll, Vapor pressure measurements of aqueous N-methyldiethanolamine solutions, *Fluid Phase Equil.* 67 (Nov. 1991) 197–201, [https://doi.org/10.1016/0378-3812\(91\)90055-C](https://doi.org/10.1016/0378-3812(91)90055-C).
- [35] E. Voutsas, A. Vrachnos, K. Magoulas, Measurement and thermodynamic modeling of the phase equilibrium of aqueous N-methyldiethanolamine solutions, *Fluid Phase Equil.* 224 (2) (Oct. 2004) 193–197, <https://doi.org/10.1016/j.fluid.2004.05.012>.
- [36] M.L. Posey, *Thermodynamic Model for Acid Gas Loaded Aqueous Alkanolamine Solutions*, 1996.
- [37] Y. Maham, A.E. Mather, L.G. Hepler, Excess molar enthalpies of (water + alkanolamine) systems and some thermodynamic calculations, *J. Chem. Eng. Data* 42 (5) (Sep. 1997) 988–992, <https://doi.org/10.1021/je960296h>.
- [38] Y. Maham, A.E. Mather, C. Mathonat, Excess properties of (alkyldiethanolamine +H<sub>2</sub>O) mixtures at temperatures from (298.15 to 338.15) K, *J. Chem. Therm.* 32 (2) (Feb. 2000) 229–236, <https://doi.org/10.1006/jcht.1999.0595>.
- [39] O. Noll, A. Valtz, D. Richon, T. Getachew-Sawaya, I. Mokbel, J. Jose, Vapor pressures and liquid densities of N-methylethanolamine, diethanolamine, and N-methyldiethanolamine, *ELDATA: Int. Electron. J. Phys.-Chem. Data* 4 (1998) 105–120.
- [40] T.E. Daubert, J.W. Jalowka, V. Goren, Vapor pressure of 22 pure industrial chemicals, *AIChE Symp. Ser.* 83 (1987) 128–156.
- [41] C. Yang, et al., "Vapor-Liquid equilibria for three binary systems of N-methylethanolamine, N-methyldiethanolamine, and ethylene glycol at P = (40.0, 30.0, and 20.0) kPa, *J. Chem. Eng. Data* 58 (8) (Aug. 2013) 2272–2279, <https://doi.org/10.1021/je400373d>.
- [42] D.M. VonNiederhausen, G.M. Wilson, N.F. Giles, Critical point and vapor pressure measurements for 17 compounds by a low residence time flow method, *J. Chem. Eng. Data* 51 (6) (Nov. 2006) 1990–1995, <https://doi.org/10.1021/je060269j>.
- [43] J.M.S. Fonseca, R. Dohrn, S. Peper, "High-pressure fluid-phase equilibria: experimental methods and systems investigated (2005–2008), *Fluid Phase Equil.* 300 (1) (Jan. 2011) 1–69, <https://doi.org/10.1016/j.fluid.2010.09.017>.
- [44] ARMINES, *Procédé et Dispositif Pour Prélever Des Microéchantillons D'un Fluide Sous Pression Contenu Dans Un Container* 2 853 414 (2003).
- [45] E.W. Lemmon, I.H. Bell, M.L. Huber, M.O. McLinden, *NIST Standard Reference Database 23: Reference Fluid Thermodynamic and Transport Properties-REFPROP*, National Institute of Standards and Technology, Standard Reference Data Program, Gaithersburg, 2018.
- [46] E.W. Lemmon, R. Span, Short fundamental equations of state for 20 industrial fluids, *J. Chem. Eng. Data* 51 (3) (May 2006) 785–850, <https://doi.org/10.1021/je050186n>.
- [47] J.G.M.-S. Monteiro, D.D.D. Pinto, S.A.H. Zaidy, A. Hartono, H.F. Svendsen, VLE data and modelling of aqueous N,N-diethylethanolamine (DEEA) solutions, *Int. J. Greenh. Gas. Cntrl.* 19 (Nov. 2013) 432–440, <https://doi.org/10.1016/j.jjggc.2013.10.001>.
- [48] D.D.D. Pinto, J.G.M.-S. Monteiro, A. Bersás, T. Haug-Warberg, H.F. Svendsen, eNRTL parameter fitting procedure for blended amine systems: MDEA-PZ case study, *Energy Procedia* 37 (Jan. 2013) 1613–1620, <https://doi.org/10.1016/j.egypro.2013.06.037>.
- [49] D.-Y. Peng, D.B. Robinson, A new two-constant equation of state, *Ind. Eng. Chem. Fund.* 15 (1) (Feb. 1976) 59–64, <https://doi.org/10.1021/i160057a011>.
- [50] C.-C. Chen, L.B. Evans, A local composition model for the excess Gibbs energy of aqueous electrolyte systems, *AIChE J.* 32 (3) (1986) 444–454, <https://doi.org/10.1002/aic.690320311>.
- [51] J.L. Oscarson, X. Chen, R.M. Izatt, A Thermodynamically Consistent Model for the Prediction of Solubilities and Enthalpies of Solution of Acid Gases in Aqueous Alkanolamine Solutions, *Gas Processors Association*, Tulsa, Oklahoma., 1995, RR-130.
- [52] T.J. Edwards, J. Newman, J.M. Prausnitz, Thermodynamics of vapor-liquid equilibria for the ammonia-water system, *Ind. Eng. Chem. Fundam.* 17 (4) (Nov. 1978) 264–269, <https://doi.org/10.1021/i160068a007>.
- [53] DIPPR, *DIPPR Chemical Database*, Design Institute for Physical Property Data American Institute of Chemical Engineers, 2004.
- [54] E.T. Hessen, T. Haug-Warberg, H.F. Svendsen, "The refined e-NRTL model applied to CO<sub>2</sub>-H<sub>2</sub>O-alkanolamine systems, *Chem. Eng. Sci.* 65 (11) (Jun. 2010) 3638–3648, <https://doi.org/10.1016/j.ces.2010.03.010>.
- [55] J. Kennedy, R.C. Eberhart, *Proceedings of IEEE International Conference on*



- Neural Networks, 1995. Perth, Australia.
- [56] S. Ghosh, S. Das, D. Kundu, K. Suresh, A. Abraham, Inter-particle communication and search-dynamics of lbest particle swarm optimizers: an analysis, *Inf. Sci.* 182 (1) (Jan. 2012) 156–168, <https://doi.org/10.1016/j.ins.2010.10.015>.
- [57] D.D.D. Pinto, CO<sub>2</sub> Capture Solvents; Modeling and Experimental Characterization, Norwegian University of Science and Technology, 2014.
- [58] B.N. Taylor, C.E. Kuyatt, NIST Guidelines for Evaluating and Expressing the Uncertainty of NIST Measurement Results. NIST Technical Note 1297." Physics Laboratory, National Institute of Standards and Technology, Sep-1994.
- [59] E.B. Rinker, O.C. Sandall, Physical solubility of hydrogen sulfide in several aqueous solvents, *Can. J. Chem. Eng.* 78 (1) (Feb. 2000) 232–236, <https://doi.org/10.1002/cjce.5450780130>.
- [60] H.A. Al-Ghawas, D.P. Hagewiesche, G. Ruiz-Ibanez, O.C. Sandall, Physico-chemical properties important for carbon dioxide absorption in aqueous methyl-diethanolamine, *J. Chem. Eng. Data* 34 (4) (Oct. 1989) 385–391, <https://doi.org/10.1021/je00058a004>.
- [61] E. Álvarez, D. Gómez-Díaz, M.D. La Rubia, J.M. Navaza, Densities and viscosities of aqueous ternary mixtures of 2-(methylamino)ethanol and 2-(ethylamino) ethanol with diethanolamine, triethanolamine, N-methyl-diethanolamine, or 2-Amino-1-methyl-1-propanol from 298.15 to 323.15 K, *J. Chem. Eng. Data* 51 (3) (May 2006) 955–962, <https://doi.org/10.1021/je050463q>.
- [62] T.T. Teng, Y. Maham, L.G. Hepler, A.E. Mather, Viscosity of aqueous solutions of N-methyl-diethanolamine and of diethanolamine, *J. Chem. Eng. Data* 39 (2) (Apr. 1994) 290–293, <https://doi.org/10.1021/je00014a021>.

# Supplementary Information

## **Hydrogen Sulfide Solubility in 50 wt.% and 70 wt.% Aqueous Methyldiethanolamine at Temperatures from 283 to 393 K and Total Pressures from 500 to 10000 kPa**

Eirini Skylogianni<sup>1</sup>, Ingvild Mundal<sup>1</sup>, Diego D.D Pinto<sup>1</sup>, Christophe Coquelet<sup>2</sup>, Hanna K.  
Knuutila<sup>\*,1</sup>

<sup>1</sup>*Department of Chemical Engineering, Norwegian University of Science and  
Technology, Sem Sælands vei 6, 7034 Trondheim, Norway*

<sup>2</sup>*Mines ParisTech - PSL University, CTP- Centre of Thermodynamics of Processes, 35  
rue Saint Honoré, 77305 Fontainebleau, France*

\* Corresponding author. E-mail: hanna.knuutila@ntnu.no

### A. Critical properties and acentric factors for pure components

The critical properties and acentric factors employed in this modeling work were taken from the DIPPR data compilation.

**Table S1.** Critical properties and acentric factors for pure components.

Components	$T_c$ (K)	$P_c$ (Pa)	$V_c$ (m <sup>3</sup> /mol)	$\omega$
H <sub>2</sub> O	647.096	2.21E+07	5.59E-05	0.344861
MDEA	675	3.88E+06	3.68E-04	1.1649
H <sub>2</sub> S	373.1	9.00E+06	9.90E-05	0.23696

### B. Model parametrization

The parameters obtained from the fitting for the MDEA-H<sub>2</sub>O system are shown in **Table S2**.

**Table S2.** Fitted energy parameters for the MDEA-H<sub>2</sub>O system.

Energy parameters, $\tau_{ij}$			
Components		Parameters	
i	j	a	b
H <sub>2</sub> O	MDEA	9.059	-1793.7
MDEA	H <sub>2</sub> O	-1.944	-198.1

The resulting parameters for the data regression for the ternary system H<sub>2</sub>S-MDEA-H<sub>2</sub>O are presented below. **Tables S3, S4** and **S5** include the adjusted parameters for Case A, B and C respectively.

**Table S3.** Fitted energy parameters for the ternary system H<sub>2</sub>S-MDEA-H<sub>2</sub>O in Case A.

Molecular parameters		
Molecule pair	a	b
H <sub>2</sub> S, MDEA	-0.664	-183.1
MDEA, H <sub>2</sub> S	4.258	-1163.2
Molecular-Salt parameters		
Molecule,salt	a	b
H <sub>2</sub> O, MDEAH <sup>+</sup> -OH <sup>-</sup>	-11.137	-1903.6
H <sub>2</sub> O, MDEAH <sup>+</sup> -HS <sup>-</sup>	-10.476	-598.0
H <sub>2</sub> S, MDEAH <sup>+</sup> -OH <sup>-</sup>	-4.771	-2060.0
H <sub>2</sub> S, MDEAH <sup>+</sup> -HS <sup>-</sup>	0.352	-284.1

MDEA, H <sub>3</sub> O <sup>+</sup> -OH <sup>-</sup>	2.403	-1310.8
MDEA, H <sub>3</sub> O <sup>+</sup> -HS <sup>-</sup>	5.673	-2656.5
MDEA, MDEAH <sup>+</sup> -OH <sup>-</sup>	0.455	-83.5
MDEA, MDEAH <sup>+</sup> -HS <sup>-</sup>	-7.215	-1907.5

Salt-Molecules parameters		
Salt pair, molecule	a	b
H <sub>3</sub> O <sup>+</sup> -OH <sup>-</sup> , MDEA	4.037	-619.4
H <sub>3</sub> O <sup>+</sup> -HS <sup>-</sup> , MDEA	6.806	-688.4
MDEAH <sup>+</sup> -OH <sup>-</sup> , H <sub>2</sub> O	4.725	-1692.1
MDEAH <sup>+</sup> -OH <sup>-</sup> , H <sub>2</sub> S	-7.238	411.1
MDEAH <sup>+</sup> -OH <sup>-</sup> , MDEA	-1.907	-1080.7
MDEAH <sup>+</sup> -HS <sup>-</sup> , H <sub>2</sub> O	9.523	-2041.1
MDEAH <sup>+</sup> -HS <sup>-</sup> , H <sub>2</sub> S	-5.145	219.8
MDEAH <sup>+</sup> -HS <sup>-</sup> , MDEA	1.587	-178.0

**Table S4.** Fitted energy parameters for the ternary system H<sub>2</sub>S-MDEA-H<sub>2</sub>O in Case B.

Molecular parameters		
Molecule pair	a	b
H <sub>2</sub> S, MDEA	-3.265	590.6
MDEA, H <sub>2</sub> S	17.920	1054.0

Molecular-Salt parameters		
Molecule,salt	a	b
H <sub>2</sub> O, MDEAH <sup>+</sup> -OH <sup>-</sup>	4.217	360.0
H <sub>2</sub> O, MDEAH <sup>+</sup> -HS <sup>-</sup>	3.594	-47.2
H <sub>2</sub> S, MDEAH <sup>+</sup> -OH <sup>-</sup>	3.405	540.3
H <sub>2</sub> S, MDEAH <sup>+</sup> -HS <sup>-</sup>	14.619	873.9
MDEA, H <sub>3</sub> O <sup>+</sup> -OH <sup>-</sup>	-3.974	844.0
MDEA, H <sub>3</sub> O <sup>+</sup> -HS <sup>-</sup>	17.788	1445.8
MDEA, MDEAH <sup>+</sup> -OH <sup>-</sup>	3.547	-40.2
MDEA, MDEAH <sup>+</sup> -HS <sup>-</sup>	-2.384	791.2

Salt-Molecules parameters		
Salt pair, molecule	a	b
H <sub>3</sub> O <sup>+</sup> -OH <sup>-</sup> , MDEA	-0.769	1070.9
H <sub>3</sub> O <sup>+</sup> -HS <sup>-</sup> , MDEA	15.586	597.2

MDEAH <sup>+</sup> -OH <sup>-</sup> , H <sub>2</sub> O	0.550	1122.8
MDEAH <sup>+</sup> -OH <sup>-</sup> , H <sub>2</sub> S	3.150	-194.2
MDEAH <sup>+</sup> -OH <sup>-</sup> , MDEA	6.254	507.4
MDEAH <sup>+</sup> -HS <sup>-</sup> , H <sub>2</sub> O	-4.342	930.1
MDEAH <sup>+</sup> -HS <sup>-</sup> , H <sub>2</sub> S	-9.752	818.3
MDEAH <sup>+</sup> -HS <sup>-</sup> , MDEA	2.999	-764.9

**Table S5.** Fitted energy parameters for the ternary system H<sub>2</sub>S-MDEA-H<sub>2</sub>O in Case C.

Molecular parameters		
Molecule pair	a	b
H <sub>2</sub> S, MDEA	1.492	162.4
MDEA, H <sub>2</sub> S	-4.406	-269.6

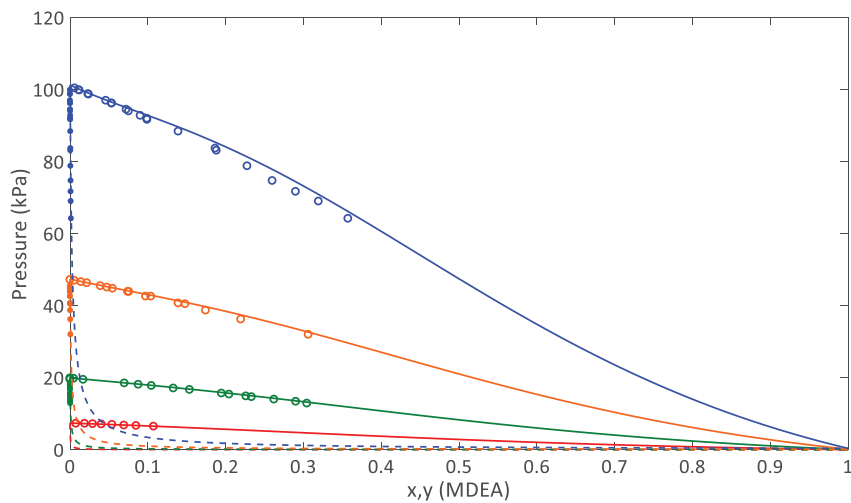
Molecular-Salt parameters		
Molecule, salt	a	b
H <sub>2</sub> O, MDEAH <sup>+</sup> -OH <sup>-</sup>	-10.686	-419.5
H <sub>2</sub> O, MDEAH <sup>+</sup> -HS <sup>-</sup>	-2.435	590.1
H <sub>2</sub> S, MDEAH <sup>+</sup> -OH <sup>-</sup>	-1.992	916.7
H <sub>2</sub> S, MDEAH <sup>+</sup> -HS <sup>-</sup>	8.735	842.3
MDEA, H <sub>3</sub> O <sup>+</sup> -OH <sup>-</sup>	-3.271	-238.3
MDEA, H <sub>3</sub> O <sup>+</sup> -HS <sup>-</sup>	1.882	323.1
MDEA, MDEAH <sup>+</sup> -OH <sup>-</sup>	0.828	-27.3
MDEA, MDEAH <sup>+</sup> -HS <sup>-</sup>	-6.721	1583.4

Salt-Molecules parameters		
Salt pair, molecule	a	b
H <sub>3</sub> O <sup>+</sup> -OH <sup>-</sup> , MDEA	3.513	387.9
H <sub>3</sub> O <sup>+</sup> -HS <sup>-</sup> , MDEA	-3.453	482.6
MDEAH <sup>+</sup> -OH <sup>-</sup> , H <sub>2</sub> O	4.356	1382.5
MDEAH <sup>+</sup> -OH <sup>-</sup> , H <sub>2</sub> S	0.356	1212.6
MDEAH <sup>+</sup> -OH <sup>-</sup> , MDEA	9.843	1455.7
MDEAH <sup>+</sup> -HS <sup>-</sup> , H <sub>2</sub> O	-2.550	1120.7
MDEAH <sup>+</sup> -HS <sup>-</sup> , H <sub>2</sub> S	-7.479	520.5
MDEAH <sup>+</sup> -HS <sup>-</sup> , MDEA	0.238	341.7

### C. Modeling results

MDEA-H<sub>2</sub>O system



**Figure S1:** P-x-y plot for the system MDEA-H<sub>2</sub>O as a function of temperature;  $\circ$  313 K,  $\circ$  333 K,  $\circ$  353 K,  $\circ$  373 K (Kim et al., 2008)

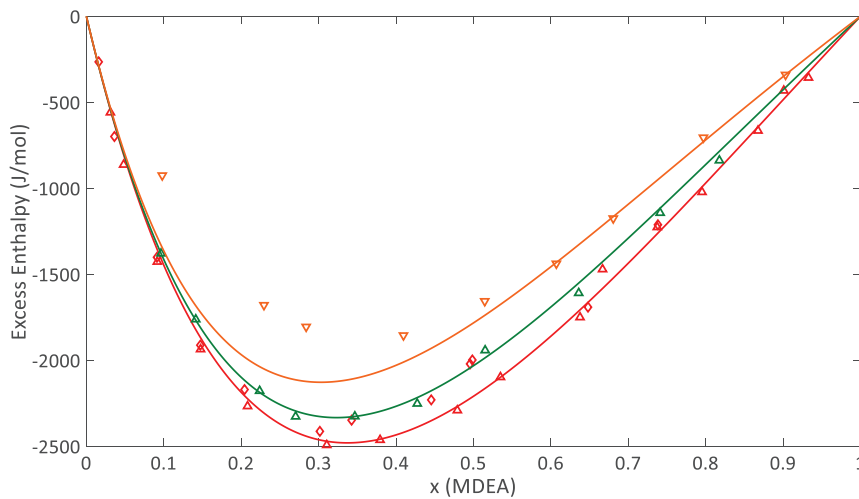


**Figure S2:** Excess enthalpy plot as a function of MDEA mole fraction and temperature;  $\Delta$  298 K (Mathonat et al., 1997),  $\diamond$  298 K (Posey, 1996),  $\Delta$  313 K (Mathonat et al., 1997),  $\nabla$  338 K (Maham et al., 2000).

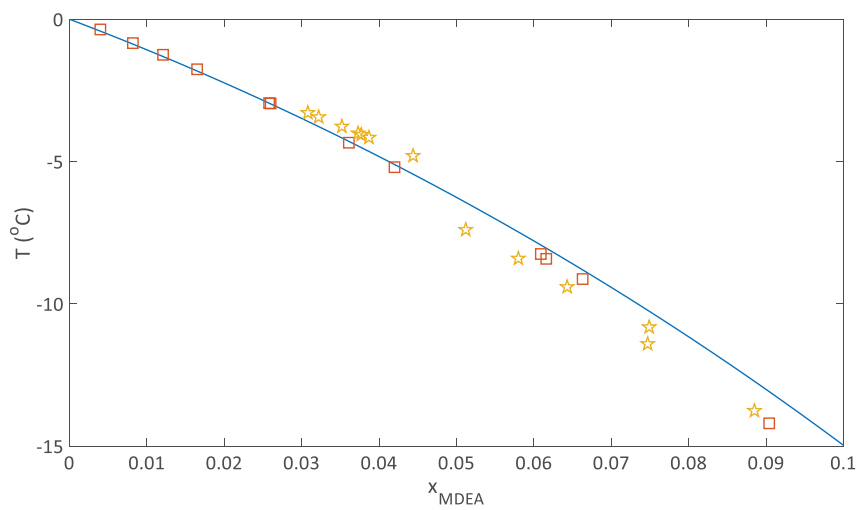


**Figure S3:** Freezing point depression plot.  $\square$  (Fosbøl et al., 2011),  $*$  (Chang et al., 1993).

Speciation graphs for 50.1 wt.% and 70 wt.% MDEA-H<sub>2</sub>O mixtures at the temperatures studied in this work are presented below.

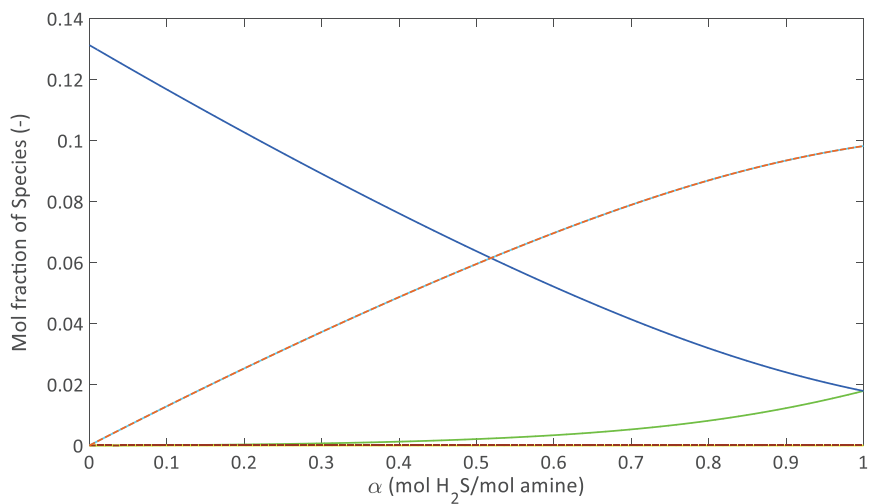


**Figure S4:** Predicted speciation of H<sub>2</sub>S, MDEA and H<sub>2</sub>O in 50.1 wt.% MDEA-H<sub>2</sub>O at 323 K. (—) H<sub>2</sub>S, (—) MDEA, (—) H<sub>2</sub>O, (—) MDEAH<sup>+</sup>, (--) OH<sup>-</sup>, (-.-) HS<sup>-</sup>.

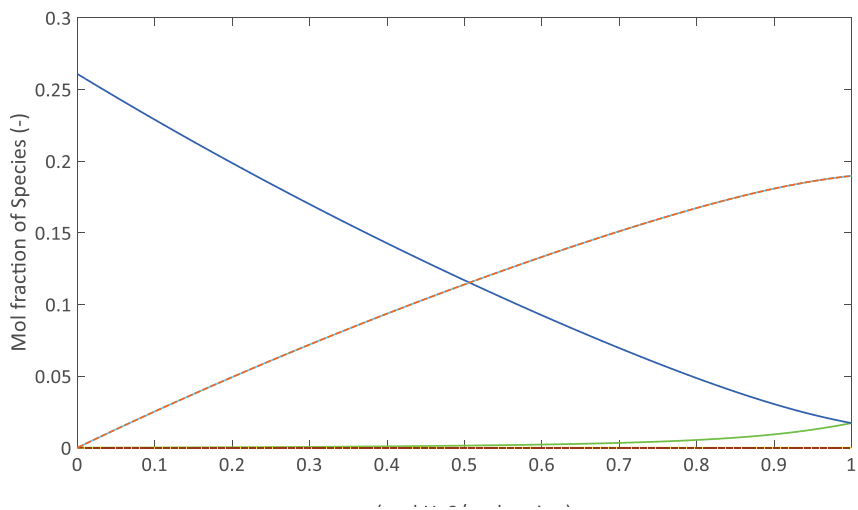


**Figure S5:** Predicted speciation of H<sub>2</sub>S, MDEA and H<sub>2</sub>O in 70 wt.% MDEA-H<sub>2</sub>O at 283 K. (—) H<sub>2</sub>S, (—) MDEA, (—) H<sub>2</sub>O, (—) MDEAH<sup>+</sup>, (--) OH<sup>-</sup>, (-.-) HS<sup>-</sup>.



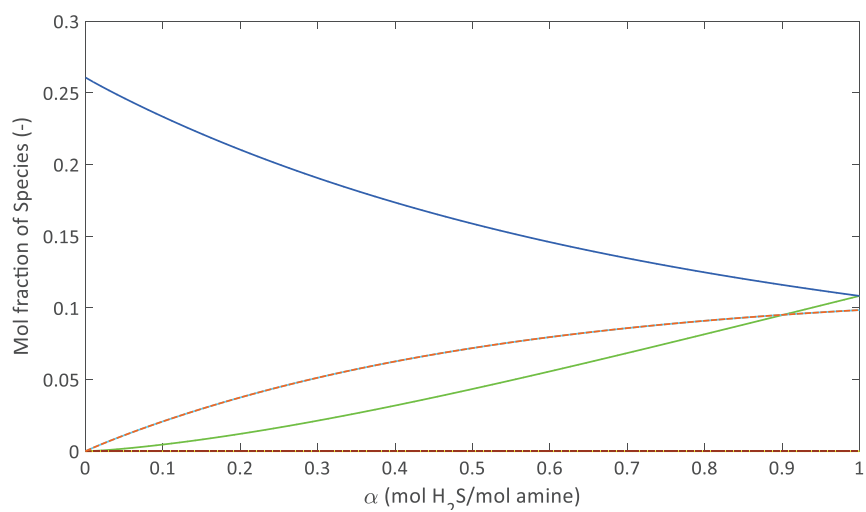


**Figure S6:** Predicted speciation of H<sub>2</sub>S, MDEA and H<sub>2</sub>O in 70 wt.% MDEA-H<sub>2</sub>O at 393 K. (—) H<sub>2</sub>S, (—) MDEA, (—) H<sub>2</sub>O, (—) MDEAH<sup>+</sup>, (- -) OH<sup>-</sup>, (- -) HS<sup>-</sup>.

## D. Experimental results

Amine concentration effect

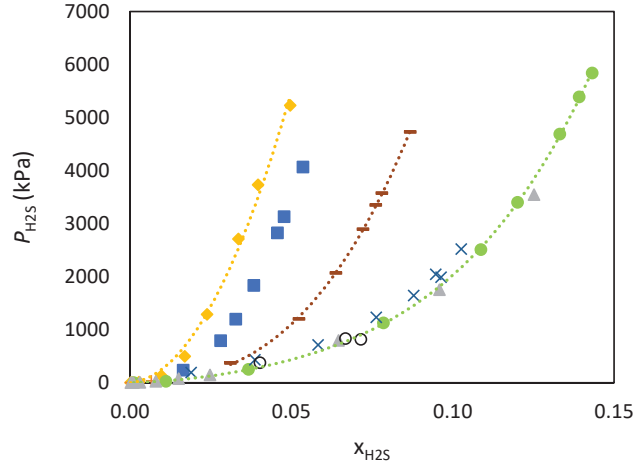


**Figure S7:** Hydrogen sulfide molar concentration in the liquid phase for the system H<sub>2</sub>S-MDEA-H<sub>2</sub>O as a function of partial pressure and amine concentration at 393 K;  $\blacklozenge$  11.8 wt.% MDEA-H<sub>2</sub>O (Jou et al., 1982),  $\blacksquare$  18.7 wt.% MDEA-H<sub>2</sub>O (Kuranov et al., 1996),  $+$  23.1 wt.% MDEA-H<sub>2</sub>O (Huang and Ng, 1998),  $-$  32.2 wt.% MDEA-H<sub>2</sub>O (Kuranov et al., 1996),  $\bullet$  48.8 wt.% MDEA-H<sub>2</sub>O (Jou et al., 1982),  $\times$  48.8 wt.% MDEA-H<sub>2</sub>O,  $\blacktriangle$  50 wt.% MDEA-H<sub>2</sub>O (Huang and Ng, 1998),  $\circ$  70 wt.% MDEA-H<sub>2</sub>O (This work).

## E. Uncertainty analysis

Uncertainty of composition expressed as weight fractions,  $w$

The standard uncertainty of the weight fractions of a binary mixture, here MDEA (1) and H<sub>2</sub>O (2), is the same for each component. Given that the weight fraction is given by:

$$w_1 = \frac{m_1}{m_1 + m_2} \quad (1)$$

where  $m$ : mass, using the Law of propagation of uncertainty, the uncertainty in weight fractions is defined as:

$$u^2(w_1) = \left(\frac{\partial w_1}{\partial m_1}\right)_{m_2}^2 u^2(m_1) + \left(\frac{\partial w_1}{\partial m_2}\right)_{m_1}^2 u^2(m_2) \quad (2)$$

The uncertainty is found:

$$u(w) = u(w_1) = u(w_2) = \frac{u(m)}{(m_1 + m_2)^2} \sqrt{m_1^2 + m_2^2} \quad (3)$$

where  $u(m)$  is the uncertainty of the mass.

The uncertainty of the mass includes both the accuracy of the scale,  $u_{scale}(m) = 1 \cdot 10^{-6}$  kg, and the purity of the chemicals used. It is calculated by the equation:

$$u(m) = \sqrt{u_{scale}^2(m) + u_{purity,i}^2(m)} \quad (4)$$

$u_{purity}(m)$  is calculated for each component, and it is equal to  $(1 - p)/\sqrt{3}$ , where  $p$ =purity% assuming uniform distribution is followed, given that no further information is available. It is assumed that the water used in this work is 100% pure.

#### Uncertainty of pressure $P$ and temperature $T$

The uncertainty of pressure and temperature refers to the measurement of pressure and temperature both in the equilibrium cell and the gas tank, accommodating hydrogen sulfide before it is introduced in the cell. The calibration method for the pressure transducers and thermoelements is described in (Dicko et al., 2010). It has been assumed uniform distribution.

**Table S6.** Expanded uncertainties in temperature with 95% level of confidence.

Cell		H <sub>2</sub> S gas tank
$U(T_{\text{upper flange}})$	$U(T_{\text{low flange}})$	$U(T_{\text{tank}})$
K	K	K
0.014	0.013	0.018

The temperature reported for every data point is the average of the temperature in the upper and the lower flange of the equilibrium cell. The uncertainty is found to be  $u(T) = 0.019$  K, expanded uncertainty with 95% confidence interval  $U(T) = 0.038$  K.

**Table S7.** Expanded uncertainties in pressure with 95% level of confidence.

Cell		H <sub>2</sub> S gas tank
$U(P_{0.3 \text{ MPa}})$	$U(P_{0.30 \text{ MPa}})$	$U(P_{\text{tank}})$
kPa	kPa	kPa
0.25	0.60	0.60

### Uncertainty of the vapor fraction of H<sub>2</sub>S, $y_{H_2S}$

The composition of the vapor phase was experimentally determined via GC analysis, assuming that there is no MDEA or water. Following the Law of propagation of uncertainty, the uncertainty of  $y_{H_2S}$  is found (Eq. 5). It is actually the same for  $y_{CH_4}$ .

$$u_c(y) = u_c(y_{H_2S}) = u_c(y_{CH_4}) = y_{H_2S} y_{CH_4} \sqrt{\left(\frac{u(n_{H_2S})}{n_{H_2S}}\right)^2 + \left(\frac{u(n_{CH_4})}{n_{CH_4}}\right)^2} \quad (5)$$

where the fractions of the argument of the square root are given by the GC calibration for the two compounds. Assuming again uniform distribution, the uncertainty of the vapor fraction of each component is given by  $u_{GC}(y) / \sqrt{3}$ . In order to take into account the repeatability of the measurement, the uncertainty is calculated by:

$$u(y) = \sqrt{u_{rep}^2(y) + u_c^2(y)} \quad (6)$$

Uncertainties related with the repeatability and the calibration are provided in the tables below.

**Table S8.** Vapor phase analysis for the system CH<sub>4</sub>-H<sub>2</sub>S-MDEA-H<sub>2</sub>O with a 50.1 wt.% aqueous MDEA solution at the studied total pressures and temperatures.  $y$  is given in a dry basis.  $\delta y$  corresponds to the standard deviation due to repeatability measurements.  $u(y)$  corresponds to uncertainties due to GC calibration.

$T$ K	$P_{tot}$ kPa	CH <sub>4</sub> $y$	H <sub>2</sub> S $y$	$\delta y$	CH <sub>4</sub> $u(y)$	H <sub>2</sub> S $u(y)$	NS
Experiment 1							
322.98	493.81	0.99381	0.00619	1.42E-04	2.3E-02	1.3E-02	9
322.98	480.01	0.97599	0.02401	5.49E-04	2.3E-02	1.3E-02	9
322.98	500.72	0.89978	0.10022	1.17E-03	2.3E-02	1.3E-02	7
322.98	604.01	0.70067	0.29933	2.60E-03	2.3E-02	1.3E-02	10
Experiment 2							
322.98	493.92	0.99462	0.00538	6.56E-05	2.3E-02	1.3E-02	6
322.98	493.50	0.95375	0.04625	2.70E-04	2.3E-02	1.3E-02	6
322.98	498.13	0.85065	0.14935	7.32E-04	2.3E-02	1.3E-02	8
322.98	530.82	0.73254	0.26746	9.70E-04	2.3E-02	1.3E-02	5
322.98	545.53	0.68501	0.31499	1.48E-03	2.3E-02	1.3E-02	9
322.98	3106.96	0.94197	0.05803	2.27E-04	2.3E-02	1.3E-02	8

**Table S9.** Vapor phase analysis for the system CH<sub>4</sub>-H<sub>2</sub>S-MDEA-H<sub>2</sub>O with a 70 wt.% aqueous MDEA solution at the studied total pressures and temperatures.  $y$  is given in a dry basis.  $\delta y$  corresponds to the standard deviation due to repeatability measurements.  $u(y)$  corresponds to uncertainties due to GC calibration.

$T$ K	$P_{\text{tot}}$ kPa	CH <sub>4</sub> $y$	H <sub>2</sub> S $y$	$\delta y$	CH <sub>4</sub> $u(y)$	H <sub>2</sub> S $u(y)$	NS
283.00	2011.87	0.99827	0.00173	3.7E-05	7.4E-03	1.5E-02	9
283.00	6030.85	0.99936	0.00064	2.4E-05	7.4E-03	1.5E-02	10
283.00	10052.50	0.99953	0.00047	8.6E-06	7.4E-03	1.5E-02	7
352.99	1976.07	0.94525	0.05475	4.0E-04	2.3E-02	1.3E-02	5
352.99	3954.66	0.97236	0.02764	2.6E-04	2.3E-02	1.3E-02	10
352.99	5957.76	0.98176	0.01824	2.5E-04	2.3E-02	1.3E-02	7
352.99	7976.36	0.98587	0.01410	1.5E-04	2.3E-02	1.3E-02	6
352.99	9988.18	0.98880	0.01120	1.9E-04	2.3E-02	1.3E-02	6
393.00	2024.40	0.80129	0.19871	2.6E-04	7.4E-03	1.2E-02	8
392.99	5979.36	0.93562	0.06438	2.0E-04	7.4E-03	1.2E-02	10
393.00	9925.29	0.96280	0.03720	7.1E-05	7.4E-03	1.5E-02	8
283.00	1975.74	0.99331	0.00665	1.4E-04	2.3E-02	1.3E-02	7
283.00	5990.55	0.99710	0.00290	1.4E-04	2.3E-02	1.3E-02	5
283.00	10045.17	0.99785	0.00215	5.0E-05	2.3E-02	1.3E-02	6
352.92	2006.00	0.86600	0.13400	3.8E-04	7.4E-03	1.5E-02	7
352.92	5980.37	0.95259	0.04741	2.6E-04	7.4E-03	1.5E-02	8
352.92	9975.23	0.96979	0.03021	1.3E-04	7.4E-03	1.5E-02	8
393.05	974.22	0.00014	0.99986	1.2E-05	2.3E-02	1.2E-02	3
393.00	2034.17	0.56816	0.43184	4.7E-04	7.4E-03	1.2E-02	8
393.01	5893.45	0.85979	0.14021	6.4E-05	7.4E-03	1.2E-02	7
393.00	9915.85	0.91721	0.08279	3.2E-04	7.4E-03	1.2E-02	9

Uncertainty of the partial pressure of H<sub>2</sub>S,  $P_{\text{H}_2\text{S}}$

The partial pressure of hydrogen sulfide was calculated by Eq. (7) and the derived uncertainty is shown in Eq. (8). It is the 1<sup>st</sup> term of the argument of the square root that decides the order of the uncertainty.

$$P_{H_2S} = y_{H_2S}(P_{tot} - P_{sol}^s) \quad (7)$$

$$u_c(P_{H_2S}) = \sqrt{(P_{tot} - P_{sol}^s)^2 u^2(y_{H_2S}) + 2 y_{H_2S}^2 u^2(P)} \quad (8)$$

where  $u(P)$  is the pressure transducer's uncertainty.

#### Uncertainty of the global loading of H<sub>2</sub>S, $\alpha_{glob}$

Given that the global loading is given by:

$$\alpha_{glob} = \frac{n_{H_2S,cell}}{n_{MDEA}} \quad (9)$$

where  $n_{H_2S \text{ in cell}}$ : moles of H<sub>2</sub>S introduced from the gas tank with known PVT and,

$n_{MDEA}$ : moles of MDEA introduced in the cell from VVP, assuming the amount of MDEA in the vapor phase is negligible due its low vapor pressure.

The uncertainty is given by Eq. (10):

$$u(\alpha_{glob}) = \alpha_{glob} \sqrt{\left(\frac{u(n_{H_2S,cell})}{n_{H_2S,cell}}\right)^2 + \left(\frac{u(n_{MDEA})}{n_{MDEA}}\right)^2} \quad (10)$$

The fraction  $u(n_{H_2S})/n_{H_2S}$  is different than the one in Eq. (5), and it can be calculated by the molar density of the gas tank before and after the pressurization of the cell with hydrogen sulfide:

$$n_{H_2S,cell} = \rho_{before}(T,P) V_{tank} - \rho_{after}(T,P) V_{tank} \quad (11)$$

For the calculation of its uncertainty, the partial derivatives of density for temperature and pressure are required and can be calculated by REFPROP<sup>®</sup> software for the pressures and temperatures recorded.

In order to calculate the fraction  $u(n_{MDEA})/n_{MDEA}$ , Eqs. (12) and (13) are used:

$$n_{MDEA} = \rho \pi r^2 \Delta l x_{MDEA} \quad (12)$$

where  $\rho$ : molar density,  $r$ : radius of the piston, and  $\Delta l$ : piston displacement.

It is found that:

$$\frac{u(n_{MDEA})}{n_{MDEA}} = \frac{\pi r^2 \Delta l \rho}{n_{tot}} \sqrt{\left(\frac{u(\rho)}{\rho}\right)^2 + \left(\frac{u(\Delta l)}{\Delta l}\right)^2} \quad (13)$$

where  $u(\Delta l)$  is the accuracy of the highly-sensitive displacement transducer, i.e.  $1 \cdot 10^{-6}$  m.

The density of the solvent was not measured; thus, its uncertainty must be also calculated according to:

$$\frac{u(\rho)}{\rho} = \sqrt{\left(\frac{u(n_{tot})}{n_{tot}}\right)^2 + \left(\frac{u(V_{solv})}{V_{solv}}\right)^2} \quad (14)$$

For the calculation of the uncertainty of the volume of the solvent  $u(V_{solv})$  through Eq. (15), the molar volumes for MDEA and H<sub>2</sub>O were retrieved by (Bernal-García et al., 2003).

$$u(V_{solv}) = \sqrt{V_{H_2O}^2 u^2(x_{H_2O}) + V_{MDEA}^2 u^2(x_{MDEA})} \quad (15)$$

where all are known.

#### Uncertainty of the liquid loading of H<sub>2</sub>S, $\alpha$

The uncertainty of the liquid loading, or simply loading, is the same as the one for global loading (Eq. (10)) except for instead of  $n_{H_2S,cell}$ , we use  $n_{H_2S} = n_{H_2S,cell} - n_{H_2S}^v$ . The total moles in the vapor phase,  $n_{tot}^v$ , as well as the moles of H<sub>2</sub>S in the vapor phase,  $n_{H_2S}^v$ , can be estimated using an accurate model like GERG EoS (Kunz and Wagner, 2012) since the pressure, temperature, volume and composition of the vapor phase are known.

$$\text{Therefore, } u(n_{H_2S}) = \sqrt{u^2(n_{H_2S,cell}) + u^2(n_{H_2S}^v)} \quad (16)$$

The first term of argument of the square root was calculated earlier, while the second term is calculated by Eqs. (17) - (19).

$$u(n_{H_2S}^v) = \sqrt{y_{H_2S}^2 u^2(n_{tot}^v) + (n_{tot}^v)^2 u^2(y_{H_2S})} \quad (17)$$

$$u(n_{tot}^v) = \sqrt{V_{vap}^2 u^2(\rho_{vap}) + \rho_{vap}^2 u^2(V_{vap})} \quad (18)$$

$$u(V_{vap}) = \sqrt{u^2(V_{cell}) + u^2(V_{solv})} \quad (19)$$

where  $u(V_{cell})$  is known from the calibration of the cell, i.e.  $5 \cdot 10^{-8} \text{ m}^3$ .

It is expected that the uncertainty of the liquid loading will be higher than the one for global loading (see Eq. (16)), since the first is also a function of the moles introduced in total in the cell from the gas tank.

## Bibliography

- Bernal-García, J.M., Ramos-Estrada, M., Iglesias-Silva, G.A., Hall, K.R., 2003. Densities and Excess Molar Volumes of Aqueous Solutions of n-Methyldiethanolamine (MDEA) at Temperatures from (283.15 to 363.15) K. *J. Chem. Eng. Data* 48, 1442–1445. <https://doi.org/10.1021/je030120x>
- Chang, H.T., Posey, M., Rochelle, G.T., 1993. Thermodynamics of alkanolamine-water solutions from freezing point measurements. *Industrial & engineering chemistry research* 32, 2324–2335.
- Dicko, M., Coquelet, C., Jarne, C., Northrop, S., Richon, D., 2010. Acid gases partial pressures above a 50 wt% aqueous methyldiethanolamine solution: Experimental work and modeling. *Fluid Phase Equilibria* 289, 99–109. <https://doi.org/10.1016/j.fluid.2009.11.012>
- Fosbøl, P.L., Pedersen, M.G., Thomsen, K., 2011. Freezing Point Depressions of Aqueous MEA, MDEA, and MEA–MDEA Measured with a New Apparatus. *J. Chem. Eng. Data* 56, 995–1000. <https://doi.org/10.1021/je100994v>
- Huang, S.H., Ng, H.-J., 1998. Solubility of H<sub>2</sub>S and CO<sub>2</sub> in Alkanolamines (No. RR-155). Gas Processors Association.
- Jou, F.Y., Mather, A.E., Otto, F.D., 1982. Solubility of hydrogen sulfide and carbon dioxide in aqueous methyldiethanolamine solutions. *Ind. Eng. Chem. Proc. Des. Dev.* 21, 539–544. <https://doi.org/10.1021/i200019a001>
- Kim, I., Svendsen, H.F., Børresen, E., 2008. Ebulliometric Determination of Vapor–Liquid Equilibria for Pure Water, Monoethanolamine, N-Methyldiethanolamine, 3-(Methylamino)-propylamine, and Their Binary and Ternary Solutions. *J. Chem. Eng. Data* 53, 2521–2531. <https://doi.org/10.1021/je800290k>
- Kunz, O., Wagner, W., 2012. The GERG-2008 Wide-Range Equation of State for Natural Gases and Other Mixtures: An Expansion of GERG-2004. *J. Chem. Eng. Data* 57, 3032–3091. <https://doi.org/10.1021/je300655b>
- Kuranov, G., Rumpf, B., Smirnova, N.A., Maurer, G., 1996. Solubility of Single Gases Carbon Dioxide and Hydrogen Sulfide in Aqueous Solutions of N-Methyldiethanolamine in the Temperature Range 313–413 K at Pressures up to 5 MPa. *Ind. Eng. Chem. Res.* 35, 1959–1966. <https://doi.org/10.1021/ie950538r>
- Maham, Y., Mather, A.E., Mathonat, C., 2000. Excess properties of (alkyldiethanolamine +H<sub>2</sub>O) mixtures at temperatures from (298.15 to 338.15) K. *The Journal of Chemical Thermodynamics* 32, 229–236. <https://doi.org/10.1006/jcht.1999.0595>
- Mathonat, C., Maham, Y., Mather, A.E., Hepler, L.G., 1997. Excess Molar Enthalpies of (Water + Monoalkanolamine) Mixtures at 298.15 K and 308.15 K. *J. Chem. Eng. Data* 42, 993–995. <https://doi.org/10.1021/je960304u>
- Posey, M.L., 1996. Thermodynamic model for acid gas loaded aqueous alkanolamine solutions.



## 4.2 Vapor-liquid equilibrium study for the system H<sub>2</sub>S-CH<sub>4</sub>-MDEA-MEG-H<sub>2</sub>O

### 4.2.1 Aim of the study

The motivation for this study was to gain more understanding regarding the effect of MEG on the absorption capacity of H<sub>2</sub>S in aqueous MDEA. An amine-glycol solution is promising for the combined desulfurization and hydrate control of natural gas subsea, where typical pressures can vary from some dozens to hundreds of bar. Therefore, this study also focused on the role of increasing total pressure in the VLE behavior of the system. Investigation of the dehydration performance of the system was not part of this work.

Vapor-liquid equilibrium data were obtained for hydrogen sulfide and a 30 wt% MDEA – 40 wt% MEG – 30 wt% H<sub>2</sub>O blend, in the presence of methane. Similar to the study in section 4.1, methane was used to simulate the composition of the natural gas as well as a pressurizing medium. The effect of total pressure was investigated by conducting experiments at 2000, 6000 and 10000 kPa and temperatures at 283, 353 and 393 K. Having produced new experimental data for this system, a comparison with aqueous MDEA systems and other MDEA-MEG-H<sub>2</sub>O mixtures reported in the literature was performed. In addition, the data were used to estimate the cyclic capacity of the solvent.

### 4.2.2 Experimental work

#### 4.2.2.1 Materials

The chemicals used in this work are presented in Table 4.1. They were used without further purification. The procedure for solution preparation was the same as presented in the previous section of the chapter, where the chemicals were mixed under vacuum. A METTLER PM1200 scale was used with an accuracy of  $1 \cdot 10^{-5}$  kg. The blend's composition was 30 wt% MDEA – 40 wt% MEG – 30 wt% H<sub>2</sub>O and the combined uncertainty for each component, including the purity of the chemicals, was found to be  $u(w_{\text{MDEA}})=0.001$ ,  $u(w_{\text{MEG}})=0.001$  and  $u(w_{\text{H}_2\text{O}})=0.001$ .

Table 4.1. Chemical Sample Table.

Component	IUPAC name	CAS	Supplier	Purity
N-methyldiethanolamine (MDEA)	2-[2-hydroxyethyl(methylamino) ethanol]	105-59-9	Sigma-Aldrich	≥ 99 wt%
Monoethylene glycol (MEG)	ethane-1,2-diol	107-21-1	Sigma-Aldrich	99.8 wt%
Water	Oxidane	-	-	Ultra-pure
Hydrogen sulfide	Sulfane	7783-06-4	Air Liquide	≥ 99.5 vol%
Methane	Methane	74-82-8	Air Liquide	≥ 99.995 vol%

#### 4.2.2.2 Experimental setup and procedure

The static-analytic apparatus presented in section 4.1 for the high-pressure VLE measurements with aqueous MDEA, was also used for the MDEA-MEG-H<sub>2</sub>O system. The main parts of the experimental rig are a variable volume press and gas tanks/bottles for introducing into the cell the solvent and the gases respectively, the equilibrium cell of approximately 34 ml volume with sampling capillaries and the gas chromatograph (GC). The temperature is controlled and monitored by means of an oil bath and thermoelements located on the upper and lower flange of the cell. The pressure is monitored inside the equilibrium cell by two pressure transducers, one for low pressure (< 3 MPa) and one for high pressure (< 30 MPa). A thermoelement and a pressure transducer are also attached to the H<sub>2</sub>S gas tank to allow for the measurement of the pressure and temperature of the tank before and after the filling the cell, therefore, allowing for the calculation of hydrogen sulfide amount via PVT data. The methodology followed to calculate the number of moles and final loading are not repeated here, since they have already been presented in the previous section. The only difference in these calculations is that the excess volume of the liquid mixture at the studied temperatures was found using the density model developed in the density study of this thesis (Chapter 3). The effect of pressure in the liquid volume was considered negligible.

Hot deionized water and ethanol were used for the cleaning of the cell, tubings and sampling capillaries. They were left to dry for at least 12 hours under vacuum. The experiment started by introducing approximately 6 ml of solvent into the cell. Once the measurement temperature was stabilized, hydrogen sulfide was added and was left to equilibrate. Equilibration was rather fast,

1-2 hours, due to the fast reaction of H<sub>2</sub>S with MDEA and water. The next step was to fill methane up to 2000 kPa and wait again for equilibrium for another 1-2 hours. Upon pressurization, vapor phase samples were withdrawn, transferred through a heated line to the GC and analyzed with a TCD detector. In the end of the analysis, the GC column was cleaned by applying 493 K, while methane was added in the cell up to the next desired pressure, i.e. 6000 kPa. The procedure was repeated for total pressure of 6000 kPa and 10000 kPa, for every studied temperature. The amount of hydrogen sulfide in the liquid phase was calculated based on the GC analysis of the vapor phase and the mass balance, as explained in detail in section 4.1 under *Experimental Procedure*.

### 4.2.3 Results and discussion

#### 4.2.3.1 Trends and effects

The high-pressure vapor-liquid equilibrium data obtained in this work with a 30 wt% MDEA – 40 wt% MEG – 30 wt% H<sub>2</sub>O solution are presented in Table 4.2, accompanied by the corresponding uncertainties. Following NIST guidelines for reporting of the uncertainty in experimental measurements, an extended uncertainty analysis was conducted based on the Law of propagation of uncertainty (Taylor and Kuyatt, 1994). Uncertainty calculations were performed according to the uncertainty analysis for the measurements with aqueous MDEA in the previous section, which is provided in detail in the Supporting Information published with the article. The only difference is the calculation of the uncertainty in the composition of the solvent, since, here, it is a ternary system. However, the equations used for this uncertainty have been listed in the uncertainty analysis conducted for the density and viscosity study presented in Chapter 3, which is also provided in the Supporting Information of the article.

Table 4.2 includes, together with the experimental data, the standard uncertainties in temperature and pressure, as they were estimated by the calibration and accuracy of the measuring devices, in addition to the combined standard uncertainties in partial pressure of hydrogen sulfide, global and liquid loading. Overall, it is observed that the uncertainties are low. Similar to the work for 70 wt% MDEA – 30 wt% H<sub>2</sub>O, the uncertainty in  $P_{H_2S}$  increases with increasing total pressure, which is the main contributor in the uncertainty  $u(P_{H_2S})$ . The uncertainty in the loadings, global and liquid, is the result of the product of the loading itself

and a term depending mainly on the uncertainty of the mol of H<sub>2</sub>S inside the cell for the global loading and the mol of H<sub>2</sub>S in the liquid phase for the liquid loading. As a result, at the higher loadings of this work, the second term of the product is lower, leading to similar loading uncertainties in all cases.

Table 4.2 Experimental vapor-liquid equilibrium data and their corresponding combined uncertainties as a function of total pressure and temperature for the system CH<sub>4</sub>-H<sub>2</sub>S-MDEA-MEG-H<sub>2</sub>O and 30 wt% MDEA – 40 wt% MEG – 30 wt% H<sub>2</sub>O<sup>a</sup>. Methane is used as makeup gas.

$T$	$P_{tot}$	$P_{H_2S}$	$u_c(P_{H_2S})$	$\alpha_{glob}$	$u_c(\alpha_{glob})$	$\alpha_{liq}$	$u_c(\alpha_{liq})$
K	kPa	kPa	kPa	mol H <sub>2</sub> S global/ mol MDEA	mol H <sub>2</sub> S global/ mol MDEA	mol H <sub>2</sub> S liquid/ mol MDEA	mol H <sub>2</sub> S liquid/ mol MDEA
283.05	1972.55	0.66	0.01	0.199	0.004	0.199	0.002
283.05	6197.73	0.79	0.05	0.199	0.004	0.199	0.002
283.03	9954.93	1.04	0.08	0.199	0.004	0.198	0.002
352.89	1730.21	28.81	0.18	0.201	0.004	0.185	0.002
352.92	6208.67	27.56	0.17	0.201	0.004	0.185	0.002
352.92	9938.67	28.55	0.18	0.201	0.004	0.184	0.002
392.99	1997.52	98.21	0.56	0.211	0.006	0.163	0.003
392.99	5984.24	99.74	0.59	0.211	0.006	0.163	0.003
392.99	9942.04	86.88	0.49	0.211	0.006	0.169	0.003
282.93	1992.95	5.26	0.04	0.513	0.006	0.509	0.003
282.92	5953.76	6.23	0.08	0.513	0.006	0.508	0.003
282.92	9976.92	6.58	0.09	0.513	0.006	0.507	0.003
352.91	1974.80	95.28	0.53	0.497	0.004	0.443	0.002
352.81	6321.59	96.73	0.60	0.497	0.004	0.443	0.002
352.91	9975.31	101.28	0.59	0.497	0.004	0.439	0.002
392.99	1996.14	276.71	1.15	0.497	0.004	0.358	0.002
392.99	5958.62	258.02	1.42	0.497	0.004	0.370	0.002
392.99	9972.70	262.00	1.44	0.497	0.004	0.367	0.002

<sup>a</sup> Standard uncertainties not included above are  $u(T) = 0.02$  K,  $u(P) = 0.6$  kPa.

The vapor fractions of hydrogen sulfide and methane measured by GC analysis with the corresponding uncertainties due to repeatability as well as due to GC calibration are provided in Table 4.3.

Table 4.3 Vapor phase analysis for the system CH<sub>4</sub>-H<sub>2</sub>S-MDEA-MEG-H<sub>2</sub>O with a 30 wt.% MDEA – 40 wt.% MEG – 30 wt.% H<sub>2</sub>O mixture as a function of total pressure and temperature.  $y$  is given in a dry basis.  $\delta y$  corresponds to the standard deviation due to repeatability measurements.  $\Delta(n)/n$  corresponds to uncertainties due to GC calibration.

$T$ K	$P_{tot}$ kPa	CH <sub>4</sub> $y$	H <sub>2</sub> S $y$	$\delta y$	CH <sub>4</sub> $\Delta(n)/n$	H <sub>2</sub> S $\Delta(n)/n$	CH <sub>4</sub> $u(y)$	H <sub>2</sub> S $u(y)$	NS
283.05	1972.55	0.99966	0.00034	2.2E-05	7.4E-03	1.5E-02	2.3E-05	1.2E-05	8
283.05	6197.73	0.99987	0.00013	2.9E-05	7.4E-03	1.5E-02	2.9E-05	1.5E-05	9
283.03	9954.93	0.99990	0.00010	2.7E-05	7.4E-03	1.5E-02	2.7E-05	1.4E-05	8
352.89	1730.21	0.98307	0.01693	1.9E-04	7.4E-03	1.5E-02	2.5E-04	1.9E-04	8
352.92	6208.67	0.99554	0.00446	3.9E-05	7.4E-03	1.5E-02	5.8E-05	4.7E-05	11
352.92	9938.67	0.99712	0.00288	2.7E-05	7.4E-03	1.5E-02	3.9E-05	3.1E-05	11
392.99	1997.52	0.94778	0.05222	3.9E-04	7.4E-03	1.5E-02	6.1E-04	5.2E-04	10
392.99	5984.24	0.98300	0.01700	1.3E-04	7.4E-03	1.5E-02	2.1E-04	1.7E-04	11
392.99	9942.04	0.99116	0.00884	3.8E-05	7.4E-03	1.5E-02	9.3E-05	8.7E-05	11
282.93	1992.95	0.99736	0.00264	4.9E-05	7.4E-03	1.5E-02	5.5E-05	3.5E-05	11
282.92	5953.76	0.99895	0.00105	4.2E-05	7.4E-03	1.5E-02	4.3E-05	2.3E-05	13
282.92	9976.92	0.99935	0.00066	3.0E-05	7.4E-03	1.5E-02	4.3E-05	1.6E-05	11
352.91	1974.80	0.95101	0.04899	2.7E-04	7.4E-03	1.5E-02	5.2E-04	4.7E-04	12
352.81	6321.59	0.98463	0.01537	1.5E-04	7.4E-03	1.5E-02	2.1E-04	1.6E-04	11
352.91	9975.31	0.98982	0.01018	6.5E-05	7.4E-03	1.5E-02	1.2E-04	1.0E-04	13
392.99	1996.14	0.8530	0.1470	2.6E-04	7.4E-03	1.2E-02	1.1E-03	1.1E-03	10
392.99	5958.62	0.95586	0.04414	2.0E-04	7.4E-03	1.5E-02	4.6E-04	4.2E-04	10
392.99	9972.70	0.97343	0.02657	6.8E-05	7.4E-03	1.5E-02	2.6E-04	2.5E-04	13

<sup>a</sup> Standard uncertainties not included above are  $u(T) = 0.02$  K,  $u(P) = 0.6$  kPa.

According to the equations for the calculation of the uncertainty in the vapor fraction  $u(y)$  (section 1.1, Equations (5) and (6) in Supporting Information), it depends on the repeatability of the measurement and the actual uncertainty due to the measurement and the GC calibration. It is concluded that the combined uncertainty  $u_c(y)$  depends equally to the GC measurement and the measurement's repeatability, since they are in most cases of the same order.

Figure 4.1 shows the H<sub>2</sub>S partial pressure against the liquid loading in the three studied temperatures and total pressure of 10000 kPa. It can be observed that an increase in the partial pressure of hydrogen sulfide leads to higher liquid loadings at isothermal conditions, as it is expected. Lower temperatures also benefit the absorption of H<sub>2</sub>S into MDEA-MEG-H<sub>2</sub>O and yield higher liquid loadings.

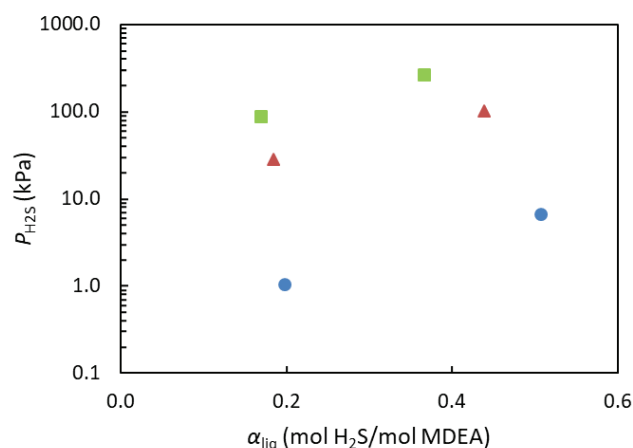


Figure 4.1 Equilibrium H<sub>2</sub>S partial pressures as a function of liquid loading and temperature for the system 30 wt% MDEA – 40 wt% MEG – 30 wt% H<sub>2</sub>O at total pressure of 10000 kPa; (●) 283 K, (▲) 353 K, (■) 393 K.

The effect of total pressure on the H<sub>2</sub>S loading of the liquid phase is discussed by aid of Figure 4.2 and Figure 4.3, where the liquid loading is plotted against total pressure for two different global loadings, i.e. 0.2 and 0.5 mol H<sub>2</sub>S/mol MDEA. The results show that an increase in total pressure from 2000 kPa up to 10000 kPa does not seem to have a significant effect on the loading of the solvent. Error bars are included for both loading and total pressure, however, the latter are too small to be visible in the scale 0 – 10000 kPa. The deviations seen at increasing pressure are within or slightly higher than the experimental uncertainty in the liquid loading, except for the measurements at 393 K. It is noted that in these measurements, it was not possible

to quantify the amount of water by GC analysis and it was calculated based on the vapor pressure of the solvent assuming that it is independent of the total pressure of the system.

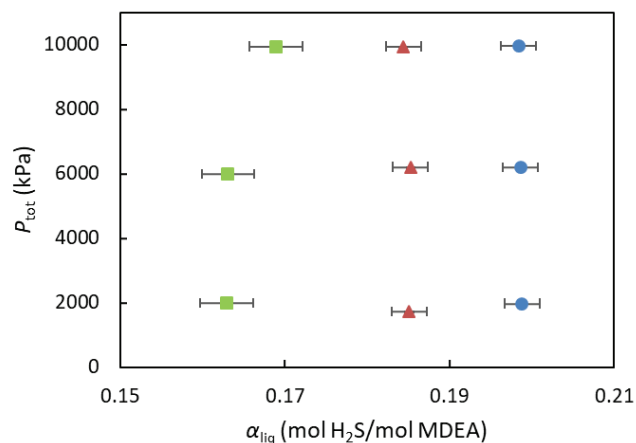


Figure 4.2 Effect of total pressure on H<sub>2</sub>S liquid loading for the system 30 wt% MDEA – 40 wt% MEG – 30 wt% H<sub>2</sub>O for approximately 0.2 mol H<sub>2</sub>S/mol MDEA global loading; (●) 283 K, (▲) 353 K, (■) 393 K. Error bars are included for x and y axis.

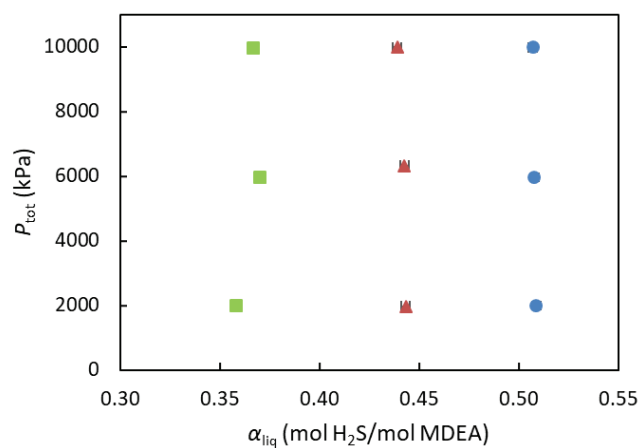


Figure 4.3 Effect of total pressure on H<sub>2</sub>S liquid loading for the system 30 wt% MDEA – 40 wt% MEG – 30 wt% H<sub>2</sub>O for approximately 0.5 mol H<sub>2</sub>S/mol MDEA global loading; (●) 283 K, (▲) 353 K, (■) 393 K. Error bars are included for x and y axis.

On the contrary to the effect of total pressure on the loading, the impact of increased total pressure on the partial pressure of hydrogen sulfide is larger than the experimental uncertainties. The fugacities were calculated at each loading and pressure and they were plotted against the liquid loadings in Figure 4.4 in order to gain more understanding of the results. The calculations were performed using TREND software (Span et al., 2015), by assuming that the water vapor fraction is equal to the ratio of the vapor pressure of the solvent to the total pressure.

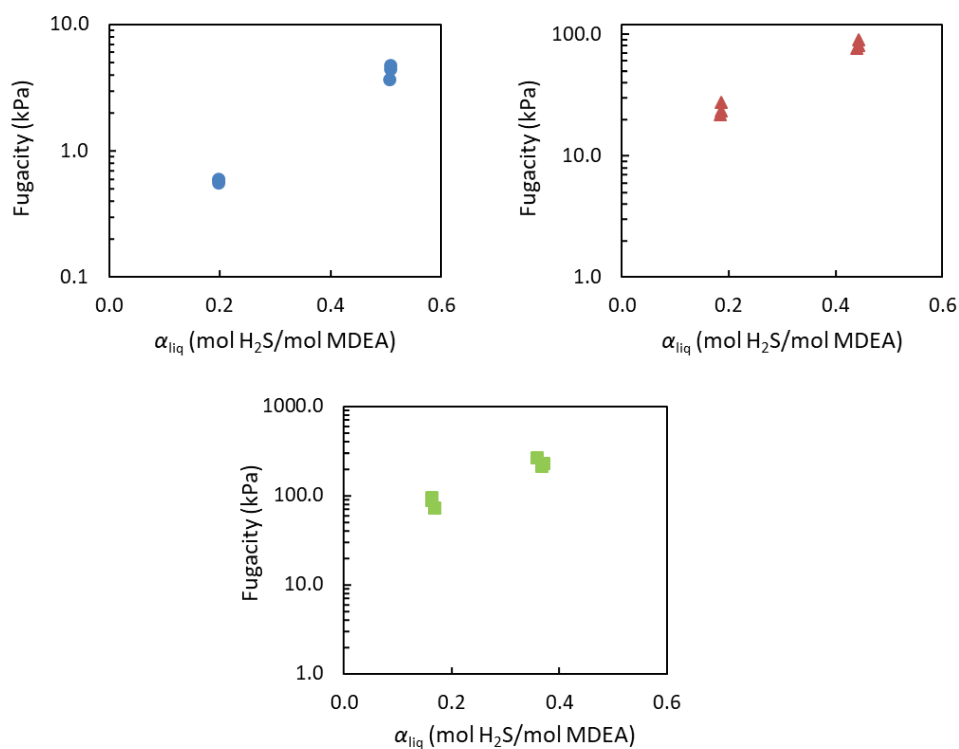


Figure 4.4 Equilibrium H<sub>2</sub>S fugacity as a function of H<sub>2</sub>S liquid loading for the system 30 wt% MDEA – 40 wt% MEG – 30 wt% H<sub>2</sub>O; (●) 283 K, (▲) 353 K, (■) 393 K.

It is observed that fugacity increases with liquid loading. At each loading, fugacity also increases with increasing total pressure at 283 K and 353 K. This is not the case at 393 K, where there is no clear behavior of increasing or decreasing fugacities. It is interesting that TREND predicted a liquid phase at 393 K and 10000 kPa for both low and high global loadings. Phase changes cannot be confirmed by the experiment since the cell was submerged in the liquid bath without possibility for visual inspection. Moreover, as mentioned earlier, there is additional



uncertainty of these data due to the fact that the water present in the liquid phase could not be quantified by GC analysis.

#### 4.2.3.2 Comparison with literature

Already in Chapter 2, where a literature review on amine-glycol systems was presented, it became evident that few studies have been carried out about MDEA-MEG solvents. To be specific, in the literature there are nine studies in total including VLE, kinetics, degradation and corrosion, three of them reporting VLE data with H<sub>2</sub>S. As part of his thesis, Jelstad measured H<sub>2</sub>S solubility in MDEA-MEG systems with focus on the effect of water (Jelstad, 1997). Poblete, also in his thesis, investigated the co-absorption of CO<sub>2</sub>/H<sub>2</sub>S in the same systems as Jelstad (Poblete, 1997). Last but not least, Xu and co-workers report VLE data for H<sub>2</sub>S, CO<sub>2</sub> and CO<sub>2</sub>/H<sub>2</sub>S mixtures in aqueous and non-aqueous MDEA-MEG (Xu et al., 2002). Since Poblete's data are obtained in the presence of carbon dioxide, only the two literature sources of Jelstad and Xu et al. were used for the comparison with the data acquired in this study.

An evaluation of each of the two individual data sets reported was performed separately prior to the comparison with each other and with our data, when possible. The density model developed in this work for aqueous and non-aqueous MDEA-MEG systems was used for the conversions concerning the solvent composition and the concentration of H<sub>2</sub>S in the liquid phase. By evaluating each of the individual sets separately, three main observations were made:

- (a) for a given partial pressure, an increase in temperature leads to lower liquid loadings,
- (b) for a given partial pressure and water content, an increase in amine concentration leads to lower liquid loadings (higher absorption capacity in mol H<sub>2</sub>S/L solution) and
- (c) for a given partial pressure, adding water to non-aqueous MDEA-MEG up to 10 wt% seems to enhance the absorption capacity of the system, though not substantially.

Observation (a) is expected due to exothermic nature of the H<sub>2</sub>S absorption reaction with amine systems. Observations (b) can be explained by the fact that more amine is available to react with hydrogen sulfide, though it is important to keep in mind that the data for 70 wt% aqueous MDEA indicated an upper limit in amine concentration which can enhance the absorption capacity of the solvent. Thus, it is emphasized that the observations (a), (b) and (c) refer to the

temperature, amine and water concentration ranges of the literature data. Observation (c) is further discussed in the following part of this section.

#### Effect of amine content on absorption capacity

The data from Jelstad (1997) and Xu et al. (2002) can be compared in terms of amine concentration effect at constant water content and 298 K (Figure 4.5). A disagreement between these two literature sources is observed. At 298 K, the data for 30 wt% MDEA – 65 wt% MEG – 5 wt% H<sub>2</sub>O by Xu et al. fall between the data obtained from Jelstad for 11 wt% MDEA and 22 wt% MDEA and constant 6 wt% H<sub>2</sub>O. This deviation is more pronounced in terms of H<sub>2</sub>S molar concentration in the liquid phase in Figure 4.6.

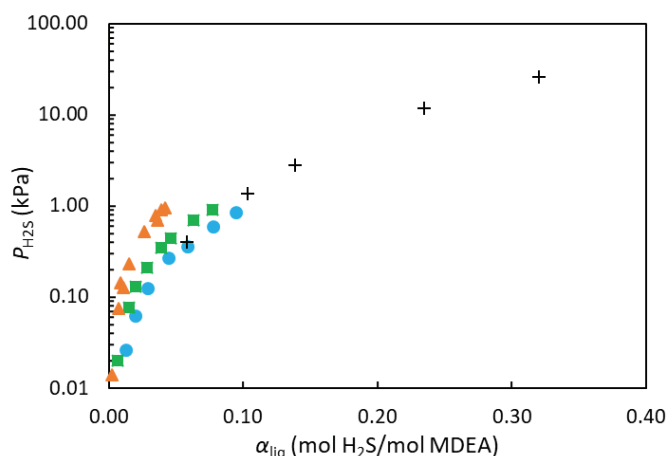


Figure 4.5 Equilibrium H<sub>2</sub>S partial pressure as a function of liquid loading and amine concentration for the system H<sub>2</sub>S-MDEA-MEG-H<sub>2</sub>O at 298 K and constant water content; (●) 11 wt% MDEA (Jelstad, 1997), (■) 22 wt% MDEA (Jelstad, 1997), (+) 30 wt% MDEA (Xu et al., 2002) and (▲) 44 wt% MDEA (Jelstad, 1997). Water content is 6 wt% for the data with 11 wt% and 22 wt% MDEA, while water content is 5 wt% for the data with 30 wt% and 44 wt% MDEA.

Figure 4.6 presents  $P_{H_2S}$  against  $x_{H_2S}$  in logarithmic scale on the left side and linear scale on the right side. On the right side, plotting up to 2 kPa allows to see more clearly some curvature on the data which is also suggested by the linear fitting with  $R^2 = 0.94$ . The non-linear relation between  $P_{H_2S}$  and  $x_{H_2S}$  testifies that the absorption is enhanced by chemical reaction.

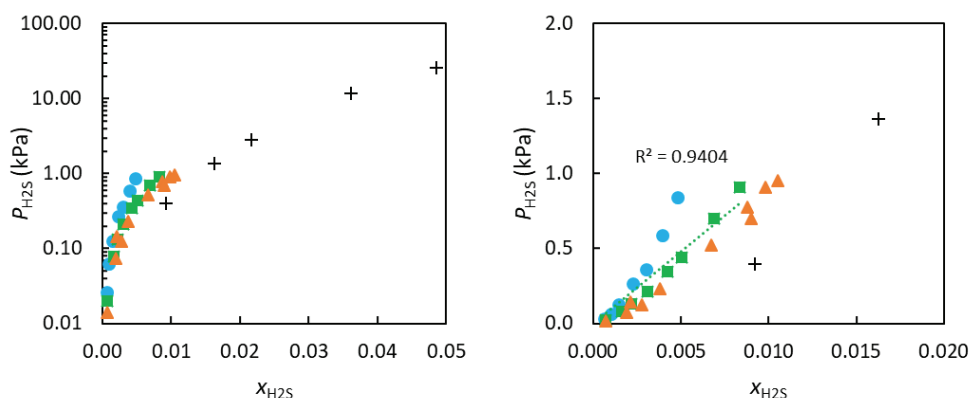


Figure 4.6 Equilibrium  $\text{H}_2\text{S}$  partial pressure as a function of  $\text{H}_2\text{S}$  liquid phase molar concentration and amine concentration for the system  $\text{H}_2\text{S}$ -MDEA-MEG- $\text{H}_2\text{O}$  at 298 K and constant water content; (●) 11 wt% MDEA (Jelstad, 1997), (■) 22 wt% MDEA (Jelstad, 1997), (+) 30 wt% MDEA (Xu et al., 2002) and (▲) 44 wt% MDEA (Jelstad, 1997). Water content is 6 wt% for the data with 11 wt% and 22 wt% MDEA, while water content is 5 wt% for the data with 30 wt% and 44wt% MDEA. Left: logarithmic scale, right: linear scale and low  $P_{\text{H}_2\text{S}}$  range.

It is important to note that both works also measured the solubility of hydrogen sulfide in aqueous MDEA to allow for a comparison with the literature. Xu et al. showed that their data are in good agreement with reported data (Jou et al., 1993; MacGregor and Mather, 1991), while the data from Jelstad were found higher than literature data, and specifically, for a given liquid concentration, their data overestimated the partial pressure. The literature source they used for comparison was not given, thus, the data were also compared to the predicted values by the VLE model developed in this work and presented in section 4.1. Indeed, the  $\text{H}_2\text{S}$  partial pressure was higher in Jelstad's measurements. This means that correction of the data would bring them closer and possibly in agreement to the data from Xu et al. Another important factor worth noting is that the data from Xu et al. were unfortunately not tabulated in the original publication, and therefore, were retrieved from graphs, adding to the uncertainty of the shown data points. Furthermore, one can notice in Figure 4.6 that the water content is either 5 or 6 wt%. Given the uncertainties discussed in this paragraph, the 1 wt% water content difference among the compared data adds only to a small degree to the observed deviations.

#### Effect of water content on absorption capacity

Reported data in the literature indicate that the presence of water enhances the absorption capacity of aqueous MDEA-MEG solvents. Jelstad investigated the VLE behavior of  $\text{H}_2\text{S}$  in

MDEA-MEG-H<sub>2</sub>O with water content from 0 to 5 wt% and showed that the water effect is small (Jelstad, 1997). The data obtained at 403 K, however, showed the opposite trend. Xu et al. increased even more the water content in their systems up to 10 wt% H<sub>2</sub>O (Xu et al., 2002). As seen in Figure 4.7, increasing the water content to 5 wt% seems to increase the absorption of hydrogen sulfide in the amine-glycol mixture though the effect is not as clear as it is in the presence of 10 wt% H<sub>2</sub>O.

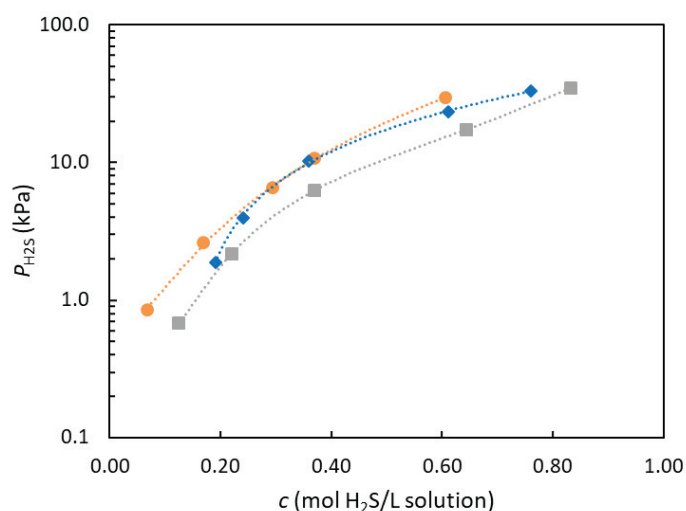


Figure 4.7 Equilibrium H<sub>2</sub>S partial pressure as a function of liquid phase concentration and water concentration for the system H<sub>2</sub>S-MDEA-MEG-H<sub>2</sub>O at 298 K and 30 wt% MDEA content; (●) 0 wt% H<sub>2</sub>O, (◆) 5 wt% H<sub>2</sub>O, (■) 10 wt% H<sub>2</sub>O (Xu et al., 2002). Trendlines are included.

Our measurements showed that the H<sub>2</sub>S loading of 30 wt% MDEA – 40 wt% MEG – 30 wt% H<sub>2</sub>O does not depend on the total pressure up to 10000 kPa, though the partial pressure of H<sub>2</sub>S changes as the total pressure increases. Therefore, a comparison of our data, which were obtained at our lowest measured total pressure, i.e. 2000 kPa, with the literature values obtained at low total pressure by Xu et al. (Xu et al., 2002), is attempted in Figure 4.8. The measurements of this study are conducted at different temperatures than the measurements of Xu et al. For this reason, the comparison is performed between the data in this work acquired at 353 K and the data from Xu et al. acquired at 363 K for the 30 wt% MDEA – 65 wt% MEG – 5 wt% H<sub>2</sub>O system (Xu et al., 2002). Figure 4.8 illustrates these data points together with VLE predictions for 30 wt% aqueous MDEA at 353 K. The predicted values were estimated by employment of

the VLE model developed in this work since, to the author's best knowledge, there are no reported data for this system at these temperatures.

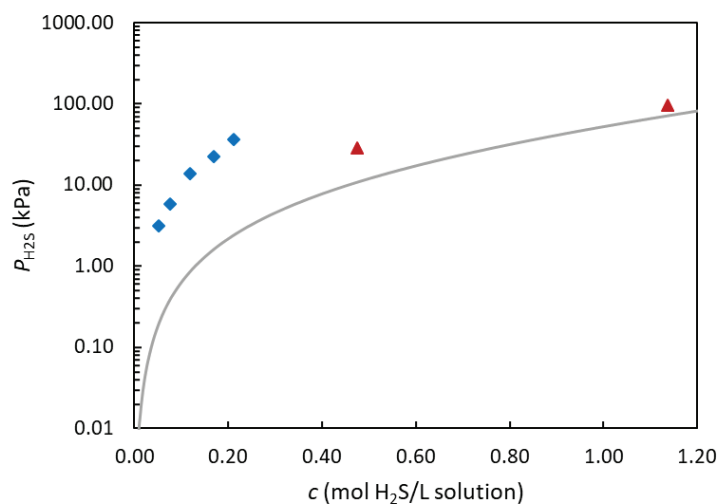


Figure 4.8 Equilibrium H<sub>2</sub>S partial pressure as a function of liquid phase concentration and water concentration for the system H<sub>2</sub>S-MDEA-MEG-H<sub>2</sub>O at constant 30 wt% MDEA content; (♦) 5 wt% H<sub>2</sub>O and 363 K (Xu et al., 2002), (▲) 30 wt% H<sub>2</sub>O at 353 K and total pressure 2000 kPa (This work), (—) 70 wt% H<sub>2</sub>O at 353 K, predicted values (This work).

It is observed that in a 30 wt% MDEA-MEG-H<sub>2</sub>O system, increasing the water content from 5 to 30 wt% H<sub>2</sub>O leads to a pronounced improvement of the H<sub>2</sub>S absorption capacity of the solvent. It is also seen that the absorption capacity of aqueous MDEA is higher than aqueous amine-glycol systems, for the same amine content. In Chapter 2 and section 2.3 Chemistry, it was mentioned that hydrogen sulfide reacts instantaneously with MDEA through a proton-transfer reaction. Therefore, the differences noticed as the water concentration increases and the glycol concentration decreases should be related to their role in the reaction mechanism and the dissolution of H<sub>2</sub>S in the solvent.

Xu et al. (Xu et al., 2002) state that the observed lower H<sub>2</sub>S solubility in MDEA-MEG solutions than that in aqueous MDEA solutions is due to the gas' lower solubility in monoethylene glycol than the one in water. However, literature data of H<sub>2</sub>S solubility in H<sub>2</sub>O and in MEG reveal the opposite. At 298 K, Henry's constant of H<sub>2</sub>S in H<sub>2</sub>O,  $H_{H_2S, H_2O}$ , is 59.4 MPa based on data from Rinker and Sandall (Rinker and Sandall, 2000) and 54.8 MPa based on the correlation proposed by Edwards et al. (Edwards et al., 1978). At the same temperature, Henry's constant of H<sub>2</sub>S in

MEG,  $H_{H_2S,MEG}$ , was calculated equal to 5.5 MPa from the data of Jou et al. (Jou et al., 1990) and equal to 7.5 MPa from the data of Afzal et al. (Afzal et al., 2012). The Henry's constant of H<sub>2</sub>S in MEG was considered equal to the slope of the linear regression between  $P_{H_2S}$  and  $x_{H_2S}$  and the deviations observed come from the different pressure ranges of the data in the two sources. Given that  $H_{H_2S,H_2O} > 50$  MPa and  $H_{H_2S,MEG} < 10$  MPa, H<sub>2</sub>S dissolves in a significantly higher extent in MEG than H<sub>2</sub>O, therefore the trend in the VLE data is not due to lower solubility in MEG.

The fact that the solubility of hydrogen sulfide is higher in MEG than in water, and yet the solubility in the mixed solvent decreases with increasing glycol concentration, can be explained by possible structural effects and/or a more complex reaction mechanism aside from the proton transfer between H<sub>2</sub>S and MDEA. The presence of water could enhance the H<sub>2</sub>S absorption through amine protonation (MDEAH<sup>+</sup>) which subsequently would react with the dissolved ionic species of H<sub>2</sub>S, HS<sup>-</sup>, causing more hydrogen sulfide to dissolve. In this system, both water and hydrogen sulfide self-ionize and produce protons (H<sup>+</sup>). According to the literature, protons can also be formed as the result of the autoprotolysis of MEG in the presence of MDEA (Eimer, 2014), which could also protonate the amine. However, even though MEG can autoprotolyze and provide H<sup>+</sup> to form MDEAH<sup>+</sup>, its molar amount is still lesser than H<sub>2</sub>O in a 30 wt% MDEA – 40 wt% MEG – 30 wt% H<sub>2</sub>O, in addition to the fact that the tendency for self-ionization is lower in MEG than water. The degree of self-ionization of solvents is informed by the autoprotolysis (dissociation) constant  $pK_{ap}$ , and the  $pK_{ap}$  of water and MEG is approximately 14 and 16, respectively (at 298 K). In other words, the proton contribution in the solvent from the autoprotolysis of glycol is lower than from the dissociation of water.

The autoprotolysis constant of triethylene glycol (TEG) is 18.5; it is higher than the one of MEG. This implies, under the assumption that the glycol undergoes autoprotolysis and participates in the reaction mechanism as a proton donor, that H<sub>2</sub>S absorption in non-aqueous MDEA-TEG would be lower than in non-aqueous MDEA-MEG, under same amine content. Indeed, Figure 4.9 shows the superior H<sub>2</sub>S absorption capacity in MDEA-MEG compared to MDEA-TEG system. Similar to the comparison between MDEA-MEG and MDEA-H<sub>2</sub>O, the trend depicted in the figure cannot be explained by the difference in solubility. Hydrogen sulfide solubility is higher in TEG than MEG and, specifically, at 298 K,  $H_{H_2S,TEG}$  is equal to 2.1 (Jou et al., 1987) while  $H_{H_2S,MEG}$  lies between 5 and 7 MPa, as shown earlier.

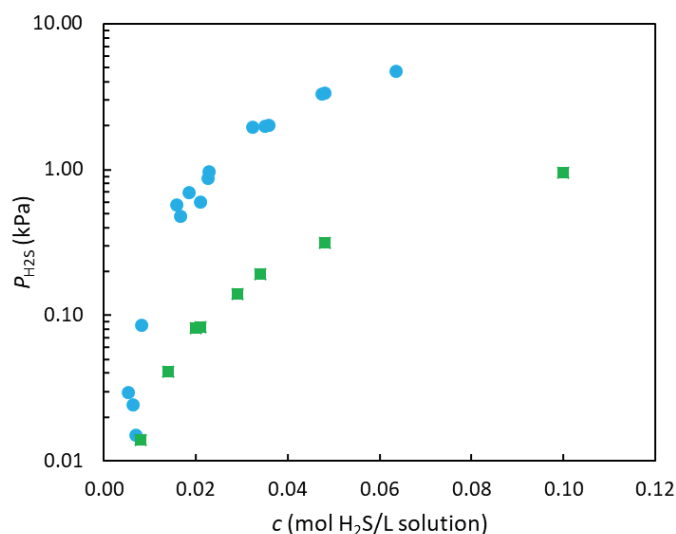


Figure 4.9 Equilibrium H<sub>2</sub>S partial pressure as a function of liquid phase concentration in non-aqueous MDEA-glycol solvent at 298 K and 11 wt% MDEA content; (●) MDEA-TEG (Eimer, 1994), (■) MDEA-MEG (Jelstad, 1997).

#### 4.2.3.3 Comparison with 70 wt% aqueous MDEA

The H<sub>2</sub>S absorption capacity in 30 wt% MDEA – 40 wt% MEG – 30 wt% H<sub>2</sub>O was compared to the one in 70 wt% aqueous MDEA, in terms of kg H<sub>2</sub>S/L solution, in order to give a more perceptible feeling of the amounts of chemicals. The comparison is performed in the basis that MDEA is a polar molecule with some affinity for water. Therefore, it is interesting to see if the substitution of the glycol with amine would be beneficial for the H<sub>2</sub>S absorption, assuming they would both achieve the required degree of dehydration in the system. Certainly, the dehydration capacity of the solvent still needs to be investigated.

The absorption capacity of each solvent was calculated for the experimental temperatures and pressures, and the results for total pressures of 10000 kPa are presented in Table 4.4. Neither the H<sub>2</sub>S concentrations in the liquid phase nor the pressures are exactly the same for the two solvents, nevertheless, it can be noticed that the solvent capacities are similar. At 283 K, at pressures 4.68 and 6.59 kPa, the capacities are 0.044 and 0.047 kg H<sub>2</sub>S/L solution for the amine-glycol and the amine blend, respectively. At 353 K and 393 K, the MDEA-MEG-H<sub>2</sub>O system seems to require lower H<sub>2</sub>S partial pressure to remove similar amounts of hydrogen sulfide.

Table 4.4 Absorption capacity of 30 wt% MDEA – 40 wt% MEG – 30 wt% H<sub>2</sub>O and 70 wt% MDEA – 30 wt% H<sub>2</sub>O mixtures at total pressures of 10000 kPa.

<i>T</i>	30 wt% MDEA – 40 wt% MEG – 30 wt% H <sub>2</sub> O		70 wt% MDEA – 30 wt% H <sub>2</sub> O	
	<i>P</i> <sub>H<sub>2</sub>S</sub>	<i>c</i> x 10 <sup>-3</sup>	<i>P</i> <sub>H<sub>2</sub>S</sub>	<i>c</i> x 10 <sup>-3</sup>
K	kPa	kg H <sub>2</sub> S/L sol.	kPa	kg H <sub>2</sub> S/L sol.
283	1.04	18.5	4.68	44.1
	6.59	47.3	21.56	102.1
353	28.55	16.3	111.42	41.2
	101.28	38.9	300.30	79.5
393	86.88	14.6	364.18	32.0
	262.00	31.7	809.32	58.6

#### 4.2.3.4 Cyclic capacity

Besides the useful information that the absorption capacity of a solvent might provide, it is common to compare the difference between the loading of the lean solvent and the rich solvent when evaluating new solvents. This difference is called cyclic capacity (Eq. 1). Its knowledge can be particularly useful since after regeneration the solvent cannot be stripped entirely from the acid gas captured and this reduced capacity of the solvent should be accounted for in the process.

$$\alpha_{cyclic} = \alpha_{rich}(T_{abs}, P_{H_2S,abs}) - \alpha_{lean}(T_{des}, P_{H_2S,des}) \quad \text{Eq. 1}$$

In the equation,  $P_{H_2S,abs}$  is the equilibrium pressure of H<sub>2</sub>S in the bottom of the absorber, and  $P_{H_2S,des}$  in the bottom of the desorber.

The cyclic capacity determines the amount of acid gas that can be absorbed for a given flow rate. Therefore, it is desired to employ solvents with high cyclic capacity in order to reduce the circulation flow rate and subsequent sensible heat loss in the stripper. Table 4.5 presents the cyclic capacity results for aqueous MDEA solutions with and without MEG.



Table 4.5 Cyclic capacity of 30 wt% MDEA – 70 wt% H<sub>2</sub>O and 30 wt% MDEA – 40 wt% MEG – 30 wt% H<sub>2</sub>O mixtures calculated at absorption temperature of 283 K and desorption temperature of 393 K. Liquid loading values in mol H<sub>2</sub>S/mol MDEA are in parentheses.

System wt%	$P_{H_2S,abs}$ kPa	$P_{H_2S,des}$ kPa	$\alpha_{cyclic}$ mol H <sub>2</sub> S/mol MDEA
30% MDEA – 70% H <sub>2</sub> O	6.6 (0.503*)	86.9 (0.246*)	0.257
30% MDEA – 40% MEG – 30% H <sub>2</sub> O	6.6 (0.507)	86.9 (0.169)	0.338

\* Predicted values

The pressures used in the cyclic capacity calculations of Table 4.5 are constrained by the experimental partial pressures of H<sub>2</sub>S; this is the reason why  $P_{H_2S}$  in the absorber is 6.6 kPa and  $P_{H_2S}$  in the desorber is 86.9 kPa. For the given conditions, the amine-glycol blend studied in this work has higher cyclic capacity (0.338 mol H<sub>2</sub>S/mol MDEA) than 30 wt% aqueous MDEA (0.257 mol H<sub>2</sub>S/mol MDEA). Although these results are optimistic, it is important to take into account a few elements. First, there are no experimental data at 283 K for any aqueous MDEA concentration; therefore, the VLE model, which was used for the calculation of absorption capacity for the aqueous MDEA, is not validated for this temperature. In addition, the calculation of the cyclic capacity is highly sensitive to the pressure and temperature selected (Bernhardsen and Knuutila, 2017). Thus, the assessment of the absorption capacity of each solvent should be performed with a case by case evaluation, and data at specific absorption and desorption conditions should be obtained. In fact, for the comparison to be fair between different solvents, it is the pressures and temperatures of the optimized process that should be used for the calculation of the cyclic capacity.

Last but not least, it should be noted that increased cyclic capacity does not automatically make a solvent better, since the pumping costs are a small part of the overall costs of acid gas removal and the column sizes are more dependent on the gas flow rates than the solvent flow rates (Raynal et al., 2011).

#### 4.2.4 Conclusions

Experimental vapor-liquid equilibrium data were measured for hydrogen sulfide in a 30 wt% MDEA – 40 wt% MEG – 30 wt% H<sub>2</sub>O blend at temperature of 283 K, 353 K and 393 K and pressures up to 10000 kPa. High pressures were obtained by using methane as makeup gas. The data show that increasing the partial pressure of hydrogen sulfide or reducing the temperature yields higher liquid loadings, as it is expected. Similar to the observations made for our measurements with 70 wt% aqueous MDEA, an increase in total pressure from 2000 kPa up to 10000 kPa for the MDEA-MEG-H<sub>2</sub>O system is accompanied by an increase in the partial pressure of hydrogen sulfide, while it seems not to have significant effect on the absorption capacity of the solvent.

It was also shown that 30 wt% aqueous MDEA has a higher absorption capacity (in mol H<sub>2</sub>S/L solution) than the studied amine-glycol system. The higher the water content is, the higher the absorption capacity of the solvent becomes, though water content as low as 5 wt% demonstrates minimal improvement. This is true besides the fact that the solubility of hydrogen sulfide is higher in MEG than in water. A reaction mechanism theory was proposed for explaining the increasing solubility of hydrogen sulfide with decreasing glycol content. Moreover, increasing the amine concentration for a given partial pressure and water content, also leads to higher absorption capacity in terms of mol H<sub>2</sub>S absorbed per liter solution. In addition, the performance of 30 wt% MDEA – 40 wt% MEG – 30 wt% H<sub>2</sub>O system was also studied against 70 wt% aqueous MDEA in order to evaluate the substitution of the glycol with amine and it was found that the absorption capacity of the comparing solvents was similar. In the end, the effect of glycol on the cyclic capacity of 30 wt% aqueous MDEA was investigated. It was found that, at the experimental pressure and temperature conditions, the amine-glycol-water system has a higher cyclic capacity than its aqueous counterpart.

### **4.3 Experimental challenges and learnings with high-pressure VLE work**

Experimental problems and time limitations did not unfortunately allow for the study of other more concentrated aqueous MDEA blends or various amine-glycol-water compositions which were initially planned and which would provide further knowledge for the thermodynamic behavior of these systems. Generally, the high-pressure VLE experiments required significantly more time to be conducted than low-pressure ones; typical number of experimental points per day is one for high-pressure and more than four for low-pressure VLE measurements.

Besides the time-consuming nature of this kind of experiments, several challenges manifested during the preparation of the experiments, the performance of the measurements and the treatment of the data. The most often problem was, by far, leakages in the equilibrium cell and the surrounding valves.

#### Leakage

The equilibrium cell consists of a sapphire tube and two flanges on each side of the tube employing O-ring seals. When leakages were detected from the O-rings, they had to be replaced. Their replacement required dismounting the cell and disconnected all the valves as well as the samplers connected to the flanges, which is a very labor-intensive procedure, prone to more leakages. Further, the apparatus is equipped with different types of valves; simple ball (ON/OFF) valves, regulating valves and non-rotating valves. The latter is the most complicated of the three (Figure 4.10). Leakages were observed, both out of the valve housing and through the valve, and many valves were replaced. However, leakage problems with the non-rotating valves often persisted. When removing and replacing the valves, grooves would often be seen in the tip of the valve needle while the PTFE seal was damaged and needed replacement. Grooves in the needle of the valve implies that the needle was rotating and this is believed to be due to inefficient mounting of the valves in the first place. It was seen that much fewer leakage problems manifested when the mounting was performed by trained personnel which was familiar with this type of valves.

Furthermore, the testing procedure for checking if pressure could be maintained was very time-consuming; the O-rings needed first to be conditioned in the temperatures to be used while the allowed rates for increasing/decreasing the pressure and temperature in the cell are 20 bar/hr

and 20 °C/hr, respectively, according to the manufacturer. Overall, maintaining vacuum or pressures up to 20 bar was possible and the leakage problems appeared at higher pressures. Experiments were conducted only after the pressure could remain stable in the cell for at least three days. Good practices include having spare valves and sealing parts, while an important learning was that combustible gas detectors used in leakage tests are much more efficient than helium detectors, flow rate detectors or soap.

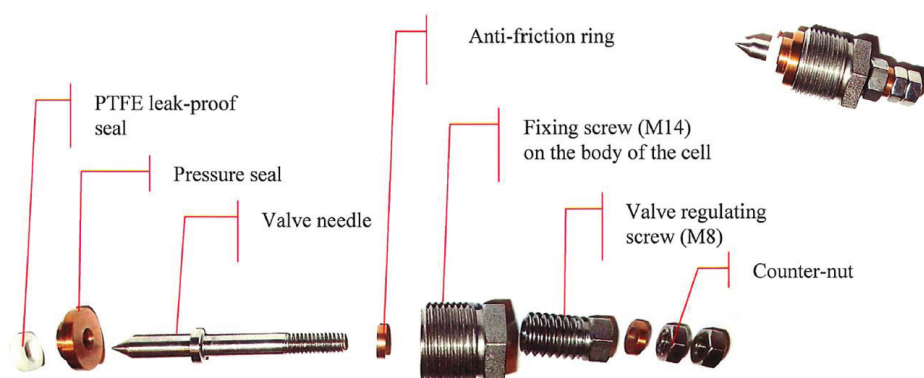


Figure 4.10 Parts consisting a non-rotating needle valve.

## HSE

Before any experiments could be conducted, various safety measures were implemented with regards to work with high pressures and, mainly, work with hydrogen sulfide. H<sub>2</sub>S detectors were installed in the fume cabinet where the apparatus is located and personal portable alarms were purchased to be used by the operator and other people while inside the room of H<sub>2</sub>S-related work. H<sub>2</sub>S masks were also purchased to be used when the gas bottle was open (during filling of the gas tank) or emergency situations. In addition, limited access was implemented, signs were put on all entrances to the lab during the experimental work with the toxic gas and all operations were performed at normal working hours. The HSE measures taken were in accordance to Statoil's HSE measures in their H<sub>2</sub>S laboratory.

## GC analysis

A common problem in GC analysis for amine systems is the amine accumulation in the column resulting in a tail on the chromatogram, decay of the column and eventually failure to perform reproducible chromatograms. This is a very costly problem due to the cost of GC columns, the

high frequency at which the column must be changed and the need to repeat the calibration for all analyzed components. These problems are more pronounced when working with viscous amines, such as MDEA. This issue can be overcome with the installation of a valve on the GC which can block the sample before the retention time of the amine and direct the rest of the sample to vent instead of the detectors. Although it solves the problem of replacing often GC columns, it is at the expense of not measuring the content of the amine. In this case, such as in the measurements reported in this thesis, it is assumed that the ratio between the water and the amine (and the glycol) remains constant during the experiment.

In order to extend the life of the column, by adding a valve in the GC which redirect the amine and the glycol to waste, a new issue rises. During the first samplings of the measurement, a new peak is identified, as can be seen in Figure 4.11 when comparing the signals with the baseline signal (blue).

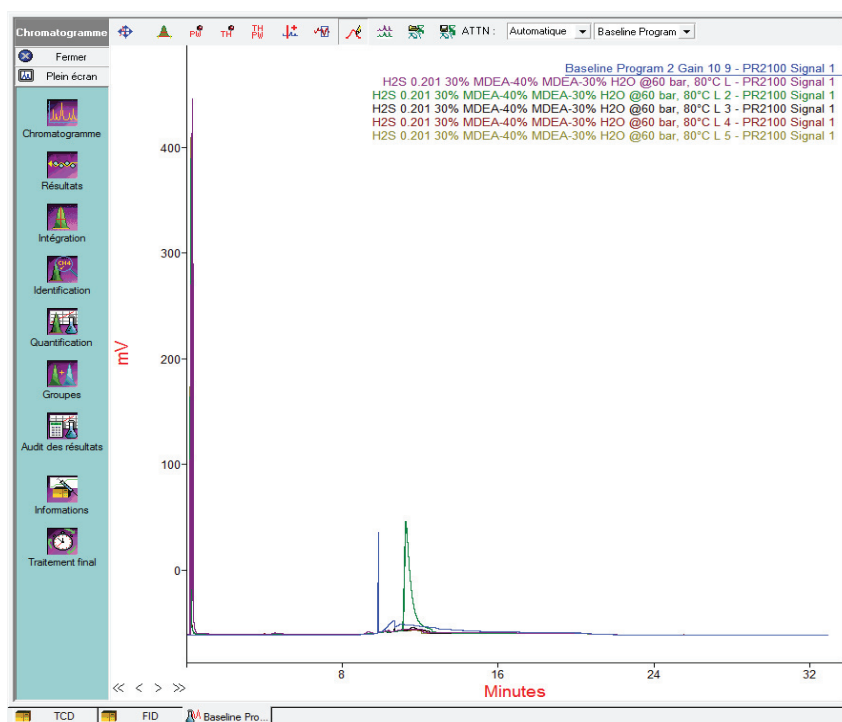


Figure 4.11 Overlapping FID chromatograms showing a peak corresponding to glycol or amine residues during liquid phase analysis with a zoom-in to the peak at 12 min.

Based on the retention time, this peak corresponds to the amine. During the baking of the column, the valve is in open position (helium flows in the main analysis column) while small amounts of amine and glycol probably remain on the side of the valve towards the vent for the amine/glycol. Taking a closer look on the chromatogram and this peak (Figure 4.12), one can notice that as more samples are analyzed in the full temperature program, the peak diminishes. The theory of residues in the valve and not in the column is supported by the fact that during the 1<sup>st</sup> sample, there is no peak, because the valve is not closing in the time between the baking of the column and the first sample withdrawal. Checking that no residues are left in the column during every analysis is good practice for ensuring high lifetime of the column.

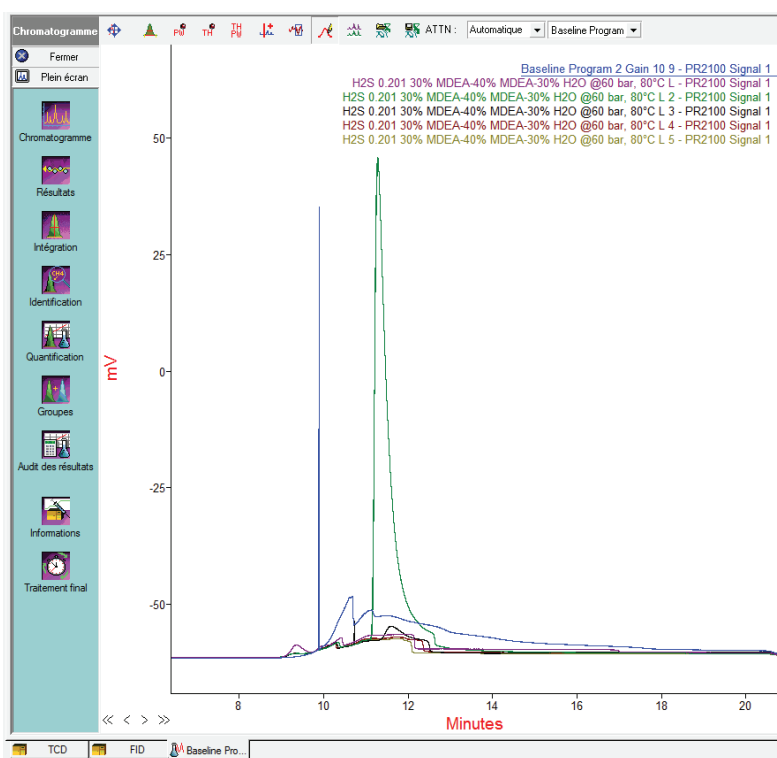


Figure 4.12 Overlapping FID chromatograms zooming at a peak corresponding to glycol or amine residues during liquid phase analysis.

At some instances, an additional peak was observed during the analysis of the vapor phase after ca. 5 min also in the FID detector (Figure 4.13). After checking and testing for contamination, it was concluded that this was not a signal corresponding to an unknown compound, ex. some degradation compound, but it was perturbation of the flame on the FID detector due to water. In the figure, the purple line corresponds to the FID signal and the blue line corresponds to the TCD signal. It is observed that the signal on the FID resembles a normal peak response and that it appears at the same time as water signal appears on the TCD.

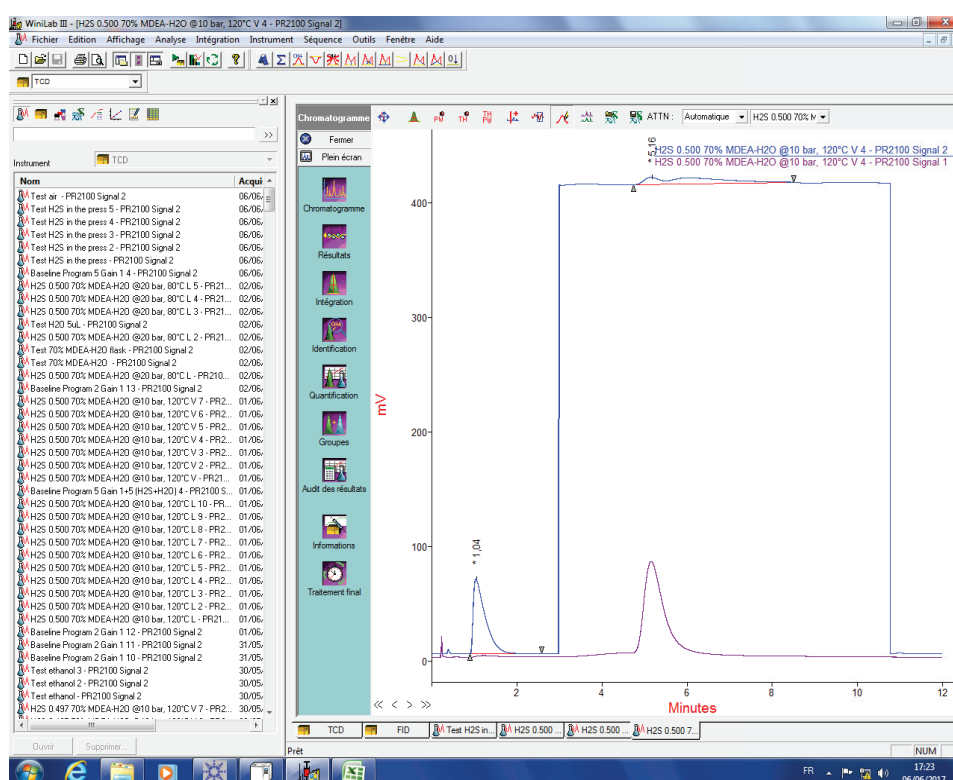


Figure 4.13 FID perturbation signal (signal 1) at 5 min, resembling a compound's peak response.

Moreover, during the course of time, retention time drifts were noticed. Operation can continue even when signal drifting appears as long as the calibration holds, there is no signal overlap and the time of the analysis is not significantly extended. In any other case, a new column is needed. An important problem encountered during the high-pressure VLE experiments was the clogging of the sampling capillary for the liquid phase. This was due to contamination inside the cell,

due to high viscosity in our systems with sample being gradually accumulated, or both. Before the sampling system failed, small black particles had been observed inside the cell which could not be removed during the cleaning procedure. These particles are believed to originate from the stirrer due to the high corrosivity in the presence of hydrogen sulfide and water. In addition, the studied systems are characterized by high viscosity. For example, the viscosity of 70 wt% aqueous MDEA at 313 K is 15.2 mPa·s (Bernal-García et al., 2004). It is, thus, possible that the combination of high viscosity and some contamination led to the clogging of the extremely thin capillaries. This problem could be solved by applying high pressure and increasing the opening (sampling) time leading to the forced removal of the blocking substance. Attention must be paid that sampling under these conditions will not lead to large amounts of sample entering the column. If this does not work, the ROLSI samplers must be disassembled to replace the capillaries.

#### Equipment failures

Other issues which happened during this work and contributed to additional labor and delays concern equipment failures. Two times it was found that the heating in the transfer line from the ROLSI samplers to the GC had unexpectedly stopped working. Since the exact time of the failure was not known, the last measurements had to be repeated. Moreover, the vacuum pump got out of order due to an unknown liquid in its interior during the first experiments and after a few months of experimental work, the TCD detector broke down. Finally, electricity stoppages caused issues with data acquisition, software operation and required time for checking the calibration of the GC as well as the pressure transducer, located in heated casings.

#### Data treatment

In the previous discussion, many challenges associated to the GC analysis concern the measurement of the liquid phase, despite the fact that the experimental results include data obtained by the GC analysis of the vapor phase and calculated liquid phase loading based on mass balance. The main challenge in the analysis was to understand why the measurement does not match the results calculated by the mass balance. Different equations of state were used to calculate the amount of H<sub>2</sub>S, without important deviations, that could explain the mismatch observed. For this reason, we decided to report only the calculated liquid phase results, omitting the measured ones. This is unfortunate since most of the time used in this work was dedicated to the liquid phase analysis. It is believed that the deviations observed are related to the



sampling procedure and it is investigated by the manufacturers of the apparatus in France, where also these experiments were carried out.

## Bibliography

- Afzal, W., Breil, M.P., Tsvintzelis, I., Mohammadi, A.H., Kontogeorgis, G.M., Richon, D., 2012. Experimental study and phase equilibrium modeling of systems containing acid gas and glycol. *Fluid Phase Equilibria* 318, 40–50. <https://doi.org/10.1016/j.fluid.2011.12.025>
- Bernal-García, J.M., Galicia-Luna, L.A., Hall, K.R., Ramos-Estrada, M., Iglesias-Silva, G.A., 2004. Viscosities for Aqueous Solutions of N-Methyldiethanolamine from 313.15 to 363.15 K. *J. Chem. Eng. Data* 49, 864–866. <https://doi.org/10.1021/jc0302250>
- Bernhardsen, I.M., Knuutila, H.K., 2017. A review of potential amine solvents for CO<sub>2</sub> absorption process: Absorption capacity, cyclic capacity and pK<sub>a</sub>. *International Journal of Greenhouse Gas Control* 61, 27–48. <https://doi.org/10.1016/j.ijggc.2017.03.021>
- Edwards, T.J., Newman, J., Prausnitz, J.M., 1978. Thermodynamics of Vapor-Liquid Equilibria for the Ammonia-Water System. *Industrial & Engineering Chemistry Fundamentals* 17, 264–269. <https://doi.org/10.1021/i160068a007>
- Eimer, D., 2014. Gas treating: absorption theory and practice. John Wiley & Sons, Inc, Chichester, West Sussex.
- Eimer, D., 1994. Simultaneous removal of water and hydrogen sulphide from natural gas (Dr. Ing thesis). NTNU, Trondheim.
- Jelstad, A., 1997. Gass-væske likevektsstudier for hydrogensulfid. Norwegian University of Science and Technology, Trondheim, Norway.
- Jou, F.-Y., Carroll, J.J., Mather, A.E., Otto, F.D., 1993. The solubility of carbon dioxide and hydrogen sulfide in a 35 wt% aqueous solution of methyldiethanolamine. *Can. J. Chem. Eng.* 71, 264–268. <https://doi.org/10.1002/cjce.5450710213>
- Jou, F.-Y., Deshmukh, R.D., Otto, F.D., Mather, A.E., 1990. Vapor-Liquid Equilibria of H<sub>2</sub>S and CO<sub>2</sub> and Ethylene Glycol at Elevated Pressures. *Chemical Engineering Communications* 87, 223–231. <https://doi.org/10.1080/00986449008940694>
- Jou, F.-Y., Deshmukh, R.D., Otto, F.D., Mather, A.E., 1987. Vapor liquid equilibria for acid gases and lower alkanes in triethylene glycol. *Fluid Phase Equilibria* 36, 121–140. [https://doi.org/10.1016/0378-3812\(87\)85018-5](https://doi.org/10.1016/0378-3812(87)85018-5)
- MacGregor, R.J., Mather, A.E., 1991. Equilibrium Solubility of H<sub>2</sub>S and CO<sub>2</sub> and Their Mixtures in a Mixed Solvent. *Can. J. Chem. Eng.* 69, 1357–1366. <https://doi.org/10.1002/cjce.5450690618>
- Poblete, A.T.C., 1997. Gass-væske likevektsstudier for hydrogensulfid. Norwegian University of Science and Technology, Trondheim, Norway.
- Raynal, L., Bouillon, P.-A., Gomez, A., Broutin, P., 2011. From MEA to demixing solvents and future steps, a roadmap for lowering the cost of post-combustion carbon capture. *Chemical Engineering Journal*, Special Section: Symposium on Post-Combustion Carbon Dioxide Capture 171, 742–752. <https://doi.org/10.1016/j.cej.2011.01.008>

- Rinker, E.B., Sandall, O.C., 2000. Physical solubility of hydrogen sulfide in several aqueous solvents. *The Canadian Journal of Chemical Engineering* 78, 232–236. <https://doi.org/10.1002/cjce.5450780130>
- Span, R., Eckermann, T., Herrig, S., Hielscher, S., Jäger, A., Thol, M., 2015. TREND. Thermodynamic Reference and Engineering Data 2.0. Ruhr-Universität Bochum, Bochum, Germany.
- Taylor, B.N., Kuyatt, C.E., 1994. NIST Guidelines for Evaluating and Expressing the Uncertainty of NIST Measurement Results. NIST Technical Note 1297.
- Xu, H.-J., Zhang, C.-F., Zheng, Z.-S., 2002. Solubility of Hydrogen Sulfide and Carbon Dioxide in a Solution of Methyl-diethanolamine Mixed with Ethylene Glycol. *Ind. Eng. Chem. Res.* 41, 6175–6180. <https://doi.org/10.1021/ie020375o>



## Chapter 5

# VLE Data for CO<sub>2</sub>-containing Systems

*This chapter presents vapor-liquid equilibrium data for CO<sub>2</sub> loaded MDEA-MEG and MDEA-MEG-H<sub>2</sub>O systems at low pressures.*

A vapor-liquid equilibrium study was conducted for CO<sub>2</sub>-MDEA-MEG and CO<sub>2</sub>-MDEA-MEG-H<sub>2</sub>O systems, in order to gain knowledge regarding the solubility of carbon dioxide in the aqueous and non-aqueous MDEA-MEG blends (journal publication III). Carbon dioxide typically co-exists with hydrogen sulfide in sour streams and its content is also controlled by transport specifications. For the process to be selective for hydrogen sulfide, the CO<sub>2</sub> absorption should be as low as possible. Due to numerous experimental challenges with the high-pressure measurements, it was decided to study the CO<sub>2</sub>-MDEA-MEG and CO<sub>2</sub>-MDEA-MEG-H<sub>2</sub>O systems at low pressures; the VLE measurements were performed at temperatures from 313 K to 393 K and pressures up to 600 kPa. The experimental apparatus is shortly described, but a more detailed description can be found in the Appendix in the end of this thesis.

In the aqueous solvents, the results indicate that the absorption capacity decreases with increasing glycol content/decreasing water content, at constant amine concentration. A comparison of the studied systems with concentrated aqueous MDEA is also performed. In the non-aqueous solvents, the solubility of carbon dioxide increases with increasing amine content up to 30-50 wt% MDEA-MEG, upon which it is reduced. Karl-Fischer titration and Nuclear Magnetic Resonance (NMR) analysis were employed for the chemical characterization of the systems and a chemical reaction between carbon dioxide and MEG was observed, in the presence of MDEA. A theory based on MEG autoprotolysis is proposed for the explanation of the results, which is also supported by additional VLE measurements of the system CO<sub>2</sub>-MDEA-TEG.

## **5.1 CO<sub>2</sub> solubility in mixtures of MDEA with MEG, MEG - H<sub>2</sub>O, H<sub>2</sub>O and TEG**

### **Journal publication III**

Skylogianni, E., Perinu, C., Cervantes Gameros, B. Y., Knuutila, H.K., 2020. Carbon Dioxide Solubility in Mixtures of Methyldiethanolamine with Monoethylene Glycol, Monoethylene Glycol – Water, Water and Triethylene Glycol. Accepted in The Journal of Chemical Thermodynamics.

(updated version)



## Paper III

The first part of the document discusses the importance of maintaining accurate records of all transactions. It emphasizes that every entry, no matter how small, should be recorded to ensure the integrity of the financial data. This includes not only sales and purchases but also expenses and income. The document provides a detailed list of items that should be tracked, such as inventory levels, accounts payable, and accounts receivable. It also outlines the necessary steps for reconciling these accounts regularly to identify any discrepancies early on.

The second part of the document focuses on the role of technology in modern accounting. It highlights how software solutions can streamline the accounting process, reduce the risk of human error, and provide real-time access to financial information. The document compares various accounting software options, discussing their features, benefits, and potential drawbacks. It also offers advice on how to choose the right software for a business's specific needs and budget.

The third part of the document addresses the importance of staying up-to-date with the latest accounting regulations and standards. It notes that the tax and financial reporting environment is constantly evolving, and businesses must adapt to these changes to remain compliant. The document provides a summary of recent regulatory updates and offers practical tips for implementing these changes within the organization. It also suggests ways to stay informed, such as attending industry conferences and consulting with professional advisors.

The final part of the document discusses the importance of effective communication in the accounting department. It stresses that accountants must be able to communicate clearly and effectively with other departments and external stakeholders. The document provides guidelines for writing clear reports, presenting data in an understandable way, and resolving conflicts. It also emphasizes the need for transparency and honesty in all financial reporting.



# Carbon Dioxide Solubility in Mixtures of Methyldiethanolamine with Monoethylene Glycol, Monoethylene Glycol – Water, Water and Triethylene Glycol

*Eirini Skylogianni<sup>1</sup>, Cristina Perinu<sup>1,2</sup>, Blanca Y. Cervantes Gameros<sup>1</sup>, Hanna K. Knuutila<sup>1\*</sup>*

<sup>1</sup> Department of Chemical Engineering, Norwegian University of Science and Technology  
(NTNU), NO-7491 Trondheim, Norway

<sup>2</sup> Department of Process, Energy and Environmental Technology, University of Southeast  
Norway, NO-3603 Kongsberg, Norway

\* hanna.knuutila@ntnu.no

**Keywords:** absorption, vapor-liquid equilibrium, MDEA, glycol, highly concentrated MDEA, NMR, alkyl carbonate

## **ABSTRACT**

The carbon dioxide solubility in non-aqueous and aqueous mixtures of methyldiethanolamine (MDEA) with monoethylene glycol (MEG) was studied due to the relevance of these solvents for the combined acid gas removal and hydrate control in natural gas treatment. Vapor-liquid equilibrium (VLE) measurements were conducted at temperatures from 303 K to 393 K and pressures up to 600 kPa. In the aqueous solvents, the effect of water content in carbon dioxide solubility was investigated. The absorption capacity of the aqueous solvents decreased with increasing glycol content and decreasing water content, at constant amine concentration. A comparison of the studied systems with concentrated aqueous MDEA was also performed. The non-aqueous solvents were studied in the whole composition range, from pure MDEA to pure MEG. The solubility of carbon dioxide increased with increasing amine content only up to 30-50 wt% MDEA-MEG, upon which it decreased. Water content determination and Nuclear Magnetic Resonance (NMR) analysis were used for the chemical characterization of the systems and explanation of the results. It was found that in the presence of MDEA, a chemical reaction occurs between carbon dioxide and MEG. A theory based on MEG autoprotolysis is proposed which is further supported by supplementary VLE data obtained in blends of MDEA and triethylene glycol.

## 1. INTRODUCTION

### 1.1 Literature Review

Main downstream processes in natural gas production are the removal of acid gases, namely carbon dioxide (CO<sub>2</sub>) and hydrogen sulfide (H<sub>2</sub>S), and the removal of water in order to meet pipeline transportation specifications, gas quality specifications and environmental requirements. Acid gases in the presence of water are highly corrosive and can jeopardize the safety of operations, both in terms of the personnel's wellbeing as well as equipment failure. The same applies in the event of hydrate formation if excess of water is present, which can lead to pipeline clogging and, in extreme cases, production shut-down.<sup>1</sup>

In offshore gas and oil wells, non-regenerative chemicals, called scavengers, are commonly used to control hydrogen sulfide content in natural gas. However, they are not ideal since their use imposes space, weight and disposal requirements, which are not friendly for offshore/subsea application<sup>2</sup>, and they cannot treat high H<sub>2</sub>S concentrations. A typical example is triazine, which is injected directly into the gas stream and is able to treat hydrogen sulfide at concentrations not higher than 200 ppmv<sup>3</sup>. As a result, fields are abandoned or not even produced due to high H<sub>2</sub>S content. In addition, oil and gas fields experience reservoir souring, i.e. increase in sulfur content, due to EOR (Enhanced Oil Recovery) activities such as water injection<sup>4</sup>. Maintaining production and safe operation in increasingly sour fields is an important industrial challenge.

A solution to the problematic high H<sub>2</sub>S concentrations in production wells is the development of a regenerative process where hydrogen sulfide and water content can be removed simultaneously. Despite the fact that the employment of a regenerative solvent requires additional equipment for its regeneration, it could enable trouble-free operations and extend the life of the field. Aqueous methyldiethanolamine (MDEA) and aqueous monoethylene

glycol (MEG) are regenerative solutions traditionally used today for the selective removal of H<sub>2</sub>S over CO<sub>2</sub> and for hydrate control, respectively. MDEA is a tertiary amine whose aqueous solutions have significantly higher reaction rates with H<sub>2</sub>S than with CO<sub>2</sub>. Therefore, mixtures of MDEA-MEG as well as highly concentrated MDEA are promising candidates for the combined removal of H<sub>2</sub>S and water vapor.

The concept of a gas treating process for combined acid gas and water vapor removal of natural gas was conceived already in 1930s and was first patented in 1939 by Hutchinson<sup>5</sup>. Process improvements were suggested in the following years<sup>6-8</sup> and the amine-glycol process found wide acceptance in the gas processing industry. An aqueous mixture of monoethanolamine (MEA) and either diethylene (DEG) or triethylene glycol (TEG) was used for the simultaneous absorption of acid gas and water from natural gas<sup>9</sup>. In spite of many advantages, severe corrosion was encountered and the process was eventually abandoned. However, MEA is known for its corrosivity issues, thus its substitution with another amine and/or the decrease in water content can potentially eliminate this problem. The years that followed until today, many researchers have studied blended aqueous and non-aqueous amine-glycol solvents, primarily in the framework of water-lean solvents, which can potentially have increased absorption capacity and reduced regeneration heating duties<sup>10-20</sup>. The majority of the literature studies concern MEA and diethanolamine (DEA) and few sources were found for MDEA-glycol system<sup>16,17,19</sup>.

Wanderley and coworkers<sup>20</sup> studied vapor-liquid equilibrium and mass transfer in MDEA – MEG – H<sub>2</sub>O among other solvents, promising for CO<sub>2</sub> capture in biogas upgrading. They observed that the solubility of CO<sub>2</sub> was decreased compared to aqueous MDEA, and they underlined the fact that higher CO<sub>2</sub> partial pressure than in aqueous MDEA was also accompanied by faster reaction rates for the same CO<sub>2</sub> pressure. Eimer<sup>19</sup> and Xu et al.<sup>16</sup> focused

on the selectivity of H<sub>2</sub>S over CO<sub>2</sub> with non-aqueous or lean-water MDEA-containing solvents. Eimer<sup>19</sup> investigated the performance of a mixture composed of MDEA and TEG aiming for the combined selective removal of H<sub>2</sub>S over CO<sub>2</sub> and dehydration. It was found that the reaction rate of H<sub>2</sub>S in the combined solvent decreases with increasing glycol content. High viscosity promotes low absorption rate and this is one of the main reasons why, in this study, we consider the far less viscous MEG as a more suitable glycol than TEG for this multifunctional solvent. Moreover, following a first screening of potential diluents which showed increased H<sub>2</sub>S selectivity in MDEA – MEG compared to aqueous MDEA, Xu et al.<sup>16</sup> measured the solubility of CO<sub>2</sub> and H<sub>2</sub>S in aqueous and non-aqueous MDEA – MEG blends. They concluded that the carbon dioxide solubility significantly decreases in MDEA – MEG than MDEA – H<sub>2</sub>O, while the solubility of H<sub>2</sub>S is only slightly lower.

## **1.2 Aim of this work**

Successful process development relies on accurate data and/or models to describe the physical properties, thermodynamic behavior and system kinetics. The first step for the evaluation of a complex multicomponent system, such as the combined hydrogen sulfide and hydrate control process, is the study of its subsystems. The aim of this work is to describe and understand the thermodynamic behavior of the subsystems CO<sub>2</sub> – MDEA – MEG and CO<sub>2</sub> – MDEA – MEG – H<sub>2</sub>O. Since carbon dioxide is generally present in natural gas with hydrogen sulfide, investigating this system is of equal importance as the absorption of H<sub>2</sub>S in the proposed solvent.

This work includes two main studies: a) an extensive study of the vapor-liquid equilibrium (VLE) behavior of CO<sub>2</sub> – MDEA – MEG systems in the whole composition range from pure MEG to pure MDEA, and b) a study of CO<sub>2</sub> – MDEA – MEG – H<sub>2</sub>O systems with focus on

the effect of water content in the system and a comparison with highly concentrated amine solutions, i.e. 70 wt% and 90 wt% MDEA – H<sub>2</sub>O. The measurements were performed at CO<sub>2</sub> pressures up to 600 kPa and temperatures from 303 to 393 K. We further investigated our VLE results through Karl-Fischer titration (for the non-aqueous systems), Nuclear Magnetic Resonance (NMR) spectroscopy, and comparison with MDEA – TEG systems in order to understand the underlying phenomena and identify possible chemical reactions undergone during the absorption of CO<sub>2</sub> into aqueous and non-aqueous MDEA-glycol blends. Density measurements were also performed as part of the VLE data processing.

## 2. MATERIALS AND METHODS

### 2.1 Materials

**Table 1** contains information for the chemicals used in this work. They were used as received from the supplier without further purification. Deionized water was used for preparation of the aqueous mixtures. The solutions were prepared gravimetrically in a METTLER PM1200 scale with an accuracy of  $1 \cdot 10^{-6}$  kg, they were sealed and let under magnetic stirring for at least 8 hours to ensure homogeneous solutions. Amine analysis by means of acid-base titration was performed in order to verify the MDEA concentration in the studied systems.

**Table 1:** Chemical Sample Table

Component	UIPAC name	CAS	Supplier	Mass fraction purity as stated by supplier
N-methyldiethanolamine (MDEA)	2-[2-hydroxyethyl(methylamino) ethanol]	105-59-9	Sigma-Aldrich	$\geq 0.99$
monoethylene glycol (MEG)	ethane-1,2-diol	107-21-1	Sigma-Aldrich	0.998

triethylene glycol (TEG)	2-[2-(2-hydroxyethoxy)ethoxy]ethanol	112-27-6	Sigma-Aldrich	≥ 0.985
carbon dioxide	carbon dioxide	124-38-9	AGA	0.99999
water	oxidane	-	-	-

## 2.2 Experimental methods

### 2.2.1 Vapor-Liquid Equilibrium measurements

Two similar setups were used to conduct the vapor-liquid equilibrium (VLE) measurements, named VLE-1 and VLE-2. The main components of the setups are a glass reactor and a storage cylinder for CO<sub>2</sub> of ca.  $1 \cdot 10^{-3}$  m<sup>3</sup> volume each, whose pressure and temperature are monitored. Measurements can be conducted at temperature range of 303 – 393 K (accuracy  $\pm 0.1$  K) and pressures 0 – 600 kPa (accuracy  $\pm 0.9$  kPa). The setups' description and instrumentation are provided in detail by Hartono et al.<sup>21</sup> Experiments were performed in two different ways, either at multiple temperatures with one CO<sub>2</sub> loading or at one temperature and multiple loadings.

Each experiment started by evacuating the reactor. The solvent was introduced and the reactor was set again to vacuum to eliminate possible air introduced with the solvent. The exact amount of solvent introduced was known by weighing the solvent holder, before and after charging the reactor. For measurements performed at multiple temperatures with one CO<sub>2</sub> loading, the temperature was set to automatically increase from 303 to 393 K with a step of 10 K. At 393 K, CO<sub>2</sub> was injected to the maximum pressure of the reactor and the temperature was decreased in reversed steps until 303 K. For the measurements performed under isothermal conditions and multiple loadings, once equilibrium was reached at the desired temperature, CO<sub>2</sub> was added. After each system equilibration, more CO<sub>2</sub> was added manually until the pressure inside the reactor was close to 600 kPa. Equilibrium in every temperature level, both for the vapor

pressure of the solution and the CO<sub>2</sub>-solvent equilibrium, required approximately 4-8 hours. The system was under constant stirring (ca. 500 rpm) and equilibrium was assumed when the temperature and pressure of the reactor were constant for 5 min.

The pressure and temperature were recorded every 5 seconds during the experiment, which lasted 3-4 days. The calculations are based on mass balances; the solvent is added from a beaker whose weight before and after the reactor filling is measured. The temperature, volume and pressure of the CO<sub>2</sub> storage vessel are known, and thus the amount of gas before and after the CO<sub>2</sub> loading of the solvent can be calculated. The amount of carbon dioxide in the vessel was calculated using Peng-Robinson equation of state<sup>22</sup>. The equilibrium pressure was calculated according to Eq. 1:

$$P_{CO_2} = P_{tot} - P_{res} \quad \text{Eq. 1}$$

where  $P_{CO_2}$ : partial pressure of CO<sub>2</sub>,  $P_{tot}$ : total pressure inside the reactor and  $P_{res}$ : residual pressure inside the reactor before CO<sub>2</sub> addition. Amine analysis was performed in the end of every experiment to verify that the amine concentration remained the same (within 2% error). CO<sub>2</sub> analysis was also performed in most of the experiments to confirm our mass balance-based calculations. The average absolute relative deviation (calculated according to Eq. 2) is 4% for all the experiments, excluding those in pure H<sub>2</sub>O, MEG and TEG where the very low values of carbon dioxide absorbed leads to large relative deviations. However, the results from those experiments are compared to and found in agreement with values reported in the literature in section 3.

$$AARD [\%] = \frac{100}{NP} \sum_{i=1}^{NP} \left| \frac{x_i^{calc} - x_i^{exp}}{x_i^{exp}} \right| \quad \text{Eq. 2}$$

where  $x$  stands for any property whose relative deviations were calculated in this work, and NP stands for number of points.



For the non-aqueous systems, the Henry's constant was calculated according to Eq. 3.  $c_{CO_2}$  denotes the concentration of CO<sub>2</sub> in the solvent and the Henry's constant  $H$  is expressed in kPa·m<sup>3</sup>·kmol<sup>-1</sup>. For the aqueous systems, the loading  $\alpha$ , expressed in mol CO<sub>2</sub>/mol MDEA, was calculated and reported.

$$H = \frac{P_{CO_2}}{c_{CO_2}} \quad \text{Eq. 3}$$

The experimental apparatuses and procedure were validated by measuring the solubility of carbon dioxide in pure water and comparing our results to the correlation provided by Carroll et al.<sup>23</sup>, as formulated by Penttilä et al.<sup>24</sup> (**Figure 1**). The experiments were repeated two times and conducted both before and during the experimental campaigns to ensure good quality data. The validation measurements are presented in **Table A. 1**. The AARD between measured and literature values was always lower than 3% for both VLE-1 and VLE-2, and the repeatability was found to be within 3% as well.

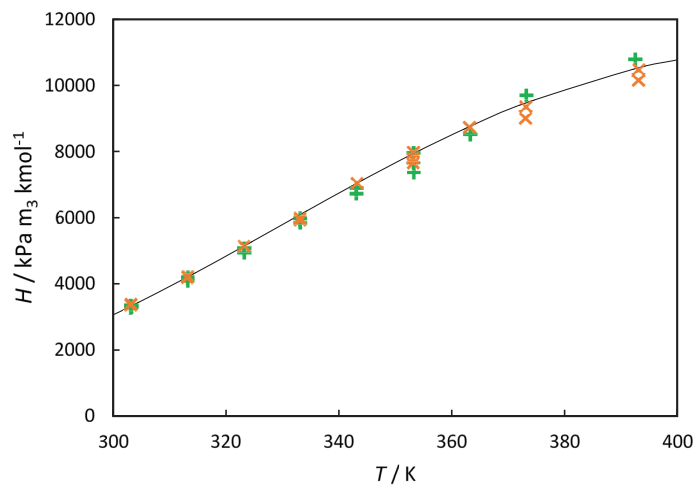


**Figure 1:** Henry's constant for CO<sub>2</sub> in water as a function of temperature. (+) Measurements in VLE-1, (x) Measurements in VLE-2, (—) Correlation by Penttilä et al.<sup>24</sup>

### 2.2.2 Density measurements

An Anton Paar Density Meter DMA 4500M was used to measure the density of the solutions used in this work, when not reported in the literature. The knowledge of the density as a function of temperature was necessary in order to calculate the volume of the solution inside the reactor, assuming that pressure effect is negligible. Calibration and validation of the apparatus was performed according to Hartono et al.<sup>25</sup> and Skylogianni et al.<sup>26</sup> An average absolute relative deviation of 0.01% was found for two repeated measurements.

### 2.2.3 Karl-Fischer titration

The presence of water in the MDEA-glycol systems was studied through Karl-Fischer titration measurements using a METHROM 831 KF coulometer. Coulometric Karl-Fischer titration is an established method for water content determination as low as a few ppm. The AARD in this work is 11%.

### 2.2.4 NMR experiments

NMR is a powerful non-invasive analytical technique for chemical analyses. Interpretation of the NMR spectra leads to the identification of the chemical structures of the molecules, including unknown products and/or side-products, and in proper performed NMR experiments the species can also be quantified<sup>27</sup>.

In this study, qualitative <sup>1</sup>H, <sup>13</sup>C and 2D NMR experiments were performed on selected liquid samples after CO<sub>2</sub> absorption to identify reaction products formed upon the addition of carbon dioxide. In particular, <sup>13</sup>C NMR spectra show the signals belonging to all the CO<sub>2</sub>-derivatives

formed upon the addition of CO<sub>2</sub>, like e.g. amine carbonate, alkyl carbonate, bicarbonate and carbonate which all contain carbon (-C) nuclei in their structure<sup>28</sup>.

Each sample was inserted in an NMR tube, together with a coaxial insert containing deuterated benzene (C<sub>6</sub>D<sub>6</sub>) for locking and referencing. The NMR experiments were performed at 300 K on a Bruker 600 MHz Avance III HD equipped with a 5-mm cryogenic CP-TCI z-gradient probe. The qualitative <sup>13</sup>C NMR spectra shown in this work were all obtained with a standard decoupling acquisition sequence with 30-degree pulse angle and Nuclear Overhauser Effect (NOE) growth (zgpg30), using a recycle delay time of 2 seconds and 1024 scans.

### 2.3 Modeling methods

Vapor-liquid equilibrium of CO<sub>2</sub> with aqueous MDEA and aqueous MDEA-MEG was modeled employing the so-called “soft model”, proposed by Brüder et al.<sup>29</sup> It is a purely empirical correlation which is described by Eq. 4- Eq. 7.

$$\ln(P_{CO_2}) = A \ln \alpha + k_1 + \frac{B}{(1 + k_2 \exp(-k_3))} \quad \text{Eq. 4}$$

where A, B are parameters and  $k_1$ ,  $k_2$  and  $k_3$  are temperature-dependent coefficients:

$$k_1 = k_{1,a} \ln\left(\frac{1}{T}\right) + k_{1,b} \quad \text{Eq. 5}$$

$$k_2 = \exp\left(\frac{k_{2,a}}{T} + k_{2,b}\right) \quad \text{Eq. 6}$$

$$k_3 = \frac{k_{3,a}}{T} + k_{3,b} \quad \text{Eq. 7}$$

$P_{CO_2}$  is expressed in kPa,  $\alpha$  in mol CO<sub>2</sub>/mol MDEA and  $T$  in K in the fitted model.

The model can predict the CO<sub>2</sub> partial pressures based only on temperature and loading and it has been employed in the past to successfully describe amine-containing reactive systems<sup>29–31</sup>. The VLE data were fitted to the correlation by minimizing the sum of the relative least square error and for each system, a different set of parameters is proposed. The binary systems, for which one or two points are obtained per temperature, were not possible to be described with the model due to the limited number of data.

### **3. RESULTS AND DISCUSSION**

#### **3.1 Analysis of the water content**

As we investigate several non-aqueous blends, it was decided to use Karl-Fischer titration for the quantification of the water present. Analysis was performed both before and after the VLE experiments for selected non-aqueous systems studied in this work. For all the systems titrated, low water amount was found before the experiment equal or lower than 0.1 wt% H<sub>2</sub>O. The detailed water concentrations and corresponding uncertainties are given in Supporting Information (Section C). It is important to note here that water was also detected in pure MEG samples even though we purchased anhydrous ethylene glycol. This signifies that some humidity was absorbed through the solution's contact with the atmosphere during solution preparation and experiment preparation.

Higher water contents were detected after the experiment was concluded. The increased water content after the experiment indicates that humidity must have been remained in the reactors or in the condenser on the top of the reactor even after their thorough cleaning and drying. The water content observed was typically below 0.2 wt% while the maximum water content was observed for pure MDEA (0.5 wt%) in the end of the experiment. The impact of the detected water is discussed on the following sections.

### 3.2 MDEA – MEG mixtures

Carbon dioxide absorption in pure MEG, pure MDEA and their blends was investigated and the data obtained are presented in the Appendix (**Table A. 2**). The measurements are reported with their respective uncertainties, calculated using the Law of propagation of uncertainty, according to the uncertainty analysis provided in Supporting Information (Section E). As explained in the experimental procedure, the solubility of a fixed CO<sub>2</sub> amount was measured at temperatures from 303 to 393 K. The densities of the MDEA – MEG blends, required for the data processing, were calculated using the model proposed by Skylogianni et al.<sup>26</sup> Density measurements of indicative systems, which were conducted to verify the model results, demonstrated maximum ARD of 1% (Section B of Supporting Information).

Several authors have reported *P-T-x* data for the binary system CO<sub>2</sub> – MEG. **Figure 2** and **Figure 3** show the mole fraction of CO<sub>2</sub> in the liquid phase against pressure at 323 K and 373 K, respectively. Literature data are also available at the studied temperatures 303 K, 333 K and 343 K and a graphical comparison can be found at Supporting Information (Figure S. 1 to Figure S. 3). It is observed that the data obtained in this work are in line with those reported in the literature. The Henry's constant values are plotted as a function of temperature in **Figure 4** for all studied blends, from pure MEG to pure MDEA.

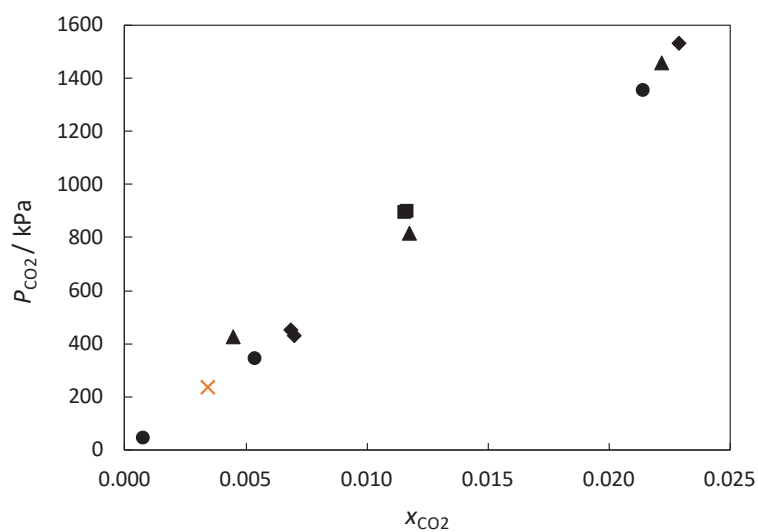


**Figure 2.** Carbon dioxide solubility in MEG expressed in mole fraction ( $x_{CO_2}$ ) as a function of pressure at 323 K. (■) Zheng et al. (1999)<sup>32</sup>, (▲) Galvao and Francesconi (2010)<sup>33</sup>, (●) Jou et al. (1990)<sup>34</sup>, (◆) Wise and Chapoy (2017)<sup>35</sup>, (×) This work.

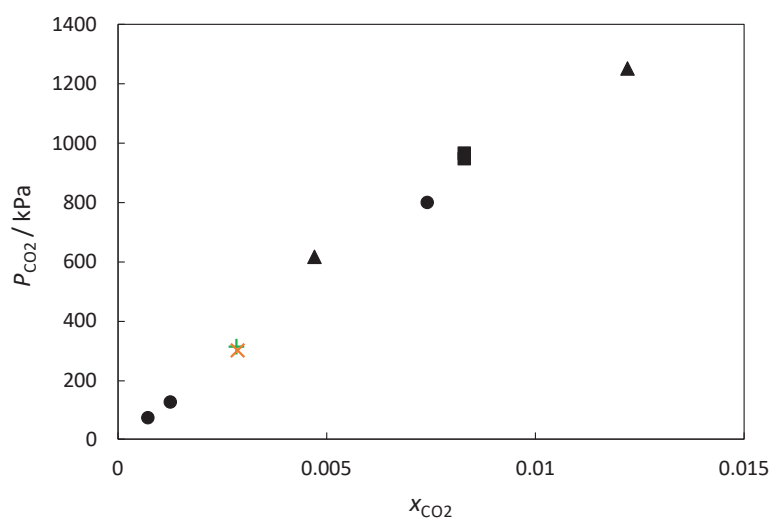


**Figure 3.** Carbon dioxide solubility in MEG expressed in mole fraction ( $x_{CO_2}$ ) as a function of pressure at 373 K. (■) Zheng et al. (1999)<sup>32</sup>, (▲) Galvao and Francesconi (2010)<sup>33</sup>, (●) Jou et al. (1990)<sup>34</sup>, (×) This work (A), (+) This work (B).

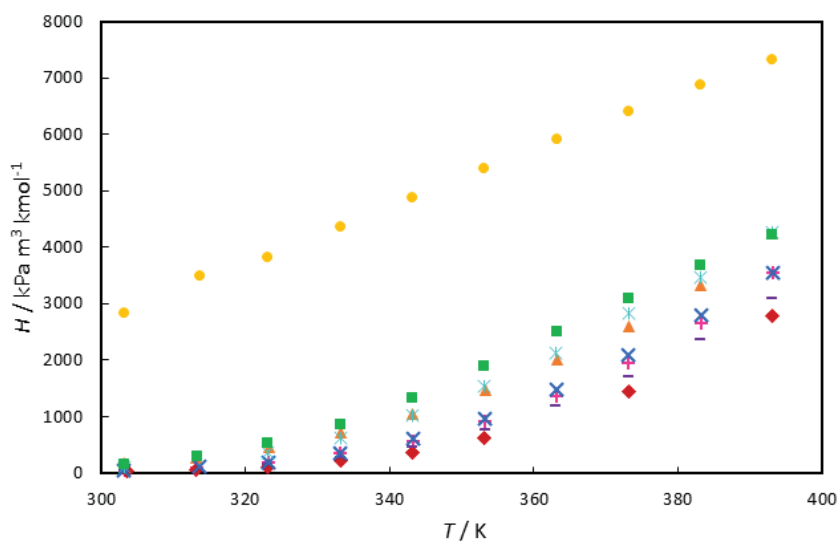


**Figure 4.** Henry's constant as a function of temperature for pure MEG, pure MDEA and their blends as measured in this work. (●) Pure MEG, (▲) 5 wt% MDEA – 95 wt% MEG, (+) 10 wt% MDEA – 90 wt% MEG, (◆) 30 wt% MDEA – 70 wt% MEG, (–) 50 wt% MDEA – 50 wt% MEG, (×) 70 wt% MDEA – 30 wt% MEG, (\* ) 90 wt% MDEA – 10 wt% MEG, (■) Pure MDEA.

As illustrated in **Figure 4**, Henry's constant increases with temperature, thus the solubility of CO<sub>2</sub> into the solvent decreases, for both unitary and binary solvents studied in this work. This is explained by the higher kinetic energy with temperature resulting to the escape of gas molecules from the liquid and in the gas phase. Moreover, it is shown that the Henry's constant of CO<sub>2</sub> in MEG is higher than the Henry's constant of CO<sub>2</sub> in MDEA. The uncertainties calculated have an average deviation from their corresponding properties of 7%. It was found that Henry's constant has higher sensitivity to the amount of CO<sub>2</sub> absorbed in the solvent, due to the propagation of errors in its calculation (Eq. S.24 in Supporting Information). Therefore, the experiments with low CO<sub>2</sub> uptake are expected to have the highest uncertainty in Henry's

constant. These experiments include mainly those experiments performed with a single loading.

An unexpected behavior was observed for the mixtures of the glycol with the amine: the solubility of carbon dioxide in mixtures of MDEA – MEG is higher than it is in its individual components. The measurements for selected blends of MDEA – MEG were repeated in order to confirm the observed trends. To be specific, the CO<sub>2</sub> solubility measurements were conducted twice in the blends of 5 wt% MDEA – 95 wt% MEG, 10 wt% MDEA – 90 wt% MEG, 30wt% MDEA – 70 wt% MEG and 50 wt% MDEA – 50 wt% MEG as well as in pure MEG. Good repeatability was found with AARD equal to 4%. The repeated measurements are given in the Appendix (**Table A. 4**).

In addition, we can observe that as amine is added in MEG, initially the solubility of carbon dioxide is increasing. Between 30 and 50 wt% MDEA content, a transition occurs, after which addition of amine leads to lower CO<sub>2</sub> solubility. As a result, the Henry's constant of CO<sub>2</sub> is similar in a rich-amine system and a lean-amine system, for example in 70 wt% MDEA – 30 wt% MEG system and 10 wt% MDEA – 90 wt% MEG system. This behavior indicates the presence of chemical effects for CO<sub>2</sub> – MDEA – MEG systems. Therefore, the solubility of CO<sub>2</sub> in MDEA – MEG may not be only physical as initially assumed.

No chemical reactions are indeed expected between CO<sub>2</sub> and neither pure MEG nor pure MDEA. MDEA is a tertiary amine which cannot react with carbon dioxide in the absence of water<sup>9,36</sup>. In order to gain an understanding of the phenomena observed, we conducted isothermal VLE experiments at 313 K and 343 K for the systems CO<sub>2</sub> – MEG and CO<sub>2</sub> – MDEA. CO<sub>2</sub> solubility in 50 wt% MDEA – 50 wt% MEG was also measured at constant temperature in order to provide more insights. The results of this study are reported in **Table**



**A. 3.** The data obtained at 313 K are plotted in **Figure 5** while a similar plot of the data at 343 K can be found in Supporting Information (Figure S. 4).

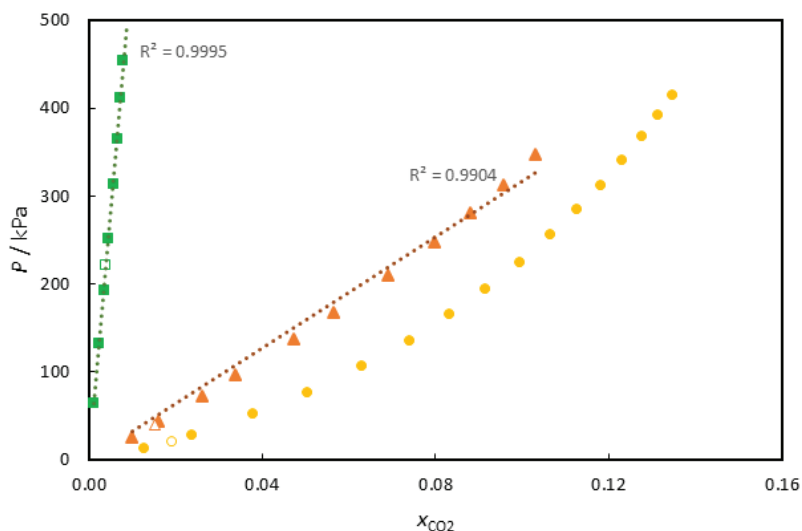


**Figure 5:** Partial pressure of CO<sub>2</sub> as a function of CO<sub>2</sub> solubility in pure MEG, pure MDEA and their 50 – 50 wt% blend at 313 K. Filled symbols denote isothermal experiment (Table A. 3) and hollow symbols denote previous experiment (Table A. 2); (■) MEG, (▲) MDEA, (●) 50 wt% MDEA – 50 wt% MEG. Dotted lines are linear trendlines; the linearity between  $P$  and  $x$  for pure MEG and pure MDEA is assessed through the coefficient of determination,  $R^2$ .

A linear relation between the partial pressure of a gas and its solubility in a solvent denotes that only physical absorption occurs, according to the simplified form of Henry's Law for ideal systems. In that case, the  $H_{\text{gas,solvent}}$ , i.e. the slope, is constant and a strong function of temperature. The linearity is assessed using the coefficient of determination,  $R^2$ . It is clear that the  $P$ - $x$  relation is linear for pure MEG with  $R^2$  equal to almost unity, i.e. 0.9995 and 0.9998 for 313 K and 373 K, respectively. This indicates that there are no chemical effects. For pure MDEA, a linear relation can be also seen at the studied conditions with a coefficient of determination 0.9904 and 0.9982 for 313 K and 373 K, respectively. One could, however, argue

that some chemical effects might be present since the coefficient of determination for MDEA data is lower and also some curvature can be observed with a naked eye, particularly at 313 K (**Figure 5**). A non-linear relationship between the partial pressure of carbon dioxide and its solubility in a 50 wt% MDEA – 50 wt% MEG blend is also pronounced in the same figure.

Chemical absorption of carbon dioxide into pure MDEA or blends of MDEA-MEG could take place if water is present in the system. Some amounts of water were detected by Karl-Fischer titration in our samples, as presented in section 3.1. Although the presence of small amount of water can explain the noticed chemical effects in pure MDEA, it does not explain the interesting behavior of increased CO<sub>2</sub> solubility up to 30 – 50 wt% MDEA-MEG and decreased solubility as the amine content further rises. For this reason, we also conducted NMR experiments to identify the species present in our loaded systems and further understand the system chemistry. The NMR results follow the VLE results for the aqueous systems.

### 3.3 MDEA – MEG – H<sub>2</sub>O mixtures

Solubility measurements of carbon dioxide into aqueous solutions of MDEA – MEG were performed with MDEA concentration in the solution kept constant at 30 wt% while the water content varied from 10 wt% to 50 wt% (**Table A. 6**). Similar to the MDEA – MEG study, the densities, which are necessary for the data treatment, were found in the literature<sup>26</sup>. Comparison between experimental and literature values at selected temperatures revealed 0.3% maximum absolute relative deviation (Section B of Supporting Information).

The partial pressure of CO<sub>2</sub> as a function of CO<sub>2</sub> loading at 313 and 343 K is shown in **Figure 6** for the 30 wt% MDEA – 60 wt% MEG – 10 wt% H<sub>2</sub>O studied mixture. The increase in loading as temperature decreases, at constant pressure, is justified by the exothermic nature of

the reaction of CO<sub>2</sub> with aqueous MDEA. One can also observe the good repeatability between two experiments, one with multiple pressurizations under isothermal conditions and one with single CO<sub>2</sub> pressurization and temperature variation, which was performed for repeatability checks and to provide data points in several temperatures (**Table A. 5**). These remarks are also valid for the additional aqueous mixtures studied in this work, as shown in Supporting Information (Figure S. 5 and Figure S. 6).

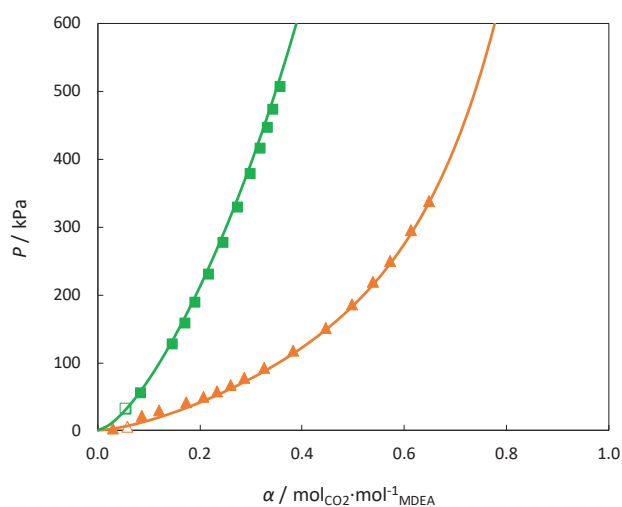


**Figure 6:** Partial pressure of CO<sub>2</sub> as a function of CO<sub>2</sub> loading in a solution of 30 wt% MDEA – 60 wt% MEG – 10 wt% H<sub>2</sub>O. Filled symbols denote isothermal experiment (Table A. 6) and hollow symbols denote repeated experiment with a single loading (Table A. 5). (▲) 313.2 K, (■) 343.2 K.

The effect of water content is illustrated in **Figure 7** and **Figure 8** for 313 K and 343 K, respectively. At 313 K, our measurements are compared with the data points reported by Shen and Li<sup>37</sup> and Xu et al.<sup>16</sup> for a 30 wt% MDEA – H<sub>2</sub>O system, for non-aqueous and aqueous MDEA – MEG blends. Although the data produced in this work for the ternary systems cover partial pressures up to 500 kPa, the y axis of **Figure 7** extends up to 140 kPa, in order for the data points at low partial pressures and loadings to be shown distinctly. The same figure

covering pressures in the whole range of this study can be found in Supporting Information (Figure S. 7). We notice that the CO<sub>2</sub> solubility in aqueous blends of MDEA – MEG is lower than the one in aqueous MDEA. The higher the water content, the higher loading at constant pressure, as shown for both 313 K and 343 K. For example, at pressure ca. 50 kPa and 313 K, the loading is approximately 0.20, 0.41 and 0.55 at water compositions 10 wt%, 30 wt% and 50 wt% respectively and constant amine content (30 wt%).

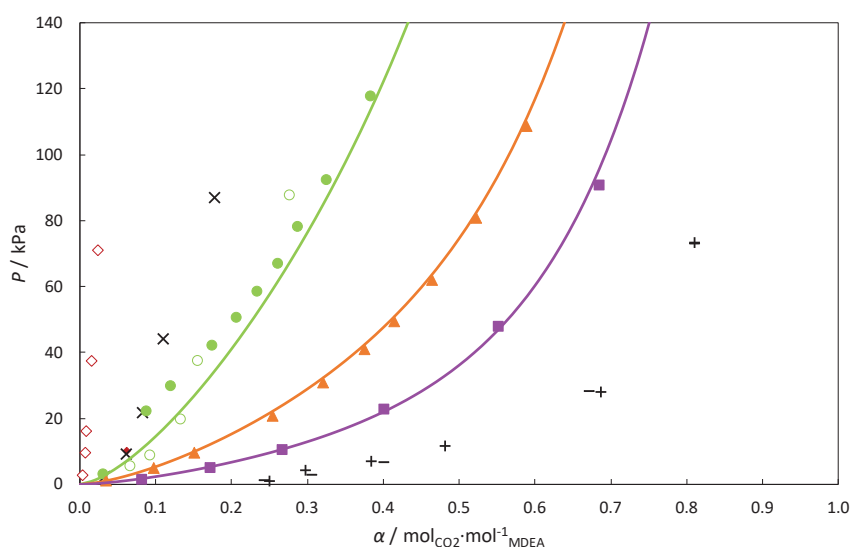


**Figure 7:** Partial pressure of CO<sub>2</sub> as a function of CO<sub>2</sub> loading in MDEA (1) – MEG (2) – H<sub>2</sub>O (3) blends at 313 K. 30 wt% MDEA – 70 wt% MEG: (♦) This work and (◊) data from Xu et al.<sup>16</sup>, 30 wt% MDEA – 65 wt% MEG – 5 wt% H<sub>2</sub>O: (×) Xu et al.<sup>16</sup>, 30 wt% MDEA – 60 wt% MEG – 10 wt% H<sub>2</sub>O: (●) This work and (○) Xu et al.<sup>16</sup>, 30 wt% MDEA – 40 wt% MEG – 30 wt% H<sub>2</sub>O: (▲) This work, 30 wt% MDEA – 20 wt% MEG – 50 wt% H<sub>2</sub>O: (■) This work, 30 wt% MDEA – 70 wt% H<sub>2</sub>O: (+) Xu et al.<sup>16</sup> and (-) Shen and Li<sup>37</sup>. The lines represent model estimations.

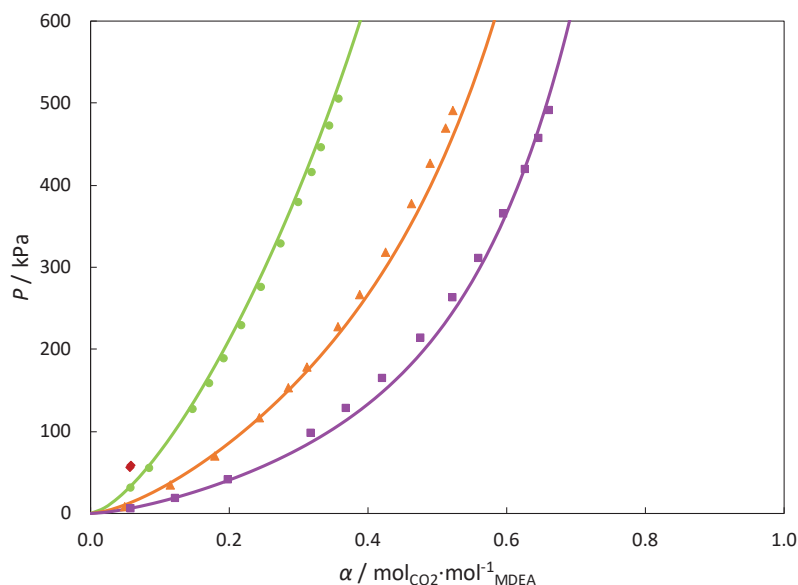


**Figure 8:** Partial pressure of CO<sub>2</sub> as a function of CO<sub>2</sub> loading in MDEA (1) – MEG (2) – H<sub>2</sub>O (3) blends at 343 K as measured in this work. (♦) 30 wt% MDEA – 70 wt% MEG, (●) 30 wt% MDEA – 60 wt% MEG – 10 wt% H<sub>2</sub>O, (▲) 30 wt% MDEA – 40 wt% MEG – 30 wt% H<sub>2</sub>O, (■) 30 wt% MDEA – 20 wt% MEG – 50 wt% H<sub>2</sub>O. The lines represent model estimations.

The presence of glycol and its substitution with water therefore leads to lower solution loadings. On the one hand, the physical solubility of CO<sub>2</sub> into pure MEG is higher than the one in water. For example, at 323 K,  $H_{\text{CO}_2,\text{water}} = 5000 \text{ kPa}\cdot\text{m}^3\cdot\text{kmol}^{-1}$  while  $H_{\text{CO}_2,\text{MEG}} = 3800 \text{ kPa}\cdot\text{m}^3\cdot\text{kmol}^{-1}$  approximately. On the other hand, the carbon dioxide uptake from MDEA due to the reaction in the presence of water is much larger than the one due to dissolution in the solvent. We can confidently say that this behavior of decreasing solution loading with increasing glycol content is true as the water content decreases down to 10 wt%. Interestingly, the data point obtained for the 30 wt% MDEA – 70 wt% MEG system at 313 K in the first experimental campaign coincides with the measurements performed in the presence of 10 wt% water (30 wt% MDEA – 60 wt% MEG – 10 wt% H<sub>2</sub>O). At 343 K and **Figure 8** though,

employment of 30 wt% MDEA – 70 wt% MEG solution yields indeed lower amine loadings. NMR analysis was therefore decided to be performed also for the aqueous systems.

As far as the comparison with literature data on MDEA – MEG – H<sub>2</sub>O and 30 wt% MDEA – 70 wt% is concerned, some disagreements can be observed. For the non-aqueous system, a significant deviation can be seen between the measured solubility and the literature one. Xu et al.<sup>16</sup> state that they performed Karl-Fischer titration but they do not inform the amount of detected water in their systems. Lower water content in Xu et al.'s samples than in ours, could explain the observed deviations. Moreover, at amine loadings lower than 0.15 mol CO<sub>2</sub>/mol MDEA, our data for a 30 wt% MDEA – 60 wt% MEG – 10 wt% H<sub>2</sub>O system fall together with literature data for a 30 wt% MDEA – 65 wt% MEG – 5 wt% H<sub>2</sub>O system. Our measurements were performed twice demonstrating a maximum ARD of 6 % at 303 K and the uncertainties of the data obtained in this study are low and cannot explain the deviations from the literature.

The solid lines in **Figure 6**, **Figure 7** and **Figure 8** are model estimations using the so-called “soft model”, as described in section 2.3. In the afore-mentioned figures, it can be seen that the model yields accurate predictions of the VLE data. The AARD is 9% for the systems 30 wt% MDEA – 60 wt% MEG – 10 wt% H<sub>2</sub>O and 30 wt% MDEA – 20 wt% MEG – 50 wt% H<sub>2</sub>O while for the 30 wt% MDEA – 40 wt% MEG – 30 wt% H<sub>2</sub>O, whose number of data points is higher than the other two systems, the AARD is 4%. The AARDs for the 70 wt% aqueous MDEA and for the 90 wt% aqueous MDEA investigated in the next section, are 3% and 5%, respectively. The model parameters are presented in Appendix B.

### 3.4 Comparison with highly concentrated MDEA solutions

After investigating the effect of water and after observing the effect of MEG concentration in CO<sub>2</sub> loading of the non-aqueous solvent, as described in section 3.2, we decided to investigate the outcome of substituting glycol with amine. In this framework, CO<sub>2</sub> solubility measurements were conducted in 70 wt% MDEA – 30 wt% H<sub>2</sub>O and in 90 wt% MDEA – 10 wt% H<sub>2</sub>O. Similar to the experiments with aqueous MDEA – MEG, the experiments were performed at 313 K and 343 K. The obtained data are reported in Appendix A (**Table A. 7**). At constant pressure, higher CO<sub>2</sub> loadings are achieved with 70 wt% aqueous MDEA than with 90 wt% aqueous MDEA. Thus, increasing amine concentrations in the solvent leads to lower absorption capacities and the CO<sub>2</sub> capture by the aqueous MDEA seems to be limited by water availability.

A comparison was performed between the amine and amine/glycol systems with constant water content, i.e. 10 wt% and 30 wt% water. **Figure 9** shows the results of the comparison between 30 wt% MDEA – 60 wt% MEG – 10 wt% H<sub>2</sub>O and 90 wt% MDEA – 10 wt% H<sub>2</sub>O in terms of CO<sub>2</sub> absorbed per kg of solution in order to give a more perceptible sense of the capacity of the solvent. One can observe that at constant pressure, the glycol-containing system demonstrates similar or better performance than the MDEA-H<sub>2</sub>O system in terms of CO<sub>2</sub> removed per kg of solution. Although CO<sub>2</sub> solubility in MDEA is higher than in MEG, some additional reactivity is observed in the aqueous MDEA – MEG system, at same water content, in line with previous observations. At 313 K, this behavior is shown for pressures lower than 200 kPa. For the systems with 30 wt% water however, aqueous MDEA outperforms the glycol-containing system (Figure S. 8 in Supporting Information). It is worth mentioning that non-aqueous systems, i.e. 90 wt% MDEA – 10 wt% MEG and 70 wt% MDEA – 30 wt% MEG, yield lower CO<sub>2</sub> concentrations than their aqueous counterparts.

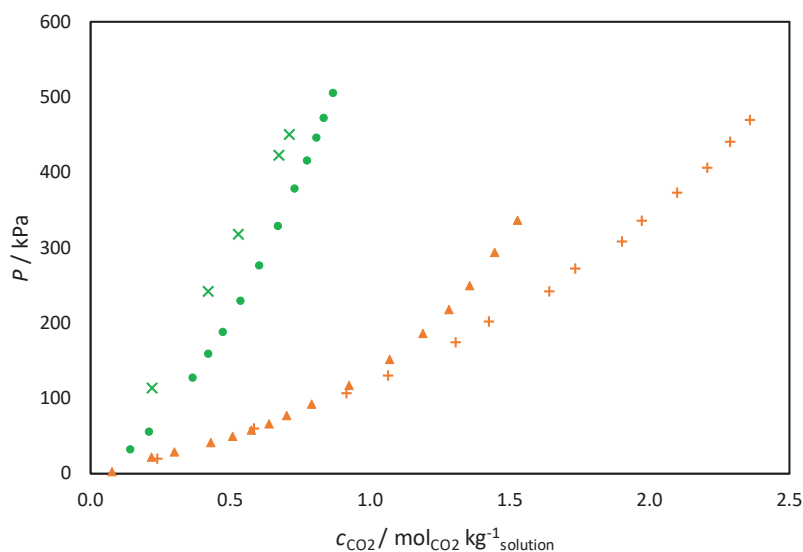
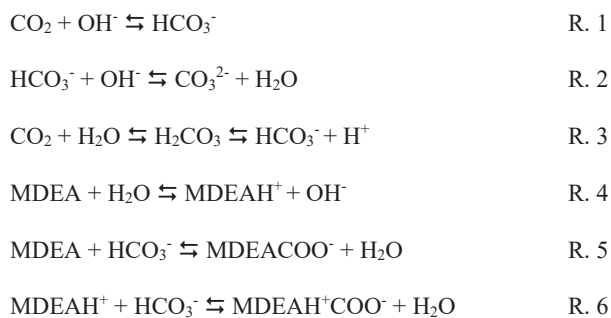


**Figure 9:** Partial pressure of CO<sub>2</sub> as a function of CO<sub>2</sub> liquid phase concentration in 30 wt% MDEA – 60 t% MEG – 10 wt% H<sub>2</sub>O and 90 wt% MDEA – 10 wt% H<sub>2</sub>O. (▲) denotes data obtained at 313 K with MDEA – MEG – H<sub>2</sub>O system, (+) 313 K with MDEA – H<sub>2</sub>O system; (●) 343 K with MDEA – MEG – H<sub>2</sub>O system and (×) 343 K with MDEA – H<sub>2</sub>O system.

### 3.5 Chemical characterization by NMR spectroscopy

Small amounts of water were detected in our non-aqueous systems signifying a possible reaction with carbon dioxide, due to the amine protonation by the water which is present. The reactions taking place in CO<sub>2</sub> – MDEA – H<sub>2</sub>O systems are listed below. Reactions R. 1 to R. 4 are usually considered in the description of chemical equilibrium, however, there are several studies in literature showing that aqueous tertiary amines can react with CO<sub>2</sub> to form alkyl carbonate<sup>38,39</sup>. In particular, Behrens et al.<sup>40</sup> showed by means of NMR analysis that, in CO<sub>2</sub> – MDEA – H<sub>2</sub>O system, more than 10 mol% of the absorbed CO<sub>2</sub> is in the form of MDEA carbonate (MDEACOO<sup>-</sup>) (Reactions R. 5 and R. 6).





With the aim of identifying possible chemical products deriving from the addition of CO<sub>2</sub> in the VLE measurements of pure MEG, pure MDEA, non-aqueous MDEA – MEG blends (5 wt% MDEA – 95 wt% MEG and 50 wt% MDEA – 50 wt% MEG) and aqueous MDEA – MEG blends (30 wt% MDEA – 60 wt% MEG – 10 wt% H<sub>2</sub>O and 30 wt% MDEA – 20 wt% MEG – 50 wt% H<sub>2</sub>O), <sup>1</sup>H and <sup>13</sup>C NMR experiments were performed, together with 2D NMR experiments. The interpretation of the spectra and their comparison allowed the structural characterization of the species in the solutions.

**Figure 10** shows the <sup>13</sup>C NMR spectra and the signal assignment of the species at equilibrium in pure MEG, pure MDEA and 50 wt% MDEA – 50 wt% MEG in the presence of CO<sub>2</sub>. In the upfield region of the <sup>13</sup>C NMR spectra, which here spans from ca. 40 to 70 ppm, the signals belonging to carbons nuclei -CH<sub>2</sub> and CH<sub>3</sub> of MDEA, MEG and their derivatives are resonating. In the downfield region, here spanning from ca. 155 to 170 ppm, the nuclei of the carbonyl carbons in the alkyl carbonates (R-O-COO<sup>-</sup>) and bicarbonate / carbonate (HCO<sub>3</sub><sup>-</sup>/CO<sub>3</sub><sup>2-</sup>) are found. The downfield region is therefore very representative of the formation of CO<sub>2</sub>-derivatives in the samples under study. It is worth mentioning that, in the <sup>13</sup>C NMR spectra, the carbons of HCO<sub>3</sub><sup>-</sup> and CO<sub>3</sub><sup>2-</sup> appear with a common signal at an averaged chemical shift. This is due to the fact that they are two species in equilibrium, and the proton exchange

between them (R. 2) is faster than the NMR time scale. The same is true for the amine and its protonated form (such as shown in R. 4 and R. 6)<sup>41</sup>.

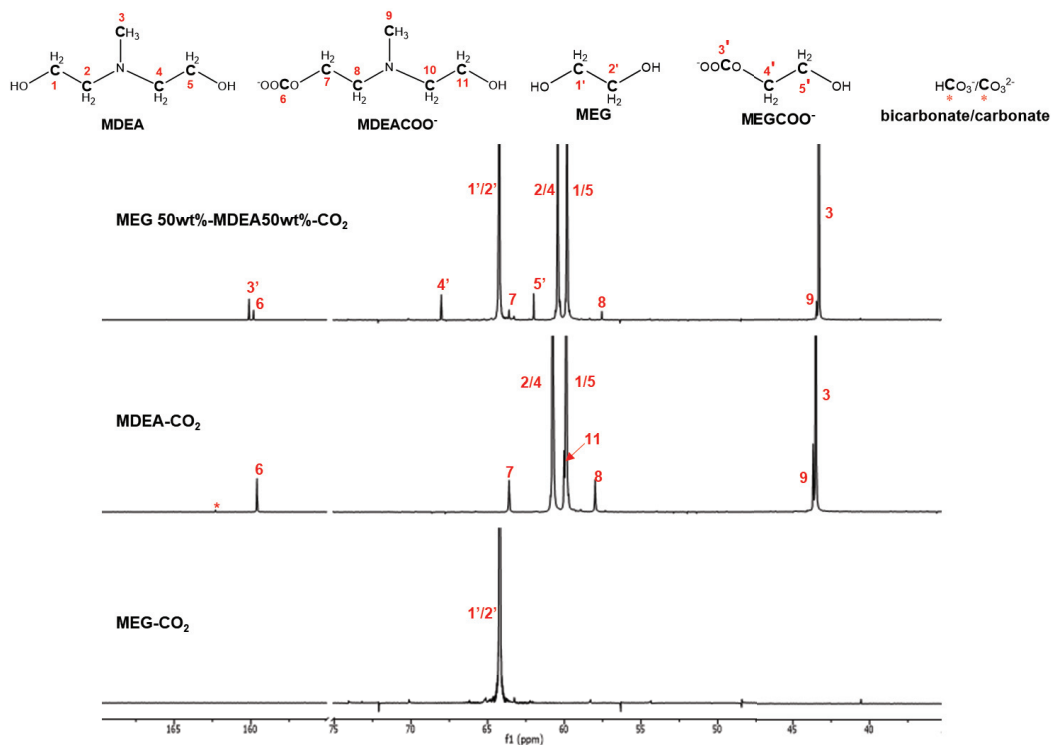


**Figure 10:** <sup>13</sup>C NMR spectra of CO<sub>2</sub> loaded pure MEG, pure MDEA, and 50 wt% MDEA – 50 wt% MEG.

Looking at the species content, we observe that in CO<sub>2</sub>-MDEA system, in addition to MDEA itself, MDEA carbonate (MDEACOO<sup>-</sup>) is formed, together with negligible traces of HCO<sub>3</sub><sup>-</sup>/CO<sub>3</sub><sup>2-</sup>. These reaction products may be the result of the presence of water traces which start a series of reactions (R. 1 to R. 6). On the contrary, in CO<sub>2</sub>-MEG system, neither MEG is chemically reacting with carbon dioxide nor HCO<sub>3</sub><sup>-</sup>/CO<sub>3</sub><sup>2-</sup> is formed. Interestingly, in the presence of MDEA, MEG is reacting to CO<sub>2</sub>, giving MEG carbonate (MEGCOO<sup>-</sup>). This is even formed in the presence of only 5 wt% MDEA (Figure S. 11 in the Supporting Information). With regard to the electroneutrality, it would be expected that the protonated form of MDEA

(MDEAH<sup>+</sup> and/or MDEAH<sup>+</sup>COO<sup>-</sup>) would act as counterion of the alkyl carbonates and HCO<sub>3</sub><sup>-</sup>/CO<sub>3</sub><sup>2-</sup>.

In **Figure 11**, the comparison of the downfield region in the <sup>13</sup>C NMR spectra of the MEG – MDEA blends in water are reported (Full spectra are available in Figure S. 12 of the Supporting Information). In the presence of water, consistent amounts of bicarbonate/carbonate are formed, and the intensity of the peak is proportional to the amount of water in the sample. In the alkyl carbonates region, the carbonyl carbon belonging to MEG and MDEA carbonates are found, and the presence of additional weak signals may suggest the formation of additional MEG-CO<sub>2</sub> and MDEA-CO<sub>2</sub> derivatives, like e.g. MEG dicarbonate (MEG(COO<sup>-</sup>)<sub>2</sub>) and/or MDEA dicarbonate (MDEA(COO<sup>-</sup>)<sub>2</sub>). However, due to weakness and/or overlapping of these signals in the spectra, these compounds were not identified.

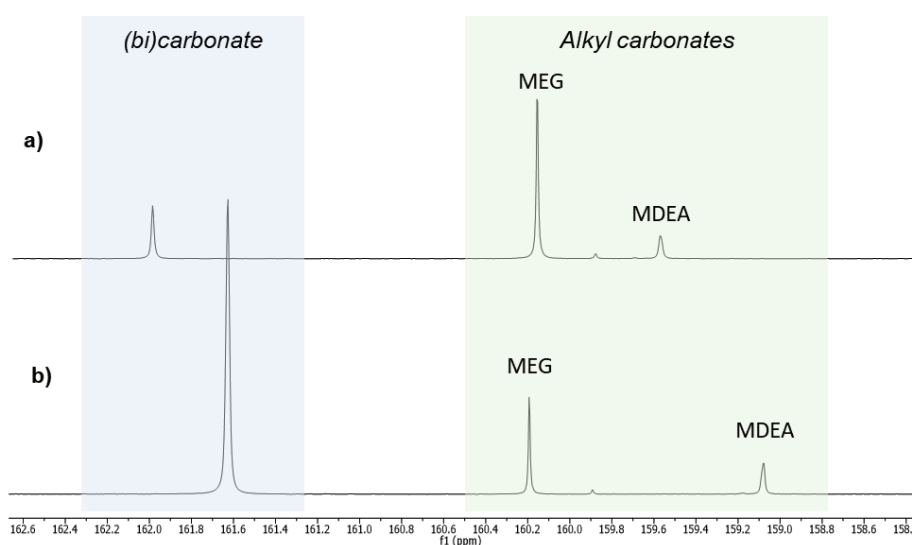


**Figure 11:** Downfield region of the <sup>13</sup>C NMR spectra of CO<sub>2</sub> loaded a) 30 wt% MDEA – 60 wt% MEG – 10 wt% H<sub>2</sub>O and b) 30 wt% MDEA – 20 wt% MEG – 50 wt% H<sub>2</sub>O; (bi)carbonate stands for HCO<sub>3</sub><sup>-</sup>/CO<sub>3</sub><sup>2-</sup>.

### 3.6 Hypothesis on reaction mechanisms of MEG with CO<sub>2</sub> in the presence of MDEA and comparison with TEG

The NMR results can explain the behavior of CO<sub>2</sub> – MDEA – MEG system as illustrated in **Figure 4**. The solubility of carbon dioxide into MDEA – MEG is higher than in pure MEG or pure MDEA because of the chemical reaction taking place between CO<sub>2</sub> and MEG in the presence of MDEA. This may be the result of autoprotolysis of MEG in the alkaline environment created by the amine<sup>42</sup>. The absence of MEGCOO<sup>-</sup> in MEG-CO<sub>2</sub> system indicates that, in the presence of MDEA, the hydroxyl group (-OH) of MEG is more prone to lose its proton, and it is then available to chemically bind carbon dioxide. As a result, in MDEA – MEG blends, both MDEA carbonate and MEG carbonate are formed. The chemical absorption of carbon dioxide into monoethylene glycol is a trade-off between the amount of amine available to offer the basicity required for MEG to autoprotolyze and the amount of MEG available for autoprotolysis.

The solvent composition between 30 and 50 wt% MDEA where we observed the reduced CO<sub>2</sub> solubility upon addition of amine, is probably the limits of this trade-off. From that point towards leaner-in-glycol systems, smaller amount of MEG autoprotolyzes and therefore the Henry's constant increases, for a given temperature. Moreover, the overlapping data for 30 wt% MDEA – 60 wt% MEG – 10 wt% H<sub>2</sub>O and 30 wt% MDEA – 70 wt% MEG discussed earlier can be attributed to the CO<sub>2</sub> – MEG reaction and MEG carbonate formation in the MDEA – MEG system which is probably in the same extent as the combined MEG carbonate and MDEA carbonate formation in the aqueous system.

Barzagli et al.<sup>43</sup> have also reported the presence of the glycol carbonate in their studies of CO<sub>2</sub> solubility into non-aqueous MDEA – MEG – propanol systems and discussed the ability of alcohols to absorb carbon dioxide when in the presence of a base. For these phenomena to take

place, only tertiary amines should serve as a base. If a primary or a secondary amine was used, the glycol carbonate formation would be hindered by the stable carbamate formation. On the contrary, tertiary amines cannot form carbamates, making them ideal for selective removal of hydrogen sulfide over carbon dioxide, since H<sub>2</sub>S can react directly with the amine. The increased reactivity of MDEA – MEG blends for the selective removal of H<sub>2</sub>S over CO<sub>2</sub> is also discussed by Dag Eimer<sup>42</sup>.

The degree of autoprotolysis of a compound is informed by its dissociation constant (autoprotolysis constant,  $K_{ap}$ ). The higher the  $K_{ap}$  (the lower the  $pK_{ap} = -\log_{10}(K_{ap})$ ), the higher the tendency of releasing a proton from the -OH group. As suggested by Eimer<sup>42</sup>, amine-MEG mixtures should have higher reactivity than amine-TEG blends, due to the lower  $pK_{ap}$  value of MEG. The  $pK_{ap}$  values for MEG and TEG are approximately 16 and 18.5, respectively<sup>42</sup>. Thus, the degree of autoprotolysis in TEG is lower than that in MEG and, it would be expected that the solubility of CO<sub>2</sub> in MDEA – TEG mixtures would be lower than in MDEA – MEG mixtures at the same concentrations.

To confirm this theory, we performed VLE experiments for the system CO<sub>2</sub> – MDEA – TEG too. The VLE data for the TEG-containing systems are presented in **Table A. 8** in the Appendix and the required for the data processing measured densities can be found in Table S. 1 in the Supporting Information. Available literature data for the density of pure TEG were compared with our measurements (**Figure 12**). The obtained experimental points follow the behavior of the literature data, except for the data of Sagdeev et al.<sup>44</sup> and Tawfik and Teja<sup>45</sup>, which are consistently higher than the rest of the data. The uncertainties reported by the different authors in most cases are higher than the deviations observed. These deviations can be attributed to the different chemical purity as well as to possible unwanted humidity absorption from the air due

to the high hygroscopicity of TEG. However, the calculated absolute relative deviations (ARD) are low, ranging from 0.01% to 0.15%.

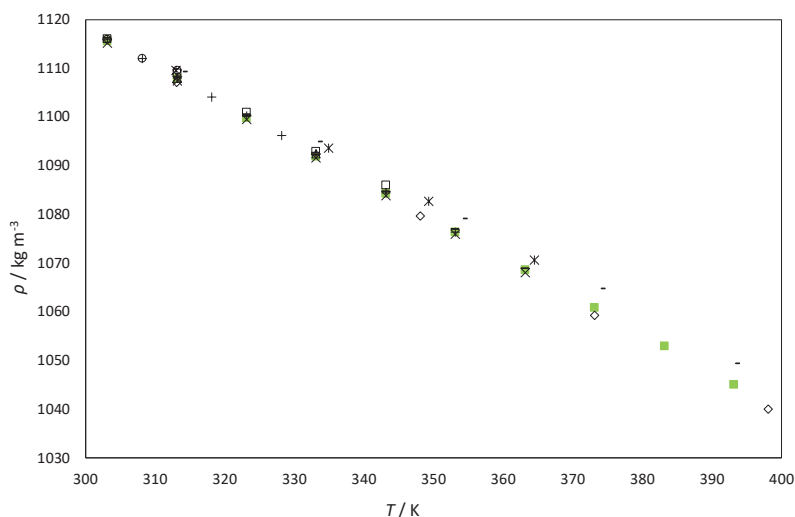


**Figure 12:** Density of pure TEG as a function of temperature at atmospheric pressure. (x) Pereira et al. (2019)<sup>46</sup>, (-) Crespo et al. (2017)<sup>47</sup>, (x) Sagdeev et al. (2011)<sup>44</sup>, (□) Tsai et al. (2009)<sup>48</sup>, (○) Sastry et al. (2008)<sup>49</sup>, (+) Valtz et al. (2004)<sup>50</sup>, (◇) Steele et al. (2002)<sup>51</sup>, (Δ) Kumagai et al. (1993)<sup>52</sup>, (-) Tawfik and Teja (1989)<sup>45</sup>, (■) This work.

In this study of TEG-containing systems, we first measured the carbon dioxide solubility in pure TEG and compared our results with literature values<sup>53,54</sup> (**Figure 13**). It is observed that the obtained data are in good agreement with the literature. Moreover, Tan et al.<sup>18</sup> reported Henry's constant of CO<sub>2</sub> in pure TEG. Their data agree with the measured Henry's constants in this work, and any small deviations observed are well within experimental uncertainty. A graphical comparison is provided in Supporting Information (Figure S. 10).

Moreover, we studied MDEA – TEG blends in two different compositions, 30 wt% MDEA – 70 wt% TEG and 50 wt% MDEA – 50 wt% TEG. These compositions were selected in order to allow for a direct comparison with MDEA – MEG mixtures at same amine weight fraction.

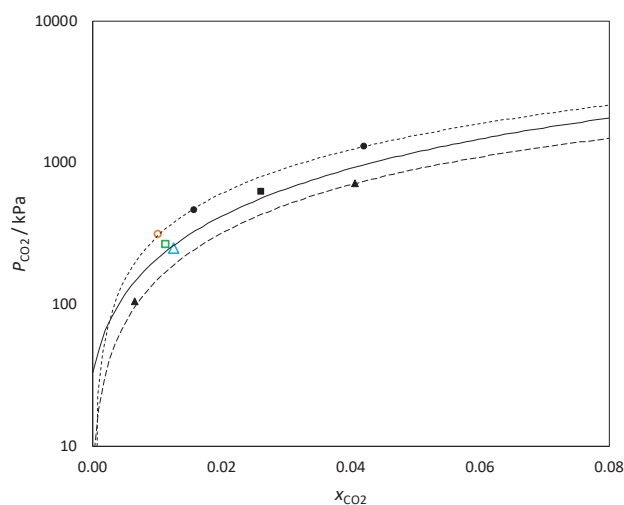


**Figure 13:** Partial pressure of CO<sub>2</sub> as a function of CO<sub>2</sub> solubility and temperature in pure TEG. Triangles denote 323 K, squares denote 343 K and circles denote 373 K. Filled symbols are literature values; (●), (▲) from Jou et al.<sup>53</sup> and (■) from Wise and Chapoy<sup>54</sup>. Hollow symbols are data obtained in this work. Tendency curves are drawn: dashed line (---) for 323 K, solid line (—) for 343 K and dotted line (⋯) for 373 K.

The following figure (**Figure 14**) depicts Henry's constant as a function of temperature and composition in MDEA – MEG and MDEA – TEG systems. Henry's constant is higher in MDEA – TEG blends than MDEA – MEG blends, while it is lower in pure TEG than in pure MEG. These results are therefore in agreement with the theory, since the degree of autoprotolysis of TEG is lower than that of MEG, leading to lower CO<sub>2</sub> solubility. In addition to this, the Henry's constant values in MDEA – TEG blends lie between the Henry's constants in pure TEG and pure MDEA suggesting that CO<sub>2</sub> is absorbed mainly physically in the solvent. However, some chemical effects are also present as indicated by the results of an isothermal experiment at 313 K for the 50 wt% MDEA – 50 wt% TEG system where a non-linear relation between  $P$ - $x$  is pronounced (Figure S. 9). Based on the NMR data obtained in this study, there is no formation of TEG carbonate (TEGCOO<sup>-</sup>) in CO<sub>2</sub> – TEG system, as it was also observed

in CO<sub>2</sub> – MEG. In CO<sub>2</sub> – MDEA – TEG systems, MDEACOO<sup>-</sup> was found, but the presence of TEGCOO<sup>-</sup> was not clear. Due to overlapping signals and crowded-signals spectra, some low-intensity signals were not assigned, but it is expected that the correspondent molecules would be in negligible amounts. Therefore, the chemical effects observed in MDEA – TEG systems are mainly due to the reaction of CO<sub>2</sub> with MDEA in the presence of water traces. All relevant spectra are available in Supporting Information (Figure S. 13).

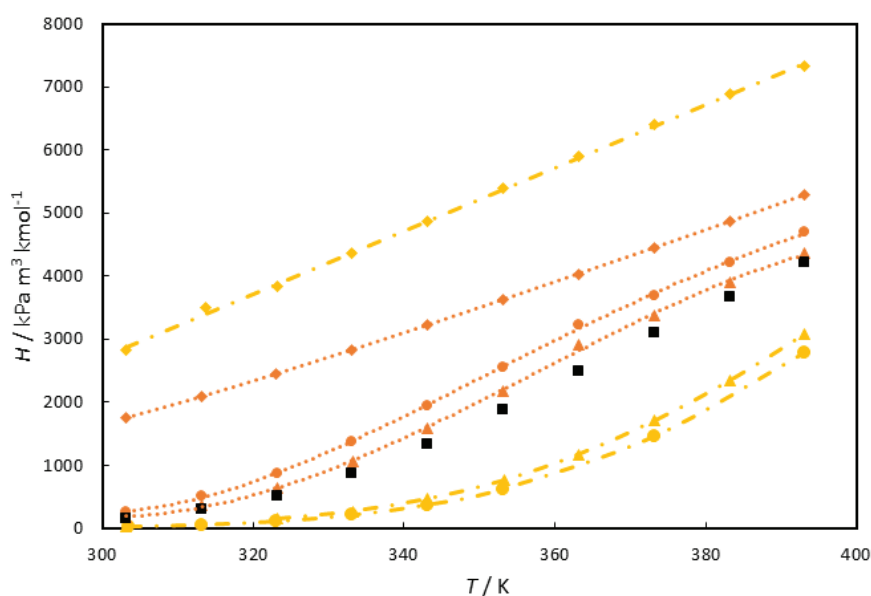


**Figure 14:** Henry's constants as a function of temperature for MDEA – MEG and MDEA – TEG systems. Tendency curves are drawn: (---, dashed dot line) MEG-containing systems, (....., dotted line) TEG-containing systems. (◆) Pure glycol, (●) 30 wt% MDEA – 70wt% glycol, (▲) 50 wt% MDEA – 50 wt% glycol, (■) Pure MDEA.

The findings of this work are important for the industrial application of an MDEA – MEG mixture for the combined hydrogen sulfide removal and hydrate control. For a successful design and trouble-free operations, the knowledge of the amount of co-absorbed carbon dioxide into the solvent through the known aqueous amine mechanism as well as through its reaction



with MEG is necessary. The importance of this work lies in the need to account for the CO<sub>2</sub> absorbed in the glycol as well in the amine during solvent regeneration. As proven from the data presented for CO<sub>2</sub> – MDEA – TEG systems, these implications are in a significantly lesser extent in the systems using TEG.

#### 4. CONCLUSIONS

Aqueous and non-aqueous solvents composed by MDEA and MEG are promising for the simultaneous H<sub>2</sub>S removal and hydrate control in natural gas. Since CO<sub>2</sub> coexists with H<sub>2</sub>S in natural gas streams, the solubility of carbon dioxide in non-aqueous and aqueous MDEA – MEG systems was investigated in this work.

VLE data were obtained at temperatures from 303 K to 393 K and pressures up to 600 kPa. It was found that the absorption capacity of the aqueous solvents decreases with increasing glycol content and substitution of water, at constant amine concentration. Increasing amine content up to 90 wt% in aqueous MDEA systems, also leads to lower solvent CO<sub>2</sub> loadings.

In the non-aqueous solvents, a transition phase was observed at compositions between 30 and 50 wt% MDEA – MEG. CO<sub>2</sub> solubility increases with amine concentration up this transition area, after which the solubility starts decreasing. This behavior is attributed to the CO<sub>2</sub> capture through chemical reaction of CO<sub>2</sub> with MEG in the presence of amine, as a result of MEG autoprotolysis in the alkaline environment of the amine. This theory is supported by supplementary VLE data obtained for MDEA – TEG systems.

NMR experiments proved the formation of glycol carbonate, both in non-aqueous and aqueous MDEA – MEG blends. MDEA carbonate was also identified both in single and blended MDEA, which is probably due to the small amounts of water found in our non-aqueous

solvents. The CO<sub>2</sub> solubility in aqueous blends of MDEA – MEG is generally higher than the one in their non-aqueous counterparts. However, similar absorption capacities can be observed for aqueous systems containing less than 10 wt% water and non-aqueous systems.

The CO<sub>2</sub> uptake by the glycol demonstrated in this work is important knowledge for the application of aqueous or non-aqueous MDEA – MEG mixtures for the combined removal of H<sub>2</sub>S and hydrate control, and specifically for the solvent regeneration.

#### ASSOCIATED CONTENT

##### **Supporting Information.**

The file (PDF) includes:

- A. Complementary data plots
- B. Density data
- C. Karl-Fischer titration results
- D. NMR spectra
- E. Uncertainty analysis

#### AUTHOR INFORMATION

##### **Corresponding Author**

\*Hanna K. Knuutila

Email: hanna.knuutila@ntnu.no

##### **Notes**

The authors declare no competing financial interest.

## ACKNOWLEDGMENT

This work was carried out as a part of SUBPRO (Subsea Production and Processing), a Research-based Innovation Centre within Subsea Production and Processing. It is funded by major industry partners, the Norwegian University of Science and Technology (NTNU) and the Research Council of Norway (RCN) [project number 237893]. Karen Karolina Høisæter is acknowledged for running some 2D NMR experiments on MDEA-TEG systems.

APPENDIX A

All VLE data obtained in this work are presented in this section.

**Table A. 1:** Measured mole fraction solubility  $x_{\text{CO}_2}$  and Henry's constant  $H$  for  $\text{CO}_2$  in water as a function of temperature  $T$  and pressure (total pressure  $P_{\text{tot}}$ , residual pressure  $P_{\text{res}}$  and their difference,  $\text{CO}_2$  partial pressure  $P_{\text{CO}_2}$ ).<sup>a</sup>

$T$	$P_{\text{tot}}$	$P_{\text{res}}$	$P_{\text{CO}_2}$	$x_{\text{CO}_2}$	$u(x_{\text{CO}_2})$	$H$	$u(H)$	$T$	$P_{\text{tot}}$	$P_{\text{res}}$	$P_{\text{CO}_2}$	$x_{\text{CO}_2}$	$u(x_{\text{CO}_2})$	$H$	$u(H)$
K	kPa	kPa	kPa	$\cdot 10^2$	$\cdot 10^2$	kPa $\text{m}^3 \text{kmol}^{-1}$	kPa $\text{m}^3 \text{kmol}^{-1}$	K	kPa	kPa	kPa	$\cdot 10^2$	$\cdot 10^2$	kPa $\text{m}^3 \text{kmol}^{-1}$	kPa $\text{m}^3 \text{kmol}^{-1}$
VLE 1															
303.1	200.3	4.6	195.7	0.108	0.015	3281	454	303.1	168.2	5.3	162.9	0.087	0.006	3389	512
313.2	224.0	7.6	216.4	0.096	0.015	4108	648	313.2	188.6	8.7	180.0	0.077	0.006	4234	727
323.2	247.0	12.4	234.6	0.086	0.015	4952	873	323.2	209.3	13.6	195.6	0.069	0.006	5145	992
333.2	271.4	19.5	251.8	0.079	0.015	5854	1141	343.2	255.8	32.3	223.5	0.058	0.006	7046	1645
343.1	298.1	30.5	267.7	0.073	0.015	6748	1435	353.2	284.5	48.5	236.0	0.055	0.006	7981	2013
353.2	329.6	46.6	283.0	0.068	0.015	7679	1770	363.2	318.8	71.9	246.9	0.053	0.006	8733	2328
363.2	366.4	69.4	297.1	0.065	0.015	8527	2100	313.2	167.2	8.0	159.2	0.069	0.013	4203	798
303.1	230.5	4.6	225.9	0.122	0.016	3345	442	333.2	206.4	20.6	185.8	0.057	0.013	6001	1401
313.2	256.5	7.8	248.6	0.108	0.016	4196	637	353.1	256.4	47.8	208.6	0.050	0.013	7802	2129
323.2	281.6	12.8	268.8	0.097	0.016	5074	866	373.1	330.3	101.7	228.5	0.046	0.014	9359	2860
333.2	307.9	20.4	287.5	0.088	0.016	5988	1135	393.2	445.7	199.7	246.0	0.045	0.015	10481	3496

343.2	336.2	31.4	304.8	0.081	0.017	6904	1432	303.2	143.9	5.3	138.6	0.075	0.014	3362	640
353.2	369.4	46.9	322.5	0.075	0.017	7956	1813	313.1	160.6	8.6	152.0	0.066	0.014	4183	905
364.7	414.1	69.4	344.7	0.067	0.016	9618	2514	333.2	196.8	21.3	175.5	0.054	0.014	5935	1584
303.2	138.9	4.3	134.6	0.073	0.016	3325	722	353.1	244.1	48.5	195.6	0.047	0.015	7656	2383
313.2	155.2	7.5	147.7	0.065	0.016	4153	1027	373.1	315.5	102.9	212.6	0.044	0.015	9011	3099
333.2	190.2	20.2	170.0	0.053	0.016	5868	1784	393.1	429.8	201.1	228.7	0.043	0.016	10154	3829
353.3	235.8	47.6	188.2	0.047	0.016	7374	2554	-	-	-	-	-	-	-	-
373.2	308.9	100.1	208.8	0.041	0.017	9689	4035	-	-	-	-	-	-	-	-
392.5	411.6	188.1	223.5	0.040	0.018	10783	4814	-	-	-	-	-	-	-	-

<sup>a</sup> Standard uncertainties are reported (level of confidence 0.68). Standard uncertainty for temperature is  $u(T) = 0.1$  K, for total and residual pressure is  $u(P_{\text{tot}}) = u(P_{\text{res}}) = 0.9$  kPa and for CO<sub>2</sub> pressure is  $u(P_{\text{CO}_2}) = 1.3$  kPa.

**Table A. 2:** Measured mole fraction solubility  $x_{\text{CO}_2}$ , loading  $\alpha$  and Henry's constant  $H$  for CO<sub>2</sub> in MDEA (1) – MEG (2) blends as a function of weight fraction  $w$  of unloaded solvent, temperature  $T$  and pressure (total pressure  $P_{\text{tot}}$ , residual pressure  $P_{\text{res}}$  and their difference, CO<sub>2</sub> partial pressure  $P_{\text{CO}_2}$ )<sup>a</sup>

$w_1$	$u(w_1)$	$T$	$P_{\text{tot}}$	$P_{\text{res}}$	$P_{\text{CO}_2}$	$x_{\text{CO}_2}$	$\alpha$	$u(x_{\text{CO}_2})$	$u(\alpha)$	$H$	$u(H)$
		K	kPa	kPa	kPa		mol <sub>CO<sub>2</sub></sub> mol <sup>-1</sup> <sub>MDEA</sub>			kPa m <sup>3</sup> kmol <sup>-1</sup>	
0.000	0.000	303.2	200.5	2.3	198.2	0.0039	0.0004	-	-	2835	284
		313.7	223.8	2.5	221.3	0.0036	0.0004	-	-	3498	389

323.2	236.8	2.8	234.0	0.0035	0.0004	-	-	3833	440
333.2	253.9	3.1	250.8	0.0033	0.0004	-	-	4355	530
343.2	270.4	3.5	266.9	0.0031	0.0004	-	-	4875	624
353.2	286.3	3.9	282.4	0.0030	0.0004	-	-	5393	720
363.2	301.7	4.5	297.2	0.0029	0.0004	-	-	5907	820
373.1	317.2	5.5	311.7	0.0028	0.0004	-	-	6406	918
383.2	332.8	7.1	325.7	0.0028	0.0004	-	-	6886	1013
393.2	348.7	9.6	339.1	0.0027	0.0004	-	-	7333	1100
0.050	0.001								
303.2	42.9	1.8	41.1	0.0141	0.0005	0.535	0.024	166	8
313.1	66.2	1.9	64.3	0.0132	0.0005	0.501	0.024	279	13
323.2	97.6	2.0	95.6	0.0121	0.0005	0.458	0.024	457	22
333.1	134.0	2.2	131.8	0.0108	0.0005	0.411	0.023	709	38
343.2	173.2	2.4	170.8	0.0096	0.0005	0.363	0.023	1048	63
353.2	212.5	2.8	209.7	0.0084	0.0006	0.318	0.023	1479	103
363.2	250.1	3.4	246.7	0.0074	0.0006	0.279	0.023	2001	161
373.1	285.4	4.4	281.0	0.0065	0.0006	0.246	0.023	2610	241
383.1	319.2	5.8	313.4	0.0058	0.0006	0.217	0.023	3321	352
393.2	354.4	8.1	346.4	0.0050	0.0006	0.190	0.024	4239	521

0.100	0.001	303.2	10.7	1.9	8.8	0.0096	0.0004	0.178	0.008	53	6
		313.2	18.8	2.2	16.5	0.0094	0.0004	0.174	0.008	103	7
		323.2	32.1	2.5	29.7	0.0091	0.0004	0.168	0.008	193	11
		333.1	52.3	2.8	49.5	0.0086	0.0004	0.159	0.008	342	19
		343.2	79.9	3.5	76.4	0.0080	0.0004	0.147	0.008	575	33
		353.1	113.6	4.6	109.0	0.0073	0.0004	0.134	0.009	909	58
		363.1	151.3	5.9	145.4	0.0065	0.0004	0.120	0.009	1365	97
		373.1	190.6	8.0	182.6	0.0058	0.0004	0.106	0.009	1948	158
		383.3	230.1	10.8	219.3	0.0051	0.0005	0.094	0.009	2667	248
		393.2	266.9	15.2	251.7	0.0044	0.0005	0.081	0.009	3557	386

0.300	0.001	303.5	7.8	2.3	5.5	0.0114	0.0004	0.063	0.003	32	5
		313.1	12.6	2.5	10.1	0.0112	0.0004	0.062	0.003	60	6
		323.1	21.7	2.7	19.0	0.0110	0.0005	0.061	0.003	115	7
		333.2	36.8	2.9	33.9	0.0106	0.0005	0.059	0.003	214	11
		343.1	59.3	3.2	56.1	0.0101	0.0005	0.056	0.003	376	19
		353.1	90.0	3.7	86.4	0.0094	0.0005	0.052	0.003	627	33
		373.2	169.2	6.0	163.3	0.0078	0.0005	0.043	0.003	1454	92
		393.2	257.4	11.1	246.3	0.0063	0.0005	0.035	0.003	2780	226

0.500	0.002	303.1	13.0	2.1	11.0	0.0200	0.0006	0.060	0.002	41	4
		323.2	39.9	2.3	37.5	0.0188	0.0007	0.056	0.002	151	6
		333.2	65.9	2.5	63.4	0.0177	0.0006	0.053	0.002	274	11
		343.2	101.5	2.7	98.9	0.0162	0.0006	0.048	0.002	471	20
		353.3	145.0	2.9	142.1	0.0144	0.0006	0.043	0.002	767	36
		363.1	192.3	3.3	189.0	0.0126	0.0006	0.037	0.002	1178	64
		373.2	239.7	4.0	235.7	0.0109	0.0006	0.032	0.002	1713	109
		383.2	283.9	5.3	278.6	0.0095	0.0007	0.028	0.002	2353	176
		393.1	324.3	7.3	317.0	0.0083	0.0007	0.024	0.002	3084	268
0.700	0.003	303.2	10.9	2.4	8.6	0.0132	0.0006	0.024	0.001	56	6
		313.6	21.1	2.6	18.5	0.0129	0.0006	0.024	0.001	126	9
		323.2	30.9	3.0	28.0	0.0125	0.0006	0.023	0.001	198	11
		333.2	50.4	3.2	47.2	0.0119	0.0006	0.022	0.001	355	19
		343.2	77.4	3.6	73.8	0.0110	0.0006	0.020	0.001	605	34
		353.2	110.7	4.0	106.8	0.0099	0.0006	0.018	0.001	975	61
		363.2	147.2	4.6	142.5	0.0089	0.0006	0.016	0.001	1472	103
		373.1	183.8	5.6	178.2	0.0079	0.0006	0.014	0.001	2090	166
		383.2	218.2	7.2	211.0	0.0070	0.0006	0.013	0.001	2796	252
		393.1	249.8	9.6	240.2	0.0063	0.0006	0.012	0.001	3549	358



0.900	0.005	303.1	18.5	1.6	16.8	0.0162	0.0006	0.0200	0.001	107	7
		323.2	53.9	2.0	51.9	0.0147	0.0007	0.0181	0.001	370	19
		333.2	83.4	2.1	81.2	0.0135	0.0007	0.0166	0.001	635	35
		343.2	119.0	2.3	116.7	0.0122	0.0007	0.0149	0.001	1024	62
		353.2	156.7	2.6	154.1	0.0108	0.0007	0.0132	0.001	1535	105
		363.2	192.5	3.1	189.5	0.0096	0.0007	0.0118	0.001	2139	166
		373.2	224.9	3.7	221.1	0.0085	0.0007	0.0104	0.001	2840	251
		383.2	253.3	4.8	248.5	0.0079	0.0007	0.0097	0.001	3465	333
		393.1	278.1	6.4	271.7	0.0071	0.0007	0.0087	0.001	4260	460
1.000	0.006	303.1	25.0	2.6	22.4	0.0160	0.0007	0.016	0.001	159	10
		313.3	42.9	2.8	40.1	0.0152	0.0007	0.015	0.001	302	17
		323.2	67.2	3.0	64.2	0.0141	0.0007	0.014	0.001	525	30
		333.2	98.4	3.2	95.2	0.0128	0.0007	0.013	0.001	868	54
		343.2	132.5	3.4	129.2	0.0114	0.0007	0.012	0.001	1331	93
		353.2	165.6	3.5	162.1	0.0102	0.0008	0.010	0.001	1888	149
		363.2	195.2	3.8	191.4	0.0092	0.0008	0.009	0.001	2494	219
		373.2	221.0	4.3	216.7	0.0085	0.0008	0.009	0.001	3103	300
		383.2	243.3	5.0	238.3	0.0079	0.0008	0.008	0.001	3681	383

393.1 263.2 6.1 257.2 0.0075 0.0007 0.008 0.001 4224 466

<sup>a</sup> Standard uncertainties are reported (level of confidence 0.68). Standard uncertainty for temperature is  $u(T) = 0.1$  K, for total and residual pressure is  $u(P_{\text{tot}}) = u(P_{\text{res}}) = 0.9$  kPa and for CO<sub>2</sub> pressure is  $u(P_{\text{CO}_2}) = 1.3$  kPa.

**Table A. 3:** Measured mole fraction solubility  $x_{\text{CO}_2}$ , loading  $\alpha$  and Henry's constant  $H$  for CO<sub>2</sub> in MDEA (1) – MEG (2) blends as a function of weight fraction  $w$  of unloaded solvent and pressure (total pressure  $P_{\text{tot}}$ , residual pressure  $P_{\text{res}}$  and their difference, CO<sub>2</sub> partial pressure  $P_{\text{CO}_2}$ ) at temperatures of 313 K and 343 K.<sup>a</sup>

$w_1$	$u(w_1)$	$T$	$P_{\text{tot}}$	$P_{\text{res}}$	$P_{\text{CO}_2}$	$x_{\text{CO}_2}$	$u(x_{\text{CO}_2})$	$\alpha$	$u(\alpha)$	$H$	$u(H)$
		K	kPa	kPa	kPa			mol <sub>CO<sub>2</sub></sub> mol <sup>-1</sup>		kPa m <sup>3</sup> kmol <sup>-1</sup>	
0.000	0.000	313.1	66.0	2.2	63.8	0.0011	0.0005	-	-	3188	1560
		313.2	133.9	2.2	131.7	0.0023	0.0008	-	-	3187	1074
		313.1	194.3	2.2	192.1	0.0034	0.0008	-	-	3158	737
		313.2	254.4	2.2	252.1	0.0045	0.0008	-	-	3145	572
		313.2	315.8	2.2	313.5	0.0056	0.0008	-	-	3157	480
		313.2	367.8	2.2	365.6	0.0065	0.0009	-	-	3173	436
		313.1	413.6	2.2	411.4	0.0072	0.0009	-	-	3186	407
		313.1	456.6	2.2	454.4	0.0079	0.0009	-	-	3209	387
		313.1	503.9	2.2	501.7	0.0087	0.0009	-	-	3219	366

343.2	61.9	2.9	59.1	0.0007	0.0005	-	-	4663	3299		
343.1	113.3	2.9	110.4	0.0014	0.0007	-	-	4663	2502		
343.2	152.4	2.9	149.5	0.0018	0.0007	-	-	4667	1865		
343.2	200.0	2.9	197.1	0.0024	0.0007	-	-	4676	1437		
343.2	251.5	2.9	248.7	0.0030	0.0007	-	-	4691	1169		
343.2	305.1	2.9	302.3	0.0037	0.0008	-	-	4721	999		
343.2	348.7	2.9	345.9	0.0042	0.0008	-	-	4704	897		
343.1	400.2	2.9	397.4	0.0048	0.0008	-	-	4701	809		
343.1	455.3	2.9	452.5	0.0055	0.0008	-	-	4739	750		
343.2	505.3	2.9	502.4	0.0061	0.0009	-	-	4742	703		
343.1	548.2	2.9	545.4	0.0066	0.0009	-	-	4738	669		
0.500	0.002	313.1	14.1	2.1	11.9	0.0129	0.0006	0.038	0.002	70	6
		313.1	29.4	2.1	27.2	0.0238	0.0008	0.071	0.003	86	4
		313.1	53.4	2.1	51.2	0.0380	0.0009	0.115	0.003	99	4
		313.1	78.7	2.1	76.5	0.0505	0.0009	0.155	0.004	110	3
		313.2	108.2	2.1	106.0	0.0631	0.0010	0.197	0.005	121	3
		313.2	137.8	2.1	135.6	0.0739	0.0010	0.233	0.005	130	3
		313.2	167.1	2.1	164.9	0.0833	0.0010	0.265	0.006	139	3
		313.2	196.0	2.1	193.9	0.0916	0.0011	0.294	0.006	147	3

313.2	226.6	2.1	224.5	0.0994	0.0011	0.322	0.007	156	4		
313.2	258.6	2.1	256.4	0.1066	0.0012	0.349	0.007	164	4		
313.1	286.7	2.1	284.6	0.1126	0.0012	0.371	0.007	172	4		
313.2	314.8	2.1	312.6	0.1182	0.0013	0.391	0.008	179	4		
313.2	342.3	2.1	340.2	0.1231	0.0014	0.410	0.008	186	4		
313.2	370.0	2.1	367.9	0.1276	0.0014	0.427	0.008	193	4		
313.2	395.0	2.1	392.8	0.1315	0.0015	0.442	0.009	199	4		
313.2	417.4	2.1	415.2	0.1348	0.0015	0.455	0.009	204	5		
1.000	0.006	313.1	27.9	2.3	25.6	0.0099	0.0010	0.010	0.001	296	34
		313.1	45.8	2.3	43.6	0.0161	0.0014	0.016	0.002	309	30
		313.1	75.1	2.3	72.8	0.0259	0.0017	0.027	0.002	318	23
		313.1	98.3	2.3	96.0	0.0337	0.0019	0.035	0.002	320	20
		313.2	139.8	2.3	137.5	0.0472	0.0020	0.050	0.002	323	16
		313.2	169.4	2.3	167.1	0.0565	0.0021	0.060	0.003	324	15
		313.1	211.6	2.3	209.3	0.0689	0.0021	0.074	0.003	329	13
		313.1	250.4	2.3	248.2	0.0796	0.0021	0.086	0.003	334	13
		313.2	284.1	2.3	281.8	0.0881	0.0022	0.097	0.003	339	12
		313.2	315.3	2.3	313.0	0.0956	0.0022	0.106	0.004	344	12
		313.1	349.2	2.3	346.9	0.1031	0.0023	0.115	0.004	351	12

343.1	58.2	4.3	54.0	0.0059	0.0011	0.006	0.001	1078	198
343.2	101.7	4.3	97.4	0.0103	0.0015	0.010	0.002	1110	164
343.1	130.2	4.3	125.9	0.0132	0.0018	0.013	0.002	1120	159
343.2	173.2	4.3	169.0	0.0174	0.0020	0.018	0.002	1132	140
343.2	222.9	4.3	218.6	0.0222	0.0022	0.023	0.002	1144	124
343.1	247.8	4.3	243.6	0.0248	0.0024	0.025	0.003	1138	122
343.2	301.9	4.3	297.6	0.0298	0.0026	0.031	0.003	1150	111
343.2	351.0	4.3	346.8	0.0344	0.0027	0.036	0.003	1159	105
343.2	372.5	4.3	368.3	0.0364	0.0029	0.038	0.003	1160	106

<sup>a</sup> Standard uncertainties are reported (level of confidence 0.68). Standard uncertainty for temperature is  $u(T) = 0.1$  K, for total and residual pressure is  $u(P_{\text{tot}}) = u(P_{\text{res}}) = 0.9$  kPa and for CO<sub>2</sub> pressure is  $u(P_{\text{CO}_2}) = 1.3$  kPa.

**Table A. 4:** Measured mole fraction solubility  $x_{\text{CO}_2}$ , loading  $\alpha$  and Henry's constant  $H$  for  $\text{CO}_2$  in MDEA (1) – MEG (2) –  $\text{H}_2\text{O}$  (3) blends in two repeated experiments as a function of weight fraction  $w$  of unloaded solvent, temperature  $T$  and pressure (total pressure  $P_{\text{tot}}$ , residual pressure  $P_{\text{res}}$  and their difference,  $\text{CO}_2$  partial pressure  $P_{\text{CO}_2}$ ).<sup>a</sup> Experiment A denotes the first experiment, also tabulated in Table A. 2 for MDEA-MEG systems and in Table A. 5 for MDEA-MEG- $\text{H}_2\text{O}$  system. Experiment B is the repeated experiment.

$w_1$	$u(w_1)$	$w_2$	$u(w_2)$	$T$	$P_{\text{tot}}$	$P_{\text{res}}$	$P_{\text{CO}_2}$	$x_{\text{CO}_2}$	$u(x_{\text{CO}_2})$	$\alpha$	$u(\alpha)$	$H$	$u(H)$
				K	kPa	kPa	kPa			$\text{mol}_{\text{CO}_2} \cdot \text{mol}^{-1}_{\text{MDEA}}$		$\text{kPa m}^3 \text{kmol}^{-1}$	
0.000	0.000	1.000	0.006					Experiment A					
				303.2	200.5	2.3	198.2	0.0039	0.0004	-	-	2835	284
				313.7	223.8	2.5	221.3	0.0036	0.0004	-	-	3498	389
				323.2	236.8	2.8	234.0	0.0035	0.0004	-	-	3833	440
				333.2	253.9	3.1	250.8	0.0033	0.0004	-	-	4355	530
				343.2	270.4	3.5	266.9	0.0031	0.0004	-	-	4875	624
				353.2	286.3	3.9	282.4	0.0030	0.0004	-	-	5393	720
				363.2	301.7	4.5	297.2	0.0029	0.0004	-	-	5907	820
				373.1	317.2	5.5	311.7	0.0028	0.0004	-	-	6406	918
				383.2	332.8	7.1	325.7	0.0028	0.0004	-	-	6886	1013
				393.2	348.7	9.6	339.1	0.0027	0.0004	-	-	7333	1100

Experiment B									
303.2	207.2	2.0	205.2	0.0042	0.0006	-	-	2749	376
313.2	223.1	2.2	220.9	0.0039	0.0006	-	-	3222	478
333.2	252.7	2.6	250.1	0.0034	0.0006	-	-	4217	720
353.2	280.0	3.7	276.3	0.0031	0.0006	-	-	5183	977
373.2	306.7	5.7	300.9	0.0029	0.0006	-	-	6139	1251
393.2	334.8	10.9	323.9	0.0027	0.0006	-	-	6991	1495

0.050 0.001 0.950 0.001

Experiment A									
303.2	42.9	1.8	41.1	0.0141	0.0005	0.535	0.024	166	8
313.1	66.2	1.9	64.3	0.0132	0.0005	0.501	0.024	279	13
323.2	97.6	2.0	95.6	0.0121	0.0005	0.458	0.024	457	22
333.1	134.0	2.2	131.8	0.0108	0.0005	0.411	0.023	709	38
343.2	173.2	2.4	170.8	0.0096	0.0005	0.363	0.023	1048	63
353.2	212.5	2.8	209.7	0.0084	0.0006	0.318	0.023	1479	103
363.2	250.1	3.4	246.7	0.0074	0.0006	0.279	0.023	2001	161
373.1	285.4	4.4	281.0	0.0065	0.0006	0.246	0.023	2610	241
383.1	319.2	5.8	313.4	0.0058	0.0006	0.217	0.023	3321	352
393.2	354.4	8.1	346.4	0.0050	0.0006	0.190	0.024	4239	521

## Experiment B

313.2	64.5	16.7	62.8	0.0128	0.0005	0.487	0.023	281	13
323.2	96.5	17.6	94.8	0.0117	0.0005	0.445	0.023	467	22
333.2	133.8	19.8	131.8	0.0105	0.0005	0.398	0.023	732	39
343.2	173.6	22.5	171.4	0.0093	0.0005	0.351	0.023	1088	66
353.2	214.0	27.6	211.2	0.0081	0.0005	0.307	0.023	1546	109
363.2	252.6	35.1	249.1	0.0071	0.0006	0.268	0.023	2104	172
373.2	288.4	45.3	283.9	0.0062	0.0006	0.236	0.023	2750	259
383.1	321.3	61.6	315.1	0.0056	0.0006	0.209	0.023	3463	371
393.1	352.4	84.9	343.9	0.0050	0.0006	0.188	0.023	4248	513

0.100 0.001 0.900 0.001

## Experiment A

303.2	10.7	1.9	8.8	0.0096	0.0004	0.178	0.008	53	6
313.2	18.8	2.2	16.5	0.0094	0.0004	0.174	0.008	103	7
323.2	32.1	2.5	29.7	0.0091	0.0004	0.168	0.008	193	11
333.1	52.3	2.8	49.5	0.0086	0.0004	0.159	0.008	342	19
343.2	79.9	3.5	76.4	0.0080	0.0004	0.147	0.008	575	33
353.1	113.6	4.6	109.0	0.0073	0.0004	0.134	0.009	909	58
363.1	151.3	5.9	145.4	0.0065	0.0004	0.120	0.009	1365	97
373.1	190.6	8.0	182.6	0.0058	0.0004	0.106	0.009	1948	158



383.3	230.1	10.8	219.3	0.0051	0.0005	0.094	0.009	2667	248
393.2	266.9	15.2	251.7	0.0044	0.0005	0.081	0.009	3557	386

Experiment B

303.2	13.0	2.2	10.8	0.0108	0.0004	0.200	0.009	58	5
323.2	40.1	2.6	37.4	0.0102	0.0004	0.188	0.008	218	11
343.2	97.4	3.2	94.2	0.0088	0.0004	0.163	0.008	639	33
353.2	135.8	3.6	132.1	0.0080	0.0004	0.148	0.008	996	56

0.300 0.001 0.700 0.001

Experiment A

303.5	7.8	2.3	5.5	0.0114	0.0004	0.063	0.003	32	5
313.1	12.6	2.5	10.1	0.0112	0.0004	0.062	0.003	60	6
323.1	21.7	2.7	19.0	0.0110	0.0005	0.061	0.003	115	7
333.2	36.8	2.9	33.9	0.0106	0.0005	0.059	0.003	214	11
343.1	59.3	3.2	56.1	0.0101	0.0005	0.056	0.003	376	19
353.1	90.0	3.7	86.4	0.0094	0.0005	0.052	0.003	627	33
373.2	169.2	6.0	163.3	0.0078	0.0005	0.043	0.003	1454	92
393.2	257.4	11.1	246.3	0.0063	0.0005	0.035	0.003	2780	226

Experiment B

303.2	7.5	2.4	5.1	0.0120	0.0005	0.067	0.003	28	5
323.2	22.7	3.0	19.7	0.0116	0.0005	0.064	0.003	113	7
343.2	62.5	3.9	58.7	0.0106	0.0005	0.059	0.003	376	19
353.1	94.8	4.7	90.1	0.0098	0.0005	0.054	0.003	628	33

0.500 0.002 0.500 0.002

Experiment A

303.1	13.0	2.1	11.0	0.0200	0.0006	0.060	0.002	41	4
323.2	39.87	2.3	37.5	0.0188	0.0007	0.056	0.002	151	6
333.2	65.9	2.5	63.4	0.0177	0.0006	0.053	0.002	274	11
343.2	101.5	2.7	98.9	0.0162	0.0006	0.048	0.002	471	20
353.3	145.0	2.9	142.1	0.0144	0.0006	0.043	0.002	767	36
363.1	192.3	3.3	189.0	0.0126	0.0006	0.037	0.002	1178	64
373.2	239.7	4.0	235.7	0.0109	0.0006	0.032	0.002	1713	109
383.2	283.9	5.3	278.6	0.0095	0.0007	0.028	0.002	2353	176
393.1	324.3	7.3	317.0	0.0083	0.0007	0.024	0.002	3084	268

Experiment B

303.1	12.5	2.1	10.4	0.0197	0.0006	0.059	0.002	39	4
313.1	22.3	2.2	20.1	0.0192	0.0006	0.057	0.002	79	4
323.1	38.9	2.2	36.6	0.0185	0.0006	0.055	0.002	150	7

343.2	100.4	2.5	98.0	0.0160	0.0006	0.048	0.002	470	20
353.1	144.4	2.7	141.6	0.0144	0.0006	0.043	0.002	766	36
363.2	193.2	3.2	190.0	0.0126	0.0006	0.037	0.002	1182	63
373.2	242.9	4.1	238.8	0.0110	0.0006	0.032	0.002	1727	107
383.1	288.8	5.5	283.4	0.0096	0.0006	0.028	0.002	2372	171
393.1	330.9	7.7	323.2	0.0084	0.0007	0.025	0.002	3100	259

0.300 0.001 0.400 0.001

Experiment A

303.1	5.3	3.3	2.0	0.0065	0.0002	0.066	0.003	11	5
313.1	8.5	5.4	3.0	0.0064	0.0002	0.066	0.003	17	5
323.2	13.8	8.6	5.1	0.0064	0.0002	0.066	0.003	29	5
343.2	36.5	21.1	15.4	0.0062	0.0003	0.064	0.003	92	7
353.2	57.9	31.9	26.0	0.0061	0.0002	0.062	0.003	162	9
363.1	89.1	46.7	42.4	0.0058	0.0002	0.059	0.003	277	15
373.2	133.0	66.4	66.5	0.0054	0.0002	0.056	0.003	467	25
383.2	190.6	94.2	96.5	0.0050	0.0002	0.051	0.003	740	42
393.1	262.1	131.6	130.5	0.0046	0.0002	0.047	0.003	1112	68

Experiment B

313.4	7.9	5.3	2.6	0.0049	0.0002	0.050	0.002	19	7
-------	-----	-----	-----	--------	--------	-------	-------	----	---

323.1	12.4	8.7	3.7	0.0048	0.0002	0.050	0.002	28	7
333.1	19.8	13.7	6.0	0.0048	0.0002	0.049	0.002	46	7
343.2	31.5	21.2	10.4	0.0048	0.0002	0.049	0.002	81	8
353.1	49.6	32.0	17.6	0.0047	0.0002	0.048	0.002	142	10
363.1	75.9	47.2	28.7	0.0045	0.0002	0.046	0.002	240	15
373.2	113.7	67.3	46.4	0.0043	0.0002	0.044	0.002	409	24
383.2	164.7	94.3	70.4	0.0041	0.0002	0.042	0.002	667	7
393.2	230.9	131.7	99.2	0.0038	0.0002	0.038	0.002	1022	41

<sup>a</sup> Standard uncertainties are reported (level of confidence 0.68). Standard uncertainty for temperature is  $u(T) = 0.1$  K, for total and residual pressure is  $u(P_{\text{tot}}) = u(P_{\text{res}}) = 0.9$  kPa and for CO<sub>2</sub> pressure is  $u(P_{\text{CO}_2}) = 1.3$  kPa.

**Table A. 5:** Measured mole fraction solubility  $x_{\text{CO}_2}$ , loading  $\alpha$  and Henry's constant  $H$  for CO<sub>2</sub> in MDEA (1) – MEG (2) – H<sub>2</sub>O (3) blends as a function of weight fraction  $w$  of unloaded solvent, temperature  $T$  and pressure (total pressure  $P_{\text{tot}}$ , residual pressure  $P_{\text{res}}$  and their difference, CO<sub>2</sub> partial pressure  $P_{\text{CO}_2}$ ).<sup>a</sup>

$w_1$	$u(w_1)$	$w_2$	$u(w_2)$	$T$	$P_{\text{tot}}$	$P_{\text{res}}$	$P_{\text{CO}_2}$	$x_{\text{CO}_2}$	$u(x_{\text{CO}_2})$	$\alpha$	$u(\alpha)$	$H$	$u(H)$
				K	kPa	kPa	kPa			mol <sub>CO<sub>2</sub></sub> mol <sup>-1</sup> <sub>MDEA</sub>		kPa m <sup>3</sup> kmol <sup>-1</sup>	
0.300	0.001	0.599	0.001	303.2	5.5	2.4	3.1	0.0084	0.0003	0.059	0.002	19	6
				313.0	9.0	3.5	5.5	0.0083	0.0003	0.059	0.002	35	6
				323.1	15.3	5.1	10.2	0.0082	0.0003	0.058	0.002	65	6

333.2	26.0	7.5	18.5	0.0080	0.0003	0.057	0.002	121	8
343.2	43.1	11.1	32.0	0.0078	0.0003	0.055	0.002	219	12
353.2	68.7	16.3	52.4	0.0074	0.0003	0.052	0.002	380	19
363.2	103.2	23.7	79.5	0.0069	0.0003	0.049	0.003	622	33
373.2	147.5	33.9	113.7	0.0063	0.0003	0.045	0.003	979	56
383.2	199.9	47.7	152.2	0.0057	0.0003	0.040	0.003	1468	95
393.1	257.7	66.3	191.4	0.0051	0.0004	0.036	0.003	2080	153
0.300	0.001	0.400	0.001	0.001	0.001	0.001	0.001	0.001	0.001
303.1	5.3	3.3	2.0	0.0065	0.0002	0.066	0.002	11	5
313.1	8.5	5.4	3.0	0.0064	0.0002	0.066	0.002	17	5
323.2	13.8	8.6	5.1	0.0064	0.0002	0.066	0.002	29	5
343.2	36.5	21.1	15.4	0.0062	0.0002	0.064	0.002	92	7
353.2	57.9	31.9	26.0	0.0061	0.0002	0.062	0.002	162	9
363.1	89.1	46.7	42.4	0.0058	0.0002	0.059	0.002	277	15
373.2	133.0	66.4	66.5	0.0054	0.0002	0.056	0.002	467	25
383.2	190.6	94.2	96.5	0.0050	0.0002	0.051	0.002	740	42
393.1	262.1	131.6	130.5	0.0046	0.0002	0.047	0.002	1112	68
0.300	0.002	0.200	0.002	0.002	0.002	0.002	0.002	0.002	0.002
303.1	5.1	4.2	1.0	0.0067	0.0003	0.048	0.003	8	7
313.1	8.1	6.9	1.2	0.0067	0.0003	0.048	0.003	9	7

323.1	12.8	11.0	1.8	0.0067	0.0003	0.048	0.003	14	7
343.2	31.8	26.9	4.9	0.0067	0.0003	0.047	0.003	40	8
353.1	48.8	40.5	8.3	0.0066	0.0003	0.047	0.003	69	8
363.1	73.3	59.6	13.6	0.0065	0.0003	0.046	0.003	116	10
373.2	108.4	85.9	22.5	0.0063	0.0003	0.045	0.003	199	14
383.2	156.8	121.1	35.7	0.0061	0.0003	0.043	0.003	329	22
393.1	221.4	168.0	53.4	0.0058	0.0004	0.041	0.003	522	36

<sup>a</sup> Standard uncertainties are reported (level of confidence 0.68). Standard uncertainty for temperature is  $u(T) = 0.1$  K, for total and residual pressure is  $u(P_{\text{tot}}) = u(P_{\text{res}}) = 0.9$  kPa and for CO<sub>2</sub> pressure is  $u(P_{\text{CO}_2}) = 1.3$  kPa.

**Table A. 6:** Measured mole fraction solubility  $x_{\text{CO}_2}$ , loading  $\alpha$  and Henry's constant  $H$  for CO<sub>2</sub> in MDEA (1) – MEG (2) – H<sub>2</sub>O (3) blends as a function of weight fraction  $w$  of unloaded solvent and pressure (total pressure  $P_{\text{tot}}$ , residual pressure  $P_{\text{res}}$  and their difference, CO<sub>2</sub> partial pressure  $P_{\text{CO}_2}$ ) at temperatures of 313 K and 343 K.<sup>a</sup>

$w_1$	$u(w_1)$	$w_2$	$u(w_2)$	$T$	$P_{\text{tot}}$	$P_{\text{res}}$	$P_{\text{CO}_2}$	$x_{\text{CO}_2}$	$u(x_{\text{CO}_2})$	$\alpha$	$u(\alpha)$	$H$	$u(H)$
				K	kPa	kPa	kPa	-	-	mol <sub>CO<sub>2</sub></sub> mol <sup>-1</sup> <sub>MDEA</sub>	mol <sub>CO<sub>2</sub></sub> mol <sup>-1</sup> <sub>MDEA</sub>	kPa m <sup>3</sup> kmol <sup>-1</sup>	kPa m <sup>3</sup> kmol <sup>-1</sup>
0.300	0.001	0.599	0.001	313.2	8.1	5.1	3.0	0.0044	0.0005	0.031	0.004	36	12
				313.2	27.2	5.1	22.1	0.0123	0.0007	0.088	0.005	93	7
				313.1	34.8	5.1	29.7	0.0168	0.0008	0.120	0.006	91	6
				313.1	47.1	5.1	42.0	0.0242	0.0009	0.175	0.007	89	4

313.1	55.6	5.1	50.5	0.0285	0.0009	0.207	0.008	90	4
313.1	63.6	5.1	58.5	0.0322	0.0010	0.234	0.009	92	4
313.1	72.0	5.1	67.0	0.0357	0.0010	0.261	0.010	95	4
313.1	83.3	5.1	78.2	0.0392	0.0011	0.288	0.011	100	4
313.1	97.4	5.1	92.3	0.0442	0.0011	0.326	0.011	105	4
313.2	122.6	5.1	117.5	0.0516	0.0010	0.383	0.012	113	4
313.2	156.5	5.1	151.4	0.0596	0.0010	0.446	0.013	125	4
313.2	191.3	5.1	186.2	0.0661	0.0010	0.498	0.013	138	4
313.2	224.1	5.1	219.0	0.0711	0.0010	0.539	0.014	150	4
313.2	254.7	5.1	249.6	0.0751	0.0010	0.572	0.015	161	4
313.2	300.0	5.1	295.0	0.0801	0.0010	0.614	0.015	178	5
313.2	342.6	5.1	337.6	0.0844	0.0010	0.650	0.016	192	5
343.2	42.8	11.1	31.6	0.0081	0.0005	0.058	0.004	206	14
343.1	66.9	11.1	55.8	0.0119	0.0006	0.085	0.005	249	15
343.2	137.9	11.1	126.8	0.0205	0.0007	0.148	0.006	324	14
343.2	169.7	11.1	158.6	0.0238	0.0008	0.172	0.007	349	15
343.1	199.6	11.1	188.5	0.0266	0.0009	0.192	0.008	370	16
343.2	240.7	11.1	229.6	0.0301	0.0009	0.218	0.009	396	16
343.2	287.3	11.1	276.2	0.0338	0.0010	0.246	0.010	423	17

343.1	340.2	11.1	329.1	0.0375	0.0010	0.275	0.010	452	17
343.1	389.9	11.1	378.8	0.0408	0.0010	0.300	0.011	477	18
343.2	427.0	11.1	415.9	0.0434	0.0011	0.319	0.011	491	18
343.1	457.5	11.1	446.4	0.0451	0.0011	0.333	0.012	506	19
343.2	484.1	11.1	473.0	0.0466	0.0011	0.344	0.013	518	19
343.1	517.1	11.1	506.0	0.0484	0.0011	0.358	0.013	533	20
0.300	0.001	0.400	0.001						
313.1	6.5	5.5	1.0	0.0034	0.0003	0.034	0.003	11	10
313.1	10.3	5.5	4.8	0.0095	0.0004	0.097	0.004	18	4
313.2	15.0	5.5	9.5	0.0146	0.0004	0.151	0.005	23	2
313.1	26.2	5.5	20.7	0.0243	0.0004	0.254	0.006	30	2
313.1	36.2	5.5	30.7	0.0306	0.0004	0.321	0.007	36	1
313.2	46.5	5.5	40.9	0.0356	0.0005	0.376	0.008	41	1
313.1	54.8	5.5	49.3	0.0391	0.0005	0.414	0.009	45	1
313.1	67.5	5.5	62.0	0.0436	0.0005	0.464	0.009	50	1
313.1	86.4	5.5	80.8	0.0489	0.0005	0.523	0.010	58	1
313.1	114.2	5.5	108.6	0.0547	0.0005	0.589	0.011	69	1
313.1	148.4	5.5	142.8	0.0599	0.0005	0.648	0.011	82	2
313.2	189.3	5.5	183.8	0.0644	0.0006	0.701	0.012	98	2
313.1	219.8	5.5	214.3	0.0671	0.0006	0.731	0.012	110	2



313.1	273.7	5.5	268.2	0.0707	0.0006	0.774	0.013	130	2
313.1	325.8	5.5	320.2	0.0733	0.0007	0.805	0.013	149	3
313.2	381.3	5.5	375.7	0.0756	0.0007	0.832	0.014	169	3
313.2	427.5	5.5	421.9	0.0771	0.0007	0.850	0.014	186	3
313.2	477.7	5.5	472.1	0.0785	0.0007	0.867	0.014	204	4
313.2	513.3	5.5	507.7	0.0794	0.0007	0.878	0.015	217	4
343.1	29.2	20.3	8.9	0.0048	0.0003	0.049	0.004	70	9
343.1	55.4	20.3	35.0	0.0111	0.0004	0.114	0.005	117	6
343.1	91.4	20.3	71.1	0.0173	0.0005	0.179	0.006	152	6
343.1	137.5	20.3	117.2	0.0233	0.0005	0.243	0.007	184	6
343.1	173.5	20.3	153.2	0.0272	0.0006	0.285	0.008	206	6
343.2	199.8	20.3	179.5	0.0298	0.0006	0.312	0.009	220	7
343.2	248.2	20.3	227.9	0.0339	0.0006	0.357	0.010	244	7
343.2	287.4	20.3	267.1	0.0368	0.0006	0.388	0.011	263	7
343.1	339.7	20.3	319.4	0.0402	0.0006	0.426	0.011	287	8
343.2	397.8	20.3	377.5	0.0435	0.0006	0.462	0.012	312	8
343.2	447.1	20.3	426.8	0.0459	0.0007	0.489	0.013	333	9
343.1	490.3	20.3	470.0	0.0480	0.0007	0.513	0.013	350	9
343.1	512.0	20.3	491.7	0.0488	0.0007	0.523	0.014	360	10

0.300	0.002	0.200	0.002	313.2	8.2	6.8	1.4	0.0061	0.0002	0.082	0.003	6	4
				313.1	11.7	6.8	4.9	0.0128	0.0003	0.173	0.005	11	2
				313.2	17.2	6.8	10.4	0.0197	0.0003	0.267	0.006	15	1
				313.1	29.4	6.8	22.6	0.0293	0.0003	0.402	0.007	21	1
				313.1	54.6	6.8	47.8	0.0399	0.0003	0.553	0.008	33	1
				313.1	97.5	6.8	90.7	0.0490	0.0004	0.685	0.009	50	1
				313.1	155.9	6.8	149.1	0.0550	0.0005	0.775	0.010	73	1
				313.1	220.3	6.8	213.5	0.0587	0.0005	0.830	0.011	98	2
				313.2	292.1	6.8	285.3	0.0613	0.0006	0.870	0.011	125	2
				313.2	379.6	6.8	372.8	0.0634	0.0006	0.901	0.012	157	2
				313.1	440.6	6.8	433.8	0.0645	0.0006	0.918	0.012	179	3
				313.1	501.8	6.8	495.0	0.0654	0.0006	0.931	0.013	202	3
				343.2	32.2	26.6	5.6	0.0043	0.0002	0.058	0.003	38	6
				343.1	45.0	26.6	18.4	0.0091	0.0003	0.122	0.005	59	4
				343.2	67.8	26.6	41.2	0.0147	0.0003	0.198	0.006	80	3
				343.1	124.3	26.6	97.7	0.0233	0.0004	0.318	0.007	119	4
				343.2	154.9	26.6	128.3	0.0270	0.0004	0.369	0.007	135	3
				343.2	192.0	26.6	165.4	0.0306	0.0004	0.420	0.008	152	3

343.2	240.7	26.6	214.1	0.0345	0.0004	0.476	0.009	174	4
343.2	290.3	26.6	263.7	0.0378	0.0004	0.523	0.010	195	4
343.2	338.3	26.6	311.7	0.0404	0.0004	0.560	0.010	216	4
343.2	391.9	26.6	365.3	0.0429	0.0004	0.596	0.011	237	5
343.2	446.5	26.6	419.9	0.0450	0.0004	0.627	0.011	259	5
343.1	484.5	26.6	457.9	0.0463	0.0004	0.647	0.012	274	5
343.1	518.1	26.6	491.5	0.0474	0.0004	0.662	0.012	288	6

<sup>a</sup> Standard uncertainties are reported (level of confidence 0.68). Standard uncertainty for temperature is  $u(T) = 0.1$  K, for total and residual pressure is  $u(P_{\text{tot}}) = u(P_{\text{res}}) = 0.9$  kPa and for CO<sub>2</sub> pressure is  $u(P_{\text{CO}_2}) = 1.3$  kPa.

**Table A. 7:** Measured mole fraction solubility  $x_{\text{CO}_2}$ , loading  $\alpha$  and Henry's constant  $H$  for CO<sub>2</sub> in MDEA (1) – H<sub>2</sub>O (3) blends as a function of weight fraction  $w$  of unloaded solvent and pressure (total pressure  $P_{\text{tot}}$ , residual pressure  $P_{\text{res}}$  and their difference, CO<sub>2</sub> partial pressure  $P_{\text{CO}_2}$ ) at temperatures of 313 K and 343 K.<sup>a</sup>

$w_1$	$u(w_1)$	$T$	$P_{\text{tot}}$	$P_{\text{res}}$	$P_{\text{CO}_2}$	$x_{\text{CO}_2}$	$u(x_{\text{CO}_2})$	$\alpha$	$u(\alpha)$	$H$	$u(H)$
		K	kPa	kPa	kPa			mol <sub>CO<sub>2</sub></sub> mol <sup>-1</sup> <sub>MDEA</sub>		kPa m <sup>3</sup> kmol <sup>-1</sup>	
0.700	0.006	313.1	9.3	5.1	4.2	0.0089	0.0003	0.034	0.004	20	4
		313.2	27.4	5.1	22.3	0.0416	0.0004	0.166	0.007	22	1
		313.2	51.2	5.1	46.1	0.0674	0.0008	0.277	0.009	27	1
		313.1	81.3	5.1	76.2	0.0935	0.0014	0.396	0.012	31	1

313.1	117.0	5.1	111.9	0.1119	0.0020	0.483	0.013	38	1		
313.2	162.3	5.1	157.2	0.1283	0.0026	0.564	0.015	45	1		
313.1	197.8	5.1	192.7	0.1373	0.0030	0.610	0.016	51	1		
313.1	261.8	5.1	256.7	0.1495	0.0036	0.674	0.017	62	1		
313.1	307.9	5.1	302.8	0.1558	0.0040	0.708	0.017	70	1		
313.1	353.9	5.1	348.9	0.1611	0.0042	0.736	0.018	77	1		
313.1	423.3	5.1	418.2	0.1672	0.0046	0.770	0.019	88	1		
313.1	477.1	5.1	472.0	0.1710	0.0048	0.791	0.020	97	1		
343.1	87.0	23.2	63.8	0.0208	0.0003	0.081	0.001	131	3		
343.1	163.7	23.2	140.5	0.0365	0.0003	0.145	0.002	161	2		
343.1	239.6	23.2	216.5	0.0491	0.0005	0.198	0.003	182	2		
343.1	310.5	23.2	287.4	0.0590	0.0006	0.241	0.003	199	2		
343.1	371.3	23.2	348.1	0.0665	0.0007	0.273	0.004	212	2		
343.2	425.9	23.2	402.8	0.0721	0.0008	0.298	0.004	225	3		
343.1	467.7	23.2	444.5	0.0763	0.0009	0.317	0.005	234	3		
343.2	499.6	23.2	476.4	0.0794	0.0010	0.331	0.005	240	3		
0.900	0.006	313.1	25.0	4.2	20.8	0.0179	0.0005	0.032	0.001	83	4
		313.2	65.1	4.2	60.9	0.0437	0.0007	0.079	0.002	98	3

313.1	111.6	4.2	107.3	0.0678	0.0010	0.126	0.003	108	2
313.1	134.5	4.2	130.2	0.0785	0.0012	0.148	0.003	112	2
313.1	178.7	4.2	174.4	0.0956	0.0015	0.183	0.003	121	2
313.2	206.7	4.2	202.4	0.1039	0.0018	0.201	0.004	128	2
313.1	247.0	4.2	242.8	0.1189	0.0022	0.234	0.004	132	2
313.1	277.5	4.2	273.2	0.1253	0.0025	0.248	0.004	140	2
313.1	313.7	4.2	309.4	0.1368	0.0029	0.275	0.005	143	2
313.2	340.4	4.2	336.2	0.1415	0.0031	0.286	0.005	150	2
313.1	377.5	4.2	373.3	0.1500	0.0035	0.306	0.005	155	2
313.1	410.6	4.2	406.4	0.1571	0.0038	0.323	0.005	160	2
313.2	445.0	4.2	440.8	0.1627	0.0041	0.337	0.006	166	2
313.2	474.4	4.2	470.2	0.1674	0.0044	0.349	0.006	172	3
343.1	78.7	13.5	65.2	0.0051	0.0005	0.009	0.001	946	103
343.2	127.0	13.5	113.6	0.0166	0.0007	0.029	0.001	505	24
343.1	150.9	13.5	137.4	0.0195	0.0008	0.035	0.002	518	25
343.1	255.9	13.5	242.5	0.0317	0.0009	0.057	0.002	557	19
343.1	332.2	13.5	318.8	0.0398	0.0009	0.072	0.002	578	18
343.1	404.1	13.5	390.6	0.0471	0.0010	0.086	0.003	593	17
343.1	436.3	13.5	422.9	0.0502	0.0010	0.092	0.003	600	17

343.1	464.5	13.5	451.0	0.0529	0.0011	0.097	0.003	606	18
343.1	488.8	13.5	475.3	0.0551	0.0011	0.101	0.003	612	18

<sup>a</sup> Standard uncertainties are reported (level of confidence 0.68). Standard uncertainty for temperature is  $u(T) = 0.1$  K, for total and residual pressure is  $u(P_{\text{tot}}) = u(P_{\text{res}}) = 0.9$  kPa and for CO<sub>2</sub> pressure is  $u(P_{\text{CO}_2}) = 1.3$  kPa.

**Table A. 8:** Measured mole fraction solubility  $x_{\text{CO}_2}$ , loading  $a$  and Henry's constant  $H$  for CO<sub>2</sub> in MDEA (1) – TEG (4) blends as a function of weight fraction  $w$  of unloaded solvent, temperature  $T$  and pressure (total pressure  $P_{\text{tot}}$ , residual pressure  $P_{\text{res}}$  and their difference, CO<sub>2</sub> partial pressure  $P_{\text{CO}_2}$ ).<sup>a</sup>

$w_1$	$u(w_1)$	$T$	$P_{\text{tot}}$	$P_{\text{res}}$	$P_{\text{CO}_2}$	$x_{\text{CO}_2}$	$u(x_{\text{CO}_2})$	$a$	$u(a)$	$H$	$u(H)$
		K	kPa	kPa	kPa			mol <sub>CO<sub>2</sub></sub> mol <sup>-1</sup> <sub>MDEA</sub>		kPa m <sup>3</sup> kmol <sup>-1</sup>	
0.000	0.000	303.1	192.5	2.3	190.3	0.0143	0.0010	-	-	1761	136
		313.1	212.2	2.3	209.9	0.0134	0.0011	-	-	2095	174
		323.1	231.3	2.4	228.9	0.0126	0.0011	-	-	2454	219
		333.1	249.6	2.6	247.1	0.0119	0.0011	-	-	2829	269
		343.2	267.3	2.7	264.6	0.0113	0.0011	-	-	3216	324
		353.2	284.3	3.0	281.3	0.0108	0.0011	-	-	3606	382
		363.1	300.7	3.3	297.3	0.0103	0.0011	-	-	3997	443
		373.2	316.7	3.7	313.0	0.0100	0.0011	-	-	4389	506
		383.2	332.2	4.3	327.8	0.0097	0.0011	-	-	4767	568

0.300	0.003	393.1	347.5	5.0	342.5	0.0095	0.0011	-	-	5148	632
		303.2	57.3	2.4	54.9	0.0256	0.0010	0.075	0.003	267	13
		313.1	95.0	2.5	92.5	0.0228	0.0010	0.067	0.003	510	26
		323.1	139.8	2.5	137.2	0.0198	0.0010	0.057	0.003	883	50
		333.1	183.8	2.5	181.3	0.0169	0.0010	0.049	0.003	1377	92
		343.2	222.6	2.5	220.1	0.0146	0.0010	0.042	0.003	1951	151
		353.2	255.1	2.6	252.5	0.0129	0.0010	0.037	0.003	2557	226
		363.1	282.0	2.8	282.0	0.0115	0.0011	0.033	0.003	3231	323
		373.2	304.9	3.1	301.8	0.0109	0.0011	0.031	0.003	3702	395
		383.2	325.2	3.8	321.4	0.0102	0.0011	0.029	0.003	4216	480
		393.2	343.7	4.6	339.1	0.0098	0.0011	0.028	0.003	4692	561
0.500	0.003	303.1	44.7	2.3	42.4	0.0279	0.0011	0.051	0.002	183	10
		313.2	77.7	2.5	75.2	0.0253	0.0011	0.047	0.002	362	20
		323.2	119.5	2.6	116.9	0.0221	0.0011	0.041	0.002	649	40
		333.2	165.1	2.8	162.2	0.0189	0.0011	0.034	0.002	1068	75
		343.2	207.2	3.2	204.1	0.0161	0.0012	0.029	0.002	1595	131
		353.2	243.3	3.5	239.8	0.0139	0.0012	0.025	0.002	2186	207
		363.2	273.4	4.4	273.4	0.0121	0.0012	0.022	0.002	2909	317

373.2	298.8	5.3	293.5	0.0113	0.0012	0.021	0.002	3371	395
383.1	320.7	6.5	314.3	0.0105	0.0013	0.019	0.002	3910	494
393.1	339.6	8.3	331.3	0.0101	0.0013	0.018	0.002	4354	578
313.1	57.4	1.6	55.7	0.0186	0.0011	0.034	0.002	367	26
313.1	104.3	1.6	102.7	0.0329	0.0015	0.061	0.003	376	22
313.1	158.2	1.6	156.5	0.0485	0.0014	0.091	0.004	383	17
313.2	213.3	1.6	211.7	0.0634	0.0013	0.121	0.004	390	15
313.1	263.8	1.6	262.2	0.0759	0.0013	0.147	0.004	398	14
313.2	303.9	1.6	302.3	0.0855	0.0013	0.168	0.005	403	14
313.2	344.1	1.6	342.5	0.0944	0.0013	0.187	0.005	410	13
313.1	375.4	1.6	373.7	0.1010	0.0014	0.202	0.005	415	13
313.1	406.5	1.6	404.9	0.1072	0.0014	0.215	0.005	421	13
313.2	431.9	1.6	430.3	0.1120	0.0015	0.226	0.006	426	13
313.2	473.3	1.6	471.6	0.1196	0.0015	0.244	0.006	433	14
313.1	505.1	1.6	503.5	0.1250	0.0016	0.256	0.006	440	14
313.1	528.3	1.6	526.7	0.1289	0.0017	0.265	0.006	444	14

<sup>a</sup> Standard uncertainties are reported (level of confidence 0.68). Standard uncertainty for temperature is  $u(T) = 0.1$  K, for total and residual pressure is  $u(P_{\text{tot}}) = u(P_{\text{res}}) = 0.9$  kPa and for CO<sub>2</sub> pressure is  $u(P_{\text{CO}_2}) = 1.3$  kPa.



## APPENDIX B

The parameters for the so-called “soft model” used to describe the VLE data in the aqueous systems studied in this work are presented in **Table B. 1**. Reference is made to equations Eq. 4 to Eq. 7. The parameters are given with their significant numbers.

**Table B. 1:** Model parameters (Eq. 4)

Systems	Parameters								
	A	B	$k_{1,a}$	$k_{1,b}$	$k_{2,a}$	$k_{2,b}$	$k_{3,a}$	$k_{3,b}$	
30 wt% MDEA – 60 wt% MEG – 10 wt% H <sub>2</sub> O	1.487	10.16	-17.924	-96.8894	-10	1.77	29	3.55	
30 wt% MDEA – 40 wt% MEG – 30 wt% H <sub>2</sub> O	1.496	10.24	-19.004	-104.0863	-10	1.56	-199	3.91	
30 wt% MDEA – 20 wt% MEG – 50 wt% H <sub>2</sub> O	1.480	10.12	-19.686	-108.8514	-10	1.27	55	2.86	
70 wt% MDEA – 30 wt% H <sub>2</sub> O	1.241	10.03	-20.083	-109.9550	-10	1.39	55	3.45	
90 wt% MDEA – 10 wt% H <sub>2</sub> O	-0.296	10.03	-18.919	-108.7841	-10	-1.04	55	0.52	

## REFERENCES

1. Stewart, M. & Arnold, K. Part 1 - Gas Sweetening. in *Gas Sweetening and Processing Field Manual* (ed. Arnold, M. S.) 1–140 (Gulf Professional Publishing, 2011).
2. Økland, O., Davies, S., Ramberg, R. M. & Rognø, H. Steps to the Subsea Factory. in *OTC-24307-MS* (Offshore Technology Conference, 2013). doi:10.4043/24307-MS.
3. GATEkeeper. H<sub>2</sub>S scavenging: Using Triazine. (2014).
4. Lioliou, M. G., Sandrød, J., Stipanicev, M. & Birketveit, Ø. Qualification and field performance of subsea H<sub>2</sub>S scavenger injection. in (2017).
5. Hutchinson, A. J. L. Process for treating gases. (1939).
6. McCartney, E. R. Gas purification and dehydration process. (1948).
7. Chapin, W. F. Purification and dehydration of gases. (1950).
8. McCartney, E. R. Extraction of acidic impurities and moisture from gases. (1951).
9. Kohl, A. L. & Nielsen, R. B. Chapter 2 - Alkanolamines for Hydrogen Sulfide and Carbon Dioxide Removal. in *Gas Purification* 40–186 (Gulf Professional Publishing, 1997).
10. Woertz, B. B. Experiments with solvent-amine-water for removing CO<sub>2</sub> from gas. *The Canadian Journal of Chemical Engineering* **50**, 425–427 (1972).
11. Sridharan, K. & Sharma, M. M. New systems and methods for the measurement of effective interfacial area and mass transfer coefficients in gas–liquid contactors. *Chemical Engineering Science* **31**, 767–774 (1976).
12. Alvarez-Fuster, C., Midoux, N., Laurent, A. & Charpentier, J. C. Chemical kinetics of the reaction of CO<sub>2</sub> with amines in pseudo m–nth order conditions in polar and viscous organic solutions. *Chemical Engineering Science* **36**, 1513–1518 (1981).
13. Oyevaar, M. H., Fontein, H. J. & Westerterp, K. R. Equilibria of carbon dioxide in solutions of diethanolamine in aqueous ethylene glycol at 298 K. *J. Chem. Eng. Data* **34**, 405–408 (1989).
14. Song, J.-H., Park, S.-B., Yoon, J.-H., Lee, H. & Lee, K.-H. Solubility of Carbon Dioxide in Monoethanolamine + Ethylene Glycol + Water and Monoethanolamine + Poly(ethylene glycol) + Water at 333.2 K. *J. Chem. Eng. Data* **42**, 143–144 (1997).
15. Leites, I. L. Thermodynamics of CO<sub>2</sub> solubility in mixtures monoethanolamine with organic solvents and water and commercial experience of energy saving gas purification technology. *Energy Conversion and Management* **39**, 1665–1674 (1998).
16. Xu, H.-J., Zhang, C.-F. & Zheng, Z.-S. Selective H<sub>2</sub>S Removal by Nonaqueous Methyl-diethanolamine Solutions in an Experimental Apparatus. *Ind. Eng. Chem. Res.* **41**, 2953–2956 (2002).
17. Park, S.-W., Lee, J.-W., Choi, B.-S. & Lee, J.-W. Absorption of carbon dioxide into non-aqueous solutions of N-methyl-diethanolamine. *Korean J. Chem. Eng.* **23**, 806–811 (2006).
18. Tan, J., Shao, H., Xu, J., Du, L. & Luo, G. Mixture Absorption System of Monoethanolamine–Triethylene Glycol for CO<sub>2</sub> Capture. *Ind. Eng. Chem. Res.* **50**, 3966–3976 (2011).

19. Eimer, D. Simultaneous removal of water and hydrogen sulphide from natural gas. (NTNU, 1994).
20. Wanderley, R. R., Yuan, Y., Rochelle, G. T. & Knuutila, H. K. CO<sub>2</sub> solubility and mass transfer in water-lean solvents. *Chemical Engineering Science* **202**, 403–416 (2019).
21. Hartono, A., Juliussen, O. & Svendsen, H. F. Solubility of N<sub>2</sub>O in Aqueous Solution of Diethylenetriamine. *J. Chem. Eng. Data* **53**, 2696–2700 (2008).
22. Peng, D.-Y. & Robinson, D. B. A New Two-Constant Equation of State. *Ind. Eng. Chem. Fund.* **15**, 59–64 (1976).
23. Carroll, J. J., Slupsky, J. D. & Mather, A. E. The Solubility of Carbon Dioxide in Water at Low Pressure. *Journal of Physical and Chemical Reference Data* **20**, 1201–1209 (1991).
24. Penttilä, A., Dell’Era, C., Uusi-Kyyny, P. & Alopaeus, V. The Henry’s law constant of N<sub>2</sub>O and CO<sub>2</sub> in aqueous binary and ternary amine solutions (MEA, DEA, DIPA, MDEA, and AMP). *Fluid Phase Equilibria* **311**, 59–66 (2011).
25. Hartono, A., Mba, E. O. & Svendsen, H. F. Physical Properties of Partially CO<sub>2</sub> Loaded Aqueous Monoethanolamine (MEA). *J. Chem. Eng. Data* **59**, 1808–1816 (2014).
26. Skylogianni, E., Wanderley, R. R., Austad, S. S. & Knuutila, H. K. Density and Viscosity of the Nonaqueous and Aqueous Mixtures of Methyldiethanolamine and Monoethylene Glycol at Temperatures from 283.15 to 353.15 K. *J. Chem. Eng. Data* **64**, 5415–5431 (2019).
27. Perinu, C., Arstad, B. & Jens, K.-J. NMR spectroscopy applied to amine–CO<sub>2</sub>–H<sub>2</sub>O systems relevant for post-combustion CO<sub>2</sub> capture: A review. *International Journal of Greenhouse Gas Control* **20**, 230–243 (2014).
28. Perinu, C., Arstad, B. & Jens, K.-J. <sup>13</sup>C NMR Experiments and Methods used to Investigate Amine-CO<sub>2</sub>-H<sub>2</sub>O Systems. *Energy Procedia* **37**, 7310–7317 (2013).
29. Brüder, P., Lauritsen, K. G., Mejdell, T. & Svendsen, H. F. CO<sub>2</sub> capture into aqueous solutions of 3-methylaminopropylamine activated dimethyl-monoethanolamine. *Chemical Engineering Science* **75**, 28–37 (2012).
30. Hartono, A. *et al.* Characterization of 2-piperidineethanol and 1-(2-hydroxyethyl)pyrrolidine as strong bicarbonate forming solvents for CO<sub>2</sub> capture. *International Journal of Greenhouse Gas Control* **63**, 260–271 (2017).
31. Bernhardsen, I. M., Trollebø, A. A., Perinu, C. & Knuutila, H. K. Vapour-liquid equilibrium study of tertiary amines, single and in blend with 3-(methylamino)propylamine, for post-combustion CO<sub>2</sub> capture. *The Journal of Chemical Thermodynamics* **138**, 211–228 (2019).
32. Zheng, D.-Q., Ma, W.-D., Wei, R. & Guo, T.-M. Solubility study of methane, carbon dioxide and nitrogen in ethylene glycol at elevated temperatures and pressures. *Fluid Phase Equilibria* **155**, 277–286 (1999).
33. Galvão, A. C. & Francesconi, A. Z. Solubility of methane and carbon dioxide in ethylene glycol at pressures up to 14 MPa and temperatures ranging from (303 to 423) K. *The Journal of Chemical Thermodynamics* **42**, 684–688 (2010).

34. Jou, F.-Y., Deshmukh, R. D., Otto, F. D. & Mather, A. E. Vapor-Liquid Equilibria of H<sub>2</sub>S and CO<sub>2</sub> and Ethylene Glycol at Elevated Pressures. *Chemical Engineering Communications* **87**, 223–231 (1990).
35. Wise, M. & Chapoy, A. Phase Behavior of CO<sub>2</sub> in Monoethylene Glycol between 263.15–343.15 K and 0.2–40.3 MPa: An Experimental and Modeling Approach. *J. Chem. Eng. Data* **62**, 4154–4159 (2017).
36. Campbell, J. M. Amine-based processes. in *Gas Conditioning and Processing* vol. 4 (1998).
37. Shen, K. P. & Li, M. H. Solubility of carbon dioxide in aqueous mixtures of monoethanolamine with methyldiethanolamine. *J. Chem. Eng. Data* **37**, 96–100 (1992).
38. Perinu, C., Bernhardsen, I. M., Pinto, D. D. D., Knuutila, H. K. & Jens, K.-J. NMR Speciation of Aqueous MAPA, Tertiary Amines, and Their Blends in the Presence of CO<sub>2</sub>: Influence of pK<sub>a</sub> and Reaction Mechanisms. *Ind. Eng. Chem. Res.* **57**, 1337–1349 (2018).
39. Nitta, M., Hayashi, K., Furukawa, Y., Sato, H. & Yamanaka, Y. <sup>13</sup>C-NMR Study of Acid Dissociation Constant (pK<sub>a</sub>) Effects on the CO<sub>2</sub> Absorption and Regeneration of Aqueous Tertiary Alkanolamine–Piperazine Blends. *Energy Procedia* **63**, 1863–1868 (2014).
40. Behrens, R. *et al.* Monoalkylcarbonate Formation in Methyldiethanolamine–H<sub>2</sub>O–CO<sub>2</sub>. *Ind. Eng. Chem. Res.* **56**, 9006–9015 (2017).
41. Perinu, C., Arstad, B., Bouzga, A. M., Svendsen, J. A. & Jens, K. J. NMR-Based Carbamate Decomposition Constants of Linear Primary Alkanolamines for CO<sub>2</sub> Capture. *Ind. Eng. Chem. Res.* **53**, 14571–14578 (2014).
42. Eimer, D. *Gas treating: absorption theory and practice*. (John Wiley & Sons, Inc, 2014).
43. Barzagli, F., Lai, S. & Mani, F. Novel non-aqueous amine solvents for reversible CO<sub>2</sub> capture. *Energy Procedia* **63**, 1795–1804 (2014).
44. Sagdeev, D. I., Fomina, M. G., Mukhamedzyanov, G. Kh. & Abdulagatov, I. M. Experimental study of the density and viscosity of polyethylene glycols and their mixtures at temperatures from 293K to 473K and at atmospheric pressure. *The Journal of Chemical Thermodynamics* **43**, 1824–1843 (2011).
45. Tawfik, W. Y. & Teja, A. S. The densities of polyethylene glycols. *Chemical Engineering Science* **44**, 921–923 (1989).
46. Pereira, M. F. V., Avelino, H. M. N. T., Caetano, F. J. P. & Fareleira, J. M. N. A. Viscosity of liquid diethylene, triethylene and tetraethylene glycols at moderately high pressures using a vibrating wire instrument. *Fluid Phase Equilibria* **480**, 87–97 (2019).
47. Crespo, E. A. *et al.* New measurements and modeling of high pressure thermodynamic properties of glycols. *Fluid Phase Equilibria* **436**, 113–123 (2017).
48. Tsai, C.-Y., Soriano, A. N. & Li, M.-H. Vapour pressures, densities, and viscosities of the aqueous solutions containing (triethylene glycol or propylene glycol) and (LiCl or LiBr). *The Journal of Chemical Thermodynamics* **41**, 623–631 (2009).

49. Sastry, N. V., Thakor, R. R. & Patel, M. C. Thermophysical Properties for Diethylene Glycol + Nitrobenzene and Triethylene Glycol + (Chloro-, Bromo-, Nitro-) Benzene Systems at Different Temperatures. *Int J Thermophys* **29**, 610–618 (2008).
50. Valtz, A., Teodorescu, M., Wichterle, I. & Richon, D. Liquid densities and excess molar volumes for water + diethylene glycolamine, and water, methanol, ethanol, 1-propanol + triethylene glycol binary systems at atmospheric pressure and temperatures in the range of 283.15–363.15 K. *Fluid Phase Equilibria* **215**, 129–142 (2004).
51. Steele, W. V., Chirico, R. D., Knipmeyer, S. E. & Nguyen, A. Measurements of Vapor Pressure, Heat Capacity, and Density along the Saturation Line for  $\epsilon$ -Caprolactam, Pyrazine, 1,2-Propanediol, Triethylene Glycol, Phenyl Acetylene, and Diphenyl Acetylene. *J. Chem. Eng. Data* **47**, 689–699 (2002).
52. Kumagai, A., Mochida, H. & Takahashi, S. Liquid viscosities and densities of HFC-134a+glycol mixtures. *Int J Thermophys* **14**, 45–53 (1993).
53. Jou, F.-Y., Deshmukh, R. D., Otto, F. D. & Mather, A. E. Vapor liquid equilibria for acid gases and lower alkanes in triethylene glycol. *Fluid Phase Equilibria* **36**, 121–140 (1987).
54. Wise, M. & Chapoy, A. Carbon dioxide solubility in Triethylene Glycol and aqueous solutions. *Fluid Phase Equilibria* **419**, 39–49 (2016).

## Supporting Information

# Carbon Dioxide Solubility in Mixtures of Methyldiethanolamine with Monoethylene Glycol, Monoethylene Glycol – Water, Water and Triethylene Glycol

*Eirini Skylogianni<sup>1</sup>, Cristina Perinu<sup>1,2</sup>, Blanca Y. Cervantes Gameros<sup>1</sup>, Hanna K. Knuutila<sup>1\*</sup>*

<sup>1</sup> Department of Chemical Engineering, Norwegian University of Science and Technology  
(NTNU), NO-7491 Trondheim, Norway

<sup>2</sup> Department of Process, Energy and Environmental Technology, University of Southeast  
Norway, NO-3603 Kongsberg, Norway

\* hanna.knuutila@ntnu.no

The file includes:

- A. Complementary data plots
- B. Density data
- C. Karl-Fischer titration results
- D. NMR spectra
- E. Uncertainty analysis

## A. Complementary data plots

MDEA-MEG mixtures

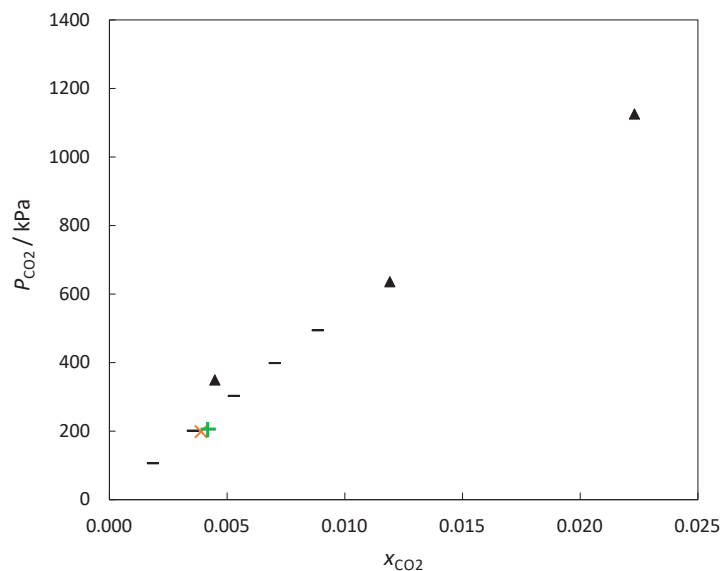


**Figure S. 1:** Carbon dioxide solubility in MEG expressed in mole fraction ( $x_{CO_2}$ ) as a function of pressure at 303.15 K. ( $\blacktriangle$ ) Galvao and Franscesconi (2010)<sup>1</sup>, ( $-$ ) Serpa et al. (2013)<sup>2</sup>, ( $\times$ ) This work (A), ( $+$ ) This work (B).

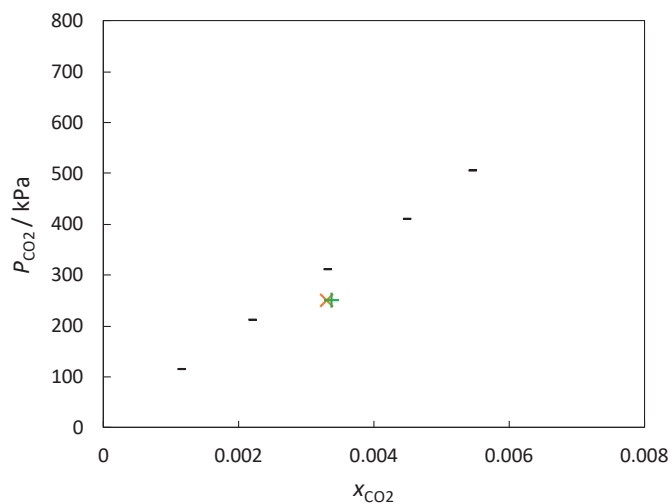


**Figure S. 2:** Carbon dioxide solubility in MEG expressed in mole fraction ( $x_{CO_2}$ ) as a function of pressure at 333.15 K. ( $-$ ) Serpa et al. (2013)<sup>2</sup>, ( $\times$ ) This work (A), ( $+$ ) This work (B).

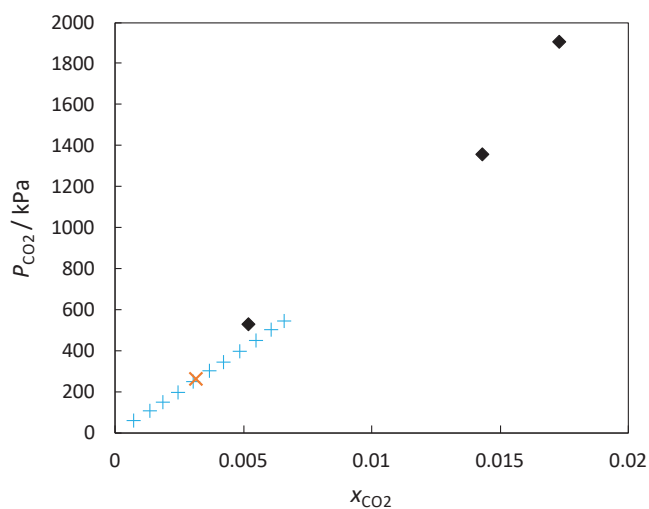


**Figure S. 3:** Carbon dioxide solubility in MEG expressed in mole fraction ( $x_{CO_2}$ ) as a function of pressure at 343.15 K. (◆) Wise and Chapoy (2017)<sup>3</sup>, (x) This work (A), (+) This work (isothermal experiment).

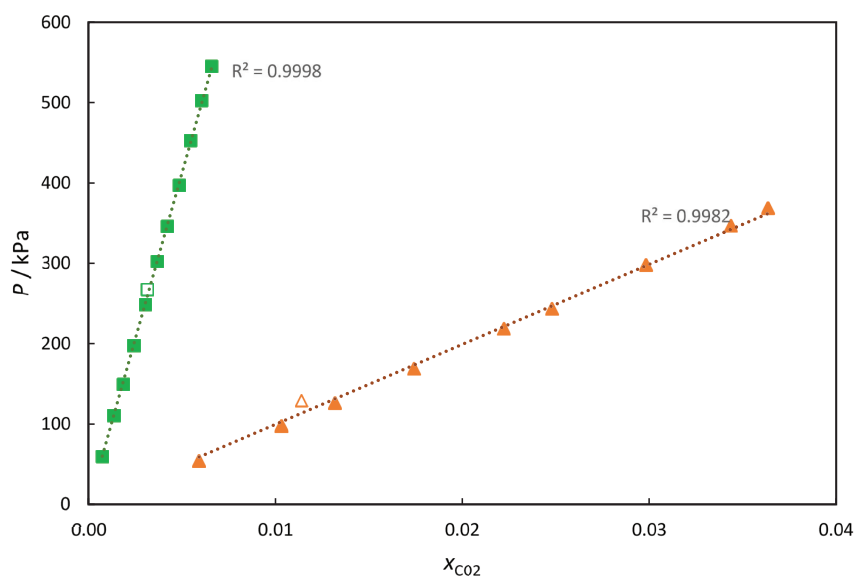


**Figure S. 4:** Partial pressure of CO<sub>2</sub> as a function of CO<sub>2</sub> solubility expressed in mole fraction ( $x_{CO_2}$ ) in pure MEG and pure MDEA at 343 K. Hollow symbols denote previous experiment (data from Table A. 2) and filled symbols denote isothermal experiment (data from Table A. 3); (■) MEG and (▲) MDEA. Dotted lines are linear trendlines; the linearity between  $P$  and  $x$  is assessed through the coefficient of determination,  $R^2$ .



### MDEA-MEG-H<sub>2</sub>O mixtures

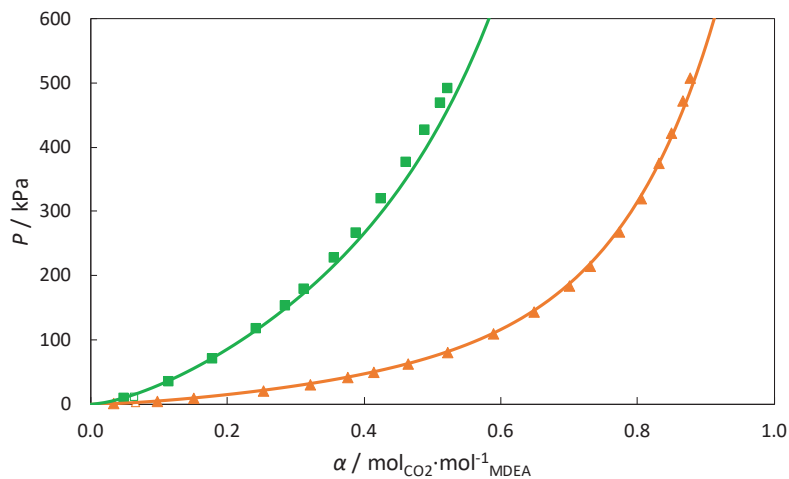


**Figure S. 5:** Partial pressure of CO<sub>2</sub> as a function of CO<sub>2</sub> loading in a solution of 30 wt% MDEA – 40 wt% MEG – 30 wt% H<sub>2</sub>O. Hollow symbols denote previous experiment (data from Table A. 5) and filled symbols denote isothermal experiment (data from Table A. 6); ( $\blacktriangle$ ) 313.2 K, ( $\blacksquare$ ) 343.2 K. The lines represent model estimations.

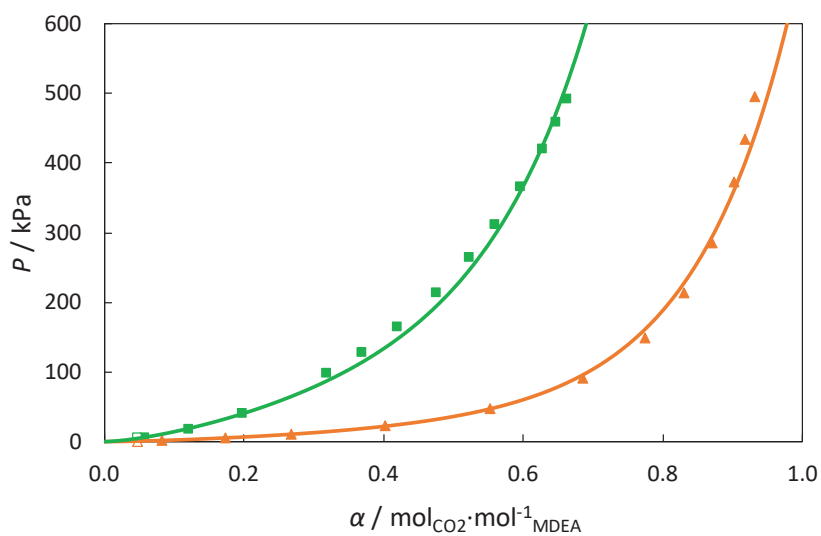


**Figure S. 6:** Partial pressure of CO<sub>2</sub> as a function of CO<sub>2</sub> loading in a solution of 30 wt% MDEA – 20 wt% MEG – 50 wt% H<sub>2</sub>O. Hollow symbols denote previous experiment (data from Table A. 5) and filled symbols denote isothermal experiment (data from Table A. 6); ( $\blacktriangle$ ) 313.2 K, ( $\blacksquare$ ) 343.2 K. The lines represent model estimations.

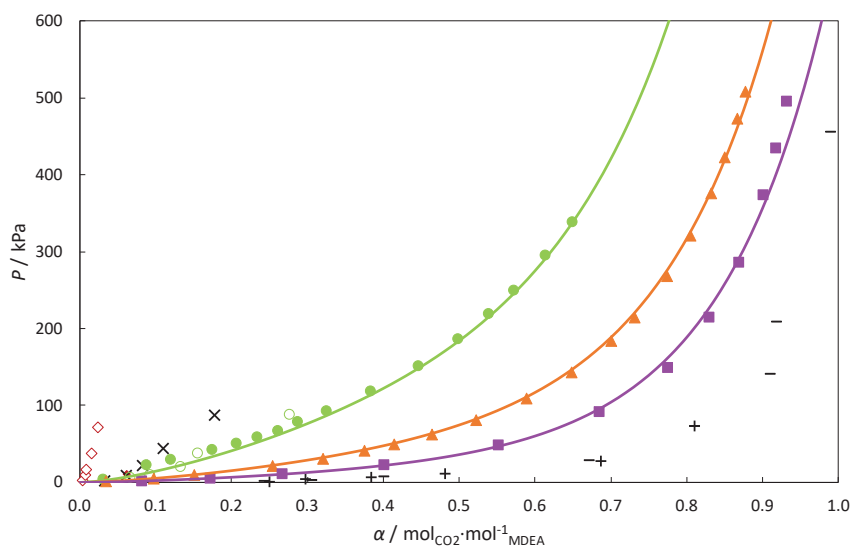


**Figure S. 7:** Partial pressure of CO<sub>2</sub> as a function of CO<sub>2</sub> loading in MDEA (1) – MEG (2) – H<sub>2</sub>O (3) blends at 313 K. 30 wt% MDEA – 70 wt% MEG: (◆) This work and (◇) data from Xu et al.<sup>4</sup>, 30 wt% MDEA – 65 wt% MEG – 5 wt% H<sub>2</sub>O: (×) Xu et al.<sup>4</sup>, 30 wt% MDEA – 60 wt% MEG – 10 wt% H<sub>2</sub>O: (●) This work and (○) Xu et al.<sup>4</sup>, 30 wt% MDEA – 40 wt% MEG – 30 wt% H<sub>2</sub>O: (▲) This work, 30 wt% MDEA – 20 wt% MEG – 50 wt% H<sub>2</sub>O: (■) This work, 30 wt% MDEA – 70 wt% H<sub>2</sub>O: (+) Xu et al.<sup>4</sup> and (-) Shen and Li<sup>5</sup>. The lines represent model estimations.

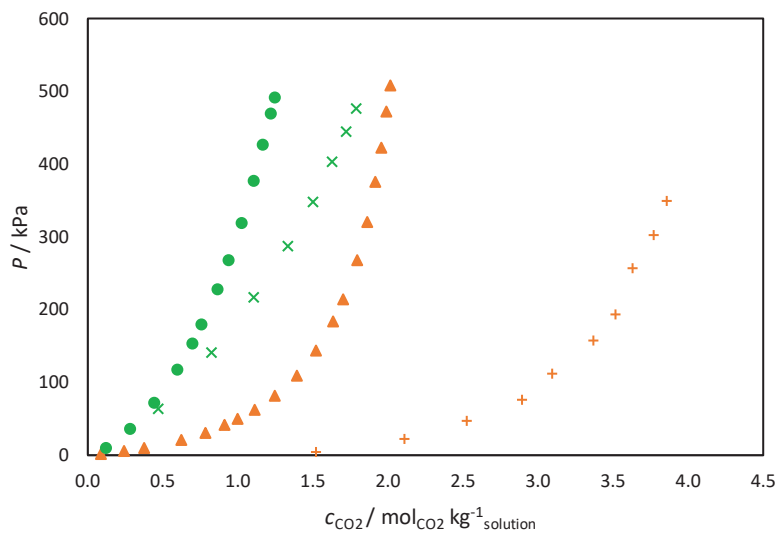


**Figure S. 8:** Partial pressure of CO<sub>2</sub> as a function of CO<sub>2</sub> liquid phase concentration in 30 wt% MDEA – 40 wt% MEG – 30 wt% H<sub>2</sub>O and 70 wt% MDEA – 30 wt% H<sub>2</sub>O. (▲) denotes data obtained at 313 K with MDEA – MEG – H<sub>2</sub>O system, (+) 313 K with MDEA – H<sub>2</sub>O system; (●) 343 K with MDEA – MEG – H<sub>2</sub>O system and (×) 343 K with MDEA – H<sub>2</sub>O system.

MDEA-TEG mixtures

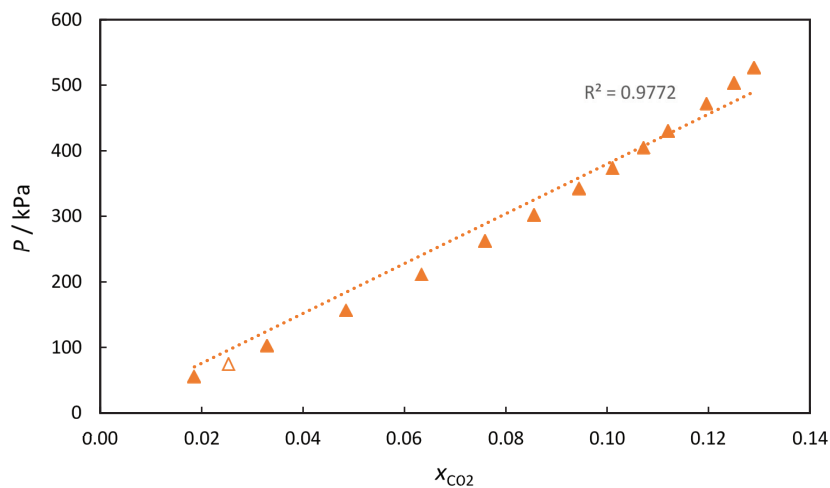


**Figure S. 9:** Partial pressure of  $\text{CO}_2$  as a function of  $\text{CO}_2$  solubility expressed in mole fraction ( $x_{\text{CO}_2}$ ) in 50 wt% MDEA – 50 wt% TEG at 313 K. Hollow symbol denotes previous experiment and filled symbols denote isothermal experiment (Table A. 8). Dotted line is linear trendline.

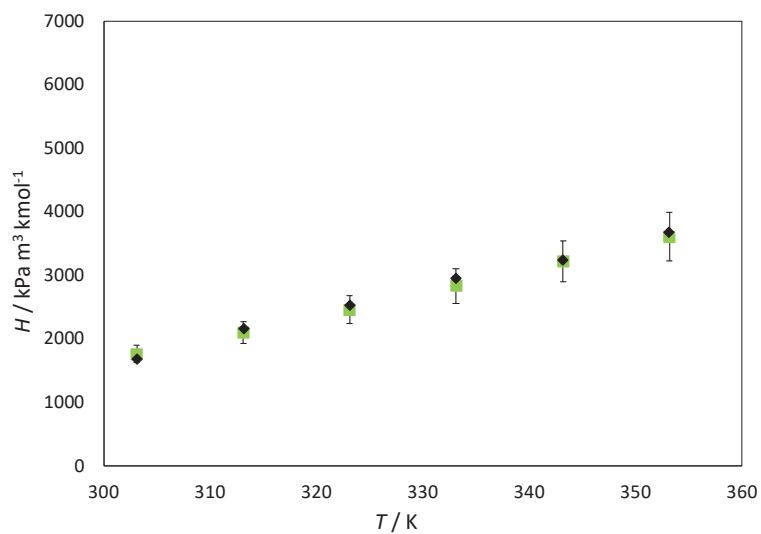


**Figure S. 10:** Henry's constant as a function of temperature for pure TEG. ( $\blacklozenge$ ) Tan et al.<sup>6</sup>, ( $\blacksquare$ ) This work. Error bars in the measured Henry's constants are included.

## B. Density data

**Table S. 1:** Density  $\rho$  in MDEA (1) – MEG (2) – H<sub>2</sub>O (3) and MDEA (1) – TEG (4) blends as a function of weight fraction  $w$  of unloaded solvent and temperature  $T$  at pressure  $P = 102$  kPa for some of the mixtures studied in this work.<sup>a</sup>

										$\rho$ (kg m <sup>-3</sup> )				
$w_1$	$u(w_1)$	$w_2$	$u(w_2)$	$w_3$	$u(w_3)$	$w_4$	$u(w_4)$	303.15 K	313.15 K	323.15 K	333.15 K	343.15 K		
0.050	0.001	0.950	0.001	-	-	-	-	1103.90*	1095.40*	1086.90*	1078.50*	1070.00*		
0.100	0.001	0.900	0.001	-	-	-	-	1106.01	1098.98	1091.72	-	-		
0.300	0.002	0.200	0.002	0.500	0.002	-	-	1097.88*	1090.19*	1082.34*	1074.31*	1066.12*		
-	-	-	-	-	-	1.000	0.006	1052.98	1046.67	1040.21	-	1025.78		
0.300	0.003	-	-	-	-	0.700	0.003	1049.93*	1044.14*	1038.23*	1032.19*	1025.98*		
0.500	0.003	-	-	-	-	0.500	0.003	1115.58	1107.82	1099.84	1091.86	1084.28		
-	-	-	-	-	-	-	-	1089.45	1081.63	1073.79	1066.24	1058.14		
-	-	-	-	-	-	-	-	1072.82	1065.08	1057.57	1050.41	1041.68		
										353.15 K	363.15 K	373.15 K	383.15 K	393.15 K
0.050	0.001	0.950	0.001	-	-	-	-	1061.50*	1052.90*	1044.30*	1035.60*	1026.80*		
0.100	0.001	0.900	0.001	-	-	-	-	1069.25	-	-	-	-		
0.300	0.002	0.200	0.002	0.500	0.002	-	-	1057.77*	1049.24*	1040.54*	1031.67*	1022.61*		
-	-	-	-	-	-	1.000	0.006	1018.12	-	-	-	-		
-	-	-	-	-	-	-	-	1019.61*	1013.05*	1006.29*	999.30*	992.09*		
-	-	-	-	-	-	-	-	1076.37	1068.73 <sup>+</sup>	1060.87 <sup>+</sup>	1053.01 <sup>+</sup>	1045.15 <sup>+</sup>		

0.300	0.003	-	-	-	-	0.700	0.003	1050.17	1042.42 <sup>+</sup>	1034.58 <sup>+</sup>	1026.73 <sup>+</sup>	1018.89 <sup>+</sup>
0.500	0.003	-	-	-	-	0.500	0.003	1033.71	1018.98 <sup>+</sup>	1010.98 <sup>+</sup>	1002.98 <sup>+</sup>	994.98 <sup>+</sup>

<sup>a</sup> Standard uncertainties are reported in composition (level of confidence 0.68). Standard uncertainties not included above are for temperature  $u(T) = 0.01$  K, for pressure  $u(P) = 3$  kPa and for density measurements  $u(\rho) = 0.09, 0.09, 0.04, 0.03, 0.05$  and  $0.05$  kg m<sup>-3</sup> at the temperatures 303.15, 313.15, 323.15, 333.15, 343.15 and 353.15 K, respectively.

\*: model by Skylogianni et al.<sup>7</sup>

+: extrapolated values

### C. Karl-Fischer titration results

**Table S. 2:** Water content  $c_w$  before and after the solubility measurements of  $\text{CO}_2$  in pure MDEA (1), pure MEG (2), pure TEG (4) and selected mixtures of them, accompanied by the corresponding standard uncertainties (level of confidence 0.68).

System				Before			After			
$w_1$	$u(w_1)$	$w_2$	$u(w_2)$	$w_4$	$u(w_4)$	$info$	$c_w$	$u(c_w)$	$c_w$	$u(c_w)$
							ppm	ppm	ppm	ppm
-	-	1.000	-	-	-	3/3 K	146	11	1857	37
1.000	-	-	-	-	-	3/3 K	1155	40	5012	156
0.050	0.001	0.950	0.001	-	-	-	610	37	1722	89
0.500	0.002	0.500	0.002	-	-	-	810	13	1599	43
-	-	-	-	1.000	-	3/3 K	340	17	1605	25
0.300	0.003	-	-	0.700	0.003	-	1048	17	1165	91
0.300	0.003	-	-	0.500	0.003	-	596	22	3371	96

D. NMR spectra

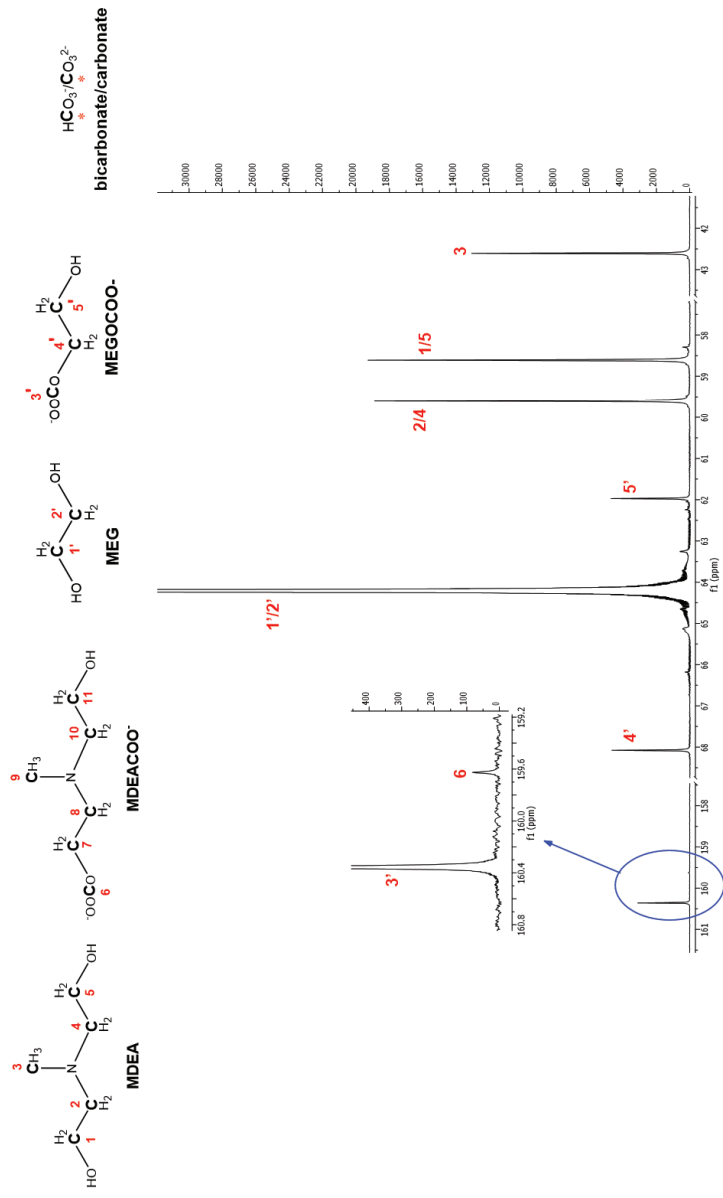


Figure S. 11: <sup>13</sup>C NMR spectrum of 5 wt% MDEA – 95 wt% MEG – CO<sub>2</sub>.

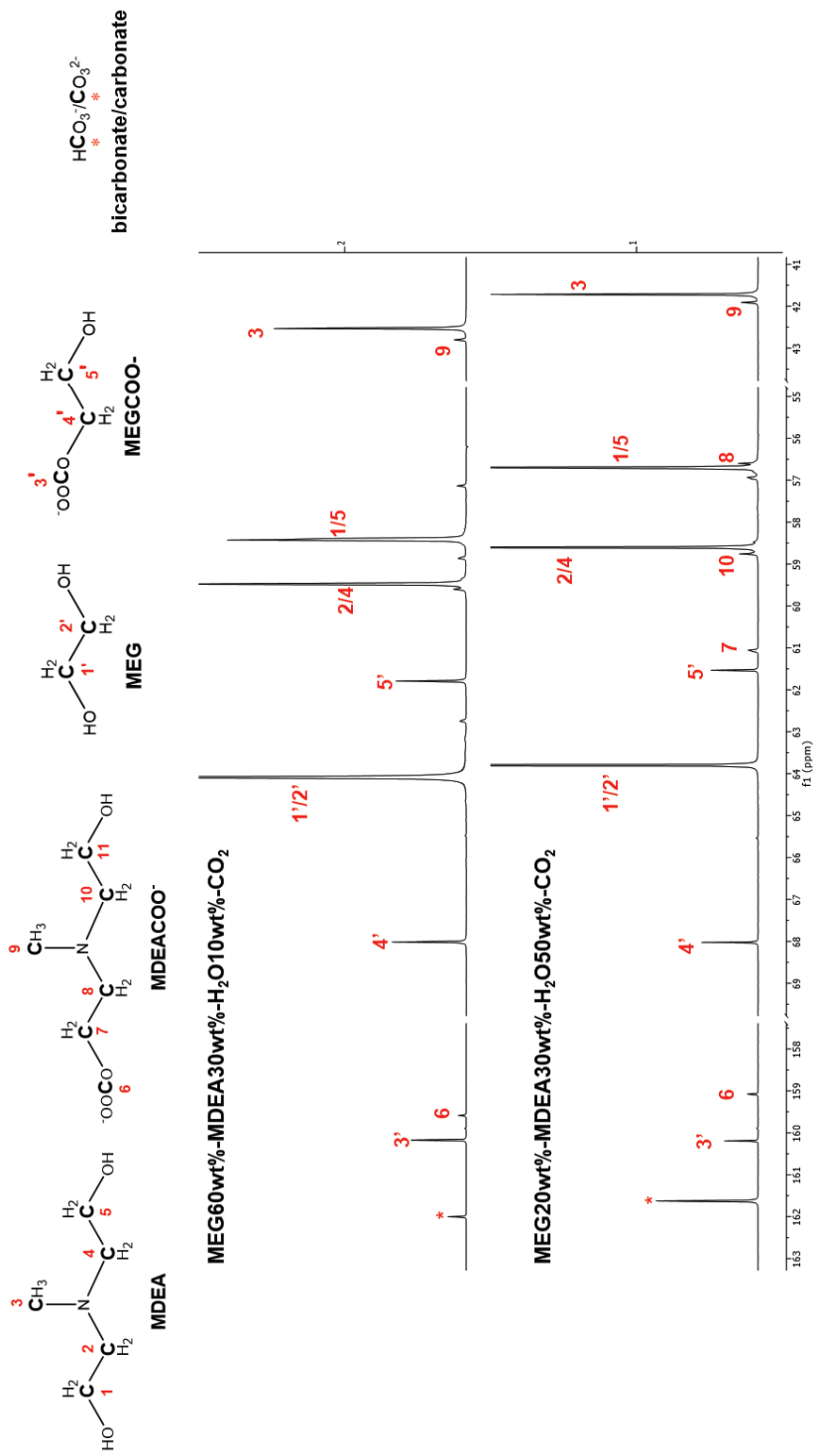
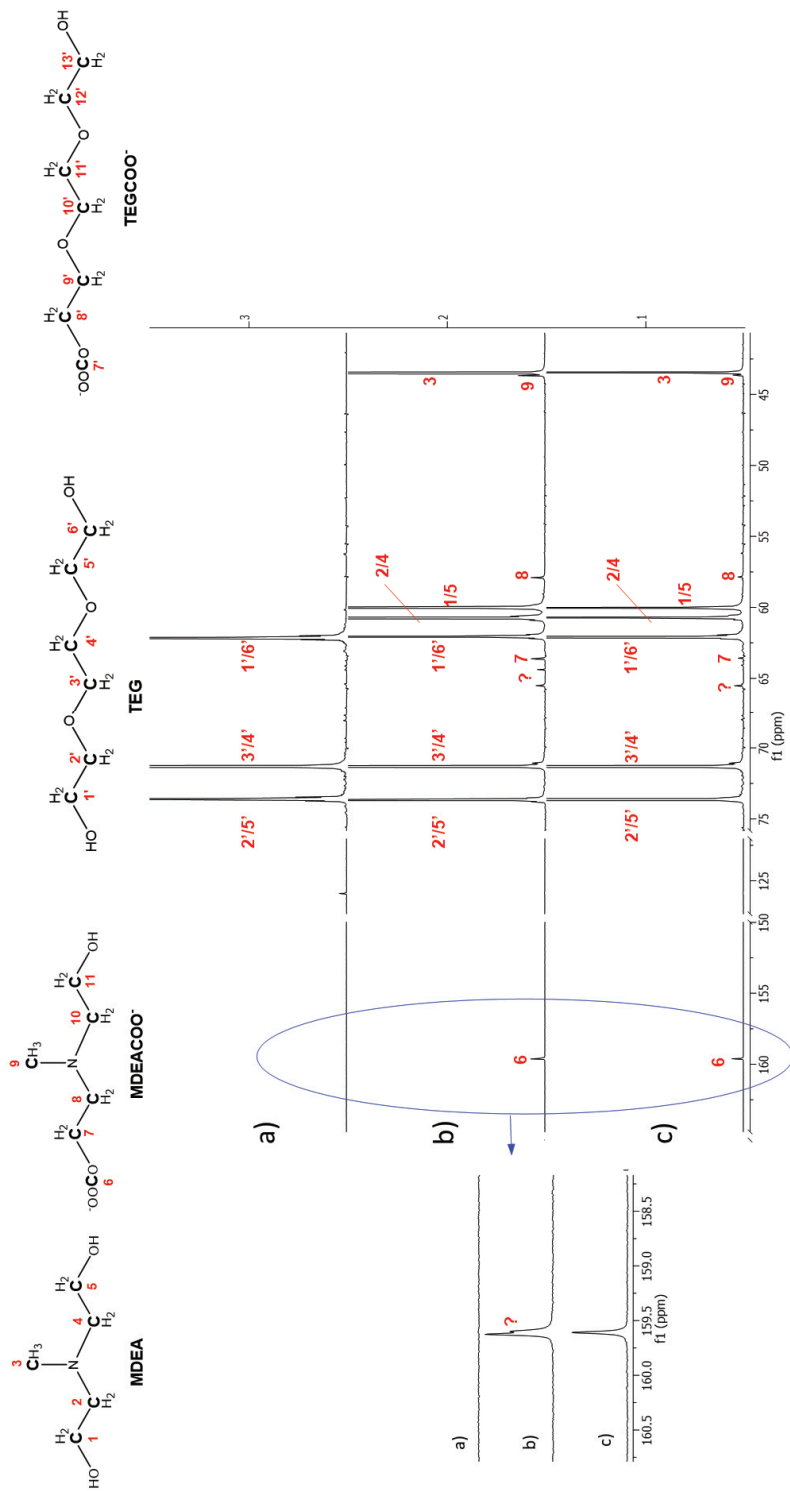


Figure S. 12: <sup>13</sup>C NMR spectrum of CO<sub>2</sub> – MDEA – MEG – H<sub>2</sub>O systems.





**Figure S. 13:**  $^{13}\text{C}$  NMR spectrum of a)  $\text{CO}_2$  - TEG, b) 50 wt% MDEA - 50 wt% TEG -  $\text{CO}_2$ , c) 30 wt% MDEA - 70 wt% TEG -  $\text{CO}_2$ .

## E. Uncertainty Analysis

In this section, the uncertainty calculations are presented. We report the standard uncertainties and combined standard uncertainties when applicable (level of confidence 0.68).

### Uncertainty of the solution composition in wt.%, $w$

The weight fraction of a binary mixture, here MDEA (1) and MEG/TEG/H<sub>2</sub>O (2), is given by:

$$w_1 = \frac{m_1}{m_1 + m_2} \quad (S.1)$$

where  $m$ : mass. The standard uncertainty of the composition of each component is equal to each other in binary mixtures. Using the Law of propagation of uncertainty, the uncertainty in weight fractions is defined as:

$$u^2(w_1) = \left(\frac{\partial w_1}{\partial m_1}\right)_{m_2}^2 u^2(m_1) + \left(\frac{\partial w_1}{\partial m_2}\right)_{m_1}^2 u^2(m_2) \quad (S.2),$$

leading to:

$$u(w) = u(w_1) = u(w_2) = \frac{u(m)}{(m_1 + m_2)^2} \sqrt{m_1^2 + m_2^2} \quad (S.3)$$

where  $u(m)$  is the uncertainty of the mass.

For a ternary system, the uncertainty of the weight fractions is found by:

$$u(w_1) = \frac{u(m)}{(m_1 + m_2 + m_3)^2} \sqrt{2 m_1^2 + (m_2 + m_3)^2} \quad (S.4)$$

$$u(w_2) = \frac{u(m)}{(m_1 + m_2 + m_3)^2} \sqrt{2 m_2^2 + (m_1 + m_3)^2} \quad (S.5)$$

$$u(w_3) = \frac{u(m)}{(m_1 + m_2 + m_3)^2} \sqrt{2 m_3^2 + (m_1 + m_2)^2} \quad (S.6)$$

The uncertainty of the mass includes both the accuracy of the scale,  $u_{scale}(m) = 1 \cdot 10^{-6}$  kg, and the chemicals' purity, according to:

$$u(m) = \sqrt{u_{scale}^2(m) + u_{purity,i}^2(m)} \quad (S.7)$$

$u_{\text{purity}}(m)$  is calculated for each component, and it is equal to  $a/\sqrt{3}$  assuming uniform distribution is followed. The numerator,  $a$ , is the maximum deviation from the measured value, i.e. purity%·mass. The purity of water is considered 100%.

**Table S. 3:** Composition in Weight Fraction  $w$  and Standard Uncertainties for the binaries {MDEA (1) + MEG (2)}, {MDEA (1) + H<sub>2</sub>O (3)} and {MDEA (1) + TEG (4)}.

$w_1$	$u(w_1) = u(w_2)$	$u(w_1) = u(w_2)$	$u(w_1) = u(w_2)$
	MDEA-MEG	MDEA-H <sub>2</sub> O	MDEA-TEG
0.000	0.000	0.000	0.000
0.050	0.001	-	-
0.100	0.001	-	-
0.300	0.001	-	0.003
0.500	0.002	-	0.003
0.700	0.003	0.006	-
0.900	0.005	0.006	-
1.000	0.006	0.006	0.006

**Table S. 4:** Composition in Weight Fraction  $w$  and Standard Uncertainties for {MDEA (1) + MEG (2) + Water (3)}

$w_1$	$w_2$	$w_3$	$u(w_1)$	$u(w_2)$	$u(w_3)$
0.300	0.200	0.500	0.002	0.002	0.002
0.300	0.400	0.300	0.001	0.001	0.001
0.300	0.599	0.101	0.001	0.001	0.001

#### Uncertainty of the partial pressure of CO<sub>2</sub>, $P_{CO_2}$

The partial pressure of carbon dioxide was calculated according to Eq. (S.8) and the derived uncertainty is shown in Eq. (S.9).

$$P_{CO_2} = P_{tot} - P_{res} \quad (S.8)$$

$$u_c^2(P_{CO_2}) = \left( \frac{\partial P_{CO_2}}{\partial P_{tot}} \right)_{P_{res}}^2 u^2(P_{tot}) + \left( \frac{\partial P_{CO_2}}{\partial P_{res}} \right)_{P_{tot}}^2 u^2(P_{res}) = 2 \cdot u^2(P) \quad (S.9)$$

where  $u(P) = u(P_{tot}) = u(P_{res})$  is the pressure transducer's uncertainty (0.15% Full Scale, i.e. 0.9 kPa). The resulted uncertainty is  $u(P) = 1.3$  kPa.

#### Uncertainty of CO<sub>2</sub> loading, $\alpha$

By definition:

$$\alpha = \frac{n_{abs}}{n_{MDEA}} \quad (S.10)$$

$$u(\alpha)^2 = \frac{1}{n_{MDEA}^2} (u(n_{abs})^2 + \alpha^2 u(n_{MDEA})^2) \quad (S.11)$$

where  $n_{abs}$  are the CO<sub>2</sub> moles absorbed in the liquid phase and  $n_{MDEA}$  the amine moles of the solution inside the reactor. It is assumed that no amine vaporization takes place which is a valid assumption due to the low vapor pressure of the MDEA.

The uncertainty  $u(n_{abs})$  as well as  $u(n_{MDEA})$  are needed.

#### Uncertainty of the number of moles of amine in the reactor, $n_{MDEA}$

The solution is prepared gravimetrically and is charged into a flask, through which it is introduced in the reactor. By weighing the flask before ( $m_{tot,flask}$ ) and after introducing the solution to the reactor ( $m_{tot,residue}$ ), the total mass introduced is known,  $m_{intr}$ .

Taking into account the molecular weight of the amine and the amount of amine introduced into the reactor,  $m_{intr} w_{MDEA}$ , the number of mols of the amine in the reactor can be known,  $n_{MDEA}$ .

$$n_{MDEA} = \frac{m_{MDEA}}{Mr_{MDEA}} = \frac{m_{intr} w_{MDEA}}{Mr_{MDEA}} = \frac{(m_{tot,flask} - m_{tot,residue}) w_{MDEA}}{Mr_{MDEA}} \quad (S.12)$$

$$u(n_{MDEA})^2 = 2 \left( \frac{w_{MDEA}}{Mr_{MDEA}} \right)^2 u_c(m_{intr})^2 + \left( \frac{m_{intr}}{Mr_{MDEA}} \right)^2 u(w_{MDEA})^2 \quad (S.13)$$

where  $u_c(m_{intr}) = 2 \cdot u(m)$  because  $m = m_{tot,flask} - m_{tot,residue}$  and  $u(m_{tot,flask}) = u(m_{tot,residue}) = u(m)$  as calculated earlier.

Uncertainty of the number of moles of CO<sub>2</sub> absorbed,  $n_{abs}$

The number of moles of CO<sub>2</sub> introduced in the reactor by the CO<sub>2</sub> cylinder is calculated by  $n_{ci} - n_{ca}$ , where  $ci$  stands for cylinder initial and  $ca$  for cylinder after. The amount of gas absorbed by the solution,  $n_{abs}$ , is the difference between the amount introduced in the reactor minus the amount of CO<sub>2</sub> that exists in the gas phase in equilibrium with the solution,  $n_{gas}$ .

Based on PVT data, the number of moles in each case was calculated, using Peng-Robinson Equation of State. In the derivations below, the compressibility factor is not shown, because its effect in the calculated uncertainties was evaluated and found negligible.

$$n_{abs} = (n_{ci} - n_{ca}) - n_{gas} \quad (S.14)$$

$$n_{abs} = \frac{p_{ci}V_c}{RT_{ci}} - \frac{p_{ca}V_c}{RT_{ca}} - \frac{p_{gas}V_{gas}}{RT_{gas}} = \frac{p_{ci}V_c}{RT_{ci}} - \frac{p_{ca}V_c}{RT_{ca}} - \frac{p_{gas,tot}(V_r - V_{liq})}{RT_{gas}} + \frac{p_s(V_r - V_{liq})}{RT_{gas}} \quad (S.15)$$

$$\begin{aligned} u(n_{abs})^2 = & \left[ \left( \frac{V_c}{RT_{ci}} \right)^2 + \left( \frac{V_c}{RT_{ca}} \right)^2 + 2 \left( \frac{V_{gas}}{RT_{gas}} \right)^2 \right] u(p)^2 + \left[ \left( \frac{p_{ci}}{RT_{ci}} \right)^2 + \left( \frac{p_{ca}}{RT_{ca}} \right)^2 \right] u(V_c)^2 \\ & + \left[ \left( \frac{p_{gas,tot}}{RT_{gas}} \right)^2 + \left( \frac{p_s}{RT_{gas}} \right)^2 \right] u(V_{gas})^2 \\ & + \left[ \left( \frac{p_{ci}V_c}{RT_{ci}^2} \right)^2 + \left( \frac{p_{ca}V_c}{RT_{ca}^2} \right)^2 + \left( \frac{p_{gas,tot}V_{gas}}{RT_{gas}^2} \right)^2 \right. \\ & \left. + \left( \frac{p_sV_{gas}}{RT_{gas}^2} \right)^2 \right] u(T)^2 \end{aligned} \quad (S.16),$$

where  $r$  denotes reactor,  $liq$  denotes the liquid phase (solvent) and  $p_s$  denotes the vapor pressure of the solvent.

Uncertainty of the molar fraction of CO<sub>2</sub> in liquid phase,  $x_{CO_2}$

By definition:

$$x_{CO_2} = \frac{n_{abs}}{n_{tot}} = \frac{n_{abs}}{n_{sol} + n_{abs}} \quad (S.17)$$

$$u(x_{CO_2})^2 = \left( -\frac{n_{abs}^2}{(n_{tot} + n_{abs})^2} \right)^2 u(n_{sol})^2 + \left( \frac{n_{sol} + n_{abs} - n_{abs}n_{sol}}{(n_{sol} + n_{abs})^2} \right)^2 u(n_{abs})^2 \quad (S.18)$$

The only unknown is the  $u(n_{sol})$ .

For its calculation, we consider the following equations:

- Binary solutions, MDEA (1) and MEG/TEG/H<sub>2</sub>O (2):

$$n_{sol} = \frac{m_{intr}w_1}{Mr_1} + \frac{m_{intr}w_2}{Mr_2} \quad (S. 19)$$

$$u(n_{sol})^2 = \left(\frac{w_1}{Mr_1} + \frac{w_2}{Mr_2}\right)^2 u(m_{intr})^2 + \left(\frac{m_{intr}}{Mr_1}\right)^2 u(w_1)^2 + \left(\frac{m_{intr}}{Mr_2}\right)^2 u(w_2)^2 \quad (S. 20)$$

- Ternary solutions, MDEA (1), MEG (2) and H<sub>2</sub>O (3):

$$n_{sol} = \frac{m_{intr}w_1}{Mr_1} + \frac{m_{intr}w_2}{Mr_2} + \frac{m_{intr}w_3}{Mr_3} \quad (S. 21)$$

$$u(n_{sol})^2 = \left(\frac{w_1}{Mr_1} + \frac{w_2}{Mr_2} + \frac{w_3}{Mr_3}\right)^2 u(m_{intr})^2 + \left(\frac{m_{intr}}{Mr_1}\right)^2 u(w_1)^2 + \left(\frac{m_{intr}}{Mr_2}\right)^2 u(w_2)^2 + \left(\frac{m_{intr}}{Mr_3}\right)^2 u(w_3)^2 \quad (S. 22)$$

#### Uncertainty of Henry's constant, $H$

Henry's constant in this work is expressed in kPa·m<sup>3</sup>·kmol<sup>-1</sup> and it is calculated as:

$$H = \frac{P_{CO_2}}{c} = \frac{P_{CO_2} V_{solv}}{n_{abs}} \quad (S. 23)$$

Its uncertainty can be calculated by:

$$u(H)^2 = \left(\frac{V_{solv}}{n_{abs}}\right)^2 u(P)^2 + \left(\frac{P_{CO_2}}{n_{abs}}\right)^2 u(V_{solv})^2 + \left(-\frac{P_{CO_2} V_{solv}}{n_{abs}^2}\right)^2 u(n_{abs})^2 \quad (S. 24)$$

where  $V_{solv}$  is the volume of the solvent inside the reactor.

Because  $V_{solv} = m_{intr}/\rho_{solv}$ ,

$$u(V_{solv})^2 = \left(\frac{1}{\rho_{solv}}\right)^2 u(m_{intr})^2 + \left(-\frac{m_{intr}}{\rho_{solv}^2}\right)^2 u(\rho_{solv})^2 \quad (S. 25).$$

#### Uncertainty of density, $\rho$

The uncertainty in density was calculated according to the analysis previously reported in the publication of Skylogianni et al. <sup>7</sup>

### Uncertainty in water content, $c_w$

The standard uncertainty in the water content was calculated by taking into account both the repeatability of the measurement,  $u_{rep}(c_w)$ , and the uncertainty deriving from the accuracy of the instrument,  $u_{cal}(c_w)$ , as defined by measuring water content standards.

$$u(c_w) = \sqrt{u_{rep}^2(c_w) + u_{cal}^2(c_w)} \quad (S.26)$$

The repeatability is calculated by the standard deviation of the means. The uncertainty of the calibration is calculated by the equation below, where  $u_{cal,rep}(c_w)$  is the repeatability of the measurement of the standards, and  $u_{cal,ref}(c_w)$  is the uncertainty of the measurement, assuming Uniform Distribution (Type B).

$$u_{cal}(c_w) = \sqrt{u_{cal,rep}^2(c_w) + u_{cal,ref}^2(c_w)} \quad (S.27)$$

The main contributor to the uncertainty is the repeatability of the measurement,  $u_{rep}(c_w)$ , resulting in significant uncertainties, as can be seen in Table S. 2.

### REFERENCES

1. Galvão, A. C. & Francesconi, A. Z. Solubility of methane and carbon dioxide in ethylene glycol at pressures up to 14 MPa and temperatures ranging from (303 to 423) K. *The Journal of Chemical Thermodynamics* **42**, 684–688 (2010).
2. Serpa, F. *et al.* Solubility and Thermodynamic Properties of Carbon Dioxide in MEG/Water Mixtures. in (2013).
3. Wise, M. & Chapoy, A. Phase Behavior of CO<sub>2</sub> in Monoethylene Glycol between 263.15–343.15 K and 0.2–40.3 MPa: An Experimental and Modeling Approach. *J. Chem. Eng. Data* **62**, 4154–4159 (2017).
4. Xu, H.-J., Zhang, C.-F. & Zheng, Z.-S. Selective H<sub>2</sub>S Removal by Nonaqueous Methyl-diethanolamine Solutions in an Experimental Apparatus. *Ind. Eng. Chem. Res.* **41**, 2953–2956 (2002).
5. Shen, K. P. & Li, M. H. Solubility of carbon dioxide in aqueous mixtures of monoethanolamine with methyl-diethanolamine. *J. Chem. Eng. Data* **37**, 96–100 (1992).
6. Tan, J., Shao, H., Xu, J., Du, L. & Luo, G. Mixture Absorption System of Monoethanolamine–Triethylene Glycol for CO<sub>2</sub> Capture. *Ind. Eng. Chem. Res.* **50**, 3966–3976 (2011).
7. Skylogianni, E., Wanderley, R. R., Austad, S. S. & Knuutila, H. K. Density and Viscosity of the Nonaqueous and Aqueous Mixtures of Methyl-diethanolamine and Monoethylene Glycol at Temperatures from 283.15 to 353.15 K. *J. Chem. Eng. Data* **64**, 5415–5431 (2019).





## Chapter 6

# Solvent Evaluation

*This chapter discusses the overall technical evaluation of MDEA-MEG-H<sub>2</sub>O solvents for combined H<sub>2</sub>S removal and hydrate control subsea and proposes a general guideline when assessing new solvents.*

The technical performance of the MDEA-MEG-H<sub>2</sub>O solvent for the combined H<sub>2</sub>S removal and hydrate control subsea is assessed by evaluating the properties measured in this work and parallel studies from the literature. In this chapter, these properties are categorized into three general groups; removal efficiency, trouble-free operations and environmental impact. Each category and property is discussed and a solvent characterization approach is suggested. A major part of this chapter is included in the conference publication #4, which also covered density, viscosity and VLE results previously presented. The full article as it is published can be found in the Appendix.

## 6.1 Solvent characterization

A simplified categorization of the properties and characteristics necessary to fully describe a solvent has been proposed. Figure 6.1 depicts the categories, i.e. removal efficiency, trouble-free operations and environmental impact, and the properties included in each one of them. Many of the properties are interconnected and may influence directly or indirectly the performance of a solvent, for example, viscosity, which falls into both removal efficiency and trouble-free operations categories. The suggested property categorization aims at providing a clear “work plan” for solvent characterization rather than oversimplifying the interactions of solvent properties. A description of each property and relevant information for the MDEA-MEG and MDEA-MEG-H<sub>2</sub>O systems are provided in the following sections.

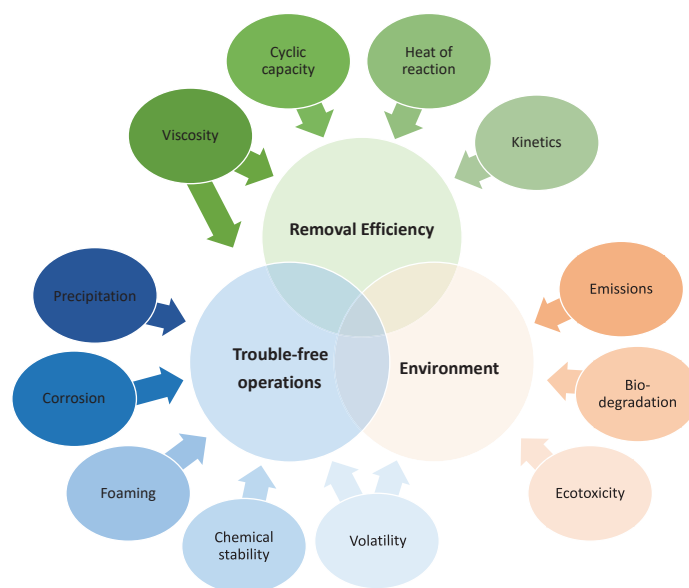


Figure 6.1. Simplified categorization of solvent characterization properties

## 6.1.1 Removal efficiency

### 6.1.1.1 Absorption capacity and cyclic capacity

The absorption capacity of a solvent provides information about how much acid gas can be removed by a given amount of solvent, or reversely, how much solvent must be used to remove the desired gas amount, under specific pressure and temperature conditions. It is often expressed in terms of loading  $\alpha$  in mol H<sub>2</sub>S/mol amine or kg H<sub>2</sub>S/kg solvent. The H<sub>2</sub>S absorption capacity of the MDEA-MEG-H<sub>2</sub>O as well as the importance of knowing the cyclic capacity of a solvent was already discussed in Chapter 4.

It was concluded that the addition of MEG in aqueous MDEA decreases the solvent's absorption capacity. This lower solvent capacity is acceptable in this process because the solvent now serves two purposes, both desulfurization and dehydration, as long as the water content specifications are also met. The cyclic capacity based on the experimental data seems to be higher in 30 wt% MDEA – 40 wt% MEG – 30 wt% H<sub>2</sub>O than in 30 wt% MDEA – 70 wt% H<sub>2</sub>O, assuming that absorption takes place at 283 K, desorption takes place at 393 K and the partial pressures at the bottom of the absorber and the desorber are 6.6 and 86.9 kPa, respectively. The H<sub>2</sub>S partial pressures are limited by the experimental data, which are not in the typical operational conditions' range. Therefore, more data are required in order to draw solid conclusions about the amine-glycol-water solvent's capacities.

Careful planning is necessary when high-pressure and HSE hazardous gases are used when performing VLE experiments. While for low-pressure measurements with CO<sub>2</sub>, it is typical to obtain around five VLE points per day, this is not the case for high-pressure experiments with H<sub>2</sub>S. In this work, three experimental points were obtained per week by performing GC analysis for both vapor and liquid phase. This time-consuming and, thus, costly experimental work becomes more challenging in the case of a chemical system acting as both H<sub>2</sub>S and water removal agent.

Co-absorption of other gases which are also present in the sour gas stream, such as carbon dioxide and hydrocarbons, should be also assessed during solvent characterization. The base case for this process is a sour gas with no requirement for carbon dioxide removal; therefore, co-absorption of carbon dioxide is minimum. For aqueous systems, a comparison between the data obtained with H<sub>2</sub>S (total pressure 2000 kPa) and CO<sub>2</sub> in a 30 wt% MDEA – 40 wt% MEG

– 30 wt% H<sub>2</sub>O is possible only at 353 K due to the different experimental methods used. For partial pressure of the acid gas at 26-28 kPa, the loadings are 0.185 mol H<sub>2</sub>S/mol MDEA (0.466 mol H<sub>2</sub>S/kg solution) and 0.062 mol CO<sub>2</sub>/mol MDEA (0.155 mol CO<sub>2</sub>/kg solution). By using a tertiary amine in the amine-glycol system, CO<sub>2</sub> absorption is expected to be minimized in non-aqueous systems. Although the measurements with CO<sub>2</sub> show that some carbon dioxide will be absorbed also in non-aqueous solutions, the amount is small. For example, in a 30 wt% MDEA – 70 wt% MEG, which showed the most pronounced chemical effects, and at 353 K, the loading of the solvent is 0.052 mol CO<sub>2</sub>/mol MDEA at partial pressure of 86 kPa. It can, therefore, be concluded that this solvent would also be applicable in cases that require removal of small CO<sub>2</sub> amounts. The knowledge of the VLE behavior of the system in the presence of both acid gases would be beneficial for better understanding of the system.

Hydrocarbon solubility into the solvent must be considered to ensure the minimization of methane loss into the solvent and other possible effects that dissolved hydrocarbons can induce. Methane solubility data in neither MDEA-MEG nor MDEA-MEG-H<sub>2</sub>O have been found. However, low methane losses are expected in these systems since MDEA is sparingly miscible with hydrocarbons (Jou et al., 1998; Kohl and Nielsen, 1997) while the solubility of CH<sub>4</sub> in MEG is low and significantly lower than TEG (Jou et al., 1994, 1987; Zheng et al., 1999), which is commonly used in natural gas dehydration.

### **6.1.1.2 Heat of reaction**

Gas sweetening is an energy intensive process with the regeneration energy requirements comprising more than 80% of the total OPEX (Raynal et al., 2011). During regeneration, heat is required in order to bring the solution to the temperature of the stripper (sensible heat), produce stripping steam (latent heat) and release the acid gas from the solvent (heat of absorption). The latter is the sum of the heat of reaction and the enthalpy change due to the physical dissolution of acid gas in the solvent, and it is the main contributor in the heat requirements. Therefore, it is an important property whose knowledge is necessary during the solvent selection and process optimization. On the one hand, the higher the heat of reaction is, the higher the temperature sensitivity of the solvent, and therefore the higher the cyclic capacity. On the other hand, the lower the heat of reaction is, the lower the heat requirement is in order to reverse the reaction release the acid gas.

Heat of absorption data for H<sub>2</sub>S-MDEA-H<sub>2</sub>O systems have been reported (Jou et al., 1982) with an indicative value of approximately 40 kJ/mol H<sub>2</sub>S for loadings up to 0.5 mol H<sub>2</sub>S/mol MDEA in a 48.9 wt% aqueous MDEA. The low heat of absorption in MDEA systems leading to low energy requirements is one of the main advantages of the MDEA process. As far as the amine-glycol system is concerned, Xu et al. calculated from VLE data the heat absorption in a 30 wt% MDEA – 65 wt% MEG – 5 wt% H<sub>2</sub>O and found that it was slightly lower than the one calculated with the same method by Jou et al. for aqueous MDEA (Jou et al., 1982; Xu et al., 2002a).

### 6.1.1.3 Kinetics

Kinetics are equally important as thermodynamic properties in the evaluation of a solvent's removal efficiency. As mentioned in the Chemistry section of Chapter 2, the choice of a tertiary amine in the amine-glycol solvent for the selective removal of hydrogen sulfide and hydrate control is reasoned on the high reaction rate with hydrogen sulfide and slow reaction rate with carbon dioxide (Kohl and Nielsen, 1997).

Xu et al. investigated nine non-aqueous MDEA solutions for selective H<sub>2</sub>S removal over CO<sub>2</sub>, among which with MEG, and showed that the selectivity is improved compared to its aqueous counterpart (Xu et al., 2002b). Furthermore, Eimer measured the absorption rate of H<sub>2</sub>S in MDEA in its blend with water and TEG in order to investigate whether the reaction is instantaneous also in the presence of TEG (Eimer, 1994). He suggested that indeed the reaction takes place in the instantaneous regime, however, there is not a clear trend between glycol content and absorption rate.

As far as CO<sub>2</sub> removal is concerned, Wanderley and his co-workers measured the mass transfer rates in MDEA-MEG-H<sub>2</sub>O, among other systems, and the results indicated that they seem to increase only minimally (Wanderley et al., 2019). Any effects due to the high viscosity of TEG, are expected to be lower with MEG. Reaction rates and mass transfer rates also influence the practical aspects of the solvent application, such as the length of the pipeline required for the sufficient removal of hydrogen sulfide and water to the desired concentration and the location of the separation system for the solvent from the natural gas stream.

## 6.1.2 Trouble-free operations

### 6.1.2.1 Viscosity

Among the physical properties of a solvent, density, viscosity and surface tension, viscosity has the most pronounced effects in mass transfer (Rochelle, 2016). High viscosity influences the diffusivity of the gas into the solvent and, therefore, the mass transfer rates. In addition, high viscosity affects the efficiency of the cross-heat exchanger, typically employed between the absorber and the stripper, leading to higher costs related to both OPEX and CAPEX.

Trouble-free operations can be ensured by verifying that the high viscosity of the solvent to be pumped to the pipeline and get separated from the gas can be tolerated by the processing equipment. A viscosity study for the binary MDEA-MEG and ternary MDEA-MEG-H<sub>2</sub>O system at ambient pressure and temperatures as low as 283 K, as presented in Chapter 3, showed that the viscosity is significantly higher compared to aqueous MDEA. At 313 K, the viscosity of the benchmark 50 wt% aqueous MDEA is approximately 5.2 mPa·s (Al-Ghawas et al., 1989; Li and Lie, 1994; Pinto et al., 2017), while for the blend 50 wt% MDEA – 50 wt% MEG is more than four times higher, 21.9 mPa·s. It has also already been discussed that the viscosity of the amine-glycol solvent is expected to decrease upon H<sub>2</sub>S loading, following the behavior of aqueous MDEA, while it is expected to slightly increase upon pressurization at 100 bar.

High viscosity systems are often encountered in the oil and gas operations, for example in TEG dehydration units, without posing operational risks (Holm, 1993). For subsea separation equipment, typical viscosity requirement is to be lower than 200 mPa·s at 277 K. Assuming that the operation will take place at 283 K, the data collected pinpoint to the aqueous and non-aqueous MDEA-MEG blends with more than 90 wt% MDEA content that may not fulfill the viscosity criterion. Additional viscosity measurements with H<sub>2</sub>S loaded and pressurized solvent and mass transfer rate measurements are required to assess the role of viscosity in the removal efficiency of the solvent and trouble-free operations.

### 6.1.2.2 Precipitation

The potential for precipitation during the actual temperature and pressure conditions of the process should be assessed based on the process under focus. For example, for onshore gas sweetening, there are some novel precipitation-based concepts for CO<sub>2</sub> removal promising for reducing the regeneration heat duties. For subsea applications, precipitation is an absolute

“showstopper” due to HSE risks if processing equipment designed for gas-liquid flow gets damaged and due to high costs during the imminent production upset and intervention. No precipitation issues have been observed or reported in the literature in the absorption of hydrogen sulfide/water in either MDEA or MEG, to the author’s best knowledge.

### **6.1.2.3 Foaming**

Foaming is the formation of stable bubbles that, in the case of amine-based gas sweetening, occur mainly in the absorber due to presence of amine degradation products, corrosion inhibitors and other contaminants. Foaming is a serious operation problem in gas sweetening and research is conducted to better understand the phenomenon and its sources in natural gas sweetening with aqueous MDEA (Alhseinat et al., 2014; Pal et al., 2015).

Foaming was observed during some of the VLE experiments with CO<sub>2</sub> and aqueous MDEA-MEG, conducted at isothermal conditions and increasing loading. However, this should not be an issue for our base case where the CO<sub>2</sub> content is low and the process is operated for the selective removal of H<sub>2</sub>S. Absorption in a co-current contactor (as in the subsea pipeline) with H<sub>2</sub>S and non-aqueous or water-lean MDEA-MEG systems should be studied in order to draw solid conclusions about possible foaming issues, though generally co-current contactors are not prone to foaming (Kohl and Nielsen, 1997).

### **6.1.2.4 Chemical stability and degradation**

The ideal solvent is chemically stable, resistant to both thermal degradation and oxidative degradation. An easily-degraded solvent is connected to high chemical costs because fresh solvent is required to be constantly fed as well as operational problems, such as the aforementioned foaming. For subsea or offshore application, the high costs associated with the fresh chemicals’ transportation and storage dictate the use of regenerative chemically stable systems.

Thermal degradation occurs mainly in the bottom of the desorber and in the cross-heat exchanger and should be studied at the relevant conditions (Vega et al., 2014). For MDEA-MEG systems, the limiting temperature in the process is the degradation temperature of MDEA, 393 K (Pandey, 2005), because it is lower than the degradation temperature of MEG, 438 K (GPSA, 2014). Although degradation studies of aqueous or non-aqueous MDEA-MEG in the presence of hydrogen sulfide have not been found, thermal stability and corrosion were studied in blends of tertiary amines and glycols in the presence of carbon dioxide by Shoukat et al.

(Shoukat et al., 2019, 2016). It was found that aqueous MDEA-MEG degrades more than aqueous MDEA or aqueous MDEA-TEG, and that other tertiary amines, 2-(Diethylamino)-ethanol (DEEA) and 3-(Diethylamino)-1,2-propanediol (DEA-1,2-PD), demonstrate better chemical stability in their blends with MEG.

Oxidative degradation is not typically a problem in natural gas sweetening, where the oxygen content is limited. At any rate, MDEA is known for its resistance to oxidation at absorber's conditions, however, if oxidized, MDEA forms diethanolamine, which can further react with nitrite and produce carcinogenic substances. In general, dissolved metals from corroded surfaces appear to act as oxidizing agents, making a solvent more prone to oxidative degradation in the presence of corrosion (Feron, 2016).

#### **6.1.2.5 Corrosion**

Corrosion is an important aspect in solvent selection considering the inherent HSE risks and the high cost of equipment replacement and production shutdown in the case of corrosion-induced material failure. Corrosion is the result of the combination of acid gases with water and the presence of aqueous amines (Kohl and Nielsen, 1997).

Namazi and Almasi studied corrosion in a gas sweetening plant in Iran using 45 wt% aqueous MDEA and found that the amine itself was not corrosive and that corrosion was detected in the stripper and the reboiler, but not in the absorber after 8 years of operation (Namazi and Almasi, 2016). Corrosion in the regeneration part of the process is expected due to the high temperatures used. At 393 K, Pal and Banat showed that, in the presence of both H<sub>2</sub>S and CO<sub>2</sub>, the solubility of iron is much higher in lean aqueous MDEA than in fresh solution, with 225 ppm opposed to 5 ppm in the fresh one (Pal and Banat, 2016). In the presence of only carbon dioxide, it has been reported that MDEA-MEG systems are more corrosive than MDEA-H<sub>2</sub>O or MDEA-TEG-H<sub>2</sub>O and that, again, DEEA and DEA-1,2-PD are less corrosive than MDEA (Shoukat et al., 2016). However, MDEA is already present in oil and gas operations and it is actually used to control corrosion, serving as a pH stabilizer. In fact, in the South Pars field in the Persian Gulf, MDEA and MEG are injected to simultaneously control the corrosion and the hydrate formation (Davoudi et al., 2014). Research is conducted on the desired pH and the effect on the glycol performance (Akhfash et al., 2017; Davoudi et al., 2014; Duan et al., 2013; Kvarekval and Dugstad, 2005).



### **6.1.2.6 Volatility**

During solvent selection and process development, knowing the vapor pressure of a chemical can help to identify possible volatility losses. High volatility can result in amine losses due to vaporization of the amine in the gas phase and, subsequently, in the sweet gas exiting the absorber. MEA is a typical example of an amine with high volatility, but for other amines traditionally used in gas purification, including MDEA, chemical losses due to high volatility is uncommon. In fact, concentrations up to 60 wt% aqueous MDEA can be used without significant amine losses (Kohl and Nielsen, 1997). MEG vapor pressure is also low, though higher than TEG (GPSA, 2014).

Vapor pressure measurements were performed for aqueous and non-aqueous MDEA-MEG in an ebulliometer, but unfortunately the results were not reproducible and, therefore, they were not reported. The lack of stirring in the ebulliometer seems to be the reason why equilibration issues occurred and, in some cases, two phases seemed to be formed in the equilibrium still.

### **6.1.3 Environment**

#### **6.1.3.1 Biodegradation and ecotoxicity**

Today, there is high focus on prevention and elimination of pollution in the environment. In gas treatment, chemicals can reach the environment through emissions and accidental spills. For offshore operations and subsea gas treatment, regulatory standards, such as the OSPAR convention in the North-East Atlantic, apply with regards to industrial waste disposal and environmental effects (OSPAR Commission, 2010). Biodegradation and ecotoxicity are two properties which can be showstoppers for a process.

Eide-Haugmo et al. conducted a biodegradability and ecotoxicity study for various amines, including MDEA (Eide-Haugmo et al., 2012). They found that it shows low biodegradability (less than 20%, which is the minimum recommended) and low ecotoxicity (EC-50 indicator is equal to 141 mg/l, while 10 is the minimum recommended). These findings are in agreement with the information from the Safety Data Sheets provided from MDEA suppliers (SIGMA-ALDRICH, 2016). According to MEG suppliers, monoethylene glycol is non-biodegradable and non-ecotoxic (SIGMA-ALDRICH, 2015). Finding a solvent that fulfills all the criteria is a

challenging task. The difficulty is demonstrated, for example, by the fact that oxidatively stable solvents are generally not biodegradable, like MDEA.

### **6.1.3.2 Emissions and aerosols**

In a traditional gas sweetening process, aerosol formation and emissions from the top of the absorber are the main environmental challenges. Besides leading to severe amine carry-over and chemical losses, amines emitted can react in the atmosphere via photo-oxidation and also via NO<sub>x</sub> reactions to form nitrosamines and nitramines, which are carcinogenic (Vega et al., 2014). However, the combined removal of hydrogen sulfide and hydrate control will take place in-line, where aerosol emissions are not an issue, but solvent carry-over and its effect on the consecutive gas processing stages should be investigated.

In a traditional dehydration process, aromatic hydrocarbons (benzene, toluene, e-benzene and o-xylene, BTEX), which are very soluble to glycols and hazardous air pollutants, are concentrated during the solution regeneration. In the MDEA-MEG process, the acid gas stream from the top of the stripper will contain mainly water vapor, hydrogen sulfide, less carbon dioxide and some aromatic hydrocarbons. Flaring is not allowed under regulations for sulfur emissions, therefore, other removal methods, such as liquid scavengers, or further processing in Claus units should be used to prevent the release of H<sub>2</sub>S to the environment (Watson, 2010). In the case of Claus units, the presence of the high molecular weight BTEX can lead to rapid catalyst deactivation and production of discolored sulfur. The solubility of BTEX in MEA-DEG is significantly higher than in the aqueous amine (Kohl and Nielsen, 1997), though BTEX solubility studies are not available for MDEA-MEG systems.

## **6.2 Solvent development approach**

Although every property plays its role in the design and development of a new process, a prioritization regarding the order in which the properties should be evaluated is necessary. It is common practice to start solvent development work by studying the properties related to removal efficiency. After a first screening of potential solvents, vapor-liquid equilibria, heat of absorption and kinetic investigations are performed. The removal efficiency criterion is based on a case-to-case evaluation, which is demanding in terms of time and resources. As long as

the removal efficiency criteria are met, the work proceeds to corrosion and chemical stability studies. Nonetheless, corrosive and easily-degraded chemicals can impair safe operations through material failure and hazardous emissions, in addition to lowering the process efficiency. It would be, therefore, a tremendous amount of time and resources wasted if to be found that an otherwise excellent solvent heavily degrades at the operating temperatures of the desorber. Especially because corrosion and degradation studies are often easier, faster and cheaper to study than vapor-liquid equilibrium experiments, for example.

It is suggested that a more practical and cost-efficient approach in solvent development is to start with a fast screening of promising solvents regarding removal efficiency, continue with corrosion, chemical stability and ecotoxicity studies, and, as long as these criteria are met and follow regulatory standards for air or marine pollution, proceed to the full thermodynamic, kinetic and physical properties investigations. In the case of hydrogen sulfide removal and hydrate control for subsea application, a significance level from 1 to 3 has been assigned to all properties in the order of appearance in the text; level 1 denotes highest significance and level 3 denotes lowest significance. Table 6.1 lists these properties, the significance level and a short comment/explanation about it, for the specific case of the combined H<sub>2</sub>S removal and hydrate control for subsea application. It is underlined that the successful solvent should fulfill the criteria for all the properties, and that this is a categorization based on the severity of the consequences it would have in case it failed to meet the process' requirements.

Precipitation, chemical stability, corrosion, biodegradation and ecotoxicity can be absolute showstoppers for the subsea removal of hydrogen sulfide and water vapor, due to intervention difficulties at long distances and deep waters as well as stringent environmental regulations. A blend of MDEA-MEG is rather stable without precipitation or corrosivity issues, at the studied temperatures and pressures, while other tertiary amines in their blends with MEG might possess higher chemical stability. Moreover, MDEA and MEG exhibit low ecotoxicity but they are not biodegradable. Despite these drawbacks, MDEA is currently used offshore as a pH stabilizer while MEG is routinely injected subsea to control hydrate formation (Davoudi et al., 2014) which would allow their use in a blend for additionally meeting H<sub>2</sub>S specifications.

Table 6.1 Property significance for solvent selection intended for the combined removal of H<sub>2</sub>S and hydrate control subsea.

Characteristic	Conditions	Significance
Absorption capacity	Removal efficiency	2
Heat of reaction	Regeneration energy requirement	3
Kinetics	Contact time can be adjusted by choosing solvent injection and collection points.	3
Viscosity	Umbilical delivery and distribution in the gas stream	2
Precipitation	Flow-assurance and revenue loss	1
Foaming	Removal efficiency and chemical loss	2
Chemical stability / degradation	Costly storage and transportation of fresh solvent offshore	1
Corrosion	HSE, high costs due to damaged equipment	1
Volatility	OPEX	3
Biodegradation/ ecotoxicity	Regulations for use offshore	1
Emissions	Regulations about BTEX, SO <sub>x</sub> for the topside processed stream from the stripper	3

Significance level 2 has been assigned to absorption capacity, viscosity and foaming, because these properties are essential for the successful employment of the solvent, but they will not compromise the safety of the operations. Rather, they would increase their cost in case of a slippage. Production streams can be mixed with other streams without hydrogen sulfide, for example, to meet transport specifications and sale requirements. In this work, it was found that the absorption capacity of the solvent decreases with MEG compared to the aqueous amine, while the effect of high pressure up to 100 bar seem to be the result of the non-ideality of the pressurized system leaving the loading of the solvent unaffected. The inferior performance of the amine-glycol blend is acceptable, as long as the solvent can also meet the water content specifications of the gas. More information is required in order to decide the solvent composition. Increasing the amine content in an aqueous or non-aqueous MDEA-MEG blend will significantly increase the viscosity of the system and affect the pumpability of the solvent.

Viscosity also affects indirectly the mass transfer properties and kinetics, which are given significance level 3. They define the length of the contactor, thus also, the injection and separation points. Since the pipeline serves as the contactor, there is great flexibility in this aspect. Furthermore, the knowledge of the heat of reaction is important together with the

regeneration scheme that would be appropriate for non-aqueous and water-lean solvents. Overall, the blend has low heat of reaction and it is believed that some water should be present to provide some steam in the reboiler. Volatility and emissions are assigned to the same significance level for two reasons. Because these are issues commonly addressed in the industry, and because MDEA-MEG solvents are not particularly volatile and chemical losses are not expected with the proposed configuration.

### 6.3 Conclusions

The properties required for solvent characterization are categorized to those related to removal efficiency, trouble-free operations and environmental impact, and the central role of the second category in solvent development was highlighted. The properties were discussed for aqueous and non-aqueous MDEA-MEG blends in the framework of simultaneous removal of hydrogen sulfide and hydrate control of natural gas subsea, assessing the solvent for its technical performance. More data, especially for the solvent's water vapor removal efficiency, process simulation and economic analysis are necessary for a complete overall evaluation of these systems.

### Bibliography

- Akhfash, M., Arjmandi, M., Aman, Z.M., Boxall, J.A., May, E.F., 2017. Gas Hydrate Thermodynamic Inhibition with MDEA for Reduced MEG Circulation. *J. Chem. Eng. Data* 62, 2578–2583. <https://doi.org/10.1021/acs.jced.7b00072>
- Al-Ghawas, H.A., Hagewiesche, D.P., Ruiz-Ibanez, G., Sandall, O.C., 1989. Physicochemical properties important for carbon dioxide absorption in aqueous methyldiethanolamine. *J. Chem. Eng. Data* 34, 385–391. <https://doi.org/10.1021/jc00058a004>
- Alhseinat, E., Pal, P., Keewan, M., Banat, F., 2014. Foaming study combined with physical characterization of aqueous MDEA gas sweetening solutions. *Journal of Natural Gas Science and Engineering* 17, 49–57. <https://doi.org/10.1016/j.jngse.2013.12.004>
- Davoudi, M., Heidari, Y., Safadoost, A., Samieirad, S., 2014. Chemical injection policy for internal corrosion prevention of South Pars sea-pipeline: A case study. *Journal of Natural Gas Science and Engineering* 21, 592–599. <https://doi.org/10.1016/j.jngse.2014.09.017>
- Duan, D., Jiang, S., Choi, Y.-S., Ne&#353, Ic, S., 2013. Corrosion Mechanism of Carbon Steel in MDEA-Based CO<sub>2</sub> Capture Plants. Presented at the CORROSION 2013, NACE International.

- Eide-Haugmo, I., Brakstad, O.G., Hoff, K.A., da Silva, E.F., Svendsen, H.F., 2012. Marine biodegradability and ecotoxicity of solvents for CO<sub>2</sub>-capture of natural gas. *International Journal of Greenhouse Gas Control* 9, 184–192. <https://doi.org/10.1016/j.ijggc.2012.03.006>
- Eimer, D., 1994. Simultaneous removal of water and hydrogen sulphide from natural gas (Dr. Ing thesis). NTNU, Trondheim.
- Feron, P.H.M., 2016. Absorption-Based Post-combustion Capture of Carbon Dioxide. Elsevier. <https://doi.org/10.1016/C2014-0-03382-5>
- GPSA, 2014. Dehydration, in: *Engineering Data Book*. Section 20. Gas Processors Suppliers Association, Tulsa, Oklahoma.
- Holm, P., 1993. Offshore TEG dehydration unit performance exceeds design. *Oil and Gas Journal* 96–103.
- Jou, F.-Y., Carroll, J.J., Mather, A.E., Otto, F.D., 1998. Solubility of Methane and Ethane in Aqueous Solutions of Methyldiethanolamine. *J. Chem. Eng. Data* 43, 781–784. <https://doi.org/10.1021/jc980003f>
- Jou, F.-Y., Deshmukh, R.D., Otto, F.D., Mather, A.E., 1987. Vapor liquid equilibria for acid gases and lower alkanes in triethylene glycol. *Fluid Phase Equilibria* 36, 121–140. [https://doi.org/10.1016/0378-3812\(87\)85018-5](https://doi.org/10.1016/0378-3812(87)85018-5)
- Jou, F.Y., Mather, A.E., Otto, F.D., 1982. Solubility of hydrogen sulfide and carbon dioxide in aqueous methyldiethanolamine solutions. *Ind. Eng. Chem. Proc. Des. Dev.* 21, 539–544. <https://doi.org/10.1021/i200019a001>
- Jou, F.-Y., Otto, F.D., Mather, A.E., 1994. Solubility of methane in glycols at elevated pressures. *Can. J. Chem. Eng.* 72, 130–133. <https://doi.org/10.1002/cjce.5450720120>
- Kohl, A.L., Nielsen, R.B., 1997. *Gas Purification*, Fifth. ed. Gulf Professional Publishing, Houston.
- Kvarekval, J., Dugstad, A., 2005. Pitting Corrosion in CO<sub>2</sub>/H<sub>2</sub>S Containing Glycol Solutions under Flowing Conditions. Presented at the CORROSION 2005, NACE International.
- Li, M.-H., Lie, Y.-C., 1994. Densities and Viscosities of Solutions of Monoethanolamine + N-methyldiethanolamine + Water and Monoethanolamine + 2-Amino-2-methyl-1-propanol + Water. *J. Chem. Eng. Data* 39, 444–447. <https://doi.org/10.1021/jc00015a009>
- Namazi, F., Almasi, H., 2016. Amine Corrosion in Gas Sweetening Plant: Causes and Minimization on Real Case Study. Presented at the CORROSION 2016, NACE International.
- OSPAR Commission, 2010. Discharges, Spills and Emissions from Offshore Oil and Gas Installations. OSPAR Commission: London, UK.
- Pal, P., AbuKashabeh, A., Al-Asheh, S., Banat, F., 2015. Role of aqueous methyldiethanolamine (MDEA) as solvent in natural gas sweetening unit and process contaminants with probable reaction pathway. *Journal of Natural Gas Science and Engineering* 24, 124–131. <https://doi.org/10.1016/j.jngse.2015.03.007>
- Pal, P., Banat, F., 2016. Comparison of thermal degradation between fresh and industrial aqueous methyldiethanolamine with continuous injection of H<sub>2</sub>S/CO<sub>2</sub> in high pressure reactor. *Journal of Natural Gas Science and Engineering* 29, 479–487. <https://doi.org/10.1016/j.jngse.2016.01.037>

- Pandey, M., 2005. Process Optimization in Gas Sweetening Unit - A Case Study [WWW Document]. URL <https://www.onepetro.org/download/conference-paper/IPTC-10735-MS?id=conference-paper%2FIPTC-10735-MS> (accessed 8.5.16).
- Pinto, D.D.D., Johnsen, B., Awais, M., Svendsen, H.F., Knuutila, H.K., 2017. Viscosity measurements and modeling of loaded and unloaded aqueous solutions of MDEA, DMEA, DEEA and MAPA. *Chem. Eng. Sci.* 171, 340–350. <https://doi.org/10.1016/j.ces.2017.05.044>
- Raynal, L., Bouillon, P.-A., Gomez, A., Broutin, P., 2011. From MEA to demixing solvents and future steps, a roadmap for lowering the cost of post-combustion carbon capture. *Chemical Engineering Journal*, Special Section: Symposium on Post-Combustion Carbon Dioxide Capture 171, 742–752. <https://doi.org/10.1016/j.ces.2011.01.008>
- Shoukat, U., Baumeister, E., Pinto, D.D.D., Knuutila, H.K., 2019. Thermal stability and corrosion of tertiary amines in aqueous amine and amine-glycol-water solutions for combined acid gas and water removal. *Journal of Natural Gas Science and Engineering* 62, 26–37. <https://doi.org/10.1016/j.jngse.2018.11.025>
- Shoukat, U., Fytianos, G., Knuutila, H.K., 2016. Thermal stability and corrosion studies of amines for combined acid gas removal and hydrate control for subsea gas treatment systems, in: 2016 Techno-Ocean (Techno-Ocean). Presented at the 2016 Techno-Ocean (Techno-Ocean), pp. 176–180. <https://doi.org/10.1109/Techno-Ocean.2016.7890641>
- SIGMA-ALDRICH, 2016. Safety Data Sheet, N-methyldiethanolamine ≥99%.
- SIGMA-ALDRICH, 2015. Safety Data Sheet, Ethylene glycol, Anhydrous 99.8%.
- Vega, F., Sanna, A., Navarrete, B., Maroto-Valer, M.M., Cortés, V.J., 2014. Degradation of amine-based solvents in CO<sub>2</sub> capture process by chemical absorption. *Greenhouse Gases: Science and Technology* 4, 707–733. <https://doi.org/10.1002/ghg.1446>
- Wanderley, R.R., Yuan, Y., Rochelle, G.T., Knuutila, H.K., 2019. CO<sub>2</sub> solubility and mass transfer in water-lean solvents. *Chemical Engineering Science* 202, 403–416. <https://doi.org/10.1016/j.ces.2019.03.052>
- Xu, H.-J., Zhang, C.-F., Zheng, Z.-S., 2002a. Solubility of Hydrogen Sulfide and Carbon Dioxide in a Solution of Methyldiethanolamine Mixed with Ethylene Glycol. *Ind. Eng. Chem. Res.* 41, 6175–6180. <https://doi.org/10.1021/ie020375o>
- Xu, H.-J., Zhang, C.-F., Zheng, Z.-S., 2002b. Selective H<sub>2</sub>S Removal by Nonaqueous Methyldiethanolamine Solutions in an Experimental Apparatus. *Ind. Eng. Chem. Res.* 41, 2953–2956. <https://doi.org/10.1021/ie0109253>
- Zheng, D.-Q., Ma, W.-D., Wei, R., Guo, T.-M., 1999. Solubility study of methane, carbon dioxide and nitrogen in ethylene glycol at elevated temperatures and pressures. *Fluid Phase Equilibria* 155, 277–286. [https://doi.org/10.1016/S0378-3812\(98\)00469-5](https://doi.org/10.1016/S0378-3812(98)00469-5)





## Chapter 7

# Conclusions and Recommendations for Future Work

### 7.1 Conclusions

The objective of this thesis was to determine the necessary thermodynamics and physical properties to characterize aqueous and non-aqueous blends of methyldiethanolamine (MDEA) and monoethylene glycol (MEG), due to their relevance for the combined hydrogen sulfide (H<sub>2</sub>S) removal and hydrate control process for natural gas subsea.

First, a literature review was conducted in order to collect information regarding the technology status in gas sweetening and hydrate control and to identify scientific and industrial challenges for this combined process. It was found that current available technologies, such as inline separation, can support a process for the combined H<sub>2</sub>S removal and hydrate control subsea. However, limited work has been performed for the solvent characterization of the promising MDEA-MEG and MDEA-MEG-H<sub>2</sub>O systems, especially in the presence of H<sub>2</sub>S. In this direction, density, viscosity and vapor-liquid equilibrium (VLE) studies followed.

The density and viscosity of the aqueous and non-aqueous MDEA-MEG blends were investigated at temperatures from 283 to 353 K and ambient pressure at various compositions. The results showed that the density of the binary mixtures of MDEA-MEG decreases with temperature and with MDEA concentration, while the viscosity increases. The same behavior applies to the ternary systems as well, provided that the amount of water in the blend is constant. The calculated excess molar volumes were negative and the viscosity deviations were positive, indicating strong non-ideality of the mixtures at the studied conditions, due to the presence of attractive intermolecular forces and structural effects in the mixtures. Both density and viscosity data were modeled using NRTL-based models, while a comparison was performed with the Aspen liquid mixture viscosity model. The models demonstrated an average absolute relative

deviation (AARD) lower than 0.4% for density and 3% for viscosity for both models. Despite the high viscosity of MDEA-MEG blends, industrial feedback and literature data ascertained that it does not pose any practical difficulties in their application subsea.

Two high-pressure VLE studies with hydrogen sulfide covered the largest part of this work; the first for the system H<sub>2</sub>S-CH<sub>4</sub>-MDEA-H<sub>2</sub>O and the second for the combined solvent in the system H<sub>2</sub>S-CH<sub>4</sub>-MDEA-MEG-H<sub>2</sub>O. Methane was used as a make-up gas since it is the main constituent of natural gas. The experiments were conducted in a high-pressure static analytic setup and the focus of the studies was the investigation of the total pressure effect on the absorption capacity of the solvent. The first study included VLE experiments with 50 wt% aqueous MDEA at temperature of 323 K and pressure up to 3000 kPa and with 70 wt% aqueous MDEA at temperature of 283 K, 353 K and 393 K and pressures up to 10000 kPa, relevant to the operational conditions. The obtained data show that increasing H<sub>2</sub>S partial pressure and decreasing temperature leads to higher solvent loadings, at constant total pressure. The effect of total pressure on the liquid loading of the solvent is within or slightly higher than the experimental uncertainties, while it was shown that the small increase of the H<sub>2</sub>S partial pressure at increasing total pressure is attributed to the non-idealities of the vapor phase. This trend was not confirmed by the measurements at 393 K. However, these measurements suffered from the lack of quantifying water content in the vapor phase, which was calculated by the vapor pressure of the solvent assuming that it is independent of the total pressure of the system.

The system H<sub>2</sub>S-MDEA-H<sub>2</sub>O was modeled employing Peng-Robinson EoS to describe the vapor phase and eNRTL activity coefficient model for the liquid phase. Due to the wide pressure and loading range and a noticeable scatter at low loadings of the existing data, it was decided to consider loadings above 0.05 mol H<sub>2</sub>S/mol MDEA. The AARD for the H<sub>2</sub>S partial pressure and for the total system pressure was found to be 18% and 16%, respectively. The effect of including in the regression the data in the presence of methane at maximum total pressure of 2000 kPa, was studied and found minimal, even when including the data obtained with 70 wt% aqueous MDEA. However, for higher total pressure and different conditions than the studied ones, the use of models taking into account the methane presence was suggested. In this work, ebulliometric measurements of pure MDEA were included and new parameters for Antoine correlation were proposed. The model was fitted to the new measurements and all available literature data, covering a wide temperature range. The AARD was found 4%.

The second high-pressure VLE study was performed with a 30 wt% MDEA – 40 wt% MEG – 30 wt% H<sub>2</sub>O solution at the same experimental conditions as the 70 wt% aqueous MDEA. The findings regarding the effect of total pressure on the loading and the H<sub>2</sub>S partial pressure were also the same. Based on the newly obtained data and data reported in the literature, the effect of glycol on the H<sub>2</sub>S removal capacity of the solvent was studied. It was shown that increasing MDEA concentration under constant water content or lowering MEG content under constant amine concentration leads to higher absorption capacity. A comparison of the amine-glycol system with 70 wt% aqueous MDEA revealed that the H<sub>2</sub>S absorption capacity of the two solvents is similar, indicating that the former has potentially higher cyclic capacity.

The thermodynamic behavior of aqueous and non-aqueous MDEA-MEG systems was also investigated in terms of carbon dioxide (CO<sub>2</sub>) absorption, since CO<sub>2</sub> often co-exists with H<sub>2</sub>S. Due to numerous experimental challenges with the high-pressure apparatus, it was decided to perform this work using two similar low-pressure VLE setups. The measurements were mass balance-based and they were conducted at temperatures from 313 K to 393 K and pressures up to 600 kPa. According to the produced data, the absorption capacity of the aqueous solvents decreases with increasing glycol content and substitution of water, at constant amine concentration. In the non-aqueous systems, the solubility of carbon dioxide increases with increasing amine content up to 30-50 wt% MDEA-MEG, upon which it is reduced. Following Karl-Fischer titration and Nuclear Magnetic Resonance analysis, it was concluded that CO<sub>2</sub> reacts with MEG in the presence of MDEA and that glycol carbonate is formed in both aqueous and non-aqueous amine-glycol systems. A theory based on the autoprotolysis of the glycol was proposed, supported by additional VLE data in MDEA-triethylene glycol systems. The importance of these findings lies in the need to account for the enhanced CO<sub>2</sub> absorption in the MDEA-MEG systems during regeneration, while the suitability of these systems for streams with low CO<sub>2</sub> content, requiring limited conditioning, comes to the fore.

In the end, an overall evaluation of the technical performance of MDEA-MEG systems for the combined H<sub>2</sub>S removal and hydrate control for subsea application was performed, based on the findings of this thesis and literature information. Both MEG and MDEA are currently employed subsea and their blends seem to possess the most important properties in terms of HSE and flow assurance. Additional information concerning both solvent characterization and process configuration are required before the technical feasibility of this process can be concluded.

## 7.2 Recommendations for future work

All the properties discussed in Chapter 6 should be known for a complete technical evaluation of the solvent. Future work should primarily focus on extending the work performed in this thesis in order to define the optimum MDEA-MEG-H<sub>2</sub>O composition for meeting H<sub>2</sub>S specifications in the gas and, equally importantly, meeting the water content specifications during the transportation of the gas. Highly concentrated aqueous MDEA solutions should also be evaluated for their ability to remove water vapor. Moreover, given the findings of this work that CO<sub>2</sub> also reacts in MDEA-MEG systems, VLE data of these solvents in the presence of both hydrogen sulfide and carbon dioxide would be beneficial for a successful process design.

Although MDEA possesses the major advantage of being already in use subsea, other tertiary amines have been identified in the literature as better alternatives in terms of chemical stability and corrosion in their mixtures with MEG and CO<sub>2</sub>. These alternatives should be evaluated in the presence of H<sub>2</sub>S, too. MDEA could then be replaced, if they would be found superior with respect to their removal efficiency, effect on trouble-free operations and environmental impact.

During the high-pressure VLE studies, several challenges arose during the preparation of the experiments, the measurements and the data processing. The most often problem in this experimental work was leakages in the equilibrium cell and the surrounding valves, therefore, training of personnel with the specific type of valves and systems is desired. Moreover, it is crucial to investigate further how low water content in the vapor phase can be quantified by GC and why the liquid phase analysis by GC did not agree with the mass balances. As far as the vapor pressure of the solvents is concerned, it was not possible to be measured by using an ebulliometer. The possibility of stirring should be added in the ebulliometer or another method should be employed for the reliable measurement of the blends' vapor pressures. Unfortunately, some parts of the low-pressure VLE apparatuses, the densitometer and the viscometer cannot tolerate H<sub>2</sub>S, and it was not possible to perform measurements with H<sub>2</sub>S-loaded solutions. Such experimental data would be advantageous for the overall technical evaluation of the solvent.

Thinking of the bigger picture for this process, it is noticed that an important missing part is the regeneration scheme. Solely thermal regeneration is not likely to succeed when using non-aqueous or highly water-lean MDEA-MEG systems due to the low content of water and the different regeneration temperatures of the amine and the glycol. Therefore, alternative regeneration schemes, for example, using stripping gas should be studied. Kinetic data and mass

transfer data are also required in order to define the length of the pipeline/contactors, the injection point and the separation point of the solvent from the gas stream. Last but not least, inline gas-liquid contact and droplet distribution studies in the pipeline are necessary to demonstrate the technology for the combined H<sub>2</sub>S removal and hydrate control for subsea application.



## **Appendix**

### **Appendix A**

#### **Experimental setups and procedures**

A detailed description of the experimental setups used in this work and the corresponding experimental procedures is presented.

#### **Amine analysis**

During solution preparation, the amine concentration was verified by acid-base titration using a Mettler Toledo G20 titrator. Approximately 0.2 ml of liquid sample is diluted with 50 ml deionized water. The solution is titrated against H<sub>2</sub>SO<sub>4</sub>; 0.05 mol/L (0.1N) H<sub>2</sub>SO<sub>4</sub> is used for the analysis of low concentrated amine systems and 0.1 mol/L (0.2N) H<sub>2</sub>SO<sub>4</sub> is used for the analysis of highly concentrated amine systems. The end point is obtained at pH 2.5. At least two parallel measurements are performed for each sample and the average is reported. The absolute relative deviation (ARD) in the analyses of this work was always lower than 3%. Typically, amine analysis was performed before and after the experiment (density, viscosity, VLE) to ensure that even at high temperatures the composition remained the same.

#### **Density meter**

An Anton Paar Density Meter DMA 4500M was used during the density study of aqueous and non-aqueous MDEA-MEG systems. The density measurement is based on the oscillating U-tube method. The apparatus is calibrated with millipore water and dry air, as explained by Hartono et al. (Hartono et al., 2014). The density meter is connected with a thermally regulated carousel which can accommodate up to 44 sample vials. 10 ml of liquid sample are charged in the sample vials which are then introduced in the measuring compartment by the Xsample 452 system for automatic filling, cleaning and drying.

The measurements were conducted in the temperature range from 283 K to 353 K and ambient pressure and the density meter was validated against pure water, MDEA and MEG. Cleaning with acetone and drying was performed after every measurement. The measurements always started with an air check and measurement of Millipore water samples. For a continuous check of the results as well as an additional cleaning media, water samples were also placed after every three samples. Both the repeatability of the density measurements and the reproducibility between freshly prepared solutions of the same composition were studied. The average absolute relative deviations (AARD) were found to be equal to 0.01% and 0.02% for the repeatability and reproducibility study, respectively.

## Viscometer

A Lovis 2000 M microviscometer was used during the viscosity study presented in this work. The viscosity measurement is based on the falling-ball method and it is actually a correlation between the rolling time of a ball inside an inclined capillary and the sample's viscosity. The measurement takes place into a temperature-controlled capillary block, containing a capillary of a  $1.59 \cdot 10^{-3}$  m diameter with a gold ball. By changing the angle of the block, the rolling time of the ball is measured, which together with the density obtained from the DMA 4500 M, are used to calculate the sample dynamic viscosity. The limits of the viscometer are 353 K temperature and 60 mPa·s viscosity. It is connected in series with the density meter, making use of the same heated carousel and the Xsample 452 system, as described under the density meter. Therefore, the same sample can be used to measure, first, its density and, secondly, its viscosity.

The measurements were conducted in the temperature range from 283 K to 353 K and ambient pressure and pure water, MDEA and MEG were used as reference fluids for the validation of the apparatus. By repeating the measurement of the same sample and of two different samples of the same composition, the repeatability and reproducibility were determined. The repeatability measurements demonstrated 0.76% AARD and the reproducibility 0.69% AARD.

## Rheometer

For viscosities close to or higher than 60 mPa·s, which is the limit of the available capillary in the microviscometer, an Anton Paar MCR 100 rheometer with a double gap measuring cell (DG-26.7) was used. It consists of two cylinders placed concentrically the one inside the other, leaving a gap for the fluid of interest to be introduced.  $3.8 \cdot 10^{-6}$  m<sup>3</sup> of sample is required, whose



temperature is controlled and maintained stable throughout the measurement by virtue of the rheometer's built-in Peltier elements with an accuracy of 0.2 K. The measurement is actually the result of rotational tests with controlled shear rate and shear stress. The slope between the shear rate and the shear stress measured corresponds to the viscosity of the sample.

The rheometer was calibrated with standard viscosity solutions from Paragon Scientific Ltd., as explained by Hartono et al. (Hartono et al., 2014) and validated against pure water, MEG and MDEA. This apparatus was used for our measurements which exhibited the highest viscosities, mainly those performed at 283 K. Repeated measurements demonstrated a maximum absolute relative deviation (MARD) of 2.05% and an AARD of 0.5%. Solutions measured in both the microviscometer and the rheometer showed 2.72% MARD and 1.07% AARD from each other.

## **Ebulliometer**

A modified Swietoslowski ebulliometer was used for the measurement of the vapor pressure of pure MDEA and pure MEG, described earlier also by Kim et al. (Kim et al., 2008). Measurements can be performed at temperatures and pressures of up to 473 K and 1 atm, respectively. The setup consists of the ebulliometer, pressure and temperature controllers, a vacuum pump and a nitrogen bottle. The temperature is measured with calibrated Pt100 resistance thermosensors with an uncertainty of  $\pm 0.05$  K. A DP1520 pressure controller from Druck<sup>TM</sup> was used, calibrated against a BeamexC5 calibrator with an accuracy of  $\pm 0.03$  kPa. Equilibrium is achieved inside a  $2 \cdot 10^{-4}$  m<sup>3</sup> glass equilibrium still, bearing two valves for the sampling of both the vapor and the liquid phase. Water was used as the reference fluid for the validation of the apparatus and a 5% maximum error from the literature was found in equilibrium pressure.

After purging nitrogen through the ebulliometer, approximately  $0.8 \cdot 10^{-4}$  m<sup>3</sup> of liquid was charged inside the still. At the desired pressure and temperature, the system was left to equilibrate. Equilibrium was assumed after 10 min of stable pressure and temperature. The vapor pressure of MDEA was measured at the temperature range of 405 – 435 K and of MEG at the range 269 – 433 K. The experiments performed in this work indicated that high viscosity mixtures pose measuring limitations mainly due to lack of solution homogeneity inside the still. A stirring option would be particularly useful for vapor-liquid equilibrium measurements of viscous systems.

## The high-pressure VLE setup

The high-pressure vapor-liquid equilibrium (VLE) setup used in this work is an in-house manufacture by ARMINES and it is developed by Laugier and Richon (Laugier and Richon, 1986). The principle of the high-pressure VLE apparatus is described as a “static-analytic” method because the gaseous and liquid components to be studied are left to equilibrate, while the measurements are performed by analysis of the vapor and liquid phase by Gas Chromatography (Fonseca et al., 2011). Measurements with acid gases and organic sulfur compounds with different solvents in a wide range of pressures, from 0.5 to 10 MPa (19.9 MPa), and temperatures, from 223 to 473 K can be conducted. Online monitoring of the pressure and temperature enables the determination of equilibrium. The apparatus is similar to the one previously presented by Dicko et al. (Dicko et al., 2010) and its schematic is shown in Figure A. 1.

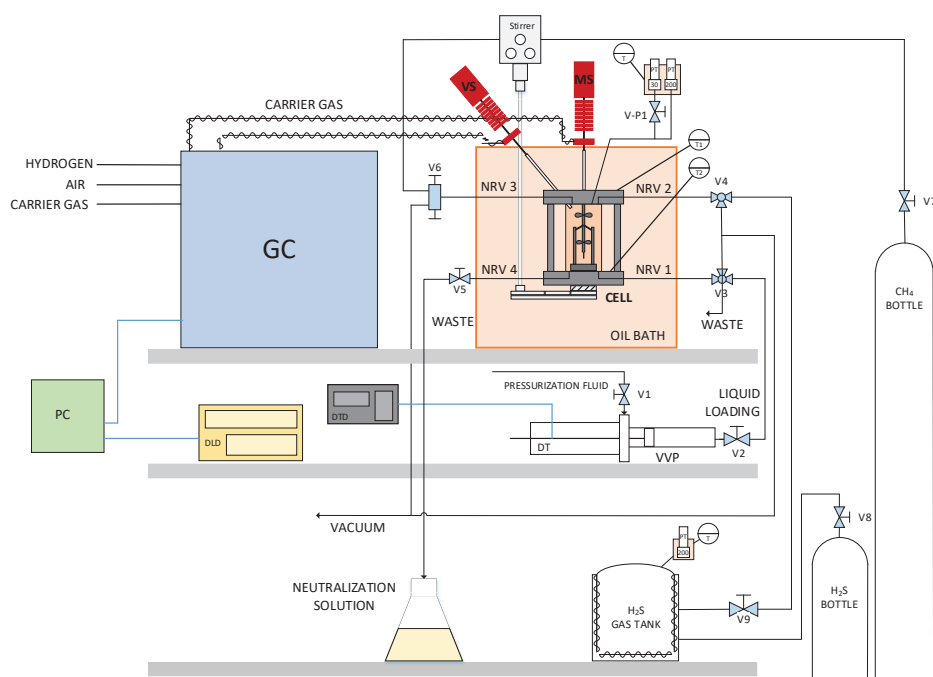


Figure A. 1 High-pressure VLE setup. DTD: Displacement Transducer Display, DLD: Data Logging Device, DT: Displacement Transducer, GC: Gas Chromatograph, MS: Mobile Sampler for the analysis of liquid phase, NRV: Non-Rotating valve, PC: Personal Computer for data acquisition, PT: Pressure Transducer, T: Thermocouple, V: Valve, VS: Vapor Sampler for the analysis of gas phase, VVP: variable volume press.

The setup consists of three distinct parts: a) the equipment for filling up the equilibrium cell, i.e. the variable volume press (VVP), the gas bottles and gas tanks, b) the equilibrium cell, including automatic samplers for the gas and the liquid phase(s) and c) the equipment for the analysis of the samples, i.e. the gas chromatograph (GC). Each of these parts consists of various valves and instrumentation. The temperatures in the equilibrium cell and gas tank are measured through 100  $\Omega$  Platinum resistance temperature detectors (Pt100) which are carefully and periodically calibrated. The Pt100 are connected to an HP data acquisition unit (HP34970A), which is connected to a personal computer through RS-232 interface.

a) The equipment for filling up the equilibrium cell.

The amount of liquid solution and gas to fill the cell with, must be known in order to be able to perform a VLE measurement. A variable volume press (VVP), composed by the variable volume pressure cell, a piston and a displacement transducer, is used to introduce the liquid solution inside the cell and record the exact displacement of the piston. Back-pressure of approximately 500 kPa is applied in order to move the piston and introduce the liquid. The piston displacement is measured and together with the knowledge of the internal diameter of the cell, the exact volume is determined.

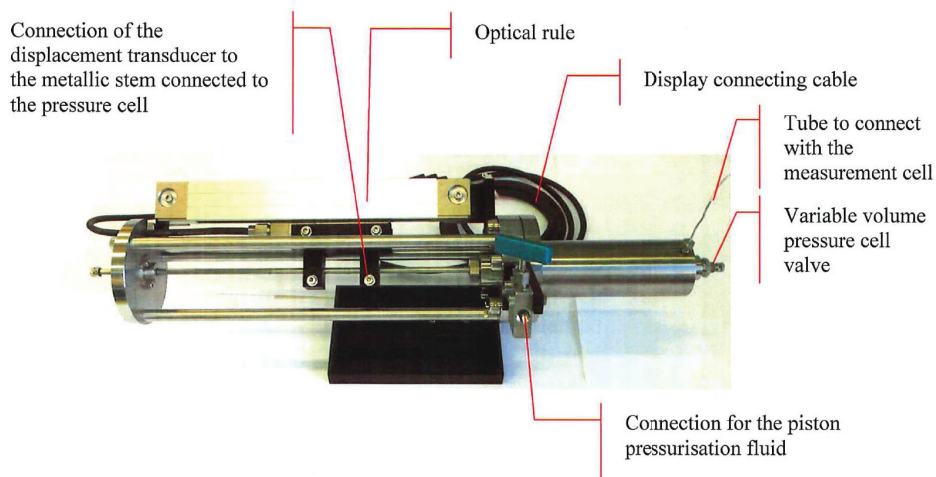


Figure A. 2 The variable volume press (Figure taken from the user manual from ARMINES).

A cylindrical gas tank with volume of  $1.61 \cdot 10^{-4} \pm 5 \cdot 10^{-8} \text{ m}^3$  was used as an intermediate gas storage between the gas bottle and the equilibrium cell. A calibrated Druck<sup>TM</sup> pressure transducer was mounted on the top of the gas tank and was connected to the HP data acquisition

unit. The transducers are maintained at constant temperature (temperature higher than the highest temperature of the study) by means of a specially made oven, which is controlled using a PID regulator (WEST, model 6100). The main reason of using gas tanks is to avoid opening the H<sub>2</sub>S bottles many times, since one pressurization of the gas tank from the bottle up to 1500 kPa was adequate for more than six experiments. In addition, direct pressurization of the cell from the H<sub>2</sub>S gas bottle was avoided, therefore, in the extreme case of a leakage, limited amount of hydrogen sulfide would be released.

#### b) The equilibrium cell

The equilibrium cell consists of a sapphire tube with two Hastelloy flanges, one on the top and one on the bottom of the tube. DuPont Kalrez O-rings which can tolerate high temperature, pressure and are resistant to sour multi-phase fluids containing H<sub>2</sub>S are used for sealing between the tube and the flanges. The upper flange accommodates two non-rotating stem loading valves, for H<sub>2</sub>S and for CH<sub>4</sub>, and the lower flange accommodates two more, only one of which was used for the loading of the liquid solution and the discharge of the cell into a caustic solution. A stirring system is integrated to the cell in order to reduce the time of equilibration and ensure phase homogeneity. Inside the cell, there is a rotating axis with one propeller mounted on the rotating axis for stirring the gas phase and a magnetic bar in the bottom of the axis for stirring of the liquid phase. A magnetic rod outside the cell causes the axis inside the cell to rotate by means of a variable speed motor.

The temperature is controlled by immersing the cell into an oil bath and it is monitored by two 100 Ω Platinum resistance temperature detectors (Pt100) with an uncertainty of ± 0.02 K. Each flange accommodates one Pt100 thermoelement. The upper flange also accommodates a cartridge heater with an integrated thermocouple to allow for additional heating of the flange to eliminate any temperature gradient within the cell. The cell is equipped with two Druck<sup>TM</sup> pressure transducers, one for 0–3 MPa and the other for 0–30 MPa pressure range, respectively, which are maintained at the temperature they were calibrated at. The uncertainty is 0.6 kPa. The cell volume when both pressure transducers are open to the cell is  $33.12 \cdot 10^{-6} \pm 5 \cdot 10^{-8} \text{ m}^3$  and, when the low-pressure transducer is isolated, it is  $32.24 \cdot 10^{-6} \text{ m}^3$ . Temperature and pressure are monitored through the HP data acquisition system. Besides connecting the equilibrium cell with the temperature and pressure measuring elements, the upper flange also serves as a support for the ROLSI<sup>TM</sup> electromagnetic samplers (ARMINES, 2003). A ROLSI sampler is shown in Figure A. 3.

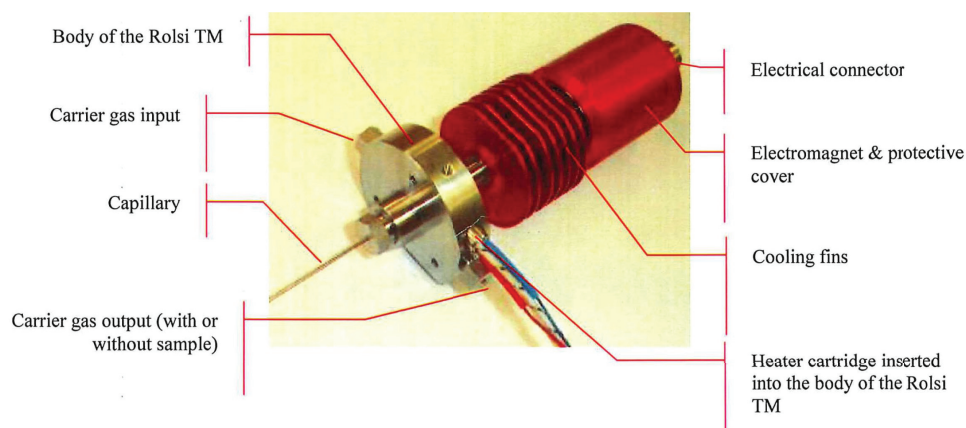


Figure A. 3 ROLSI™ sampler (Figure taken from the user manual from ARMINES).

Two capillaries, with designated diameter and level inside the cell, allow for the automatic sampling of the vapor and liquid phase each. The gas phase capillary enters at an angle while the liquid phase capillary enters vertically. The latter serves as a guide for the stirring axis inside the cell too. The body of the ROLSI™ practically separates the moving part of the sampler and the fixed capillary. The moving part consists of a polymer part in its lower end and a soft iron nucleus and a return spring in the upper end. When electromagnetic force is applied, the moving part is drawn up and unseals the upper part of the capillary for sample withdrawal. The carrier gas from the GC flows through the body and the upper part of the capillary and transfers the sample to the GC column for analysis, via a heated transfer line.

The size of the samples taken, especially under conditions of a given pressure and temperature, is in direct proportion to the duration of the sampling time. Pressures, temperatures and thus viscosities varied greatly in our work, thus the sampling time had to be adjusted every time in order for the sample concentration to be within the range of the GC calibration. Generally, the sampling time was highest at the lowest pressure and decreased at higher pressures, at constant temperature. The sampling times for vapor sample covered the range 0.13-0.50 s at 2000 kPa bar, 0.06-0.13 s at 6000 kPa and 0.04-0.08 s at 10000 kPa, while for the liquid phase covered the range 0.20-1.10 s at 2000 kPa, 0.08-0.50 s at 6000 kPa and 0.07-0.40 s at 10000 kPa. It is worth noting that the diameter of the two capillaries are different.

### c) The gas chromatograph

This setup contains a PERICHROM (model PR-2100) gas chromatograph equipped with a thermal conductivity detector (TCD) and a flame ionization detector (FID), which were operated at 453 K and 523 K, respectively. The analysis column is a Porapak-R column R80/100 mesh (length 2 m, diameter 2 mm) from RESTEK. Helium was used as a carrier gas at a flow rate of 20 ml/min. A valve is installed on the GC which acts as a divider of the column in two parts, the first part where the sample is injected (pre-column) and the second part where the analysis takes place (main column). The valve can automatically close at a requested time in order to redirect towards the waste undesired components, instead of letting them pass in the main column. Undesired components are those which accumulate in the column, resulting in a tail on the chromatogram, decay of the column and eventually failure to obtain reproducible chromatograms. In our case, these components are MDEA and MEG which are not measured, but calculated assuming constant ratio with water. The software used for GC acquisition and treatment is WINILAB III.

After careful testing and calibration of the detectors, temperature programs were created for the vapor phase analysis, liquid phase analysis, baking of the column and stand-on mode. A constant temperature program at 333 K was used for the quantification of both methane and hydrogen sulfide in the vapor phase. Analysis at 373 K was also performed to check for water presence in the vapor phase. For the liquid phase analysis, the temperature program was extended and set to 373 K for the measurement of water. The last temperature level was always 503 K for baking the column in order to remove any possible remaining sample. The temperature and duration of each one of them were decided based on the retention time of the components, the carrier gas flow rate, the ramp rate of the oven temperature and the clarity of the signal in the chromatogram. By injecting known amounts of gases in the GC, a calibration correlation between the peak area in the chromatogram and the number of moles was found. The gases were injected using an automatic syringe (SGE eVol XR syringe) and the liquids using manual syringes.

The TCD was calibrated for all components measured, i.e. methane, hydrogen sulfide and water, while the FID only for methane, since the rest cannot be detected. Although methane is also detected by the TCD, FID is more sensitive and suitable for detecting low methane concentrations. Therefore, the FID was used for the measurement of methane in the liquid phase, while it was saturated during the sampling of the vapor phase whose main component is

methane. Moreover, the amount of hydrogen sulfide and methane differed significantly at different experiments. In some cases, the option of increasing the sensitivity of the detector was used. For example, the TCD was calibrated for both sensitivity level “Gain 1” and “Gain 5” in order for the H<sub>2</sub>S amount in the sample to be always within the calibration range. This was necessary because adjusting the sampling time was not in all cases sufficient. A typical chromatogram where both detector sensitivities were employed is shown in Figure A. 4.

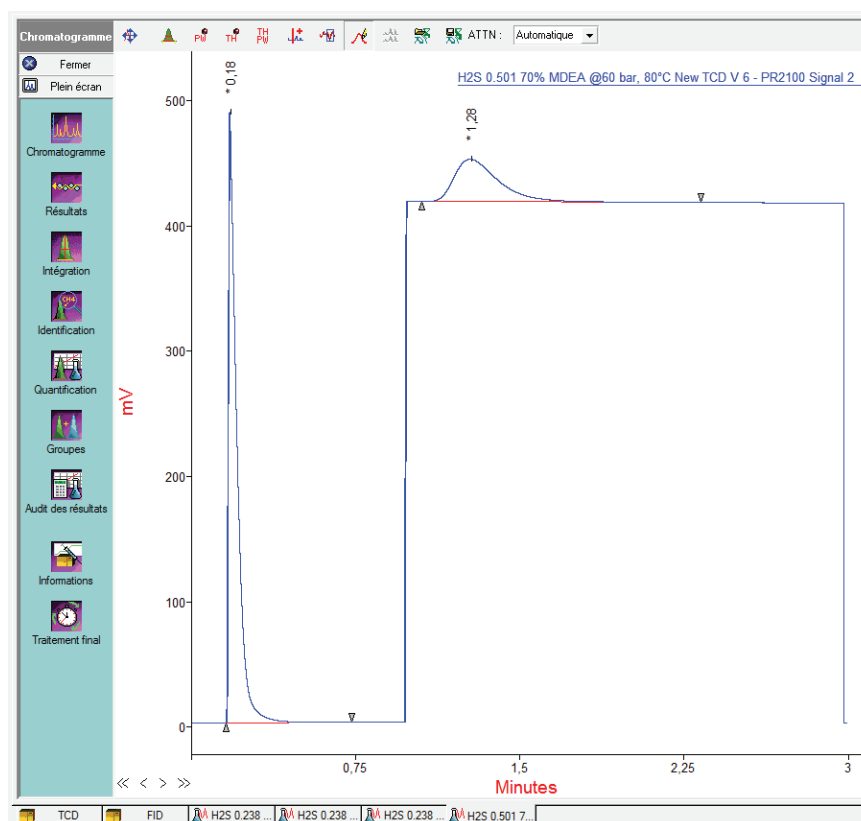


Figure A. 4 Typical TCD chromatogram of vapor phase analysis using gain 1 for methane up to ca. 0.9 min and gain 5 for hydrogen sulfide afterwards.

It was found that manual integration of the peaks in the chromatogram shows higher repeatability than the automatic one. Therefore, all the peaks were integrated manually in this work. In order to check the repeatability of the measurements and to perform uncertainty analysis, five samples at least were withdrawn, the first two of them usually were required to saturate the transfer lines in terms of adsorption. Disturbance to equilibrium was considered negligible due to the small volume of each sample.

The experimental procedure starts with the cleaning of the cell and the tubings using hot deionized (DI) water and ethanol, drying, and setting it to vacuum for at least 10 hours. The solution is prepared under vacuum directly inside the VVP and can be used for multiple experiments. The solution is introduced inside the cell, and the end displacement position is recorded, so as the exact amount of solution added can be calculated. Then, the cell is immersed into the liquid bath, the stirrer is set on and the desired temperature of the experiment is set. Temperature stabilization requires approximately 30-60 min, after which the vapor pressure of the solution is recorded.

Most of the experiments were conducted by first deciding the global loading, i.e. mol of H<sub>2</sub>S inside the cell per mol of amine, inside the cell. Based on the PVT conditions of the H<sub>2</sub>S gas tank before and after the filling of the cell, the amount of H<sub>2</sub>S introduced can be determined. Knowing the moles of H<sub>2</sub>S introduced in the cell, the global loading can be calculated based on Eq. A. 1 and Eq. A. 2. In this work, REFPROP software (Lemmon et al., 2018) and, specifically, a Helmholtz energy-based equation of state developed by (Lemmon and Span, 2006) for pure H<sub>2</sub>S were used.

$$n_{H_2S} = n_{H_2S,tank}^{before} - n_{H_2S,tank}^{after} \quad \text{Eq. A. 1}$$

$$\alpha_{glob} = \frac{n_{H_2S}}{n_{MDEA}} \quad \text{Eq. A. 2}$$

In order to perform experiments with increasing H<sub>2</sub>S loading, small amount of H<sub>2</sub>S are introduced in steps and, in every step, samples are withdrawn upon equilibration for GC analysis. Such is the case of the experiments of this work performed with 50.1 wt% MDEA aqueous solution. Due to limitations of the ROLSI<sup>TM</sup> sampler, the total pressure should be minimum 500 kPa, thus, makeup gas should be used. Higher loadings are reached by adding more H<sub>2</sub>S into the cell and repeating the above-mentioned procedure. For the systems 70 wt% MDEA – 30 wt% H<sub>2</sub>O and 30 wt% MDEA – 40 wt% MEG – 30 wt% H<sub>2</sub>O, two series of experiments were conducted based on the global loading, one for 0.2 and one for 0.5 mol H<sub>2</sub>S/mol MDEA. The experimental procedure varies in the way that after equilibrium is reached, makeup gas is added at isothermal conditions and a VLE measurement is conducted at increasing total pressures. Typically, performing this type of experiments lasts approximately one week for one temperature and three different pressure levels.



In this work, the liquid phase concentrations reported were calculated based on the mass balances and the vapor phase analysis, due to the fact that the liquid phase analysis did not match the mass balance. Knowing the pressure, temperature and the composition of the vapor phase, the density of the vapor phase was estimated using REFPROP software (Lemmon et al., 2018). Eq. A. 3 to Eq. A. 6 show the calculations for the determination of the liquid loading from the vapor phase density.

$$n_{tot}^v = \rho^v \cdot V^v \quad \text{Eq. A. 3}$$

$$n_i^v = n_{tot}^v \cdot y_i \quad \text{Eq. A. 4}$$

$$n_i^l = n_{tot} - n_i^v \quad \text{Eq. A. 5}$$

$$\alpha = \frac{n_{H_2S}^l}{n_{MDEA}} \quad \text{Eq. A. 6}$$

where  $\rho^v$  is the molar density of the gas mixture, calculated using REFPROP and  $V^v$  is the volume of the vapor phase. The volume of the vapor phase is calculated by subtracting the volume of the liquid solvent from the volume of the cell, which is known. Knowing the mass introduced in the cell at ambient temperature, the liquid phase volume can be calculated by a suitable density correlation.

## The low-pressure VLE apparatus

The low-pressure vapor-liquid equilibrium measurements in this work for CO<sub>2</sub>-MDEA-MEG and CO<sub>2</sub>-MDEA-MEG-H<sub>2</sub>O systems were conducted using two similar setups, named VLE-1 and VLE-2. A schematic has been drawn by Hartono and his co-workers (Hartono et al., 2017) and is shown in Figure A. 5. It can be seen that the setup consists of a glass reactor, a storage cylinder for CO<sub>2</sub>, a condenser, a vacuum pump and the gas bottles. The volume of the glass reactor and the storage cylinder is approximately  $1 \cdot 10^{-3} \text{ m}^3$  and their pressure and temperature are constantly monitored and logged. The only difference between VLE-1 and VLE-2 is that the reactor in VLE-1 is connected with one pressure transducer (PCE-28, 0-600 kPa) while the reactor in VLE-2 employs two pressure transducer, one for low pressures (PTX7517-1, 0-200 kPa) and one for higher pressures (PTX5072, 0-600 kPa). The same type of pressure transducers

is used in each set up for the reactor and the storage cylinder. The temperature is monitored by Pt100 resistance thermosensors and it is controlled a Julabo ME6 heat circulator using ethylene glycol as a heating medium. Silicon-heating tapes are used for the heating of the lid of the reactors. The apparatus can be operated pressures 0 – 600 kPa (accuracy  $\pm 1.27$  kPa) and at temperature range of 303 – 393 K (accuracy  $\pm 0.1$  K).

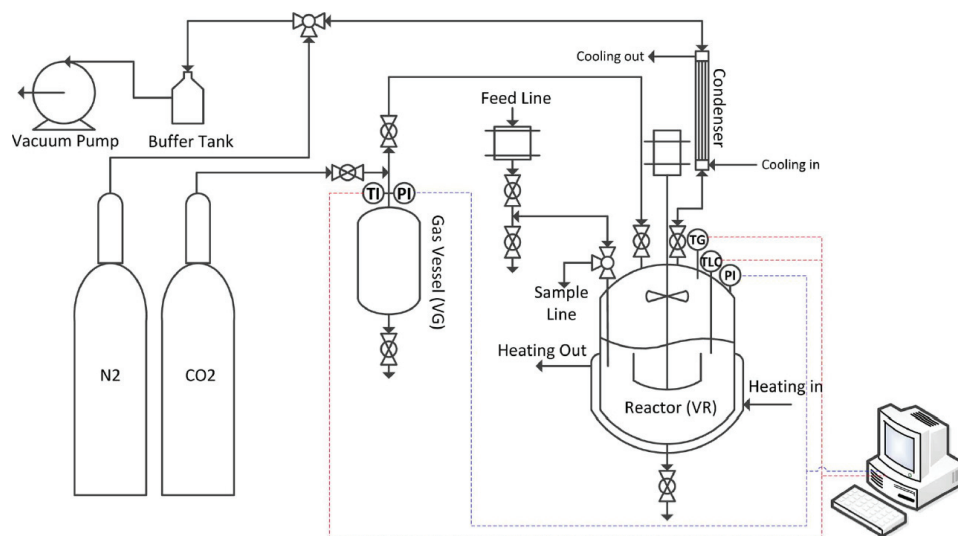


Figure A. 5 Illustration of the low-pressure VLE apparatus. TI: Temperature Indicator, PI: Pressure Indicator, TG: Temperature Gas phase, TLC: Temperature Liquid phase Control (Figure taken from Hartono et al., 2017).

The experimental procedure includes evacuation of the reactor, introduction and degassing of the solvent, and performance of the measurement. The measurements can be performed either at multiple temperatures with one CO<sub>2</sub> loading or isothermally with multiple loadings. In the first case, the temperature is set to automatically increase from 303 to 393 K with a constant step, 10 K in this work. At 393 K, CO<sub>2</sub> is injected to the maximum pressure of the reactor. The temperature is then decreased in reversed steps until 303 K. In the second case of isothermal experiment, once equilibrium is obtained at the desired temperature, CO<sub>2</sub> is added. After each system equilibration, more CO<sub>2</sub> is added until the pressure inside the reactor is close to 600 kPa. Equilibration required approximately 4-8 hours. The system was under constant stirring (ca. 500 rpm) and equilibrium was assumed when the temperature and pressure of the reactor were constant for 5 min.

The calculations are based on mass balances. The exact amount of solvent introduced was known by weighing the solvent holder, before and after charging the reactor.  $P$ - $V$ - $T$  data are known for the CO<sub>2</sub> storage vessel, thus the amount of gas before and after the CO<sub>2</sub> loading of the solvent can be calculated. An equation of state, here Peng-Robinson (Peng and Robinson, 1976), is used for estimating the amount of carbon dioxide in the vessel. The equilibrium pressure is calculated by Eq. A. 7:

$$P_{CO_2} = P_{reactor} - P_{start} \quad \text{Eq. A. 7}$$

For the aqueous systems, where pronounced chemical effects were expected, the experiments were conducted isothermally with multiple loadings and the loading in mol CO<sub>2</sub>/ mol MDEA was calculated and reported. For the non-aqueous systems, where only physical solubility was expected, the experiments were conducted at multiple pressure with a single carbon dioxide addition and the Henry's constant was calculated and reported. The Henry's constant can be calculated according to Eq. A. 8, where  $c_{CO_2}$  stands for the concentration of CO<sub>2</sub> in the solvent.

$$H_{CO_2} = \frac{P_{CO_2}}{c_{CO_2}} \quad \text{Eq. A. 8}$$

The validation of the experimental methodology was performed by measuring the solubility of carbon dioxide in pure water and comparing our results to the correlation provided by Carroll et al. (Carroll et al., 1991), as formulated by Penttilä et al. (Penttilä et al., 2011). The AARD between measured and literature values was always lower than 3% for both VLE-1 and VLE-2. Moreover, various experiments were conducted twice and showed that the AARD between two repeated experiments was also lower than 3%.

## CO<sub>2</sub> analysis

CO<sub>2</sub> analysis was performed at the end of VLE experiments with CO<sub>2</sub>-containing systems in order to verify the mass balance-based calculations for the CO<sub>2</sub> content in the liquid phase. The analysis was conducted in the Total Organic Carbon TOC-L analyzer provided by Shimadzu, which allows for the determination of the Inorganic Carbon (IC) species (CO<sub>2</sub>, HCO<sub>3</sub><sup>-</sup>, CO<sub>3</sub><sup>2-</sup>). The content of IC is determined by acidification using H<sub>3</sub>PO<sub>4</sub> (25 wt% solution) and sparging of the sample with synthetic air. The IC is released completely as CO<sub>2</sub> and it is afterwards

detected with a non-dispersive infrared (NDIR) sensor, by measuring the amount of IR radiation of the specific wavelength at which CO<sub>2</sub> absorbs. Standard solutions (sodium hydrogen carbonate, NaHCO<sub>3</sub>) were used for the calibration of the analyzer.

The analyzer is connected to a carousel which can accommodate up to 68 sample vials of 40 ml each. The liquid sample to be measured was diluted by a factor of 100 using Millipore water and sample homogeneity was ensured by using a vial shaker, prior to placing them in the carousel. The measurements always started and ended by measurement of standard solutions. Standard solutions were also placed after every three samples for a continuous check of the calibration curve. Two parallel measurements were performed for each sample and the average was reported. The AARD was 4%.

### **Karl-Fischer titration**

Coulometric Karl-Fischer titration is an established method for low water content determination and it was used in this work for identifying and quantifying the presence of water in the MDEA-glycol systems. The measurements were performed in a METHROM 831 KF coulometer which allows for water measurement down to 10 ppm. The method utilizes a methanolic solution of iodine, sulfur dioxide and a base as a buffer. Certified water standard solutions were used to check the accuracy of the instrument prior to the measurements. Typically, 0.03-0.06 g were injected in the titrator using one-time use syringes for each sample. The end point is defined voltammetrically by application of an alternating current of constant strength to a double Pt electrode. At least three parallel measurements are performed for each system and the average is reported. Since the systems of this work are highly hydrophilic, leaving the samples open to atmosphere even for a short time gave a pronounced effect on the measurement. The AARD in this work was 11%.

## Paper IV

The first part of the document discusses the importance of maintaining accurate records of all transactions. It emphasizes that every entry, no matter how small, should be recorded to ensure the integrity of the financial data. This includes not only sales and purchases but also expenses, income, and transfers between accounts.

Next, the document outlines the various methods used to collect and analyze financial data. It mentions the use of spreadsheets, accounting software, and manual ledgers. Each method has its own advantages and disadvantages, and the choice depends on the size and complexity of the business.

The document then delves into the process of reconciling accounts. This involves comparing the company's records with the bank statements to identify any discrepancies. It provides a step-by-step guide on how to perform a reconciliation, including how to handle errors and adjustments.

Finally, the document discusses the importance of regular financial reviews. It suggests that businesses should conduct a thorough review of their financial statements at least once a month. This allows them to identify trends, spot potential problems, and make informed decisions about their financial future.

## Appendix B

### Conference publication #1

Skylogianni, E., Lilleng, M.I., Knuutila, H., 2016. Combined hydrogen sulfide removal and hydrate control for subsea application: Simulation study, in: IEEE 2016 Techno-Ocean (Techno-Ocean) Proceedings. Presented at the 2016 Techno-Ocean (Techno-Ocean), pp. 28–34. <https://doi.org/10.1109/Techno-Ocean.2016.7890757>.

© 2016 IEEE. Reprinted, with permission, from Skylogianni, E., Lilleng, M.I., Knuutila, H., Combined hydrogen sulfide removal and hydrate control for subsea application: Simulation study, in: 2016 Techno-Ocean (Techno-Ocean) Proceedings, October 2016.

# Combined Hydrogen Sulfide Removal and Hydrate Control for Subsea Application

## Simulation Study

Eirini Skylogianni, Mari I. Lilleng and Hanna Knuutila\*

Department of Chemical Engineering  
Norwegian University of Science and Technology (NTNU)  
Trondheim, Norway

\*Corresponding author: hanna.knuutila@ntnu.no

**Abstract**—The feasibility of the combination of hydrogen sulfide removal and dehydration is investigated in this work using Aspen Plus simulation software. First, the simulation model is validated against experimental data from the literature. Secondly, two process configurations are examined for the simultaneous removal of hydrogen sulfide and water vapor, and Aspen Plus limitations are discussed. Pressure of 100 bar was used in the absorption simulation, in order to simulate subsea high pressure while three different natural gas compositions, with increasing hydrogen sulfide content, were studied. The absorption performance using a mixed methyldiethanolamine (MDEA)-monoethylene glycol (MEG) solvent in one contactor was not possible due to convergence problems. Absorption of H<sub>2</sub>S and CO<sub>2</sub> in aqueous MDEA, and H<sub>2</sub>O in aqueous MEG, including regeneration of the solvents, was therefore simulated separately and further analysis was performed. The specific reboiler duties required to meet the H<sub>2</sub>S content specification for trouble-free gas transportation in the sweet gas, using an aqueous MDEA solution for optimum Liquid-to-Gas ratio in the absorber, are in agreement with values reported in the literature. Gas dehydration in order to meet the water dew point specifications was also investigated.

**Keywords**—hydrogen sulfide removal; dehydration; Aspen Plus simulations; subsea

### I. INTRODUCTION

The trend in the oil and gas sector is towards subsea production and processing and the exploitation of subsea wells has witnessed significant developments since the start of the offshore era. More and more fields are found in greater distances from the shore and in greater depths than the ones under production so far. As a result, the need for more compact and lighter installations has risen in order to meet the technological and economic demands onshore and offshore. Research is conducted towards increased modularity of process equipment and reduced weight, size, complexity and footprint, i.e. process intensification [1]. The combination of two well-established processes in natural gas treatment into one can lead to more compact, smaller installations with lower energy requirements.

In this direction, our work focuses on the development of a process for the combined hydrogen sulfide removal and hydrate control. Acid gas removal and hydrate inhibition are

key-processes for natural gas treatment in order to ensure trouble-free operations and fulfil environmental requirements. Commonly, acid gases, such as hydrogen sulfide and carbon dioxide, are removed with alkanolamine solutions by chemical absorption. For hydrogen sulfide removal, a solution of the tertiary amine N-methyldiethanolamine (MDEA) is an excellent solvent due to, among other, its ability to selectively absorb H<sub>2</sub>S over CO<sub>2</sub>, the low heat of reaction with H<sub>2</sub>S and CO<sub>2</sub>, and low corrosive and highly resistant to thermal and chemical degradation nature [2]. Direct injections of concentrated solutions of monoethylene glycol (MEG) into the gas pipelines is a widely applied technique for hydrate inhibition. Concentrated MEG solutions physically absorb the water in order to prevent hydrate formation. MEG is preferred over other glycols and methanol due to its lower cost, lower viscosity, and lower solubility in liquid hydrocarbons [3], [4]. A combined solvent composed by MDEA, MEG and H<sub>2</sub>O thus seems promising for such application.

The concept for the simultaneous acid gas and water vapor removal exists already since 1939 when Hutchinson [5] patented such a gas treating process. In this patent, he claims a process in which acidic gases, such as CO<sub>2</sub> and H<sub>2</sub>S, and water vapor are removed simultaneously from a gas stream by means of absorption of these impurities into a liquid absorbent. Similarly to the typical amine-based acid gas removal, the gas is contacted in a tower counter-current with the liquid absorbent which removes the acid gases and the water vapor. The absorbent is a mixture of a glycol, an amine and water. The glycol-amine solution leaves the bottom of the absorber to enter a desorber where it is regenerated by providing sufficient heat to release the absorbed water vapor and acidic gases in a cyclic operation. The following years, more patents were granted based on Hutchinson's idea, from McCartney [6], [7] and Chapin [8].

Subsea application could be realized by spraying inline the solvent into the transport pipeline while the regeneration of the solvent could take place topside. The regeneration requires high temperatures and subsea regeneration could be challenging due to the low temperatures occurring at the seabed. In this work, the removal capacity of a combined solvent composed by MDEA, MEG and H<sub>2</sub>O is investigated in an absorber at the high pressure of 100 bar, in order to simulate



the high pressure experienced subsea. More specifically, the simulation aimed to the removal of H<sub>2</sub>S down to 4 ppm and the removal of water to achieve a water dew point of -18°C at 70 bar, according to typical gas transport specifications for the Norwegian Continental Shelf [9].

In this work two different process configurations were investigated using the available model in Aspen Plus process simulator. One of them concerned the removal of H<sub>2</sub>S and water with a mixed solvent in one absorption column and one concerned the removal of H<sub>2</sub>S and the removal of water in two different absorbers. Due to convergence issues with the first configuration, further analysis was performed for the latter one. The effect of the MDEA concentration and the MEG concentration on the removal capacity of the solvent was studied. In addition, the energy required for the regeneration of the solvent for three different compositions of natural gas was investigated. The composition for the three cases, with increasing hydrogen sulfide content, is shown in Table I. The inlet temperature of the sour gas was set to 25°C.

TABLE I. SOUR GAS COMPOSITIONS IN MOL% FOR THE THREE CASES STUDIED

	Case 1	Case 2	Case 3
Hydrogen sulfide	50 ppm	500 ppm	4.5 %
Carbon dioxide	5.6 %	5.6 %	8.0 %
Water	921 ppm	921 ppm	973 ppm
Methane	rest	rest	rest

## II. METHODOLOGY

The chemical process simulator software Aspen Plus version 8.6 and the template “ElecNRTL\_Rate\_Based\_MDEA\_model” are used for the simulation of the combined hydrogen sulfide removal and hydrate control. The template was used without any modifications on its thermodynamic model while equilibrium calculations were defined for the absorber and the desorber. In a first stage, the available model was validated against experimental vapor-liquid equilibrium (VLE) data found in the literature. In a second stage, different process configurations were studied and further analysis was performed.

### A. Validation

Validation of the simulation software Aspen Plus is crucial for the correct evaluation of the simulation results. Therefore, an extensive validation of the Aspen Plus model employed in this work has been performed. The systems studied consist of the components of main interest which are the impurities to be removed from the gas stream, water and H<sub>2</sub>S, the constituents of the removing solvent, MDEA and MEG, and the gas components having an effect on the removal capacity, CO<sub>2</sub> and CH<sub>4</sub>. The study of the CO<sub>2</sub> solubility is significant as MDEA is chosen for this simulation study because of its selectivity towards H<sub>2</sub>S over CO<sub>2</sub>, as mentioned earlier. Moreover, one of the criteria for solvent selection is the hydrocarbon losses into

the solvent, primary methane, as significant losses deteriorate the quality of the gas and, thus, its heating value. Therefore, the capability of Aspen Plus model to predict the solubility of methane in aqueous MDEA and in aqueous MEG was also studied.

Table II presents the sub-systems for which the validation was performed as well as the sources of VLE data used for the validation. The data used cover various solvent concentrations, pressures and temperatures in order to simulate the high pressures/low temperatures of absorption and the low pressures/higher temperatures required for desorption.

Fig. 1, for example, shows the predicted equilibrium curves with Aspen Plus model against H<sub>2</sub>S solubility experimental data available at the literature from Jou et al. [10] for a 50.1 wt.% MDEA solution. It is observed that, for the given pressure and temperature range, the predicted VLE curves follow the trend of the experimental data. Further study for H<sub>2</sub>S solubility in different solution concentrations revealed that there are lower deviations for a 11.9 wt.% MDEA solution or a 23.7 wt.% MDEA solution.

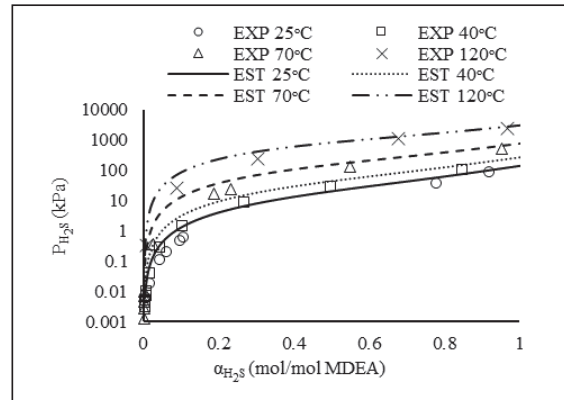


Fig. 1. Estimated and experimental [10] partial pressure of hydrogen sulfide on log scale as a function of the loading of hydrogen sulfide in the liquid phase of a 50.1 wt.% aqueous MDEA solution at 25°C, 40°C, 70°C and 120°C.

The solubility of CO<sub>2</sub>, H<sub>2</sub>S, CH<sub>4</sub> in MDEA and in MEG as well as the solubility of H<sub>2</sub>O in MEG was studied and the results were found satisfactory. However, large deviations were observed between the predicted VLE curves and the literature data [20] for the combined MDEA-MEG-H<sub>2</sub>O solvent, as demonstrated in Fig. 2. A possible explanation for the large deviations observed is the fact that on the template used for this study, the reaction of H<sub>2</sub>S with MDEA is defined requiring the presence of water. In reality, the reaction of hydrogen sulfide with MDEA is a proton transfer, which does not require water to take place [21]. This is the reason why MDEA is known for selective removal of H<sub>2</sub>S over CO<sub>2</sub>, as mentioned earlier. On the other hand, carbon dioxide cannot react with an amine without the presence of water. Naturally, by replacing the water in an MDEA solution with another compound, in our case MEG, should in theory improve the selectivity of the solvent

TABLE II. OVERVIEW OF THE VLE DATA USED FOR THE VALIDATION OF ASPEN PLUS MODEL

System	Solvent Concentration (wt.%)	Temperature (°C)	Pressure (kPa)	Literature source
H <sub>2</sub> S-MDEA	11.9% - 50.1% MDEA	25-120	0.0013-5840	Jou et al. [10]
	23.7% MDEA	40	0.52-1600	MacGregor and Mather [11]
CO <sub>2</sub> -MDEA	11.9% - 50.1% MDEA	25-120	0.001-6570	Jou et al. [10]
	23.7% MDEA	40	1.17-3770	MacGregor and Mather [11]
	35% MDEA	40, 100	0.004-236	Jou et al. [12]
CH <sub>4</sub> -MDEA	34.7% MDEA	25-130	95-13210	Jou et al. [13]
H <sub>2</sub> S-MEG	99.5% MEG	25-125	3.5-6750	Jou et al. [14]
CO <sub>2</sub> -MEG	99.5% MEG	25-125	29.3-20290	Jou et al. [14]
	99.8% MEG	50-125	425.5-5421	Galvão and Francesconi [15]
	99.9% MEG	50-125	895-38400	Zheng et al. [16]
CH <sub>4</sub> -MEG	99.8% MEG	30-150	1367.4-13726.4	Galvão and Francesconi [15]
	99.9% MEG	50-125	200-39617	Zheng et al. [16]
H <sub>2</sub> O-MEG	99.99% MEG	60	0.28-19.92	Horstmann et al. [17]
	99.5% MEG	50	0.316-12.082	Gonzales and Van Ness [18]
	99%MEG	60	0.543-19.428	Villamañan et al. [19]
CO <sub>2</sub> /H <sub>2</sub> S-MDEA-MEG	30% MDEA + 65% MEG	40-90	1.1-70.75	Xu et al. [20]

for H<sub>2</sub>S over CO<sub>2</sub>. Further analysis was performed in order to investigate the effect of the water content in the solvent. As H<sub>2</sub>O is added, the solubility of H<sub>2</sub>S is increased and the experimental points are better approached. This shows that, as more water is becoming available, more H<sub>2</sub>S can react with the amine solvent, reinforcing the aforementioned discussion. The analysis was based on the experimental points from Xu et al. [20], which to our best knowledge is the only literature source available with VLE measurements for the system H<sub>2</sub>S/CO<sub>2</sub>-MDEA-MEG-H<sub>2</sub>O. Moreover, further uncertainty during validation exists since only five experimental points for each solvent composition are provided, which were in addition

retrieved directly from the charts due to the fact that the solubility data were not reported.

### B. Process Configuration

The investigation of a process configuration consisting of one absorption column (*Fig. 3a*) in which both H<sub>2</sub>S and water are removed with a combined MDEA-MEG-H<sub>2</sub>O solvent was attempted. However, convergence issues did not allow for the investigation of the removal capacity of the mixed solvent when small amounts of water were available. The use of a solvent with 80% diethylene glycol, 15% triethanolamine and 5% water is suggested in the literature [5] for the simultaneous removal of hydrogen sulfide and water vapor, and solvents with higher water concentrations were not the scope of this work. In addition, the results from the validation of Aspen Plus model showed that the model fails to predict accurately the thermodynamic behavior of the combined system with 0 to 10 wt.% water, unless a substantial amount of water is added. Thus, this process configuration was not investigated further.

Analysis was, therefore, performed using two different absorption towers for the removal of hydrogen sulfide and the removal of water subsequently (*Fig. 3b*) in order to study the absorption process at 100 bar and the corresponding energy requirements. During this investigation, the regeneration of the two separate solvents was also simulated. In this configuration, water saturated gas enters the first absorber to contact a MDEA solution in order to meet the H<sub>2</sub>S specification. Afterwards, the sweet gas leaving the first absorber enters the second absorber where it is contacted with a MEG solution in order to meet the water content specification. The effect of the H<sub>2</sub>S content of the gas and MDEA concentration of the amine solvent on the Liquid-to-Gas (L/G) ratio and energy required for the regeneration was investigated. Moreover, a preliminary

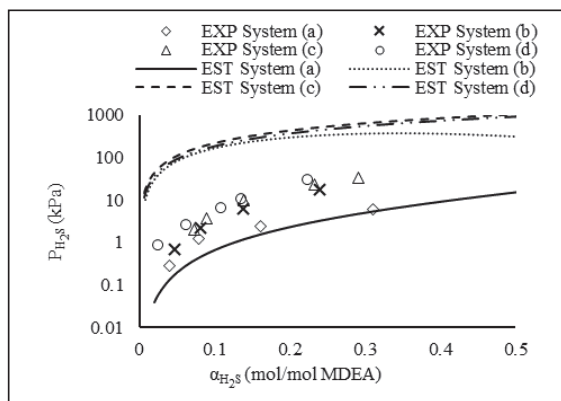


Fig. 2. Estimated and experimental [20] partial pressure of hydrogen sulfide on log scale as a function of the mole ratio of hydrogen sulfide in the liquid phase at 40°C for system (a) 30 wt.% MDEA + 70 wt.% H<sub>2</sub>O, system (b) 30 wt.% MDEA + 60 wt.% MEG + 10 wt.% H<sub>2</sub>O, system (c) 30 wt.% MDEA + 65 wt.% MEG + 5 wt.% H<sub>2</sub>O and system (d) 30 wt.% MDEA + 70 wt.% MEG.

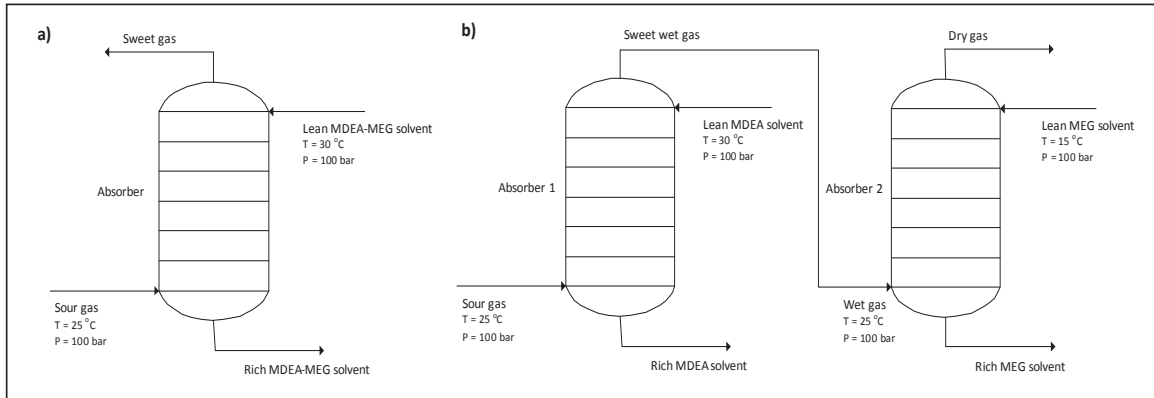


Fig. 3. Investigated set-ups implemented in Aspen Plus for  $H_2S$  and water removal a) with a combined solvent of MDEA-MEG- $H_2O$  and b) with a MDEA solution and a MEG solution in two absorption columns, respectively.

analysis was performed regarding the MEG concentration required for the dehydration of the sweet gas. The findings of the analysis performed using this process configuration are presented and discussed in the next section of this work.

### III. RESULTS AND DISCUSSION

The results from the second configuration, where the removal of  $H_2S$  and the removal of water with an MDEA solution and a MEG solution, respectively, are examined separately, are presented in this section. The absorption for both acid gas and for water vapor takes place at 100 bar while 8 stages are used in both absorbers. The desorbers consist of 8 and 4 stages for the desulfurization and dehydration process, respectively.

#### A. $H_2S$ Removal

- MDEA Concentration Effect

The effect of the MDEA concentration on the L/G ratio required to reach the  $H_2S$  specification was studied. The MDEA concentration varied from 15 to 55 wt.% MDEA due to convergence issues during the simulations outside this concentration range. The temperature of inlet lean amine solution was set to 30°C during the analysis. The regeneration section was not included in this study. Fig. 4 shows the effect of MDEA concentration on the L/G ratio required for Case 1. As the concentration increases, the L/G ratio decreases since less amount of solvent is required when more MDEA is available for reacting with the same amount of hydrogen sulfide.

Based on the simulation results, one could assume that, if the trend depicted in Fig. 4 is similar for higher MDEA concentrations than 55 wt.%, the higher the MDEA concentration, the lower the L/G required. However, it is reported in the literature that concentrations of MDEA above 50-55% are not recommended [2]. Higher concentration can lead to corrosion issues and higher viscosity, leading to higher

pumping cost. However, the effect of viscosity could not be studied using equilibrium based Aspen Plus model.

- $H_2S$  Concentration Effect

Three cases for different gas compositions have been investigated in terms of Liquid-to-Gas (L/G) ratio and its effect on the energy requirements, in terms of specific reboiler duty during the regeneration of the amine solution. A 45 wt.% MDEA solution was used for  $H_2S$  removal down to 4 ppm, according to the operating data of a MDEA process in a plant in Qatar [22]. Fig. 5 shows the specific reboiler duty,  $Q_s$ , required for various L/G ratios in order to reach the gas purification specifications. It is observed that the L/G ratio increases as the amount of acid gas increases in the sour gas. In addition, as the L/G ratio increases, the specific reboiler duty decreases until a plateau is reached. Convergence issues did not allow for further analysis to higher L/G ratios than 0.8 for Case 1.

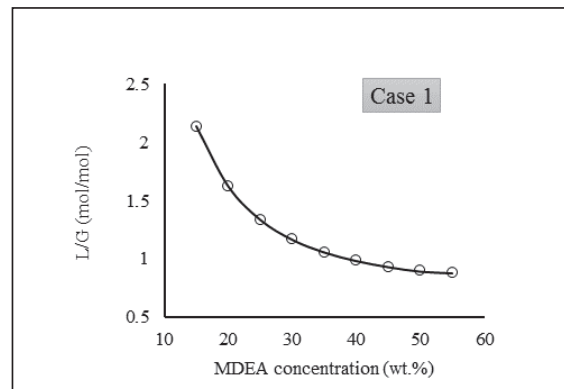


Fig. 4. Estimated L/G ratios required for obtaining 4 ppm in the sweet gas as a function of the MDEA concentration in wt.% for Case 1.

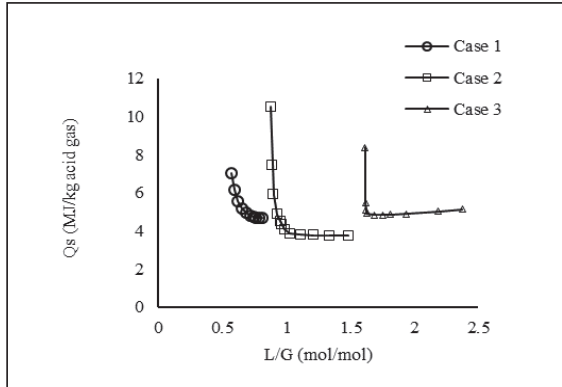


Fig. 5. Specific reboiler duty as a function of L/G ratio for the three cases studied.

For all three cases, a Liquid-to-Gas ratio is proposed based on the specific reboiler duty,  $Q_s$ , the loading of the lean and rich amine (Fig. 6) and the acid gas removal. Typical acid gas rich loadings for a 50-55 wt.% MDEA solution is 0.45-0.50 mol/mol while maximum lean loading should be 0.004-0.010 mol/mol, according to DuPart et al. [23] for both  $H_2S$  and  $CO_2$  in terms of corrosion. It is observed that as the L/G ratio increases, the rich loading for  $H_2S$  and  $CO_2$  decreases for all three cases. This behavior is expected as more MDEA is available to react with the acid gas, assuming constant amount of acid gas to be removed. Loadings for Case 1 exhibit a slight increase at higher L/G ratios while, for Case 2, at L/G ratios below 0.92  $H_2S$  rich and lean loading present a sharp increase, indicating  $H_2S$  stripping from the solvent in the absorber. As far as the lean loading is concerned, for Case 1, increase in the L/G ratio leads to a slight increase, in the order of  $10^{-4}$ , of the lean loading. For Case 2 and 3, the same trend is followed for the lean loading, except for L/G lower than 0.92 for Case 2, where the loading is increasing. Case 3, where the high  $H_2S$  content of 4.5% is set, exhibits a gradual increase of the loadings as the L/G ratio increases while the loading of lean MDEA for  $CO_2$  is significantly lower than in Cases 1 and 2.

Aiming for low energy requirements in the reboiler, operational areas are decided for all cases to allow for further analysis. The L/G ratio is chosen slightly after the plateau is observed in order to avoid unnecessary high liquid flowrates. The proposed L/G ratios for operation in each case are presented in Table III. The corresponding specific reboiler duties are in accordance to reported values in the literature from Sakwattanapong et al. [24]. He reported specific reboiler duties from 1 to 6 MJ/kg  $CO_2$  for lean loadings of MDEA from 0 to 0.1 mol/mol.

In addition, Table III presents the reboiler temperature,  $H_2S$  and  $CO_2$  loadings for the lean and rich MDEA and acid gases' recoveries for the operational areas chosen. It is worth mentioning that, in Case 1, both lean and rich loadings of MDEA for  $CO_2$  exceed the maximum recommended values of 0.01 and 0.5 respectively for all L/G ratios examined. The degradation temperature of MDEA is  $130^\circ C$  thus amine degradation may occur in Case 3 [25]. Bulk removal of  $CO_2$  takes place despite the known selectivity of MDEA for  $H_2S$

TABLE III. EFFECT OF SOUR GAS COMPOSITION ON THE OPTIMUM L/G RATIO AND SPECIFIC REBOILER DUTY FOR THE REGENERATION OF THE AMINE SOLUTION

	Case 1	Case 2	Case 3
Optimum L/G ratio (mol/mol)	0.75	1.11	1.69
Specific duty (MJ/kg acid gas)	4.72	3.80	4.96
$\alpha_{H_2S,lean}$ [mol $H_2S$ /mol MDEA]	0.0005	0.0033	0.0086
$\alpha_{CO_2,lean}$ [mol $CO_2$ /mol MDEA]	0.1277	0.0302	8.61 E-07
$\alpha_{H_2S,rich}$ [mol $H_2S$ /mol MDEA]	0.0009	0.0074	0.2493
$\alpha_{CO_2,rich}$ [mol $CO_2$ /mol MDEA]	0.6155	0.4915	0.4280
$H_2S$ recovery [%]	92.1	98.8	98.3
$CO_2$ recovery [%]	93.4	99.5	99.3
Reboiler temperature ( $^\circ C$ )	106	131	140

over  $CO_2$ . An explanation for this is the fact that the simulations were equilibrium based and the selectivity is based on rate of absorption kinetics of these two components. Another reason for this behavior might be the fact that the direct reaction of  $H_2S$  with MDEA, in the absence of water, is not defined in the Aspen Plus model, as discussed in II.A.

#### B. Dehydration

ASPEN Plus simulations based on a typical dehydration unit [4] were performed and further analysis was conducted by using a concentrated MEG solution at  $35^\circ C$  for the absorption of water at 100 bar. Different operations in the  $H_2S$  absorber will result in different temperature and water content in the wet gas out of the absorber, thus, requiring different operating conditions in the dehydration process. The results showed that, with respect to L/G ratio, concentrations above 99 wt.% MEG were required in order to reach the water content specifications, which is higher than the ones usually required for the regeneration of MEG for hydrate inhibition [3]. The 99 wt.% MEG purity requirement lead into unfeasible reboiler temperatures; temperatures above MEG degradation temperature of  $165^\circ C$  [3].

#### IV. CONCLUSION

The feasibility of the simultaneous removal of hydrogen sulfide and water vapor at 100 bar has been studied using Aspen Plus simulation software. Validation of the Aspen Plus model used in this work revealed the capability of the model to satisfactorily predict the solubility data of the different binary sub-systems studied, while failing to predict the vapor-liquid equilibrium behavior of the combined system. Two configurations were examined; one for the removal of  $H_2S$  and  $H_2O$  with a mixed solvent of MDEA-MEG- $H_2O$  in one absorber, and another for the removal of  $H_2S$  and  $H_2O$  separately, using an MDEA solution and a MEG solution, respectively, in two subsequent absorbers. During the investigation of the first configuration, convergence issues arose when low amount of water was present in the solvent, thus, this process configuration was not investigated further. Analysis using the second configuration showed that the higher the  $H_2S$  content of the gas, the higher the L/G ratio required for meeting the  $H_2S$  specifications when employing a 45 wt.%

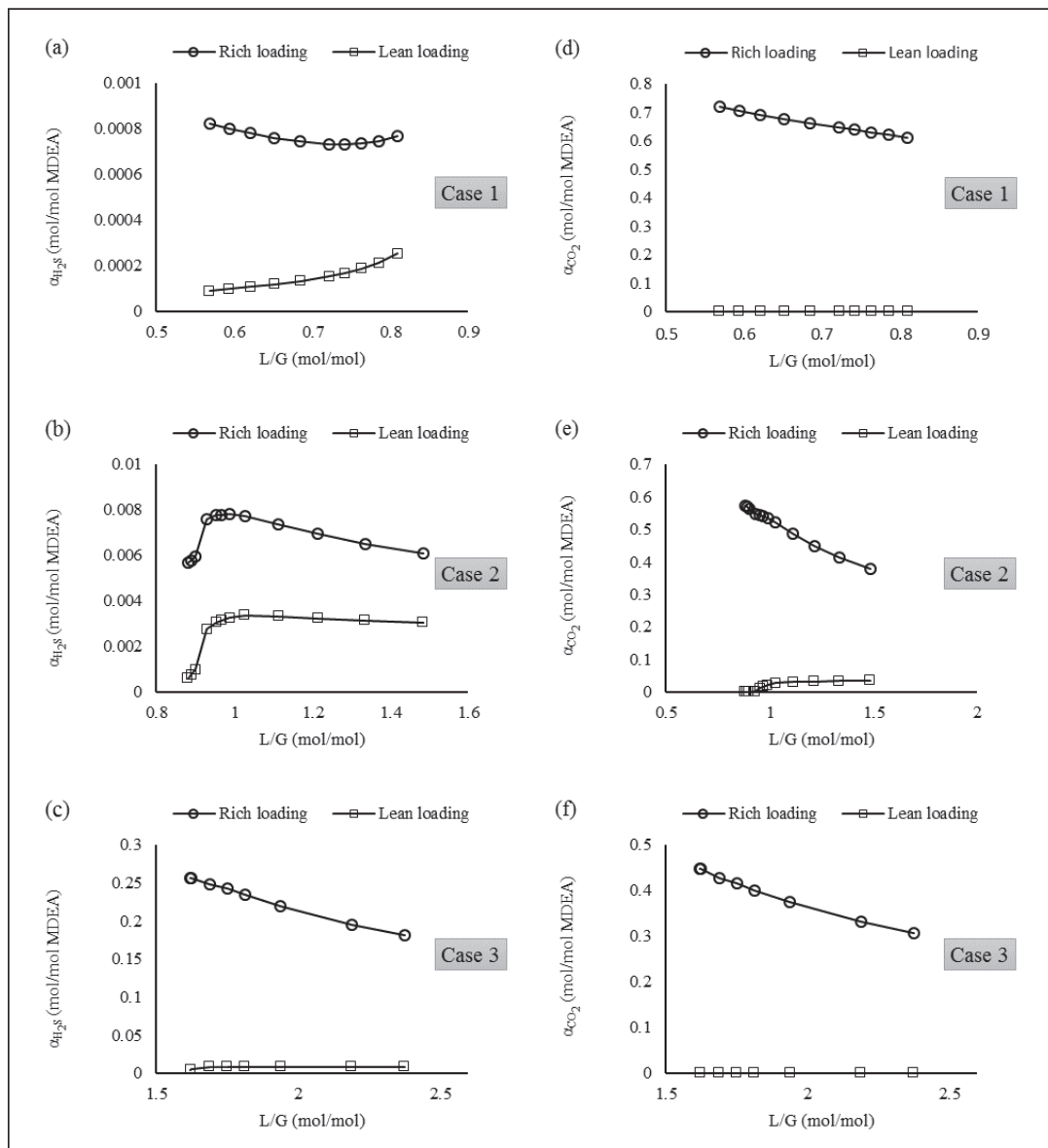


Fig. 6. Estimated lean and rich loadings of MDEA for H<sub>2</sub>S (a, b, c) and CO<sub>2</sub> (d, e, f) for the three cases studied.

MDEA solution. L/G ratios were proposed for operation and the specific reboiler duties found are in agreement with values reported in the literature. Gas dehydration was investigated for the three cases and a concentrated glycol of 99 wt.% MEG at 35°C was required to meet the water content specifications. However, the reboiler temperatures significantly exceeded the MEG degradation temperature.

#### ACKNOWLEDGMENT

The authors acknowledge the financial support from the Subsea Production and Processing (SUBPRO) center for research based innovation, which is a collaboration between NTNU, the Research Council of Norway and major industrial players in the field.

## REFERENCES

- [1] O. Økland, S. Davies, M. Ramberg, and H. Rogno, "Steps to subsea factory," Offshore Technology Conference Proceedings, October 2013.
- [2] A.L. Kohl and R.B. Nielsen, Gas Purification, 5th ed. Gulf Professional Publishing, 1997.
- [3] GPSA, Engineering Data Book, 13th ed., section 20. Gas Processors Suppliers Association, 2014.
- [4] J.M. Campbell, Gas Conditioning and Processing, 8th ed., vol 2. John M. Campbell and Company, 2004, pp. 333-372.
- [5] A.J.L. Hutchinson, Process for treating gases. United States Patent Office, October 1939.
- [6] E.R. McCartney, Gas purification and dehydration process. United States Patent Office, January 1948.
- [7] E.R. McCartney, Extraction of acidic impurities and moisture from gases. United States Patent Office, August 1951.
- [8] W.F. Chapin, Purification and dehydration of gases. United States Patent Office, August 1950.
- [9] A.O. Fredheim, C. Gotaas Johnsen, E. Johannessen, and G. Pedersen Kojen, "Gas-2-Pipe™, A Concept for Treating Gas to Rich Gas Quality in a Subsea or Unmanned Facility," Offshore Technology Conference Proceedings, May 2015.
- [10] F.Y. Jou, A.E. Mather, and F.D. Otto, "Solubility of hydrogen sulfide and carbon dioxide in aqueous methyldiethanolamine solutions," Ind. Eng. Chem. Process Des. Dev., vol. 21, pp. 539-544, October 1982.
- [11] R.J. MacGregor, and A.E. Mather, "Equilibrium solubility of H<sub>2</sub>S and CO<sub>2</sub> and their mixtures in a mixed solvent," Can. J. Chem. Eng., vol. 69, pp. 1357-1366, December 1991.
- [12] F.Y. Jou, J.J. Carroll, A.E. Mather, and F.D. Otto, "The solubility of carbon dioxide and hydrogen sulfide in a 35 wt% aqueous solution of methyldiethanolamine," Can. J. Chem. Eng., vol. 71, pp. 264-268, April 1993.
- [13] F.Y. Jou, J.J. Carroll, A.E. Mather, and F.D. Otto, "Solubility of methane and ethane in aqueous solutions of methyldiethanolamine," J. Chem. Eng. Data, vol. 43, pp. 781-784, 1998.
- [14] F.Y. Jou, R.D. Deshmukh, F.D. Otto, and A.E. Mather, "Vapor-liquid equilibria of H<sub>2</sub>S and CO<sub>2</sub> and ethylene glycol at elevated pressures," Chem. Eng. Comm., vol. 87, pp. 223-231, 1990.
- [15] A.C. Galvao, and A.Z. Francesconi, "Solubility of methane and carbon dioxide in ethylene glycol at pressures up to 14 MPa and temperatures ranging from (303 to 423) K," J. Chem. Thermodyn., vol. 42, pp. 684-688, January 2010.
- [16] D.Q. Zheng, W.D. Ma, R. Wei, and T.M. Guo, "Solubility study of methane, carbon dioxide and nitrogen in ethylene glycol at elevated temperatures and pressures," Fluid Phase Equilibria, vol. 155, pp. 277-286, 1999.
- [17] S. Horstmann, H. Gardeler, M. Wilken, K. Fischer, and J. Gmehling, "Isothermal vapor-liquid equilibrium and excess enthalpy. Data for the binary systems water + 1,2-ethanediol and propene + acetophenone," J. Chem. Eng. Data, vol. 49, pp. 1508-1511, May 2004.
- [18] C. Gonzalez, and H.C. Van Ness, "Excess thermodynamic functions for ternary systems. 9. Total-pressure data and G<sup>E</sup> for water/ethylene glycol/ethanol at 50°C," J. Chem. Eng. Data, vol. 28, pp. 410-412, 1983.
- [19] M.A. Villamanan, C. Gonzalez, and H.C. Van Ness, "Excess thermodynamic properties for water/ethylene glycol," J. Chem. Eng. Data, vol. 29, pp. 427-429, 1984.
- [20] H.J. Xu, C.F. Zhang, and Z.S. Zheng, "Solubility of hydrogen sulfide and carbon dioxide in a solution of methyldiethanolamine mixed with ethylene glycol," Ind. Eng. Chem. Res., vol. 41, pp. 6175-6180, November 2002.
- [21] G.F. Versteeg, L.A.J. Van Dijck, and W.P.M. Van Swaaij, "On the kinetics between CO<sub>2</sub> and alkanolamines both in aqueous and non-aqueous solutions. An overview," Chem. Eng. Comm., vol. 144, pp. 113-158, February 1996.
- [22] H.E. Alfadala, and E. Al-Musleh, "Simulation of an acid gas removal process using methyldiethanolamine; an equilibrium approach," 1st Annual Gas Processing Symposium Proceedings, Elsevier, January 2009.
- [23] M.S. DuPart, T.R. Bacon, and D.J. Edwards, "Understanding corrosion in alkanolamine gas treating plants. Part 1&2.," Hydrocarb. Process. pp. 75-80, 89-94, April and May 1993.
- [24] R. Sakwattanapong, A. Aroonwilas, and A. Veawab, "Behavior of reboiler heat duty for CO<sub>2</sub> capture plants using regenerable single and blended alkanolamines," Ind. Eng. Chem. Res., vol 44, pp. 4465-4473, 2005.
- [25] M. Pandey, Process optimization in gas sweetening unit - A case study," International Petroleum Technology Conference, November 2005.

## Paper V

...the ...

...the ...

...the ...

...the ...

...the ...

...the ...

...the ...

...the ...

...the ...

...the ...

...the ...

...the ...

...the ...

...the ...

...the ...

...the ...

...the ...



## Appendix C

### Conference publication #4

Skylogianni, E., Knuutila, H.K., 2019. Process intensification: H<sub>2</sub>S and hydrate control for subsea application. Presented at the GPA Europe Spring Conference, Gas Processors Association Europe, Amsterdam, the Netherlands.

<https://gpa-europe.com/library/secure/process-intensification-h2s-and-hydrate-control-subsea-application>.

Reprinted (adapted) with permission from the Gas Processing Association.

## **Process intensification: Hydrogen sulfide and hydrate control for subsea application**

Eirini Skylogianni and Hanna K. Knuutila  
Norwegian University of Science and Technology

### **Abstract**

The trend in the oil and gas sector is towards subsea production and processing, where increased modularity of process equipment and reduced weight, size, complexity and footprint are key elements. SUBPRO is a Norwegian center for research-based innovation within subsea production and processing, which together with the most important industrial players in the subsea field aims to address challenges for subsea applications.

Today on a typical topside platform, acid gas removal, dehydration and glycol injection take place, giving three different chemical systems. We are working on the development of a new regenerative process for simultaneous removal of H<sub>2</sub>S and water from the natural gas, which could lead to a more compact, smaller installation with lower energy requirements as well as allow for production from high H<sub>2</sub>S-concentration gas fields. The feasibility investigation of such complex process requires knowledge of the thermodynamic behavior and physical properties of the proposed system, which can only be obtained by experimental data. Time-consuming and demanding experiments at high pressures have been conducted and provided the basis for the development of models and tools to be used by the industry for the evaluation of this combined process.

# Process intensification: Hydrogen sulfide and hydrate control for subsea application

## Introduction

As the oil and gas industry is forced to extend its exploration activities in longer distances and depths offshore in order to meet the future energy demands, subsea processing has naturally gained grounds. The installation, maintenance and retrieval of the subsea equipment play now a significantly more important role than for onshore/topside facilities, thus reduced weight, size, complexity and footprint as well as increased modularity are key requirements.

In the emerging battle for increased efficiency in the current use of fossil fuel, the industrial and academic community have joined forces to tackle the challenges of the new oil and gas subsea era. One of these joint efforts is realized by Subsea Production and Processing (SUBPRO) center for research-based innovation established in the Norwegian University of Science and Technology (NTNU), which together with the most important industrial players in the subsea field aim to address challenges for subsea applications [1]. SUBPRO is active within field architecture, system control, safety & reliability, as well as separation research area.

Technological advancements in the field aim to the development of the missing parts for the realization of the subsea factory (subsea pumps and compressors, oil-water separators) and on finding solutions to the challenges associated with subsea production and processing. One such example is the increasingly important *field souring*. The term denotes the increasing concentration of hydrogen sulfide (H<sub>2</sub>S) observed in the course of production of a reservoir. The presence of hydrogen sulfide can compromise the efficiency and safety of the operations. Although the scientific community has not yet fully understood the mechanism of this souring, it is established that seawater injection for increased recovery leads to increasing levels of H<sub>2</sub>S [2], [3]. Addressing this issue in combination with the already established hydrate control norms is one of the ways forward. The core challenge for the simultaneous hydrogen sulfide and hydrate control process is the determination of a chemical compound, which will serve both as a hydrate inhibitor and as an H<sub>2</sub>S removal agent.

This paper presents the work performed within SUBPRO and NTNU in the framework of a doctoral degree. It focuses on the steps followed for the characterization of the proposed multifunctional chemical and can merely be used as a general guideline for solvent selection when a new process is developed or an existing one is optimized.

## Status today – Concept

### The motivation

The presence of hydrogen sulfide in produced gas creates safety hazards for operations, increases corrosion and sulfide-stress cracking risks, and results in an export gas of lower value. Its toxicity presents further risks both for humans and animals; exposure to 100 ppm of H<sub>2</sub>S can be fatal [4]. Furthermore, it has been observed that mitigation strategies, for example addition of nitrate in the seawater before injection, do not perform as expected and the H<sub>2</sub>S concentration keeps increasing [5]. Good HSE practices impose the removal of H<sub>2</sub>S in an as early stage as possible.

### Current technologies

Acid gases, carbon dioxide (CO<sub>2</sub>) and H<sub>2</sub>S, are removed from natural gas ordinarily in absorption towers utilizing amine-based solvents. The process of acid gas removal is referred to as “gas sweetening”. Absorption with aqueous amines is a mature technology with the important advantage of being regenerative, i.e. acid gas absorption into the amine-solution (rich-solvent) is followed by the reversed process, acid gas desorption from the amine-solution, such that it can be recovered and re-used (lean-solvent). The acid gases are absorbed through an exothermic chemical reaction with the amine-solvent, and afterwards by means of temperature swing, the reaction is reversed and gas is released from the solvent [6]. A reboiler is used to provide the heat required in the desorber. In case selective removal of the hydrogen sulfide is desired and if H<sub>2</sub>S is present alone in reasonably small quantities, the normal

procedure today is to remove it using the so-called “scavengers”. Offshore, hydrogen sulfide removal is most commonly performed with a liquid non-regenerative scavenger, triazine or its blends [7].

Besides acid gases, water vapor is also a natural gas impurity that is necessary to control in order to ensure trouble-free operations. The reason is the well-known flow assurance issue of hydrate formation and water condensation during gas processing and transportation. Moreover, water presence enhances corrosion. Methanol or monoethylene glycol (MEG) are used as hydrate inhibitors being injected in the transportation pipeline to physically absorb water and suppress the water dew point of the system. When complete dehydration is sought, triethylene glycol (TEG) is used in a similar process as acid gas absorption into amines. The glycol can then be regenerated and re-used.

### Process Intensification

A solution to the problem of gradual reservoir hydrogen sulfide increase can be the merge/integration of acid gas removal process into the well-established glycol injection system used for hydrate control. An H<sub>2</sub>S removal agent would then be injected together with MEG in the pipeline, which would act as the absorption tower, increasing the liquid volume dispersed and made available for mass transfer. Important criterion for the proposed process is to be regenerative. On the one hand, the transportation and handle of the fresh and then spent chemical is eliminated, but on the other hand, the need for topside regeneration is emerged due to the high temperatures required in the regeneration stage. However, newly developed technologies for underwater production and processing, such as “subsea on a stick” [8], could support the proposed concept. Pumps and other separation systems should be employed for the collection and re-injection of the chemical in the pipeline.

To meet the criterion of a regenerative solvent, automatically the non-regenerative solvents currently used, such as triazine, are excluded from the potential candidates and amine solvents dominate. The proposed chemical in this work is a mixture of methyl-diethanolamine (MDEA), MEG and water. MDEA is known for selective removal of H<sub>2</sub>S over CO<sub>2</sub> and has been used for hydrogen sulfide removal from natural gas [9], [10]. An amine-glycol process was once extensively used for the combined acid gas removal and dehydration of natural gas. The concept was initially conceived by Hutchinson already in 1839 [11], and improvements were suggested later [12]–[14], leading to lower energy requirements and excellent purification from H<sub>2</sub>S and CO<sub>2</sub>. The process was soon abandoned mainly due to severe amine vaporization losses and corrosion problems in the stripper caused by the low water content in the solvent, thus high reboiler temperatures. However, the amine used was monoethanolamine (MEA), which is known for its high volatility and corrosivity issues [6].

The characterization of the proposed solvent is the backbone in this process intensification attempt, leading to advancement of the scientific knowledge, thereby, the proposed process aims to reach Technology Readiness Level 1. Solvent characterization includes all those properties, physical and chemical, that the solvent should possess for its successful application. The work performed and impact on the industry are shown Figure 1.

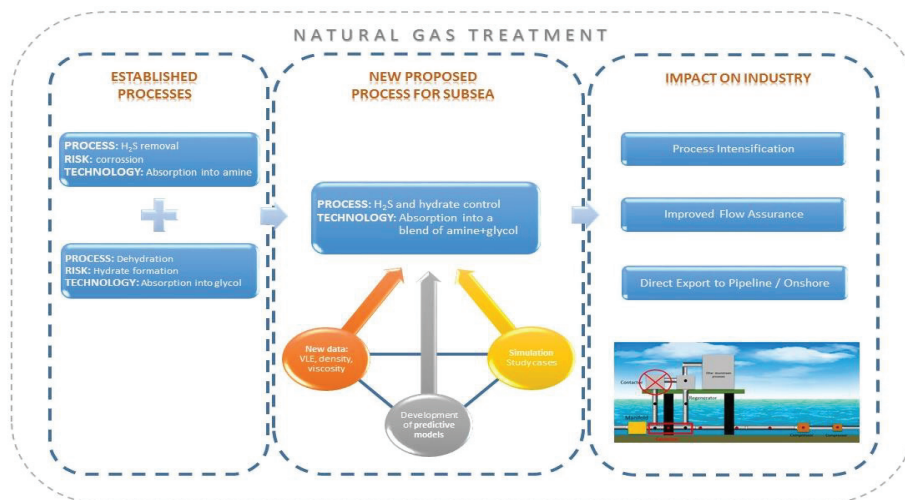


Figure 1: Schematic of process intensification work in alignment with industrial strategies

## Solvent characterization

To evaluate the suitability of a selected solvent for its designated application, here the combined removal of hydrogen sulfide and water vapor, properties regarding the removal efficiency, trouble-free operations and the impact to the environment must be assessed. Removal efficiency concerns all those properties that the solvent must possess in order to meet the gas purification requirements, such as the solubility of the gas into the solvent, the thermodynamics and the kinetics of the system. All the characteristics associated to the practical aspects of application, for example corrosion issues, constitute the trouble-free operations-related properties. Impact to the environment includes emission control and chemical ecotoxicity. Because one property may influence in more aspects the process, the above-mentioned categorization is the authors' attempt to simplify the complicated interactions of the various properties, and should be treated as such. Each property is explained below accompanied with the relevant information for the proposed solvent in our case, while also underlying the challenges faced.

### Removal efficiency

#### Cyclic capacity

Necessary for the development of the thermodynamic models employed during the design and operation of the absorption and regeneration units, are vapor-liquid equilibrium (VLE) data over pressure and temperature range relevant for the process. In the figure below the measured vapor-liquid equilibrium curve at 50°C for a 50.1 wt.% MDEA-H<sub>2</sub>O solution is shown.

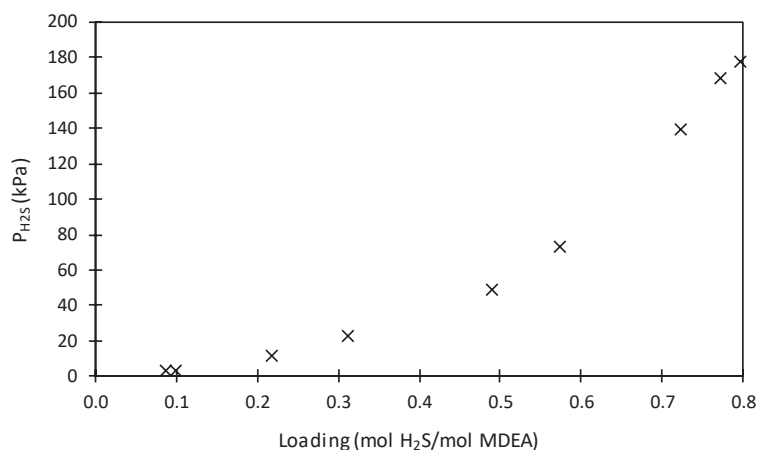


Figure 2: Vapor-liquid equilibrium data showing H<sub>2</sub>S partial pressure as a function of H<sub>2</sub>S loading in a 50.1 wt.% aqueous MDEA at 50°C

The amount of gas absorbed in a solvent is called capacity of the solvent. The capacity is usually expressed in terms of "loading",  $\alpha$ , in mol H<sub>2</sub>S/mol amine or kg H<sub>2</sub>S/kg solvent. The capacity of a solvent provides information of how much gas can be removed, or reversely how much solvent must be used to remove the desired gas amount.

Besides the useful information that the capacity of a solvent might provide, it is the difference between the loading of the lean-solvent and the rich-solvent that shows the real amount of gas that can be removed in a real process. This difference is called cyclic capacity and it is essential since after regeneration the solvent cannot be stripped entirely from the acid gas captured. Therefore, it is the cyclic capacity that should be assessed during the screening of different potential solvents for an application. The higher the cyclic capacity, the more H<sub>2</sub>S can be absorbed for a given solvent flowrate. In our case, it is of interest to study the influence of MEG presence in the H<sub>2</sub>S-removal capacity of the solvent, since the successful application of aqueous MDEA for H<sub>2</sub>S removal from natural gas is already proven. Cyclic capacity results are shown in Table A.

Table A: Cyclic capacity of aqueous amine solutions with and without glycol calculated at absorption temperature of 10°C and desorption temperature of 120°C. Loading values in mol H<sub>2</sub>S/mol MDEA are in parenthesis.

System (wt.)	P <sub>H<sub>2</sub>S, absorption</sub> (kPa)	P <sub>H<sub>2</sub>S, desorption</sub> (kPa)	α <sub>cyclic</sub>
30% MDEA - 70% H <sub>2</sub> O	5.3 (0.518)	20.0 (0.105)	0.413*
30% MDEA - 70% H <sub>2</sub> O	5.3 (0.518)	98.2 (0.250)	0.268*
30% MDEA - 40% MEG - H <sub>2</sub> O	5.3 (0.509)	98.2 (0.163)	0.346

\*No experimental data are available in the literature at 10°C for 30 wt.% aq. MDEA. The tabulated values are predicted with an in-house model developed for H<sub>2</sub>S-MDEA-H<sub>2</sub>O systems.

It is important to state as realistic conditions as possible for calculating the cyclic capacity because its estimation is highly sensitive to the pressure and temperature selected [15]. However, it should be noted that increased cyclic capacity does not automatically make the solvent better, since the pumping costs are very small part of the overall costs of acid gas removal and the column sizes are more dependent on the gas flow rates than the solvent flow rates [16].

The pressures used in this cyclic capacity calculation are constrained by the experimental partial pressures of H<sub>2</sub>S; this is the reason why a high value, 98.2 kPa, is chosen. The results show that the cyclic capacity increased from 0.268 to 0.346 with the addition of glycol at the given composition and conditions compared to its aqueous counterpart. Although the results are optimistic, it is important to take into account that there are no experimental data at 10°C for any MDEA concentration; therefore, the model is not validated for this temperature. The only data available in the literature for H<sub>2</sub>S absorption close to 30 wt.% aq. MDEA are those from Li and Shen (30.35 wt.% MDEA solution) [17] which can be compared with our data obtained at the same temperature, 80°C. At 80°C and partial pressure of 91 kPa, the loading is 0.473, while in our solvent with MEG at slightly higher partial pressure of 95.5 kPa, the loading is 0.444 showing small deterioration. Although the experimental data from Li and Shen are regarded as inconsistent [18], this trend is in agreement with the findings for CO<sub>2</sub> removal from Wanderley et al. [19]. They report lower absorption of CO<sub>2</sub> with the addition of glycol, though the variation is more significant than in our work. This however can be explained since H<sub>2</sub>S can react directly with the amine, while CO<sub>2</sub> requires the presence of water in case of MDEA. Xu et al. [20] also investigated acid gas removal with a blend of MDEA-MEG(-H<sub>2</sub>O) and our measurements follow the trends depicted in their work.

Vapor-liquid equilibrium experiments with the very toxic hydrogen sulfide, especially at high pressures related to natural gas processing and subsea application, are very challenging and time-consuming. In our work, the composition of the vapor and the liquid phase were measured by gas chromatography (GC). Obtaining 3 experimental VLE points in one week has been typical. This is an enormous increase in the required time compared to low pressure applications with CO<sub>2</sub>, where we can typically produce up to 5 VLE points per day. This time-consuming and costly experimental work is made even more challenging in case of chemical system acting both as an H<sub>2</sub>S and water removal agent. The dual function of the solvent increases the amount of data needed to be generated (different amounts of H<sub>2</sub>S, in different MDEA-MEG-H<sub>2</sub>O blends). Thus, careful planning of experimental work is required.

Moreover, it is not only the solubility of acid gas into the solvent that is important, but also the solubility of hydrocarbons. Hydrocarbon solubility into the amine solution must be considered to ensure mainly the minimization of methane loss into the solvent, and other impact that dissolved hydrocarbons can induce. MDEA is sparingly miscible with hydrocarbons [6].

### Heat of reaction

Gas sweetening is an energy intensive process due to the regeneration stage, whose optimization requires among other the knowledge of the heat of reaction. The heat of reaction or heat of absorption provides information regarding the amount of heat per mole absorbed, which must be offered in the stripper in order to reverse the reaction and regenerate the solvent. For CO<sub>2</sub> capture from flue gases, the energy requirements for the solvent regeneration only, constitute more than 80% of the total operational expenditure (OPEX) [16]. High heat of reaction is desired in order to have high temperature sensitivity and achieve high rich loadings. At the same time, it is important that the heat of reaction is low in order to reduce the energy required to reverse the reaction and strip the solvent from the absorbed gas.

Heat of reaction data for H<sub>2</sub>S reaction with aqueous MDEA is available in the literature [21], [22] and a simple correlation dependent on amine concentration and temperature has been drawn. The low heat of reaction of MDEA, and therefore low energy requirements, is one of the main advantages of the MDEA process. Heat of reaction data for the combined 30% MDEA-65% MEG-5% H<sub>2</sub>O in weight base system is reported and compared to aqueous MDEA by Xu et al. [20]. Heat of reaction in the blend with MEG is lower than in MDEA-H<sub>2</sub>O solvent, which can be explained by the fact that the degree of solvation in an organic solvent is lower than in water. Moreover, internal data for other tertiary amines with MEG show slightly lower heat of reactions, but within the experimental uncertainty of the measurement.

### Mass transfer

VLE and kinetics go hand-by-hand in the evaluation of the removal efficiency of a solvent. Kinetics, reaction rates and mass transfer coefficients, will also define the practical aspects of the solvent application, meaning the length of the pipeline required for the removal of hydrogen sulfide and hydrate control, the location of the separation system for the solvent from the natural gas stream etc.

One aims for high reaction rates between the impurity to be removed and the solvent, in our case high H<sub>2</sub>S reaction rate with MDEA-MEG-H<sub>2</sub>O. In addition, in the case where the selective removal of H<sub>2</sub>S is desired over CO<sub>2</sub>, the solvent should have low CO<sub>2</sub> reaction rate, a property of tertiary amines like MDEA. The reaction rate of H<sub>2</sub>S with aqueous MDEA is high, while research conducted on the effect of replacing water with MEG in blends with MDEA indicated that the selectivity of H<sub>2</sub>S over CO<sub>2</sub> is improved [20]. Mass transfer properties seem to remain unaffected using a MDEA-MEG-H<sub>2</sub>O blend compared to its aqueous amine as far as CO<sub>2</sub> removal is concerned [19]. In his dissertation, Eimer [23] investigated the effect of water and MDEA concentration in a blend with TEG, on the reaction rate of H<sub>2</sub>S with the amine. He found that increasing the glycol content at either constant water or amine concentration, the rate of reaction decreases. However, we should bear in mind that the high viscosity of TEG is expected to affect the mass transfer at a higher degree than MEG.

### Trouble-free operations

#### Viscosity

The physical properties of a solvent, such as density, viscosity and surface tension, all influence its removal efficiency through their indirect effect on the diffusivity, and thus the mass transfer of the system. From those, viscosity, denoted by  $\eta$ , is the most important physical property to consider because high viscosity signifies low diffusivity and mass transfer [24] as well as high heat duties and equipment costs due to the severely affected heat exchanger's operation.

Amine concentration of 50 wt.% MDEA is considered the benchmark for selective H<sub>2</sub>S removal from natural gas, exhibiting viscosity of ca. 5.2 mPa·s at 40°C [25]–[27]. In this work we measured the density and viscosity of the binary MDEA-MEG and ternary system MDEA-MEG-H<sub>2</sub>O at various concentrations, various temperatures as low as 10°C to simulate subsea conditions and at ambient pressure. Viscosity data for the non-aqueous solvent is shown in Figure 3.

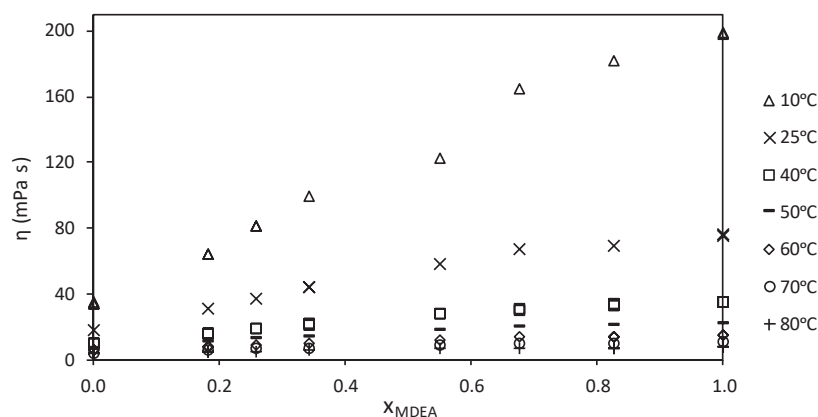


Figure 3: Viscosities of MDEA-MEG blends as a function of temperature and amine concentration (mol basis)

We observe that the viscosity increases in its blend with MEG, as expected due to the higher viscosity of MEG than the one of water. At 40°C, 50 wt.% MDEA-MEG exhibits high viscosity of 21.9 mPa·s, more than four times higher than its aqueous solution. However, the viscosity is expected to be lowered at the high pressures of the proposed process, as reported by Sobrino et al. [28]; the viscosity of 30 wt.% aq. MDEA drops from 3.1 mPa·s [26], [27] to 2.1 mPa·s at 100 bar. In addition, the viscosity of the solvent is expected to decrease with H<sub>2</sub>S loading [29].

The reason why viscosity is included under the properties related to trouble-free operations, although it significantly influences the removal efficiency of a solvent, is the fact that it can be a showstopper if pumps and other processing equipment cannot handle its viscosity. Luckily, viscous fluids, like the proposed, are not considered problematic for subsea application. Dehydration units using TEG have been operated at or near 0°C successfully without encountering viscosity-related issues [30]. TEG viscosity is comparable to the viscosity of, for example, 50 wt.% MDEA-MEG, with 19.5 mPa·s for TEG and 21.9 mPa·s for the blend at 40°C [31]. Experimental data at subsea conditions and at hydrogen sulfide loadings relevant to the process are required to get a better understanding of the viscosity encountered in such system, though.

#### *Modelling work*

Common simulation tools used in the industry, for example Aspen Plus, provide correlations and models for density and viscosity prediction. The complexity of the models required to accurately predict these physical properties increases when more components are added and when applicability concerns wide pressure and temperature ranges. The precision requirements depend on the importance of the effect that the studied property has on the process.

In this work, we compared the Aspen Plus liquid viscosity model and the NRTL-DVIS model [32], developed in our group. The latter was found superior to the Aspen Plus model for the given MDEA-MEG(-H<sub>2</sub>O) blend and temperature range, especially due to the low temperature of 10°C, relevant for subsea. We fitted our data to the two models and observed an average absolute relative deviation (AARD) of 4.25% for the Aspen model and of 2.86% for the NRTL-DVIS.

#### **Volatility**

Solvents with low viscosity, which enhance the mass transfer as explained earlier, usually have high volatility. High volatility means that the chemical has a high tendency to vaporize, thus easily escape in the vapor phase, and eventually lead to carry-over in the purified gas stream and chemical loss. Knowing the vapor pressure of the chemical can help to identify chemical losses during the design and development of a process.

Low volatility is one of the main advantages for MDEA allowing for as high as 60 wt.% aqueous MDEA concentration without significant amine losses in gas sweetening [6]. MEG volatility is also very low, making its blend with MDEA practically non-volatile.

#### **Precipitation**

For subsea applications, precipitation risks must be eliminated to ensure safe and trouble-free operations. No precipitation issues have been reported in the absorption of hydrogen sulfide/water in either MDEA or MEG, to our best knowledge.

Generally, precipitation issues render a solvent unsuitable for typical absorption / desorption systems. For example, a main disadvantage in using the otherwise promising aqueous piperazine (PZ) for CO<sub>2</sub> removal, is its risk of precipitation in both low and high loadings [33]. However, novel precipitation-based concepts for CO<sub>2</sub> removal are proposed in the literature [34] for onshore gas sweetening and are claimed to overcome the main bottleneck of solvent regeneration, i.e. the high energy requirement.

#### **Foaming**

Foaming is a critical issue in traditional gas sweetening operations, and research is conducted to define the sources and their contribution to the phenomenon [35]. Although not studied yet, foaming problems in the proposed process with a co-current absorber/pipeline and utilizing an amine-glycol solvent are not expected.



### **Chemical stability and degradation**

Chemical stability and degradation are important aspects in solvent selection, since easily degraded chemicals have a direct impact on the cost of the process, mainly through the chemical replacement cost. Degradation can be the result of chemical exposure to oxygen (oxidative degradation) or at high temperatures (thermal degradation). Especially in the case of offshore/subsea application, fresh chemicals' transportation and storage requirements should be minimized due to the limited accessibility and space/weight constraints.

MDEA is quite resistant to oxidation at absorber's conditions, however, if oxidized, MDEA forms diethanolamine. Diethanolamine is a secondary amine whose reaction with nitrite leads to carcinogenic products [36]. Thermal degradation in our case should be studied at the desorber's operation temperature. For the proposed combined solvent of MDEA-MEG, it is the degradation temperature of MDEA which will dictate the maximum temperature in the stripper because it is lower, 130°C [37], than the one of MEG, 165°C [38]. Shoukat et al. [39], [40] studied thermal stability and corrosion in aqueous CO<sub>2</sub>-loaded tertiary amines and its blends with MEG or TEG. As far as MDEA is concerned, its blend with MEG showed lower chemical stability than its aqueous solutions or its mixtures with TEG. Promising tertiary amines which demonstrated higher chemical stability in their blends with MEG are 2-(Diethylamino)ethanol (DEEA) and 3-(Diethylamino)-1,2-propanediol (DEA-1,2-PD).

The ideal solvent, in terms of chemical stability and degradation, is one that is prone to neither thermal nor oxidative degradation, while at the same time is non-toxic to the environment and biodegradable. However, it is seen that oxidatively stable solvents are not biodegradable, like MDEA. Degradation is linked with corrosion, since dissolved metals appear to act as oxidizing agents, making a solvent more prone to oxidative degradation in the presence of corrosion [36].

### **Corrosion**

Corrosion is a much more important issue when considering solvent selection than chemical stability. Although the latter is a continuous additional cost, it is far less significant than the cost of equipment replacement and production shutdown in the case of corrosion-induced material failure.

According to Namazi et al. [10] who published corrosion results of a gas sweetening plant in Iran using 45 wt.% aqueous MDEA, the amine itself is not corrosive and corrosion was not detected in the absorber after 8 years of operation. Corrosion was detected in the desorber (or stripper) and the reboiler, which is expected due to the high temperatures used. More precisely, Pal and Banat's work [41] indicate that at 120°C and in the presence of both H<sub>2</sub>S and CO<sub>2</sub>, iron solubility is much higher in lean solution than fresh solution, with 225 ppm opposed to 5 ppm in the fresh one. Furthermore, research conducted on tertiary amine-induced corrosivity shows that, in the presence of CO<sub>2</sub>, the combination of MDEA with MEG is more corrosive than the aqueous amine or its blend with TEG [39]. The study, found that other tertiary amines, such as 2-(Diethylamino)ethanol (DEEA) and 3-(Diethylamino)-1,2-propanediol (DEA-1,2-PD), yield better results.

The acid gases in water cause corrosion in equipment and pipelines, and various corrosion inhibitors can be used during natural gas transportation. The injection of MDEA and MEG to simultaneously control the corrosion and the hydrate formation has been used in the industry, an example being in the South Pars field in the Persian Gulf [42]. MDEA serves as a pH stabilizer, and research on the desired pH and the effect on the glycol performance is on-going [42]–[45].

## **Environment**

### **Biodegradation and Ecotoxicity**

In today's constantly increasing interest of industrial waste to the environment, the knowledge of the biodegradation and ecotoxicity of a chemical is necessary. Especially in those occasions where there is a risk for a slip into the environment, such as the chemical transfer subsea in long distances and deep waters, environmental effect can play a decisive role in solvent selection. Regulatory standards apply with regards to prevention and elimination of pollution from, among other, the offshore oil and gas industry, for example in the North-East Atlantic, according to the OSPAR convention [46].

Biodegradation and ecotoxicity data for different amines in the marine environment, including MDEA, is presented by Eide-Haugmo et al. [47]. They reveal that MDEA is far less biodegradable than the minimum recommended 20% biodegradability. They also show that tertiary amines have low ecotoxicity, with MDEA demonstrating an EC-50 equal to 141 mg/l. EC-50 is a concentration indicator, whose minimum recommended value for ecotoxicity is 10. Safety Data Sheets provided from MDEA suppliers support these findings. MEG suppliers characterize the chemical as non-biodegradable and non-ecotoxic. To put this in perspective, EC-50 measured in water fleas for MDEA is reported 233 mg/l (48h), while for MEG 74 000 mg/l (24h) [48], [49]. To our best knowledge, biodegradability and ecotoxicity tests for the combined MDEA-MEG solvent are not reported.

### Emissions and aerosols

In traditional absorption towers, aerosol formation and emissions are the main environmental challenge. Various impurities in the gas as well as degraded amine form small droplets, aerosols, whose emission present health and environmental risks, while also lead to severe amine carry-over and amine loss [50]. However, the proposed intensified process utilizes the pipeline as the gas-liquid contactor, where aerosol emissions is not an issue, but solvent carry-over and its effect on the consecutive gas processing stages should be investigated.

Deploying a multifunctional chemical for the selective removal of hydrogen sulfide and water vapor means that a stream rich in H<sub>2</sub>S will be discharged from the top of the stripper. This stream will need to be processed since flaring it is not an option under regulations for sulfur emissions. Depending on the amount of the hydrogen sulfide removed, liquid scavengers, redox solutions or even Claus units would be used topside to process and refrain the hydrogen sulfide from the atmosphere [51]. In North America, H<sub>2</sub>S treatment units using the liquid scavenger triazine have been integrated to existing amine facilities to assist to conform to gas specifications and stringent sulfur emission regulations [52]. Aromatic hydrocarbons (benzene, toluene, e-benzene and o-xylene, BTEX), which are hazardous air pollutants and very soluble to glycols [49], will probably also constitute the acid gas stream. Their presence and impact on the sulfur treating units should be also evaluated.

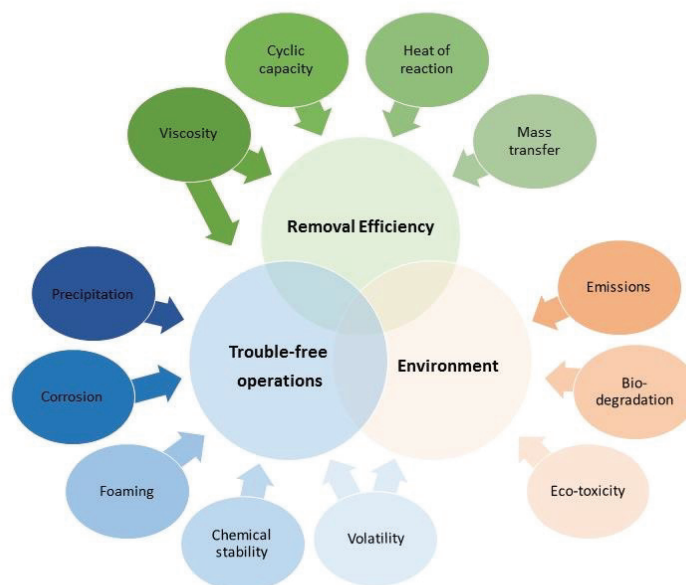


Figure 4: Simplified categorization of solvent characterization properties

## Solvent development

Each of the aforementioned properties play their role for the successful solvent selection. Traditionally, solvent development starts with the investigation of the properties related to removal efficiency. A first screening of potential chemicals is performed, often followed by vapor-liquid equilibria, cyclic capacity, mass transfer and kinetics investigation. The chemicals that are successful are thereafter studied in terms of corrosion, followed by degradation/biodegradation and ecotoxicity studies. However, issues related to safety, construction materials and of course the environment, can be absolute showstoppers even if the removal capacity of the chemical is excellent. Thus, fully characterizing a promising solvent in terms of its capture efficiency would be a waste of resources, time and funding, if found out later that it heavily degrades thermally at temperature levels commonly used during regeneration. Degradation and ecotoxicity, not only are they highly prioritized in the decision-making of solvent application, but they are also easier, faster and cheaper to test than vapor-liquid equilibrium experiments.

A more practical approach is to focus from the start to those properties that pose insurmountable obstacles on a chemical's use. Initially, a fast screening regarding removal efficiency should be performed, with corrosion, chemical stability and ecotoxicity studies performed before the full thermodynamic, kinetic and physical properties investigations. Moreover, regulations concerning gas and liquid emissions differ depending on location, thus it is of paramount importance that knowledge of those regulations will be in place on the first stages of the process development. In an attempt to distinguish those properties that are absolute showstoppers under specific operational conditions, an importance level from 1 to 3 has been assigned to them, 1 denoting highest significance and 3 lowest. Table B lists all the properties in the order of appearance in the text and indicates their significance in the specific case of the combined H<sub>2</sub>S removal and hydrate control for subsea application, based on the successive discussion.

Table B: Property significance for solvent selection intended for the combined removal of H<sub>2</sub>S and hydrate control for subsea

<i>Characteristic</i>	<i>Conditions</i>	<i>Significance</i>
Cyclic Capacity	Simultaneous H <sub>2</sub> S and hydrate control	2
Heat of reaction	Related to regeneration energy requirement	3
Mass transfer	Contact time can be adjusted by choosing solvent injection and collection points.	3
Viscosity	Important in the injection and distribution in the gas stream	2
Volatility	Influences OPEX, no emissions to air	3
Precipitation	Revenue loss due to intervention urgency	1
Foaming		2
Corrosion	High cost due to damaged equipment	1
Chemical stability / degradation	Costly storage and transportation of fresh solvent offshore	1
Biodegradation/ ecotoxicity	Regulations for use offshore	1
Emissions	Regulations about BTEX, SO <sub>x</sub> for the topside processed stream from the stripper	3

Absolute showstoppers for the investigated process are the properties related to trouble-free operations and the environment, namely precipitation, corrosion, chemical stability, biodegradation and ecotoxicity. A blend of MDEA-MEG is rather stable without precipitation or corrosivity issues. Both MDEA and MEG exhibit low ecotoxicity but they are not biodegradable. However, these components are already individually in use for subsea natural gas processing, MDEA as anti-corrosion agent [42] and MEG as a hydrate inhibitor. As discussed earlier, chemical stability of the proposed blend is inferior to other amine-glycol blends that have potential as simultaneous H<sub>2</sub>S and H<sub>2</sub>O removal agents. This is an important disadvantage whose extent requires further investigation and could lead to the replacement of the chosen amine.

The removal capacity of both hydrogen sulfide and water vapor from natural gas down to the transportation specifications is certainly the most essential requirement for the developed solvent. The absorption capacity of the proposed solvent with MEG is reduced compared to the aqueous amine that

is commonly used for H<sub>2</sub>S removal. This is expected due to the lower diffusivity of H<sub>2</sub>S in MEG than H<sub>2</sub>O, but it is acceptable since now the solvent serves two purposes and this comes at the price of reduced H<sub>2</sub>S removal capacity. Because the concentration affects the absorption capacity, the composition of the solvent must be carefully chosen. The concentration of water in the solvent will dramatically affect the viscosity which if lowered, will facilitate the use in pumps, injection and collection systems. Foaming is not expected to be a problem in this co-current contactor scheme.

Viscosity also affects indirectly the mass transfer properties. In this case, they play a less significant role because the limitation of the absorption column size is not an actual problem for subsea, where the pipeline serves as the contactor. Long pipeline allows for higher contact time and reaction of the hydrogen sulfide with the solvent. It is important, however, to mention that under high contact time, the advantage of H<sub>2</sub>S selectivity over CO<sub>2</sub> will be lost if water is present in the solvent. This is because CO<sub>2</sub> will also react with the MDEA, though in a lower rate. The regeneration scheme must be investigated in order to draw conclusions regarding the content of the water in the solvent and the energy requirements. Overall, the blend has low heat of reaction and it is believed that some water should be present to provide some steam in the reboiler. From the top of the stripper, an H<sub>2</sub>S-rich stream will be produced which will have to be further processed with similar technologies as used today for produced acid gases offshore and the emissions should be controlled according to the relevant regulations. Last but not least, the proposed solvent is not volatile and no chemical losses are expected due to volatility with the proposed configuration.

## Conclusion

A solvent development practice has been suggested focusing on the practical aspects of the solvent application from an early stage, such as corrosion and degradation. The solvent selection steps have been discussed in the framework of process development for the simultaneous removal of hydrogen sulfide and hydrate control of natural gas subsea. The paper concerns the technical performance of a solvent, which accompanied by an economic analysis, determines the final decision for the selected solvent.

Managing hydrogen sulfide removal and hydrate control with one chemical would lead to process intensification and could ensure higher energy efficiency and better utilization of resources. The feasibility of the process relies on the existence of a solvent with the dual function for H<sub>2</sub>S and H<sub>2</sub>O removal. The proposed solvent is a blend of aqueous or non-aqueous methyldiethanolamine (MDEA) and monoethylene glycol (MEG), which although demonstrates satisfactory properties in terms of removal efficiency, trouble-free operations and environmental considerations, requires further investigation. The investigation should mainly focus on the regeneration scheme of such multifunctional solvent as well as the gas-liquid contact and droplet distribution in the pipeline.

## Acknowledgements

The authors greatly acknowledge the financial support by the Research Council of Norway through the Subsea Production and Processing Center for Research Based Innovation (SUBPRO, Project 237893), which is a collaboration between the Norwegian University of Science and Technology and major industrial players in the field, including Equinor, Lundin Norway, Neptune Energy, AkerBP, Aker Solutions, DNV GL and Kongsberg ([www.ntnu.edu/subpro](http://www.ntnu.edu/subpro)).

## References Cited

- [1] C. Fossen, "SUBPRO." [Online]. Available: <https://www.ntnu.edu/subpro/>. [Accessed: 13-Mar-2019].
- [2] Z. I. Khatib and J. R. Salanitro, "Reservoir Souring: Analysis of Surveys and Experience in Sour Waterfloods," presented at the SPE Annual Technical Conference and Exhibition, 1997.
- [3] A. F. Mitchell and S. Asa, "10248: A REVIEW OF RESERVOIR SOURING FOR THREE NORTH SEA FIELDS.," p. 8.

- [4] M. K. Amosa, I. A. Mohammed, and S. A. Yaro, "Sulphide Scavengers in Oil and Gas Industry—A Review," *Nafta*, vol. 61, pp. 85–92, 2010.
- [5] A. F. Mitchell, I. Skjevrak, and J. Waage, "A Re-Evaluation of Reservoir Souring Patterns and Effect of Mitigation in a Mature North Sea Field," in *SPE International Conference on Oilfield Chemistry*, Montgomery, Texas, USA, 2017.
- [6] A. L. Kohl and R. B. Nielsen, "Chapter 2 - Alkanolamines for Hydrogen Sulfide and Carbon Dioxide Removal," in *Gas Purification*, 5th ed., Houston: Gulf Professional Publishing, 1997, pp. 40–186.
- [7] GATEkeeper, "H<sub>2</sub>S scavenging: Using Triazine," May-2014.
- [8] "UWP/Subsea on a Stick®," *Kvaerner - UWP/Subsea on a Stick®*. [Online]. Available: <https://www.kvaerner.com/Products/Subsea-on-a-Stick/>. [Accessed: 13-Mar-2019].
- [9] H. E. Alfadala and E. Al-Musleh, "Simulation of an Acid Gas Removal Process Using Methyl-diethanolamine; an Equilibrium Approach," in *Proceedings of the 1st Annual Gas Processing Symposium*, vol. 1, H. E. Alfadala, G. V. Rex Reklaitis, and M. M. El-Halwagi, Eds. Amsterdam: Elsevier, 2009, pp. 256–265.
- [10] F. Namazi and H. Almasi, "Amine Corrosion in Gas Sweetening Plant: Causes and Minimization on Real Case Study," presented at the CORROSION 2016, 2016.
- [11] A. J. L. Hutchinson, "Process for treating gases," 24-Oct-1939.
- [12] E. R. McCartney, "Gas purification and dehydration process," US2435089 A, 27-Jan-1948.
- [13] W. F. Chapin, "Purification and dehydration of gases," US2518752 A, 15-Aug-1950.
- [14] E. R. McCartney, "Extraction of acidic impurities and moisture from gases," US2547278 A, 03-Apr-1951.
- [15] I. M. Bernhardsen and H. K. Knuutila, "A review of potential amine solvents for CO<sub>2</sub> absorption process: Absorption capacity, cyclic capacity and pK<sub>a</sub>," *Int. J. Greenh. Gas Control*, vol. 61, pp. 27–48, Jun. 2017.
- [16] L. Raynal, P.-A. Bouillon, A. Gomez, and P. Broutin, "From MEA to demixing solvents and future steps, a roadmap for lowering the cost of post-combustion carbon capture," *Chem. Eng. J.*, vol. 171, no. 3, pp. 742–752, Jul. 2011.
- [17] M. H. Li and K. P. Shen, "Solubility of hydrogen sulfide in aqueous mixtures of monoethanolamine with N-methyl-diethanolamine," *J. Chem. Eng. Data*, vol. 38, no. 1, pp. 105–108, Jan. 1993.
- [18] P. J. G. Huttenhuis, N. J. Agrawal, and G. F. Versteeg, "The solubility of hydrogen sulfide in aqueous N-methyl-diethanolamine solutions," *Int. J. Oil, Gas and Coal Technology*, vol. 1, no. 4, pp. 399–424, 2008.
- [19] R. R. Wanderley, Y. Yuan, G. T. Rochelle, and H. K. Knuutila, "CO<sub>2</sub> solubility and mass transfer in water-lean solvents (in press)," 2019.
- [20] H.-J. Xu, C.-F. Zhang, and Z.-S. Zheng, "Solubility of Hydrogen Sulfide and Carbon Dioxide in a Solution of Methyl-diethanolamine Mixed with Ethylene Glycol," *Ind. Eng. Chem. Res.*, vol. 41, no. 24, pp. 6175–6180, Nov. 2002.
- [21] J. L. Oscarson and R. M. Izatt, *Enthalpies of Solution of H<sub>2</sub>S in Aqueous Methyl-diethanolamine Solutions*. Gas Processors Association, 1990.
- [22] F. Y. Jou, A. E. Mather, and F. D. Otto, "Solubility of hydrogen sulfide and carbon dioxide in aqueous methyl-diethanolamine solutions," *Ind. Eng. Chem. Process Des. Dev.*, vol. 21, no. 4, pp. 539–544, Oct. 1982.
- [23] D. Eimer, "Simultaneous removal of water and hydrogen sulphide from natural gas," Dr. Ing thesis, NTNU, Trondheim, 1994.
- [24] G. T. Rochelle, "3 - Conventional amine scrubbing for CO<sub>2</sub> capture," in *Absorption-Based Post-combustion Capture of Carbon Dioxide*, P. H. M. Feron, Ed. Woodhead Publishing, 2016, pp. 35–67.
- [25] D. D. D. Pinto, B. Johnsen, M. Awais, H. F. Svendsen, and H. K. Knuutila, "Viscosity measurements and modeling of loaded and unloaded aqueous solutions of MDEA, DMEA, DEEA and MAPA," *Chem. Eng. Sci.*, vol. 171, pp. 340–350, Nov. 2017.
- [26] M.-H. Li and Y.-C. Lie, "Densities and Viscosities of Solutions of Monoethanolamine + N-methyl-diethanolamine + Water and Monoethanolamine + 2-Amino-2-methyl-1-propanol + Water," *J. Chem. Eng. Data*, vol. 39, no. 3, pp. 444–447, Jul. 1994.
- [27] H. A. Al-Ghawas, D. P. Hagewiesche, G. Ruiz-Ibanez, and O. C. Sandall, "Physicochemical properties important for carbon dioxide absorption in aqueous methyl-diethanolamine," *J. Chem. Eng. Data*, vol. 34, no. 4, pp. 385–391, Oct. 1989.
- [28] M. Sobrino, E. I. Concepción, Á. Gómez-Hernández, M. C. Martín, and J. J. Segovia, "Viscosity and density measurements of aqueous amines at high pressures: MDEA-water and MEA-water mixtures for CO<sub>2</sub> capture," *J. Chem. Thermodyn.*, vol. 98, pp. 231–241, Jul. 2016.

- [29] M. Shokouhi and R. Ahmadi, "Measuring the density and viscosity of H<sub>2</sub>S-loaded aqueous methyldiethanolamine solution," *J. Chem. Thermodyn.*, vol. 102, pp. 228–236, Nov. 2016.
- [30] P. Holm, "Offshore TEG dehydration unit performance exceeds design," *Oil and Gas Journal*, pp. 96–103, Jan. 1993.
- [31] T. Sun and A. S. Teja, "Density, Viscosity, and Thermal Conductivity of Aqueous Ethylene, Diethylene, and Triethylene Glycol Mixtures between 290 K and 450 K," *J. Chem. Eng. Data*, vol. 48, no. 1, pp. 198–202, Jan. 2003.
- [32] D. D. D. Pinto and H. F. Svendsen, "An excess Gibbs free energy based model to calculate viscosity of multicomponent liquid mixtures," *Int. J. Greenh. Gas Control*, vol. 42, pp. 494–501, Nov. 2015.
- [33] L. Li *et al.*, "Amine blends using concentrated piperazine," *Energy Procedia*, vol. 37, pp. 353–369, Jan. 2013.
- [34] E. Sanchez-Fernandez, F. de M. Mercader, K. Misiak, L. van der Ham, M. Linders, and E. Goetheer, "New Process Concepts for CO<sub>2</sub> Capture based on Precipitating Amino Acids," *Energy Procedia*, vol. 37, pp. 1160–1171, Jan. 2013.
- [35] P. Pal, A. AbuKashabeh, S. Al-Asheh, and F. Banat, "Role of aqueous methyldiethanolamine (MDEA) as solvent in natural gas sweetening unit and process contaminants with probable reaction pathway," *J. Nat. Gas Sci. Eng.*, vol. 24, pp. 124–131, May 2015.
- [36] P. H. M. Feron, *Absorption-Based Post-combustion Capture of Carbon Dioxide*. Elsevier, 2016.
- [37] M. Pandey, "Process Optimization in Gas Sweetening Unit - A Case Study," 2005. [Online]. Available: <https://www.onepetro.org/download/conference-paper/IPTC-10735-MS?id=conference-paper%2FIPTC-10735-MS>. [Accessed: 05-Aug-2016].
- [38] GPSA, "Dehydration," in *Engineering Data Book. Section 20.*, 13th ed., Tulsa, Oklahoma: Gas Processors Suppliers Association, 2014.
- [39] U. Shoukat, G. Fytianos, and H. K. Knuutila, "Thermal stability and corrosion studies of amines for combined acid gas removal and hydrate control for subsea gas treatment systems," in *2016 Techno-Ocean (Techno-Ocean)*, 2016, pp. 176–180.
- [40] U. Shoukat, E. Baumeister, D. D. D. Pinto, and H. K. Knuutila, "Thermal stability and corrosion of tertiary amines in aqueous amine and amine-glycol-water solutions for combined acid gas and water removal," *J. Nat. Gas Sci. Eng.*, vol. 62, pp. 26–37, Feb. 2019.
- [41] P. Pal and F. Banat, "Comparison of thermal degradation between fresh and industrial aqueous methyldiethanolamine with continuous injection of H<sub>2</sub>S/CO<sub>2</sub> in high pressure reactor," *J. Nat. Gas Sci. Eng.*, vol. 29, pp. 479–487, Feb. 2016.
- [42] M. Davoudi, Y. Heidari, A. Safadoost, and S. Samieirad, "Chemical injection policy for internal corrosion prevention of South Pars sea-pipeline: A case study," *J. Nat. Gas Sci. Eng.*, vol. 21, pp. 592–599, Nov. 2014.
- [43] M. Akhfash, M. Arjmandi, Z. M. Aman, J. A. Boxall, and E. F. May, "Gas Hydrate Thermodynamic Inhibition with MDEA for Reduced MEG Circulation," *J. Chem. Eng. Data*, vol. 62, no. 9, pp. 2578–2583, Sep. 2017.
- [44] J. Kvarekval and A. Dugstad, "Pitting Corrosion in CO<sub>2</sub>/H<sub>2</sub>S Containing Glycol Solutions under Flowing Conditions," presented at the CORROSION 2005, 2005.
- [45] D. Duan, S. Jiang, Y.-S. Choi, Ne&#353, and S. Ic, "Corrosion Mechanism of Carbon Steel in MDEA-Based CO<sub>2</sub> Capture Plants," presented at the CORROSION 2013, 2013.
- [46] "OSPAR Convention," *OSPAR Commission*. [Online]. Available: <https://www.ospar.org/convention>. [Accessed: 25-Mar-2019].
- [47] I. Eide-Haugmo, O. G. Brakstad, K. A. Hoff, E. F. da Silva, and H. F. Svendsen, "Marine biodegradability and ecotoxicity of solvents for CO<sub>2</sub>-capture of natural gas," *Int. J. Greenh. Gas Control*, vol. 9, pp. 184–192, Jul. 2012.
- [48] SIGMA-ALDRICH, "Safety Data Sheet, N-methyldiethanolamine ≥99%." 2016.
- [49] SIGMA-ALDRICH, "Safety Data Sheet, Ethylene glycol, Anhydrous 99.8%." 2015.
- [50] S. M. Fulk, M. R. Beaudry, and G. T. Rochelle, "Amine Aerosol Characterization by Phase Doppler Interferometry," *Energy Procedia*, vol. 114, pp. 939–951, Jul. 2017.
- [51] J. F. Watson, "Sulfur Recovery Processes Modified For FPSO Topside Installations," presented at the Offshore Technology Conference, 2010.
- [52] M. Schulz, "Integration of H<sub>2</sub>S scavengers with amine plants," presented at the Laurance Reid Gas Conditioning, 2013.

